AGARD-CP-368

AGARD

ADVISORY GROUP FOR AEROSPACE RESEARCH & DEVELOPMENT

7 RUE ANCELLE 92200 NEUILLY SUR SEINE FRANCE

AGARD CONFERENCE PROCEEDINGS No.368

Engine Cyclic Durability by Analysis and Testing

NORTH ATLANTIC TREATY ORGANIZATION

DISTRIBUTION AND AVAILABILITY ON BACK COVER

AGARD-CP-368

NORTH ATLANTIC TREATY ORGANIZATION

ADVISORY GROUP FOR AEROSPACE RESEARCH AND DEVELOPMENT

(ORGANISATION DU TRAITE DE L'ATLANTIQUE NORD)

AGARD Conference Proceedings No.368

ENGINE CYCLIC DURABILITY BY ANALYSIS AND TESTING

Papers presented at the Propulsion and Energetics Panel 63rd (B) Specialists' Meeting,
in Lisse, Netherlands, 30 May — 1 June 1984.

THE MISSION OF AGARD

The mission of AGARD is to bring together the leading personalities of the NATO nations in the fields of science and technology relating to aerospace for the following purposes:

— Exchanging of scientific and technical information;

— Continuously stimulating advances in the aerospace sciences relevant to strengthening the common defence posture;

— Improving the co-operation among member nations in aerospace research and development;

— Providing scientific and technical advice and assistance to the North Atlantic Military Committee in the field of aerospace research and development;

— Rendering scientific and technical assistance, as requested, to other NATO bodies and to member nations in connection with research and development problems in the aerospace field;

— Providing assistance to member nations for the purpose of increasing their scientific and technical potential;

— Recommending effective ways for the member nations to use their research and development capabilities for the common benefit of the NATO community.

The highest authority within AGARD is the National Delegates Board consisting of officially appointed senior representatives from each member nation. The mission of AGARD is carried out through the Panels which are composed of experts appointed by the National Delegates, the Consultant and Exchange Programme and the Aerospace Applications Studies Programme. The results of AGARD work are reported to the member nations and the NATO Authorities through the AGARD series of publications of which this is one.

Participation in AGARD activities is by invitation only and is normally limited to citizens of the NATO nations.

Published September 1984

ISBN 92-835-0362-7

Printed by Specialised Printing Services Limited
40 Chigwell Lane, Loughton, Essex IG10 3TZ

RECENT PUBLICATIONS OF THE PROPULSION AND ENERGETICS PANEL

Conference Proceedings

Testing and Measurement Techniques in Heat Transfer and Combustion
AGARD Conference Proceedings No.281, 55th A Meeting, May 1980

Centrifugal Compressors, Flow Phenomena and Performance
AGARD Conference Proceedings No.282, 55th B Meeting, May 1980

Turbine Engine Testing
AGARD Conference Proceedings No.293, 56th Meeting, September/October 1980

Helicopter Propulsion Systems
AGARD Conference Proceedings No.302, 57th Meeting, May 1981

Ramjets and Ramrockets for Military Applications
AGARD Conference Proceedings No.307, 58th Meeting, October 1981

Problems in Bearings and Lubrication
AGARD Conference Proceedings No.323, 59th Meeting, May/June 1982

Engine Handling
AGARD Conference Proceedings No.324, 60th Meeting, October 1982

Viscous Effects in Turbomachines
AGARD Conference Proceedings No.351, 61st A Meeting, June 1983

Auxiliary Power Systems
AGARD Conference Proceedings No.352, 61st B Meeting, May 1983

Combustion Problems in Turbine Engines
AGARD Conference Proceedings No.353, 62nd Meeting, October 1983

Hazard Studies for Solid Propellant Rocket Motors
AGARD Conference Proceedings No.367, 63rd A Meeting, May 1984

Working Group Reports

Aircraft Fire Safety
AGARD Advisory Report 132, Vol.1 and Vol.2. Results of WG 11 (September and November 1979)

Turbulent Transport Phenomena (in English and French)
AGARD Advisory Report 150. Results of WG 09 (February 1980)

Through Flow Calculations in Axial Turbomachines
AGARD Advisory Report 175. Results of WG 12 (October 1981)

Alternative Jet Engine Fuels
AGARD Advisory Report 181 Vol.1 and Vol.2. Results of WG 13 (July 1982)

Suitable Averaging Techniques in Non-Uniform Internal Flows
AGARD Advisory Report 182 (in English and French). Results of WG 14 (June/August 1983)

Lecture Series Publications

Non-Destructive Inspection Methods for Propulsion Systems and Components
AGARD LS 103 (April 1979)

The Application of Design to Cost and Life Cycle Cost to Aircraft Engines
AGARD LS 107 (May 1980)

Microcomputer Applications in Power and Propulsion Systems
AGARD LS 113 (April 1981)

Aircraft Fire Safety
AGARD LS 123 (June 1982)

Operation and Performance Measurement of Engines in Sea Level Test Facilities
AGARD LS 132 (April 1984)

Ramjet and Ramrocket Propulsion Systems for Missiles
AGARD LS 136 (September 1984)

Other Publications

Airbreathing Engine Test Facility Registe
AGARD AG 269 (July 1981)

THEME

Research on gas turbine engine development during the past decade in NATO nations has concentrated heavily on obtaining a better understanding of the relationship between material characteristics, failure mechanisms, structural analysis and validation testing to gain increased service life.

The meeting surveyed the current state-of-the-art in technological areas related to improving engine life and considered the technical and economical problems and possibilities of advanced cyclic testing in the development of engines. Relationships between engine utilization and failure modes, accelerated mission testing (AMT) development, critical material characteristics, component life assessment methods, recent results of component and engine cyclic testing, and future requirements were discussed.

The topic was coordinated with the Structures and Materials Panel which has contributed papers. The meeting took place the week prior to the 1984 ASME Gas Turbine Conference thus enabling attendance at both conferences with one business excursion.

* * * *

Les recherches effectuées par les pays de l'OTAN, au cours de ces dix dernières années, dans le domaine du développement des moteurs à turbine à gaz, ont été essentiellement orientées vers une meilleure compréhension des relations entre caractéristiques du matériel, mécanismes des défaillances, analyse des structures et essais de validation, l'objectif poursuivi étant l'accroissement de la durée de vie.

Au cours de la réunion, les conférenciers ont examiné l'état de l'art dans les domaines technologiques qui sous-tendent l'amélioration de la longévité des moteurs. Ils ont étudié les problèmes et les possibilités techniques et économiques que présentent, au stade du développement des moteurs, les essais avancés aux divers régimes. Ils ont traité des sujets suivants: relation entre l'exploitation des moteurs et les modes de défaillance, mise au point d'essais accélérés en vue de missions spécifiques, caractéristiques critique des matériaux, méthodes d'évaluation de la durée de vie des composants, résultats récents d'essais de moteurs et de composants aux différents régimes, et impératifs futurs.

Ce thème a fait l'objet d'une coordination avec le Panel des Structures et Matériaux qui a fourni certaines des communications présentées. La réunion a eu lieu au cours de la semaine précédant la Conférence sur les Turbines à Gaz organisée par l'ASME en 1984, pour permettre aux personnes intéressées d'assister successivement aux deux manifestations au cours d'un même voyage.

PROPULSION AND ENERGETICS PANEL

PROGRAMME COMMITTEE

HOST NATION COORDINATOR

PANEL EXECUTIVE

ACKNOWLEDGEMENT

The Propulsion and Energetics Panel wishes to express its thanks to the Dutch National Delegates for the invitation to hold this meeting in Lisse, Netherlands, and for the facilities and personnel which made the meeting possible.

CONTENTS

*Not available at time of printing.

TECHNICAL EVALUATION REPORT

by

J.R.Nelson

1. INTRODUCTION

Powerplant capability has historically been the pacing item in aeronautical system capability. Since the advent and application of the turbine engine to aircraft systems, improvements in overall system capability have been impressive and continuous. A commonly held view of this progress is that it has generally been in terms of engine performance improvement at the expense of life and durability. A careful review of the history of turbine engine applications reveals this common view is not accurate. For example, in the mid 1940s, the first qualified US military jet engines exhibited major overhaul periods and some component lives of 10 to 15 hours, yet by the early 1950s, those early engines and the newer designs were providing 1 0-hour periods between major overhauls which was equivalent to the life/durability of reciprocating engine designs of the time as used in fighter applications. Some reports of that time note that improving life, durability and safety were of top priority, followed very closely by the need to improve fuel consumption characteristics. Since that time, while performance in terms of thrust, thrust-to-weight and specific fuel consumption has improved dramatically, so too has engine durability and life, having increased well beyond the best ever experienced for reciprocating engines in fighter/bomber applications and by thousands of hours compared to reciprocating engines in transport/airline applications.

However, due to sharply increasing engine acquisition costs and very large overall costs of ownership, it is essential that engine life be further increased. Almost as important as this increase in life is a requirement that life values be accurately predicted at initial fleet introduction for the engine and its components. In addition, usage must be tracked carefully in order to maintain a close relationship not only between predicted and actual life, but also between predicted and actual support requirements. This latter point is central not only to fleet readiness to insure stability of operations, but also to controlling support costs which, aside from the expense of fuel itself, are still several times the initial acquisition cost and are very sensitive to unexpected durability/reliability shortfalls.

It was very timely, then, that this NATO-AGARD Propulsion and Energetics Panel (PEP) specialists' meeting concentrated on summarizing recent activity and progress in Engine Cyclic Durability by Analysis and Testing. Great progress has been made in improving engine durability analysis and testing. Futhermore, not only does significant data and experience exist, but it is being accumulated at an increasing rate. The breadth of activity and interest was apparent in the contributed papers of this session and by the approximately 100 attendees. Recognizing the critical role of materials characteristics in engine durability, it was appropriate to present recent propulsion materials work in this session, including a summary of the AGARD Structures and Materials Panel (SMP) work over the past decade. Very close coordination and continuing dialogue between the PEP and SMP is highly desirable and important in all areas related to engine life and durability.

The meeting was organized around four sessions with 19 invited papers presented. Attendance was excellent at all sessions and considerable dialogue ensued, as evidenced by the questions and answers at the close of each presentation, which are included as part of this report. An initial technical evaluation summary was presented by the author to the attendees at the close of the last session.

This report will provide a condensed summary of the meeting, a detailed discussion of the contents of the papers and finally some conclusions/recommendations. The reader will note the detailed comments section (Section 3) is organized in three general areas involving: durability parameter measurement, modeling and analysis techniques, and recent engine cyclic testing results. Although the meeting was organized in four sessions, the content of the papers seemed to lend itself to grouping in the three areas noted.

Also, there is frequent reference in this report to the US Air Force terms, Accelerated Mission Testing (AMT) and Engine Structural Integrity Program (ENSIP). This frequent reference is not intended to emphasize AMT and ENSIP at the expense of other important related concepts presented at this meeting. Rather it reflects deep involvement by the author with the development of these concepts and the activities in these areas and thus they are used as a framework of reference for similar concepts and parallel activities presented in the papers and discussions.

2. SUMMARY

This 63rd (B) Specialists' Meeting of the Propulsion and Energetics Panel provided a diverse selection of topics that

generally described the status of where the NATO gas turbine engine industry stands in analysis, testing, and materials characterization technologies. A significant outcome of this meeting is the general concurrence on technology areas where the industry needs to make further progress to better understand engines and to be able to produce them more efficiently with higher performance and better durability.

The concept of Accelerated Mission Testing (AMT), by this and other names, is becoming well accepted throughout the industry both in civil and military programs. This approach is a significant improvement over past qualification testing techniques. However, AMT does not provide the total capability to avoid durability problems, but does provide a good method for identification and correction of what would otherwise become fleet introduction, or "infant mortality", problems. AMT also does an excellent first assessment of susceptibility to hot section distress, as well as providing identification of some wearout indications and HCF envelope clearance.

Understanding of temperature and load induced stress on critical engine components is essential in making life predictions for thermally sensitive parts. A major problem is that there is no simple correlation between primary recordable engine parameters and the resultant response at the component locations. This leads to questions as to the volume of data required as well as the needed accuracy for meaningful life prediction capability. For the measurement of these parameters, some manufacturers and users have an interest in recording and real-time processing of in-flight data. The purpose here is to have a real-time understanding of engine life usage. The US Air Force is committed to onboard engine health monitoring and has required this capability on all new engines both for tracking events/usage and for understanding overall engine trending and fleet support management. However, the level, format, and volume of data to be presented to maintenance personnel for effective maintenance action is the subject of intense interest and activity with no accepted solution as yet.

The need for improved capability materials continues to be a major requirement for improved durability and in recent years progress in the Powder Metallurgy (PM) concept has been most significant in this regard. Initially, these PM compounds exhibited a generic inability to provide consistent quality hardware due mainly to contamination problems in the powder preparation process. Today, through improved controls to assure "clean" powder, followed by use of extruding, forging and hot isostatic pressing manufacturing processes, the PM contaminants are reducing in number and dispersed to an acceptable level of concentration. However, with these new PM alloys, the heretofore used "safe life" approach cannot be used cost effectively. The "safe life" approach is based on the statistics of the achievement of a measurable crack in one member in a total population of a given material/component design. This measurable crack size is equal to the threshold measurement capability of the inspection process used. Based upon the time to occurrence of the crack in this one defective (minimum) member, the entire population is scrapped. The use of PM technology, however, is based on the fact that the growth rate of the crack is a more critical parameter than the time to initiation of a measurable crack. Therefore, a crack growth management of the design ("damage tolerance" philosophy) must be applied in establishing valid life numbers for PM materials specifically, and, of course, in general where "damage tolerance" is to be used rather than "safe life".

The role of protective coatings in modern gas turbine engines was re-emphasized in this session. They are essential in preventing erosion, corrosion, oxidation and overall wear. The selection of the best coating process is, however, a compromise typical of most unique design processes. Coating durability, adherence, environmental protection, and the impact of the coating on base metal mechanical properties must be considered and iterated to reach the best solution.

Several papers discussed the capabilities and limitations of current analytical modeling techniques. There is general agreement that significant strides have been made in the last two decades in the development of engine structural analysis modeling techniques and design tools. However, the application of these tools, as presented and discussed at this meeting, highlights the need for further development. Some of the earlier models did not accurately assess the complex loading relationships of gas turbine engine components. These shortcomings are now being addressed to some degree. The General Electricity Company and Pratt & Whitney, for example, have each developed empirical models to address this complex loading problem. These models are simple in nature and do not yet address multiple crack initiation that occurs in actual practice. The occurrence of these and other real life events requires that continued development of analytical techniques be vigorously pursued. Furthermore, resolution of additional questions is needed in the general areas of: boundary constraints and their accurate measurement necessary for determination of local stress fracture analyses and the required materials property data for these analyses (especially with PM materials), and how to ultimately combine these considerations into a life determination.

As previously mentioned, the "safe life" concept of life management of field hardware has been the approach used in the past to set component life limits although it resulted in high operating and support costs. For example, this approach can result in throwing away 90 percent of a turbine disc population that still has more than 50 percent of life remaining. Further, the other 10 percent of these discs remaining in service are at some risk of premature failure. The alternate "damage tolerance" approach is of course attractive in that it promises continued usage of expensive hardware if the defects or the damage is within certain specified limits. As a result, the gas turbine industry is becoming more receptive to this approach in the light of growing knowledge regarding fracture initiation and growth characteristics in various engine materials. This "damage tolerance" approach is an integral part of the US Air Force Engine Structural Integrity Program (ENSIP) philosophy.

A new life prediction verification method being utilized by the US Air Force for experimental component and engine testing is called Life Assessment Testing (LAT). Its purpose is to validate the analytical tools of life prediction and establish an early baseline durability value for engine components of advanced design. The concept requires testing components "to failure" in an efficient manner. This is accomplished by controlling temperature and stresses at critical areas of the test components. The approach promises to be cost effective in providing early evaluation of the entire design system with more

efficient use of test assets and thus could reduce and, or eliminate portions of the expensive AMT full engine testing now required as part of ENSIP.

The use of AMT and ENSIP has had significant impact on the development process of US Air Force military gas turbine engines. Intensive Cyclic Endurance (ICE) testing is a similar approach described by Ponsford (Paper 15) for the Rolls Royce RB211 engine. In either approach, this engine testing provides only a limited statistical data base, but, as previously noted, it is a powerful tool in identifying engine/component "infant mortality" problems and identifying possible distress areas in the engine hot section.

The ENSIP method provides a structured program for total engine development and it includes a durability and damage tolerance assessment, a durability and damage tolerance control plan, and a structural maintenance plan. It is also of significance to note both AMT and ENSIP/ are now part of all US Air Force initial engine development programs and are required to be carried forward through the life of the engine program in order to accommodate field usage changes, multiple system applications, engine upgrades, etc. The total process will produce more durable, reliable engines with much better defined support requirements.

The requirement for extended gas turbine engine durability has grown dramatically in the last decade. The future requirements for analysis and testing techniques must keep pace with these engine and component configuration advancements in a cost effective manner. AMT has contributed to the efficiency of test, but other additional improvements should be considered. For instance, the LAT approach previously discussed offers significant payoff. Testing efficiency can be improved also via the use of updated test facilities like the 'core engine' test facility at Pratt & Whitney (described in Paper 20) in which full engine operating conditions are cost-effectively simulated while only the core engine is on test. Improvements in the capability of instrumentation will also help satisfy the need for more accurate engine data. Improved slip ring technology, improved telemetry, noncontacting instrumentation, and optical pyrometers are typical state-of-the-art sensors/systems that must be fully exploited in order to achieve safe and efficient monitoring of test engines. The advancements achieved in finite element analysis, understanding of creep/fatigue interaction, crack growth model analysis, etc., have all been verified by engine experience. As prediction and measurement techniques improve, continued engine correlations will be required. Meetings like the AGARD meeting summarized in this document, are necessary to ensure not only current understanding of these fast-developing areas of technology, but also a healthy dialogue and critique of new approaches to improve turbine engine durability and reliability while continuing to improve performance. Extensive, duplicative effort can thus be avoided other than where needed to demonstrate consistency of results. New areas for consideration can also be identified. In that light, some recommendations are made in Section 4 of this report.

3. CONTENT OF THE MEETING

As previously noted, the subject of this meeting was rather thoroughly covered and the 19 papers plus the related questions and answers were wide ranging. However, it is useful to organize and comment on the content by division into three major topic areas. (1) In-flight measurement of critical parameters and their analysis (2) New and expanded approaches to component modeling and analytical techniques, and (3) Recent results of engine cyclic testing and correlation with field experience. In addressing the area of in-flight measurement and analysis, Paper 1 by Breitkopf and Speer emphasized there is no simple correlation between primary engine operating parameters and critical component life limiting locations for thermally sensitive parts. This leads to a strong need for accurate data measurement for life prediction and the conclusion that real time analysis by use of on board recording and processing equipment for rapid approximation of stresses is possible. An algorithm correlating flight measurable parameters and calculated versus actual stresses was presented. Paper 2 by Edmunds and Lawrence also made the point that variability and complexity of actual usage and the related thermal transients requires on board data recording. This latter paper also emphasized that an acceptable compromise between computational power and accuracy must be established. A simplified model was discussed wherein parameters causing thermal stress were determined by curve fitting measured data to known results of thermal stress analysis. Considerable discussion ensued regarding the accuracy of the approaches presented in these two papers. Also discussed was the amount of data to be acquired to assure "life accuracy". It may be said here that current US Air Force experience in advanced augmented turbofan engine designs would indicate a vast amount of data would be required to address all thermally sensitive parts with real time analysis. The need for accurate data is unquestioned, but the need and the capability for real time calculation of transient thermomechanical stresses for all parts is still to be resolved. Also to be resolved is the value of on board real-time calculations as the basis for follow-on maintenance action. In fact, extensive dialogue is underway in the US Air Force to establish the level and format of data to be presented to maintenance personnel. However, it can also be said that the US Air Force is committed to the need for on board engine health monitoring and diagnostic systems and each new engine currently being acquired will have a system with extensive capabilities in these areas. These systems are essential to the concept of engine life tracking and management as part of the overall ENSIP approach. In flight measurement of critical parameters and their analysis then, is an important area in which progress is being made. This area is of overall interest for engine life management in both military and commercial engines and concentrated effort should continue to be exerted in order to resolve the questions of on-board data volume, level of processing, and required accuracy and eventual use in engine development and the life management.

In addressing the second area, that of component modeling and analytical techniques, it can be said that component modeling is at best a science that is directed by agency policy that is itself based upon past success, intuitive feelings and fear of failure of achieving the required product. The major scientific aspects of modeling an engine component with the end result of producing a meaningful durability assessment of the engine itself can be categorized as follows.

(a) *Boundary Constraints.* The boundary constraints on a component are the temperature, pressure and body forces. It is necessary to determine these items as accurately as possible in order to have a "valid model result". This point was repeated by Papers 1, 2, 8, 10, 12, 14, 15, 17, 18, 19, and 20. In each of these papers, the point took on different forms such as: duty cycle effects on components, on-board recording of data, degradation effects, etc. However for valid results the theme was the same — one must either measure the environment or accurately predict it in order to achieve a durability assessment that is meaningful.

(b) *Stress Analysis.* The second category is the determination of the stresses that the component local area experiences as a function of the different fluctuations of the boundary constraints during the actual flights. The need for this is pointed out succinctly by Paper 17 — "a 10 percent lower stress can produce a 60 percent higher life". The major problem to be addressed is embodied in the questions. "How much stress analysis is required? — What level of acuracy is required?" Paper 1 states that a "rapid approximation of stress" is required for any "real time" life processing system. Papers 5, 8, 9, 10, 12, 13, 17, 18, 19, and 20 expressed the same need for accurate stress analysis. The problem ultimately results in an answer of "How much money and time is available to accomplish the stress analysis?" Perhaps Paper 12 summarized it best with the statement that an acceptable compromise between computational power, accuracy and cost is required when doing a stress analysis. During any specific engine design and development, the intent is to require the minimum effort to accomplish the minimum level of acceptable accuracy. Also, an important facet of durability analysis is the assessment of the design for fracture potential. In order to do this, a fracture mechanics analysis must be conducted using the calculated stress values as primary input.

(c) *Fracture Analysis.* The technology of conducting detailed fracture analyses is perhaps the fastest growing technology in the turbine engine industry. This was discussed in detail in Paper 5, and pointed out as a need generated by the onset of powder metallurgy in Papers 6, 7, 9, 19, and 20. Paper 19 pointed out the need to consider the environmental and synergistic effects of stress sequence and temperature in conducting a detailed fracture assessment of an engine component. However, one must keep in mind that basic to the fracture assessment is the all important "material property" generation at the appropriate environmental conditions and with material specimens of proper metallurgical condition. This fact was presented by Papers 5, 6, 9, 10, 12, 14, 17, 19, 20, and especially Paper 7 which showed grain size alone has significantly different effects on crack growth rates in the same material composition. In addition, the location of the crack in the component (surface or subsurface) and the surrounding stress gradient play a very important role in the resultant final fracture life value. But, perhaps the last facet of the durability assessment is the area where considerable effort has been put forth, but with essentially nonconclusive results to date. This area is the actual life determination based upon cumulative damage models and related agency policy (or nonpolicy).

(d) *Life/Durability Determination.* The process of determining the actual life of a component is very dependent upon the answers to some basic, but key questions — "What is a failure? What is safe? How sensitive is the life number to mistakes and input variations?" The answers to these questions can be given in statistical terms, historical precedence, legal considerations of responsibility of premature "failure" or a host of other terms. A good life analyst can generate a variety of answers to the life question dependent upon the degree of liability that the agency is willing to accept. This is perhaps why this PEP session had so many discussions dealing with "accuracy", "sensitivity", "economical aspects", "failure definition", and life "philosophy" after each of the papers. Papers 1, 3, 9, 11, 17, 19 and 20 all discussed different aspects of life determination and methods used for accounting for damage accumulation. What can be said about each is that all were different and none were totally wrong! In fact, this independent activity and discussion of areas of disagreement as to parameter validity, sequencing, correction factors, creep characteristics, use of classical models, etc., is healthy and needs further encouragement. If durability could be considered to be "the measure of the design life achieved without significant maintenance cost", then it is very evident how important the assessment of the life value is through either component or engine testing. In addition, the agency which can supply this test assessment most cost effectively will win out in the market place. Papers 1, 3, 4, 15, 17, 18, 19, and 20 pointed out this fact quite clearly.

(e) Of importance to note is the fact that in this area of analysis and modeling, there was a dearth of discussion on the subject of multiple cracking. There was but one short discussion of multiple cracking and then only with respect to a given single location. While this case is of interest and should be modeled and analyzed for cause and effect, the case of multiple cracking must be addressed wherein second, third, etc., cracks appear in remote locations of a single structure, e.g., first in a bolt hole of a turbine disc then in a second bolt hole or the web nonadjacent to the first crack. While this analysis may be difficult, it does represent real experience with some evidence that secondary remote cracking may delay or otherwise affect initial crack growth in some structures. Such sophisticated analysis is an area which should be reviewed for progress and focused effort.

The third major topic area covered recent results of engine cyclic testing and correlation with field experience. Presentations by Ponsford, Guibert, and Clayton reviewed extensive cyclic testing of RB211, CFM56, and F101 engines. In the case of the RB211, this commercial in-service engine developed a turbine blade life problem which was resolved by redesign resulting from iterative tailoring of an "intensive cyclic endurance" test until distress seen in the test cycle could be correlated with that seen in the field. The test was designed to demonstrate full service life in this case, which prior endurance testing to initial certification requirements did not accomplish. The need for careful control of test conditions was stressed, since it was found that local environmental conditions gave initial test results nonrepresentative of usage. For the CFM56, Guibert described the careful modeling done as part of the fan design to satisfy bird strike requirements. Screening tests and photoelastic techniques were used (Paper 3). Correlation between AMT cycles and field usage is excellent due to continuous tracking of usage and resultant AMT updates. Using this data and analysis techniques, AMTs for new engines are structured based upon projected usage and its relationship to prior usage in similar applications. Although these AMTs are only as valid

as their relative similarity to the initial application in the field, enough experience now exists to expect reasonable correlation wherein initial distress seen in the field will be quite predictable and thus maintenance planning and support activities can be accomplished at levels close to the expected. This leads to orderly introduction of engines into service and, importantly, orderly introduction of design improvements rather than the disorder of early and unexpected failures, followed by interim fixes, redesign, ultimate fixes, all on a time constrained basis. However, even with the growing confidence of the engine community in the validity of AMT and ENSIP philosophy, it is also true that AMT is expensive. Therefore, it is highly desirable that improved, more extensive analysis in the areas mentioned be accelerated to reduce the amount of required testing and thus reduce test costs. Farmer's paper (Paper 20) emphasized the need for more efficient test technique to keep development costs down and described the "core engine" test facility now in use at Pratt & Whitney which allows for proper full engine environmental testing of the core outside of full engine tests. Both he and Clayton emphasized efficient use of test time focused on those parameters which drive life limits. The previously discussed LAT testing also shows excellent potential to reduce total test costs. Both Clayton and Farmer also emphasized the need for improved inspection techniques which are usable in the field in order to assure proper engine life management according to established inspection criteria.

Finally, the author's summary comments covered two areas not previously discussed in the meeting, but of significant importance to engine structural analysis and testing. First discussed was the area of facilities for AMT. This extensive cyclic testing, especially of augmented turbofans, has required redesign of facility hardware, both for creation of the proper environmental test conditions and for durability of facility hardware itself. Particular attention must be paid now to fuels, oils, and horsepower extraction equipment in order to assure temperatures and flows appropriate to engine AMT conditions are maintained. Strengthened test stand frames, inlet screens and louvres, and exhaust diffusers are required. Overall facility maintenance costs are increased. Attention is required to devise means of reducing these costs. The second of these final areas of discussion emphasized that engine qualification still involves extensive sea level testing, testing in altitude facilities and flight testing, with all this testing done essentially to demonstrate capabilities other than that for durability. There needs to be some investigation of how to relate the extensive instrumented performance/operability testing done in altitude test facilities with the sea level AMT type testing. Selection of some key operating points and test parameters which can be related between sea level and altitude tests is needed to assure valid performance and durability relationships. These relationships must be established in order to acquire improved levels of both at acceptable cost.

4. CONCLUSIONS AND RECOMMENDATIONS

Progress in improving turbine engine durability since the initial applications of this powerplant to aircraft systems in the 1940s has been impressive. In fact, a good argument can be made that there is no area of total aircraft system design where progress has been so significant as that for engines, in terms of both performance improvement and durability improvement. However, it is also true that engines are expensive to acquire and even more expensive to maintain. A major reason for this high total cost of ownership has been due not only to engine life being less than desired, but even more significantly engine/component part lives being less than predicted. The resultant instabilities in the engine support system, especially at initial fleet introduction have caused significant, unplanned cost variances as well as shortfalls in system reliability and availability for the mission, whether military or civilian in application.

This situation has led to intense management interest and research and engineering effort to improve not only engine life itself but the ability to accurately assess and predict engine and engine component life/durability characteristics. Progress in the past decade in both testing and analysis techniques has been significant, particularly in the improved understanding of the major impact of low cycle fatigue (LCF) on engine/engine part life, especially with respect to engine hot section part life.

Considering this historical background, it was very timely to conduct this specialists' meeting to review status and progress in engine cyclic durability and the related analysis and test techniques. This section summarizes the conclusions of the review of what is a very broad area of aero-thermo-mechanical technical disciplines demanding the most sophisticated and advanced analysis and test techniques.

As a first conclusion, the concept of Accelerated Mission Testing, by this and other names (e.g., ICE — Intensive Cyclic Endurance) has become well accepted for both military and civil applications. Data summarizing three different in-service engines, RB211, CFM56, F101, were presented as well as a paper summarizing US Air Force application of AMT as part of a specified engine qualification process. Excellent correlation between engine component distress seen both in field usage and in AMT is being achieved. Special care must be taken to assure tests are representative of field conditions, which requires both that field usage be measured and tracked consistently for any changes and that test conditions be carefully controlled to assure valid environmental representation. Experience in structuring AMTs based on projected field usage is expected to give good correlation with initial field experience for new engines in new applications. This is extremely important in introducing engines to the field with proper support in terms of spare engines, spare parts, and maintenance actions. It is important to note, however, that AMT does not provide all answers for engine life and durability predictions. It is most effective at, and principally focused toward, early identification of hot section distress, although it does provide excellent information on early part wearout characteristics and related maintenance actions, performance degradation characteristics, and high cycle fatigue (HCF) responses. AMT, to be most effective, needs to be part of an iterative process of Durability and Damage Tolerance Assessment (DADTA), test and analysis, redesign, etc., which is embodied in the US Air Force ENSIP philosophy.

The need for an iterative process of test and analysis leads to a second conclusion. Engine and engine component structural analysis and the related modeling techniques have also made great strides in the past two decades. However, further improvement is needed in several areas. Early models missed many of the complex loading relationships and a large

number of the papers, as well as the most extensive discussions dealt with synergistic effects of sequencing loads/stresses, sensitivity of life calculations to boundary constraints and input variations, and safety/failure thresholds for damage accumulation accounting. Central to modeling and analysis is the generation of materials properties under proper environmental and metallurgical conditions. Potentially of greatest impact to engine life management in the field is to move toward the "damage tolerant" philosophy as opposed to the conservative "safe life" approach historically used for turbine engines in aircraft applications. The "damage tolerant" concept will significantly increase useful component lives with resultant major reduction in support costs. It is central to the US Air Force DADTA, AMT, and ENSIP approach, but is absolutely dependent upon accurate materials properties, related fracture analysis of crack growth from some threshold crack size, and controlled test verification.

Also noted as needed major improvements in expanded analysis capability are: attention to multiple cracking wherein analysis of the effects of the appearance of second, third, etc., cracks is needed for component locations remote from the initial crack, and addition of "secondary" part/design detail analysis to models which currently address essentially only major or primary parts. The latter level of sophistication will address seals, blade retainers, flanges, shrouds, etc., in addition to "primary" structures such as discs, blades, cases, ducts, and struts. Premature and unpredicted failure of these "secondary" structures is typical of current experience. Furthermore, failures of these structures, their related secondary damage, and resultant engine removal rates are driven as much or more by these "secondary" structures than by the "primary" structures.

The disagreements evidenced in the papers and discussions as to level of effort, specific areas of concentration and improvement in this general area of modeling and analysis is healthy and a fertile field for further intense and focused effort.

It is recommended that AGARD give consideration to a combined SMP/PEP session to expand the dialogue and, hopefully, accelerate understanding and convergence of solutions in the area of modeling and analysis techniques.

If AMT has been accepted as a valid test technique and component analysis/modeling has made great strides in the past decade, so there has also been great progress in data acquisition and test techniques. Both valid AMT and improved modeling are absolutely dependent on accurate measurement of temperature and load-induced stresses. A problem exists in the fact there is no direct correlation between recordable engine parameters and component time-related response. Therefore, there is a question as to the volume of data needed and levels of accuracy of the various component data to gain valid life assessments and predictions for specific engine designs. This question applies to all testing and analysis, but is of special importance to in-flight engine data acquisition and analysis. While on-board engine health monitoring systems are necessary for engine maintenance and overall management, the level of data acquired for, and the amount of, on-board analysis and diagnostics is in question. The capability for real-time calculation of transient thermomechanical stresses would appear to require very extensive data storage and high levels of accuracy to provide valid life prediction and analysis. As these systems are widely applied not only in airline usage, but in more diversified military usage — the US Air Force is requiring them as part of all new engine acquisitions — the question of data volume, level of processing and required accuracy for engine life management in the field will be resolved.

It is recommended that future PEP meetings include papers and progress reports on this area from both military and civil applications. As in the general area of modeling and analysis previously discussed, the acceptable compromises among computational power, accuracy, and cost must be established.

Since cost is always of high importance, an important conclusion of this session is that improved efficiency of test and modeling techniques is required. While good correlation of AMT and field usage-related distress is being achieved, AMT adds significantly to test hours of a typical engine development with resultant increased cost of hardware, fuel and test support. Also, AMT being essentially a cyclic test series, is very hard on the test facilities used. Test cell durability itself and the cost of its upkeep and repair as well as that of ancillary test equipment is increased. Equipment for fuel and oil handling and power extraction must be more closely designed and controlled to assure valid engine and component test conditions. Approaches to reduce required test time are thus needed. The LAT approach and "core engine" testing described in this meeting are typical of improved test approaches which promise to reduce required AMT hours. Also, AMT is but one type of overall qualification testing. Extensive testing is also accomplished to establish sea level and altitude performance capabilities of an engine and its components. Selection of some key operating points and test parameters to cross-correlate and validate performance and durability test data is needed. Some portions of each type of testing and analysis may thus be shortened and models improved along with overall cost effectiveness.

It is recommended that PEP review current efforts to utilize and cross-correlate the various test data acquired in component, engine qualification activities for potential areas of improved understanding of performance/durability trades and overall test efficiency.

A final comment — performance and durability goals are not necessarily opposed, they can be complementary in today's advanced engine designs. For instance, durable seals, retainers, nozzle actuators, as well as primary gas path parts are mandatory for good performance retention which is now clearly recognized as being important enough to trade for peak initial performance. Reliable, predictable performance retained for long periods at slightly less than the maximum performance available from a new engine is of far more operational value than a maximum performance level which quickly deteriorates to significantly lower levels. This has brought us to a period of engine design wherein we must treat performance and durability as inseparable from the moment of initial design and throughout the useful life of an engine. As noted in these Conclusions and Recommendations, much progress has been made in engine durability through improvements in design, analysis, and test. It is apparent much work is yet to be done and meetings such as this 63rd (B) Specialists' Meeting of the PEP with SMP support can be very fruitful in helping to focus and prioritize NATO research and development energies in

IN-FLIGHT EVALUATION OF LCF LIFE CONSUMPTION OF CRITICAL ROTOR COMPONENTS SUBJECTED TO HIGH TRANSIENT THERMAL STRESS

G. E. Breitkopf and T. M. Speer
Motoren- und Turbinen-Union München GmbH
Dachauer Strasse 665
8000 Munich 50
West Germany

SUMMARY

Utilization of the full life potential of critical gas turbine engine rotor components is possible only subject to adequate knowledge of the actual engine usage.

There is no simple correlation between the primary operating parameters and the stresses at critical points for components subjected to thermal stresses. For these components, the individual on-board calculation of the life consumption for each critical point during the flight is the most accurate and handiest method.

An essential part of the method is a speedy and adequately accurate approximation procedure for determining the transient temperatures and thermal stresses.

An algorithm for computing LCF-life consumption on this basis is introduced, which can be included in a microprocessor for on-board in-flight evaluation.

The principle behind the method consists in that the heat-conductive structure is taken to be a multidimensional transfer system, with the temperature being the system variable, and speed, gas temperature and gas pressure being the control parameters. The transfer characteristics are determined by finite-element analysis of appropriate test signals.

Nomenclature

T	temp. distribution, field, profile (absolute)
θ	temp. distribution, field, profile (rel. to gas temp.)
T_G	gas temperature across the disk
p_G	gas pressure across the disk
N	speed
t	time
Δt	time interval
n	number of "distinctive" points
α	time scaling factor
λ	weight factor

Subscripts

j	denotes the j-th basic function

1 Introduction

The durability and reliability of highly-stressed turbine rotors of modern jet engines can be assured only when based on a design system that takes into consideration both the design and the utilization phases.

The essential components of such a system and their interactions are described elsewhere, for example see Tiffany et al.[1].

According to the crack initiation-based safe life concept usual today, a specific life is determined for each critical point of the highly-stressed components in terms of reference cycles, where a failure probability can be allocated for each number of cycles completed. To the number of cycles on which approval for usage is based there belongs, in particular, an accepted residual failure probability. If this number of cycles is exceeded during usage, the probability of failure increases.

By way of example, figure 1 shows the conditions at the bore of a high-pressure compressor disk, where 3,000 load cycles corresponds to a failure probability of 0.1%. If this figure is exceeded by 10%, the failure probability increases from 0.1% to 0.28%, that is to say almost threefold.

Similarly, with a retirement for cause concept the reliability depends on the knowledge of the actual number of cycles completed. It depends on the certainty of cracks being discovered in good time by inspection. The intervals between inspections depend on the usage.

However, the load history of turbine rotors in military aircraft engines is seldom known. This means that the number of cycles completed must usually be taken to be a stochastic value, for which there exists an estimate of

The reason for this weak spot of the system is attributable to the fact that there is no simple, clear relationship between easily available parameters from usage, especially flight duration and nature of mission, and the corresponding number of cycles completed.

It is much easier to make such allocations if standardized operating sequences which include typical characteristics of actual flights, e. g. AMT cycles[2] can be used as a yardstick of the fatigue strength of a component, rather than using simple min./max. reference cycles. However, there are also no simple correlations for converting flights into the equivalent number of such standard sequences.

There are three basic methods for determining the usage:

- The use of overall cyclic exchange rates for converting the flying hours into the number of completed reference cycles or sequences;
- The use of different cyclic exchange rates depending on the nature of the mission flown, and
- Calculation subsequent to each flight on the basis of the time history of the relevant flight and engine parameters.

Experience shows that the life consumption based on flying hours varies considerably for the same type of aircraft and engine in military usage, for example see May et al.[3]. Differences of a factor of 10 from flight to flight are not uncommon.

Hence, for reasons of both economy and safety, the use of overall cyclic exchange rates can be acceptable only when the mission mix of all the aircraft is known and all engines undergo the same mission mix, and when the life consumption for this mission mix is known. Generally, all three prerequisites are not sufficiently met, meaning that high exchange rates must be used.

In the case of the safe-life concept, the proportion of the inherent cyclic strength of components, which is not used by the average engine, consequently considerably exceeds the value which is already high as it is, for example see Annis et al.[4]. With retirement for cause, on the other hand, very short inspection intervals are obligatory.

Evaluation of the flown missions using different cyclic exchange rates is probably the most commonly used method. In contrast to the method of using the overall cyclic exchange rates, this procedure offers the chance of appreciably greater accuracy.

If flown missions are classified according to specific characteristics and the relevant cyclic exchange rates are determined on a broad data basis for each class, this method can have sufficient accuracy for cold section parts, and it can be the optimal solution for such components in respect of the contradictory aspects of safety and life cycle costs.

But this is not very probable when it comes to the hot section components, since appropriate classification of flights in this case is very elaborate.

2 Acquisition of life consumption of hot section parts

Essentially, cold section components are stressed by centrifugal forces, which depend linearly on the square of the rotor speed. Consequently, for these components there is a clear correlation between the speed characteristics and the load history.

In contrast, the stressing of the hot section components results only from the superimposition of the centrifugal force stresses on the thermal stresses.

The thermal stresses are a function of the temperature distribution in the relevant components. As a result, in comparison with all primary operating parameters, such as thrust, gas temperature, speed and gas pressure, these stresses exhibit the same complex time behaviour as the rotor temperatures.

With values of between 1 and 1,000 seconds, the time constants of the dynamic temperature behaviour are several orders of magnitude greater than the time constants of the operating parameters. Consequently, any clear relationship to the time behaviour of the operating parameters becomes lost in the load history of the hot section parts. Furthermore, the load characteristics of the various critical areas of the rotor are no longer similar. This is made clear in figures 2, 3 and 4.

Figure 2 shows the behaviour of the gas temperature in a rear stage of a high-pressure compressor and the temperature behaviour at two points of the disk for a tactical air/air mission.

It is recognizable that at its rim, the disk temperature follows fluctuations in the gas temperature, which is closely related to the speed, whereas the disk bore reacts to temperature fluctuations with considerable sluggishness.

The relevant loading for the two typical, critical areas rim and bore is plotted in the form of the maximum principal stress over the time in figure 3 and 4.

During the departure phase, high thermally-induced compressive stresses occur in the rim, giving rise to a negative overall stress here. Deceleration causes corresponding thermal tensile stresses to occur, to which the likewise positive centrifugal force stresses are added. On the other hand, during accelerations thermal tensile stresses, and thus high positive overall stresses, occur at the bore, whilst thermally-induced compressive stresses occur during decelerations.

Although there exist similar general patterns of the stress-time characteristics for other critical areas of rotor disks as well, the time behaviour of the loading at a critical point nevertheless in detail represents a sequence of stress maxima and minima with continuously varying mean stress and temperature, whose relationship to the primary operating parameters is not immediately clear.

Therefore, classification of the flights must be made on the basis of the individual characteristics of the time behaviour of the primary operating parameters, which exert a significant influence on the stresses at the critical points.

Figure 5 represents the general course of a flight on the basis of the time behaviour of the rotor speed, as also used as a tool for TURBISTAN[5].

Apparently the beginning and end of the flight, including the elements ground time and departure, and landing and taxi, respectively, are of a deterministic character, with regard to both the succession of the elements and the pattern of the elements. However, the beginning and end of the flight include a number of parameters, such as duration of warm-up period or number of checks, whose value is shown to be random. In contrast, with the centre manoeuvring elements, it is their number, sequence and length as well as the pattern of their time function which are random.

The figure shows the main characteristics which exert the greatest influence on the stress behaviour of the hot section parts, and consequently on the life consumption during the flight. In principle, the influence of any single parameter cannot be regarded separately from that of the others.

As an example of the influence of these parameters, a duty cycle with three different warm-up periods of 3, 10 and 20 minutes is represented in figure 6. The thermal stress behaviour is plotted with the speed behaviour for a high-pressure compressor disk, where the stress minimum and maximum of the main cycle are identified for the three periods. The shorter the warm-up phase, the lesser is the stress minimum and the greater is the span of the main cycle. With a warm-up period of 3 minutes in comparison to 20 minutes, the life consumption during this flight increases by 52%.

As highlighted in table 1, the flight characteristics, which are at first random, are determined by the conditions of the flight. A distinction is made between conditions that principally affect the mission mix and those that particularly affect the life consumption of a mission of a specific nature, as well as those which chiefly lead to discrepancies in the accumulated life consumption of a specific rotor with average consumption of the collective.

It becomes clear that the method of different cyclic exchange rates is likely to provide only a very limited degree of accuracy as long as just a few of the many important flight conditions, such as the mission profile of the formation and geographical conditions of the operation area, are considered. Furthermore, it is apparent that the criteria number of throttle excursions, number of full thermal cycles and engine hot time, previously often used, will not suffice for suitably accurate assessment of flights.

On the other hand, experience shows that under the conditions of actual operation, the large number of influences in no way means that a lengthy operating time of each engine will always result in a mean life consumption within an acceptable scatter, see Koschel[6]. Thus, with simultaneous high utilization of the inherent life of the components, the risk of overshooting the approved usage period could be avoided only when the missions actually flown are assessed on the basis of the numerous pertinent criteria.

However, in all probability this would be practicable only as an interim solution. Instead, the on-line computation of the life consumed during the flight, and individually for each engine, out of the measured relevant flight and engine parameters offers itself as the best solution. This procedure is appreciably more accurate, is less cumbersome and avoids the large logistical

expenditure required by the on-ground evaluation of recorded flight data, for example see Bertolina[7].

The general procedure is illustrated in figure 7, where the flight is processed in steps in real time. First, the gas temperatures and pressures for each step are determined from the relevant flight parameters speed, altitude and outside temperature and from the engine parameters speed and turbine section gas temperature. Next, the momentary temperature distribution in the hot section parts is calculated. From this the momentary thermal stresses are derived. The centrifugal force stresses are calculated as a function of the engine speed, and are superimposed on the thermal stresses to give the overall stresses. The time functions of the overall stresses are broken down into cycles, and the corresponding damage for each cycle is worked out and accumulated.

Because the thermal stresses have very great influence on the life consumption, they must be calculated with great accuracy. In particular, the determination of the time behaviour of the temperature distribution in the critical components, necessary to achieve this high accuracy, presents a problem. There is no known analytical solution of the partial differential equations, which describe the temperature time behaviour of the rotor structure, for complex geometries. Moreover, precise numerical methods (finite-element or difference methods), which would otherwise be used, do not come into question because of the time and the amount of computer hardware they require. Consequently, a rapid and accurate approximation procedure must be used.

Such a procedure is described below. A suitable method for the on-line calculation of the accompanying thermal stresses is also given.

3 Temperature approximation

3.1 Rotor as transfer system

The heat-conducting structure of a gas-turbine rotor may be regarded as a transfer system, as illustrated in figure 8.

If the operating parameters are held constant for a time, a quite specific temperature distribution in the rotor at the end of this period will result from the temperature distribution at the beginning of the period and from the value of the operating parameters. This final temperature distribution may be regarded as being the response to the input signals "operating parameters" and "initial temperature distribution".

The search is for the system response at any time to any initial temperature distribution and any value of the operating parameters. In principle, the procedure in the method presented here is that, first, the system response to a set of selected values of the input variables is ascertained once and for all. Then, to carry out a time step, the actual vector of the input variables is represented in suitable manner by the selected input signals. This occurs essentially by superimposing the initial temperature distributions of the set. The system response is then in the form of an analogous superimposition of the corresponding known system responses. Thus, it is possible to deduce the actual temperature development from known temperature developments, resulting from specific initial temperature distributions, commencing with the given temperature distribution in the rotor.

3.2 Basic functions

Thus, the basis of the approximation method consists in a set of initial temperature distributions, for which the eventual temperature development - the system response - is known. This response is known from a finite-elemen. analysis of the rotor, which is based on rig tests. Using this numerical model, the temperature development of the rotor with constant operating parameters up to steady-state condition is calculated in time-steps for selected initial temperature distributions. Every momentary transient temperature distribution, occurring here, is available for the approximation as an input signal in the above sense, since the response - the eventual temperature distribution after an interval of arbitrary duration - is known. Each of these calculated temperature-time relationships is called a "basic function".

The information about the behaviour of the complete heat-conducting structure is provided for the approximation by means of these basic functions.

3.3 Remarks

The continuous behaviour of the operating parameters is replaced by a step-by-step constant behaviour, where the values of the operating parameters at the end of an interval are taken to be constant for the whole interval. This approaches the real situation accurately enough, since the intervals under consideration are short. The duration of the shortest interval is 0.5 seconds; longer intervals are acceptable with slight operating parameter gradients.

The individual rotor stages are treated separately insofar as their temperature fields are approximated individually. This is possible for two reasons:

- The thermal coupling between the disks is far smaller than the heat convection from the disks to the ambient gas and than the heat transfer within a disk;
- The information about the thermal coupling between the disks is contained fully in the basic functions, and is used by the algorithm for the approximation of the temperature field of the disk under consideration.

Below, 'temperature distribution' is used for denoting the temperature at all points of the complete rotor, and 'temperature field' for the temperature of a disk.

The temperature development of a disk is determined by the initial temperature field of this disk as well as by the operating parameters:

- Speed N
- Temperature of the gas T_G across the disk
- Pressure of the gas p_G across the disk

The speed N is generally present as a measured quantity. The values T_G and p_G are calculated from the measured operating parameters 'total condition' at the engine intake and in the turbine section and speeds, from relationships, which arise out of the engine performance map.

3.4 Summarized algorithm

The transient temperature field development of a disk is evaluated time step by time step. In each time step the known quantities are the initial temperature field of the disk and the values of the operating parameters. The sought-after quantity is the temperature field following the elapse of the time-interval Δt.

The calculation requires a number of steps (figure 9):

- From every basic function, determination of that momentary temperature profile which corresponds best to the actual temperature profile
- Representation of the actual temperature profile as a linear combination of some of the best corresponding temperature profiles
- Adaptation of the time scales of the basic functions to the actual values of the operating parameters
- Combination of the temperature changes in the basic functions in accordance with the linear combination found, in order to proceed by the time interval Δt.

3.5 Principle behind algorithm

The starting-point of the temperature approximation for a time step is characterized by the temperature field at the beginning of the time step and by the operating parameters taken as constants for the whole interval.

For the further temperature development, it is the position of the initial temperature field in relation to the gas temperature that is relevant, rather than the absolute level of the field. Hence, instead of the 'absolute' temperature fields T, the 'relative' temperature fields $\theta = T_G - T$ are considered. Similarly, the basic functions T_j are converted into $\theta_j = T_{G,j} - T_j$, with the gas temperature $T_{G,j}$ being used as a basis in their calculation.

The influence of the initial temperature field and of the operating parameters on the eventual temperature development - i. e. on the transfer characteristics of the rotor - can be kept largely separate. The eventual temperature field is continuously and, within limits, linearly dependent on the initial temperature field. This is to say, for a given fixed initial temperature field, the non-linear transfer system will be approximated by a linear one for initial temperature fields, adjacent to the given one. For a given rotor structure, the time constants which determine the transfer characteristics change mainly in dependence on the operating parameters.

3.5.1 Determination of most suitable temperature profile from basic functions

The system behaviour subject to constant operating parameters is contained in the basic functions. If there is a point in one of the basic functions at which the (relative) temperature field coincides with the actual (relative) temperature field, the further temperature development can be read directly from this basic function. However, this is generally not the case. Consequently, the times at which the temperature field of the basic function and the actual temperature field exhibit the best possible agreement, i. e. minimum

of squares sum of the differences in the temperature at the individual points of the rotor system, are evaluated from all basic functions.

The shape of a temperature field of a disk can be characterized with sufficient accuracy by the temperatures at a few points. This is explained by figure 10, which as an example shows a high-pressure turbine disk and the temperature plotted versus disk radius for characteristic steady states and transient states, covering the whole spectrum of the operating conditions.

All these fields can be represented by the temperature of just three marked "distinctive" areas rim, web and bore. However, more complex shapes of disks may require a somewhat higher number (n) of distinctive areas.

If two temperature fields at the distinctive areas correspond, i. e. have the same 'temperature profiles', their subsequent development will also be the same, subject to the operating parameters being the same. Thus, at any time in the future, the temperature changes at all points, referred to the initial temperature, will approximately agree.

Hence, in the search for similar temperature fields of the basic functions, it is sufficient to concentrate on the temperature differences at the distinctive points. For every basic function there will then be a temperature profile which best approximates the actual temperature profile.

3.5.2 Representation of actual temperature profiles as convex linear combination

Selecting the n+1 best temperature profiles and isolating any duplicates, the actual temperature profile is represented by a convex linear combination of these n+1 profiles. By definition a linear combination is convex when none of the coefficients concerned is negative and their sum equals 1. The following geometrical approach may be of assistance here: the temperature profiles give the temperatures at n points of the disk. Each profile represents an n-dimensional vector or a point in an n-dimensional space. In the above case of n=3, the thus-determined four temperature profiles form the corners of a tetrahedron (three-dimensional space), in the interior (including boundary) of which lies the point of the actual temperature profile (precisely then the linear combination is convex).

3.5.3 Interpolation of eventual temperature

Having obtained such a linear combination, one proceeds with the aid of the known temperature development of the basic functions whose temperature profiles go into the linear combination: for every point on the disk, the temperature change is represented for the time in question by a linear combination of the known changes in these temperature fields, using the same linear combination as in the representation of the initial temperature profile.

This procedure is based on the local linearization of the transfer system. This is illustrated geometrically by the fact that the relative position of the actual temperature profile in the above-described tetrahedron is maintained for short intervals during the temperature development. Expressing it more formally, this means that for each point under consideration, the temperature after a short interval is a function of the initial temperature profile. If this profile changes, the consequent change in the eventual temperature is linearly dependent on this change in the initial profile.

This linear interpolation of the eventual temperature is permissible because, firstly, the assumed linearity of slight changes in the initial temperature profile can be confirmed on the basis of known temperature - time behaviour and, secondly, it is ensured that the temperature profiles processed are not far removed from one another, since they all lie close to the actual profile.

If none of the possible linear combinations, used for representing the actual temperature profile, is convex, the above procedure corresponds to a linear extrapolation, which in certain circumstances can lead to considerable inaccuracies. The procedure to be followed in this situation is described in section 3.5.5.

3.5.4 Transformation of time scale

When interpolating the future temperature development, it must be remembered that the time constants of temperature field changes depend on the operating parameters (N, T_G, p_G).

Essentially, this is a consequence of the dependence of the heat transfer coefficients on the operating parameters. Consideration of the future temperature development of identical relative temperature fields with differing operating parameters reveals that the individual temperature - time characteristics can be made to coincide approximately by modifying the time scaling. Based on the nature of the functional relationship between the operating parameters and the coefficients of heat transfer, the time scaling factors

can be evaluated as being proportional to appropriate powers of the operating parameters.

In tracing the temperature development of the disk back to that of the basic functions, the difference between the actual operating parameters and the operating parameters associated with the basic functions must be borne in mind. For this, the time scales of the basic functions are adapted to the actual operating parameters by means of the time axis scaling factors.

To determine the eventual temperature of the individual points used for the interpolation, one proceeds in these shortened or lengthened basic functions by the actual period under consideration.

3.5.5 Treatment of profiles with no possible convex linear combination

If no convex linear combination can be obtained for representation of the actual temperature profile, in the case of n=3 the profile will be located outside the tetrahedron spanned by the basic function temperature profiles.

Comparisons have shown that as long as temperature profiles are not too far removed from one another, the ratio of actual to future temperature is nearly constant point by point. Consequently, the eventual temperature of the actual temperature profile can be calculated safely point by point from the future temperature of that profile on the surface of the tetrahedron adjacent to the actual profile.

4 Computation of transient thermal stresses

The thermal stresses are a function of the momentary temperature distribution for a given rotor structure.

Experience shows that very simple set-ups, such as linear combinations of characteristic temperatures, for example, can be found for representing the thermal stresses from the temperatures.

For example the thermal stresses in all critical areas of the disk shown in figure 10 can be optimally represented out of a linear combination of the three typical areas bore, web and rim.

5 Accuracy

The applicability of any fast method of approximating transient temperatures and stresses to a great extent depends on the accuracy of the method.

An accuracy estimation of the method under discussion on an analytical basis would involve considerable difficulties, and has therefore not been attempted so far.

However, the accuracy of the method can be estimated by examining sample applications.

Such a sample flight is shown in figure 11. The sequence of events includes the take-off phase, various cruise and manoeuvring elements and the landing. Intermittent constant conditions have been assumed for this flight. This means that the work involved in modelling the boundary conditions in the exact numerical model remains acceptable without diminishing the validity of the statement from the comparison of exact temperatures (FE full analysis) and approximated temperatures.

The temperature behaviour of the disk depicted in figure 10 is shown for the areas rim, web and bore. The maximum error in modelling the temperatures amounts to 25 K. The differences between the three characteristic temperatures are approximated with a maximum error of 35 K. These maximum errors are typical maximum values, and in principle they can be reduced at will by increasing the number of applied basic functions.

For assessing the accuracy of the stress modelling with given temperature distribution, the error is shown in figure 10 as the difference between exact thermal stress (finite element calculation) and approximated values for the critical area bore. The maximum error is 2.1% of the maximum thermal stress that occurs.

Finally, for the critical area bore, the exact overall stress and the stress determined by the temperature and stress approximation are represented in figure 12 for the example sequence shown in figure 11. The maximum error amounts to 6%, which is likewise a typical maximum value.

6 Calculation effort

Next to the accuracy, the most important criterion concerning the applicability of an approximation method is the amount of effort required.

The computational work involved in the method under discussion is nearly negligible in comparison with the time required for a full numerical finite-element analysis.

Furthermore, the storage requirements are such that the method can be applied using a microprocessor, enabling the LCF of a rotor to be computed on-board during the flight. With the 16-bit processors available today, this means that all critical areas of the rotor subjected to high thermal stress can be processed within a period of 0.5 seconds, thus guaranteeing real-time computation.

7 Conclusions

The calculation procedure under review offers the opportunity of a rapid approximation of transient temperatures and thermal stresses in the rotor structure of a gas turbine engine.

The method can be implemented with the aid of a microprocessor system, permitting the LCF life consumption of components subject to considerable thermal stresses, such as HP turbine and compressor stages, also to be calculated with good accuracy in flight.

In view of the large scatter in the life consumption per hour flown and the large number of influencing parameters, concerning the hot section components, calculation of the life actually consumed per flight on completion of the flight would seem to be the only method that is simultaneously simple to handle and sufficiently accurate to enable the cyclic strength of the components to be used to the full.

References

1 Tiffany, C.F.; Cowie, W.D.: Progress on the ENSIP Approach to Improved Structural Integrity in Gas Turbine Engines.
ASME 78-WA/GT-13

2 Turnbull, R.C.: Recent General Electric engine development testing for improved service life. SAE Paper 780990

3 May, R.J.; Chaffee, D.R.; Stumbo, P.B.; Reitz, M.D.: Tactical aircraft engine usage - a statistical study.
J. Aircraft, Vol. 20 (1983), No. 4, pp 338-344

4 Annis, C.G.; Vanwanderham, M.C.; Harris, J.A.; Sims, D.L.
Gas turbine engine disk retirement for cause: An application of fracture mechanics and NDE.
ASME 80-GT-127

5 TURBISTAN: International working group activity for developing standardized gas turbine load sequences for purposes of materials testing.

6 Koschel, W.: Operational engine usage.
AGARD-CP-324 Engine handling

7 Bertolina, E.: Flight parameters recording for safety monitoring and investigations.
AGARD-CP-347 Flight mechanics and system design lessons from operational experience

Characteristic affected	Flight conditions exerting influence on life consumption	Relevant characteristics during flight
Mission mix	Mission profile of formation	Manoeuvring element parameters (sequencing of elements)
Life consumption per mission of certain type	Geographical conditions of operation area	Duration of warm-up Duration of departure Duration of taxi
	Position of aircraft in formation Pilot's experience	Manoeuvring element parameters (No. of throttle excursions)
	Ground-handling procedures	Ground time parameters Duration of taxi
	Variations in a mission, e.g. repeated touch/go, length of mission components	Manoeuvring element parameters Landing parameters
Discrepancy between usage of individual engine and mean value	Condition of engine concerned (settings, clearances, etc.)	Max. stress 100 % stress
	Operation planning	Manoeuvring element parameters
	Incidents during operation	All parameters

TAB. 1 SENSITIVITY OF LCF LIFE CONSUMPTION TO RELEVANT USAGE ITEMS

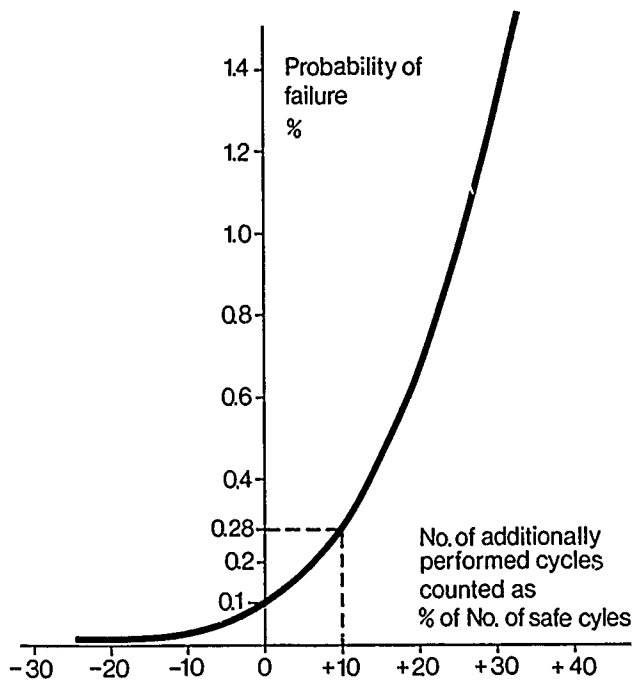

FIG. 1 PROBABILITY OF FAILURE VS EFFECTIVE CYCLES

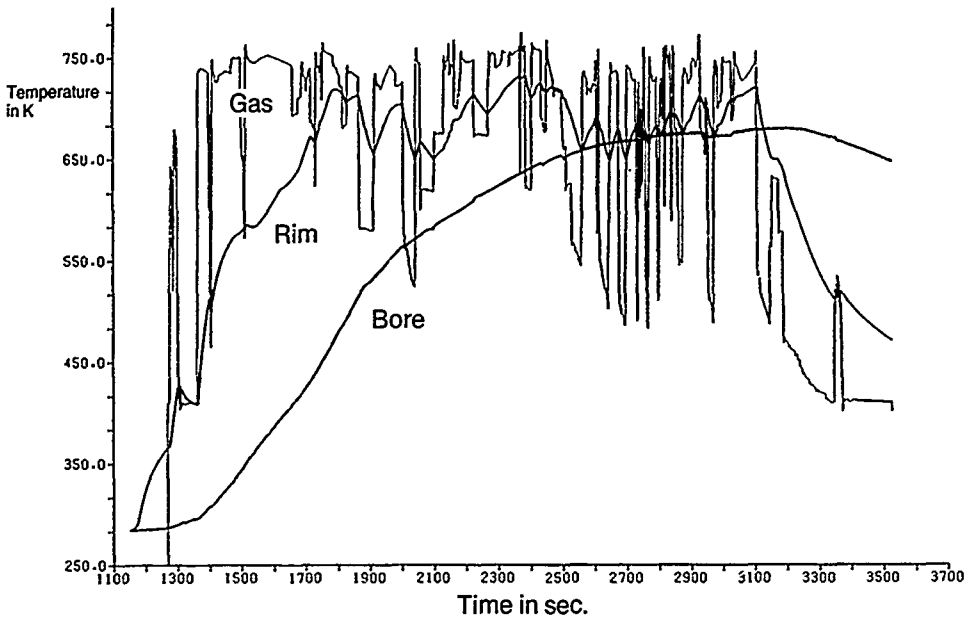

FIG. 2 TACTICAL AIR/AIR MISSION
HPC DISK TEMPERATURE HISTORY

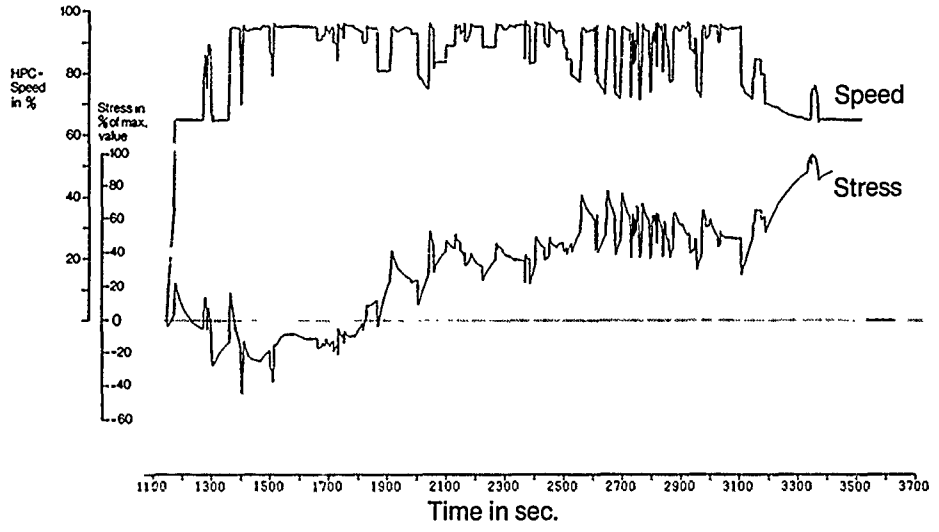

FIG. 3 TACTICAL AIR/AIR MISSION
HPC DISK RIM CRITICAL AREA. STRESS HISTORY

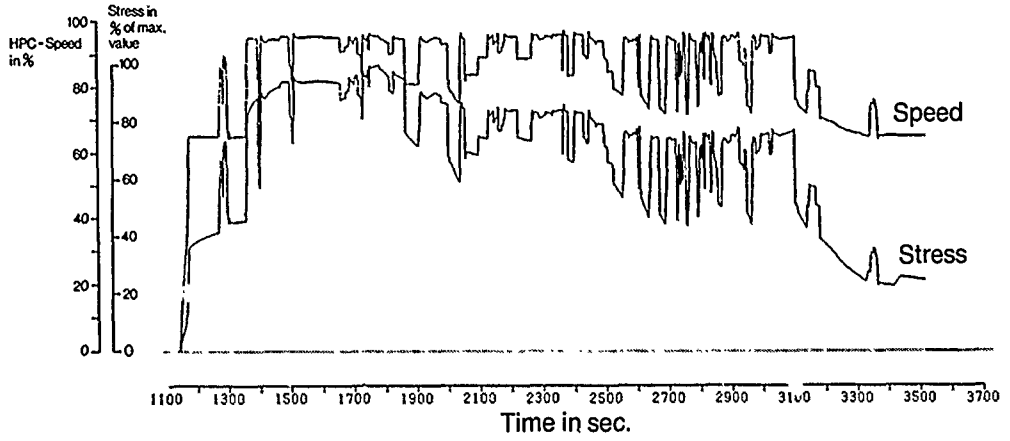

FIG. 4 TACTICAL AIR/AIR MISSION
HPC DISK BORE CRITICAL AREA. STRESS HISTORY

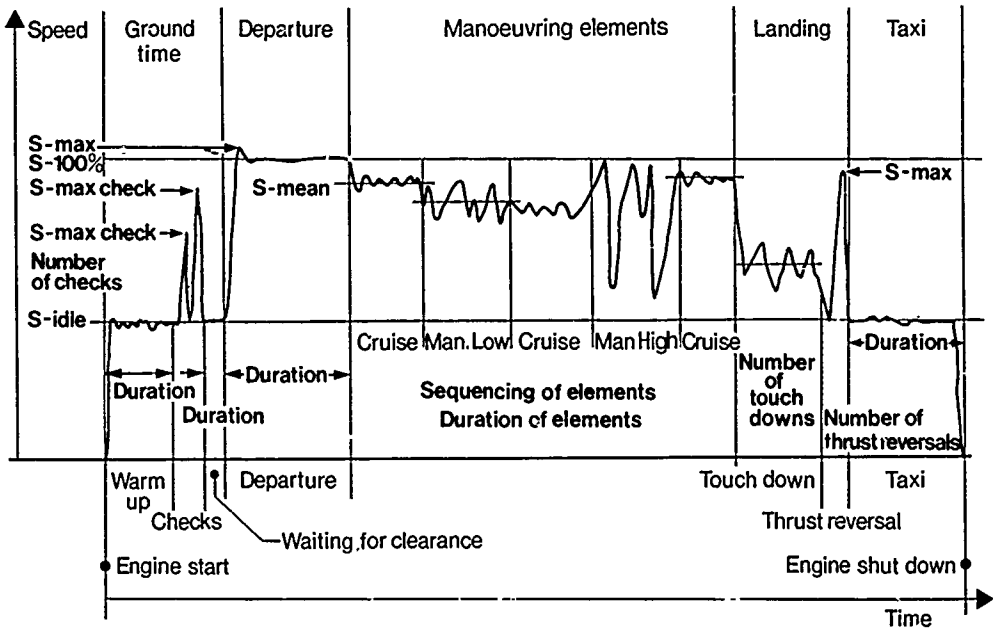

FIG. 5 GENERAL MISSION PATTERN WITH LCF-RELEVANT MAIN PARAMETERS

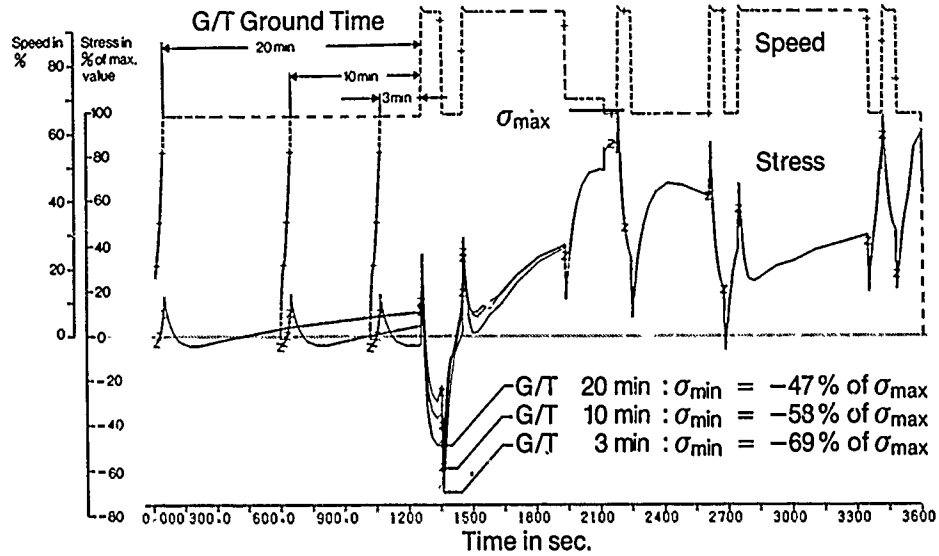

FIG. 6 DIFFERENCE IN HPC DISK RIM STRESS HISTORY DUE TO DIFFERENT GROUND TIMES

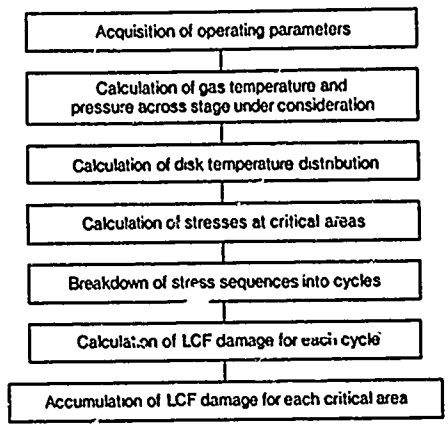

FIG. 7

FLOW CHART
MISSION ANALYSIS

CALCULATION OF
LCF-LIFE CONSUMPTION

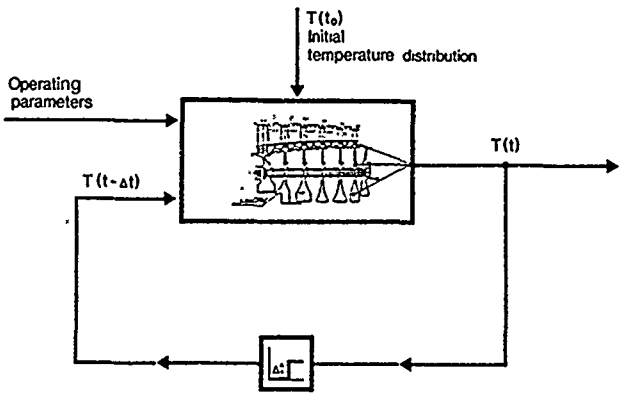

FIG. 8 GT-ROTOR AS TRANSFER SYSTEM

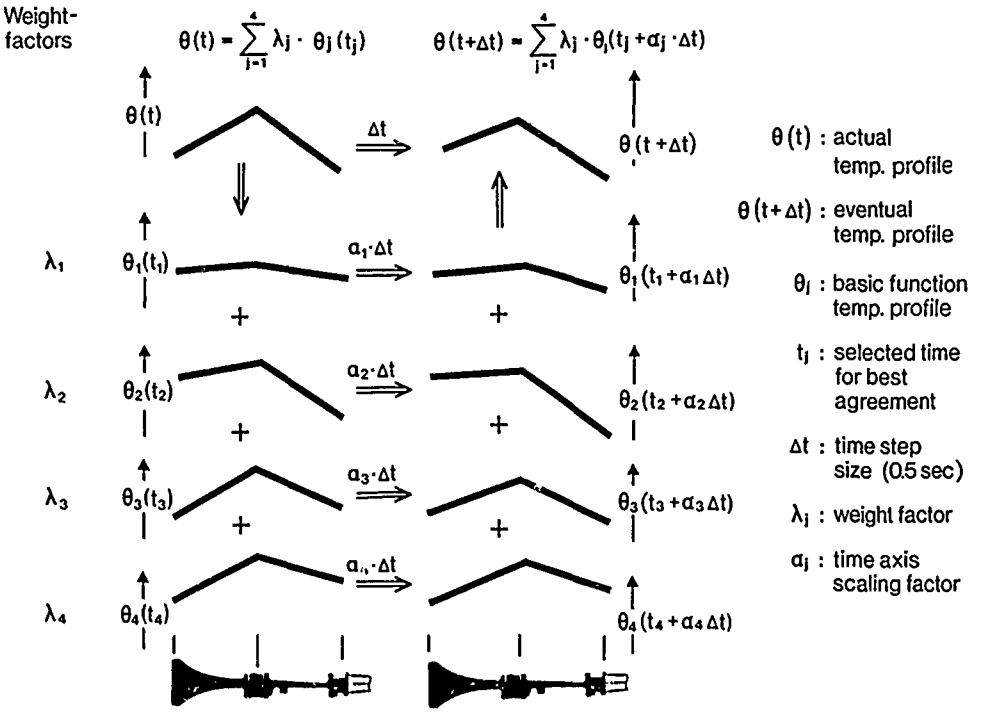

FIG. 9 MODELLING OF TEMPERATURE FROM TEMPERATURE PRO. .LES OF BASIC FUNCTIONS

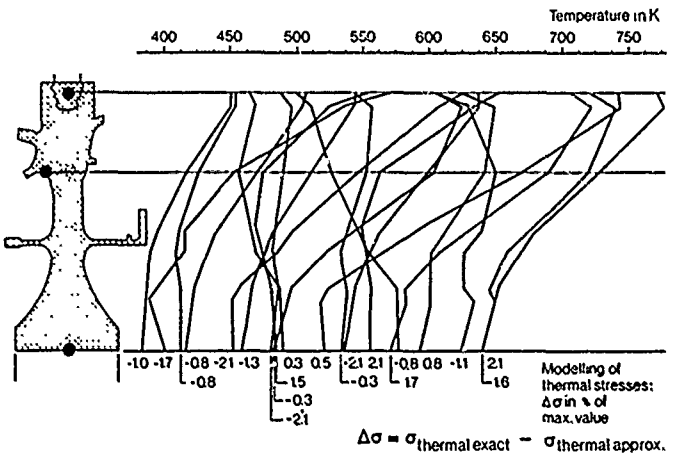

FIG. 10 GT DISK SPECTRUM OF TRANSIENT TEMPERATURE DISTRIBUTIONS

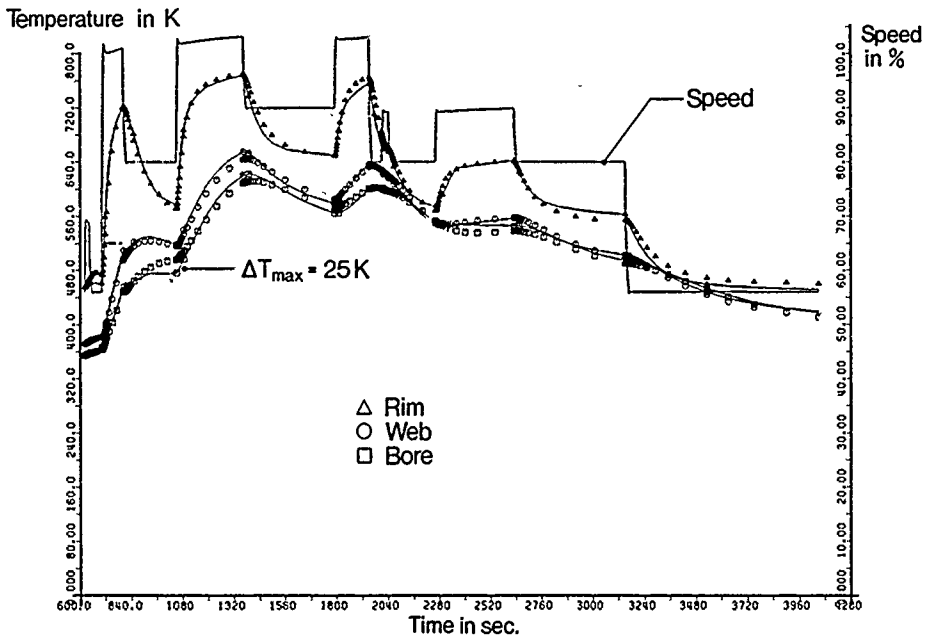

FIG. 11 GT DISK TEMPERATURE HISTORY
APPROX. COMPARED WITH EXACT

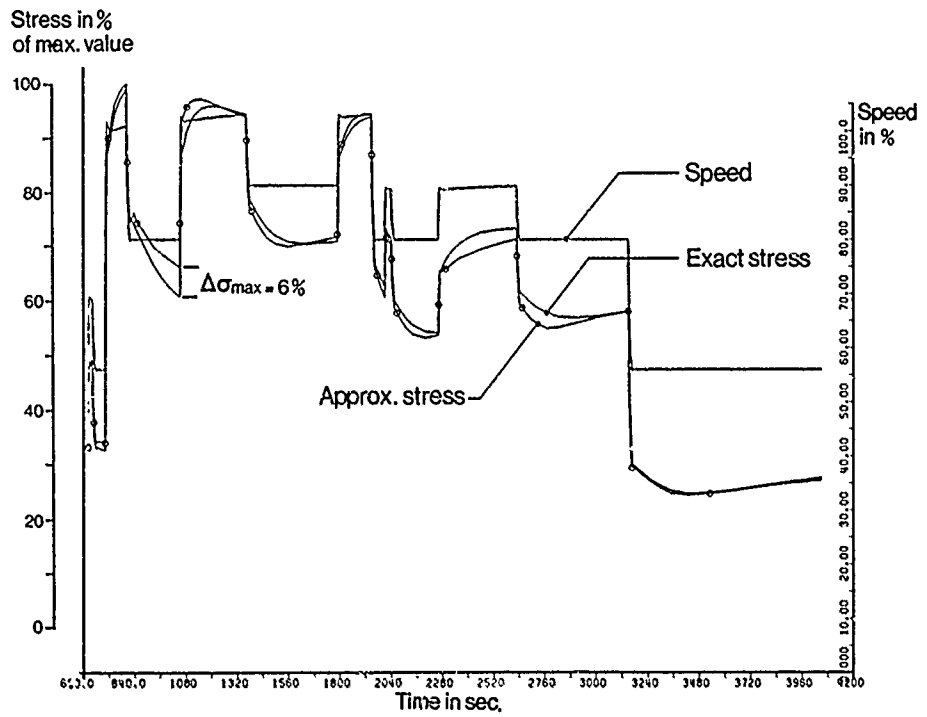

FIG. 12 GT DISK BORE. TOTAL STRESS HISTORY
APPROX. COMPARED WITH EXACT

DISCUSSION

R.Tadros, Ca

Could you elaborate on your statement regarding thermal stress — "there is no known solution for the temperature distribution in a component." I prefer that you say there is no closed form analytical solution. Do you agree with me?

Author's Reply

Yes.

R.Tadros, Ca

On the basic function approach for temperature simulation, I consider this a special function that can be derived easily from the finite element approach using either a steady or time-related shape function — do you agree?

Author's Reply

The basic functions are derived from complete finite element (F.E.) solutions for the whole rotor structure. They reflect the temperature distribution and its development at time intervals at constant operating conditions. A direct relation to the "shape function" is not given.

R.Tadros, Ca

On your comments of accuracy of stress calculations showing figures of 6% difference between calculated and measured stress results, I would like to say that this 6% can be dramatic with respect to life estimation and a 100% reduction in life due to a 6% difference in stress should not be a surprise — do you agree?

Author's Reply

We agree that an error of 6% in the maximum stress of a flight cycle could result in a very bad estimation of the related life consumption. However, based on the nature of our approach, the maximum error occurs at random during the flight. Thus, the probability that it (max. error) coincides with a peak or a trough in the stress history is very remote, particularly with regard to those of the maximum cycle.

P.Ramette, Fr

In your presentation you used temperature curves which depend only on the radius (of the disk). Don't you think that, for cooled turbine disks for example, the calculation of the variation of temperature with the depth (axial depth) in the disk should lead to more precise results for the stresses?

Author's Reply

One must distinguish between the "distinctive points" of a disk and those points, the temperatures of which, are used for the calculation of the thermal stresses in the individual critical areas. The former points are chosen with respect to a sufficient representation of the temperature distribution within the disk. The latter points are selected so that they best suit their purpose. Therefore, we work with surface points as well as with inner points, depending on the results of these selection processes.

D.W.Hoeppner, Ca

Can you briefly discuss the methood (with assumptions) that you used related to the calculation of LCF damage as well as the accumulation of LCF damage after you get the temperature-stress as you have described?

Author's Reply

The method presented here provides the basis for every kind of damage evaluation technique since it gives the stress-temperature history in the critical areas. The discussion of those techniques is undoubtedly very necessary, but we feel it is too complex to be adequately covered by just the few words possible here. Most of us will do this (damage calculations) by some linear accumulation method.

H.I.H.Saravanamuttoo Ca

How many temperatures in the gas path are actually measured in determining the temperatures in the various disks?

Author's Reply

We need the total conditions at the engine intake which we get from the measured parameters. Outer air temperature, Altitude, Flight speed, and Rotor speed. In addition one turbine section gas temperature is required. The actual parameter used is a turbine blade temperature in one case and an exhaust gas temperature in another. It depends on what is available on the engine under consideration.

R.Tadros, Ca

With respect to the question asked by Dr Hoeppner (University of Toronto) regarding life calculation, the way I look at it is using the damage caused by each stage in the mission given temperature and stress, and using Minor's Rule for life calculation, and knowing the material LCF curves, the total life of the component can be calculated — do you agree?

Author's Reply

Yes. This is a common approach in the LCF life consumption evaluation technique that Dr Hoeppner has referred to.

A.A.Martino, US

What material properties do you use in your method/model and when do you obtain this data?

Author's Reply

All required information about the time temperature-stress behaviour of the rotor structure is provided by the "basic function" and related stresses in the critical areas. This data is derived from the same numerical (F.E.) models which are used for the component design and lifing procedure. More precisely we use the temperature coefficient of the material and other material properties normally available to an engine manufacturer.

Mr Bergmann, Ge

What are the stresses you are calculating? Are they elastic stresses, equivalent stresses, multi-axial stresses or what is it?

Author's Reply

For the example shown, we calculated an elastic stress and concentrated on the main principal stresses.

MONITORING ENGINE THERMAL STRESSES

T.M.EDMUNDS AND R.A.LAWRENCE

Rolls-Royce Limited,
P.O. Box 3,
Filton
Bristol
England

SUMMARY

The high performance and rapid response of modern military engines means that transient thermal stresses make a significant contribution to the fatigue life utilisation of critical rotating components. This, coupled with the variability of actual usage, raises a requirement for calculating transient thermal stresses from flight recorded data.

This paper describes a computationally efficient procedure for meeting this requirement. The analysis is based on a simplified model of the heat transfer and mechanics of the engine that is tuned with results of more sophisticated finite difference and finite element computations.

Applications to an engine disc are described using data collected by on-board recordings. The results are validated by comparisons with more detailed theoretical analyses - practical constraints preventing a direct measurement of in-flight stresses.

The integration of the results into the overall lifing procedure is also briefly described.

1. THE SAFE LIFE METHOD

The finite, safe life method of ensuring engine cyclic durability is based on a combination of analysis and testing. The low cycle fatigue endurance of each potentially critical location is ascertained by cyclic testing. The safe life is then determined as the number of zero-to-maximum reference stress cycles at which the probability of occurance of an 'engineering crack' is acceptably small. This reference stress, and its associated temperature, is chosen to be representative of the expected once per flight maximum. However, due to the variability and complexity of actual usage, the resulting safe cyclic life cannot be used directly.

In order to be of use, the manufacturer's cyclic life needs to be expressible in terms of the usage parameter that the operator records. This is achieved by monitoring a sample of service operation and computing the stresses and temperatures experienced by each critical feature. These time histories are converted to an equivalent number of reference cycles using a modified rainflow cycle extraction procedure, a correction for the temperature at which the peak stress occurs and linear summation of damage. This leads to a cyclic damage rate which, coupled with usage records, allows the fatigue life usage of critical components to be controlled.

The necessary approximations and algorithms for calculating fatigue damage from engine data are discussed in reference 1. However, this paper only considers centrifugal and steady state thermal stresses and a major area of recent concern has been the role played by transient thermal stresses. These stresses inevitably make a substantial contribution to the low cycle fatigue life usage of modern military engines due to the rapid response and high temperatures involved. The heat transfer rates necessary to reproduce the stresses are difficult, if not impossible, to achieve on a cyclic rig and the technical problems of engine measurement are equally formidable. The only practical methods of including them in the lifing procedure are based on calculation.

To summarise, there is a requirement to calculate the temperatures and transient thermal stresses from flight recorded data. This requirement is equally valid in alternative lifing methods.

2. ANALYSIS OF TEMPERATURE AND STRESS

The numerical analysis tools for the prediction of engine temperatures and transient thermal stresses are well established. Starting from a description of the flight in terms such as spool speeds, forward air speed and altitude the steps involved are:

2. ANALYSIS OF TEMPERATURE AND STRESS (Cont'd)

i) Compute gas stream temperatures, pressures and velocities from the known performance characteristics of the engine.

ii) Compute the secondary air flows, such as cooling bleeds.

iii) Compute the gas/metal heat transfer coefficients from the above.

iv) Apply these temperatures and heat transfer coefficients to a transient heat conduction model of the structure to predict the metal temperatures through the flight.

v) Transfer these temperatures to a structural analysis model and predict the stresses through the flight.

Various levels of sophistication are possible in the models used. A typical, intermediate level, is illustrated in section 4 where a two dimensional analysis of a high pressure turbine assembly is discussed.

The numerical analysis models all require substantial computational power and storage and can only be effectively used on a mainframe installation. However, a major restraint on the service monitoring operation is the requirement to operate on a mini-computer at a maintenance base and, ultimately, on an on-board micro-processor. The use of the above tools is impractical in these environments and hence, in order to meet the previously established requirement, it is necessary to construct a simplified heat transfer/stress analysis model that represents an acceptable compromise between computational power requirements and accuracy. The remainder of this paper is concerned with such a model.

3. THE SIMPLIFIED MODEL

The characteristic response time for some areas (defined as the time to achieve 90% of the stabilised temperature) can be as long as 8 minutes for a turbine disc cob centre whereas the mean time between major throttle movements can be as short as 30 seconds during some phases of operation. This means that a large number of transient events start from a non-stabilised state and/or themselves are interrupted by a further change in engine conditions. As a consequence methods based on the identification and stressing of discrete transient events have been rejected.

The approach adopted is to construct a very simple model of the mechanism causing thermal stress and determine its parameters by curve fitting to the results produced by more detailed models. These detailed models will already have been analysed for some representative transients or datum flight as part of the normal lifing procedure. The process of curve fitting to the results can be seen as a way of condensing the vast amount of data involved in these analyses.

The actual model used includes several assumptions about the behaviour of temperatures and stresses:

i) Temperatures always decay exponentially towards the asymptotic value that they would achieve if the current engine conditions were held indefinately. These asymptotic values are linearly related to a local gas stream temperature.

ii) The characteristic constant of the decay depends on the engine conditions. Higher gas pressures and velocities being associated with larger heat transfer coefficients.

iii) The thermal stress at a particular location is linearly related to the temperatures of a small number of thermal masses.

For a particular critical location, these assumptions lead to a thermal stress given by:

$$\sigma(t) = \sum_i K_i^5 T_i(t)$$

where i sums from 1 to N- the number of thermal masses that significantly influence this location. The temperatures of these masses, Ti(t), are given by the numerical solution of the differential equation

$$dT_i/dt = H_i (T_{ia} - T_i)$$

with an appropriate initial condition at the start of the flight. The heat transfer coefficients, Hi, are taken as

$$H_i(t) = K_i^3 \left(N P / T_c^{.7} \right)^{K_i^4}$$

3. THE SIMPLIFIED MODEL (Cont'd)

where N,P and Tc are spool speed and representative local gas stream pressure and temperature respectively and the functional form used is based on experimental correlations. The asymptotic temperatures, Tia, are assumed to be linearly related to gas stream temperature by

$$T_{ia}(t) = K_i^1 T_c + K_i^2 .$$

This model has 5N parameters, K_i^j , but some simple manipulation shows that only 4N of them are independent - K_i^1 can be set to an arbitrary value without effecting the possible forms of $\sigma(t)$.

In addition to stress, fatigue is dependent on metal temperature at the critical location. This is predicted using exactly the same equations as above - the only difference being the units of K_i^5 and the replacement of $\sigma(t)$ by T(t).

In the simplest case of a thermal flight between two discrete structural elements, N would be 2 for stress prediction and the K^5 constants would be equal and opposite. Similarly, the simplest temperature case would have N as 1. It has been found in practice that acceptable predictions can usually be obtained by increasing N to 3 for stress prediction and 2 for temperature prediction.

The curve fitting process used to determine K_i^j is a standard one that aims to minimise

$$\Sigma \left(\sigma_{\substack{\text{FULL} \\ \text{MODEL}}} - \sigma_{\substack{\text{SIMPLE} \\ \text{MODEL}}} \right)^2$$

with a similar expression for temperature. This problem is non-linear, least squares minimisation that is solved using a commercial Levenberg-Marquardt finite difference algorithm. Starting from an initial guess, each parameter is varied in turn and a linear least suqares approximation to the local behaviour of Σ is constructed. From this a new estimate of the optimum parameters is made and the procedure is repeated. This continues until successive estimates of all the parameters are within 0.1%. The final values and the above algorithm then form the simplified model for one particular critical location.

The parameters determination process is numerically very sensitive and standard techniques for solving the differential equation for Ti(t) have proved inadequate. In order to obtain reliable results a complex, semi-analytic solution procedure has had to be developed. When applying the resulting model this complexity is unnecessary and simpler methods are adequate.

4. VERIFICATION

In order to demonstrate the ability of the simplified model to adequately reproduce the results from a more detailed analysis, the high pressure turbine assembly of a military engine has been analysed. The steps involved are:

1. Analyse the temperatures and thermal stresses occurring during transients between zero and ground idle, ground idle and combat and combat back to ground idle.

2. Use the procedure of section 3 to construct simplified models from these results.

3. Apply these simplified models to a nominal, representative mission and check its predictions against a detailed analysis of this mission. The comparison is done on thermal stress.

The second flight was deliberately chosen to include features not in the original analysis. In particular, transients to and from different engine states and transients away from non-stabilised conditions were included. These provide some qualitative checks on the physical reasonableness of the underlying assumptions.

The detailed heat transfer model is shown in figure 1. A comparitively simple structural model, figure 1a, is used to follow the movements and growths of the components through a flight. These are then used to compute the various secondary air flows which then provide the boundary conditions for the heat transfer model, figure 1b. This is an 1100 variable finite difference model that includes non-linear material properties and automatic time-stepping control.

4. VERIFICATION (Cont'd)

The detailed structural analysis model is shown in figure 2. This is a 6000 variable finite element model consisting of axisymmetric and plane stress second order isoparametric elements. The loading consists of rotational forces and the temperatures interpolated from the results of the heat transfer model. The temperature dependence of Young's modulus has a significant effect on the stress response and hence it is necessary to reform and solve the stiffness matrix for each time point.

Following step 1 of the verification procedure, these models are subjected to the transients shown in figure 3. The temporal variation of the results is discussed later and the spatial variation is illustrated in figure 4. This shows the hoop stresses and metal temperatures 30 seconds after the start of the acceleration to combat rating. There are internal cold areas in the central bulk of the disc and coverplate giving rise to tensile stresses in these areas. Additionally, the front arm has heated more than the disc and there is a significant radial fight between them giving rise to bending stresses in the front arm which, through a Poisson's ratio effect, give rise to the hoop bending stresses shown.

In order to condense the vast amount of data, four critical stresses are selected to bracket the various response types seen. These are:

i) Hoop stress at the cob centre
ii) Nominal hoop stress at the disc rim
iii) Concentrated in-plane stress at front arm disc fillet
iv) Nominal hoop stress in the coverplate attachment flange

and their locations are shown in figure 2.

Step 2 of the verification procedure is followed for these four areas using an arbitrary but reasonable initial guess for the parameters. The ability to correlate the thermal stresses is shown in figure 5. The response rate of the cob centre when the engine is idling is the most marked discrepancy.

The thermal stresses in the cob and rim are dominated by the basic radial temperature distribution of the disc and those in the arm by the radial fight between the rapidly responsing shaft and the slowly responding disc. The flange is more complex in that each change of engine condition causes two stress extremes. Examination of the detailed results in this area shows that early in the transient the dominant temperature difference is between the coverplate shaft and disc shaft. At later times this reduces and the difference between the disc shaft and its attachment flange becomes dominant.

Similarily, the ability of the simplified model to correlate metal temperatures is shown in figure 6. The most marked discrepancy here is for the front arm fillet where the stabilised values are in error by $10^{o}C$.

These correlations are satisfactory and the models are then applied to the more representative mission shown in figure 7 (step 3). The resulting thermal stress and temperature histories are then compared at 80 time points with the results from the detailed model, figures 8 and 9. The comparison is visually good and is quantified by selecting the four major events in the flight that cause transient stresses. These are marked on figure 7 and can be described as:

i) Take off

ii) In flight acceleration from cruise to maximum unreheated rating.

iii) In flight deceleration from Mach.9 cruise to Mach.5 cruise, via flight idle.

iv) Thrust reverse.

The actual times at which the comparisons are made vary from location to location due to the different response rates involved. The differences in thermal stress between the simple model and the detailed model are shown in table 1. These have been expressed as a percentage of the stress range experienced at each location.

4. VERIFICATION (Cont'd)

	Take-Off	Cruise Max	.9 .5	Thrust Reverse
Cob Centre	-1.5	+1.1	+2.5	+3.3
Disc Rim	+5.3	+2.6	+2.0	+3.9
Front Arm	+5.6	+1.6	+1.8	+4.1
Flange	0.0	-0.6	0.0	0.0

TABLE 1 - Stress Errors, % of range

Similarly, the differences in metal temperatures are shown in table 2 for the three events that cause distinct temperature extremes.

	Take-Off	.9 .5	Thrust Reverse
Cob Centre	-4	18	-31
Disc Rim	-4	4	-11
Front Arm	2	-6	15
Flange	-2	-1	3

TABLE 2 - Temperature Errors, ^{o}C.

The root mean square errors are 2.8% and 12^{o}C respectively. Although no conservatism has been delibrately built in, the simple model tends to over-predict stress.

As an illustration, the four critical locations characterised in the previous section have been stressed using flight recorded data. The 90 minute flight included manoeuvring at altitude and is an extreme example of the complexity of actual usage.

An on-board digital system records the air temperature, altitude and air speed for the aircraft and two spool speeds and compressor delivery pressure for each engine. The recording rate for the various parameters varies up to 16 per second but the post flight analysis locally smooths the data and converts it all to half second intervals. Further processing then detects and removes electronic 'spikes' from the data. Standard performance calibrations are then used to calculate the gas stream temperatures and pressures needed by the stress prediction algorithm.

Figure 10 shows the variation of the square of the high pressure spool speed for one of the engines during this 90 minute flight. This gives the time variation of the centrifugal component of stress and in the absence of other mechanisms, such as thermal stress, would give the stress history for all critical locations on the high pressure spool. The pattern is typical of military flights in that it has a major, zero-maximum-zero, envelope with a large number of complex sub-cycles that essentially achieve the same maximum.

The predicted total stresses at each of the critical locations is shown in figure 11. This emphasises the different stress histories that can be seen on a single component. In particular, the front arm fillet experiences a stress reversal when the engine speed falls.

The temperatures at each critical location are shown in figure 12. The responses range from the cob centre where short time excursions in engine conditions are barely felt to the coverplate attachment flange where nearly all the detail of figure 10 is apparent.

5. CONCLUSIONS

1. Using the results from earlier, detailed analyses ensures that the exchange rate monitoring exercise is compatible with the overall lifing procedure. Attention is particularly focussed on the transient event causing the once per flight maximum stress.

2. Over a representative range of critical locations and transient events the approximations introduce RMS errors of 2.8% for stress and 12°C for temperature.

3. Section 4 only demonstrates the ability to efficiently reproduce the behaviour of detailed models. The absolute accuracy of the results is a separate issue that could only be finally resolved by in flight stress and temperature monitoring.

4. The computational requirements of the method are reasonable. Each critical location requires ~30 storage locations and ~100 floating point operations for each time frame.

5. In addition to the computation of exchange rates from flight recorded data, the models allow a rapid assessment of the damage done by proposed alternative sorties provided that the actual engine handling can be anticipated.

6. The major unsolved problem is the incorporation of fatigue models that adequately handle sequencing effects for the extremely complex stress and temperature histories experienced in service.

REFERENCES

1. M. Holmes
"Application of Engine Usage Analysis to Component Life Utilisation"
AGARD conf. 248 Cleveland, Ohio. 1978

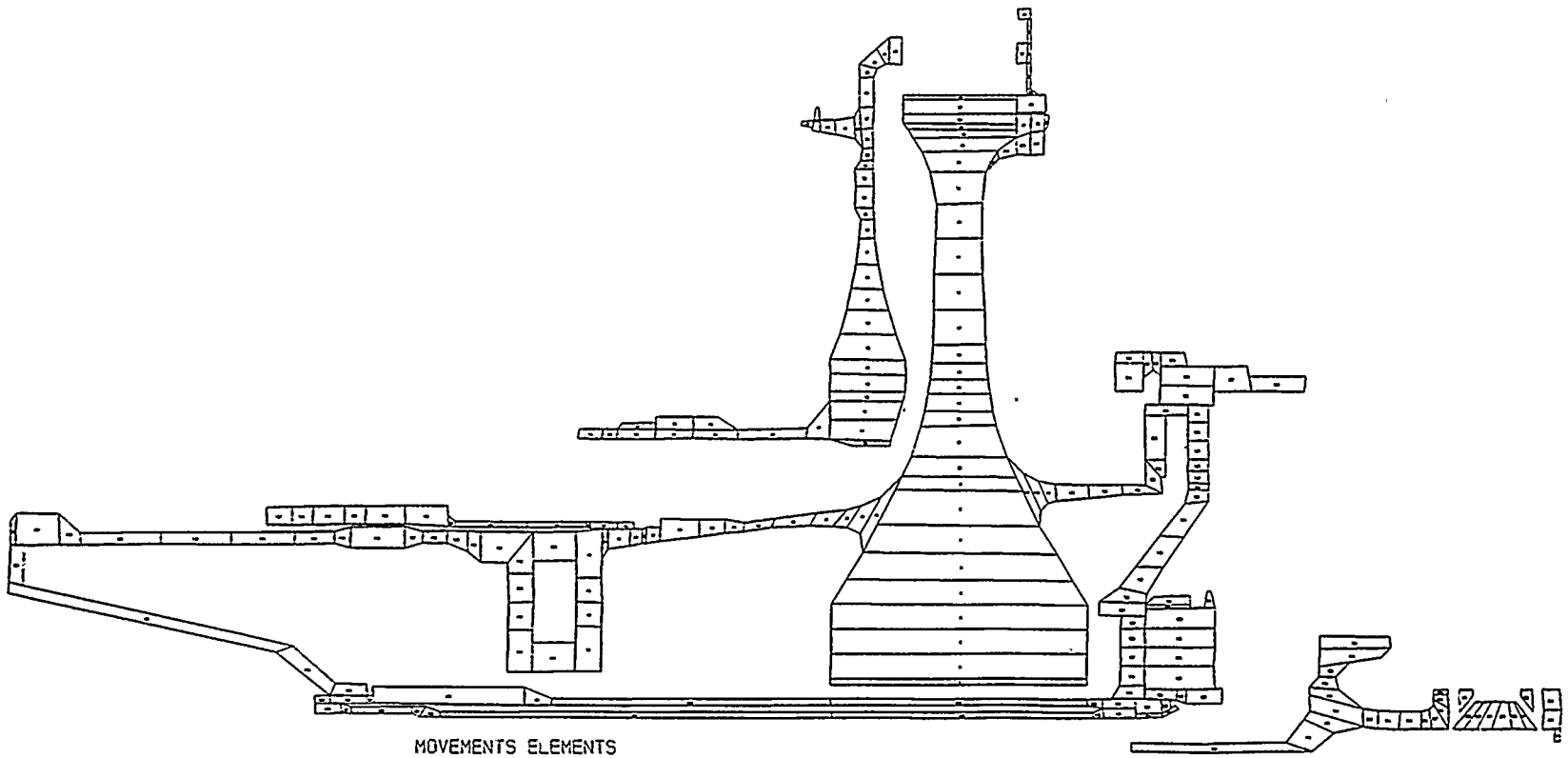

FIGURE 1A SECONDARY AIR FLOW MODEL

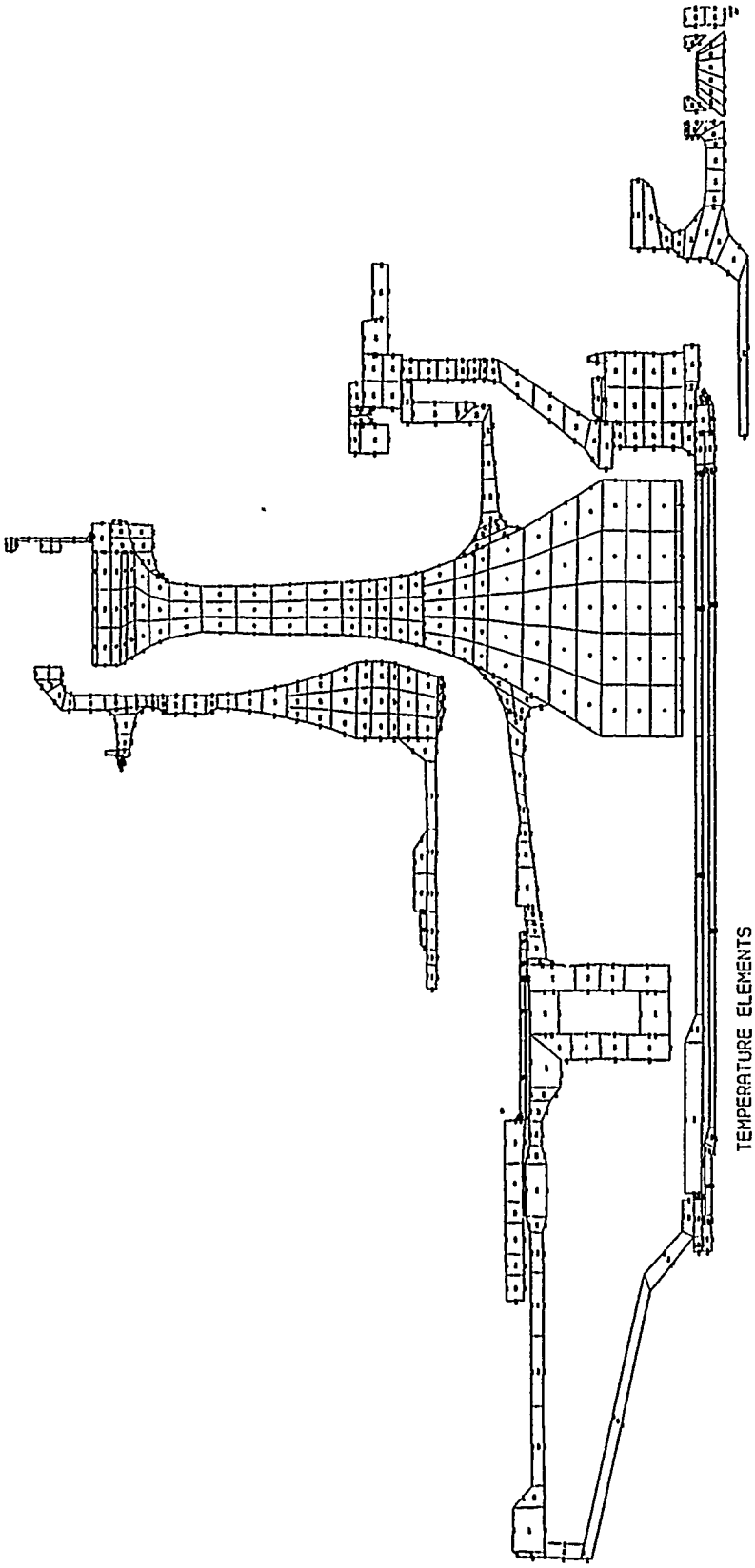

FIGURE 1B METAL TEMPERATURE MODEL

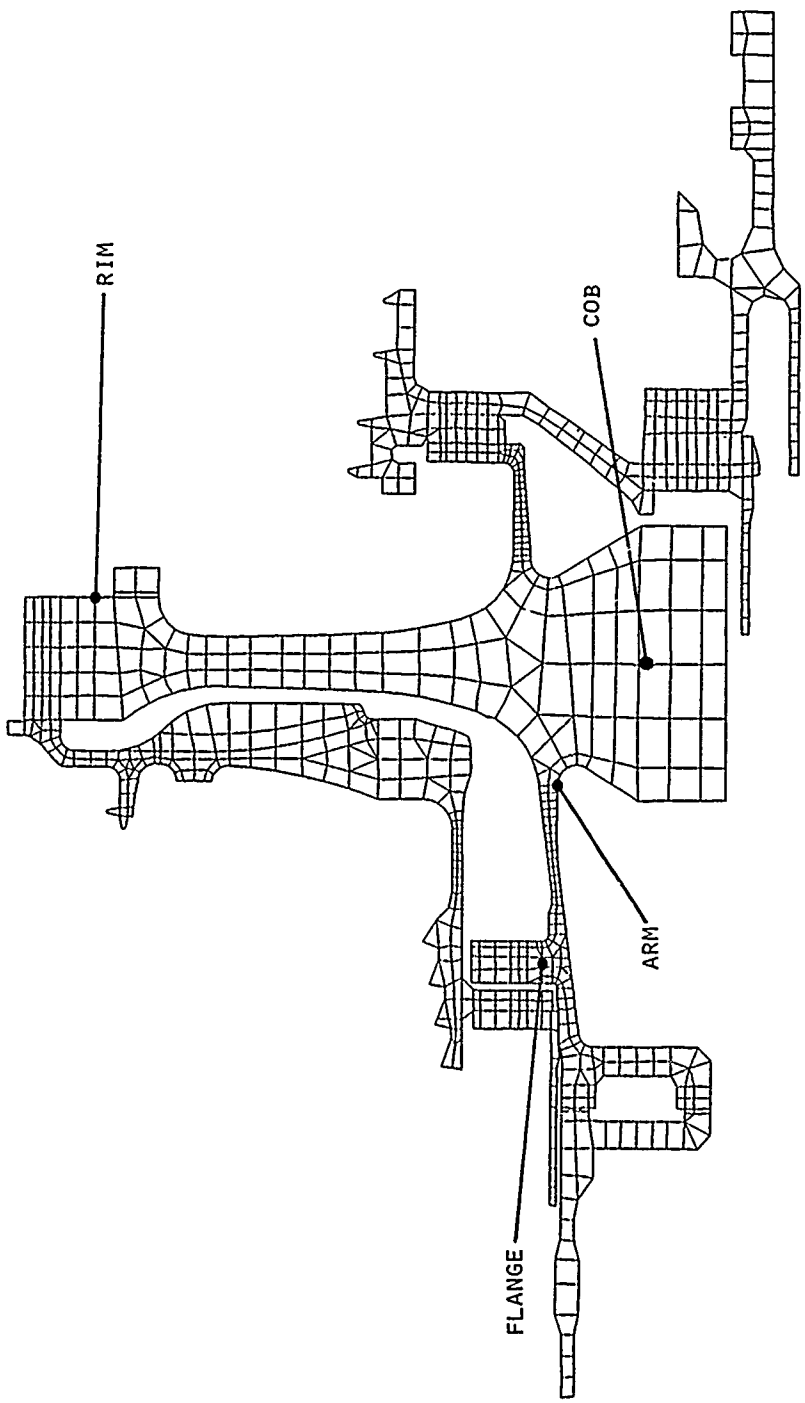

FIGURE 2 STRESS MODEL AND CRITICAL LOCATIONS

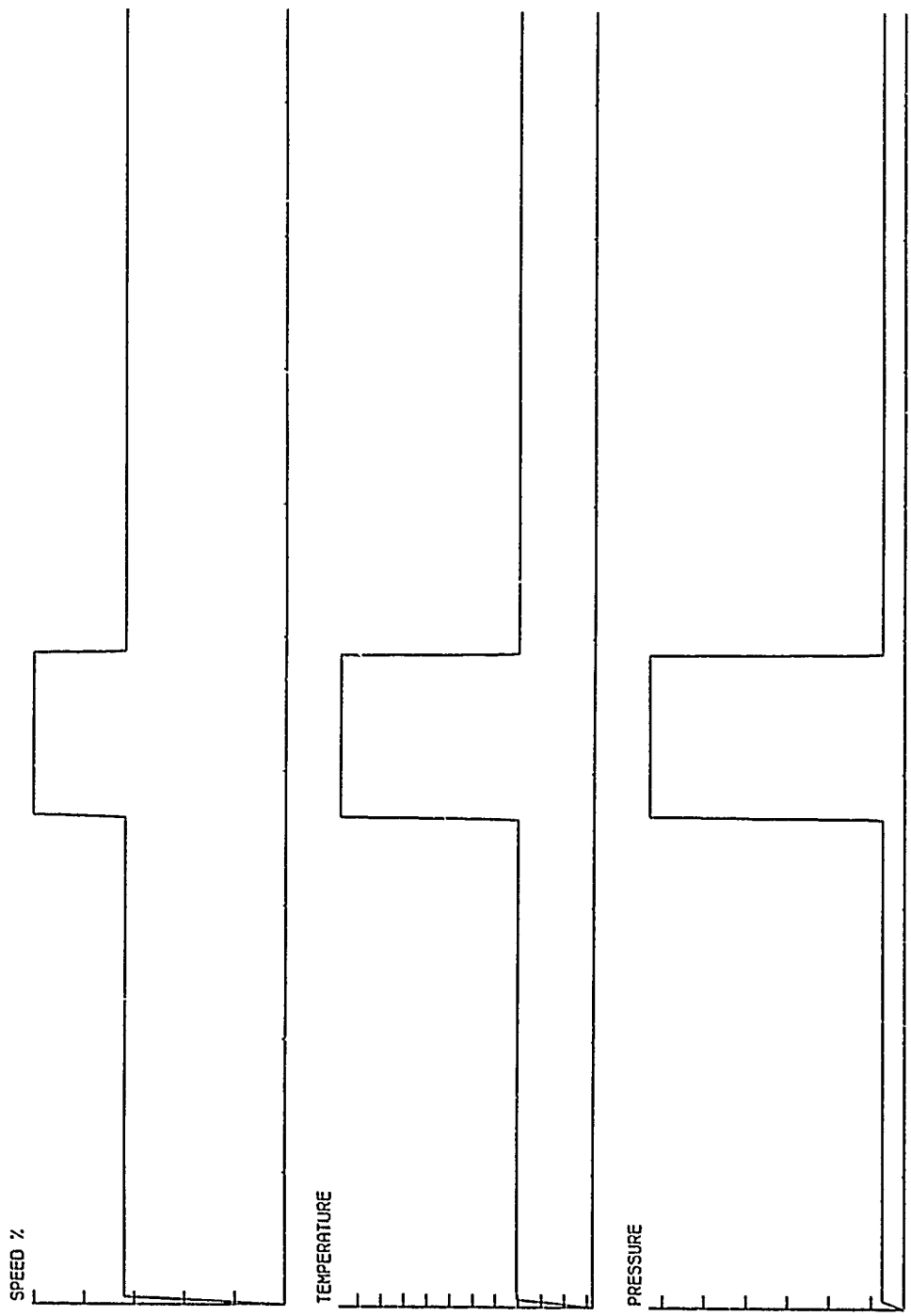

FIGURE 3 INITIAL TRANSIENTS

HOOP STRESS

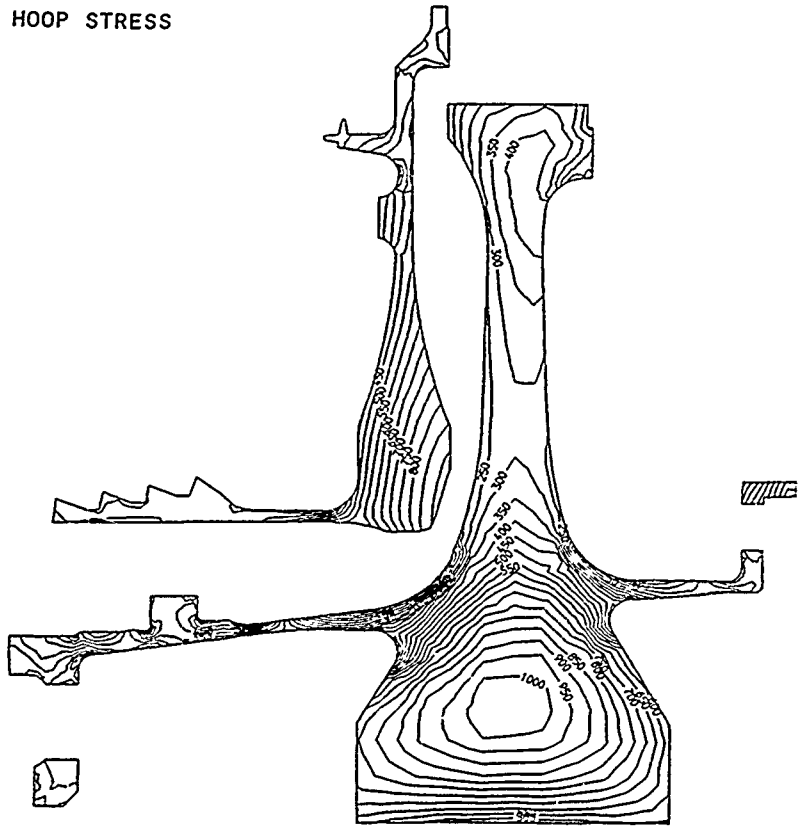

TEMPERATURE

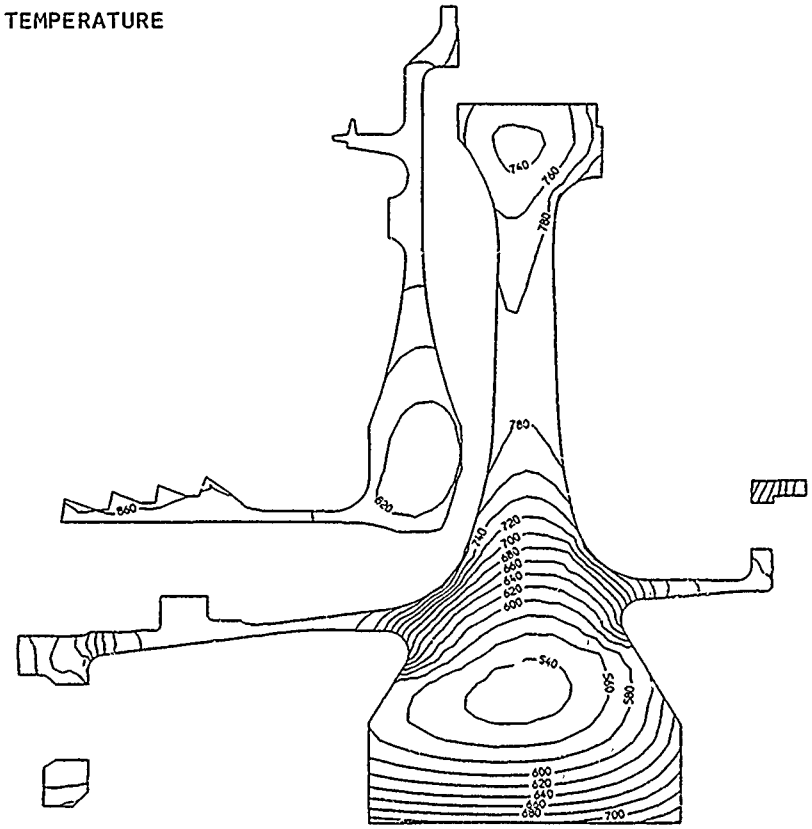

FIGURE 4 HOOP STRESS AND TEMPERATURE 30 SECS AFTER ACCELERATION

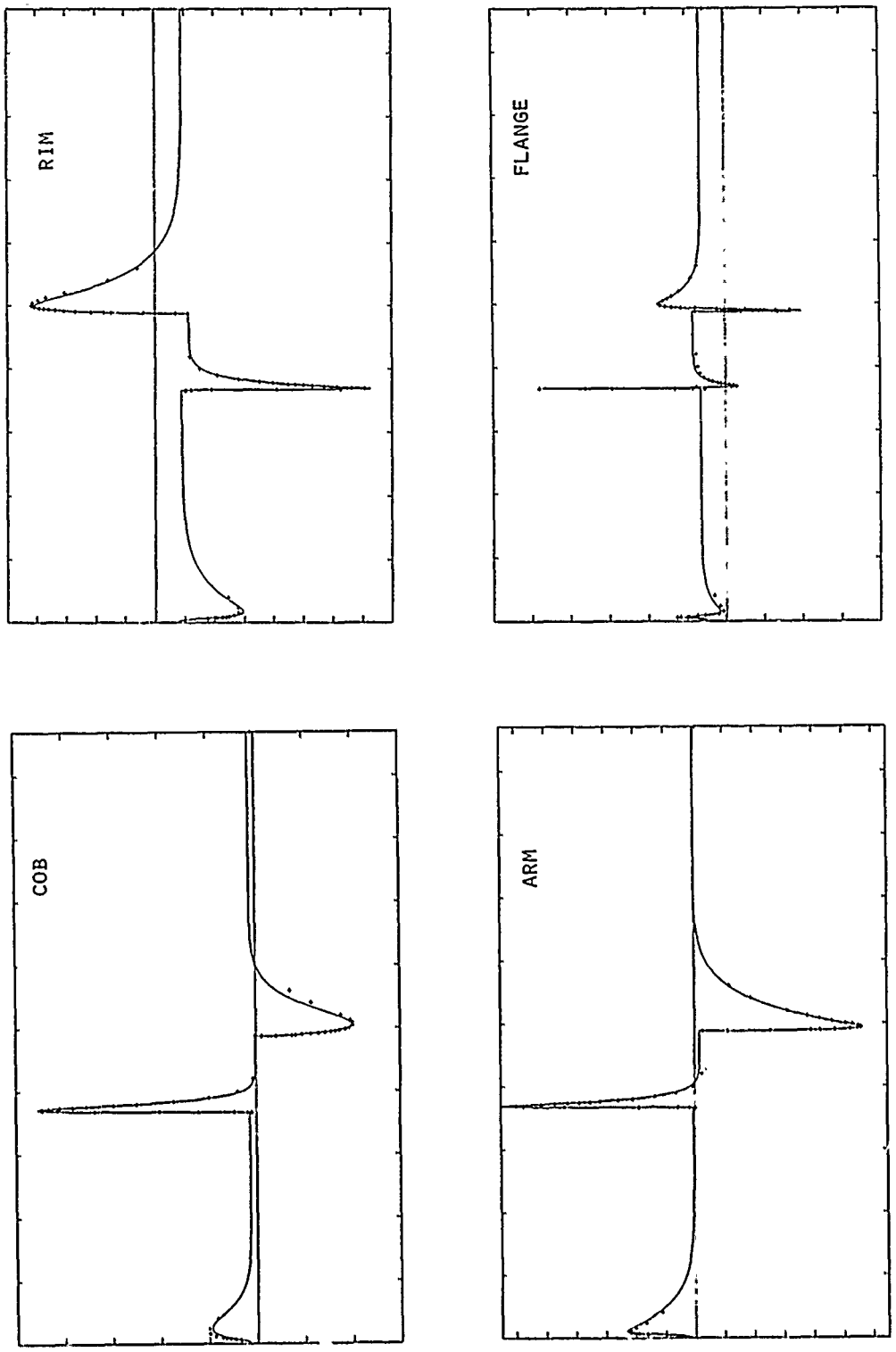

FIGURE 5 STRESS CORRELATION FOR INITIAL TRANSIENTS

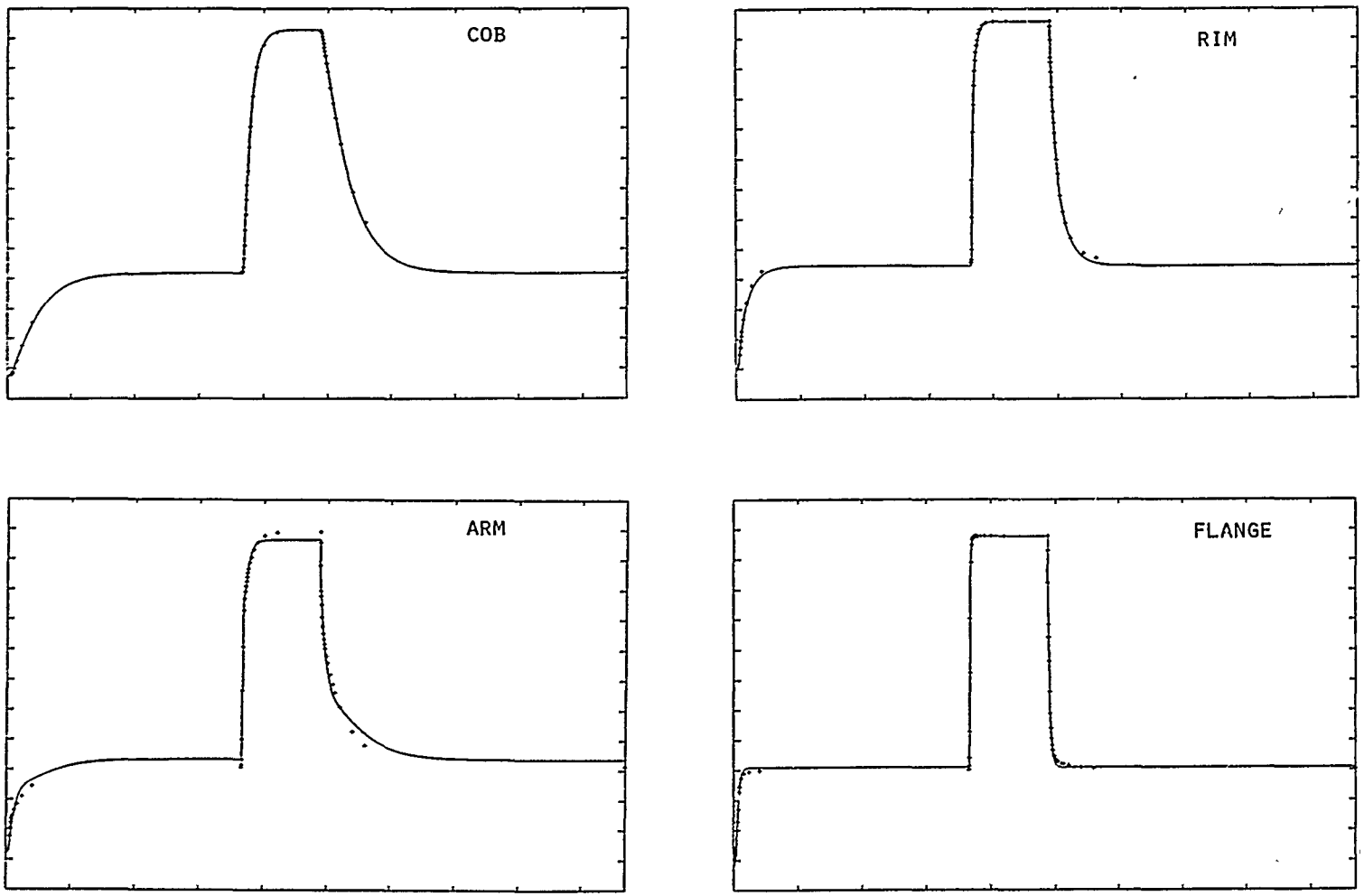

FIGURE 6 TEMPERATURE CORRELATION FOR INITIAL TRANSIENTS

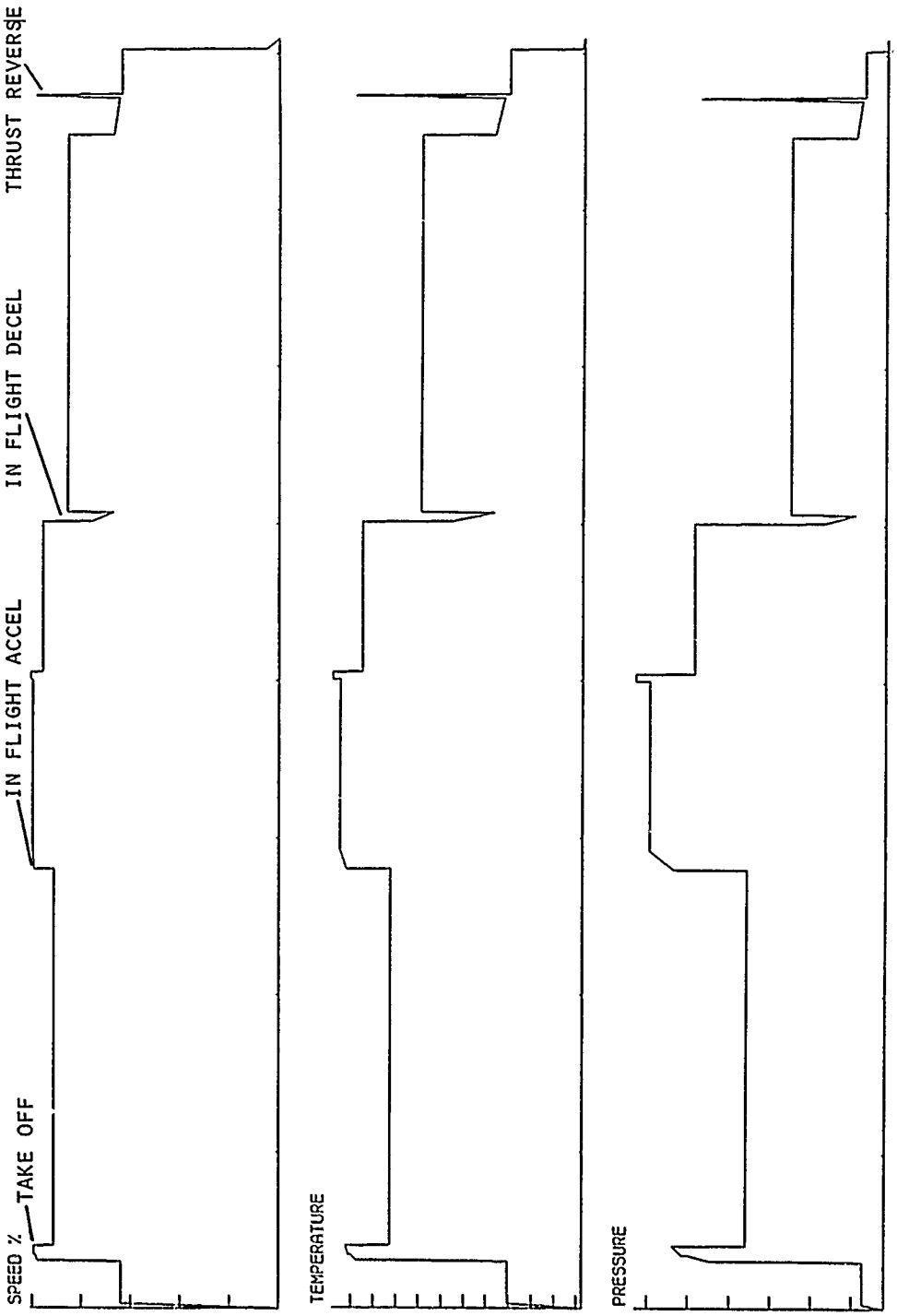

FIGURE 7 NOMINAL MISSION AND TRANSIENT EVENTS

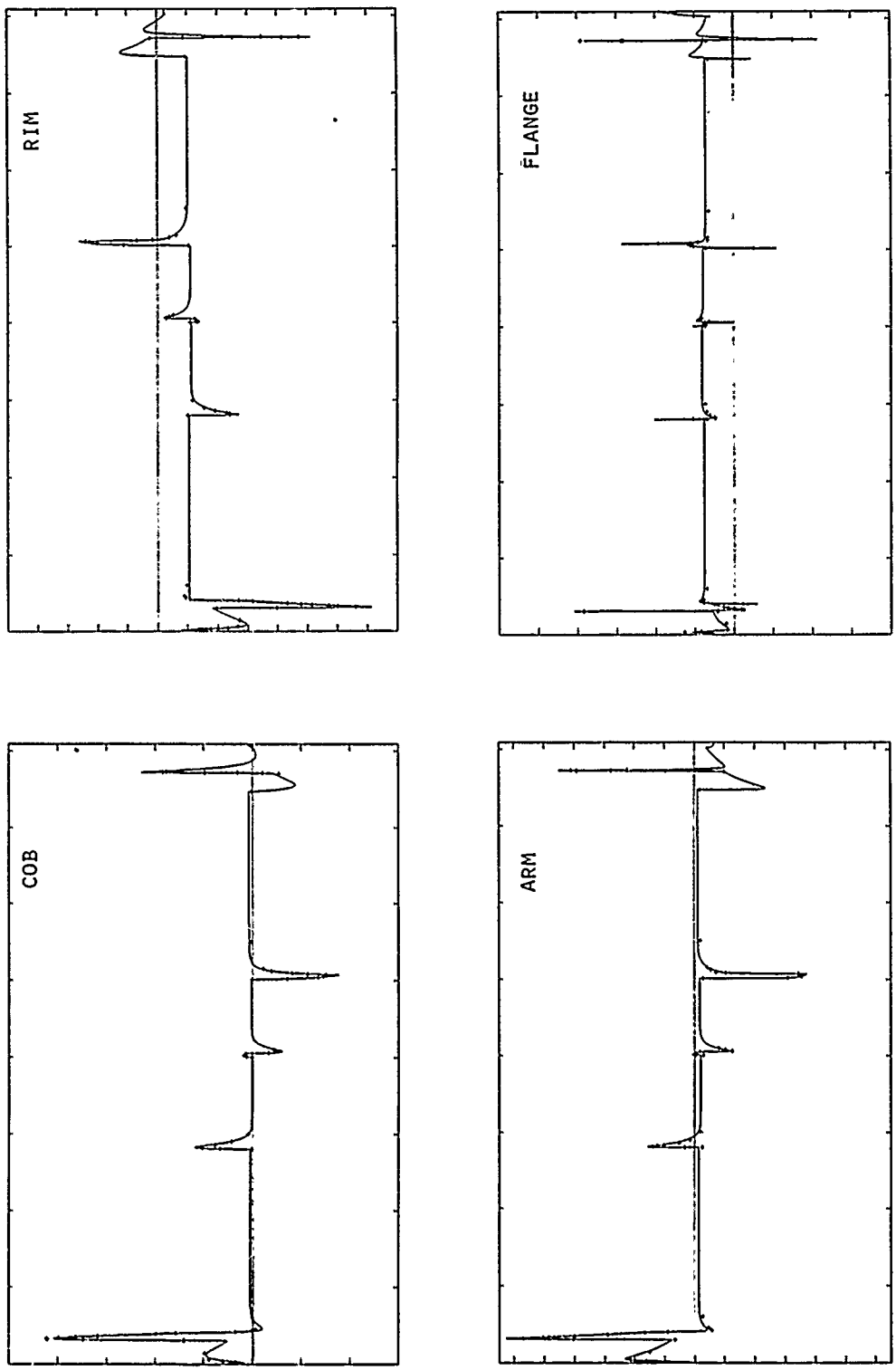

FIGURE 8 STRESS COMPARISON FOR NOMINAL MISSION

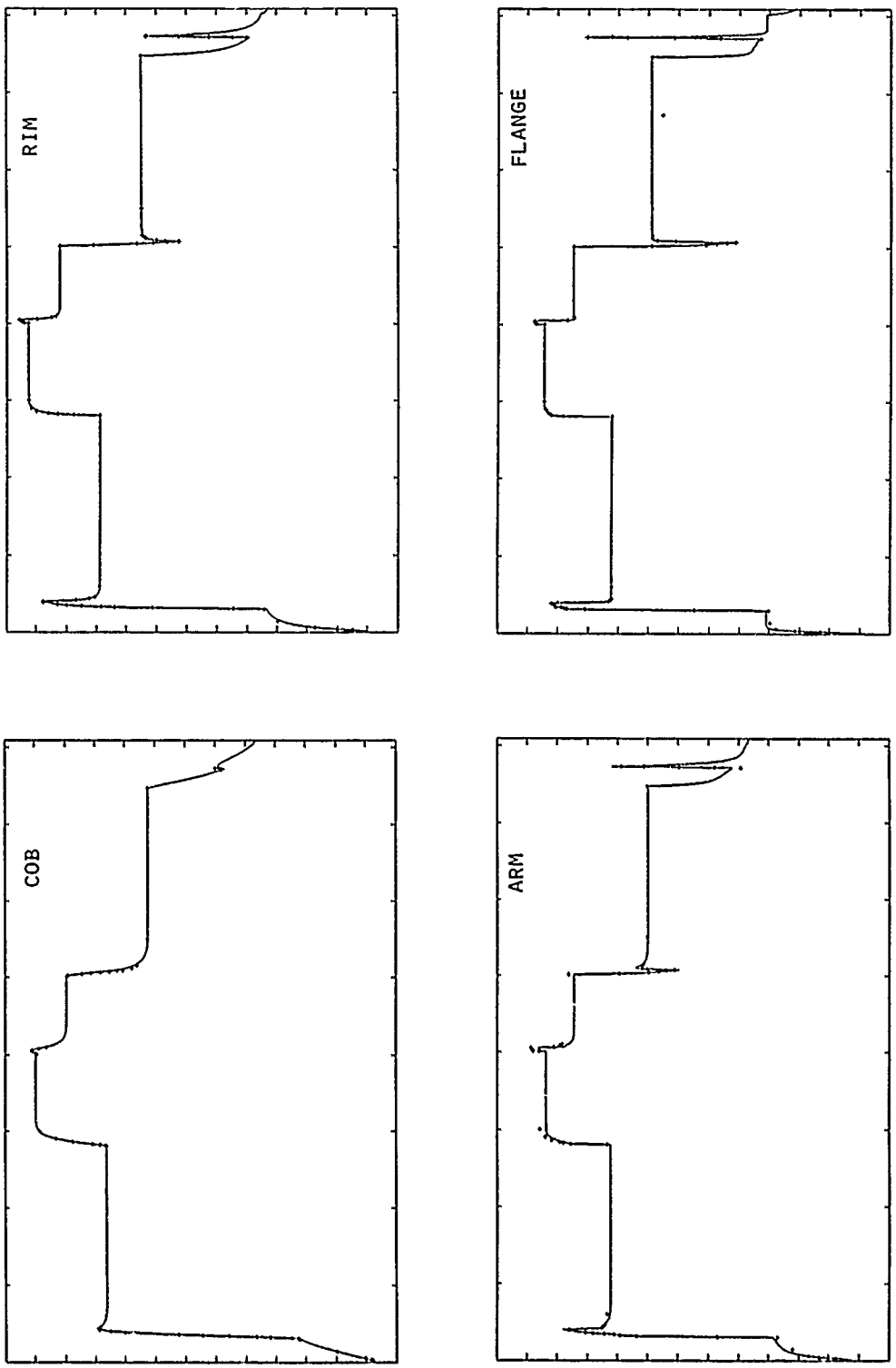

FIGURE 9 TEMPERATURE COMPARISON FOR NOMINAL MISSION

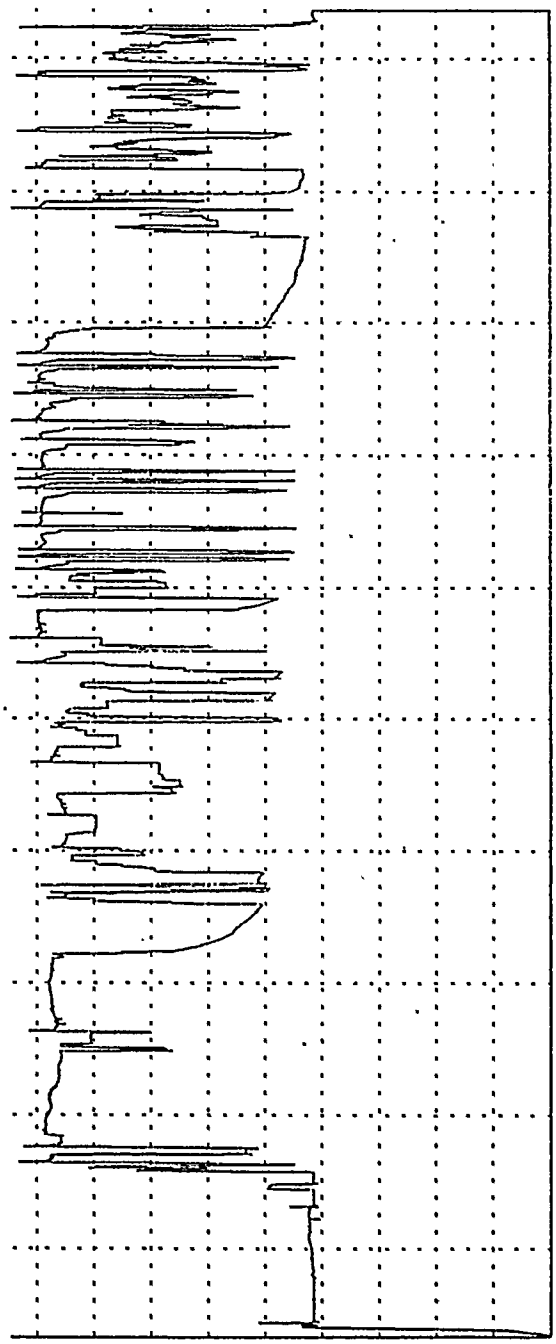

FIGURE 10 SPEED SQUARED VARIATION FOR ACTUAL MISSION

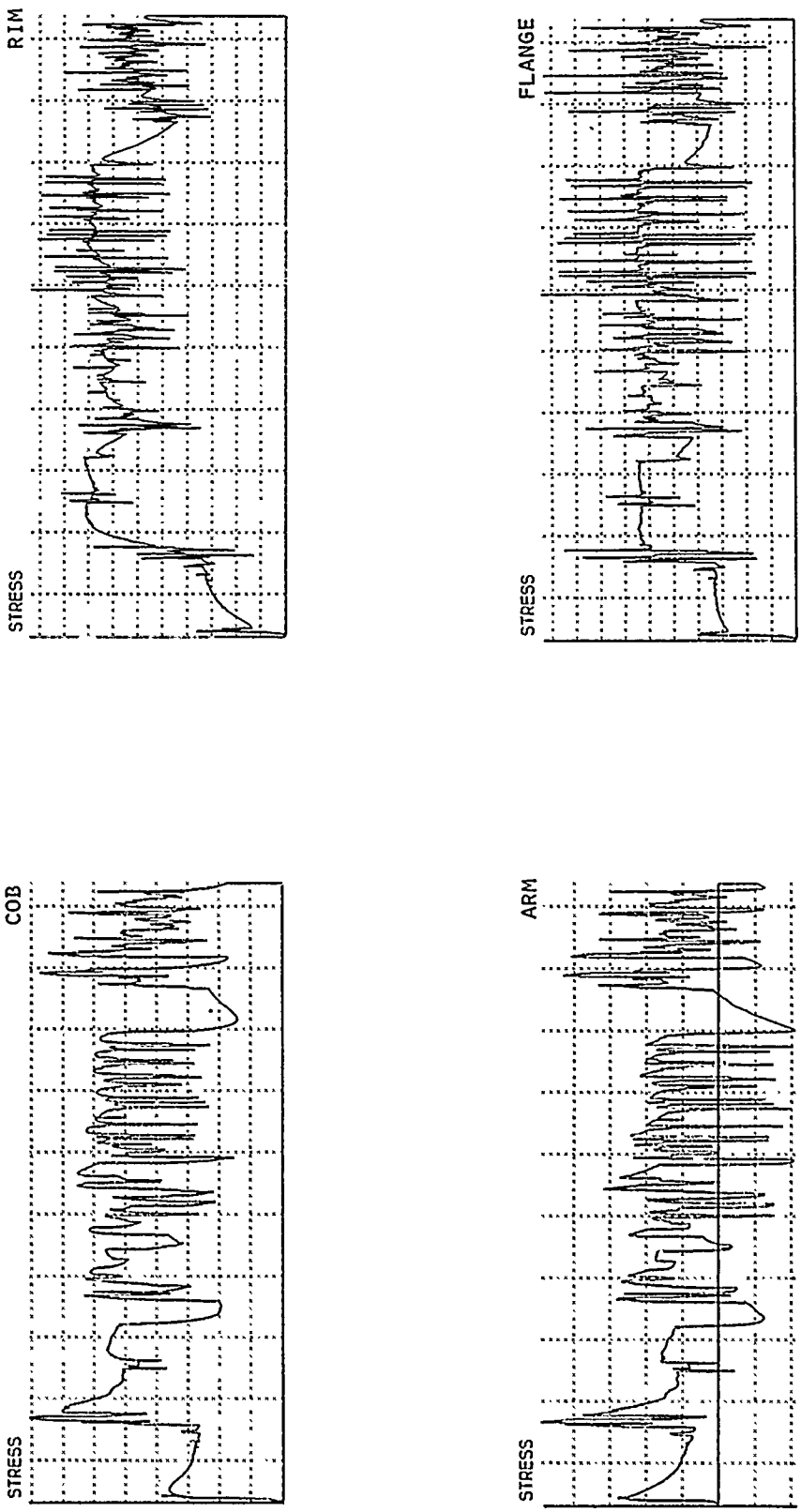

FIGURE 11 STRESS PREDICTION FOR ACTUAL MISSION

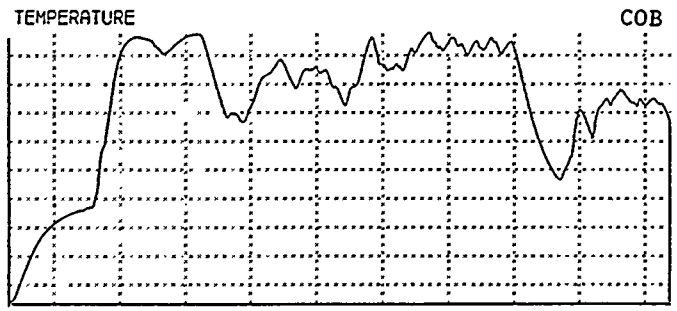

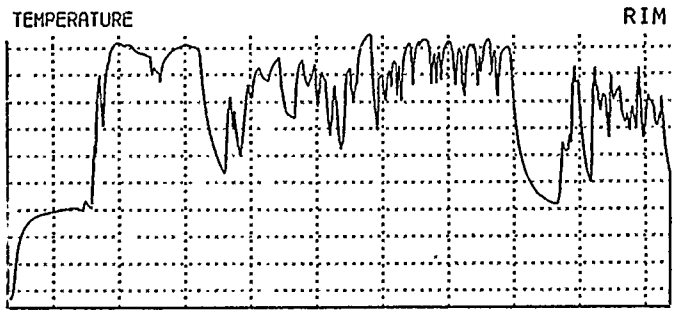

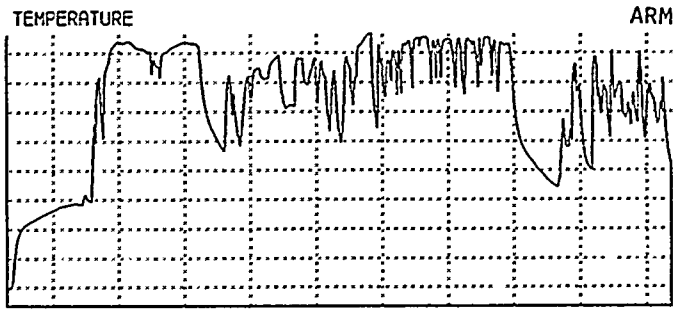

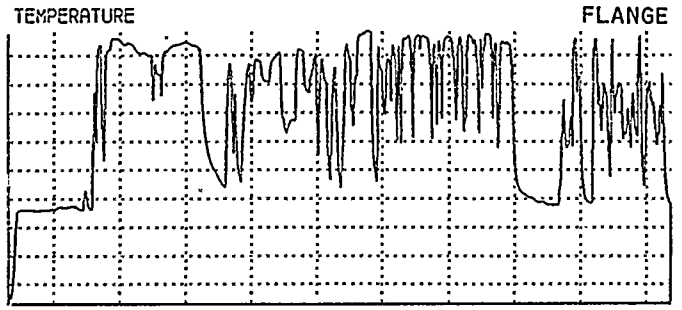

FIGURE 12 TEMPERATURE PREDICTION FOR ACTUAL MISSION

DISCUSSION

T.E.Farmer, US

What is your recommendation for the number of critical locations to be tracked?

Author's Reply

The use of four critical locations (as per this example) on a single component is typical. Each case has to be considered on its merits.

D.W.Hoeppner, Ca

At the conclusion of your talk you made the point that the development of realistic fatigue models and the evaluation of your calculations is necessary. With respect to this, how do we know the analysis/calculation/measurements of temperatures and stresses is necessary, or indeed practical, without more information on the fatigue models. Could you comment on this point?

Author's Reply

Currently available fatigue models are known to be inadequate for handling histories, as shown in figures 11 and 12. However, the analysis is still worthwhile even in the absence of absolute fatigue predictions. For example, the results can be used with some confidence for quantifying the relative damages of different usage (e.g. AMET and services) and for assessing the variability of these peak mission stresses.

ACCELERATED MISSION ENDURANCE TESTING (AMET)

Wilson R. Taylor - Aerospace Engineer
United States Air Force
Aeronautical Systems Division (ASD/YZEE)
Wright-Patterson Air Force Base, OHIO 45433

ABSTRACT

The cost of ownership of gas turbine aircraft engines today makes it imperative that the development process produce a production engine that will minimize life cycle cost. We have recognized this problem and one of the most significant changes that has been made in the last 10 years is the incorporation of AMET into our development programs. In the past, engine designs were qualified for production release when it successfully completed a 150 hour "model" test. However, as these engines accumulated service time, problems arose that were not discovered in factory test. It was apparent that the durability of these engines were not well understood. In 1973, the US Air Force, Navy, and Detroit Diesel Allison incorporated a new test cycle in their TF41 engine development program that was representative of the aircraft usage. The success of this effort encouraged us to incorporate this test method into other engine development programs. Today, the US Air Force uses factory test cycles for design verification and qualification that have been derived from known or projected aircraft usages. The background of mission related testing, test cycle derivation, data sources, key parameters, limitations and benefits will be discussed in this paper.

BACKGROUND

The concept of engine endurance testing has been with us for a long time, as evidenced by the Army-Navy turbo jet engine specification AN-E-32 dated 14 June 1946 (figure 1). This specification was superceded by MIL-E-5009 and subsequently replaced by our most recent specification MIL-E-5007D. The engine development requirements today are generally based on the requirements of MIL-E-5007D, but have been augmented by the AMET concept and the soon to be released Engine Structural Integrity Program (ENSIP). These requirements will be incorporated into one new Mil-Prime Engine Specification.

The AN-E-32 specification test cycle contained 60 engine transients from idle power to maximum power and back to idle power and 15 transients from cruise power to maximum power and back to cruise and 20 somewhat small transients (figure 2). As will be shown later, by todays standards not a very demanding test. But when you consider that the engines of this mid-1940's vintage were 25-50 hours of life, this test was likely a very stringent test.

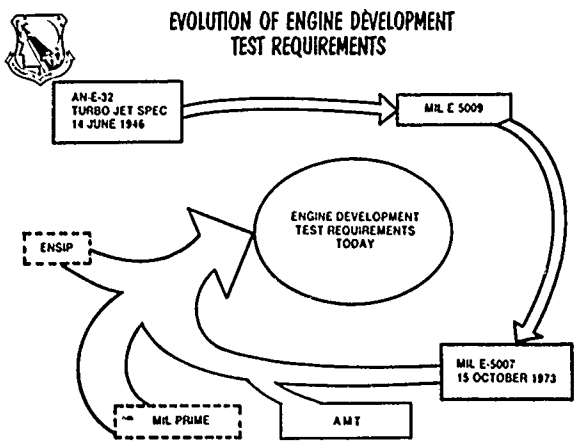

figure 1

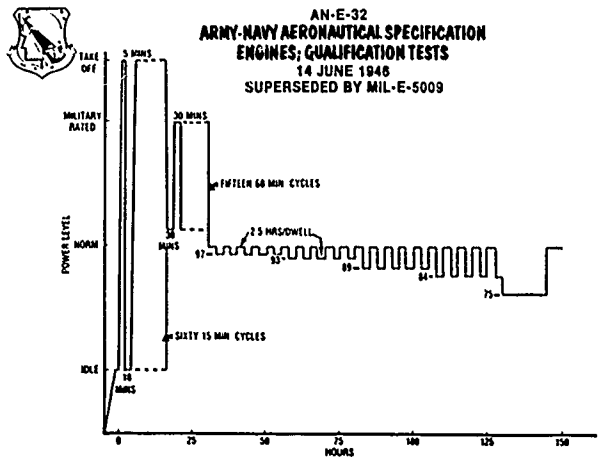

figure 2

The test cycle shown in figure 3 is from the MIL-E-5007 engine specification. This cycle was designed to cover all engine applications. This generalized "model" test was used as a qualification requirement for all military engines. The problem being that a large diversity of engine usage exist in fighter, bomber, transport and trainer aircraft missions. This 6 hour test was run 25 times for a total of 150 hours during which 300 idle-max-idle and 25 zero-max-zero engine transients. The test is much more severe than that of the earlier AN-E-32 test profile.

In the early 1970's the TF41 engine was experiencing field problems resulting in the loss of aircraft. It became apparent from these failures that there was a strong need to devise an endurance test program that would provide good correlation between

factory engine test and field engine experience and reliably uncover engine problems on the test stand before they become serious field problems. So the engine manufacturer jointly with the US Air Force and Navy conducted a fleet wide usage survey. From these data, a typical flight of mission profile was derived. The complexity of the control system adjustments required to trim the engine provide a very severe ground test cycle (figure 4). The engine test cycle was then determined (figure 5) and incorporated in all subsequent testing. This was the first program of many to adopt this philosophy.

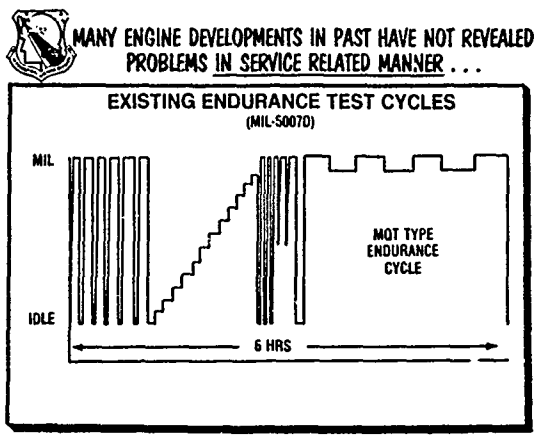

figure 3

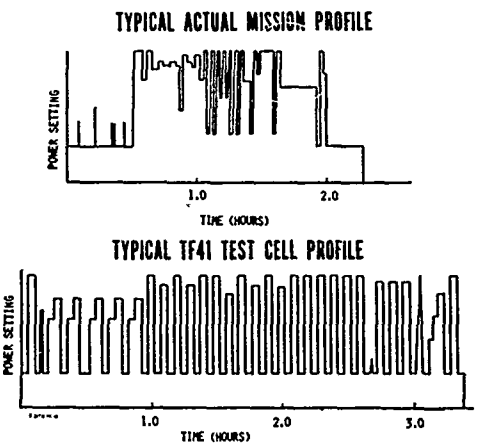

figure 4

PHILOSOPHY

As other engine development programs began to incorporate this method of test into their programs, each one had its own acronym and definition of what mission related testing was to be defined as and called. To prevent confusion within the Air Force and standard acronym and definition was adopted. Accelerated Mission Testing (AMT) is defined as:

> "An engine test conducted in a ground test facility in which the test profile bears a direct relationship to mission usage. The profile accounts for all significant throttle excursions and time at high power that would typically be seen in a composite operational mission."

The key points to be emphasized are 1) That AMT directly relates to field usage and 2) That AMT accounts for major throttle excursions and time at high engine power settings. AMT is primarily a structural durability test and it is important that the detrimental portions of the mission be included in the test. The major throttle excursions drive low cycle fatigue and thermal fatigue failure modes. The dwell time at high power conditions contributes to creep, stress rupture and erosion failure phenomenon.

APPROACH

Since the major intent of AMT is to reveal field related problems and distress in the factory test engines, it is imperative that an understanding of the aircraft usage be obtained. For new aircraft/engine systems the main source of usage information comes from user projections and review of mission data from aircraft flying similar missions. For existing systems usage surveys, recorded flight data, flight logs, test cell logs, pilot and ground crew interviews are used when nothing else is available. All aspects of engine usage must be considered, i.e., flight missions, ground trim runs, and test cell runs. This data is reviewed to assure that nothing significant is omitted from the AMT plan. Experience has shown that not only the correct number of cycles and dwell time at high power is required to derive a good AMT plan, but the following must also be considered. Some of our engines require periodic adjustment of allowable turbine control temperature in order to maintain required thrust. This temperature is set on the fuel control by the number of "clicks." A typical example of field experience is shown in figure 6. To assure the AMT is representative of this field exposure this adjustment schedule is carried throughout the testing of this engine. Since aircraft operate in a variety of climates and consequently a wide range of ambient temperatures, it has been found necessary to heat the inlet air of the test engine to assure demonstration of the hot environmental effects on the engine. Another significant finding is that dwell times at the idle and low power settings has a large impact on the stress range of some rotating parts and significant reduction in their part lives. Analysis has shown that horsepower extraction (accessory loads, aircraft bleed air, etc.) impacts the turbine cooling air flow and must also be demonstrated during AMT. The influence of high mach number aircraft missions must also be included in the AMT because of its life impact. These special considerations are the major parameters to be considered when setting up an AMT plan.

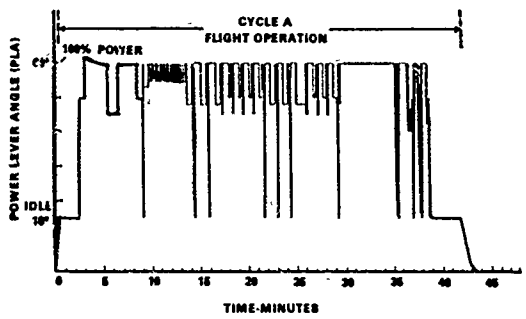

figure 5

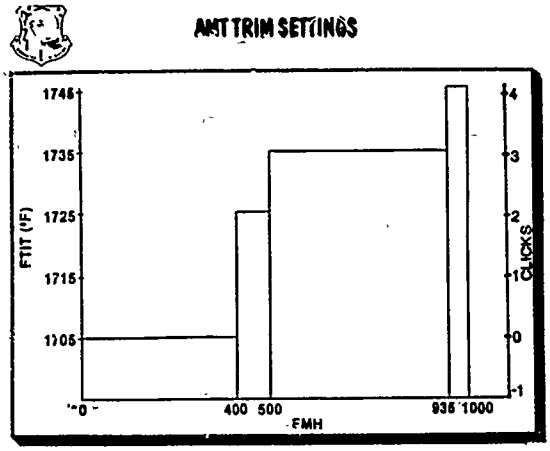

figure 6

Finally, after all available usage data is gathered a series of mission profiles can be constructed. These profiles can then be combined into a single composite mission or set of missions representing an average aircraft mission usage. The composite are then reduced by the elimination of part power dwell times and minor throttle transients that do not contribute to the overall life consumption of the engine (figure 7). The relative damage of the dwell times and minor cycles that are eliminated is usually determined by analysis. This elimination process is the key step in obtaining an optimized AMT cycle because it reduces expensive and superfluous test cell time.

BENEFITS/LIMITATIONS

Accelerated Mission Testing addresses a large portion of the failure modes as they relate to engine structural durability (figure 8). These primary failure modes are stress rupture, creep, low cycle fatigue, high cycle fatigue and in some cases, erosion and wear related distress.

However, all damaging conditions are not fully simulated during this type of testing, particularly those parts that are sensitive to total engine run time, flight maneuver loads, and installation effects such as external pressure and vibratory induced loads. For example, engine bearings are sensitive to total engine operation and flight maneuver loads neither of which are simulated fully in these static ground tests. Another example is external nozzle flaps which respond to the aircraft external flow field that imposes pressure and vibratory loads on the flaps not duplicated in AMT. Additionally, engine accessories and control components are generally life limited by total engine run time. They are normally bench tested for design verification.

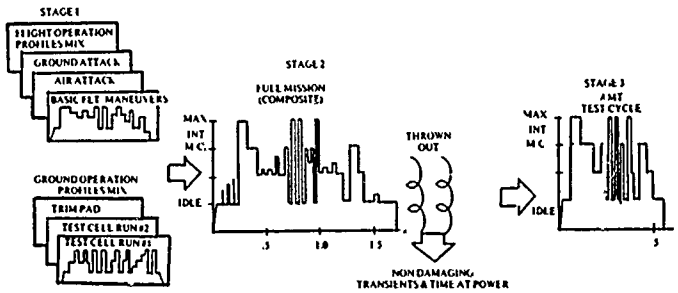

Fig. 7 Three stages of AMT cycle derivation.

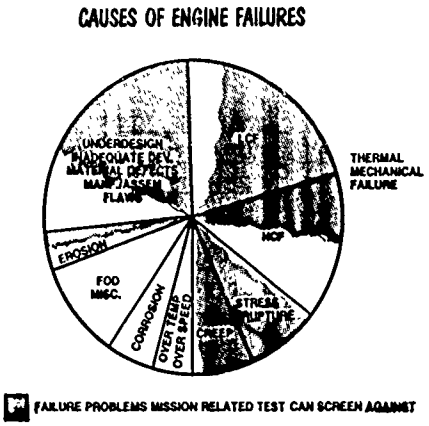

figure 8

RESULTS

Today, the F-15 and F-16 aircraft have the usage audited annually in order to assure that the AMT cycles being used in the factory are representative of the current field usage. The current F100 (F-15 and F-16 aircraft) AMT test profiles are shown in figure 9. There are five separate profiles: air combat, air to surface, functional check flight, ground test, and high cycle fatigue (HCF) profile. Since a large portion of the part power time has been eliminated for AMT profiles, any engine part that is sensitive to part power engine frequencies is not fully tested. Therefore, the HCF test has been added to "run-out" any high cycle fatigue induced responses in the engine parts sensitive to part power engine frequencies.

The requirements to qualify a typical 4000 flight hour engine is significantly more severe today compared to the earlier engine specification as shown below:

THROTTLE TRANSIENTS	AN-E-32 (1946)	MIL-E-5007 (1970)	AMT (Today)
0-Max-0	1 cycles	25 cycles	3,000 cycles
Idle-Max-Idle	60 cycles	300 cycles	20,000 cycles
Cruise-Int-Cruise	15 cycles	0 cycles	24,000 cycles
Time at Intermediate Power and Above	12 hours	89 hours	680 hours

A complete accounting of AMT revealed problems since its incorporation is beyond the scope of this paper and is difficult to present equitably. In one program or another all of the failures mode mentioned previously were identified in an AMT. Suffice it to say that the concept of AMT is accepted by every major American engine manufacturer for military development programs as evidence by the list of engines that have run or are currently running AMT's (figure 10).

SUMMARY

The past 10 years of AMT experience has shown that it correlates well with field usage in life demonstration. It is a useful tool for design substantiation and revealing problems that require redesign. AMT is also useful for establishing field and overhaul limits and the verification of rework procedures. There are limitations associated with this type of testing. AMT cannot completely address performance degradation because of the flight conditions not simulated in this static test. The total answer to engine structural durability is not provided due to the stochastic nature of engine component life and synergistic effects between the simulated and nonsimulated failure mechanisms.

It is important to realize that AMT does not provide the total answer to engine structural durability and there is a definite need for good design criteria, bench and component test, continued update of mission usage, and "lead the fleet programs." AMT is a major life management tool that is a useful tool in promoting safety, reducing cost and system readiness.

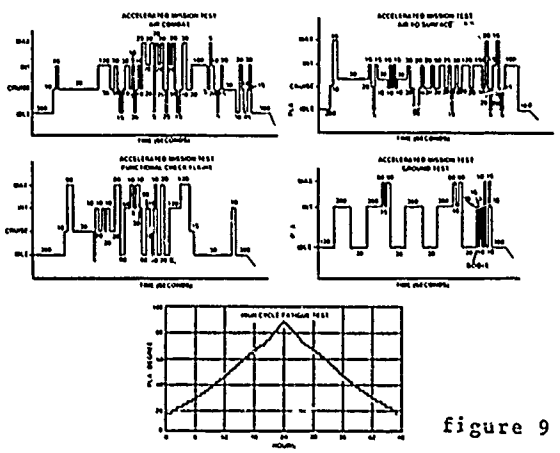

figure 9

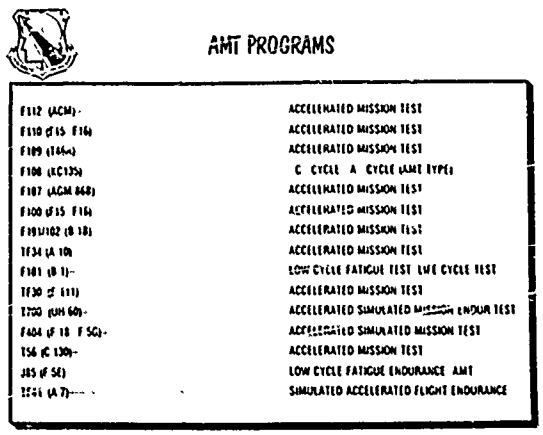

figure 10

REFERENCES

1. Accelerated Mission Testing of Gas Turbine Engines; Wilson R. Taylor and Jon S. Ogg. Wright-Patterson Air Force Base, OH; AIAA Paper Number 77-992.
2. Accelerated Mission Test Summary and Conclusions at 4000 EMH. Pratt & Whitney Aircraft Report, July 1979.
3. TF41 Component Improvement Program Report, Detroit Diesel Allison Division, Feb 1980.

DISCUSSION

W.J.Evans, UK

What failures do you produce with accelerated mission testing that do not appear in actual service and therefore cause unnecessary modifications?

Author's Reply

I do not know that we have done this to date. AMT does lead the fleet by substantial times to permit significant analysis.

A.J.A.Mom, Ne

You mentioned that you leave out small "non-damaging" cycles — how do you determine which ones qualify?

Author's Reply

Transients are left out only after analysis shows no significant portion of damage is attributed to them. We do recognize that we do miss such things as wear, but the gains associated with compressing the test time outweigh the disadvantages.

A.J.A.Mom, Ne

How many dwell times (length, temperature) do you incorporate into an AMT?

Author's Reply

All cycles included are what the engine will actually feel. We don't intentionally lengthen or shorten any dwell times unless an extensive analysis regarding the stress range on the particular component has been conducted.

P.Ramette, Fr

With AMT, could clearance variations cause unrealistic rubbing (interferences)?

Author's Reply

To avoid these undesirable situations one must be very careful in the design of the AMT cycle. Our current testing has not experienced this problem.

G.Breitkopf, Ge

When designing AMT cycles one has to reduce the representative real time operating sequence with respect to the time scale. This must be done on different rules according to the critical areas or features one is addressing to. So, do you use different AMT's, for example, for cold section parts and hot section parts testing?

Author's Reply

Yes. Currently AMT's are basically developed to investigate hot section durability.

EXIGENCES DE CONCEPTION ET D'ESSAI POUR DEVELOPPER LES MOTEURS D'AUJOURD'HUI

Jacques FRESCO
Sté TURBOMECA - Bordes
64320 Bizanos - FRANCE

1 – PREAMBULE

Pour s'adapter aux exigences toujours plus grandes de sécurité et de rentabilité du transport aérien, le moteur doit remplir deux fonctions de nature souvent opposées : performances et durabilité.

Si la compétition pour les performances constitue un aiguillon constant pour les constructeurs, jamais autant que maintenant la recherche d'une durabilité élevée n'a parue aussi impérieuse dès la mise en service.

La combinaison de ces deux lignes de force : performances traduites en termes de consommation de carburant ou de puissance et de durabilité conduisent à l'objectif final de réduction générale des coûts, pris au sens large. Aujourd'hui, dès la mise en service d'un nouveau moteur, il est nécessaire de garantir des potentiels élevés, du même ordre, sinon supérieurs, à ceux de moteurs en exploitation ayant déjà accumulé plusieurs millions d'heures de vol.

Dans cet exposé, nous analyserons les différents moyens permettant d'atteindre l'objectif de durabilité, comment ils interviennent dans la conception, quels sont les essais qui permettent de reproduire au mieux les phénomènes d'endommagement et nous donnerons quelques exemples qui se rapportent plus particulièrement aux moteurs de petite taille.

2 – DEFINITION DE LA DURABILITE

Le terme de la durabilité se définit de lui-même, c'est "l'aptitude à durer" (en anglais : ability).

Nous pouvons relier deux fonctions chiffrables à cette notion, lesquelles, combinées, représentent la durabilité, soit : la fiabilité et la durée d'utilisation.

Selon les cas, la fiabilité et la durée d'utilisation sont rapportées au moteur, au module ou au composant.

La fiabilité s'exprime en valeurs de probabilité issues de l'analyse statistique des résultats en service d'une flotte existante, en termes de :
- probabilité d'arrêt en vol ;
- probabilité de dépose non programmée.

La durée d'utilisation s'exprime :
- soit en durée entre révisions : retour en atelier,
- soit en durée entre visites : dépose sur terrain par action de maintenance,
- soit encore en durée de vie : dépose obligatoire d'une pièce critique.

Les outils disponibles permettant de prédire des valeurs réalistes pour chacun de ces postes sont de plus en plus performants, qu'il s'agisse de calcul, d'analyse ou d'essai.

Nous exposerons plus loin comment ces différents domaines interviennent dans la conception et les méthodes d'essai, ainsi que pour quantifier la probabilité des paramètres de durabilité dès la phase de développement.

3 – CARACTERISTIQUES D'UTILISATION

La base de départ pour toutes les études relatives à la durabilité est constituée par la définition des caractéristiques d'utilisation, c'est-à-dire :
- le cycle de référence
- le ou les profils de mission.

Cycle de référence (Figure 1)

Le cycle de référence sert de base aux différentes phases de la vie du moteur :

- lors de la conception, pour le calcul des contraintes et durées de vie, principalement des pièces tournantes critiques, pour l'évaluation des jeux en fonctionnement, etc... ;

- lors des essais pour déterminer le ou les cycles types d'essai de fatigue au banc des composants et du moteur ;

- en service, pour la comptabilisation des cycles réels effectués.

La détermination du profil du cycle de référence est particulèrement importante pour la distribution des contraintes dans les pièces tournantes fortement chargées. La partie initiale du cycle constituée par le démarrage est primordiale car elle impose les transitoires mécaniques et thermiques et selon que le démarrage est lent (environ 1 minute), ou rapide (inférieur à 40 secondes), la durée de vie du disque de turbine HP par exemple peut être divisée par un facteur 2.

Sur un hélicoptère bimoteur, les profils de démarrage du moteur gauche et du moteur droit sont différents, il faut donc en tenir compte.

Le choix de la température d'entrée turbine maximale du cycle est également très importante parce qu'elle constitue un étalon d'endommagement, notamment en fluage. On choisit en général le régime de décollage correspondant à un fonctionnement à des conditions ambiantes supérieures au Standard.

Profil(s) de mission (Figure 2)

La détermination d'un profil de mission type permet :
- lors de la conception, d'évaluer un potentiel prévisionnel ;
- lors des essais, de fixer le profil d'essai du moteur au banc pour vérifier les hypothèses d'endommagement, faire la démonstration du potentiel revendiqué et mettre au point les opérations de maintenance.

La détermination de ce profil n'est pas une tâche aisée surtout lorsqu'il s'agit de turbomoteurs d'hélicoptères. Les différents types d'utilisation de l'hélicoptère : transport, liaison plateformes de forage pétrolier, travail à l'élingue, "saut de puce", recherche et sauvetage... représentent chacun un profil d'utilisation des moteurs différents.

Il faut en plus intégrer les conditions ambiantes d'altitude et température pour finalement obtenir un profil d'essai sous la forme d'une combinaison des différentes missions que l'on pourra ensuite rapporter au profil moyen ou a chacun des profils d'utilisation possibles par un coefficient de corréiation.

Il est possible également d'évaluer la relation entre le cycle de référence et le profil de mission type.

4 – EXIGENCES DE DURABILITE LORS DE LA CONCEPTION

Les choix techniques lors de la conception sont déterminants pour la durabilité. Ces choix correspondent toujours à des compromis entre plusieurs solutions qui prennent en compte les différents aspects : performance, résistance, poids et coût.

C'est donc là qu'il faut veiller à intégrer la fonction durabilité qui pourrait se trouver négligée pour satisfaire les objectifs à court terme.

C'est d'abord au plan des principes de construction que s'établit cette fonction et nous examinerons successivement les différentes parties du moteur à cet égard.

Entrée d'air : l'influence de la conception de l'entrée sur la durabilité se traduit par l'homogénéité ou l'hétérogénéité de l'écoulement, c'est-à-dire par une distorsion de pression au plan d'entrée compresseur. Cette distorsion est fonction des obstacles et de la géométrie, elle peut engendrer une alimentation discontinue du compresseur et entraîner des vibrations de pale et même du pompage.

Pour un moteur d'hélicoptère avec réducteur placé à l'avant, une entrée d'air radiale est une solution acceptable pour remplir les objectifs énoncés ci-desus. L'alimentation d'une telle entrée a été réalisée sur le turbomoteur TM 333 par une volute rapportée, comme indiqué sur la Figure 3.

La géométrie a fait l'objet d'études et d'essais en soufflerie et une optimisation de la forme de la volute permet d'alimenter l'entrée d'air radiale du moteur avec le minimum de perte de charge. Elle permet également d'installer sur la volute tout dispositif de protection tel que séparateur de particules si nécessaire.

Compresseur axial : L'architecture de la plupart des moteurs TURBOMECA est constituée par une association axial + centrifuge (Figure 4).

Une des caractéristiques principales est une corde de profil longue, ce qui entraîne un nombre réduit de pales c'est-à-dire des épaisseurs importantes. Mis à part les avantages vis à vis de la marge au pompage, la durée de vie des pales est augmentée par rapport à des profils minces. En effet, pour des tolérances de fabrication données identiques Δe, la variation d'épaisseur relative $\Delta e/e$ est plus faible et la dispersion en fréquence également.

Autres avantages des profils épais, une meilleure résistance à l'érosion, à l'abrasion et aux impacts, ce qui est important pour les compresseurs axiaux.

Une autre caractéristique des compresseurs qui constitue un élément fondamental pour la durabilité est la construction pales/disque intégrale (blisk = blade and disk). Ce choix qui n'a pas que des objectifs de durabilité mais aussi de coût permet de supprimer tout système d'attache des pales : brochage, trou, queue d'aronde, c'est-à-dire d'éviter tout coefficient de concentration de contraintes donc d'avoir des roues peu chargées et par conséquent des durées de vie importantes : des vies limites supérieures à 10 000 cycles sont usuelles sur ce type de pièce.

En plus de la durée de vie potentiellement plus élevée de ce type de roue, l'absence de système d'attache élimine tout problème d'usure, de tolérances de fabrication et les risques de panne inhérents au système.

Ce type de construction n'est pas exempt d'inconvénients (manque d'amortissement) et, à cet égard le choix du matériau est important afin d'éviter une sensibilité à l'érosion qui conduirait à déposer les roues pour cette raison avant d'avoir atteint la vie limite.

Compresseur centrifuge (Figure 4) : les compresseurs étant de plus en plus chargés et l'effet de la température n'étant plus négligeable comme pour les axiaux, le dessin des centrifuges doit faire appel à des méthodes de calcul très élaborées, minutieuses, qui requièrent une optimisation par un grand nombre d'itérations.

Le sens de circulation de l'air derrière le rotor est à considérer avec attention pour son effet sur la température au moyeu, ce qui a une conséquence directe sur la durée de vie.

L'augmentation des vitesses périphériques et par conséquence des charges aérodynamiques et mécaniques et l'accroissement des taux de pression sont les caractéristiques de l'évolution récente des compresseurs centrifuges. Parallèlement, une amélioration significative des rendements et une maitrise des circulations secondaires ont permis de compenser en partie l'élévation de température consécutive à l'augmentation du taux de pression permettant ainsi d'utiliser des alliages classiques de titane.

L'optimisation de ces différentes caractéristiques a, de cette façon, un impact direct sur la durée de vie du rotor de compresseur centrifuge.

Chambre de combustion (Figure 5): les éléments majeurs à considérer sont le matériau et le type de refroidissement de paroi.

Cet ensemble nécessite une étude mais surtout une mise au point par des essais de composants.

La technique classique de refroidissement par film est réalisée sur les chambres TURBOMECA soit par perçage incliné dans l'épaisseur des tôles par bombardement électronique, soit par film rapporté, soit par une combinaison des deux.

Les peintures "thermocolors" constituent maintenant un des outils précis et fiable qui permettent par une visualisation des températures de paroi d'optimiser rapidement le refroidissement et le profil de sortie d'une chambre.

Turbines (Figure 6) : ce qui a été exposé ci-avant pour le calcul des rotors de compresseur centrifuge est encore plus aigu pour les turbines. Mais les méthodes de calcul de durée de vie en fatigue oligocyclique, en fatigue à haute fréquence, en fatigue vibratoire, en fluage, le calcul des transferts de chaleur, la mécanique de la rupture permettent une approche de plus en plus précise des phénomènes d'endommagement. Chacun d'eux constitue un vaste domaine d'investigation et de recherche continues.

Un point mérite d'être souligné, il s'agit de la ventilation interne. Cet aspect est d'autant plus important que pour les moteurs de petite taille les disques sont courts et trappus et sont soumis à de forts gradients thermiques. Une optimisation de la ventilation interne entre compresseurs et turbines permet un gain significatif en température et en gradient de température dans les disques et par conséquent en durée de vie des turbines.

L'augmentation de la charge des turbines a un effet indirect sur la durée de vie. Il est possible en réduisant le nombre d'étages d'obtenir un gain important en température moyennant un compromis acceptable sur les contraintes et ainsi d'éviter le refroidissement des pales de turbine. Le résultat se traduit immédiatement à température et performances égales en matière de simplicité, compacité et coût, la simplicité étant un des élément clé de la durabilité.

Le nombre de pales étant faible et les cordes axiales relativement grandes, les disques sont massifs au moyeu, ce qui entraîne une biaxialité des contraintes importante dans les phases transitoires et c'est pourquoi une définition précise du cycle de référence doit être effectuée tandis qu'une corrélation avec les essais est indispensable.

On peut ainsi obtenir avec des turbines fortement chargées assurant des performances élevées, une durabilité compatible avec les exigences actuelles.

Réducteur : pour les turbomoteurs et turbopropulseurs le réducteur constitue un organe particulièrement important et son intégration avec le générateur de gaz doit être préparée par une étude mécanique approfondie.

En particulier pour les moteurs de petite taille, la vitesse d'entrée dans le réducteur étant élevée, et compte tenu des dimensions disponibles, les charges radiales sur les roulements sont importantes. Il faut donc une architecture et des roulements capables de supporter ces efforts.

Le calcul des dentures doit être optimisé afin d'augmenter le rendement de la pignonnerie, ce qui a pour effet de diminuer la dissipation d'énergie en chaleur. Cette optimisation s'effectue en recherchant une combinaison des différents paramètres : pression de Hertz, vitesse de glissement, température éclair pour conserver dans les conditions extrêmes l'intégrité du film d'huile.

Toutes choses égales par ailleurs, on obtient un abaissement de la température d'huile qui permet de garantir des durées de vie de plusieurs milliers d'heures pour les pignons et roulements.

Régulation (Système de contrôle du débit de carburant) (Figure 7) : le choix du principe de régulation du moteur est également important pour la durabilité. Sur les moteurs TURBOMECA, ce choix est basé sur la régulation tachymétrique.

Ceci signifie que pour un régime donné : maxi d'urgence, décollage ou maxi continu, pour une valeur de vitesse N_G du générateur de gaz de consigne, la puissance minimale nécessaire à ce régime est disponible dans tout le domaine de vol (température, altitude-pression). La température d'entrée turbine varie dans ce domaine jusqu'à la valeur maximale qui correspond en principe au niveau de la mer à la température ambiante maximale.

Par rapport à un moteur régulé en température et pour lequel la valeur de consigne (valeur maximale) pour le décollage par exemple est affichée à chaque vol, un moteur régulé en vitesse N_G ne fonctionnera à la valeur maximale de température qu'en limite du domaine d'utilisation. Les marges sont donc plus importantes sur un moteur piloté en N_G et permettent d'obtenir par le principe même une durabilité potentielle plus élevée que pour un moteur piloté en température.

L'apparition de l'électronique et des microprocesseurs pour la régulation des moteurs modernes ouvre des perspectives intéressantes pour enregistrer le fonctionnement du moteur et en quantifier l'endommagement. Toutefois, il reste du travail à faire avant de pouvoir transposer ces résultats en diagnostic sur l'état de tel ou tel élément.

5 – EXIGENCES DE DURABILITE POUR LES ESSAIS

Les choix sur la conception étant effectués, les bases pour la durabilité du moteur et de ses éléments sont alors fixés. Il reste à les vérifier par les essais et apporter des améliorations ou modifier certains choix si c'est possible.

Nous distinguerons les essais de composants et les essais sur moteur.

5.1. Essais de composants

Une planification rigoureuse des essais de composants permet en même temps de vérifier les hypothèses de conception et de limiter au strict nécessaire les essais sur moteur qui sont plus longs à mettre en oeuvre, coûteux et qui nécessitent d'avoir le bon standard au bon moment.

Hormis les essais de composants spécifiques aux performances, ceux plus spécialement axés sur la durabilité sont essentiellement les essais d'endurance sur bancs spéciaux (Figure 8).

Des essais partiels bien conçus permettent de figer rapidement la configuration des moteurs prototypes et donc de commencer très tôt dans le programme de développement, les essais de durabilité.

Essais en cycles de fatigue :

Les rotors de compresseurs, axiaux et centrifuge, les turbines sont soumis à des essais d'endurance en fatigue oligocyclique basés sur le cycle de référence.

Le cycle d'essai est déterminé pour chaque pièce afin de reproduire un état de sur-contraintes mécaniques et thermiques par rapport au cycle type de référence défini précédemment.

Cette simulation implique de réaliser des moyens de chauffage des pièces en essai qui reproduise d'une façon aussi proche que possible la distribution des températures en transitoire et en valeurs stabilisées mini et maxi. Il importe à cet effet de faire des mesure de température sur moteur par thermocouples et peinture thermosensible ou par tout autre moyen plus sophistiqué. La Figure 9 montre une coloration obtenue sur une chambre de combustion, sur les turbines on utilise à la fois des mesures par sondes

thermosensibles et peinture "thermocolore".

Il est possible aussi lorsque l'on ne dispose pas du champ de température d'ajuster les vitesses de rotation mini et maxi d'essai pour obtenir l'équivalent à froid des contraintes à chaud.

La détermination des paramètres d'essai est faite par calcul sur la zone la plus chargée.

Des essais en fatigue vibratoire sont mis en oeuvre en tenant compte des diagrammes d'excitation vibratoire des pales. Le banc doit alors être équipé des obstacles tels que redresseur, bras de carter, etc... qui sont les sources possibles d'excitation et tourner en stabilisant la vitesse sur la fréquence correspondant à la résonance tout en mesurant l'amplitude par jauge extensométrique.

Essais de survitesse :

Toujours pour les rotors, des essais de survitesse sont effectués au puits sous vide, afin de vérifier les marges de calcul jusqu'à rupture.

Ces essais sont particulièrement importants pour les éléments de turbine libre surtout si l'on a choisi de justifier en certification que le risque en cas de survitesse est couvert par la rupture des pales et la rétention des débris en cas de survitesse.

Ce choix conduit à mesurer avec exactitude la vitesse de rupture au banc, corrigée éventuellement par les effets de la température et de démontrer que le blindage contient les débris éjectés.

Bien que n'étant pas des essais directement applicables à la durabilité, ils constituent le complément nécessaire aux essais d'endurance en évaluant les marges permettant de garantir qu'à l'intérieur des durées de vie en fatigue, le risque de rupture présente une probabilité suffisamment faible et d'autre part, que s'il y a rupture, il n'y a pas de danger pour l'aéronef.

Essais des arbres de transmission, paliers, roulements :

Les phénomènes de fatigue en flexion, torsion et flexion/torsion combinées sont reproduits sur des bancs d'arbres de transmission. Des essais d'endurance peuvent donc être mis en oeuvre jusqu'à la rupture pour vérifier les durées de vie calculées.

Des bancs spéciaux d'arbres munis de leurs paliers et roulements sont destinés aux essais de vitesse critique et de susceptibilité au balourd. Ces essais permettent de mettre au point les jeux de palier, de mesurer les amplitudes de réponse du système dynamique en cas d'usure de roulement, d'impact sur une pale pouvant engendrer un balourd et même de simuler la rupture d'une pale entière : profil et plateforme. La Figure 10 montre l'amortissement d'un système arbre/paliers avec un balourd de 50 cm/g. L'instrumentation du système permet de mesurer la déformation et le déphasage en différents points de l'arbre, la contrainte dans la cage du palier et les caractéristiques d'amortissement.

Essais d'endurance des réducteurs :

Les bancs "dos à dos" (back to back) permettent de charger les réducteurs selon un programme déterminé, ils permettent d'étudier le comportement des pignons et des roulements en faisant varier les différents paramètres de fonctionnement : température, pression et débit d'huile ainsi que les différentes spécifications d'huile : 3 cSt, 5 cSt et 7,5 cSt.

Ces essais sont surveillés par analyse spectrographique de l'huile et si nécessaire, par des moyens plus sophistiqués.

Essais des systèmes :

Sans entrer dans le détail des essais innombrables qui sont effectués sur les systèmes et leurs accessoires à la fois pour l'endurance et l'influence de l'environnement, nous citerons seulement pour mémoire, ceux qui se rapportent au système de carburant. TURBOMECA conçoit et développe ses propres systèmes : pompe, filtre, régulation et est donc équipé de banc d'essais spéciaux.

Les essais de simulation à partir de modèles mathématiques représentant l'ensemble : moteur-transmission mécanique au rotor d'hélicoptère (ou à l'hélice, ou à l'alternateur pour les G.A.P.) permettent la mise au point des boucles de régulation, l'étude des transitoires et le comportement en modes de panne.

Les essais d'endurance sous des conditions variées d'environnement permettent de vérifier les choix de construction.

L'avènement des régulations électroniques digitales à autorité totale rend ces différents essais encore plus importants avant même le montage sur moteur.

La Figure 11 montre le boitier électronique du turbomoteur TM 333 en cours de certification.

5.2. Essais sur moteur

Les essais de composants s'imbriquent dans le programme des essais de développement au banc sur moteur qui de toutes façons permettent de faire un diagnostic plus précis sur la validité des choix de conception.

Les essais sur moteur qui ont pour objet la vérification de la durabilité sont constitués essentiellement par les essais d'endurance au banc, mais aussi, par certains essais en vol qui permettent de compléter les résultats des essais de composants et des essais sur moteur.

Essais en cycles de démarrage - arrêt :

Ces essais basés sur le cycle de référence constituent, avec les essais de composants du même type (essentiellement les compresseurs), la base pour le calcul des vies limites initiales de service et éventuellement pour l'extension de ces mêmes vies limites.

Essais en cycles de mission accélérée :

Après avoir défini le profil du cycle ainsi qu'il est indiqué au paragraphe 3, les essais propremens dits sont effectués au banc sur un moteur se rapprochant le plus possible du standard série. Ce type d'essais est particulièrement important pour la durabilité parce qu'étant effectué avec un coefficient d'accélération du temps relativement important, on précipite la formation des défauts, les conditions de pannes potentielles et l'examen attentif des résultats d'essai : usures, criques, déformations, etc. permet d'apporter à temps les modifications nécessaires.

La Figure 12 donne un exemple de cycle avec la représentation de la variation de la température et des contraintes en différents points d'un disque de turbine.

Essais d'endurance à haute température :

Ces essais d'un caractère particulier, permettent de vérifier le comportement des parties chaudes, de caractériser le moteur en fluage en vue d'applications spéciales (régimes d'urgence à durée limitée) et de déceler par anticipation les zones de défaillance possibles.

Essai d'endurance de type de 150 heures :

Cet essai consacré par l'usage est le point clé des programmes d'homologation et de certification. Bien que les enseignements que l'on tire des essais cités précédemment soient d'une façon générale plus précieux pour le constructeur, il constitue néanmoins une référence qui permet de valider les limites de fonctionnement du moteur et reste de toutes façons le "juge de paix" du programme.

Essais d'endurance spéciaux :

Les moteurs TURBOMECA à turbine liée font l'objet d'essais en cycles ou en continu accouplés à un alternateur dans une des centrales électriques de nos usines. A vitesse constante, la charge est produite par la variation de puissance électrique, elle se traduit par des variations de débit carburant de la régulation, c'est-à-dire, par une variation de la température d'entrée turbine. L'avantage du système est de pouvoir annuler la puissance fournie par un délestage électrique complet permettant de simuler par exemple des régimes de descente rapide d'un turbopropulseur.

Certains moteur TURBOMECA tels le TURMO ou l'ASTAZOU ont des applications industrielles, notamment ferroviaires dont l'utilisation dépasse couramment 10 000 heures et qui permettent de mettre à jour des types d'endommagement particuliers. L'application des modifications consécutives sur les moteurs aéronautiques permet d'améliorer la durabilité.

Essais en vol :

La possibilité de confirmer pour des essais en vol des résultats obtenus au banc, même par un fonctionnement limité constitue un avantage majeur pour le développement. Les conditions d'environnement réelles en vibrations, température sous capot, facteurs de charges, etc... sont des éléments essentiels à prendre en compte pour la durabilité du moteur et des équipements.

6 – ANALYSE DES RESULTATS D'ESSAI

Les résultats d'essai constituent la sanction des choix de conception, il en est du reste de la durabilité comme des autres domaines. Il importe donc d'analyser les résultats avec une grande finesse, en premier lieu afin d'apporter les correctifs et améliorations nécessaires en temps utile, en second lieu afin d'en tirer des enseignements sur la durabilité du moteur en service.

L'analyse des évènements et incidents même mineurs qui arrivent lors des essais de composants et surtout lors des essais du moteur au banc ou en vol doivent être enregistrés pour être ensuite exploités.

Cette exploitation doit être basée sur le principe suivant : l'incident aurait-il provoqué en service :

- une action de maintenance de routine
- une dépose moteur non programmée
- un arrêt en vol.

Chacun de ces postes est ensuite traduit en chiffres de fiabilité ou plus précisément en taux par 1 000 heures. Un taux cumulé et un taux périodique (3 mois, 6 mois ou 1 an) sont tracés sur un diagramme qui permet de suivre l'évolution de la fiabilité réelle et prévisionnelle pendant le développement.

La Figure 13 montre un exemple de cette évolution. Le diagramme peut être établi pour le moteur dans son ensemble, il peut aussi être éclaté en éléments principaux : (compresseurs, turbines, réducteur ...) et équipements importants (régulation, partie hydro-mécanique, boitier électronique ...).

La comparaison entre les études prévisionnelles de fiabilité, les objectifs et les résultats même limités tirés de l'expérience du développement permet de juger à priori de la durabilité du moteur.

7 – CONCLUSION

Le duel constant entre la recherche de hautes performances et la durabilité constitue un challenge particulièrement difficile pour les constructeurs.

Les choix à faire lors de la conception engagent l'avenir du moteur et il importe de trouver des compromis satisfaisants.

L'effort à fournir pour mener à bien ce double objectif doit être constant pendant tout le programme.

Les composantes de la durabilité sont multiples et complexes, or il ne semble pas qu'à court terme, un saut technologique important soit possible par les matériaux. Il faut donc s'attacher à améliorer chacune des composantes afin d'assurer une sécurité de fonctionnement toujours plus grande.

Les méthodes de prévision par calcul et analyse sont de plus en plus précises et fiables. Assitées par les essais de composants elles permettent d'obtenir plus rapidement les objectifs de performance et de dégager ainsi dans un programme de développement un temps plus long à consacrer aux démonstrations de durabilité sur moteur.

Dans un avenir proche, l'utilisation des microprocesseurs ouvre des perspectives intéressantes pour une meilleure connaissance du comportement des moteurs en service, avec une incidence bénéfique sur la conception et une adéquation des essais de simulation au banc.

PROCEDURE TYPE DE DEMARRAGE SUR HELICOPTERE BI-MOTEUR

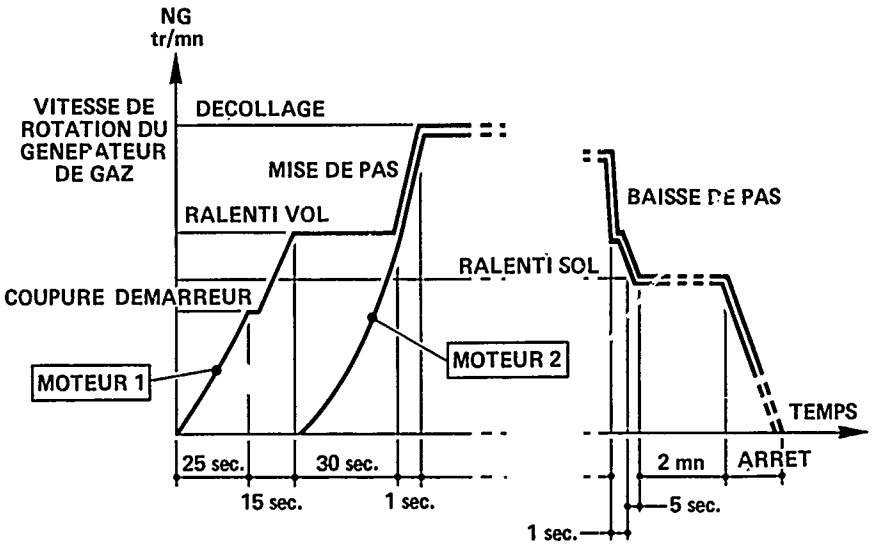

CYCLE DE REFERENCE

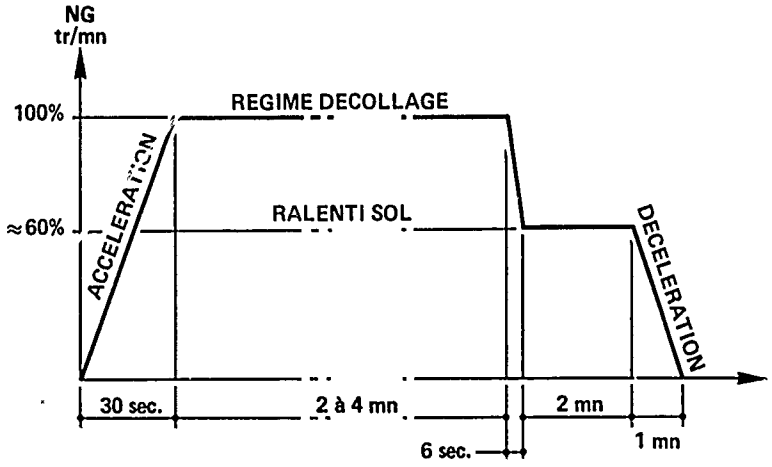

FIGURE 1

PROFILS DE MISSION

TURBOMOTEURS D' HELICOPTERE

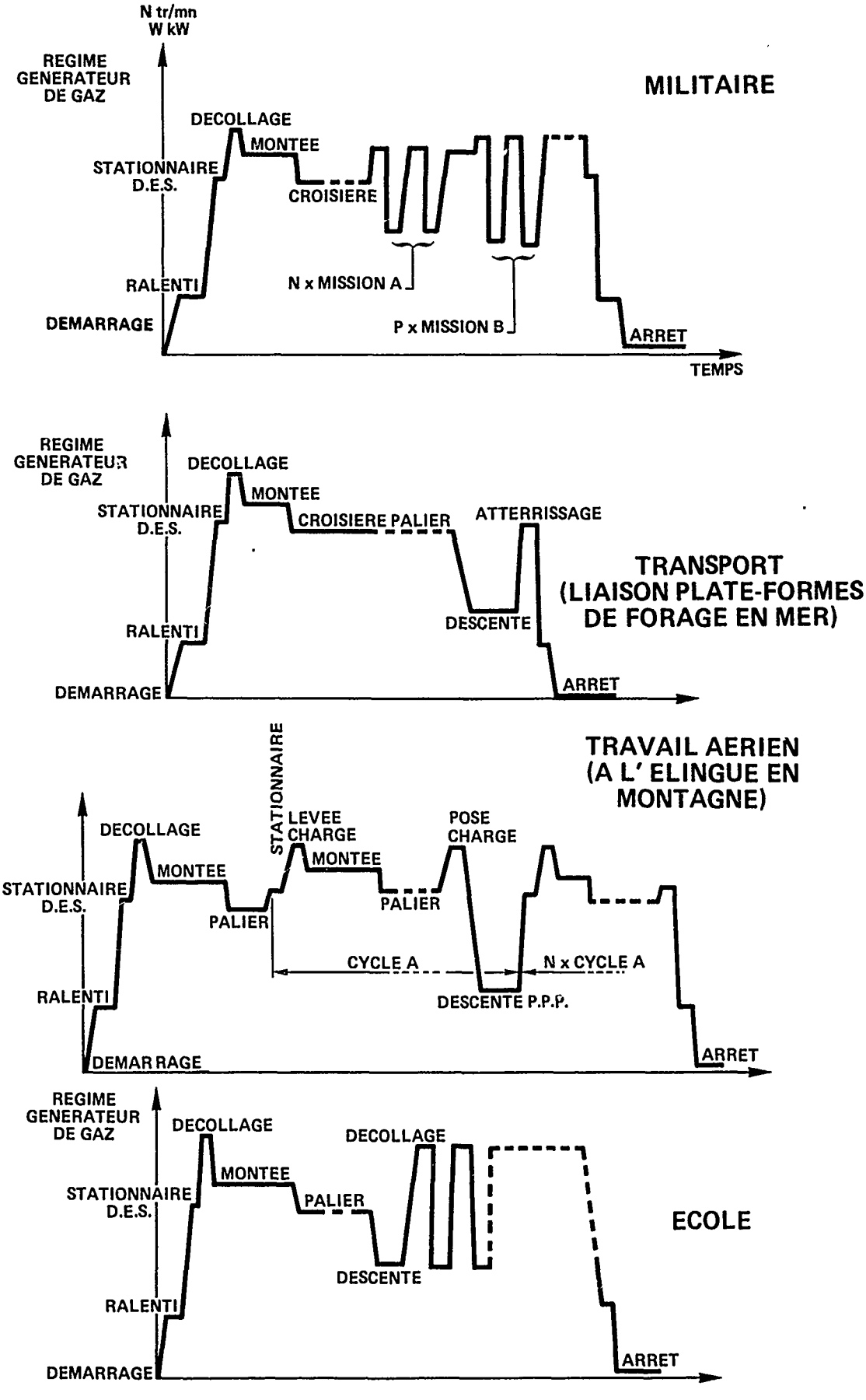

FIGURE 2

FIGURE 3

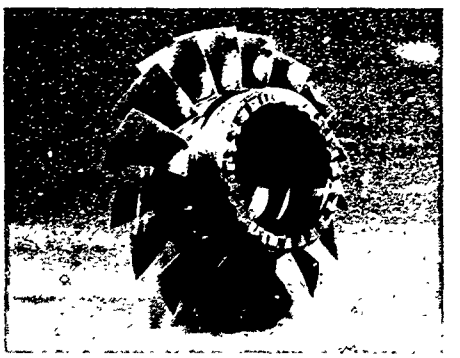

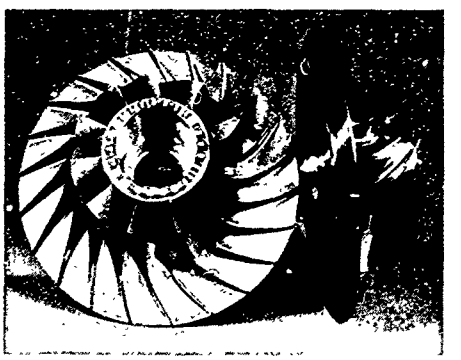

FIGURE 4

FIGURE 5

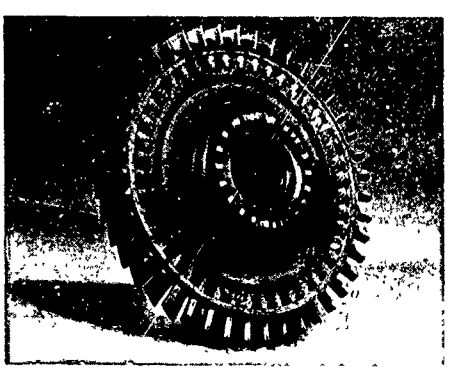

FIGURE 6

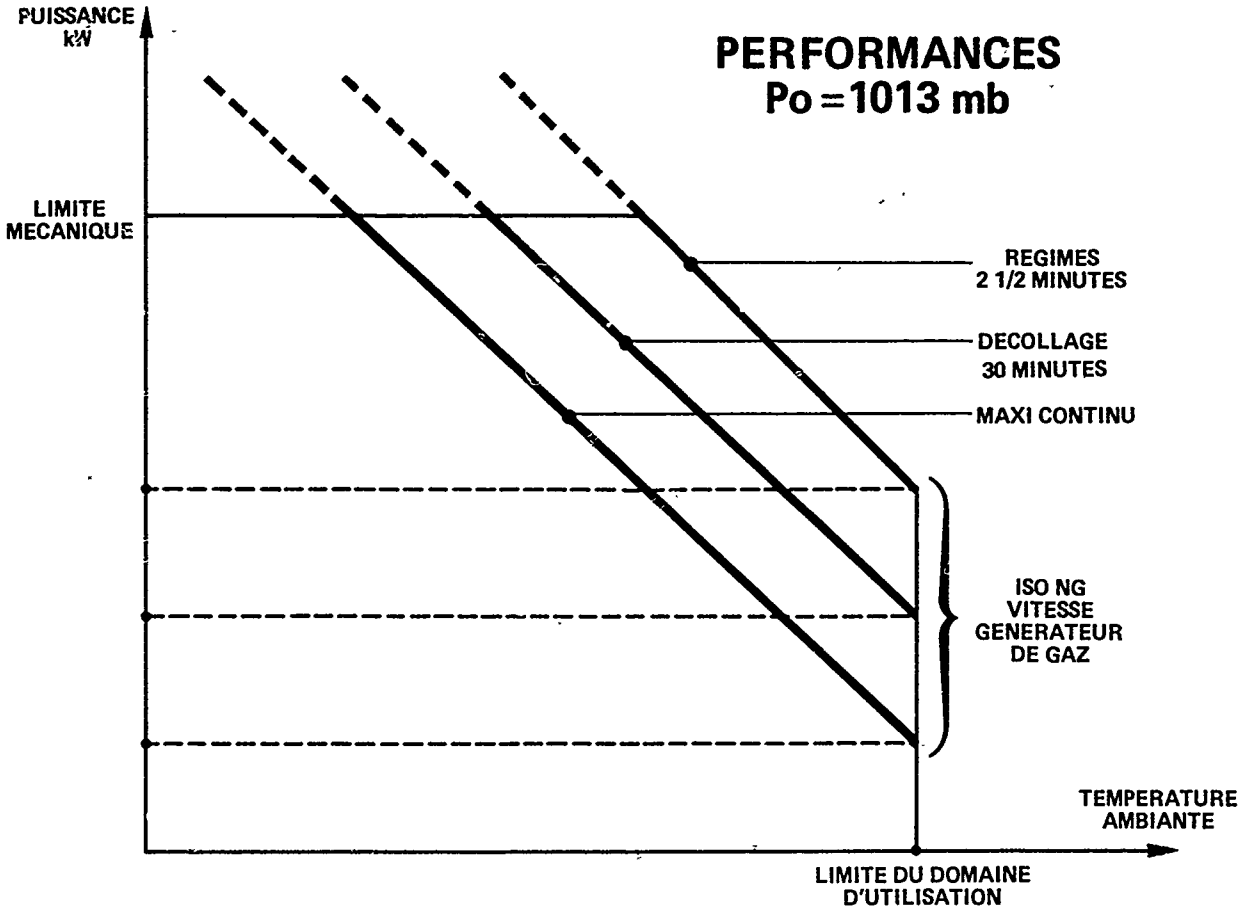

FIGURE 7

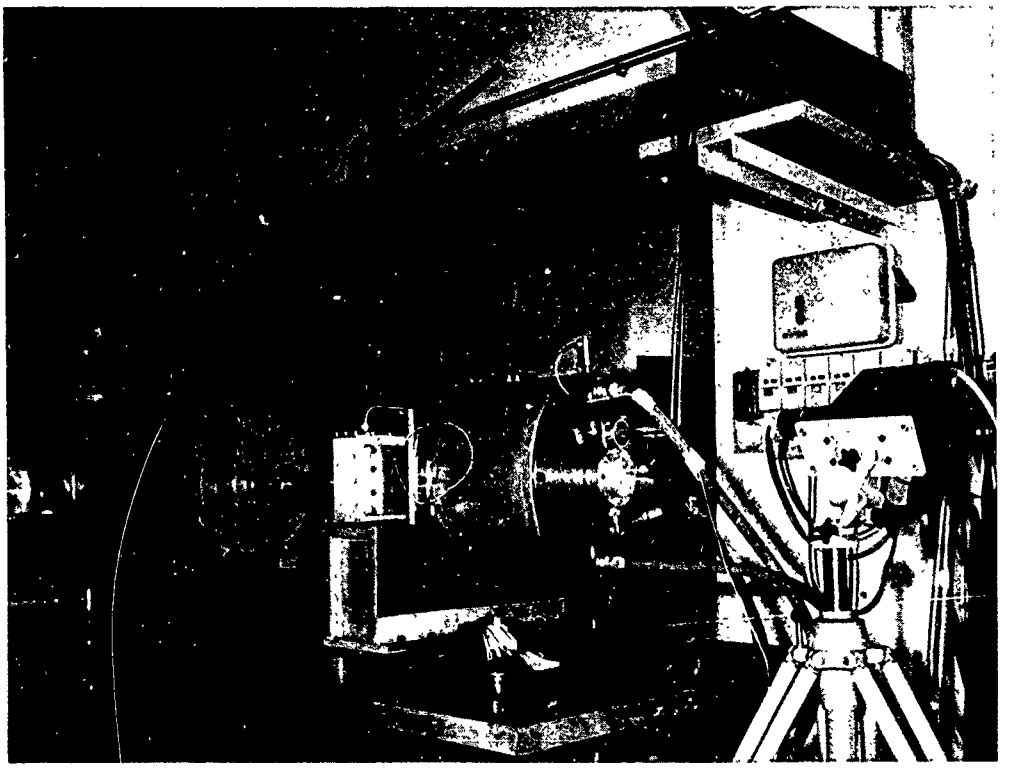

FIGURE 8

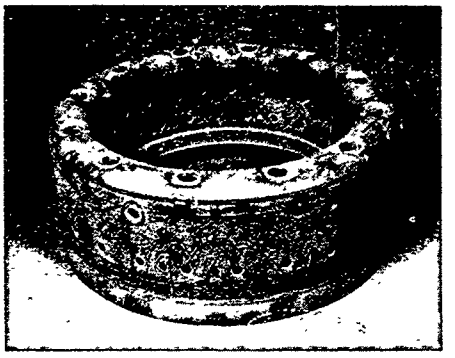

FIGURE 9

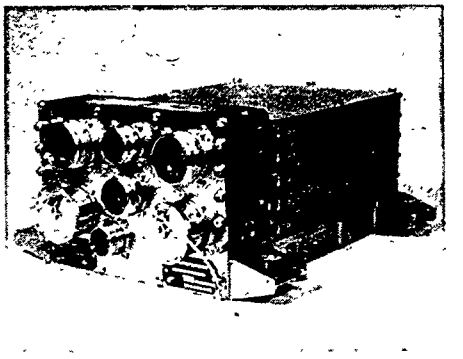

FIGURE 11

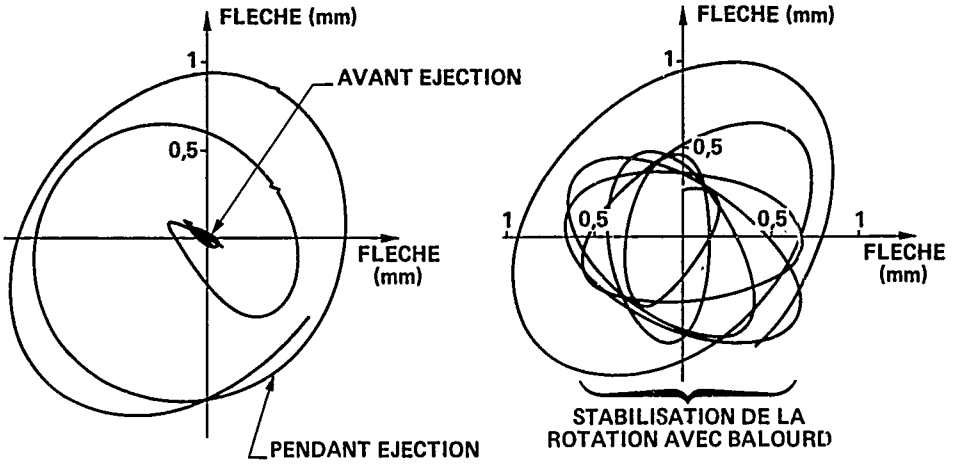

FLECHE DU MILIEU DE L' ARBRE, EJECTION D'UNE MASSELOTTE
REPRESENTANT ENVIRON 1/2 PROFIL DE PALE DE TURBINE LIBRE

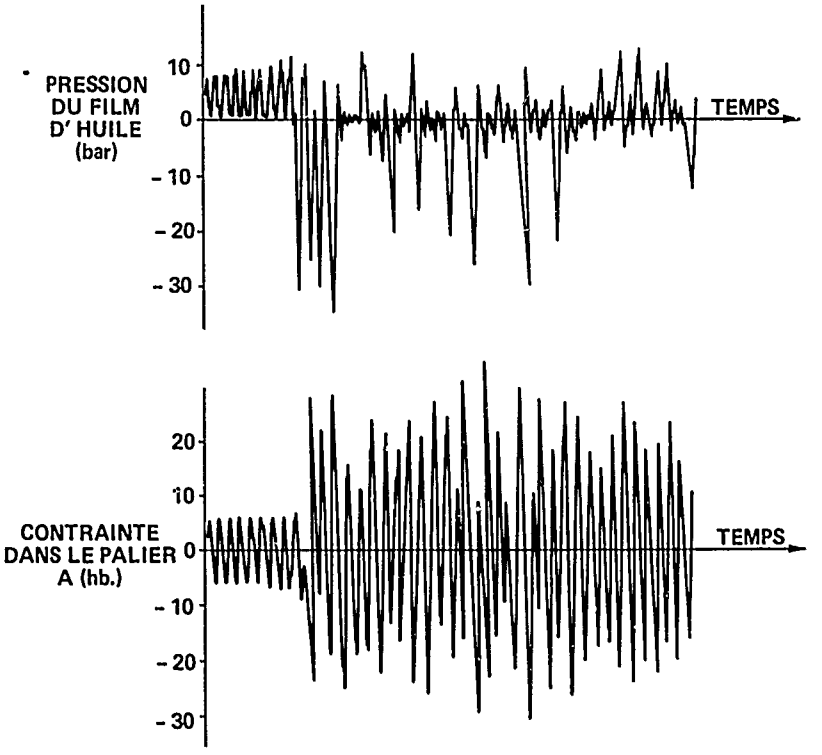

FIGURE 10

PROFIL CYCLE MISSION ACCELEREE

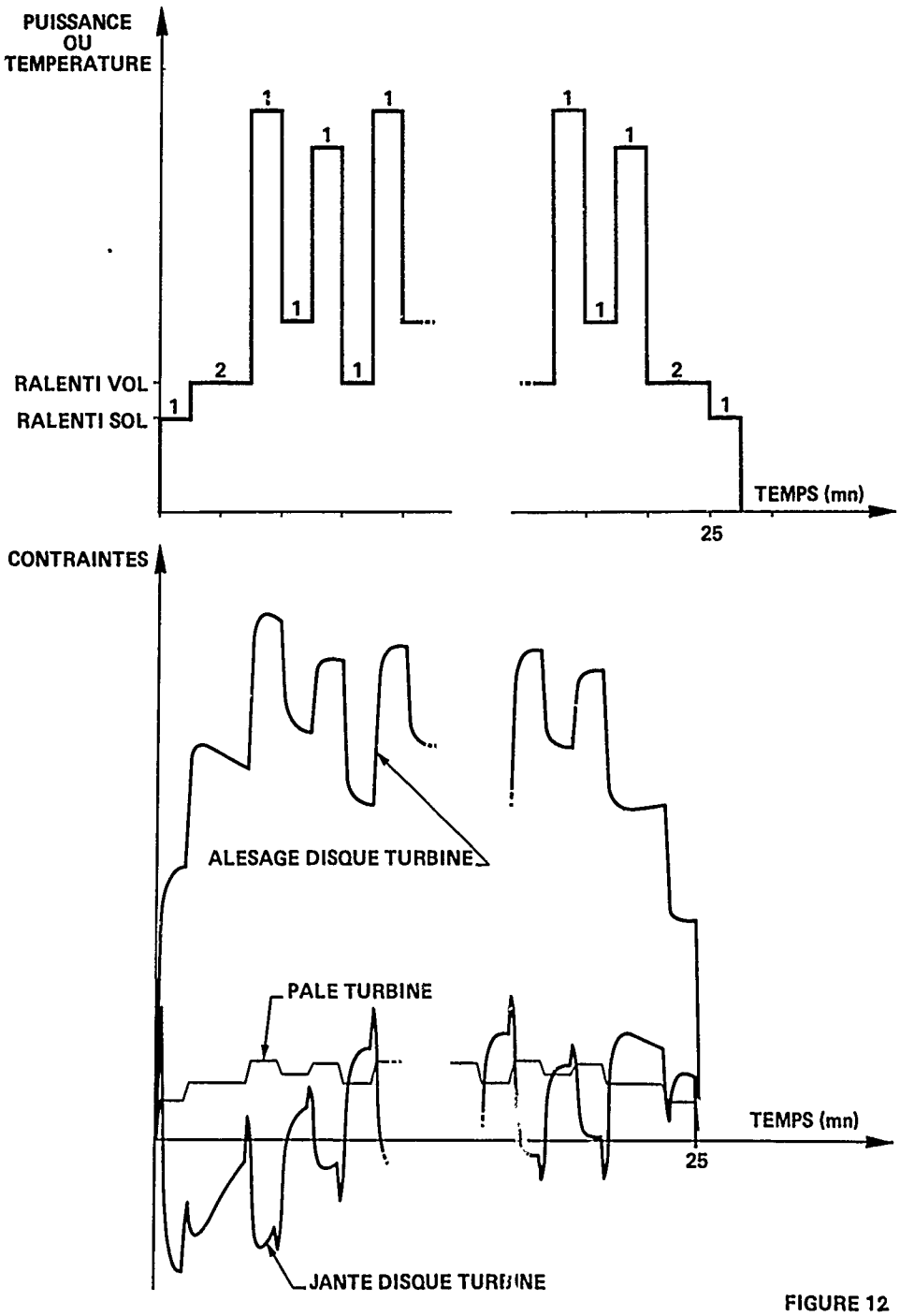

FIGURE 12

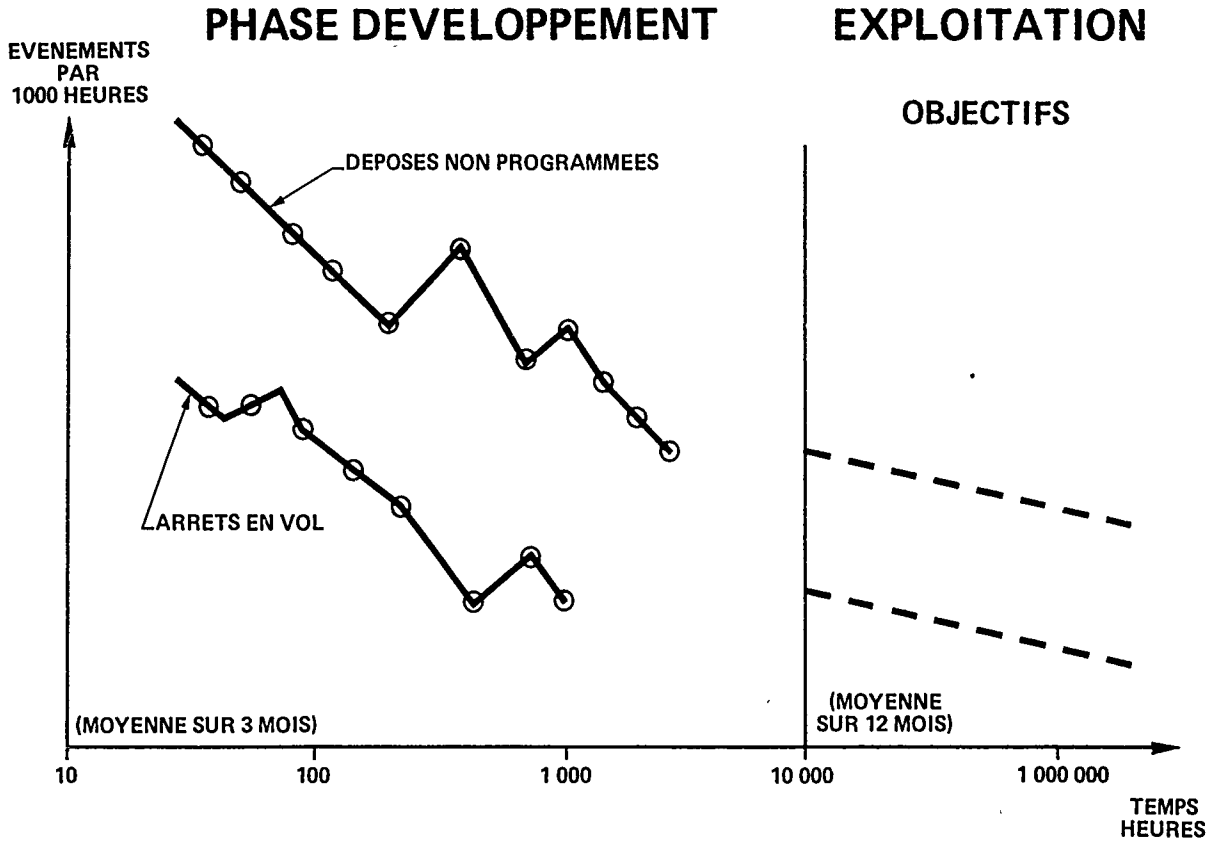

FIGURE 13

DISCUSSION

R.Tadros, Ca

You spoke of titanium material. Exactly what type of material are you talking about at approximately 1000°F, and 2000 feet per second centrifugal rotors run speed.

Author's Reply

Classical types of titanium alloys – processed under vacuum. I don't know the US classification. For advanced projects titanium is not adopted. What I wanted to say was that with an improvement in output of special work on internal cooling, you can consider titanium alloys.

OVERVIEW OF THE AGARD SMP ACTIVITIES ON TURBINE ENGINE MATERIALS TECHNOLOGY IN THE 1972 - 1982 PERIOD

A.J.A. Mom
National Aerospace Laboratory NLR
Anthony Fokkerweg 2, 1059 CM Amsterdam
The Netherlands

SUMMARY

This paper presents an overview of the AGARD Structures and Material Panel activities on turbine engine technology over the last 10 years. These activities cover most of the material related aspects in gas turbine technology from the initial design stage up to the final retirement of components. Topics which have been discussed over the last years can be brought under different headings:
1) the development and application of advanced materials, 2) material properties and behaviour, 3) material processing and fabrication techniques, 4) maintenance and repair and 5) life prediction methods.
With respect to the advanced materials and fabrication techniques attention will be given in this paper to the directionally solidified in-situ composites, the ceramic materials and the PM materials, and their different processing aspects. New fabrication techniques like hot isostatic pressing, superplastic forming and surface treatments are included. Furthermore the corrosion behaviour and low cycle fatigue characteristics of engine materials, including methods to predict creep and fatigue behaviour, like e.g. the strain range partitioning method, are discussed.
Finally, attention will be given to maintenance, repair and life prediction of engine components. Emphasis is directed to the introduction of damage tolerance concepts to make a more economic use of inherently available component life than is presently done by the safe life philosophy.

1. GENERAL INTRODUCTION

Figure 1 gives a schematic view of the links between materials technology-related topics such as materials selection, development, processing, maintenance and repair and the basic steps in gas turbine engine technology: design, production and operation.
The AGARD Structures and Materials Panel is paying increasing attention to the highly interesting area of materials for aero gas turbines. In the last 10 years all subjects indicated on the right hand side of figure 1 have been addressed:

- the development and application of advanced materials, in particular directionally solidified eutectics and ceramics
- materials properties and behaviour, e.g. corrosion behaviour
- materials processing and fabrication techniques
- maintenance and repair and
- life assessment and prediction methods.

In this paper reviews will be presented from the various Specialists Meetings on the above subjects organised in the 1972-1982 period.

2. HIGH TEMPERATURE CORROSION OF AEROSPACE ALLOYS

2.1 Introduction

When a component is operating at high service temperatures very serious consideration should be given to its corrosion and oxidation behaviour under the appropriate working conditions. Not only strength and fatigue properties but often corrosion properties determine the suitability of a particular material for a specific application. Oxidation for example prevents the application of Ti-alloys above 550 °C; hot corrosion strongly affects the service life of Ni- and, to a lesser extent, Co-alloys in the 700-1000 °C temperature range; and at temperatures above 900 °C oxidation becomes a life limiting factor for Ni- and Co-alloys.
A number of questions arise when dealing with the problem of high temperature corrosion:

- what are the different types of high temperature corrosion and under what conditions do they occur?
- what is the relative corrosion resistance ranking of present and future alloys?
- which factors determine the resistance of alloys against corrosive attack and would it be possible to modify alloys to improve their corrosion resistance?
- would it be possible to modify the environment to prevent the occurrence of corrosion promoting conditions?

The above questions, addressed during the 1972 AGARD Specialists Meeting [1], will be discussed in more detail below.

2.2 High temperature corrosion processes in gas turbine engines

Two different corrosion processes can be distinguished:

1) oxidation; this process of converting metal into metal oxides is characterised by an increasing oxidation rate with increasing temperature. Oxidation becomes important at temperatures above 900 °C.
2) hot corrosion; an accelerated form of oxidation due to the presence of molten alkali-metal sulphates on the surface of the component. This type of corrosion usually occurs in the 700-1000 °C temperature range.

Because the air/fuel ratio in gas turbines is about 50:1 by weight [2] strong oxidising conditions generally exist. The rate of oxidation can be controlled (often very satisfactorily) by material alloying or the use of coatings. This will be discussed in a later section.

A more serious problem, especially at intermediate temperatures, is encountered by the occurrence of hot corrosion. This type of attack manifests itself by a very rapid, and sometimes even catastrophic attack of the component. Uncorroded parent metal is often left behind the rapidly advancing corrosion front (figure 2).
A necessary condition for the occurrence of hot corrosion is the presence of molten sulphate, generally Na_2SO_4, on the surface. The salt may come from:

a) the intake air; Na_2SO_4 is present in seawater and hence in coastal areas is also present in the air

b) a reaction between Na- and S-compounds. Sulphur may be present in the fuel or in the intake air as SO_2 or SO_3. Na is sometimes present in the fuel but can also be ingested via the intake air (NaCl).

The formation of Na_2SO_4 is possible by e.g. the following reaction:

$$2NaCl + SO_2 + \tfrac{1}{2} O_2 + H_2O \rightarrow Na_2SO_4 + 2HCl$$

For normal gas turbine operating conditions the thermodynamic equilibrium of the reaction lies on the far right hand side. Therefore a nearly complete NaCl conversion may be expected if residence time is long enough. However, residence times are often very short (only milliseconds) and this may imply that this process of gas phase sulphation occurs only on a limited scale. Nevertheless, Na_2SO_4 deposits (whatever their origin) are often found on turbine blades.

Because molten sulphates are a prerequisite for hot corrosion the temperature region in which it occurs might be thought to be bordered on the lower side by the melting point of Na_2SO_4 (884 °C) and on the upper side by its dewpoint, which depends on the Na_2SO_4 partial pressure. Figure 3 [3] shows the relation between dewpoint, pressure and concentration of salt in the intake air. Note that seasalt concentration rather than the Na_2SO_4 partial pressure has been plotted along the horizontal scale. Seasalt contains about 12 % Na_2SO_4. The dark upper bands in the figure indicate (for both pressure conditions) the dewpoint when all NaCl has been converted to Na_2SO_4.
From the above considerations it could be concluded that hot corrosion will not occur below 884 °C, the melting point of Na_2SO_4. However, this melting point shifts downwards when other compounds dissolve into the melt: the eutectic melting point of a Na_2SO_4/NaCl mixture is 630 °C [4]. In presence of V_2O_5 this point shifts to even lower values: the Na_2SO_4/V_2O_5 eutectic point is at about 525 °C [5]. Seasalt itself has a melting point of 757 °C [2].

2.3 The effect of contaminants and use of thermodynamics

Several authors [2,6,7] at the meeting directed attention to the aspects of fuel and intake air contaminants. Restall [6] mentions that the permitted sulphur level in aero engine fuels is about 0.2 % (in general the mean S-level is about 0.05 % [8]); Vanadium content is probably less than 2 ppm and Na-content should be less than 1 ppm. A decrease in S-level might be considered: however, even very low levels, e.g. lower than 0.01 % S, may not prevent hot corrosion [9] especially in coastal or industrial environments. This is because intake air contaminants play a very serious role in hot corrosion. Condé [2] presented data on seasalt concentrations in the intake air, finding 0.1 ppm in a marine environment and even up to 0.01 ppm at 160 km inland. With figure 3 in mind this clearly shows that even without any fuel contaminants hot corrosion is likely to occur. Also, intake air leads to a third source of contaminants: salt deposits on compressor components. These deposits may periodically break off and enter the turbine section. It turns out, based on recent measurements [10], that these deposits often consist mainly of Na_2SO_4, and so they directly generate hot corrosion-prone conditions in the turbine without the sometimes disputed conversion of NaCl into Na_2SO_4.

The role of carbon, leading to carburisation and possibly the "green-rot" type of attack [6]; chloride, which effects the integrity of the oxide scale and the wetting properties of Na_2SO_4 deposits [2]; and vanadium, which strongly affects the corrosion rate ([2],[7] and [1], p. 265) were all discussed in the indicated references. Furthermore, attention was focussed on the importance of the local micro-environment at the gas/metal interface, instead of the overall environment [11] and also on the importance of the use of thermodynamic equilibrium diagrams [12]. Although these do not give an indication about reaction kinetics they enable at least the prediction of which chemical species are stable, metastable or unstable under certain environmental conditions (temperature, pressure, gas phase composition).

2.4 Factors affecting corrosion resistance

If current Ni-base gas turbine alloys are compared in terms of hot corrosion resistance a ranking order like that in table 1 is obtained [13]. There are ranking orders for other material combinations also [14,15,16]. They all have in common that the Cr-content is of prime importance. For oxidation protection the Al-content is more important because it forms, assisted by Cr, a stable, dense and adherent oxide scale. Under oxidising conditions, especially at high temperatures, the Cr_2O_3 scale is less suitable because it will further oxidise into CrO_3 and evaporate. However, the Cr_2O_3 oxide layer is still important because it provides the necessary conditions for the initial formations of the Al_2O_3-scale.
Several authors addressed in detail the factors which are important for the formation of a stable and protecting oxide scale and the factors which determine its characteristics: the kinetics of early oxidation, the effect of surface preparation on oxide scale behaviour, diffusion processes and the mechanical behaviour of oxide scales under stress (cycles). Thus, in general, basic research topics were discussed.
A new development which received attention [17] was the introduction of alloys which contain oxide dispersions of rare earth elements or additions of rare earth elements themselves. Figure 4 shows the drama-

tic effect of the addition of Sc and especially ThO_2 on the cyclic oxidation of Ni-20Cr alloys. This effect is caused by a much lower growth rate of the oxide scale on alloys with the rare earth type additions, by enhanced selective oxidation of chromium in the alloy and by an improved oxide adherence during thermal cycling.

3. DIRECTIONALLY SOLIDIFIED IN-SITU COMPOSITES (Specialists Meeting, Washington, April 1974 [18])

3.1 Introduction

The directionally solidified (DS) eutectic materials, also called DS in-situ composites, offer a very attractive approach towards still higher turbine temperatures in the aircraft engine. These materials consist of a matrix phase which is reinforced by platelets or fibres of a strengthening second phase. The material is created in-situ by directional solidification out of a eutectic melt. With regard to present superalloys the DS in-situ composites offer considerable advantages. The currently best Ni-base superalloys are limited in their useful operating temperature range because the γ' ($Ni_3(Ti,Al)$)-strengthening phase dissolves at very high operating temperatures. The DS in-situ composites are, because of their eutectic composition, stable up to the melting temperature. Other possible alternatives for the present superalloys, like refractory metals, W-fibre reinforced superalloys and ceramics still have so many drawbacks, especially in the areas of oxidation/corrosion resistance and ductility, that their prognoses for the near future are not as good as for the eutectics.

Most development work has been done on two families of eutectics: Pratt and Whitney concentrated on the Ni_3Nb reinforced lamellar eutectics, like γ'-δ (Ni_3Al-Ni_3Nb) and γ/γ'-δ (Ni/Ni_3Al-Ni_3Nb) whereas GE and ONERA developed the monocarbide (e.g. TaC or NbC) reinforced alloys. Figure 5 [19,20] shows the microstructure of two alloys belonging to the above families. Many data have been gathered on these systems, both with regard to mechanical properties as to processing parameters. Figure 6 [21] shows a comparison of tensile strength at different temperatures for a number of eutectic alloys and two of the best current superalloys. Even more interesting is the comparison of stress rupture properties, see figure 7 [21], clearly showing the gain in temperature capability (or stress capability) which might be obtained by using in-situ composites.
Apart from strength considerations, however, other properties should also be evaluated before application as a turbine blade material. Ductility, oxidation and corrosion resistance, impact strength and fabrication possibilities are also essential. In the following sections the most promising eutectic alloys will therefore be discussed in greater detail. Table 2 gives an overview of some of the properties of these alloys [21,22,23,24]. For comparative purposes two well-known superalloys are included.

3.2 Lamellar DS eutectics

The γ'-δ and γ/γ'-δ lamellar alloys can be classified as ductile-semiductile systems in which the ductile matrix, consisting of γ' (Ni_3Al) or γ/γ' (the normal Ni-superalloy matrix strengthened by γ' precipitates), is strengthened by the semiductile lamellar intermetallic delta phase Ni_3Nb. The γ'-δ alloy (figure 5a), with the composition Ni-23.1Nb-4.4Al, contains 44 v/o Ni_3Nb lamellae; a particular γ/γ'-δ alloy with the composition Ni-20Nb-6.0Cr-2.5Al contains about 37 v/o Ni_3Nb lamellae. The γ'-δ alloy has better tensile properties than γ/γ'-δ above 1000 °C (figure 6 [21]) and superior stress rupture characteristics over the entire temperature region, see figure 7 [21]. However, γ'-δ is highly anisotropic and it has considerably less strength in transverse directions than in the growth direction. For example, up to 800 °C the transverse strength is only one-third of the longitudinal strength. Under transverse bending the alloy is brittle at room temperature and ductile at 1093 °C [21]. Although the ductility of γ'-δ is very low the impact strength at room temperature is comparable to that of superalloys as MarM200. The γ/γ'-δ alloy has much better ductility than γ'-δ: 2-5 % at room temperature compared to less than 1 % for γ'-δ [22]. It has also a less marked tensile anisotropy. The impact strength at room temperature is comparable to that of MarM200. Furthermore the γ/γ'-δ offers more compositional flexibility than γ'-δ. This might result in future alloy improvements. Finally, the γ/γ'-δ alloy shows greater oxidation resistance than γ'-δ. This combination of properties makes the γ/γ'-δ alloy more attractive for turbine blade alloy application than γ'-δ, despite the former's lower stress rupture strength.

3.3 Fibrous DS eutectics

The carbide fibre reinforced DS eutectic alloys can be classified as ductile-brittle eutectic systems. These alloys are characterised by a great flexibility in alloy composition. The ductile matrix may be a Ni or Co-superalloy matrix which can be solid solution strengthened or, as in the case of a Ni-matrix, also precipitation strengthened by adding elements like Al. The reinforcing brittle fibres may consist of monocarbide MC fibres, with a volume fraction of up to about 16 %, or of M_7C_3-carbide fibres with a higher (30 v/o) fibre percentage.
The M-MC class of alloys mostly contain TaC fibres, although NbC fibres are also studied (Fig. 5b). The fibre diameter is about 1 micron. One of these alloys, Co-20Cr-10Ni-12.7Ta-0.75C has greater rupture strength than γ'-δ at high values of the Larson-Miller parameter (Fig. 7). Furthermore, the M-MC eutectics show good transverse strength in relation to the lamellar γ'-δ and γ/γ'-δ alloys. (They also show good ductility: a fracture strain at room temperature between 10 and 30 % [22,25] and good impact resistance.) The only moderate strength at lower temperatures may, however, impose a serious design limitation (Fig. 7). Of the M_7C_3-fibre reinforced alloys the alloy 73C has a chemical composition of Co-41Cr-2.4C. The reinforcing phase is faceted and more irregular in comparison with the MC-fibres. Because of its high volume fraction of fibres the M_7C_3-reinforced eutectic tends to be more anisotropic than the M-MC type of alloy; however, they are both less anisotropic than the lamellar γ'-δ and γ/γ'-δ alloys [21].

Another aspect which should be brought to attention is the large thermal expansion mismatch between the monocarbide fibres and the matrix phase. This might affect thermal fatigue behaviour, although some authors do no consider this to be a major problem [25]. However, cyclic temperature experiments have indicated that some fibre degradation occurred, especially when the maximum cycle temperature rises above 1100 °C [23], resulting in a lower stress rupture life. In contrast to the carbide reinforced fibrous eutectics the δ-reinforced lamellar eutectics seem to exhibit a much greater thermal cycling stability, which is explained to be the result of their physiochemical stability and the relatively low thermal expansion mismatch between the two phases [23].

3.4 Design and production

In the past decades it has been shown that if the maximum allowable blade metal temperature rises by e.g. 10 °C the turbine entry temperature may rise by 25 °C because the blade is air cooled. Therefore, to gain the full potential capabilities out of the DS eutectic alloys they should be necessarily applied in sophisticated, highly cooled blades [26]. This requires the development of methods to produce blades with a complex cooling configuration out of DS eutectics. Figure 8 shows various possibilities for blade production [27]. At present it has been shown that DS eutectic blades can indeed be produced by directional solidification in a precision investment casting mould. However, serious consideration should be given to contamination effects produced by the mould (especially valid for the very high melting M-MC alloys), the difficulty of producing planar front growth, especially in complex cooled blades, and the ability to achieve the desired structure in every location of the blade. In this respect it is important to recognise that the material properties may be manipulated by growth speed variations [21] and this will enable optimization of a specific structure in particular blade locations, e.g. a more cellular, ductile structure in the blade root and a strong, fully aligned structure in the airfoil. Also, blade fabrication by directional solidification of simple shapes and their subsequent assembly by e.g. brazing may be possible [27]. All these techniques should, however, be explored in more detail.

4. LOW CYCLE HIGH TEMPERATURE FATIGUE (LCHTF)

4.1 Introduction

The subject of LCHTF addresses itself to the explanation and prediction of material behaviour under conditions in which both creep and fatigue occur. The spring 1984 AGARD Specialists Meeting on Low Cycle High Temperature Fatigue [28] in Washington covered this subject, which is very important from the viewpoint of predicting component performance under real engine operating conditions. With regard to the title of the subject it is probably necessary first to define the term low cycle fatigue in relation to high cycle fatigue.
Low cycle fatigue (LCF) is often defined as the deterioration or cracking of metals in less than 50,000 cycles [29]. However, this limit is very arbitrary - values of 10^4 and 10^5 cycles have also been mentioned. A more rational approach has been proposed by Manson [30] who regards LCF "as implying that a high plastic strain exists over a microscopic region (say several grain diameters), while "high cycle" implies that the microscopic strain is elastic or involves very small plasticity". In practice this means that LCF plastic strains develop over a part of a cross-section of a component, e.g. at a notch, while-on the contrary - during HCF the strains are elastic apart from a very small region immediately ahead of a crack tip (or stress concentration).

4.2 Necessary steps for life calculation

Components in aircraft engines operate under a combination of complex loading and temperature cycling which makes it extremely difficult to predict a safe life, the prime intention of the designer. Calculation of a safe life is difficult especially because the fatigue and creep contributions to life may not be simply added up, even if it proved to be possible to distinguish between these simultaneously occurring effects anyhow. The different views on the LCHTF problem, from the designers standpoint and from the materials scientists side are very well expressed in the paper of Harrison and Cockcroft [31]. Some of the other views in this paper are also presented below.
The LCHTF problem can generally be approached from two sides. The first approach is that component life is calculated based on available low temperature fatigue life relations. Time and temperature effects are incorporated in those relations to account for operation at elevated temperature or to account for thermal cycling conditions. The other approach is based on available creep life equations which are adapted to take into account the effect of cyclic loading conditions. It may be expected that both methods work best in their original area. The fatigue approach lends itself most to fatigue dominated conditions: life is highly dependent on the number of cycles, and frequency or time effects are less dominant. In that case failure occurs mostly by crack initiation at the surface followed by transgranular crack propagation. The creep approach is most appropriate for creep dominated conditions: life is strongly dependent on time at temperature. The failure mode is characterized by intergranular void formation and crack nucleation.

Before the various life prediction methods are discussed an indication will be given of the methods to determine a real stress or strain history in a component [32]. First a thermokinetic study is performed to determine the temperature distribution in a component at any moment of the cycle. For this purpose heat transfer coefficients, the emissivity of the component surface, thermal conductivity and specific heat should be well known. It should be recognised that already during this calculation errors are inevitable due to e.g. small differences in cooling air flow. Subsequently a calculation is made of stresses and strains in the component owing to mechanical loading and temperature differences. For this calculation elastic behaviour is assumed; this means that the thermal expansion coefficient α, the Young's modulus E and the Poisson's ratio ν are assumed to totally determine the material behaviour.

Plasticity effects, occurring at notches or geometric discontinuities where stresses may exceed the yield stress of the material, are then taken into account. The Neuber rule provides a means for the calculation of stresses and strains under these conditions if the cyclic stress-strain curve of the material is known:

Neuber: $K_t^2 = K_\sigma . K_\varepsilon$ with K_t = theoretical elastic stress concentration factor at notch.

$$K_\sigma = \frac{\sigma_{local}}{\sigma_{mean}} = \text{actual stress concentration factor}$$

$$K_\varepsilon = \frac{\varepsilon_{local}}{\varepsilon_{mean}} = \text{actual strain concentration factor.}$$

Rewriting the above equation and substituting ε_{mean} by $\frac{\sigma_{mean}}{E}$ gives:

$$\frac{K_t^2 . \sigma_{mean}^2}{E} = \sigma_{local} . \varepsilon_{local}$$

The two unknown right hand terms in this equation are related by the cyclic stress-strain curve of the material.
Using the above simplified approach it is thus possible to calculate the stress and strain history for any location of the component, provided that no temperature or time dependent effects induce stress or strain relaxation. A life prediction should now be made based on the stress and strain history and also the accompanying temperature history, i.e. creep effects (if any) are introduced in the life prediction model.

4.3 Life prediction methods

The papers by Harrison and Cockcroft [31], Brunetaud and Thiery [32], Manson [33] and McEvily and Crosby [34] all contained reviews of life prediction methods for conditions where creep/fatigue interactions occur. Recently Halford [35] published a review of life prediction methods developed at NASA. This review is also extremely useful for those who wish to know the present status of this subject. In the following the various methods are briefly reviewed.

Extension of low temperature fatigue life relations

The first life prediction method in the area of low temperature low cycle fatigue was introduced in the early 1950's and became known as the Manson-Coffin Law. It relates inelastic strain range to number of cycles to failure:

$$\Delta\varepsilon_{in} = C . N_f^{-0.5} \qquad (1)$$

In this equation C is a constant which is directly related to the tensile ductility of the material. In fact this equation may be regarded as a life relation valid for the low cycle fatigue governed part of the total fatigue curve. A general equation for the total fatigue curve has been proposed by Manson [36], the so called Method of Universal Slopes:

$$\Delta\varepsilon_t = \Delta\varepsilon_p + \Delta\varepsilon_e = D^{0.6} . N_f^{-0.6} + \frac{3.5\ \sigma_u}{E} . N_f^{-0.12} \qquad (2)$$

in which $\Delta\varepsilon_t$ = total strain range
$\Delta\varepsilon_p$ = plastic strain range
$\Delta\varepsilon_e$ = elastic strain range
D = measure of fatigue ductility = $\ln \frac{100}{100-RA}$
RA = reduction in area in a tensile test
N_f = number of cycles to failure
σ_u = ultimate tensile strength
E = Young's modulus

The method is illustrated in figure 9 which also shows the original Manson-Coffin law for low cycle fatigue (equation (1)). In comparing the two equations it is clear that the slope of the plastic line differs: -0.5 in the Manson-Coffin law and -0.6 for the Universal Slope Method. However, Manson [36] explained that there was no basic conflict because the -0.5 line was mostly based on the life necessary to generate a certain crack whereas the -0.6 line regarded final fracture as the fatigue life.
The universal slopes equation has been shown to be valid for a wide range of materials: only in extreme cases does the predicted value differ from the actual value by a factor of 10 [35,36]. The ease of the method is that to predict life only the tensile strength, ductility and Young's modulus of the material is needed.
It has been tried to modify the universal slopes equation to extend its use also for elevated temperatures. A "10 percent rule" was proposed by Manson and Halford [37]. This states that the number of cycles predicted by the universal slopes equation (calculated for the actual temperature) should be reduced by a factor of 10 to account for oxidation and creep effects. Although this rule has shown to be effective over a range of temperatures, it overestimated life especially at very high temperatures and also at low frequency or when hold time effects were considered. A modification to the 10 percent rule, to account for these effects, was proposed by Manson. Based on creep rupture curve slopes Harrison and Cockcroft [31] simplified Manson's modification to

$$N_f' = \frac{N_f}{1 + \frac{K}{FA}} \qquad (3)$$

where N_f' = revised number of cycles in relation to 10 percent rule
K = fraction of cycle time at peak load

F = frequency
A = time to rupture on a stress rupture curve.

Harrison and Cockcroft stated that the same result could have been obtained by applying the 10 percent rule to a somewhat modified universal slopes equation: changing of the exponent of the elastic part of this equation from -0.12 to -0.24 would suffice.

Coffin extended the low temperature Manson-Coffin relation, eq. (1), into an elevated temperature form by introducing a frequency term. The addition of the elastic component, which is also frequency dependent, resulted in the following Coffin's frequency modified fatigue relation [38] (Note: the original literature [38] contained printing errors which subsequently resulted in errors in the derived literature [31,33]; the following equations (4) and (5) are the corrected ones):

$$\Delta\varepsilon_t = \Delta\varepsilon_p + \Delta\varepsilon_e = C_2(N_f.\nu^{k-1})^{-\beta} + \frac{AC_2^n}{E}.N_f^{-\beta n}.\nu^{k_1'} \qquad (4)$$

where ν = frequency
β = slope of plastic curve, no hold time
n = cyclic strain hardening exponent
C_2 = constant in Manson-Coffin law (eq. 1)
A,k,k_i,k_1' = material constants; $k_1' = -\beta n(k-1) + k_1$

It is easy to see that this equation transforms into the universal slopes equation if the frequency effects are eliminated ($k = 1$, $k_1' = 0$ ($\Leftrightarrow k_1 = 0$)), $C_2 = D^{0.6}$, $\beta = 0.6$, $A = 3.5\,\sigma_u/D^{0.12}$ and $n = 0.2$.
The elastic and plastic terms in the Coffin relation are represented by straight lines if plotted in a double logarithmic $\Delta\varepsilon$ - N_f figure. The frequency effect causes a parallel shift of the curves. Manson [33] covered this subject broadly by reviewing a lot of literature showing also a rotational effect of the strain versus life curves at different frequencies or hold times. This would imply that the frequency term in the Coffin relation, apart from being just a multiplier, should also be introduced into the exponent of the life relation. However, for these modifications we refer to the paper of Manson [33]. Results of the Coffin approach are shown in figure 10 [39].
Coffin's frequency modified relation provides the opportunity to relate N_t, the transition fatigue life, to the applied frequency. The transition fatigue life is the life at the intersection of the plastic and elastic lines in the fatigue life relation (see e.g. figure 9b). In the Coffin approach N_t is given by (by equating the elastic and plastic terms in equation (4)):

$$N_t = \left\{\frac{AC_2^{n-1}}{E}\right\}^{1/\beta(n-1)} .\nu^{k_1'-\beta(1-k)/\beta(n-1)} \qquad (5)$$

Coffin [38] emphasizes strongly the value of N_t. It determines the method of testing and the analytical procedures to be used for the handling of the problem. If the design life $N_d \gg N_t$, then high cycle fatigue information is most meaningful, mean and residual stresses have a great effect on life and linear elastic stress analysis and fracture mechanics should be applied. If $N_d \lesssim N_t$ then low cycle fatigue data are required, mean stresses will relax during cycling and elastoplastic solutions are required for design.

An interesting aspect is that the Coffin relation (eq. (4)) can also be written in a "creep" form (see [31]) by replacing N_f/ν by the time to failure t_f:

$$\Delta\varepsilon_t = C_2.t_f^{-\beta}.\nu^{-k\beta} + \frac{AC_2^n}{E}.t_f^{-\beta n}.\nu^{k_1'-\beta n} \qquad (6)$$

For hold-time testing the frequency can be replaced by the inverse of the hold time τ:

$$\Delta\varepsilon_t = C_2.t_f^{-\beta}.\tau^{k\beta} + \frac{AC_2^n}{E}.t_f^{-\beta n}.\tau^{\beta n-k_1'} \qquad (7)$$

As above, the constants k and k_1' determine whether frequency effects are important. If $k = 1$ and $k_1' = 0$, at low temperatures, then eq. (7) transforms into the universal slopes equation (2): material behaviour is then only cycle dependent. At the other end of the scale, substituting $k = 0$ and $k_1' = \beta n$ the equation (7) becomes only time dependent. The conditions are now creep dominated. Only in between these values is the material behaviour frequency dependent. This type of behaviour is illustrated in figure 11, showing results of Conway et al. [40].
A list of the above mentioned coefficients, calculated from test data, was prepared by Coffin for a number of materials, see table 3 [38]. The frequency modified relationship may be quite useful, especially under those conditions which resemble the conditions for which the constants were calculated. However, a lot of input data is required: for each temperature at least 6 coefficients should be determined.

Linear damage summation

Linear damage summation, also called time and cycle fraction summation, is another well known method of life prediction. This method, first proposed by Taira [41], combines Miner's fatigue damage rule and Robinson's creep damage rule to

$$\sum_{j=1}^{p} \frac{n_j}{N_j} + \sum_{k=1}^{q} \frac{t_k}{T_k} \leq D \qquad (8)$$

where n_j = number of cycles at load level j; p = number of load levels
N_j = number of cycles to failure at load level j
t_k = time duration at load level k
T_k = creep rupture time at load level k
D = total damage factor

In this approach it is assumed that the damage fraction occurring in fatigue (the cycle fraction) and the damage fraction occurring in creep (time fraction) may be simply added up; in this case the value of D would be 1 (fig. 12 [35]). Although the relation has been successful there are also serious limitations; in particular different loading conditons are not well predicted. Furthermore there are limitations with respect to compressive loading [42] and hold time effects [43]. The effect of different loading conditions is illustrated in figure 13 [44]. This figure shows the stress rupture curve of the virgin material (continuous line) whereas the dotted lines represent the stress rupture curves (also called constant damage lines) for specimens which have been previously exposed to a certain fraction (points 1 and 2) of the creep life. If the time fraction rule applied then all lines would be parallel. However, if the stress is increased then a lower life is found (points 1A and 2A) than predicted on the basis of the life fraction rule. The opposite effect occurs when the stress is decreased. No such behaviour is observed when, instead of the stress, the temperature is changed. In the latter case the life fraction rule remains valid.

Ductility exhaustion model

Polhemus [45] developed a model in which the total initial available ductility is gradually exhausted due to the accumulated damage contributions of cycling and creep. In this model the damage occurring in every cycle is converted into an equivalent creep time. This equivalent creep time is added to the actual creep time in the cycle. The procedure in fact calculates at any cycle the position along the static creep curve. The stepwise progression is followed until failure occurs, which is the case when the remaining ductility is zero, thus when the total strain equals the fracture strain of the creep rupture curve.

Before we go over to the last life prediction model to be reviewed in this paper: the strain range partitioning method, some additional remarks will be made about the 1974 LCHTF AGARD conference. In the above life prediction methods no clear distinction has been made between crack initiation and propagation. Only the total fatigue life (defined as the life to complete failure (Manson) or the life to an "engineering" size crack in the case of Coffin) was predicted. Well's paper [46] addressed the subject of crack initiation and propagation from the materials side: failure modes, processing quality, residual stress effects etc. Manson [33] showed some equations for crack growth which may also be used in the high temperature regime. Also in this case relations are often based on low temperature relations, e.g. the Paris law: $\frac{da}{dN} = C.(\Delta K)^n$, which have been modified for use at elevated temperatures. Another crack growth life prediction method is a variant of the strain range partitioning method. However, for all these methods we refer to the literature [33].
Lastly, short mention is made of the paper by Krempl [47] which addressed the problem of multiaxial fatigue failure criteria, and the paper by Smith [48] which was actually a review paper on the precision of LCHTF testing methods. Constitutive testing and component testing, as extremes of the total test spectrum, were described including the test variables which should be known and controlled for making valuable test results.

The strain range partitioning (SRP) method

The SRP method - introduction

The strain range partitioning approach as a means for life prediction was broadly discussed during the 1974 Specialists Meeting on LCHTF. As a result of that meeting Mr. Hirschberg of NASA suggested a cooperative testing programme to evaluate the ability of the SRP method to predict life. Several laboratories participated in the programme and its final results were presented at the 1978 AGARD Specialists Meeting on Characterization of Low High Temperature Fatigue by the Strain Range Partitioning Method [49]. In the first instance the background and basic concept of the SRP method will be presented and then we will discuss the ability of the method to predict life, as was done during the 1978 meeting. The SRP method of life prediction was first proposed in 1972 by Manson, Halford and Hirschberg [50] as a result of their efforts to improve the linear damage summation (time and cycle fraction) model. In doing so their attempts finally resulted in the basically new SRP method. The SRP model is in essence based on the assumption that there are two forms of inelastic strain: plasticity and creep. Creep is the thermally activated, diffusion controlled and time dependent component, whereas plasticity is the time independent component (the immediately occurring plastic strain only as the result of the application of a load). Because in a simple cycle inelastic deformation can take place in either the tensile part or the compressive part of the cycle we arrive at a maximum of four strain components: plasticity in tension, plasticity in compression, creep in tension and creep in compression. By combining these 4 basic strain components the following inelastic strain range components are created: $\Delta\varepsilon_{pp}$, $\Delta\varepsilon_{pc}$, $\Delta\varepsilon_{cp}$ and $\Delta\varepsilon_{cc}$. The two components denote the types of strain in tension and compression respectively, so $\Delta\varepsilon_{pc}$ depicts a strain cycle in which during the tensile part only plasticity occurs and in compression only creep. The four generic types of strain ranges are shown in figure 14. Only three of these; $\Delta\varepsilon_{pp}$, $\Delta\varepsilon_{cc}$ and one of the mixed strain ranges $\Delta\varepsilon_{pc}$ or $\Delta\varepsilon_{cp}$ can, by definition, occur simultaneously in one cycle. $\Delta\varepsilon_{cp}$ and $\Delta\varepsilon_{pc}$ cannot coexist, otherwise a further splitting up into $\Delta\varepsilon_{pp}$, $\Delta\varepsilon_{cc}$ and either $\Delta\varepsilon_{pc}$ or $\Delta\varepsilon_{cp}$ would be possible.
A visualisation of what might actually happen in a component during the completion of a cycle is shown schematically in figure 15 [51] for component $\Delta\varepsilon_{cp}$. During the tensile part of the cycle creep processes

like grain boundary sliding and void formation in the grain boundaries occur. The load is assumed to be too low to activate the slip plane EF. During the compression part of the cycle, when the net external strain is returned to the initial value, rapid loading is assumed (no creep effect). Therefore high stresses develop, the slip plane EF is activated and slipping occurs along that and other parallel crystallographic planes. Although the outer dimensions are the same, internal damage has been introduced. During continuous cycling an accumulation of damage occurs until the material is not capable any more to accommodate more strain and a crack develops.

The SRP method - application

The SRP method now says that any complex loading cycle can be split up into one or more of the 4 generic components. This is visualised in figure 16, showing a strain cycle with rapid tensile loading, followed by a load hold and subsequently a rapid compressive loading and a load hold in compression until the cycle is closed. By analysing this cycle it turns out that $\Delta\varepsilon_{pp}$ = BD, $\Delta\varepsilon_{cc}$ = CD and $\Delta\varepsilon_{pc}$ = AB-CD. If the life relationships of the 4 basic components are known, and these should be established by appropriate tests, then a simple linear damage rule can be applied for the calculation of the complex cyclic loading life. The life relationships of the 4 basic strain range components can indeed be determined, see figure 17 [42]. It turns out that the PP curve is usually the highest and the CP curve is usually the lowest. This allows upper and lower bounds of life easily to be established without the need for partitioning a complex cycle, and this may be sufficient for a specific purpose.
Another important aspect of the life relationships shown in figure 17 is that they are reasonably independent of temperature. The relationships are valid between 540 °C and 870 °C [52]. A particular strain range applied at different temperatures results in the same life. However, this need not be true in general: if the creep or plastic ductility of a material is sensitive to temperature or time of application then no temperature or time independence may be expected.

If the individual life relationships of the generic strain range components are known then a simple linear damage rule would apply:

$$\frac{1}{N_{pp}} + \frac{1}{N_{cc}} + \frac{1}{N_{pc}} + \frac{1}{N_{cp}} = \frac{1}{N_f}$$

where N_{pp} = the number of cycles to failure if only $\Delta\varepsilon_{pp}$ is applied, etc.

However, an "interaction damage rule" has been found more easy to use:

$$\frac{F_{pp}}{N_{pp}} + \frac{F_{cc}}{N_{cc}} + \frac{F_{pc}}{N_{pc}} + \frac{F_{cp}}{N_{cp}} = \frac{1}{N_f}$$

in which $F_{pp} = \dfrac{\Delta\varepsilon_{pp}}{\Delta\varepsilon_{in,total}}$, etc.

and N_{pp} = the number of cycles to failure if the total $\Delta\varepsilon_{in}$ is assumed to be $\Delta\varepsilon_{pp}$.
Both methods are illustrated in figure 18 [42]; they differ from each other in the sense that for the second method the life N for a particular type of strain range should have to be known only for the entire inelastic strain range involved. E.g. in the case of figure 18 N_{pp} and N_{cc} have only to be known for $\Delta\varepsilon_{in}$ = 0.01. This prevents the necessity of accurately establishing the life relations at very low strain ranges; e.g. for point B as was necessary in the case of the linear damage rule.

The SRP method - procedure for partitioning

The procedure of partitioning a strain range is for a simple case illustrated in figure 19 [42]. In this case a symmetrical loading pattern (a constant strain rate both in tension and in compression) was applied at different frequencies. The total inelastic strain range was held constant at 0.47 %. Because of the symmetrical loading only $\Delta\varepsilon_{pp}$ and $\Delta\varepsilon_{cc}$ are present. The wide hysteresis loops shown in figure 19 are the continuous cycling loops containing both $\Delta\varepsilon_{pp}$ and $\Delta\varepsilon_{cc}$. To obtain only the plasticity strain range $\Delta\varepsilon_{pp}$ rapid loading should be performed between the maximum load reversal values; this results in the thinner loops shown in the same figure. The creep strain range $\Delta\varepsilon_{cc}$ is obtained by subtracting the plasticity loop from the outer, total inelastic strain range loop.
For the test conditions shown in the figure the life was computed with the aid of the above mentioned linear damage rule and the interaction damage rule. There is no great difference in the prediction capability of the two rules, and it is still uncertain which of the rules give better results [42]. Again, this figure shows the frequency independence of life at very low and very high frequencies.
For more complex asymmetrical loading the strain range can also be partitioned. We therefore refer to Manson et al. [52].
Before the as above determined strain range fractions can be applied for life calculation the basic strain range life values (fig. 17) have to be generated. This can be done in appropriate tests, using rapid loading patterns, so excluding creep effects, and on the other hand using e.g. long hold times at constant stress, to exclude plasticity.

In the AGARD cooperative testing programme to evaluate the SRP method each laboratory carried out the above mentioned tests to generate the baseline strain range/life relations. It turns out that fatigue tests in which the total inelastic strain range consists of $\Delta\varepsilon_{pp}$ are easily performed by selection of a high strain rate. However, all the other tests, designed to give primarily a cp-, pc- or cc-type of loading still contained a pp component. This means that before the three other individual relationships can be drawn the interaction damage rule should be applied in the reverse manner.

The SRP method - predictive capability

Verification tests with more complex loading were performed to check how well the established SRP life re-

lationships could be used to predict cyclic lives [53]. In this paper we will not go into further detail with respect to all individual findings and applications of the SRP method. We refer therefore to the available proceedings [49]. However, it may be stated that the SRP method had in general a reasonably good predictive capability (within a factor of 2) for specimen lives under more complex loading situations. Drawbacks were that in a number of cases the application of the SRP method resulted in negative life values for N_{cp}, N_{pc} and N_{cc} (see e.g. [54,55]). This is attributed to the effect of mean stresses which is not accounted for by the SRP method. The SRP method in its present form only accounts for the strain range and not for the mean (or maximum) tensile stress in the cycle.
Another question which arose during the Specialists Meeting was the ability of Ductility Normalised SRP relationships to predict life. This approach introduced by Halford, Hirschberg and Manson [56], involves the normalisation of the strain range by dividing by the ductility D. The $\Delta\varepsilon_{pp}$ and $\Delta\varepsilon_{pc}$ strain ranges are divided by the plastic ductility as measured in a tensile test, whereas $\Delta\varepsilon_{cp}$ and $\Delta\varepsilon_{cc}$ are divided by the creep ductility, determined in a creep test both at the appropriate temperature and environmental conditions.
The resulting ratios, e.g. $\Delta\varepsilon_{pp}/D_p$ are then plotted against number of cycles. Halford et al. [57] showed that using this approach universalised equations for the four basic strain ranges could be formulated:

$$\Delta\varepsilon_{pp} = 0.50.D_p.N_{pp}^{-0.6}$$

$$\Delta\varepsilon_{pc} = 0.25.D_p.N_{pc}^{-0.6}$$

$$\Delta\varepsilon_{cp} = 0.20.D_c^{0.6}\,N_{cp}^{-0.6}$$

$$\delta r = 0.10\,D_c^{0.6}\,N_{cp}^{-0.6}$$

$$\Delta\varepsilon_{cc} = 0.25.D_c^{0.6}\,N_{cc}^{-0.6}$$

Knowledge of the ductility of the material under the appropriate conditions would then be enough to estimate the position of the four basic life relationships and this would be extremely useful, of course. However, there was at the meeting considerable reluctance to accept ductility as the overriding parameter in describing fatigue behaviour of a wide range of materials. This aspect, together with others mentioned above, therefore still requires more consideration.

5. POWDER METALLURGY

5.1 Introduction

The production of engine components (and also aircraft structural components) out of superalloy or titanium powders has received considerable attention in recent years. Powder Metallurgy (PM) offers considerable potential advantages: in large components a much better uniformity in properties can be obtained then by conventional forging of ingot material. Furthermore the technique also offers a considerable cost reduction potential because of (near) net shape forging by hot isostatic pressing (HIP) capabilities. AGARD therefore organised a Specialists Meeting on this subject in Ottawa in the Spring of 1976 [58]. During this meeting all aspects related to PM processing were handled: powder production, canning techniques, powder consolidation, secondary forging operations, heat treatment, non destructive inspection, mechanical properties and economics. In addition, during the 1978 AGARD Specialists Meeting on Advanced Fabrication Processes [59] PM metallurgy and near net shape powder production techniques again received considerable interest. A short review of both meetings on this subject will be presented below.

5.2 Powder production

High quality superalloy and titanium powders can be produced in several ways. Figure 20 ([58], pp. SC1-3 and SC6-1) shows two of those: the rotating electrode process (REP) and the vacuum atomisation process. In the REP-process an electric arc is struck between a non rotating W-cathode and a rotating, consumable electrode made of the alloy which should be atomised. By the centrifugal action the molten material flies off from the rotating anode forming very small droplets which solidify in the inert environment. In the vacuum atomisation process the molten master alloy, supersaturated with hydrogen gas, explodes into a vacuum tank forming very fine powder particles. Table 4 [60,61] gives an overview of the various production processes, some of their characteristics and the resulting powder properties.
Some processes, e.g. the REP and the CSC processes, make use of an inert environment, which increases cooling speed and so allows for smaller chamber dimensions (molten droplets should preferably be prevented from hitting the walls). The inert environment (e.g. He or A) is of course not capable of improving the quality of the starting material. The electron beam processes, which use vacuum as environment, offer the possibility of melt refining by the evaporation of interstitial elements; however, compositional variation also results and furthermore droplet cooling is only possible by radiation, which requires a long solidification path.
The rotating electrode process is most widely used for Ti-powder production. One of the drawbacks however, is the contamination of the powder with W-particles originating from the "non-consumable" W-cathode. This contamination may result in inferior fatigue properties (see later). Work is in progress to replace the W-cathode by a co-consumable Ti-cathode of the desired powder composition.
The Argon atomisation process is preferably used for the production of superalloy powders. One of the problems with this process is that argon is picked up and entrapped by the powder particles, especially the larger ones. This results in the development of internal pores after post-consolidation heat-treatments. Therefore the maximum particle size to be used is restricted to 180 μm. In that case still acceptable A-levels occur (< 2 ppm A) [60].
In general powder handling is considered of vital importance to prevent gaseous contamination (especially valid for small particle size powders) and foreign particle contamination. All handling (e.g. classification, storage, canning etc.) is therefore mostly done in vacuo or in an inert environment.

5.4 Powder consolidation

Before consolidation the powder is filled into (mostly) steel cans which are evacuated and outgassed before they are tightly welded. Consolidation may be carried out by several processes: extrusion, pressing and sintering, explosive impaction and hot isostatic pressing (HIP). HIP offers a variety of opportunities for powder consolidation: ranging from the simple production of billet stock, which can subsequently be processed by conventional forging methods, down to near net shape forging of the final component. This latter process is especially attractive because it avoids a number of forging and machining steps and leads to a considerable cost reduction. This is illustrated in figure 21 [62] showing a comparison between three production methods for engine discs: 1) conventional forging in various steps starting from ingot material, 2) HIP processing of powder to an intermediate preform or 3) HIP processing of powder directly to near net shape. For additional clarification figure 22 [63] shows the total powder processing route leading to a disc preform. The much more efficient material usage obtained by PM processing with respect to conventional forging is clearly illustrated in figure 21 and this may be an additional advantage for processing strategic materials.

5.4 Mechanical properties

As already mentioned, one of the main reasons for the introduction of the PM technology is that uniform properties can be obtained throughout large components. In the case of conventional production processes via ingot casting and subsequent forging operations it is nearly unavoidable that macro-segregation occurs resulting in microstructural changes and therefore property changes in different cross-sections. Defects as a result of inclusions, slag etc. are also difficultly to avoid. PM materials, because of their better controllable process steps, may thus offer substantial improvement over conventional processes. However, at present there are still many problems to overcome. For example: it turned out that the mechanical properties of Ti-powder alloys were about equivalent to those of their wrought counterparts, with the exception of fatigue properties. Vaughan et al. [64] showed that the LCF data on PM Ti-6Al-4V were inferior to the wrought product data and that there was considerable scatter also in the PM data. These observations are similar to results of Keinath [65] who showed that for the same alloy the notched as well as smooth specimen fatigue lives for HIP-processed material were lower then those for the normally forged alloy. Both studies indicate that W-inclusions (from the cathode in the REP process) are the cause of crack initiation. Eliminating these W-inclusions by a change in electrode material would very likely result in improvement in fatigue behaviour. The study of Vaughan et al. [64] also concluded that the amount of reduction during the HIP-route is considerably smaller than the work done in the conventional forging route. It was suggested that this would also contribute to the inferior fatigue behaviour of the PM material. Other papers [66,67] indicate that also for PM Ni-superalloys the amount of reduction is very important for the improvement of mechanical properties. This seems to be underlined by the papers of Allen [68] and Symonds and Thompson [69]. Allen described the production of F100 turbine discs with emphasis on the fact that the IN 100 superalloy powder is first consolidated by extrusion to a very fine grain size and is subsequently hot isothermally forged (superplastically forged) to the near net sonic shape used for non destructive inspection. Symonds and Thompson mention thermoplastic processing, the basis of which is that the powder is heavily cold-worked before compaction, as a means of simplifying subsequent HIP and forging operations and possibly improving the material properties. In general it may be stated that the combination of deformation operations and thermal treatments is of upmost importance for the production of the desired structures and therefore the desired material properties.

5.5 Other PM developments

Apart from the above mentioned items several other aspects of PM material were treated like e.g. weldability of PM Ti-6Al-4V [70], the production of airframe components from Ti [71], Co-base PM materials [72]and the production of a composite turbine blade made of PM MarM200 and reinforced W-fibres [73]. A most interesting new approach is the introduction of extremely high solidification rates during powder atomisation ($> 10^5$ K/s) by rapid quenching of a molten stream of fine particles in a high mass flow of He [74]. Especially at smaller particle sizes (~ 60 µm), where solidification rates approach 10^6 K/s, an almost complete homogeneity is obtained. After extrusion of the powders the structural uniformity is striking, leading for MarM200 to an incipient melting point increase of 90 K over the conventionally processed alloy. This means that the normal alloying boundaries can be expanded and new alloys may be developed. Indeed, new Ni-Al-Mo material compositions for turbine blade application were tested and, although only in a preliminary stage of development, these showed superior strength at temperature over the presently used directionally solidified superalloys. This strength increase, shown in figure 23 [74], may also be translated in a 110 K improvement in high temperature capability.

In summary the following advantages can be expected from the PM approach (see also [64]):

- Billet stock, preforms and final forgings may be produced free from defects, with a uniform and fine grain size and no compositional variation
- mechanical properties should be at least equal to those obtained by conventional forging
- considerable cost reduction should be possible because of fewer forging and machining steps
- a more efficient material usage due to near net shape forming techniques
- new alloys, with properties beyond those of convential ingot metallurgy alloys, can be developed.

6. ADVANCED FABRICATION PROCESSES

During the 1978 Advanced Fabrication Processes Meeting [59] aspects other than PM metallurgy were also handled. An interesting paper was presented on net shape processing of non-oxide ceramics [75]; however this subject will be discussed in more detail in the next section. Some papers presented overviews of the effect of cutting and grinding parameters on tool life and residual stresses: others described present automatic milling and 5-axis automatic drilling equipment.

Various surface treatment processes e.g. to improve corrosion and wear resistance were presented. Advanced coating deposition techniques are ion vapour deposition [76], sputter ion plating [77] and ion implantation [77]. The first two processes involve deposition of a partly ionised source (coating) material on a substrate (which acts as a cathode), assisted by inert gas ion-bombardment for densification. The described processes differ with respect to evaporation of the source material: in the case of ion vapour deposition the source material (e.g. Al) is evaporated by resistance heating, whereas in sputter ion plating the source material is "sputtered off" (by ion bombardment) from a second cathode consisting of the coating material. The third process, ion implantation, involves the bombardment of a component surface with very high energy ions of the element to be implanted. These ions penetrate the upper substrate layer (to about 1 µm) to give a higher surface content of the particular element.
The deposition of Al by ion vapour deposition on fasteners and engine components made out of steel may prevent serious drawbacks of cadmium-electroplating like hydrogen embrittlement and ecological side effects because of the toxicity of Cd [76].
Sputter ion plating of TiC and TiN has been applied to produce very hard coatings for wear and erosion resistance. MCrAlY coatings may be deposited by this method for improved high temperature corrosion resistance.
C- or N-ion implantation provides much better wear characteristics of cutting tools and extrusion dies. Furthermore ion implantation of Al, Cr, and Y may offer better high temperature corrosion behaviour [77].
Wear resistant surfaces can also be created by plasma spraying of a layer consisting of a dispersion of carbides in a metal matrix, e.g. WC in a Co-matrix [78].

An interesting new approach is the use of lasers: they may e.g. be used to modify a surface structure by heat treatment or to change the surface composition and structure by treatment of previously applied coatings [79]. They are also suitable for all sort of metal working, such as deep penetration welding, hole drilling and cutting operations [80].

Finally, superplastic forming and diffusion bonding may also be considered as advanced production processes. Two papers were presented on these subjects [81,82] both showing the capabilities of these methods with respect to production of complex Ti-components. The first process is based on the finding that several Ti-alloys exhibit superplastic behaviour at temperatures around 950 °C, see figure 24 [81] in which the process is schematically illustrated. At the same temperature and under pressure (e.g. 2 hours at about 15 bar) atomic diffusion occurs between two adjacent Ti-interfaces and a strong bond nearly equal to the parent metal strength is obtained. The combination of superplastic forming and diffusion bonding allows the production of fairly complex parts, see figure 25 [81]. Although mainly aircraft structural parts have been made until now, it seems likely that also engine components (e.g. hollow fan blades [83]), engine casings or the engine support structure can be fabricated in this way.

7. CERAMICS

7.1 Introduction

The demand for higher turbine entry temperatures and lower material costs has strongly stimulated the development of ceramics for turbine engine applications. This was the reason why AGARD organised in 1979 a Specialists Meeting on Ceramics for Turbine Engine Applications [84]. The papers presented at this meeting can be roughly categorized into three areas: (1) requirements and criteria for application of ceramics in gas turbines, (2) fabrication aspects and properties of ceramics, and (3) actual ceramic component development and evaluation.
The most attractive properties of ceramics are their high temperature capability with respect to both stress and environmental resistance, their low cost manufacturing potential and the superabundance availability of raw materials. On the other hand, ceramics also show serious drawbacks: their inherent brittleness makes them vulnerable to thermal and mechanical shocks; material yielding in order to smooth out stress concentrations is not possible, and there are great problems with mechanical interface matching. In the following a short overview is presented of the above mentioned aspects dealt with during the meeting.

7.2 Classification, fabrication and properties

Ceramics may be defined as inorganic, non-metallic materials which are first processed to shape at about room temperature and which obtain their final characteristics by a heat treatment which is normally carried out above 800 °C. Ceramics can be classified into various families of which the silicon nitride based family and the silicon carbide based family are considered as the most likely potential candidates for gas turbine engine application (see also [85-89]):

Silicon nitride based ceramics

The silicon nitride family consists of:

hot pressed silicon nitride	(HPSN)
reaction bonded silicon nitride	(RBSN)
sintered silicon nitride	(SSN)
β' SiALON's	(SiMON)
Chemically vapour deposited silicon nitride	(CVD-SN)

Hot pressed silicon nitride (HPSN) is produced by normal, uniaxial pressing or by hot isostatic pressing. Starting material is an α-Si_3N_4 powder and a densification aid, like e.g. MgO, Y_2O_3, ZrO_2 and CeO, which acts as a lubricant (a liquid-forming oxide) during compaction. Strength depends on the quality of the starting powder and phase composition, pre-processing (milling, mixing) and hot pressing parameters like time and temperature (normally about 1700 °C). In general, however, HPSN shows with respect to other types of ceramics, superior strength at intermediate temperatures (up to 1000 °C), high K_{Ic}, good thermal shock resistance and excellent erosion resistance. HPSN is normally produced in simple preforms. Because of the

high machining costs for the production of complex components out of billet material research has been initiated in the area of near net shape hot pressing of Si_3N_4. Examples of HPSN materials are NC-132, HS 130 and NCX-94.

Reaction bonded silicon nitride (RBSN) is produced by nitridation of a Si-metal preform. The preform is e.g. made by slip casting, flame spraying, injection moulding or green pressing of silicon powder. Nitridation in a N_2 or $N_2 + H_2$ atmosphere at about 1350 °C by the reaction $3Si + 2N_2 \rightarrow Si_3N_4$ results in a material which maintains its strength to beyond 1400 °C. A 23 % volume increase occurs during the nitridation process. However, the dimensions of the mould remain practically unchanged (~ 0.1 %) because the pores in the Si-preform will be filled up. This provides the possibility of production of accurately sized components without extra machining steps. The creep rate of RBSN is significantly lower than that for HPSN; however because of the inherent porosity of RBSN (more than 10 %) it is less oxidation resistant and less strong than HPSN at intermediate temperatures. Well known materials in this class are NC-350, FORD RBSN and KBI-RBSN.

Sintered silicon nitride (SSN) is a more recently developed material in which by the addition of suitable additives (MgO, Y_2O_3) and use of very high temperatures (~ 1600-1800 °C) sintering may be achieved without the application of pressure (unlike HPSN). Densities of more than 95 % have been obtained. It has been shown that sintering of RBSN preforms can also be performed, resulting in lower shrinkage than obtained by sintering of powder preforms. An example is GTE sintered Si_3N_4 which contains 6 % Y_2O_3.

The SiAlON's are materials in which metal oxides form a solid solution in a distorted β-Si_3N_4 lattice, thus creating a β'-Si_3N_4 lattice. In fact the material is formed by a simultaneous replacement of Si and N by Al (or another metal) and O. Originally Al_2O_3 was used (hence the name SiAlON), however other oxide additions (MgO, BeO, Y_2O_3) are also effective. β'-SiAlON can be fabricated by hot pressing (to fully dense bodies) and by pressureless sintering to up to 98 % theoretical density. The low temperature strength of the SiAlON's is higher than the strength of sintered Si_3N_4 but considerably lower than the strength of HPSN. However, many SiAlON's show higher oxidation resistance than HPSN. Because the different phases in SiAlON's play a major role in controlling grain boundary behaviour (which strongly controls HPSN and SSN strength) future improvements in mechanical properties may be expected by better chemistry and phase composition control.

Silicon carbide based ceramics

The SiC-based ceramics include:

Hot pressed SiC	(HP-SiC)
Reaction sintered (bonded) SiC	(RS-SiC)
Sintered SiC	(S-SiC)
SiC/Si composites	(Sil/comp)
Chemically vapour deposited SiC	(CVD-SiC)

Hot pressed SiC. In general, processing is similar to that of HPSN. Mostly Al_2O_3 is used as a densification aid but only small amounts are necessary because of the much higher hot pressing temperature (above 2200 °C). HP-SiC is less strong than HPSN at low temperatures but it retains its strength to about 1400 °C.

Reaction sintered SiC. Although there are many variations in this process the first step is generally the formation of a plastic body consisting of SiC, graphite and plasticizer, which is subsequently formed to a green shape by e.g. pressing, extrusion, or injection moulding. The plasticizers are burned off or converted to a porous char. Then silicon is intruded into the green body via the gas phase or as molten Si forming SiC with the graphite or char, so that reaction bonding is obtained. RS-SiC is necessarily porous because of the passage of Si through the body. However, excess Si may be used to fill up the pores to create a more dense structure. In that case the maximum use temperature will not be higher than about 1400 °C, the melting point of Si. During processing the overall volume remains constant so that near net shape part production is possible.

Sintered silicon carbide (S-SiC) is a recent development. At about 2000 °C SiC can be pressureless sintered to near full density when extremely fine powder and small amounts of boron and carbon additives are used. Complex shapes can be made by slip casting, die pressing and extrusion. SiC is easier to machine then Si_3N_4; however it is far more brittle than Si_3N_4, and this makes it somewhat less attractive for engineering applications. Table 5 contains an overview of the mechanical and physical properties of the aforementioned types of ceramics.

Fabrication aspects

An important question in the production of ceramic parts is how closely the final dimensions can be achieved using a preform which still must undergo thermal treatments [85]. Shrinkage of up to 18 % during heat treatment might occur for sintered products and this makes net shape processing very difficult. Of course machining to final dimensions may be performed, however, because of the high hardness of the ceramics, the costs of such production steps are excessive. Gugel [85] gave an overview of the various processes of shaping of ceramic components including an indication of time, complexity, accuracy and cost of tools of these methods. At low temperature dry pressing, injection moulding, warm moulding, extrusion and slip casting are the basic shaping methods, which are normally followed by a "burnout" (the removal of the organic binder) and a sintering step. At high temperatures hot pressing is nearly the only method of shaping ceramics. Very high temperatures are employed (1700 °C for Si_3N_4 and above 2100 °C for SiC) but the pressure is relatively low owing to limitations set by the strength of the graphite dies. Under these conditions the flow properties of the ceramic powder are only marginal, so complex parts cannot be produced in this way.

7.3 Requirements for ceramics for gas turbine applications

Figures 26 and 27 show the strength versus temperature relationships of the types of ceramics discussed above. The same figures also contain the design stress/temperature requirements for vanes, blades, combustors, shrouds and thermal barrier coating applications for a generic helicopter or limited life engine with a turbine inlet temperature of 1200-1370 °C [86,91].
In order to compare the 4-point modulus of rupture (MOR)-strength of the ceramics with the design stresses noted for the engine components (these are principle tensile stresses) the tensile strength is (conservatively) considered to be half of the MOR strength. Katz and Lenoe [86] show in their paper that nearly all materials (except one of the RBSN types) satisfy the basic strength requirement for vanes. However, HPSN is not suitable because of its inability to be near net shaped, thus use of HPSN will lead to very high machining costs. Furthermore SiC-ceramics containing free Si are also not acceptable because they cannot withstand occasional overtemperatures, if above the melting point of Si. A similar approach for selection of candidate rotor blade materials results in the conclusion that presently only HPSN or HP-SiC are suitable blade materials based on the strength requirements for the dovetail section. Of course machining of blades out of a hot pressed Si_3N_4- or SiC-preform will be very expensive although significant progress in cost reduction seems possible [92]. If the strength of some sintered Si_3N_4 and SiC materials could be further increased by about 25-50 % then these would be attractive alternatives.
Apart from short term strength requirements time dependent properties should also be considered. Creep and oxidation will further limit material suitability. Strength is seriously affected during high temperature exposure. Although not very many creep data exist, some have been incorporated in table 5 and figure 26. The data show the large reduction in strength of HPSN under creep exposure which makes it unattractive as a blade material. Nevertheless, ceramics offer considerable improvement in creep strength over superalloys (fig. 28 [91]). Oxidation behaviour may also limit the applicability of some ceramics. A 4000 hr life requirement for turbine vanes would e.g. rule out RBSN as a candidate material.

A most important aspect of ceramic materials, their inability to deform plastically and therefore to smooth out high local stresses, makes them very vulnerable to failure. Failure may occur due to the presence of all kinds of internal or external (surface) defects. Failure may also occur owing to unforgiving high design stress concentrations, imperfect surface fits (e.g. blades in a disc) or thermally induced stresses. In a proper design the latter problems may eventually be overcome: components can be geometrically designed such that thermal and mechanical stress concentrations are brought back to an acceptable level and the use of compliant layers at ceramic interfaces may help in the reduction of peak stresses. However, there still remains the probabilistic nature of the material failure mechanism which often results in an extreme strength variability. This is illustrated in figure 29 [93] showing the materials probability of failure as a function of surface stress. This probability is a function of e.g. the flaw distribution in a component and is therefore dependent on size. The slope of the line, given by the Weibull modulus m, determines the strength variability. The higher the Weibull modulus m the smaller the strength variability, hence resulting in a higher acceptable stress at a given probability of failure, e.g. 0.1 %. The combination of the failure probability curve for test specimens, which is only valid for the particular flaw distribution in the test specimens, the real flaw distribution in a component and the stress distribution in a component determine the probability of success for that component. Therefore knowledge of these characteristics is essential in the design of a ceramic component: this is a very difficult problem.

7.4 Actual ceramic component development

Many papers presented at the meeting [84] described the actual development and testing of engine components such as vanes, blades and combustors. It has been shown that these components can be fabricated out of ceramics and some were tested with reasonable success. In the framework of this paper it is impossible to deal with all the often very interesting aspects concerning component development and testing. However, some general comments will be made. For the rotor several concepts are possible:

- a metal disc/ceramic blading concept, see e.g. [92,93]. In this case HPSN blades were inserted in a superalloy metal disc using Pt-compliant layers between the blades and the disc, or the blades were attached to the disc by hot isothermal forging [92].
- a duo-density design concept, consisting of a HPSN rotor hub and an RBSN blade ring [94]. The rotor hub is simultaneously densified and diffusion bonded by hot pressing to the blade ring.
- an all HPSN-rotor, machined out of a HPSN billet [95].
- an innovative compression loaded rotor [96] consisting of an RBSN rotor blade ring surrounded by a cooled band of carbon fibre reinforced epoxy.

Developmental work was also performed on vanes or nozzle segments using HPSN and HP-SiC [97], or RBSN, SSN, RS-SiC and S-SiC [98]. The latter study impressively showed how component stresses can be reduced by several factors by design optimisation.

Because present NDI techniques seem not to be able to sort out and reject parts on the low end of the statistical strength distribution, proof tests are considered as vital classification tools for ceramic components. If the proof test stress level is chosen high enough than this will greatly decrease the statistical failure probability in service. Of course an economic balance should be made between the number of parts rejected by a proof test and the probability of a service failure.

In conclusion it may be stated that for future application of ceramics improved strength properties and especially long term stability are needed. To obtain reliable data for engine usage testing should be performed under realistic conditions. Furthermore new, improved processes for manufacturing of complex components are a necessity, as well as reliable techniques for part qualification. Another important aspect is the introduction and optimisation of brittle material design. Such new design approaches are really necessary for a reliable introduction of ceramics. The most likely future applications are to be sought firstly in the areas of automotive, truck and industrial gas turbines and in the area of unmanned aerospace vehicles.

8. MAINTENANCE AND REPAIR OF ENGINE COMPONENTS

8.1 Introduction

Modern maintenance of aircraft gas turbines is becoming extremely complex. It requires detailed knowledge of very different materials (Al, Ti, steels, superalloys), chemical processes for e.g. cleaning and plating, NDI procedures and their backgrounds (reliability, confidence), insight in service history, component tracking systems, life prediction methods and engine testing, as well as many other aspects. Furthermore it requires detailed knowledge about all sorts of repair processes. Some of the above mentioned aspects were addressed during the 1981 Specialists Meeting on "Maintenance in service of high temperature parts" [99].
In the first instance general maintenance procedures for military [100] and civil aero engines [101] were discussed. Present maintenance concepts are often a mixture of life on condition maintenance and a fixed life philosophy. During on condition maintenance a part is replaced depending on its physical condition, service history and risk potential with respect to aircraft integrity. In the fixed life philosophy the design prescribes a maximum service life (mostly indicated in cycles) which may not be exceeded and after which the component should be retired. The particular concept used in practice is often dependent upon the type of component or the particular engine type: a disc is normally a lifed component whereas a combustion liner is maintained on condition. The degree to which the on condition philosophy can be applied to e.g. rotating components depends on the type of service monitoring equipment which is available and hence on the accuracy with which the real component history can be deduced. This will be discussed later in this section.

8.2 Repair

Several papers dealt with the subject of life extension of components via the repair route. Weld repair of combustion chambers, ducting, seals, vanes and even blades (blade tips) is now common practice. Undersized components (because of wear) are again brought to design dimensions by welding or plasma spraying. A relatively new development is the application of repair brazing techniques such as "diffusion healing". This technique enables a homogeneous structure to be obtained and also that broad gaps and cracks with a width of approximately 1 mm can be repaired, which would not be possible by conventional brazing. The technique involves in its most simple form isothermal solidification of the braze joint and a subsequent diffusion heat treatment for homogenisation, see figure 30 [102]. For bridging broad gaps the technique is adapted by the addition of superalloy powder to the low melting point braze filler metal. These techniques have clear advantages over other repair techniques like welding because no thermal gradients and hence thermal stresses develop in the component, thereby preventing the occurrence of weld-induced cracking.
Rejuvenation of turbine parts by hot isostatic pressing (HIP) was shown by some authors [103-106] to be a a major possibility for life extension. During the HIP-treatment service induced creep damage (e.g. voids or even internal cracks) may be healed (fig. 31 [105]) and additionally the heat treatment may regenerate the material microstructure and thus reverse microstructural degradation occurring in service. It was concluded [107], however, that the most important problem still is the selection of a suitable heat treatment cycle for each individual alloy, because temperature has a marked effect on the dissolution of the γ'-phase and other precipitates and on grain coarsening. Also the cooling rate at the end of the HIP-process itself or during reheat treatment cycles is a major factor. A more fundamental knowledge of the combined effect of heat and pressure seems to be necessary to gain the full potential from this very promising technology.
The application of coatings will also result in considerable life extension of turbine components. Hauser et al. [108] presented results on the effect of coatings on the mechanical properties of superalloys. Furthermore some comparative data were presented on coating performance on Ni-base superalloys with respect to hot corrosion, LCF and HCF and stress rupture [109].

8.3 Disc lifing concepts

One of the most interesting and basically new areas in aero engine maintenance is the introduction of damage tolerance (= retirement for cause = life on condition) concepts for critical rotating parts like discs. Present lifing methods are still based on the so-called safe-life approach. The LCF life, after which a disc is retired from service, is in that approach defined as the life after which a 1/32 inch surface crack has developed with a statistical probability of 1 in every 1000 discs. In practice this means that 999 out of every 1000 discs are rejected although considerable service life may still be left. This is clearly shown in the paper of Harris et al. [110] in which remaining life times were calculated for these 999 discs after the LCF life was reached, see figure 32. When the damage tolerance approach is applied then only those discs are withdrawn from service which actually have a life limiting crack instead of the statistical probability of a crack, see figure 33. Such an approach of course offers from economic and material conservation considerations a considerable improvement over the present safe-life philosophy. However, there are some basic requirements before the damage tolerance lifing approach can be successfully incorporated:

1. The operational loading history of discs should be very well known.
2. Material crack growth data should be available for the appropriate loading conditions.
3. NDI or other techniques should be available which can reliably detect cracks down to a certain minimum size (sometimes as low as 0.1 mm!).

Jeal [111] also addressed this subject but more specifically emphasized the need for improved lifing procedures. Present discs are so highly loaded that even with current NDI standards undetectable defects can be malignant in some cases. Improved lifing procedures have been developed for various stages in the total life: crack nucleation, crack growth to grain size and large crack growth. Such an approach requires an enormous amount of information on initial defect size, type and orientation and on capabilities of NDI techniques for detection of such defects. Further it requires knowledge about behaviour of these defects in the very early, microstructure related stage of life. If adopted fully, such an approach should be able to lead also to the introduction of a damage tolerance concept for disc life extension.

An interesting aspect with respect to disc life extension, apart from the application of the damage tolerance approach, is the use of de-rated take off procedures by civil airlines [101]. Such de-rated take offs should result in a longer safe (LCF) life for discs. However, it did not become clear whether such life extension methods are already implemented and supported by the engine manufacturers and approved by the aviation authorities.

9. CONCLUSIONS

In overviewing the 1972-1982 period it may be concluded that aspects related with life prediction and life extension of gas turbine engine components received most attention in the AGARD Structures and Materials Panel activities. The various life prediction methods when dealing with low cycle fatigue were reviewed. A most interesting new development is the introduction of damage tolerance lifing concepts for engine parts. This is a considerable step forward with respect to the conventional safe-life philosophy. Attractive other areas also got serious attention. Powder metallurgy and hot isostatic pressing have been introduced and will further be developed to gain their full potential benefits for material quality improvements and reduction of materials processing costs.

10. REFERENCES

1. Stringer, J., Jaffee. R.I., Kearns, T.F. (editors), High temperature corrosion of aerospace alloys, Proceedings of the Specialists Meeting held in Lyngby, Denmark, 1972; AGARD CP-120, 1973.
2. Condé, J.F.G., What are the separate and interacting roles of sulphur, sodium and chloride in hot corrosion, in: AGARD CP-120 [1], pp. 203-219.
3. Bessen, J.J., Fryxell, R.E., Proceedings of the Gas Turbine Materials Conference; Naval Ship Engineering Center, Washington D.C., 1972, pp. 73-84.
4. Stringer, J., High temperature corrosion of aerospace alloys, AGARD AG-200 (1972), p. 26.
5. Hancock, P., The use of laboratory and rig tests to simulate gas turbine corrosion problems, Corrosion Science, 22, 1982, pp. 51-65.
6. Restall, J.E., The environment encountered by high temperature components of the aircraft gas turbine, in: AGARD CP-120 [1], pp. 11-29.
7. Williams, K.J., Parry, P.J., Can fuel ash corrosion by vanadium be combatted by alloying or coating without the use of fuel additives? in: AGARD CP-120 [1], pp. 255-264.
8. Friedman, R., Recent trends in aviation turbine fuel properties, NASA TP-2056, 1982.
9. Beltram, A.M., Shores, D.A., Hot corrosion, in: The Superalloys, ed. C.T. Sims and W.C. Hagel, John Wiley & Sons, (1972), pp. 317-339.
10. Kolkman, H.J., Mom, A.J.A., Corrosion and corrosion control in gas turbines, part I, The compressor section, in: Proceedings of the 29th Int. Gas Turbine Conference, Amsterdam, 1984.
11. Rosner, D.E., Environmental effects on gas/metal reactions at elevated temperatures, in: AGARD CP-120, [1], pp. 129-143.
12. Pourbaix, M., What are the advantages and limitations in the use of equilibrium thermodynamics for the treatment of complex high temperature corrosion reactions, in: AGARD CP-120 [1], pp. 63-76.
13. Mom, A.J.A., Kolkman, H.J., Corrosion and corrosion control in gas turbines, part II, The turbine section, in: Proceedings of the 29th Int. Gas Turbine Conference, Amsterdam, 1984.
14. Brunetaud, M., Matériaux couramment employés dans la pièces à haute température des turbines à gaz aéronautiques, in: AGARD CP-120 [1], pp. 31-42.
15. Wheatfall, W.L., Are cobalt-base alloys intrinsically more resistant to hot corrosion than alloys based on nickel, in: AGARD CP-120 [1], pp. 237-254.
16. Davin, A., Coutsouradis, D., What are the effects of alloying elements singly or in combination on hot corrosion, in: AGARD CP-120 [1], pp. 221-233.
17. Pettit, F.S., On the effect of oxide dispersions and rare earth type elements on the oxidation of Cr- and Al-containing alloys, in: AGARD CP-120 [1], pp. 155-170.
18. Thompson, E.R., Sahm, P.P., Directionally solidified in-situ composites, Proceedings of the Specialists Meeting held in Washington, April 1974; AGARD CP-156, 1974.
19. Thompson, E.R., George, F.D., Kraft, E.H., Investigation to develop a high strength eutectic alloy with controlled microstructure, Final Report UARL-J910868-4 East Hartford Conn., United Aircraft Corp., July 1970.
20. Bibring, H., Matériaux d'avenir pour turbines à haute température, in: AGARD CP-229, High temperature problems in gas turbine engines, 1978, paper 20, pp. 1-10.
21. Ashbrook, R.L., Directionally solidified composite systems under evaluation, in: AGARD CP-156 [18], pp. 93-111 .
22. Bibring, H., Perspectives des composites réfractaires élaborés par solidification unidirectionelle, in: AGARD CP-156 [18], pp. 141-155.
23. Gell, M., Thermal stability of directionally solidified composites, in: AGARD CP-156 [18], pp. 117-124.
24. Lawley, A., The mechanical metallurgy of directionally solidified composites. Strengthening fundamentals, tensile, creep, fatigue and toughness properties, in: AGARD CP-156 [18], pp. 21-33.
25. Jahnke, L.P., Bruch, C.A., Requirements for and characteristics demanded of high temperature gas turbine components, in: AGARD CP-156 [18], pp. 3-12.
26. Cockcroft, M.G., Crowley, P.H., Component design with directionally solidified composites, in: AGARD CP-156 [18], pp. 157-161.
27. Alexander, J.A., Graham, L.D., Forming useful directionally solidified composite shapes, in: AGARD CP-156 [18], pp. 67-76.
28. Low Cycle High Temperature Fatigue, Proceedings of The Specialists Meeting held in Washington, April 1974; AGARD CP-155, 1974.
29. Spera, D.A., Thermal fatigue of materials and components, in: ASTM STP 612, 1976, p. 3.
30. Manson, S.S., Metal Fatigue Damage, in: ASTM STP 495, 1971, p. 254.
31. Harrison, G.F., Cockcroft, M.G., The effect of cycle parameters on high temperature low cycle fatigue, in: AGARD CP-155 [28], pp. 4/1-13.
32. Brunetaud, R., Thiery, J., Les problèmes de fatigue oligocyclique à chaud dans les turboréacteurs aéronautiques, in: AGARD CP-155 [28], pp. 1/1-10.

33. Manson, S.S., An overview of high temperature metal fatigue; aspects covered by the 1973 international conference on creep and fatigue, in: AGARD CP-155 [28], pp. 2/1-44.
34. McEvily, A.J., Crosby, S.R., Lifetime prediction methods for elevated temperature fatigue, in: AGARD CP-155 [28], pp. 6/1-16.
35. Halford, G.R., High-temperature fatigue in metals - A brief overview of life prediction methods developed at the NASA Lewis Research Center of NASA, SAMPE Quarterly, April 1983, pp. 17-25.
36. Manson, S.S., Fatigue: A complex subject - some simple approximations, Exp. Mechanics, Vol. 5, No. 7, 1965, pp. 193-226.
37. Manson, S.S., Halford, G.R., A method of estimating high temperature low cycle fatigue behaviour of materials, Proc. of Int. Conf. on thermal and high strain fatigue, Met. and Metall. Trust, London, 1967, pp. 154-170.
38. Coffin, L.F., Fatigue at high temperatures, in: Fatigue at elevated temperatures, ASTM STP 520, 1973, pp. 5-34.
39. Henry, M.F., Solomon, H.D., Coffin, L.F., A comprehensive characterization of the high temperature fatigue behaviour of A 286, in: Proc. of the Int. Conf. on Creep and Fatigue in Elevated Temperature Applications, Philadelphia 1973, Sheffield 1974, Vol. 1, pp. 182/1-7.
40. Conway, J.B., Berling, J.T., Stenz, R.H., Strain rate and holdtime saturation in low cycle fatigue: design parameter plots, in: Fatigue at elevated temperatures, ASTM STP 520, 1973, pp. 637-647.
41. Taira, S., Lifetime of structures subjected to varying load and temperature, in: Creep in structures, Hoff, Nicholas Ed.,Acad. Press, New York, 1962, pp. 96-124.
42. Manson, S.S., The Challenge to unify treatment of high temperature fatigue - A partisan proposal based on strain range partitioning, in: Fatigue at elevated temperatures, ASTM STP 520, 1973, pp. 744-782.
43. Jaske, C.E., Mindlin, H., Perrin, J.S., Combined low cycle fatigue and stress relaxation of alloy 800 and type 304 stainless steel at elevated temperatures, in: Fatigue at elevated temperatures, ASTM STP 520, 1973, pp. 365-376.
44. Woodford, D.A., A critical assessment of the life fraction rule for creep rupture under non-steady stress or temperature, in: Proc. of the Int. Conf. on Creep and Fatigue in Elevated Temperature applications, Philadelphia 1973, Sheffield 1974, Vol. 1, pp. 180/1-6.
45. Polhemus, J.F., Spaeth, C.E., Vogel, W.H., Ductility exhaustion model for prediction of thermal fatigue and creep interaction, in: Fatigue at Elevated Temperatures, ASTM STP 520, 1973, pp. 625-636.
46. Wells, C.H., Design procedures for elevated temperature low cycle fatigue, in: AGARD CP-155 [28], pp. 7/1-8.
47. Krempl, E., Multiaxial fatigue. Present and future methods of correlation, in: AGARD CP-155 [28], pp. 5/1-10.
48. Smith, E.M., Precision in LCHTF testing, in: AGARD CP-155 [28], pp. 3/1-17.
49. Characterization of Low Cycle High Temperature Fatigue by the Strainrange Partitioning Method, Proceedings of the Specialists Meeting held in Aalborg, Denmark, April 1978, AGARD CP-243, 1978.
50. Manson, S.S., Halford, G.R., Hirschberg, M.H., Creep fatigue analysis by strain-range partitioning. Symp. on Design for Elevated Temperature Environment, ASME, 1971, pp. 12-28 (NASA TM-X-67838, 1971).
51. Manson, S.S., The development and application of strainrange partitioning as a tool in the treatment of high temperature metal fatigue, in: AGARD CP-243 [49], 1978, pp. K/1-11.
52. Manson, S.S., Halford, G.R., Nachtigall, A.J., Separation of the strain components for use in strain-range partitioning, paper presented at the ASME Pressure Vessels and Piping Conference, San Francisco, 1975 (NASA-TM-X-71737).
53. Halford, G.R., Nachtigall, A.J., Strainrange partitioning behaviour of the Nickel-base superalloys Renē 80 and IN 100, in: AGARD CP-243 [49], 1978, pp. 2/1-14.
54. Day, M.F., Thomas, G.B., Creep-fatigue interaction in Alloy 738LC, in: AGARD CP-243 [49], 1978, pp. 10/1-13.
55. Hyzak, J.M., An analysis of the low cycle fatigue behaviour of the superalloy Renē 95 by strainrange partitioning, in: AGARD CP-243 [49], 1978, pp. 11/1-25.
56. Halford, G.R., Hirschberg, M.H., Manson, S.S., Temperature effects on the strainrange partitioning approach for creep fatigue analysis, in: Fatigue at elevated temperatures, ASTM STP 520, 1973, pp. 658-669.
57. Halford, G.R., Saltsman, J.F., Hirschberg, M.H., Ductility normalised strain range partitioning life relations for creep-fatigue life predictions, NASA-TM-73737, 1977.
58. Advanced fabrication techniques in powder metallurgy and their economic applications, Proceedings of the Specialists Meeting held in Ottawa, Canada, April 1976, AGARD CP-200, 1976.
59. Advanced fabrication Processes, Proceedings of the Specialists Meeting held in Florence, Italy, September 1978, AGARD CP-256, 1979.
60. Sutcliffe, P.W., Final summary, part I - powder production, in: AGARD CP-200, 1976, pp. FS 1/1-4.
61. Stephen, H., Schmitt, H., Ruthardt, R., Production of high purity metal powders by electron beam techniques, in: AGARD CP-256, 1979, pp. 17/1-11.
62. Arnold, D.B., Renē 95 powder metallurgy opportunities for gas turbine applications, in: AGARD CP-200, 1976, pp. P6/1-6.
63. Evans, D.J., Manufacture of low cost PM Astroloy turbine discs, in: AGARD CP-200, 1976, pp. P4A/1-6.
64. Vaughan, R.F., Blenkinsop, P.A., Morton, P.H., Comparative evaluation of forged Ti-6Al-4V bar made from shot produced by the REP and CSC process, in: AGARD CP-200, 1976, pp. P11/1-7.
65. Keinath, W., Some comments on the mechanical properties of HIP titanium, in: AGARD CP-200, 1976, pp. SC8/1-12.
66. Betz, W., Huff, H., Track, W., Investigations for manufacturing turbine discs of Ni-base superalloys by powder metallurgy methods, in: AGARD CP-200, 1976, pp. P7/1-19.
67. Lescop, P., Marty, M., Walder, A., Influence sûr les caractéristiques mêchaniques des conditions de mise en oeuvre de poudres de superalliages à base de nickel, in: AGARD CP-200, 1976, pp. P8/1-12.
68. Allen, M.M., Iso-forging of powder metallurgy superalloys for advanced turbine engine applications, in: AGARD CP-200, 1976, pp. P5/1-15.
69. Symonds, C.H., Thompson, F.A., Nickel superalloy powder production and fabrication to turbine discs, in: AGARD CP-200, 1976, pp. P3/1-14.
70. Geissendorfer, R.F., Clark, L.P., Greenfield, M.A., Weldability of hot isostatically pressed prealloyed titanium 6Al-4V powders, in: AGARD CP-200, 1976, pp. SC10/1-5.
71. Witt, R.H., Near net powder metallurgy airframe structures, in: AGARD CP-200, pp. P12/1-8.

72. Drapier, J.M., Viatour, P., Coutsouradis, D., Habraken, L., High strength powder metallurgy cobalt base alloys for use up to 650 °C, in: AGARD CP-200, 1976, pp. P10/1-14.
73. Mazzei, P.J., Vandrunen, G., Hakim, M.J., Powder fabrication of fibre-reinforced superalloy turbine blades, in: AGARD CP-200, 1976, pp. SC7/1-16.
74. Cox, A.R., Moore, J.B., Reuth, E.C. van, Rapidly solidified powders, their production, properties and potential applications, in: AGARD CP-256, pp. 12/1-11, 1979.
75. Gugel, E., Net-shape processing of non-oxide ceramics, in: AGARD CP-256, 1979, pp. 14/1-16.
76. Fannin, E.R., Ion vapour deposited aluminium coatings for improved corrosion protection, in: AGARD CP-256, 1979, pp. 5/1-8.
77. Coad, J.P., Physical vapour deposition and ion beam techniques for surface durability, in: AGARD CP-256, 1979, pp. 7/1-9.
78. Norris, L.F., et al. Metal bonded carbides for wear resistant surfaces, in: AGARD CP-256, 1979, pp. 8/1-12.
79. Bacci, D., Tosto, S., Surface treatments by high power laser on nickel base superalloys, in: AGARD CP-256, 1979, pp. 9/1-10.
80. Walther, H.H., Basic trends in advanced fabrication processes, in: AGARD CP-256, 1979, pp. K/1-12.
81. Stacher, G.W., Weisert, E.D., Concurrent superplastic forming/diffusion bonding of B-1 components, in: AGARD CP-256, 1979, pp. 15/1-10.
82. Swadling, S.J., Fabrication of titanium at high temperatures, in: AGARD CP-256, 1979, pp. 16/1-17.
83. Doak, R.A., Diffusion bonded titanium alloy hollow fan disc, AFML-TR-72-192, 1972.
84. Ceramics for Turbine Engine Applications, Proceedings of the Specialists Meeting held in Porz Wahn, Köln, Germany, October 1979, AGARD CP-276, 1980.
85. Gugel, E., Net-shape processing of non-oxide ceramics, in: AGARD CP-256, 1979, pp. 14/1-16.
86. Katz, R.N., Lenoe, E.M., Ceramics for small airborne engine applications, in: AGARD CP-276, 1980, pp. 2/1-13.
87. Godfrey, D.J., Reaction-bonded, SiALON and CVD Si_3N_4 ceramics for engineering applications, in: AGARD CP-276, 1980, pp. 21/1-6.
88. Campo, E., Martinengo, P.C., Development in sintered silicon nitride, in: AGARD CP-276, 1980, pp. 24/1-8.
89. Dutta, S., State of the art of SiAlON materials, in: AGARD CP-276, 1980, pp. 16/1-15.
90. Kennedy, P., The fabrication and properties of Refel silicon carbide in relation to gas turbine components, in: AGARD CP-276, 1980, pp. 10/1-13.
91. Brooks, A., Bellin, A.I., Benefits of ceramics to gas turbines, in: AGARD CP-276, 1980, pp. 1/1-25.
92. McLeod, S.A., Walker, B.H., Mendelson, M.I., Development of an integral ceramic blade-metal disc with circumferential blade attachment, in: AGARD CP-276, 1980, pp. 7/1-10.
93. Wallace, F.B., et al., Silicon nitride turbine blade development, in: AGARD CP-276, 1980, pp. 5/1-12.
94. Baker, R.R., McLean, A.F., Duo-density ceramic turbine rotor-concepts, materials processes and test results, in: AGARD CP-276, 1980, pp. 6/1-19.
95. Tiefenbacher, E., Investigations of a hot pressed silicon nitride turbine rotor, in: AGARD CP-276, 1980, pp. 8/1-9.
96. Kochendörfer, R., Compression loaded ceramic turbine rotor, in: AGARD CP-276, 1980, pp. 22/1-19.
97. Napier, J.C., Arnold, J.P., Development of ceramic nozzle section for small radial gas turbine, in: AGARD CP-276, 1980, pp. 12/1-10.
98. Burfeindt, H., Langer, M., Development of a ceramic turbine nozzle ring, in: AGARD CP-276, 1980, pp. 13/1-8.
99. Maintenance in service of high temperature parts, Proceedings of the Specialists Meeting held in Noordwijkerhout, The Netherlands, Sept./Oct. 1981, AGARD CP-317, 1982.
100. Hedgecock, R.B.G., Military maintenance policies and procedures for high temperature parts; will they be adequate, in: AGARD CP-317, 1982, pp. 1/1-7.
101. Stroobach, J.Ph., Maintenance experience with civil aero engines, in: AGARD CP-317, 1982, pp. 4/1-3.
102. Honnorat, Y., Lesgourgues, J., Turbine stator parts repair by diffusion brazing, in: AGARD CP-317, 1982, pp. 9/1-12.
103. Cheung, K.L. et al., Rejuvenation of used turbine blades by hot isostatic pressing and reheat treatment, in: AGARD CP-317, 1982, pp. 10/1-6.
104. Vet, W.J. van der, HIP-processing, potentials and applications, in AGARD CP-317, 1982, pp. 11/1-16.
105. Tipler, H.R., Regeneration of the creep properties of a cast Ni-Cr base alloy, in: AGARD CP-317, 1982, pp. 12/1-6.
106. Huff, H., Wortmann, J., Repair and regeneration of turbine blades, vanes and discs, in: AGARD CP-317, 1982, pp. 13/1-7.
107. Mom, A.J.A., Recorder's report, session II, in AGARD CP-317, 1982, pp. R2/1-2.
108. Hauser, J.M., Duret, C., Pichoir, R., Influence des traitements de protection sûr les propriétés méchaniques des pièces en superalliages, in: AGARD CP-317, 1982, pp. 8/1-11.
109. Snide, J.A., Schulz, W.J., Engine depot maintenance repair technology, in: AGARD CP-317, 1982, pp. 2/1-19.
110. Harris, J.A., et al., Engine component retirement for cause, in: AGARD CP-317, 1982, pp. 5/1-9.
111. Jeal, R.H., Defects and their effects on the behaviour of gas turbine discs, in: AGARD CP-317, 1982, pp. 6/1-15.

Table 1
Hot corrosion ranking of some Ni-base alloys

	Alloy	Cr-percentage
increasing hot corrosion resistance ↓	B 1900	8
	IN 100	10
	Nimonic 100	11
	713 C	12.5
	Udimet 700	15
	Nimonic 105	15
	IN 738	16
	Nimonic 90	20
	Udimet 500	19
	Waspaloy, Hastelloy, Nimonic 80 A, IN 939	19.5/22/20/22.5

Table 2
Comparison of properties between present superalloys and more promising DS eutectics [21-24]

Alloy	γ'- δ	γ/γ'- δ	Co-TaC	Ni-TaC	MarM200	MarM302
composition	Ni-23.1Nb-4.4Al	Ni-19.7Nb-6.0Cr-2.5Al	Co-20Cr-10Ni-12.7Ta-0.75 C	Ni-20Co-10Cr-γ'-Tac	Ni-9Cr-10Co-12.5W-1Nb	Co-21Cr-10W-9Ta
second phase and volume percentage	44	37	16	10	-	-
σ_y* 25°	1020	1190	950	1300	840	700
σ_u* 25°	1230	1230	1090	1610	945	945
σ_y* 816 °C	870	950	700	915	810	360
σ_u* 816 °C	900	970	700	985	905	520
endurance limit* 10^7 cycles, 25 °C	690			450	275	
fracture strain(%) 25 °C	0.5-0.8	2.9- 5	29	11.2	7	2
fracture strain(%) 816 °C	5.8-8.4	5.1-10.5	7.1	10.8	3.6	9.5
density (10^3 kg/m^3)	8.5	8.5	9		8.53	9.21
solidus temp. (°C)	1280	1244	1365		1315	1315
thermal expansion coefficient; mean value 20-910 °C (10^{-6}/°C)	13.2	14.4	14.7		15.85	15.68
appr. thermal expansion mismatch (10^{-6}/°C)	1.6	6.1	9.9	8.1	-	-
thermal conductivity (W/m °K) at 20 °C			14.7 13.5		14.0	18.7
thermal conductivity (W/m °K) at 930 °C			20.6 20.0		23.9	24.2

* All strength values indicated in MN/m^2

Table 3
Coefficients for high-temperature fatigue equations for several materials [38]

	A 286		AISI 409	AISI 304		AISI 316		AISI 348		Udimet 500
	air	vacuum								
temperature °C	595	595	427	650	816	650	816	650	816	816
A' (MN/m^2)	308	476	86	156	47	149	68	105	61	111
β'	0.12	0.16	0.052	0.187	0.094	0.143	0.117	0.102	0.131	0.132
k_1'	0.045	0.12	0.007	0.089	0.071	0.074	0.091	0.038	0.127	0.075
A^1(MN/m^2)	295	632	81	148	44	184	65	126	74	359
n	0.122	0.35	0.064	0.258	0.105	0.24	0.151	0.191	0.224	0.185
k_1	0.0026	0.116	0.0013	0.053	0.053	0.052	0.079	0.015	0.115	0.057
C_2^1	1.32	0.37	2.65	1.108	1.72	0.354	1.081	0.382	0.365	0.0736
k^2	0.65	0.99	0.889	0.81	0.81	0.86	0.90	0.77	0.92	0.864
β	0.97	0.44	0.831	0.707	0.87	0.57	0.74	0.527	0.56	0.712
E (10^{10}N/m^2)	17.3	17.3	18.7	14.9	13.0	15.1	12.7	15.0	13.1	17.3

$A' = AC_2^n$ $\quad \beta' = n\beta$ $\quad k_1' = -\beta n(k-1) + k_1$

Table 4
Powder Production Processes [60,61]

process	method	start material			atomisation atmosphere	melting rate kg/min	present capacity 10^3kg/year	powder properties				material utilisation
		type	form	quantity kg				size range µm	mean size µm	tap density %	contamination	%
Electron Beam Rotating Electrode (EBRE)	centrifugal atomisation of rotating electrode	Ti	electrodes 50mm dia. 200mm long	2	Vacuum 10^{-4} torr	0.5	7	50-1000	400	-	C from bouncing sheet	78-85 (spheres < 1000 µm)
Rotating Electrode Process (REP)	centrifugal atomisation of rotating electrode	Ti	electrodes 62mm dia. 1.5m long	35	He ~latm	-	100/ machine	50-500	225	65	W of cathode	85-95
Electron Beam Rotating Disc (EBRD)	centrifugal atomisation from rotating disc	Ti	electrode up to 150 mm dia. 800mm long	64	Vacuum	1-2	-	50-700	-	60	-	70-85
Centrifugal Shot Casting (CSC)	centrifugal atomisation from rotating crucible	Ti	electrode up to 76mm dia. 600mm long	12	He/A ½-latm	1	1-3	50-1000	300-400	65	-	30-60 (spherical fraction)
Argon atomisation	atomisation of molten stream by argon jets	Ni	vacuum induction melt	500	Argon > latm	-	> 500	5-500	-	64 (< 150 µm)	ceramics of crucible/ nozzle; O_2+A	~70 (<150 or 180 µm)
Vacuum atomisation	exposure of supersaturated solution of H_2 in melt to vacuum	Ni	vacuum induction melt	200	Vacuum/ H_2	~ 100	> 150	1-200	10-50	60-65	ceramics of crucible/ nozzle; O_2 from wall	-

Table 5
Physical and mechanical properties of various ceramic materials

Type	Ref.	density	Modulus of rupture (4-point flexural strength) MN/m²			Young's modulus	hardness	Thermal characteristics				300 hr stress rupture strength	thermal shock resistance**	K_{Ic}***
								thermal expansion	thermal conductivity W/m °C		thermal shock parameter at 500°C			
		10^3kg/m³	RT	1000°C	1400°C	GN/m²	kg/mm²	10^{-6}/°C	*	500°C	1200°C	W/m	at 1200°C	°C	MN/m$^{3/2}$
HPSN	90	3.2	690			310	2500-3500	3.2		17.5	14	12,000			
HPSN NC-132	86		690	620	275	320		3.0	30-15				245	750	5-8
RBSN	90	2.6	240			220	900-1000	3.2		15	14.2	5,500			
RBSN NC-350	86	2.45	210	350	370	168		2.8	6-3				345	460	
SSN	86		660	590	255	280		3.2	28-12						
SiAlON	90	3.2	550			304	2500-3500	3.2		15.3	11.5	8,500		320(HP)	1-6
SiAlON	89	3.1-3.2	400-500	400-500	150-225									510(sint)	
HP-SiC NC-203	86		655	585	520	450		4.5	85-35				410	415	
HP-SiC	85	3.2	550	550	450	420		4.6							
RS-SiC NC-435	86		380	415	<275	350		4.4	100-50				315		
RS-SiC Refel	90	3.1	525			413	3000	4.3		83.6	38.9	25,000		305	
RS-SiC	85	2.7	250	250	250	280		4.5							
RS-SiC(Si-imp)	85	3.1	400	500	250	360		4.3							
S-SiC (α)	86		310	310	310	410		4.8	100-50				280		
S-SiC (β)	86		440	520	470										
S-SiC	85	3.0	500	450	400	400		4.6							

* no temperature interval indicated
** data from reference [89], reported values not specified within each class
*** data from references [86] and [89].

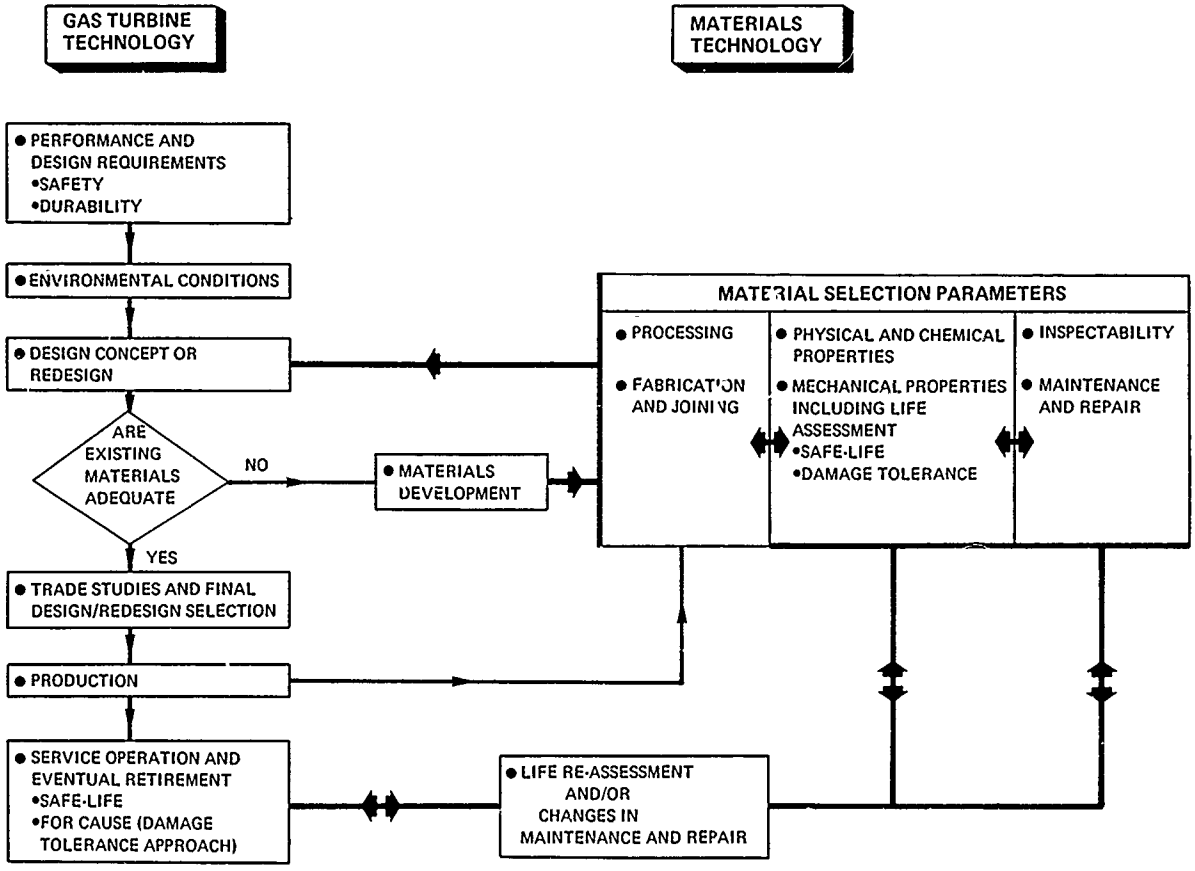

Fig. 1 An illustration of the relationships between gas turbine engine technology and materials technology

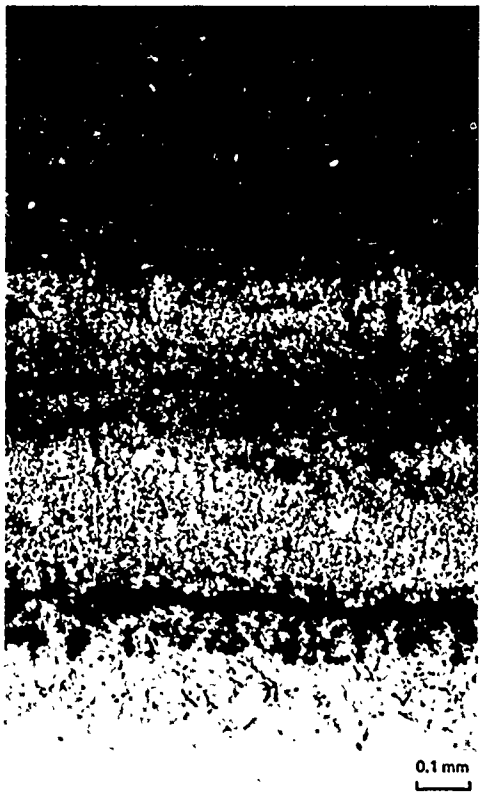

Fig. 2 Cross sectional microstructure appearance of hot corrosion in an industrial gas turbine blade

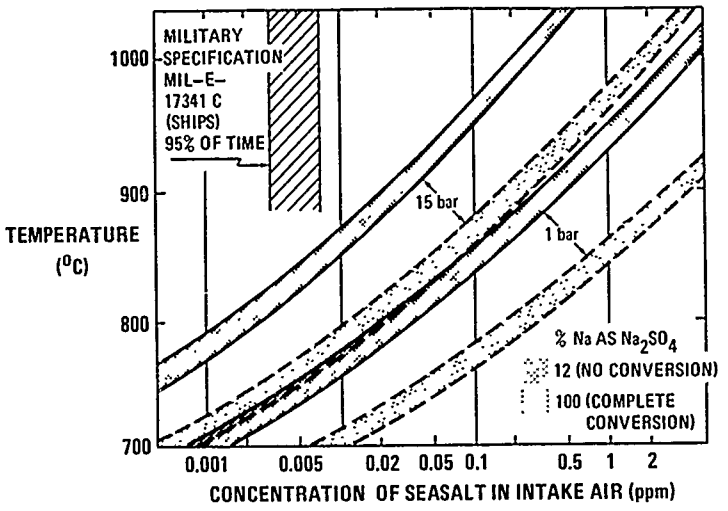

Fig. 3 Dewpoint of Na_2SO_4 as a function of seasalt concentration and pressure.
N.B.: For each pressure two bands are indicated. The upper band represents the dewpoint curve in the case of complete conversion of NaCl to Na_2SO_4 [3]

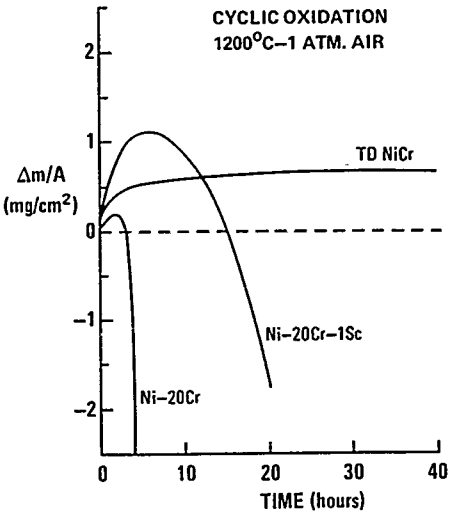

Fig. 4 Cyclic oxidation results for Ni-20Cr, TD NiCr ($Ni-22Cr-2ThO_2$) and Ni-20Cr-1Sc in air at 1200°C (2 hr. cycles) [17]

LONGITUDINAL

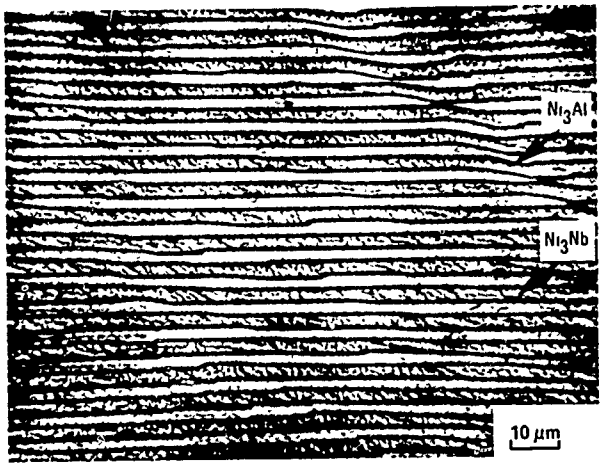

Figure 5a

TRANSVERSE

Figure 5a

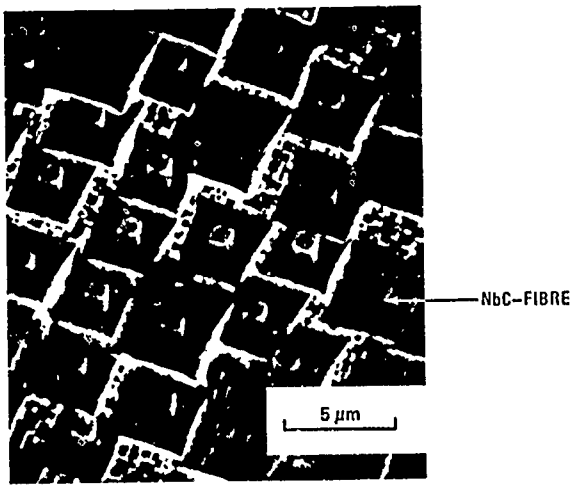

Figure 5b

Fig. 5 Microstructures of DS eutectic alloys;
a) Lamellar γ'-δ (Ni_3Al-Ni_3Nb) [19]
b) Fibrous NiCo-NbC eutectic [20]

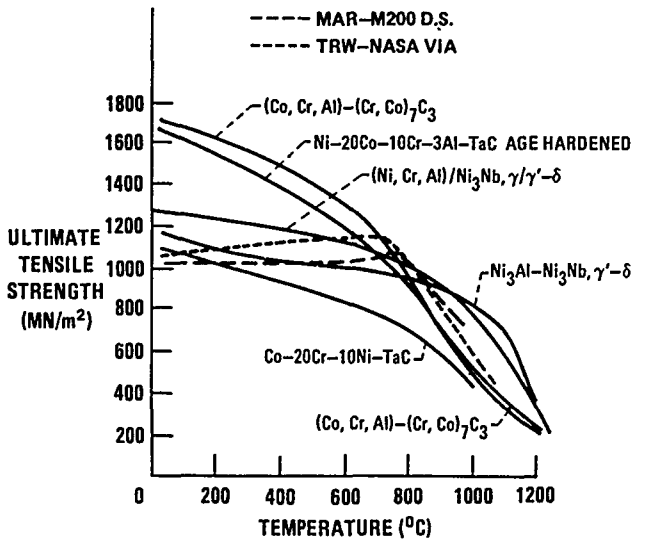

Fig. 6 Ultimate tensile strength versus temperature for eutectic alloys and two superalloys [21]

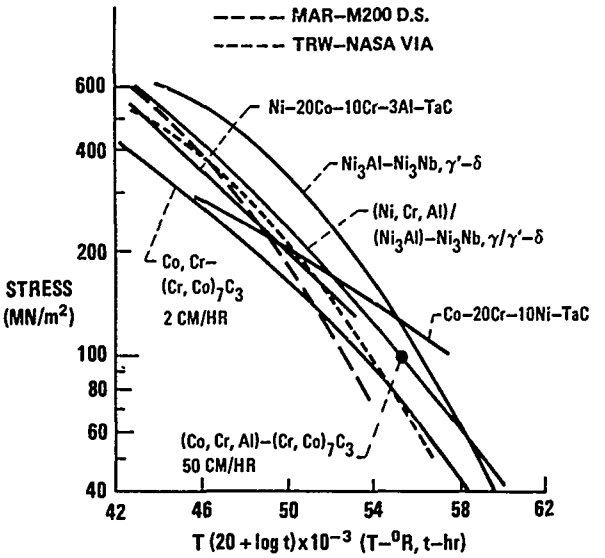

Fig. 7 Stress-rupture comparison of eutectic alloys and two superalloys [21].
For some alloys the growth rate during solidification is indicated

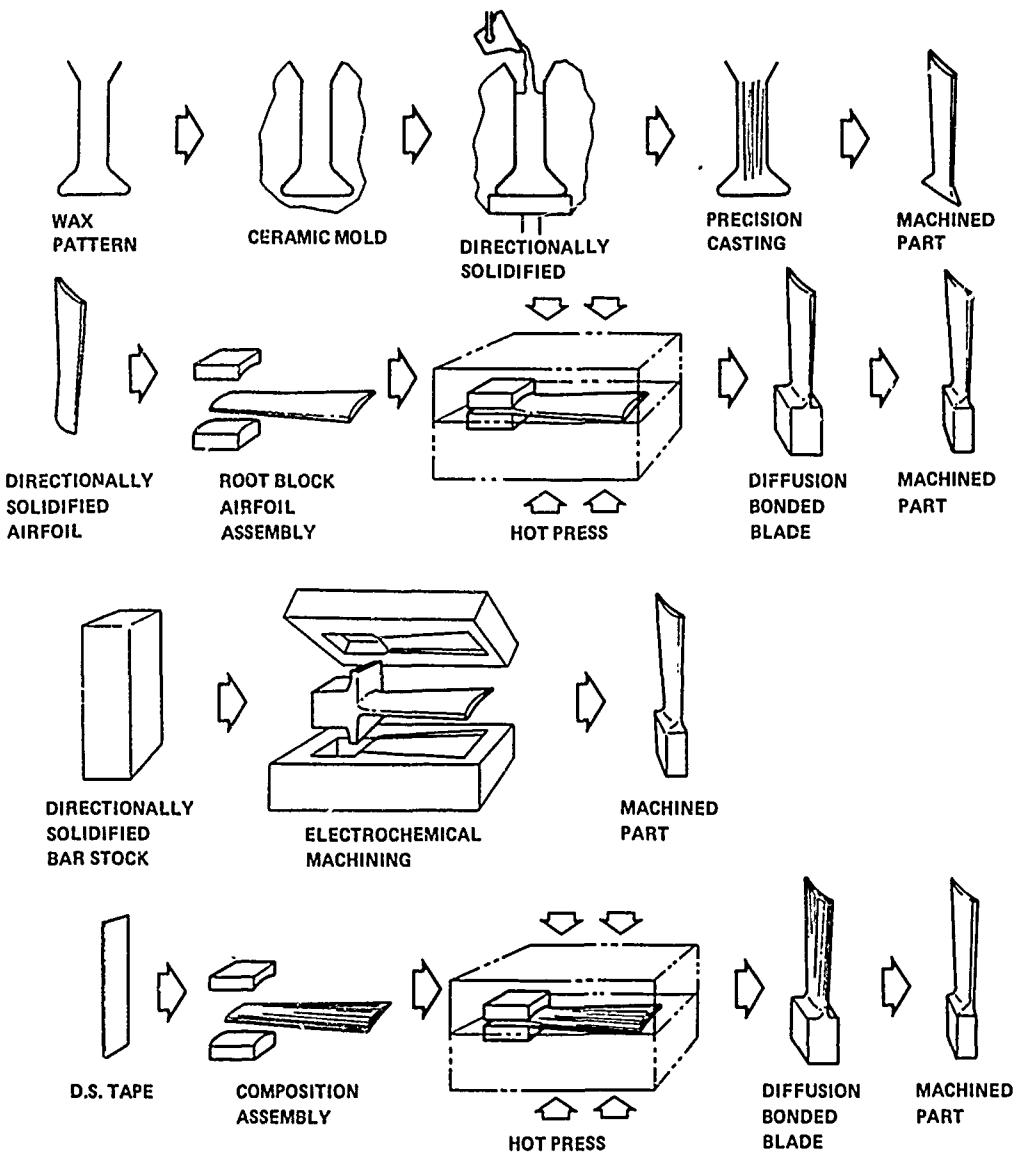

Fig. 8 Examples of DS eutectic blade processing options [27]

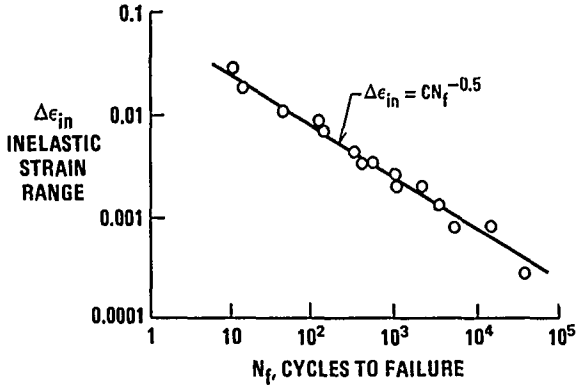

Figure 9a

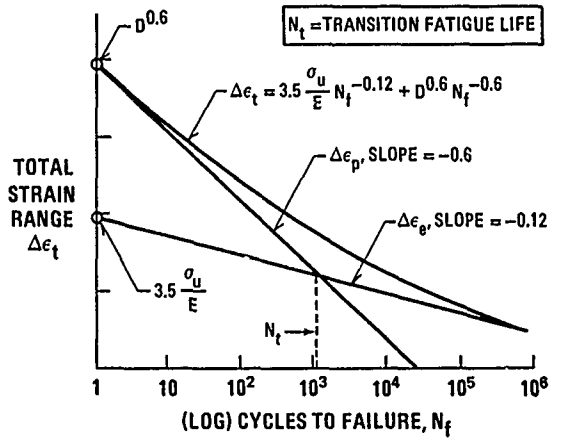

Figure 9b

Fig. 9 Figures illustrating Manson-Coffin relationship (fig. 9a) and universal slope method (fig. 9b) [35]

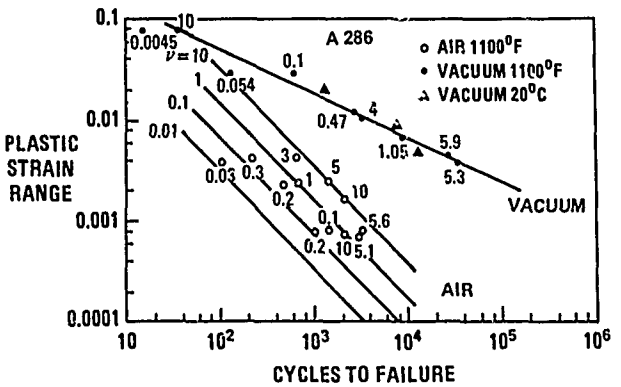

Fig. 10 Comparison of test data and predicted life, based on Coffins frequency modified life relation [39]

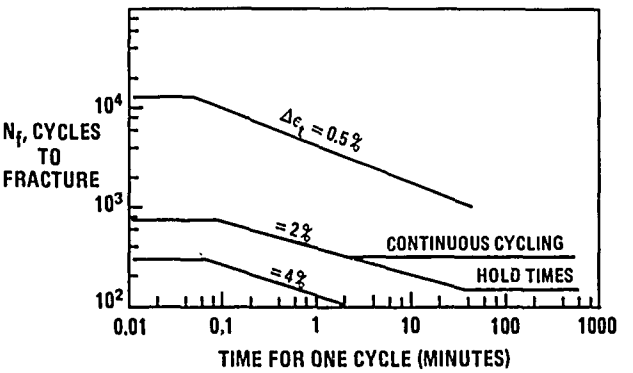

Fig. 11 Life curves of AISI 304 at 650°C showing frequency independence at very low and very high frequency [40]

TIME AND CYCLE FRACTION METHOD		
FAILURE MODE	STRESS–TIME–DEPENDENT	STRAIN–CYCLE–DEPENDENT
FAILURE CRITERION	CREEP RUPTURE FAILURE 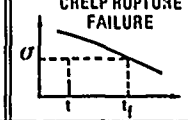	FATIGUE FAILURE 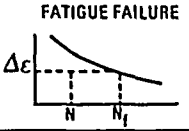
MEASURE OF DAMAGE	LIFE FRACTION t/t_f	LIFE FRACTION N/N_f
ACCUMULATION OF DAMAGE	LINEAR SUMMATION TO $\sum \frac{t}{t_f} = 1$ (AT FAILURE)	LINEAR SUMMATION TO $\sum \frac{N}{N_f} = 1$ (AT FAILURE)
COMBINATION	$\sum \frac{t}{t_f} + \sum \frac{N}{N_f} = 1$ (AT FAILURE)	

Fig. 12 Time and Cycle Fraction Method [35]

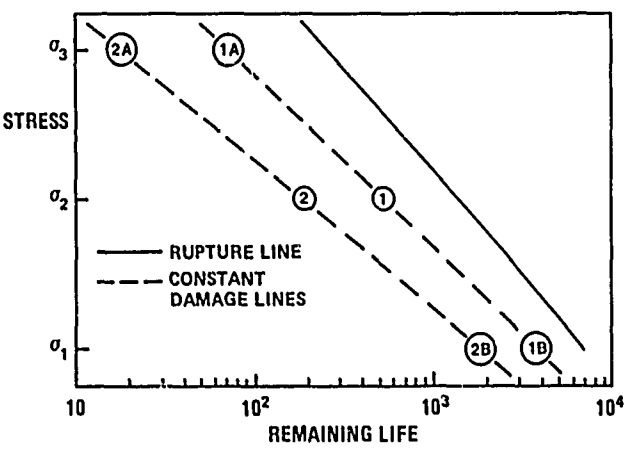

Fig. 13 Schematic plot illustrating construction of constant damage lines in terms of remaining life for different stresses [44]

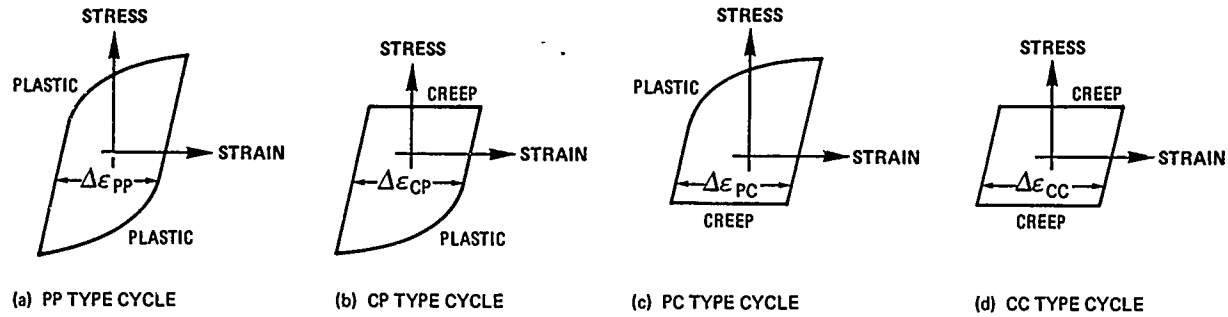

(a) PP TYPE CYCLE (b) CP TYPE CYCLE (c) PC TYPE CYCLE (d) CC TYPE CYCLE

Fig. 14 The four generic types of strainranges

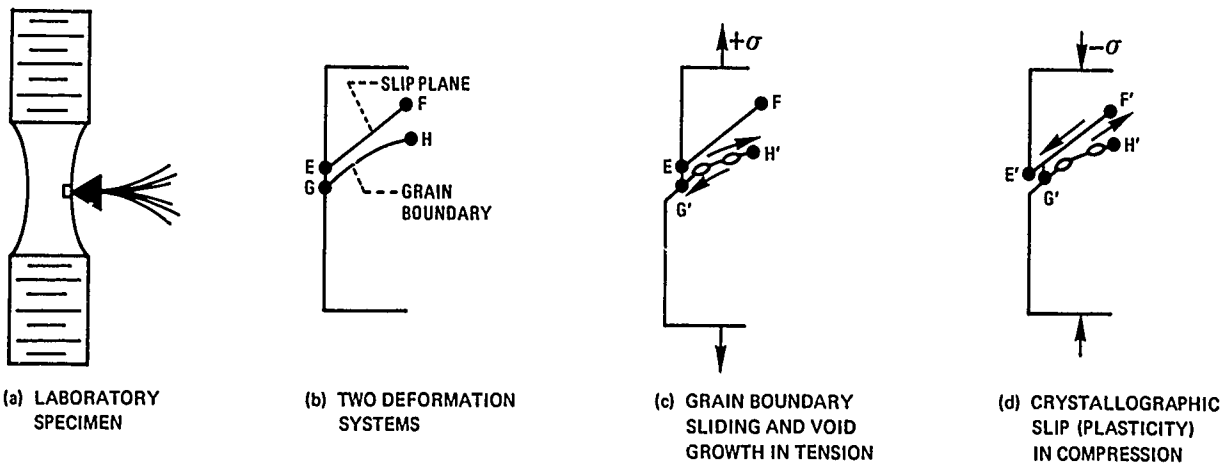

(a) LABORATORY SPECIMEN (b) TWO DEFORMATION SYSTEMS (c) GRAIN BOUNDARY SLIDING AND VOID GROWTH IN TENSION (d) CRYSTALLOGRAPHIC SLIP (PLASTICITY) IN COMPRESSION

Fig. 15 Simplified schematic illustration of the creep-fatigue interaction occurring when tensile creep occurring along grain boundaries is reversed by compressive plasticity occurring along crystallographic slip planes [51]

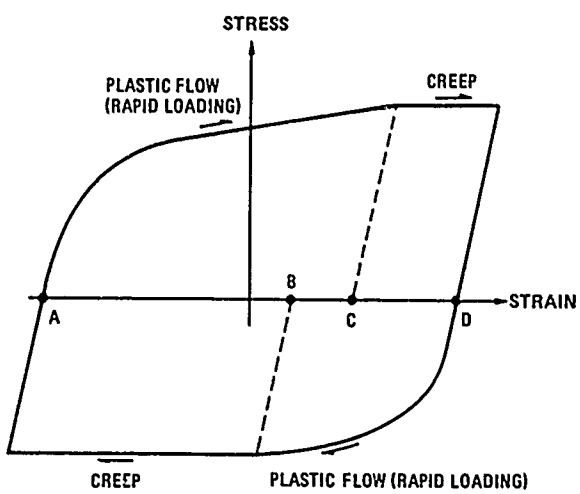

Fig. 16 Hysteresis loop with creep and plasticity

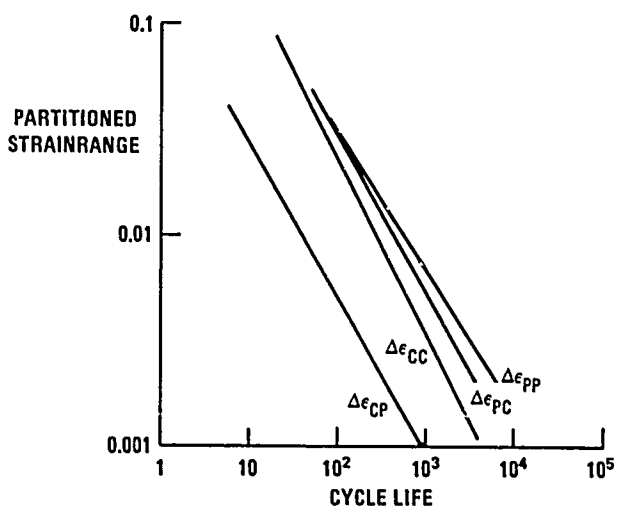

Fig. 17 Life relationships for generic strainrange components for 316 stainless steel at about 700°C [42]

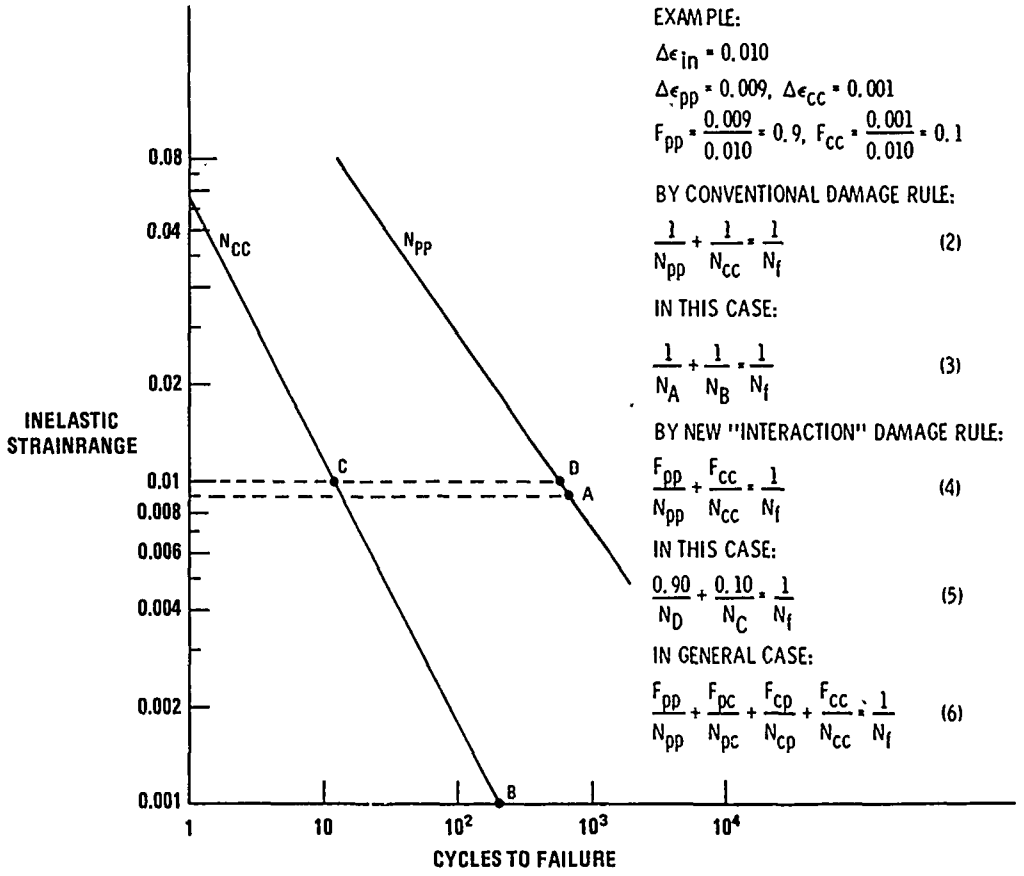

Fig. 18 Relationships for determining life when two or more strainrange components are present [42]

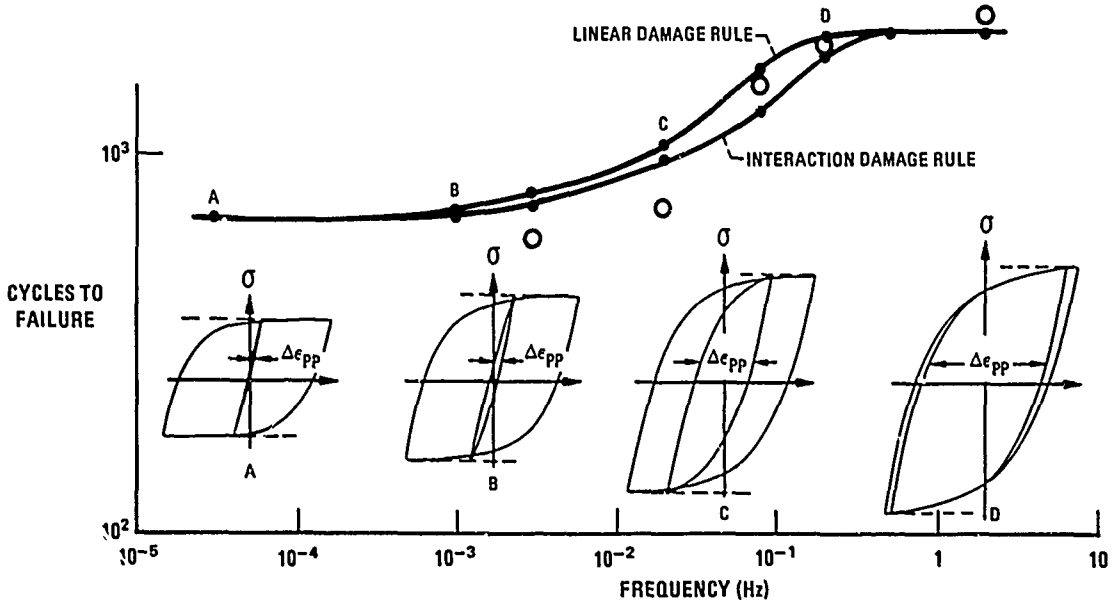

Fig. 19 Method of partitioning using real-time hysteresis loop and rapid-cycling hysteresis loop between same stress limits. Data for 316 stainless steel tested at 815°C, $\Delta\epsilon_{in} = 0.0047$, triangular strain waveform [42]

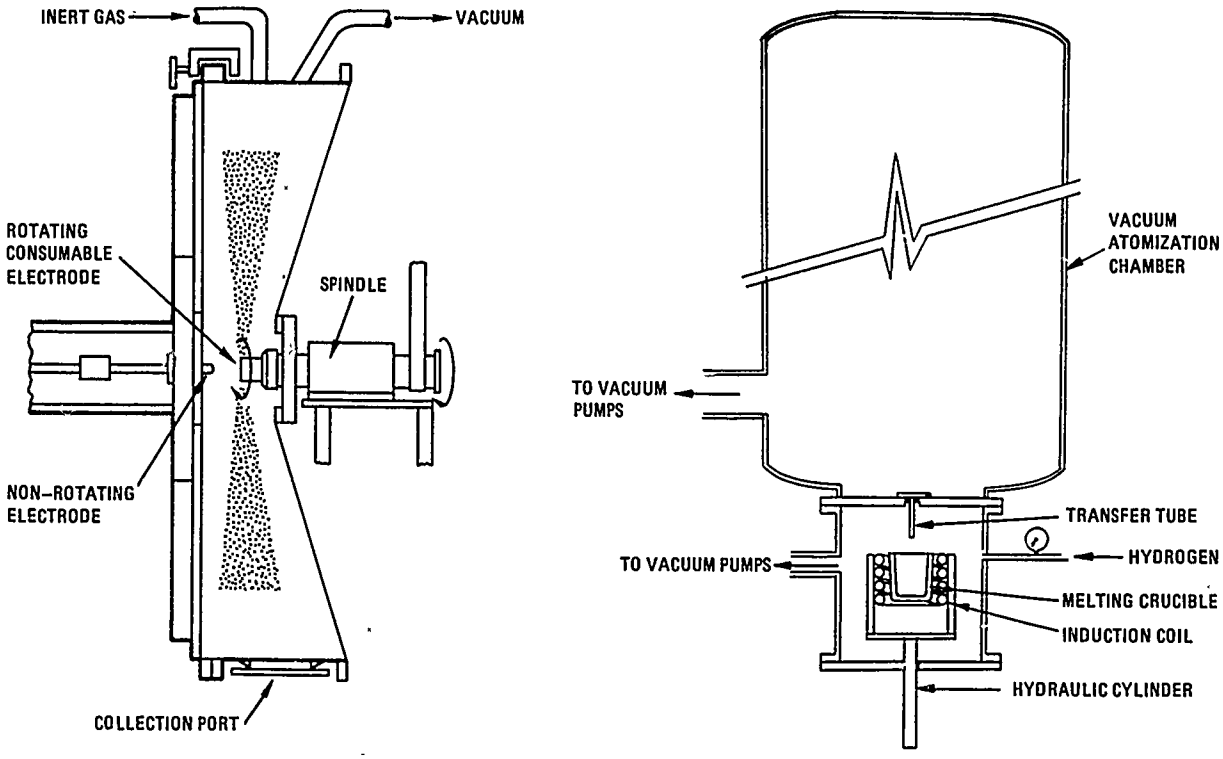

Fig. 20 Two powder production processes; left REP-process, right vacuum atomization process [58, pp SC 1/3 and SC 6/1]

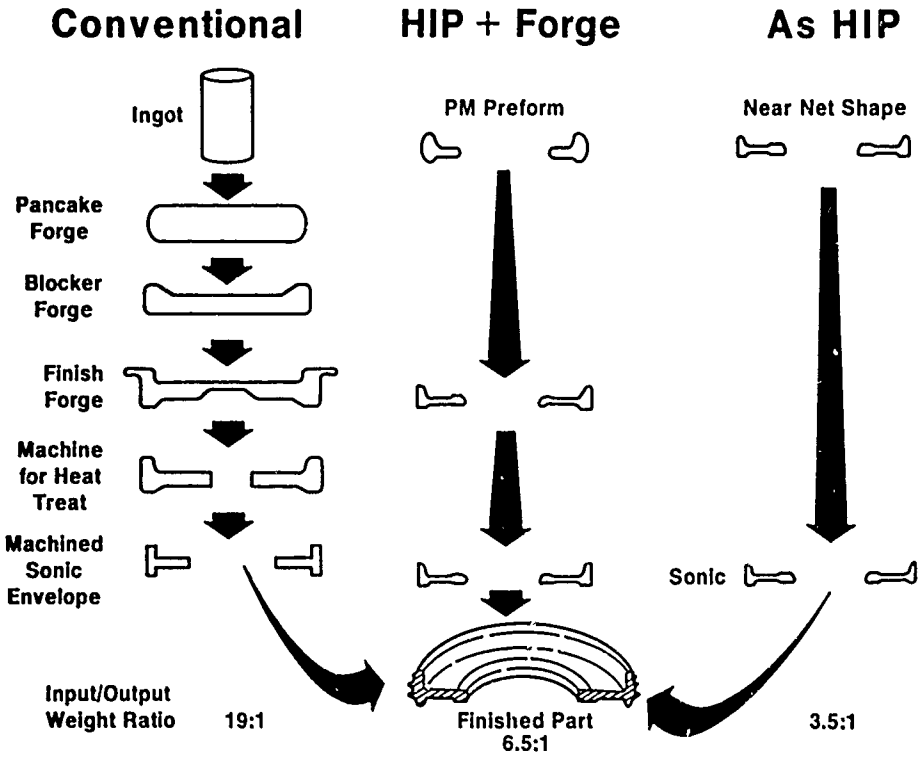

Fig. 21 Comparison of manufacturing methods of René 95 disk [62]

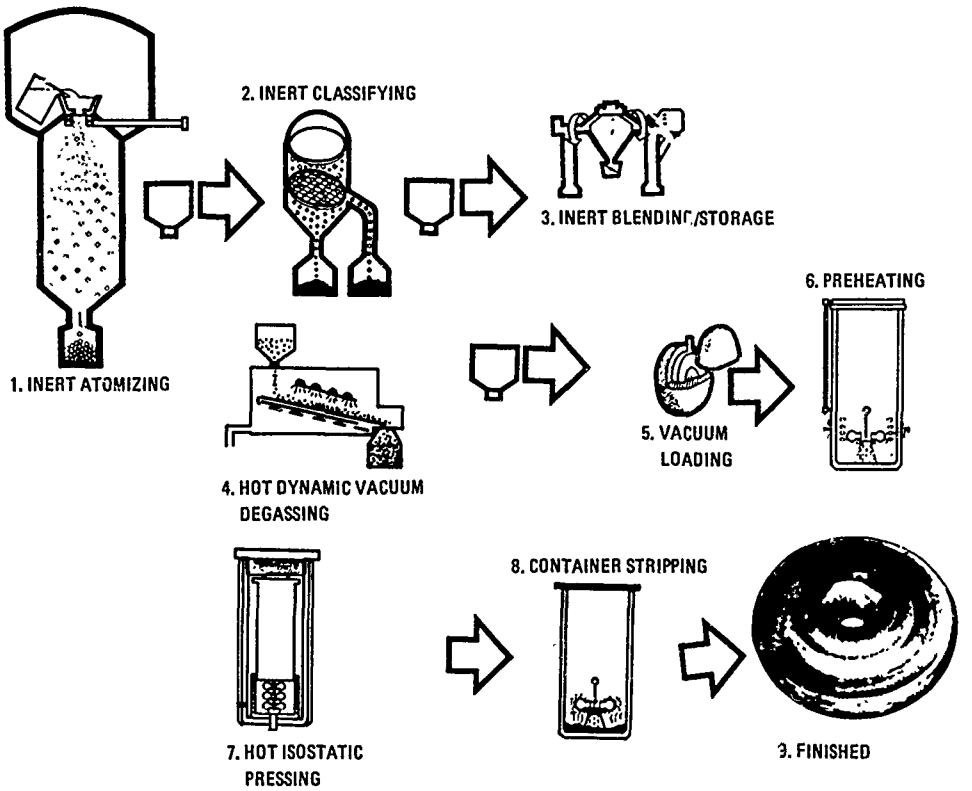

Fig. 22 Schematic powder processing route for HIP production of disc preforms [63]

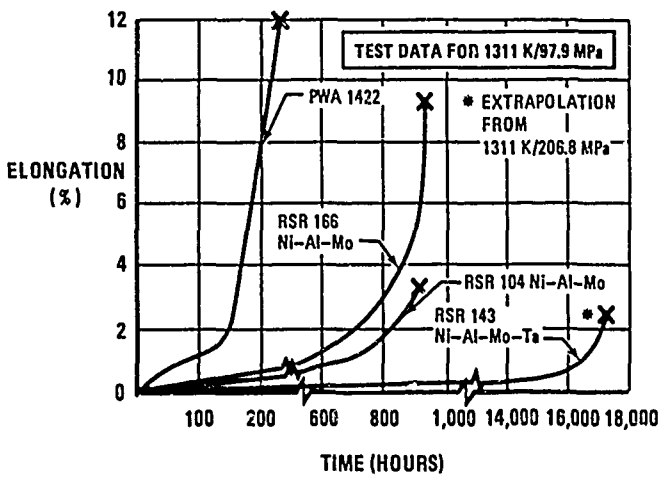

Fig. 23 Creep deformation of rapidly solidified (RSR) Ni-Al-Mo alloys in comparison with directionally solidified MarM200 + Hf (PWA 1422) [74]

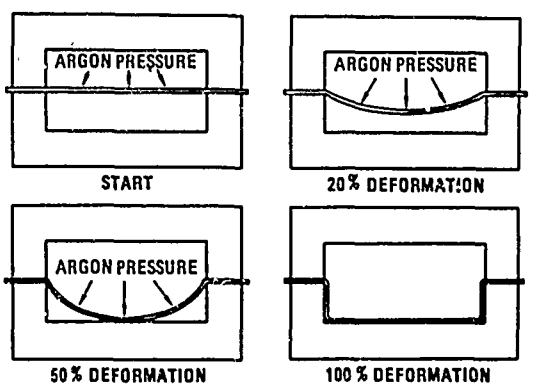

Fig. 24 Schematic illustration of superplastic forming process [81]

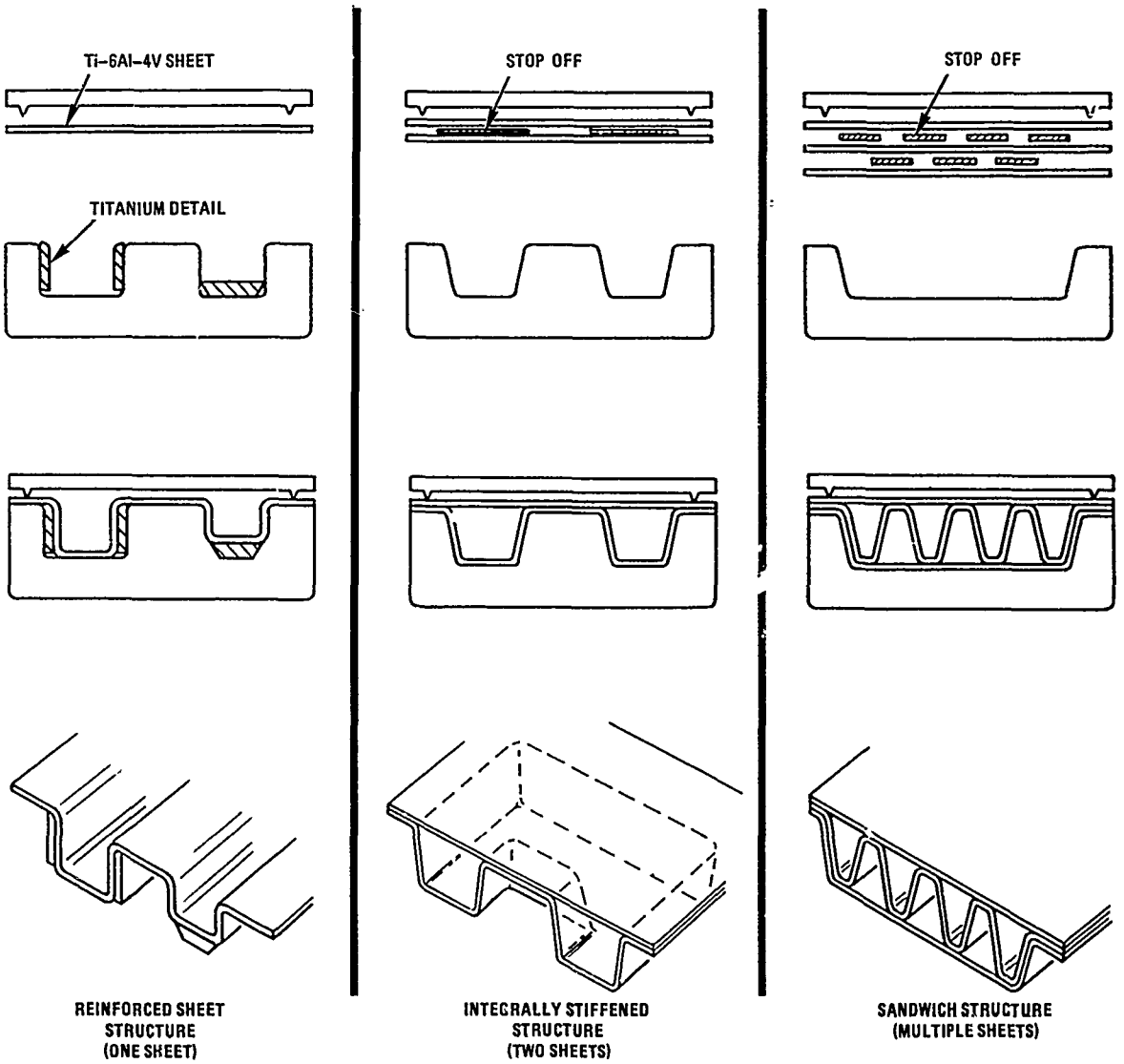

Fig. 25 Three types of structures produced by a combination of superplastic forming and diffusion bonding; note: stof off is applied to prevent bonding in certain areas [81]

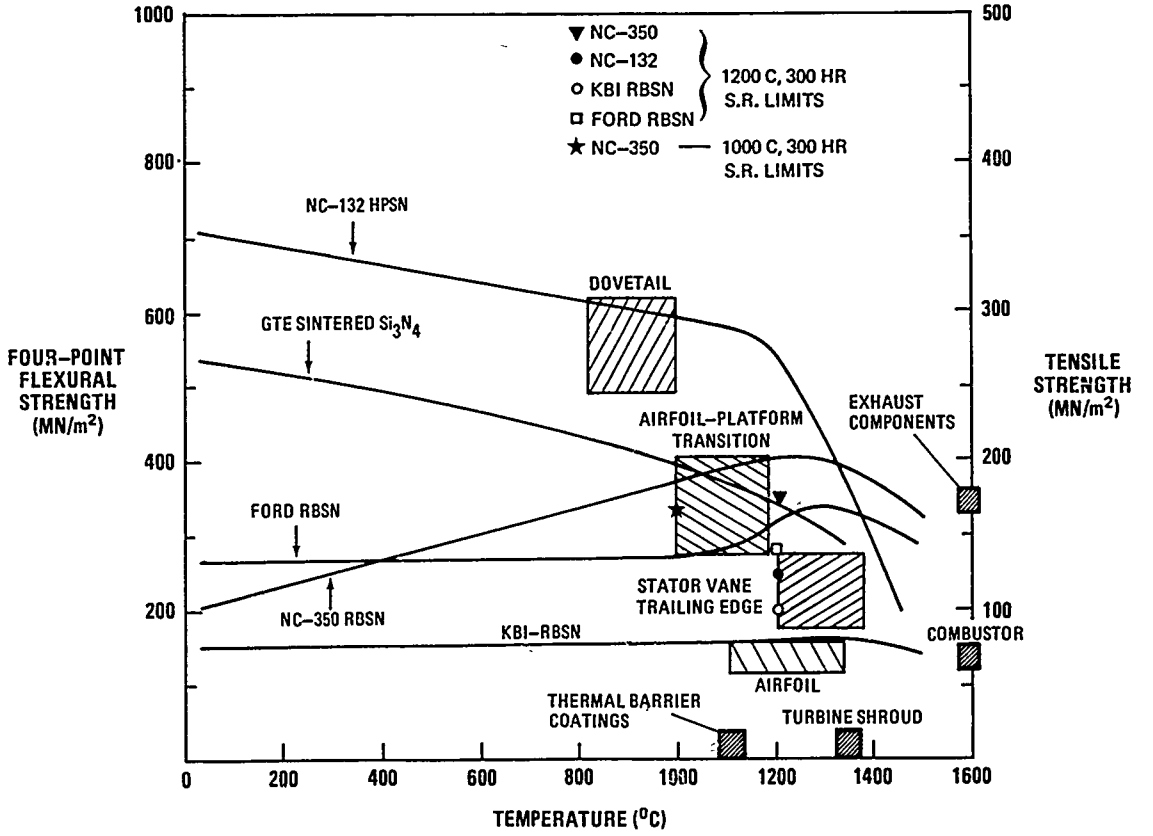

Fig. 26 Flexural strength of silicon nitride materials versus required strengths for blades, vanes and other components [86, 91]; some 300 hr stress rupture data points are also included

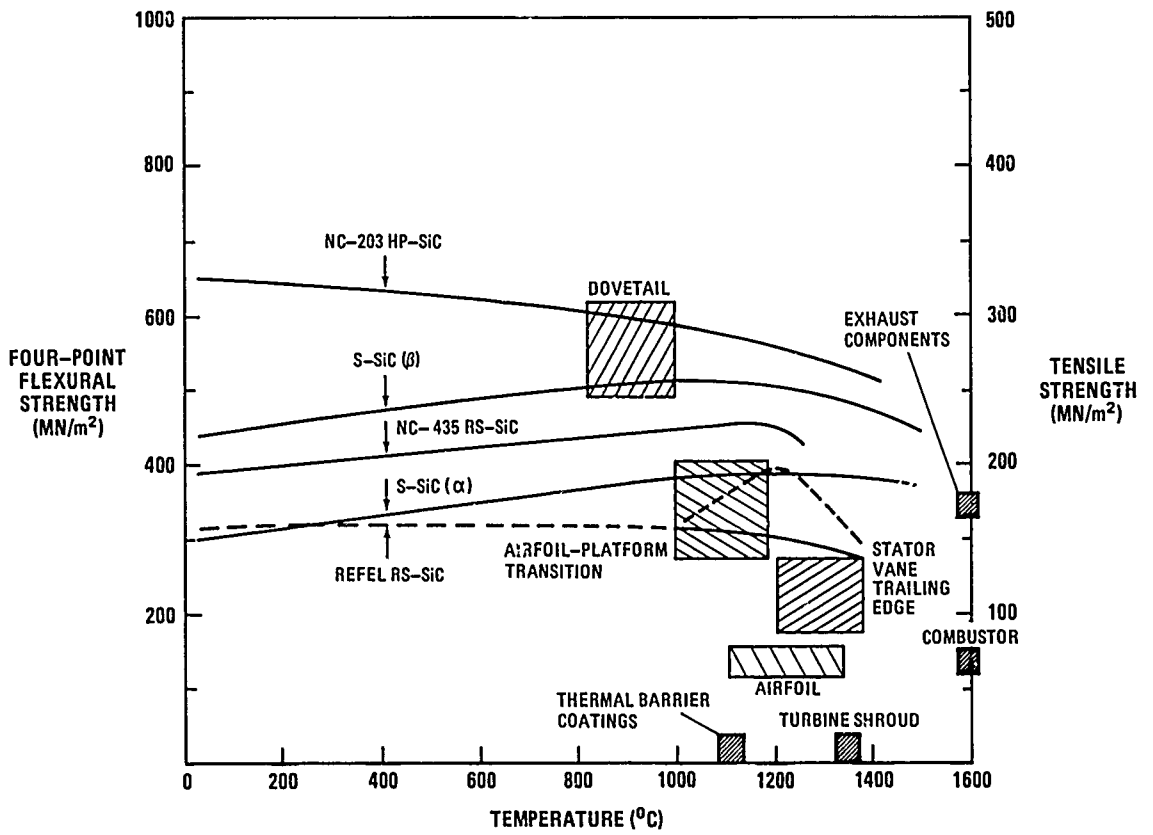

Fig. 27 Flexural strength of silicon carbide materials versus required strengths for blades, vanes and other components [86, 91]

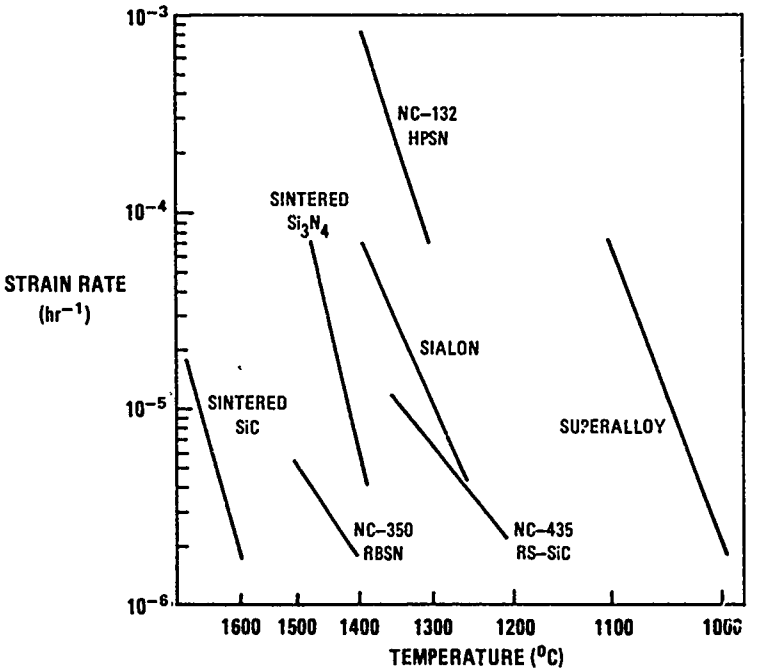

Fig. 28 Comparison of creep behaviour of ceramics versus a superalloy [91]

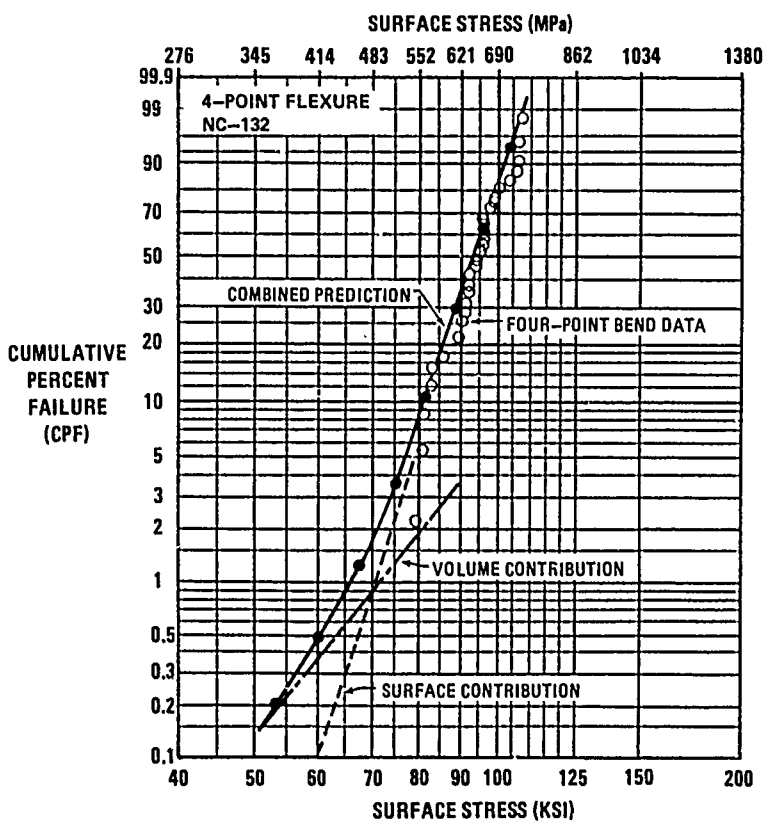

Fig. 29 Weibull distribution for 4-point flexural specimen failures [93]

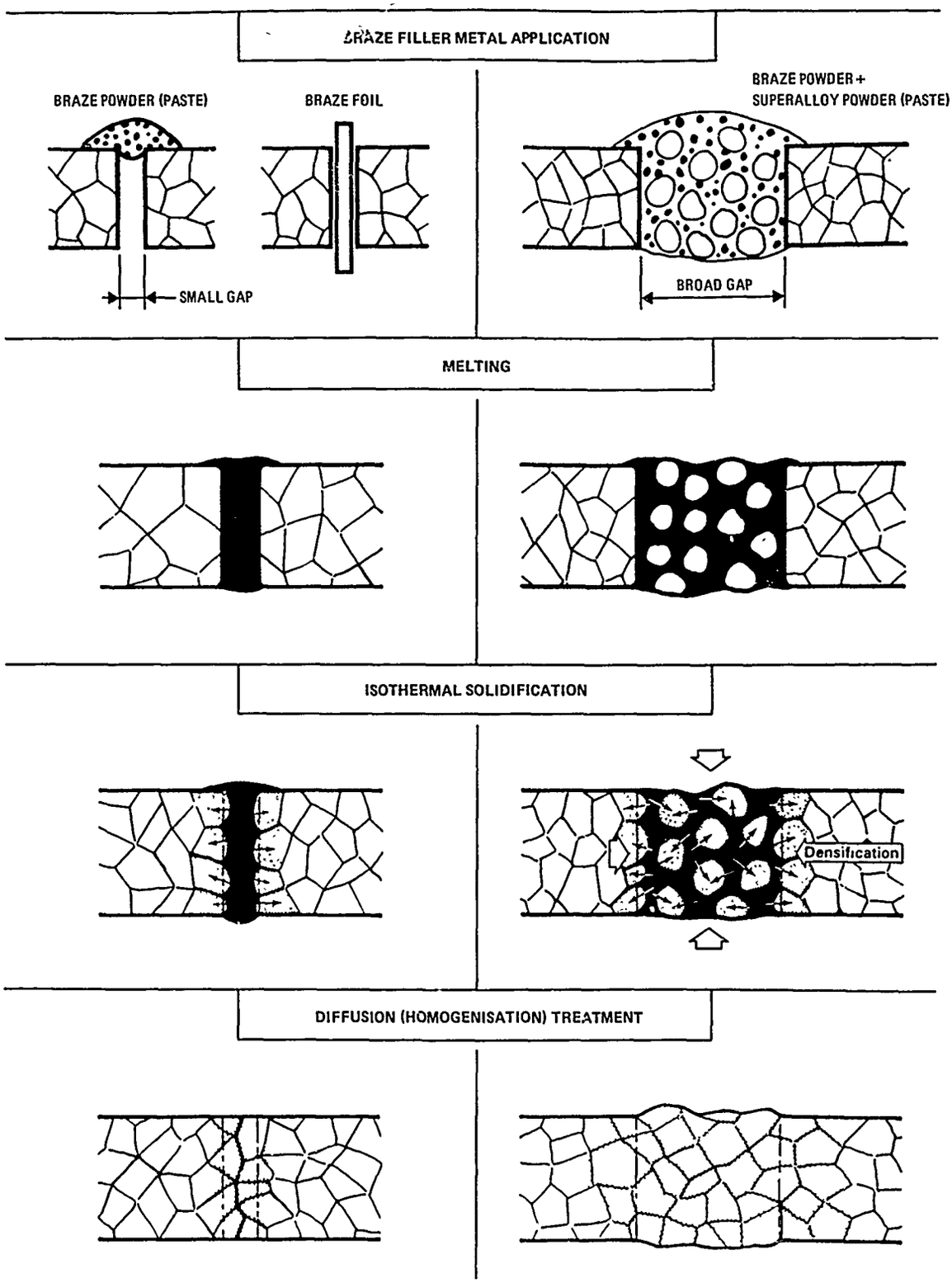

Fig. 30 Diffusion brazing process with and without the addition of superalloy powder to bridge broad gaps [102]

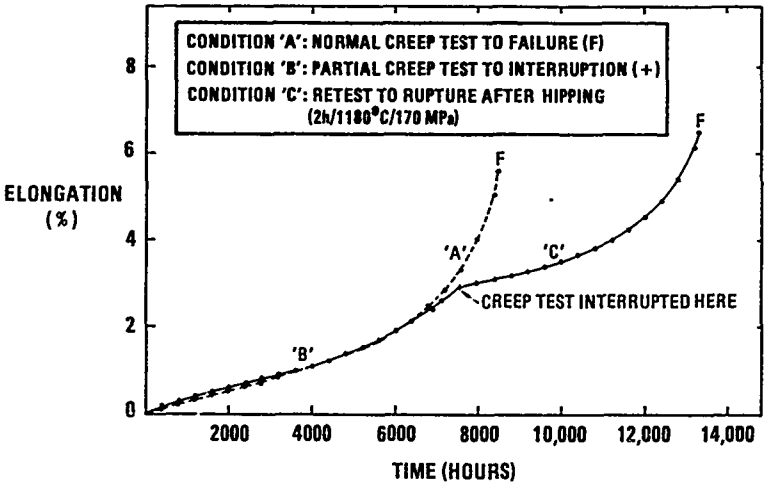

Fig. 31 Effect of hipping on creep behaviour of IN738LC in test stopped in tertiary creep prior to rupture at 170 MPa and 850°C [105]

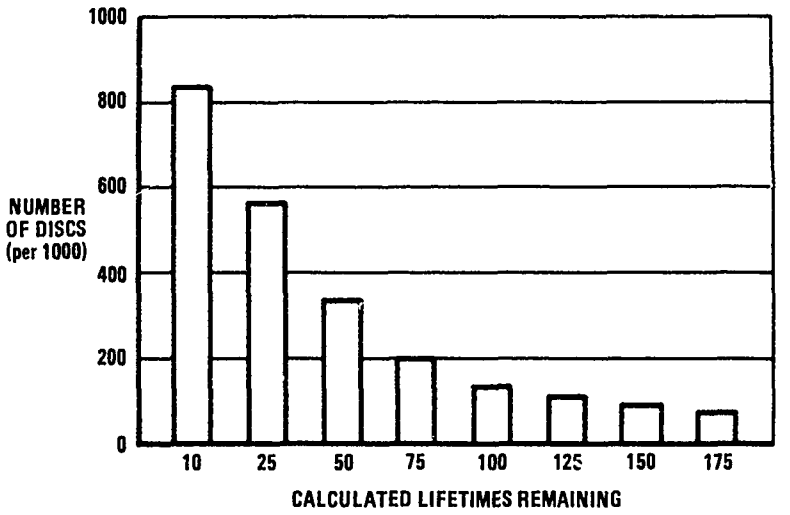

Fig. 32 Remaining lifetimes of discs (after LCF life has been reached) in the current safe-life approach [110]

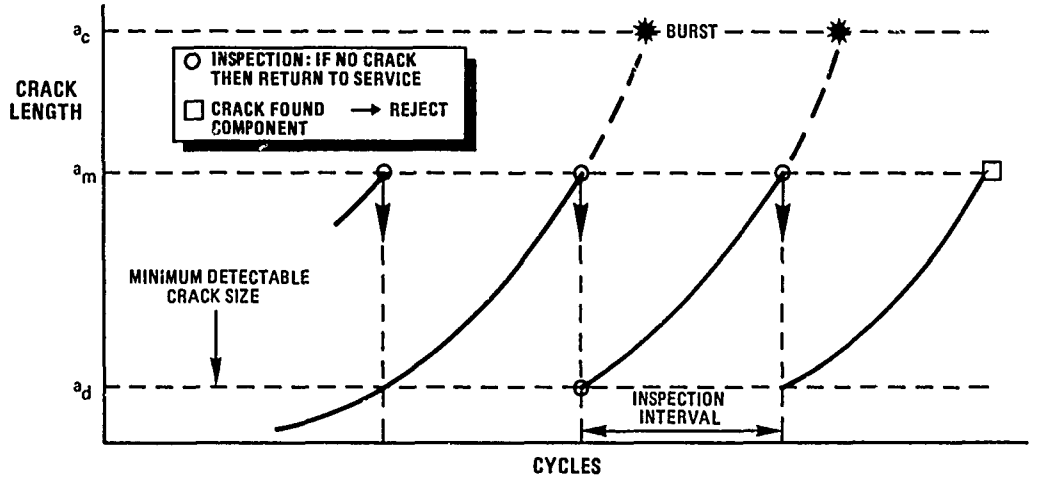

Fig. 33 Schematic of damage tolerance lifing approach
a_c = critical crack size
a_m = maximum allowable crack size in service
a_d = crack detection limit

DISCUSSION

P.Ramette, Fr

Sintered ceramics (silicon carbide) yield stress is higher in compression than tension. Can this property be used in turbine engines?

Author's Reply

Indeed, because ceramics show very good compressive strength, one could think about the development of compression loaded rotors. In my paper I have referred to a very interesting German study in that field (96). Furthermore, I can refer to a French study, which is also of particular interest, see reference (84), pages 4/1—13.

P.Ramette, Fr

Did the SMP consider composite ceramics in gas turbine engines?

Author's Reply

Ceramic composite materials may offer a potential for improved toughness, high-temperature strength and oxidation resistance. However, the development of these types of materials is only in a very exploratory stage. At the time of the conference (1979) nearly no information existed on these materials and even nowadays information is only limited. In this respect, I would like to refer to a National Materials Advisory Board Report, NMAB — 376, 1981.

R.Tadros, Ca

In your discussion on material applicability at high temperature you made a statement that ceramic has been considered after the Eutectic material. Can I ask why you have not considered other materials, for example, single crystal?

Author's Reply

I have only addressed he subject of ceramics because this was the main subject of an AGARD SMP specialists' Meeting in Cologne, in 1979. I agree with you that single crystals have a much higher short-term probability of being incorporated in aircraft engines than ceramics. In fact single crystals are now already being used in advanced engines. However, the topic of single crystals was not addressed in great detail during the 10-year period which I reviewed and therefore was outside the scope of the paper. This is somewhat unfortunate.

R.Tadros, Ca

You have made a blunt statement saying that the Safe-Life Approach (SLA) for LCF life estimation should not be used and the Damage Tolerance Approach (DTA) will definitely be the tool to be used. You have focussed on the point that when using the safe-life approach we will be throwing away 999 components in each 1000 lot, therefore it is not cost efficient. I am quite sure that the author realizes that the DTA is based on crack propagation data produced for a certain type of crack, deviation or void, at a certain location and in a certain direction, which is not necessarily representative of actual crack propagation in full-size components exposed to complex stress and temperature cyclic conditions. Unless more representative data are developed and the NDT techniques are developed to identify cracks in the field with a high degree of accuracy, and until one can identify clearly during inspection where to look for cracks (10 locations or 1000 locations), the DTA approach is not safe to use. Adding to that, using the DTA approach you have to control the da/dn curve, and therefore lower stress in components and therefore increasing weight in some cases. Do you know that the DTA approach was not able to detect a crack of 6 inches long due to inability to locate its position? I don't want to sound negative about the DTA approach, but such a statement made can be misleading in many respects. Besides, we are not throwing away 999 components for every 1000. Extensive component and residual life testing prove that large scatter exist in the lifing of components, and that the SLA is sound, safe, and cost-effective.

Author's Reply

Your last argument that a large scatter exists in the life of components is just the reason that the damage tolerance approach has been developed and is considered as a means to much better usage of the real available life of a component and to reduce the cost of ownership of engines. Of course, many problems still have to be overcome before the damage tolerance approach can be fully implemented. Such problems are e.g. (as also stated in the paper) the development of reliable crack detection techniques. As you are aware the USAF and your colleagues of Pratt & Whitney in West Palm Beach are already implementing the damage tolerance approach for the F100 engine. In that case cracks of 0.1 mm should be found with confidence (cryogenic proof tests!).

Furthermore, not only in the damage tolerance approach but also in case of the safe life philosophy you need to know where cracks are likely to develop, otherwise you would base your life prediction approach on locations which are not critical, leading to a higher risk potential in service. It is in fact to the credit of the DTA approach that it explicitly requires the identification of critical areas: this is not the case with the safe life approach as it is currently approached.

A last point is that, with reference to the damage tolerance approach, the questioner stresses the importance of actual crack propagation data in full size components exposed to complex stress and temperature cyclic conditions. However, the generation of life data under actual operating conditions in full size components should be at least as important in the safe life philosophy, whereas current practice shows that life data are mostly based on specimen testing.

T.E.Farmer, US

Could you please briefly explain the difference between the a_m field crack size limit versus the critical crack limit a_c?

Author's Reply

a_c is the critical crack size at which the disc fails in service. a_m is what I call the maximum allowable crack size in service. If a_m is smaller than a_c then this gives a kind of safety factor if one were to allow for only one inspection during the inspection interval indicated in figure 33. In general, however, at least 2 NDI inspections are considered necessary between a_d and a_m. In that case the position of a_m below a_c would represent an additional safety factor, which, however, is of secondary importance to the concept of having at least two inspections.

G.Cailletaud, Fr

I would appreciate your comment on the applicability of the creep-fatigue rupture prediction methods that you have presented, in the case of multi-axial, eventually out-of-phase loading.

Author's Reply

The problem of multi-axial fatigue is a very complex one. A literature survey on this subject and some considerations regarding multi-axial failure laws were presented in the paper of Krempl (see reference 47 of the paper).

G.Cailletaud, Fr

In my opinion, it is important to note that there exists some alternative methodology for these predictions: Continuum Damage Mechanics has now been developing for at least 15 years and has showed its efficiency to predict the life of specimens or components in complex creep fatigue operating conditions.

Author's Reply

I am not sure what you mean by 'Continuum Damage Mechanics'. However, I can say that fracture mechanics may be a tool for lifing of components. In that case we think about the crack propagation stage of life only. The crack nucleation phase cannot be predicted by fracture mechanics. The present lifing procedures in the safe life philosophy account for the crack nucleation phase and the phase of early crack formation until a 'detectable' crack has been developed.

COMPARISON BETWEEN THE PROPERTIES OF CONVENTIONAL WROUGHT AND POWDER METALLURGICAL ALLOYS FOR TURBINE DISC APPLICATIONS

by

G.W. König

Materials Laboratory

MTU

8000 Munich 50

West Germany

SUMMARY

Mechanical properties of powder-metallurgical nickel-base superalloys (e.g. U700PM; René 95) were evaluated in order to predict the behaviour of advanced aero-engine discs in comparison with conventional wrought nickel-base (e.g. Waspaloy; IN 718) discs. The assessment includes tensile strength, crack initiation and propagation fatigue life as well as the influence of mean stress. Special emphasis was put on the question about the scatter in fatigue lives resulting from defects in the material (e.g. oxide inclusions) and on the surface (e.g. grooves). The tolerance with respect to these defects was estimated on the basis of fracture mechanics methods.

1. INTRODUCTION

The development of advanced turbine engines with improved engine thrust and fuel economy has increased the demand for turbine disc materials with improved strength and fatigue properties at high temperatures.Pronounced segregation and limited forgeability make it difficult to utilize conventional wrought nickel-base alloys with high alloying content. One way to overcome these difficulties are powder metallurgical (PM) alloys where prealloyed atomized superalloy powders are consolidated by hot isostatic pressing (HIP)[1] which may be followed by forging.This paper discusses some aspects related to the potential and the limitations of PM nickel-base alloys for aero-engine disc applications.

2. TENSILE STRENGTH

Fig. 1 represents typical curves of the yield stress as a function of temperature for conventional wrought as well as PM alloys. From the diagram it is obvious that the potential in tensile strength up to high temperatures of the PM alloys (AP1 and René 95) is equal or superior compared with the two conventional alloys (Waspaloy and IN718) which are in wide use today. Important microstructural features responsible for the higher strength are a larger amount of the precipitation hardening phase γ' ($(Ni_3(Al, Ti))$ and a finer grain structure. Waspaloy contains only about 20 volume percent of γ', while high-strength alloys such as René 95 contain more than 50 volume percent.The fine grain structure (compare Fig. 2) of high-strength alloys usually leads to a rather homogeneous structure and a small scatter in the monotonic tensile material data.

3. STRESS-STRAIN CHARACTERISTICS

The effect of the material strength on the cyclic stress-strain characteristics can be observed by comparing the behaviour of Waspaloy and René 95 (Fig. 3) in strain controlled tests (strain ratio $R = \varepsilon_{min} / \varepsilon_{max} = 0$). For René 95 the stress range follows the elastic straight line up to high strain ranges and the maximum stress curve is at a significantly higher level than for Waspaloy. The consequence is an appreciable higher mean stress at a given imposed strain range for the high-strength alloy.

4. CRACK INITIATION LIFE

The different mean stress characteristic is also reflected in the crack initiation life behaviour.It is generally found[2] that strain controlled smooth specimen tests yield superior fatigue properties with increasing material strength (Fig. 4).The advantage decreases with decreasing fatigue life (i. e. at high loads). At very short lives the ranking usually becomes reversed. Information about the effect of mean stress on fatigue life can be obtained from a comparison between the curves of strain ratio 0 (including tensile mean stress) and -1 (no mean stress).Due to the larger mean stress the loss in fatigue life is much higher for René 95 than for Waspaloy. In consequence, the advantage of high-strength materials with respect to crack initiation life is somewhat diminished when tensile mean stresses (which actually occur at critical sites of engine components due to operating and residual stresses) are taken into account. High strength alloys, on the other hand, have a large potential of improvement by producing compressive residual stresses on purpose (for example by shot peening or cold expansion of holes). Similar to strain controlled test data, improved fatigue performance with increasing strength is also found in stress controlled tests with smooth specimens (Fig. 5).

5. CRACK PROPAGATION LIFE

Contrary to the crack initation behaviour, a completely different situation is envisaged when the crack propagation behaviour is considered[2,3,4] (Fig. 6):At high temperatures the crack propagation rate of high-strength alloys is significantly higher compared with materials of less strength. One important reason for this is the enhanced tendency to fast intergranular crack propagation when the grain structure gets finer. This effect becomes even more pronounced when the loading includes a dwell period. At lower temperatures and high loading frequencies, on the other hand, the linear part of the crack propagation rate-stress intensity curve of different nickel-base alloys is often found to fall into a single scatter band.

In summary, high-strength nickel-base alloys offer clear advantages with respect to monotonic tensile properties and to fatigue crack initiation life under stress control as well as under strain control at low strain ranges, whereas there is no advantage with respect to the fatigue life at high strain ranges and to the crack propagation life.Since the useful life of most aircraft discs is limited by fatigue, it is important for the assessment of disc alloys to know whether the favourable or detrimental effects are prevailing under service conditions.

6. FATIGUE LIFE AT HOLES

The most common feature to produce high strain ranges in discs are notches, such as bolt holes, cooling holes or blade slots.A suitable way to obtain material data for the behaviour of this type of notches are tests using specimens with an internal hole. Fig. 7 shows that there is no appreciable difference in the fatigue lives between nickel-base alloys of different strengths. Though the statistical basis of these measurements is too small to justify far-reaching conclusions, the results suggest that the advantage of high-strength alloys for notched structures is less than for smooth structures under conditions when high local strain in the notch root occurs.

7. EFFECT OF SMALL DEFECTS ON FATIGUE LIFE

7.1 INHERENT MATERIAL DEFECTS

An important source of high (local) strain range and reduced crack initiation life are small defects which may occur in the material (as from inclusions[5-13]), segregations, pores[14] etc.) or on the surface[15] (machining marks, scratches, etch pits etc.). Fig. 8 shows as an example of inherent material defects a nonmetallic inclusion of about 200 microns diameter in the neighbourhood of an eccentric hole of a model disc. The effect of the defect was a significant decrease in the crack initiation life of the disc in a cyclic spin test and the shift of the crack initiation site away from the more severely loaded root of the eccentric hole.
The development of modern PM-alloys has been successful in limiting the concentration of defects such as inclusions to a very low level. This is the reason why the chance of getting information about the influence of inclusions on fatigue life by investigating a comparatively small volume of specimens and components with standard material quality is rather limited. In engineering practice, however, the safety of a very large number (and hence volume) of components has to be guaranteed. Due to the size effect the likelihood of failures at defects increases with the volume. Thus the assessment of the risk caused by defects at critical sites of components requires the knowledge of a) the type, concentration, size and shape of all potentially harmful defects, and b) the effect of these defects on the mechanical properties under service loading conditions.

An effective method to determine the effect of inclusions on fatigue life are tests with specimens which are deliberately provided with defects. As an example, Fig. 9 shows results of fatigue tests performed with PM-specimens which were doped before hipping with nonmetallic inclusions of different types and sizes. It is clearly visible that the inclusions result in a reduction of the fatigue strength. The results refer to near-surface defects. Defects in the interior were also found to decrease fatigue life but to a less degree.

One observation of these doping experiments was that at high-stress ranges inclusions virtually eliminate the crack initiation stage such that the fatigue life nearly coincides with the pure crack propagation life. Fig. 10 represents a fracture mechanics simulation of the propagation behaviour of a crack with an initial size and shape similar to the nonmetallic inclusion shown in the micrograph. The life increment between two half-ellipses in the diagram is 1000 cycles. The predicted crack propagation life is in good agreement with the total experimental fatigue life. As demonstrated in Fig. 11, the strain-life curve of a doped PM-alloy can be fairly well predicted by the crack propagation life curve obtained from fracture mechanics. It is important for economical reasons that the detrimental effect of defects is significant only when a certain minimum size is exceeded. This minimum size depends on the material and on the loading conditions and can be estimated by fracture mechanics[8].

7.2 SURFACE DEFECTS

An important origin of small harmful defects are surface marks inadvertantly produced by machining or handling. The effect of a small groove on the fatigue life of a turbine disc is illustrated by the following case history. A turbine disc of the PM-alloy U 700 was tested in a laboratory cyclic spin test until bursting occurred after 3100 cycles. The experimental life was less than one-third of the life predicted on the basis of smooth specimen material data. Failure analysis revealed that the failure was due to a fatigue crack starting from a groove in the disc bore (Fig. 12). The depth of the groove is about 35 microns. In order to evaluate the effect of grooves of this size fatigue tests were performed using round bar specimens with a circumferential machining groove (Fig. 13). The tests were performed under conditions similar to the strain in the disc bore during the cyclic spin test.The life of the grooved specimen was found to be in good agreement with the disc life (Fig. 14). To investigate the influence of the choice of the material similar tests were performed with alloys of different strengths. As expected, the smooth specimen life which is dominated by the crack initiation portion increases appreciably with growing yield stress. The life of the grooved specimens, on the other hand, where the crack propagation life range is prevailing, shows a much less influence of yield stress and even tends to decrease when yield strength increases(Fig. 14).

8. SCATTER IN FATIGUE LIFE

The weak sensitivity of the crack propagation behaviour (excluding the range of high temperatures and long dwell times where time-dependent processes become important) and strong sensitivity of crack initiation behaviour to material strength has an important influence on the scatter in fatigue life. This is schematically illustrated by the stress-life curves in Fig. 15. The diagram is based on the assumption that the materials contain a defect population with a maximum defect size of 0,1 mm. This maximum defect size roughly defines a single minimum life curve for all alloys considered. The level of the upper limit of the scatter band is strongly raised with increasing strength of the material leading to a broadening of the scatter band. Fig. 16 shows an example of the large scatter band found with the PM-alloy APl. It is important to note that the increase in scatter of high-strength materials is primarily caused by an extension of the scatter band to long lives while minimum life depends solely on the maximum defect size. This is the reason why the treatment of the scatter by applying symmetrical distribution functions may lead to wrong conclusions. Fig. 17 shows a statistical evaluation of LCF results in a logarithmic Gaussian plot. Though all measured points of René 95 are to the right of those of MTS 1024, the extrapolation to a small probability of failure gives preference to René 95. Actually, the defect size and distribution in both alloys were about the same and so the minimum life curves are also expected to be roughly the same.

9. USABLE LIFE

Most of the methods which are currently used for the design of engine discs are based on a safe life approach, where the safe life is determined from a statistical evaluation of the crack initiation behaviour in specimen and component tests as well as from the experience in service. With increasing stress crack propagation life becomes more and more important and the safe life is no longer related to the crack initiation life determined with defect free test pieces but primarily to mechanical laws governed by the defect structure and loading conditions. This calls for new design methods[16-20] as well as criteria for the selection and development of materials based on fracture mechanics, defect tolerance and volume dependent failure propability.

The influence of the material production process on the minimum fatigue life is due to the variations in type, size, shape and population of the resulting defects. In this respect materials produced by hipping offer obvious advantages because gross defects such as segregations or forging cracks can be avoided. Techniques such as water elutriation result in a very high purity level. By screening of the powders the maximum foreign particle size can be limited to diameters which are well below 100 microns and a high standard of the homogeneity as well as the fineness of the microstructure leads to increased capabilities to find small defects by non destructive testing.
However, even if it would be possible to cope with the problem of detrimental inherent material defects, the difficulty with inadvertant surface marks as life limiting defects remains. Anyhow, the future progress in increasing the safe live of disc materials will be decisively influenced by the maximum defect diameter that can be warranted at critical sites of components.

An alternative approach to safe live design is the "life on condition" or "retirement for cause" concept[21,22]. According to this concept, components are kept in service until a defect is indicated by non destructive testing. Under these circumstances the useful life is given by the individual life of each component. It is evident that this concept favours materials with long mean fatigue life such as high-strength PM-alloys. High operating stresses, on the other hand, result in short crack propagation lives and short critical crack lengths for failure. The consequences are large expenditures for inspections. Thus there is an optimum stress level, where the retirement for cause concept yields maximum gain.

10. CONCLUDING REMARKS

The potential of advanced nickel-base superalloys with respect to static strength and fatigue life is superior to that of currently used conventional wrought disc materials. It has been shown that the most important requirement for the use of this fatigue potential is a high quality standard which limits the maximum size of defects both in the material and on the surface. The now available knowledge of the variables influencing the reliability of disc materials enables an optimization to obtain improved service behaviour. Furthermore, the strength and quality of materials as well as the manufacturing process can be fitted to the requirements of each type of component.

11. REFERENCES

1) Symonds, C.H., Eggar, J.W., Lewis, G.J., Siddal, R.J.: Properties and structures of hot isostatic pressed and hot isostatic pressed plus forged superalloys; powder metallurgy international 1 (1983) 30-35.

2) Cowles, B.A., SIMS, D.L., WARREN, J.R., Miner, R.V.: Cyclic behaviour of turbine disk alloys at 650°C. Journal of engineering materials and technology, 102 (1980) 356-363

3) Gayda, J., Miner, R.V.: Fatigue crack initiation and propagation in several nickel-base superalloys at 650°C; Int. J. Fatigue; Vol 5; 3 (1983) 135-143

4) Gayda, J., Miner, R.V.: The effect of microstructure on 650°C fatigue crack growth in P/M Astroloy; Met. Trans. 14 A (1983) 2301-2308

5) Jablonski, D.A.: The effect of ceramic inclusions on the low cycle fatigue life of low carbon astroloy subjected to hot isostatic pressing, materials science and engineering, 48 (1981) 189-198

6) Betz, W., Track, W.: Structural defects govering the potential use and limitations of powder metallurgy nickel base materials, 109th AIM annual meeting, Las Vegas, (1980)

7) Law, C.C., Blackburn, M.J.: Effects of ceramic inclusions on fatigue properties of a powder metallurgical nickel-base superalloy, proceedings of the 1980 international powder metallurgy conference, Washington D.C.

8) König, G., Track, W., Betz, W.: Assessment of the LCF behaviour of a PM nickel-base alloy for turbine disk application, metal powder report, 38 (1983) 19-25

9) Betz, W., Track, W.: Living with defects in powder metallurgy materials; Powder metallurgy international Vol. 13, 4 (81) 195-198

10) Hicks, M.A., Newley, R.A., Towill, B.P.: The cyclic behaviour of powder Ni-base superalloys; in: Proceeding of the twelfth international committee on aeronautical fatigue held at Toulouse, France, May 1983, Centre d'Essais Aeronautique de Toulouse.

11) Hyzak, J.M., Bernstein, I.M.: The effect of defects on the fatigue crack initiation process in two P/M superalloys: Part I, fatigue origins; Met. Trans 13A (1982) 33-43

12) Hyzak, J.M., Bernstein, I.M.: The effect of defects on the fatigue crack initiation process in two P/M superalloys: Part II, surface-subsurface transition, Met. Trans 13A (1982) 45-52

13) Tompson, F.A., Cutler, C.P., Sidall, R.J.: The influence of inclusions on the low cycle fatigue properties of the nickel-based superalloy APK1 produced via the powder route; in proc. 108th AIME annual meeting, New Orleans (1979)

14) Miner, R.V., Dreshfield, R.L.: Effects of fine porosity on the fatigue behaviour of a powder metallurgy superalloy; Met. Trans. 12A (1981) 261-267

15) König, G.W.: Fracture mechanics analysis of the influence of machining marks on the LCF life of the nickel-base alloy IN 718; intended to be presented on the 5th European conference on fracture, Lisbon (1984)

16) Huff, H., König, G.: Damage tolerance of aero-engine disks; in proceeding of the twelfth international committee on aeronautical fatigue held at Toulouse, France, May 1983, Centre d'Essais Aeronautique de Toulouse

17) Eßlinger, P.: Bewertungskriterien für Werkstoffe des Flugtriebwerkbaues; Metall, 36 (1982) 654-659

18) Jeal, R.H.: Defects and their effect on the behaviour of gas turbine disks; in: Maintenance in service of high temperature parts, AGARD-CP-317, 1982

19) Cruse, T.A.: Engine components; in: Practical application of fracture mechanics, AGARD-AG-257, 1982

20) Hoepner, D.W.: Application of damage tolerance concepts to "short cracks" in safety critical components; in: Proc. of the 12th international committee on aeronautical fatigue held at Toulouse, France, May 1983, Centre d'Essais Aeronautique de Toulouse

21) Harris, Jr. J.A., Amnis, JR.C.G., Vanwanderham, M.C., Sims, D.L.: Engine component retirement for cause;
in: Maintenence in service of high temperature parts, AGARD-CP-317, 1982

22) Bergmann, J., Operparleitner, W., Schütz, W.:
Retirement for Cause-Beschreibung und Bewertung des Verfahrens; IABG-Report TF-1420

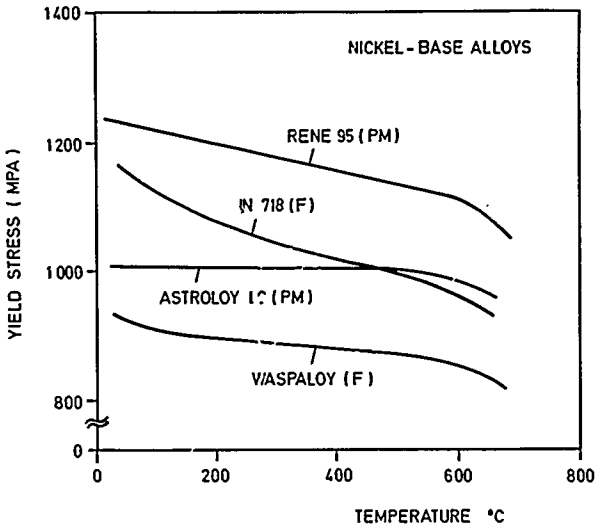

Fig. 1 Yield strength of conventional forged (F) and powdermetallurgical (PM) nickel-base alloys

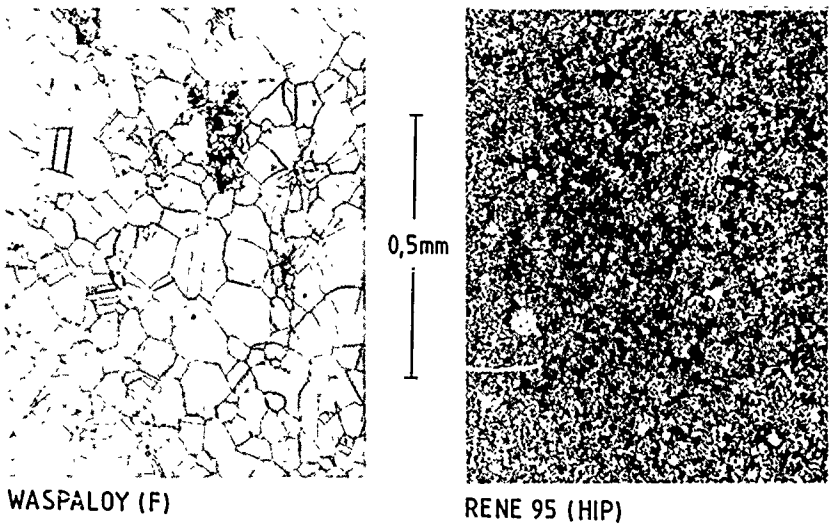

Fig. 2 Microstructure of Waspaloy and Rene 95

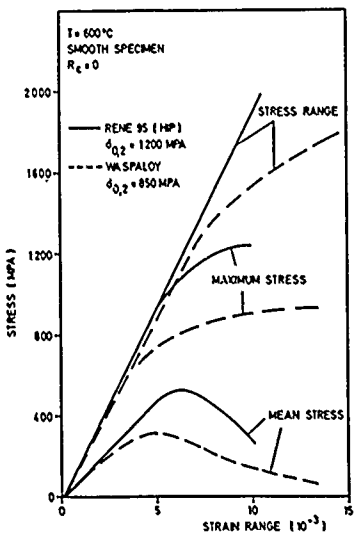

Fig. 3 Cyclic stress-strain curves of Waspaloy and Rene 95

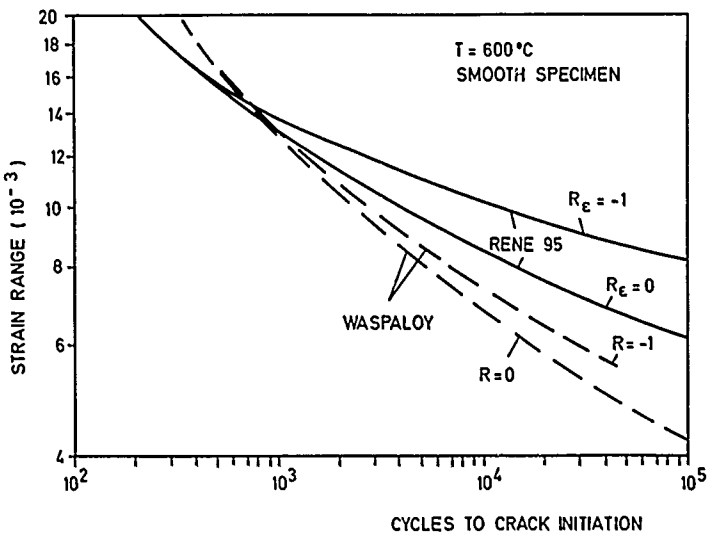

Fig. 4 cyclic strain-life curves of Waspaloy and Rene 95

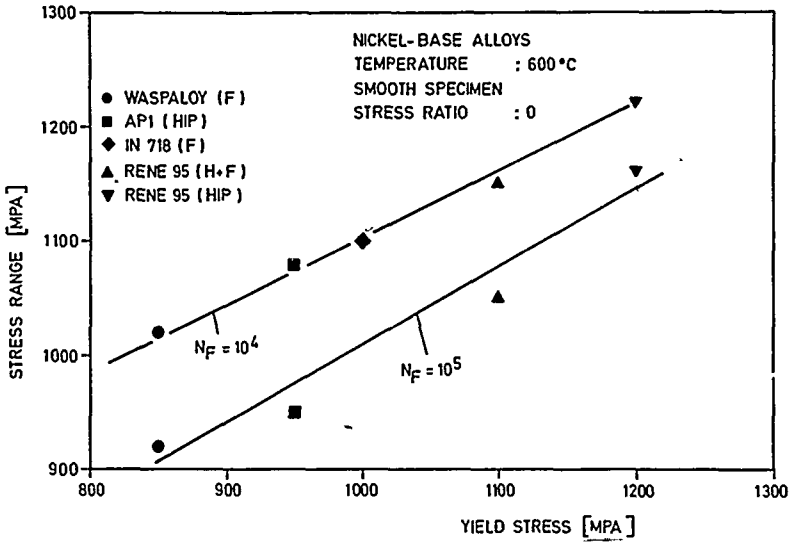

Fig. 5 Increase in fatigue strength (N_F indicates the cycles to fracture) with growing yield stress

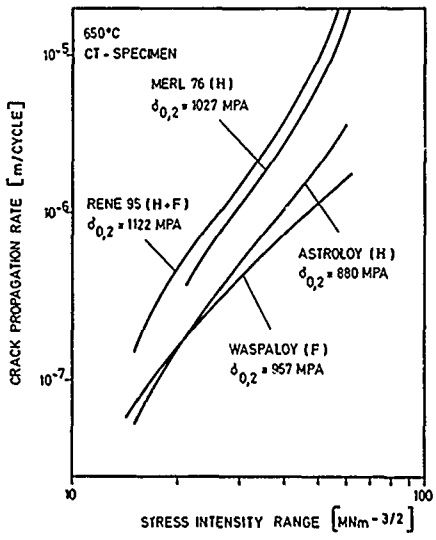

Fig. 6 Crack propagation behaviour of nickel-base alloys of different strength (from Gayda and Miner[3])

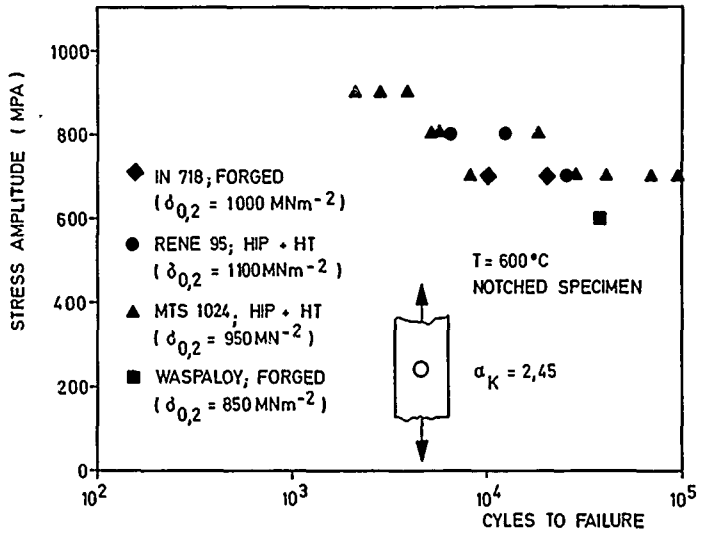

Fig. 7 Fatigue life of notched specimens

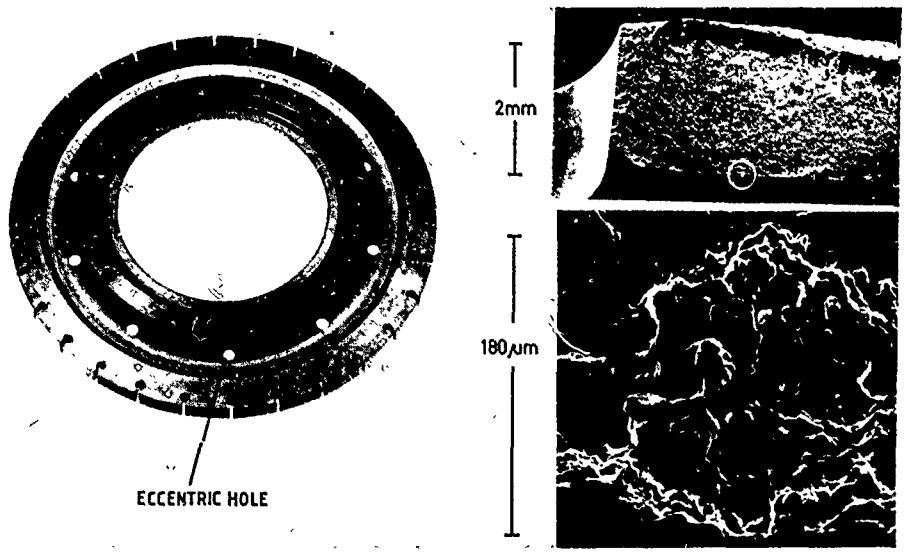

Fig. 8 Crack initiation at a nonmetallic inclusion 2 mm distant of an eccentric hole of a model disc[16)]

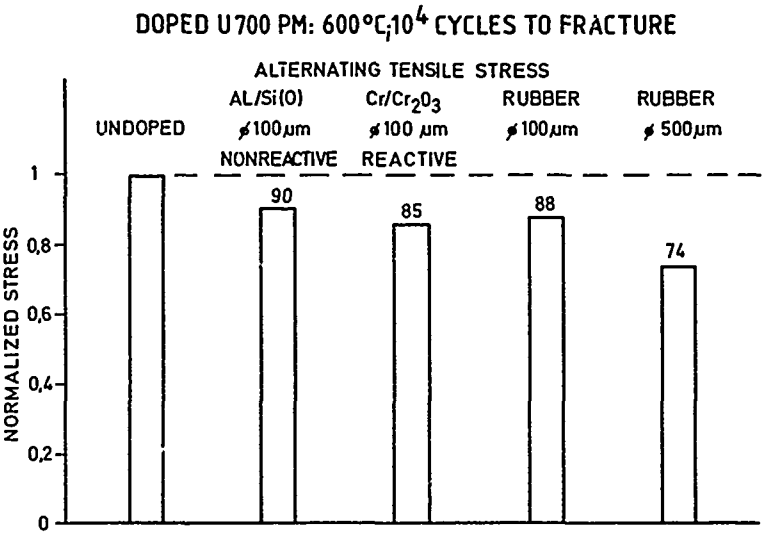

Fig. 9 Effect of doping particles on fatigue strength

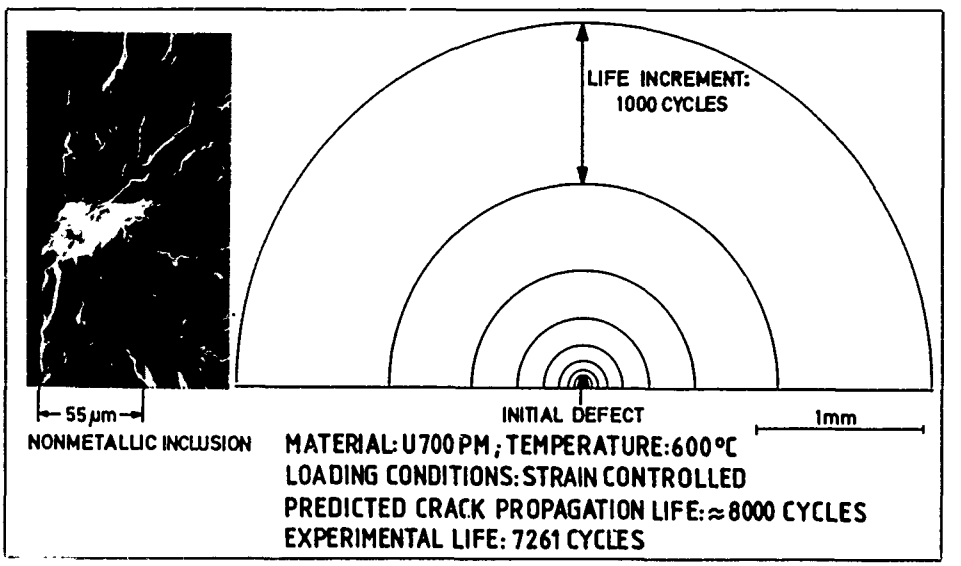

Fig. 10 Simulation of the propagation behaviour of a crack initiated at an inclusion

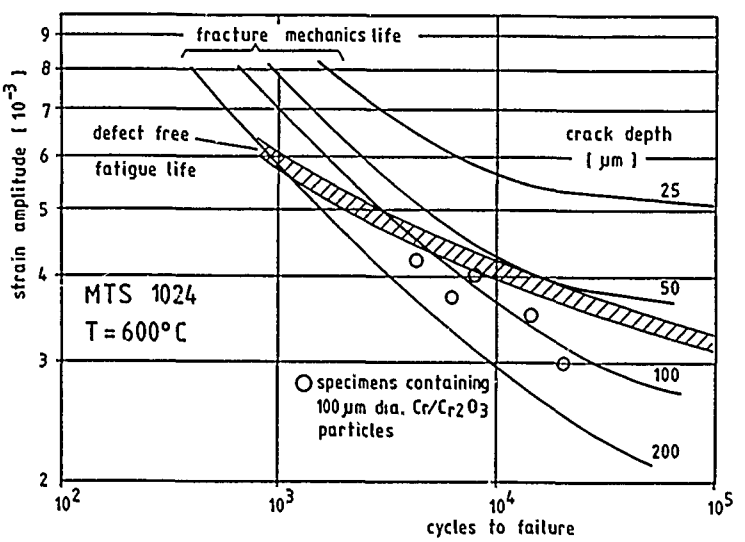

Fig. 11 Comparison of calculated and observed effects of inclusions on fatigue life[8)]

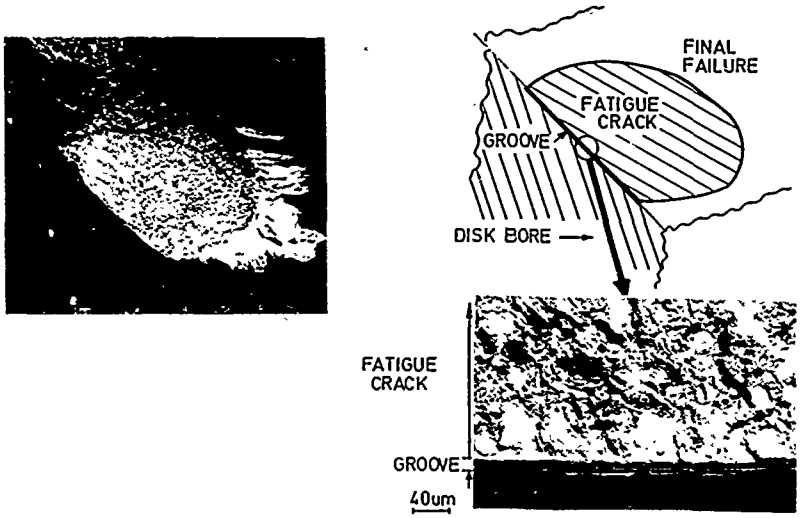

Fig. 12 Fatigue crack starting at a groove[15)]

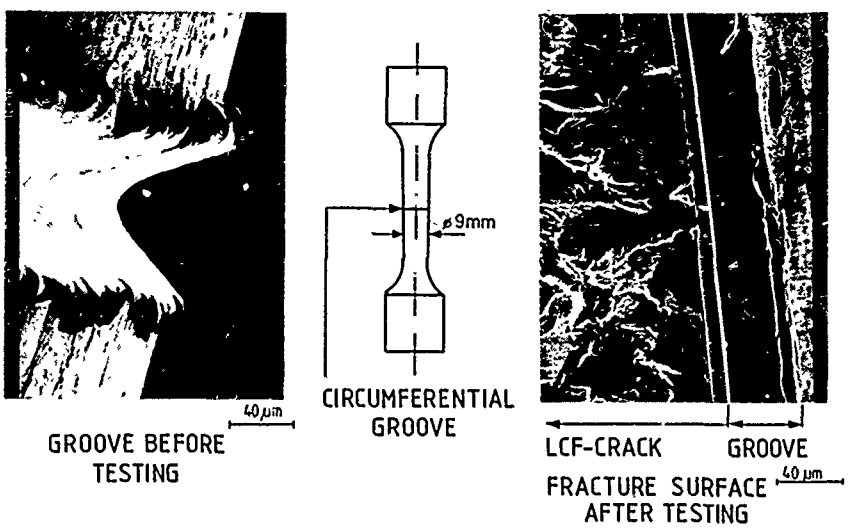

Fig. 13 Round bar specimen with circumferential groove[15)]

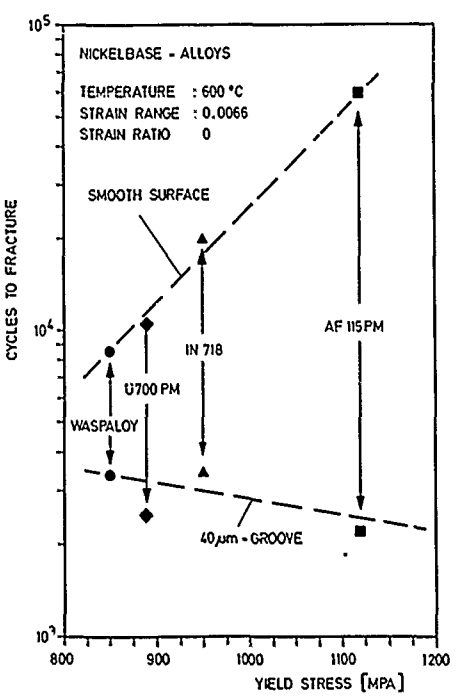

Fig. 14 Effect of a 40 microns deep groove on fatigue life[15)]

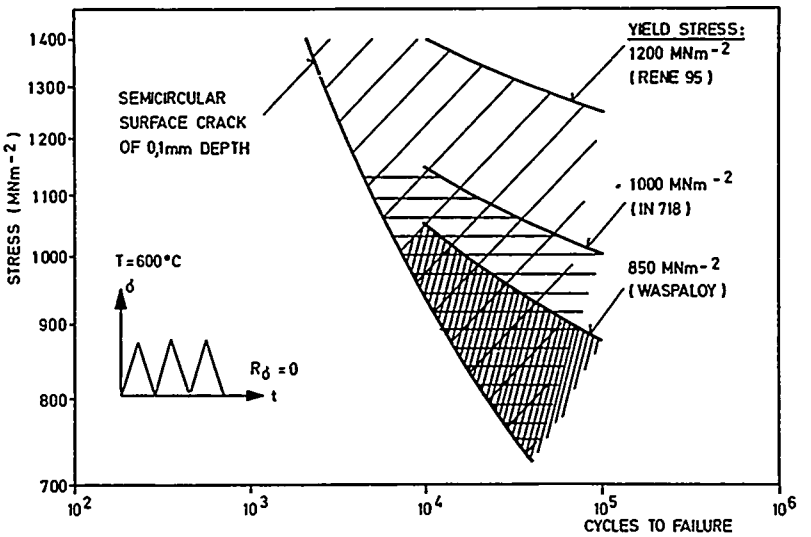

Fig. 15 Scatter in fatigue lives resulting from a defect population with a maximum size of 0,1 mm (schematic).

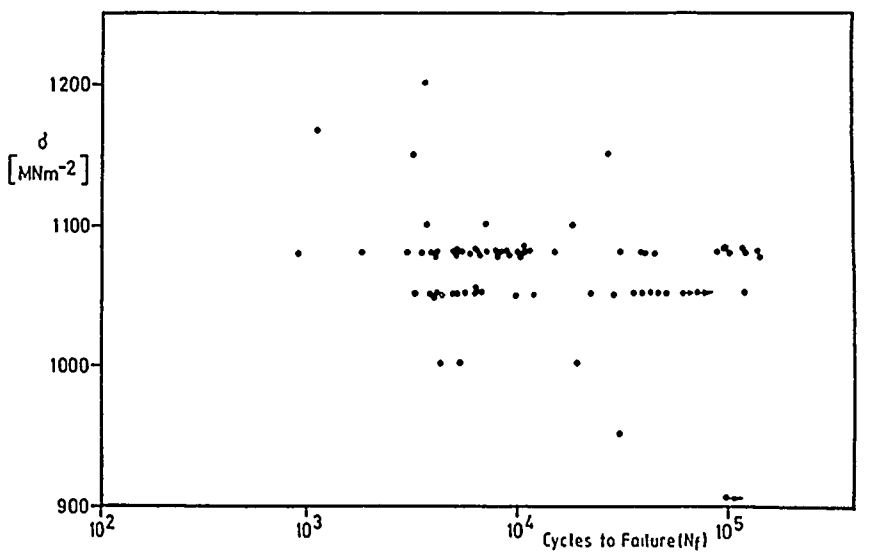

Fig. 16 Scatter in fatigue lives found with AP1[9] including both undoped and doped (maximum foreign particle diameter: 400 microns) specimens

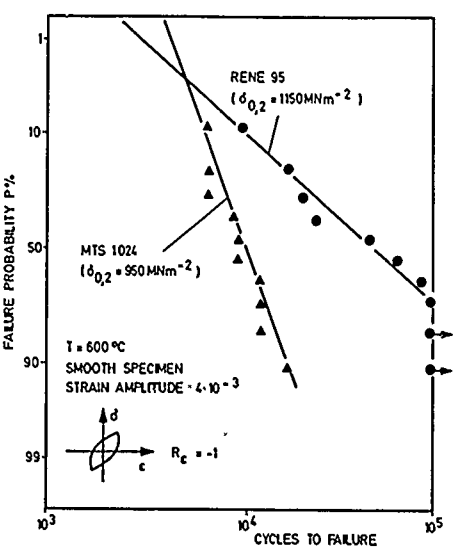

Fig. 17 Statistic evaluation of fatigue tests performed with MTS1024 (similar to AP1 or U700 PM) and René95.

DISCUSSION

M.Y.Nazmy, Switzerland

I would like to address the problem of crack propagation. Do you believe that it is legitimate to use crack propagation data, obtained by testing of CT specimens, to predict lives of components that have about 50 microns size inclusions or grooves.

Author's Reply

It is well known that, at given stress intensity range, small defects and large cracks may behave quite differently. This is the reason why fatigue tests were performed using specimens with small defects of technical relevant sizes located in the interior (e.g., inclusions) or on the surface (e.g., grooves or 'thumbnail' cracks). The results of these tests were compared with the fracture mechanics prediction based on CT-specimen data. It was found that there is a good agreement between the crack propagation rate of CT-specimens and of small cracks larger than 100 microns. Below a crack depth of 100 microns the applied methods (potential drop, striation count) were unable to monitor the crack propagation rate. In these cases the experimental life was compared with the predicted crack propagation life. It was always found that the experimental life is about equal or larger (due to incubation processes) than the predicted life. Thus, fracture mechanics is able to give a conservative estimate of the fatigue life of a defective component. These results refer to fine-grained (grain size smaller than the defect size), high-strength nickel-base alloys and should not be extrapolated to coarse-grained materials.

RESISTANCE A LA PROPAGATION DE FISSURES DE L'ALLIAGE INCONEL 718

L. PORET (1) - J.Y. GUEDOU (1) - A. PINEAU (2)

(1) S.N.E.C.M.A. Laboratoire des Matériaux et Procédés - B.P. 81
91003 EVRY Cedex - FRANCE

(2) Ecole des Mines de PARIS - Centre des Matériaux - B.P. 87
91003 EVRY Cedex - FRANCE

RESUME

La résistance à la propagation de fissures a été étudiée sur diverses nuances d'alliage INCONEL 718 à haute température (550 - 650° C) en fatigue, fluage et fatigue-fluage. Les essais ont été effectués sous vide et à l'air. Une sensibilité notable aux effets de temps de maintien a été observée. Elle dépend de la microstructure de l'alliage (distribution des carbures, taille et forme des grains, présence ou non de la phase β, écrouissage) ainsi que des effets dus à l'oxydation. Les données de base relatives aux vitesses de propagation ont été appliquées à un disque d'essai sur lequel un amorçage prématuré a conduit à la propagation d'une fissure jusqu'à rupture. A partir d'un calcul de contraintes par éléments finis, l'utilisation des courbes obtenues par essais sur éprouvettes, dans des conditions représentatives des sollicitations de la pièce, a permis de rendre compte des observations expérimentales (nombre de cycles de propagation déterminés par comptage de stries).

INTRODUCTION ET PRESENTATION DE L'ETUDE

Le premier souci des motoristes concernant les alliages pour disques, est d'améliorer leur tenue à l'amorçage des fissures provoquées par des sollicitations de fatigue oligo-cyclique. Cela a conduit les métallurgistes à développer des nuances de superalliages à base de nickel à haute limite d'élasticité, et dotées de caractéristiques en fatigue oligocyclique élevées jusqu'à des températures de l'ordre de 650° C. Alors que de nouvelles nuances sont en voie de développement rapide, l'alliage forgé INCONEL 718 (NC 19 FeNb), mis au point depuis une vingtaine d'années, reste encore largement employé. Le travail présenté dans cette étude concerne précisément cet alliage.

La première partie est consacrée à l'étude expérimentale de la propagation des fissures de fatigue à haute température (550° - 650° C) et à la présentation de résultats récents concernant l'influence de la structure métallurgique de cet alliage. Dans cette partie, nous avons rassemblé un grand nombre de résultats expérimentaux publiés dans la littérature, en mettant plus particulièrement l'accent sur l'effet d'un temps de maintien à 650° C. On observe en effet, comme cela est illustré par la figure 1, que l'examen des données publiées et rassemblées en (1) fait ressortir une "dispersion" très importante. Nous montrerons qu'une large partie de cette dispersion doit être attribuée à des effets microstructuraux et à l'influence de l'environnement.

A cause de cette dispersion, le calcul de la propagation d'une fissure éventuelle dans un disque se trouve entaché d'une forte incertitude. Nous montrerons cependant dans la deuxième partie que ce calcul peut être mené avec une bonne précision à condition d'utiliser les courbes représentatives de la matière employée pour une fabrication spécifique. Cette illustration est faite à propos du calcul d'un disque d'essai.

1 - RESULTATS EXPERIMENTAUX

Comme nous l'avons indiqué précédemment, l'alliage base nickel INCONEL 718 a fait l'objet de nombreuses études. Il a en particulier été largement caractérisé en propagation des fissures dans différentes conditions. La figure 1 regroupe les résultats de la littérature recensés par A. PINEAU (1), concernant des essais de fissuration en fatigue continue, d'une part à froid, d'autre part à 650° C, température limite d'emploi de ce matériau. Les résultats à la température ambiante présentent sans doute une certaine dispersion, mais celle-ci est faible en comparaison des écarts relevés à chaud : pour une valeur de ΔK comprise entre 20 et 40 Mpa $\sqrt{m}$, les vitesses de fissuration mesurées à 650° C peuvent varier de deux ordres de grandeur. Une telle imprécision apparaissant dans le domaine d'emploi du matériau, mérite un examen approfondi afin de réduire les incertitudes qui en résultent pour les calculs de fissuration sur pièce.

Cette dispersion des résultats, mise en évidence essentiellement à chaud, peut être imputable en premier lieu à des écarts dans la structure métallurgique de l'alliage. On constate en effet, dans les cas où le matériau utilisé est décrit, que les différentes études ont été réalisées sur des microstructures non semblables. La taille de grain, la répartition des précipités et des carbures en particulier, interviennent sur les caractéristiques du matériau.

L'influence de la microstructure a été étudiée à partir d'essais réalisés sur trois structures différentes obtenues dans un même lot matière, par des traitements thermomécaniques appropriés : une structure à grains fins (6 à 8 ASTM), une structure à gros grains (3 à 4 ASTM) et une structure duplex à collier constituée de gros grains (3 à 4 ASTM) entourés de plus petits (6 à 8 ASTM). Ces trois alliages, de même composition chimique, présentent des caractéristiques de traction différentes comme l'indique le tableau I : la structure à grains fins offre les caractéristiques les plus élevées, celle à gros grains les plus faibles.

Les résultats de fissuration à 650° C (2) sont présentés sur la figure 2. La figure 2.a reproduit les résultats obtenus à l'air en fatigue continue (fréquence 20 hz) et en fatigue-fluage (cycle trapèzoïdal 10 s - 300 s - 10 s). A fréquence élevée (20 hz), les trois microstructures conduisent à des vitesses de fissuration sensiblement identiques. Par contre, lorsqu'un temps de maintien (300 s) est superposé à charge maximale au cycle lent de fatigue (cycle triangulaire 10 s - 10 s), la structure en collier présente une résistance à la propagation de fissures nettement meilleure. La structure à grains fins, dont les caractéristiques de traction sont voisines de la précédente, conduit à des vitesses de propagation supérieures de plus d'un ordre de grandeur. Par ailleurs, les essais menés sur des éprouvettes prélevées dans deux sens métallurgiques différents, font apparaître la sensibilité des caractéristiques de fissuration à l'anisotropie du matériau.

Des écarts identiques entre les trois microstructures sont également observés sur des essais de fluage pur (figure 2.b) réalisés à l'air.

La similitude entre les résultats de fatigue-fluage (10 s - 300 s - 10 s) et ceux de fluage à 650° C suggère qu'un temps de maintien long fait intervenir des mécanismes essentillement contrôlés par le temps, du même type que le fluage ou l'oxydation. Lorsque les essais de fatigue-fluage sont conduits sous vide (5.10^{-6} Torr), cet effet de microstructure disparaît presque totalement (figure 2.c) et les vitesses de fissuration mesurées diminuent considérablement, pour un même type de chargement. Il apparaît donc nettement que l'environnement joue un rôle très important dans la propagation des fissures à chaud du matériau. Cet effet se traduit par une fragilisation des joints de grains par l'oxygène, ce qui conduit à des faciès de rupture intergranulaire.

La figure 3 présente, pour une valeur de ΔK fixée (20 MPa $\sqrt{m}$) les vitesses de fissuration mesurées à deux températures pour des cyclages de période plus ou moins longue, en fonction de cette période. Les données sont issues de résultats de la littérature (1). On observe sur ce diagramme que l'accroissement des vitesses de fissuration résultant d'un temps de maintien sous charge, s'accompagne du passage à un mode de fissuration intergranulaire. La transition a lieu pour un cycle de 10 s à 550° C, et elle apparaît avant 1 s à 650° C. De même, l'augmentation des vitesses de fissuration est beaucoup plus importante à 650° C qu'à 550° C. Pour une période supérieure à 10 s, la vitesse est sensiblement proportionnelle à la période, ce qui signifie que la propagation des fissures dans ces conditions, est essentiellement régie par le temps.

Cet examen des données expérimentales fait clairement ressortir l'importance des facteurs métallurgiques et de l'environnement. Par ailleurs, il montre également la nécessité de prendre en compte l'influence de la période et du temps de maintien à charge maximale.

2 - CALCUL DE LA FISSURATION DANS UNE PIECE ROMPUE EN ESSAI

L'utilisation des données de base relatives aux vitesses de propagation est illustrée par l'analyse de la rupture d'un disque d'essai et la simulation numérique de la fissuration (3).

2.1. Analyse de la rupture d'un disque d'essai

Les résultats d'essais sur éprouvettes sont utilisés en premier lieu dans le calcul de durée de vie des pièces. Toutefois, des essais au banc sur disque sont réalisés pour reproduire des effets qui ne sont pas restitués sur éprouvettes :

. sollicitations d'un volume de matière important, ce qui est particulièrement intéressant dans les études de dispersion (métallurgie des poudres)

. représentativité des états de contraintes dans les disques (biaxialité, gradients dans les zones à forte épaisseur...)

Un disque d'essai en INCONEL 718, de taille de grain moyenne 30 à 50 µm (6 ASTM), a subi des cycles de fatigue oligocyclique à 550° C en fosse de survitesse. La variation des contraintes est réalisée par cyclage des vitesses de rotation entre 1500 et 24700 tr/mn (fig. 4). Ce disque est instrumenté de thermocouples soudés sur un dépôt de plasma et démontés avant essai. Un contrôle périodique est prévu en cours d'essai. Le disque a effectué 16160 cycles avant éclatement.

L'expertise a montré que la crique ayant conduit à la rupture s'est amorcée sous une bande de plasma d'épaisseur insuffisante, à l'aplomb d'un point de soudure électrique nécessaire au maintien des pontets métalliques qui assurent le cheminement des fils d'instrumentation. La propagation s'est effectuée suivant un plan radial, comme le montre la figure 5. Une analyse microfractographique de la cassure a mis en évidence plusieurs zones semi-circulaires :

. une zone directement affectée par la soudure ($r < 0.2$ mm)
. une zone dentritique où le matériau fondu s'est resolidifié ($0.2 < r < 0.3$ mm)
. une zone affectée thermiquement, avec un faciès de rupture fragile ($0.3 < r < 0.36$ mm)
. la matrice

Les mesures de microdureté effectuées dans la zone endommagée (fig. 6) montrent que les propriétés mécaniques du matériau sont affectées sur une profondeur de 0.8 mm environ, qui est supérieure à celle de la zone affectée thermiquement.

A partir de ces observations, il a été tenté de reconstituer la fissuration du disque. L'objet de cette estimation est d'établir la courbe qui relie le nombre de cycles réalisés N à la profondeur de fissure a mesurée sur la pièce. La méthode consiste à corréler les comptages de stries sur le disque et sur une éprouvette de type CT prélevée dans le disque, soumise à un chargement similaire et avec laquelle une courbe de fissuration $\frac{da}{dN}$ (ΔK) a été tracée.

Les mesures d'interstries sur la cassure ont été effectuées au microscope électronique à balayage. La courbe interstrie-profondeur fissurée i(x) présente une certaine dispersion dans les premiers millimètres de fissuration (fig. 7) : cela est dû à la difficulté de mesurer l'interstrie dans une zone très perturbée proche du point de fusion.

Afin de corréler avec précision les mesures d'interstrie et la vitesse de propagation, une éprouvette de type CT a été prélevée dans le disque suivant un plan de propagation radial, à une distance de l'alésage proche du rayon de la zone critique : cela assure une structure très proche de celle du disque dans la zone de propagation et on peut estimer obtenir, dans ces conditions, une bonne caractérisation du matériau rompu. Ce point est essentiel, comme nous l'avons souligné dans la première partie.

Le relevé de la distance d'interstrie sur éprouvette i (ΔK) ainsi que la courbe de propagation $\frac{da}{dN}$ (ΔK) permettent de déterminer (fig. 8) la vitesse de propagation ainsi que le facteur d'intensité de contrainte pour chaque longueur de fissure a dans le disque (à laquelle est associée une distance d'interstrie i). Une intégration simple permet ensuite de tracer la courbe reliant la profondeur moyenne de la fissure au nombre de cycles subis par le disque (fig. 9). A cause de l'incertitude sur les mesures de distance entre stries, deux courbes de fissuration extrêmes ont été établies. Elles tendent vers une valeur asymptotique qui permet d'évaluer le nombre de cycles à rupture pour des profondeurs de criques supérieures à 8 mm. La valeur expérimentale (16160 cycles) se situe bien entre les valeurs extrêmes de 14000 et 18000 cycles correspondant aux deux estimations faites.

2.2. Simulation numérique de la rupture

Le calcul vise à reconstituer la progression de la crique à travers le disque, c'est-à-dire à déterminer la courbe N (a) précédemment établie de façon empirique.

Le modèle de calcul utilise un barreau équivalent dont les dimensions et la position sont cohérentes avec la géométrie et la répartition des contraintes dans le disque. Dans cet élément de volume, on fait propager une crique semi-elliptique. Le programme se déroule de la manière suivante :

1. Après définition des conditions initiales (taille de crique, barreau, chargement), le facteur d'intensité de contrainte KI est calculé suivant les deux axes de l'ellipse a et c.

2. Pour un incrément de longueur da appliqué, une augmentation du nombre de cycles dN est obtenue, ainsi qu'un accroissement de l'autre longueur dc de l'ellipse.

3. A partir de la nouvelle configuration de la crique, un nouveau calcul de KI est effectué et le processus est itéré jusqu'à la valeur KIC critique.

Le problème de la détermination des conditions initiales est très important. Il consiste à définir le chargement, le barreau équivalent, la configuration initiale de la crique ainsi que la formulation de KI appropriée au cas de calcul.

Le disque a été modélisé en éléments finis axisymétriques à 3 ou 4 noeuds (fig.10) Un calcul élastique des contraintes suivant les 3 axes principaux (contraintes tangentielle, axiale et radiale) a été effectué (code SAMCEF développé par le L.T.A.S. de LIEGE). Seule, la contrainte tangentielle gouverne l'ouverture des lèvres de la fissure en mode I. Pour évaluer la redistribution des contraintes lorsque la fissure avance, des calculs successifs sont réalisés pour des configurations évolutives de la crique. La discontinuité de matière qui en résulte est modélisée en annulant les termes de la matrice de HOOKE qui déterminent la contrainte tangentielle : cette contrainte vaut 550 MPa en début de la propagation (au point de soudure) et augmente jusqu'à 650 MPa lorsque la crique atteint 8 mm.

Les dimensions du barreau équivalent, ainsi que sa position dans le disque, doivent tenir compte de la localisation de la crique et aussi de l'homogénéité de la contrainte, ainsi que de la sensibilité de KI à la largeur du barreau. Une étude complète de ces paramètres (3) conduit à un barreau de 14 mm de largeur et 15 mm d'épaisseur pour une crique de taille maximale 7 mm (fig. 11). En fin de propagation, un deuxième barreau (longueur 80 mm et épaisseur 25 mm) est adopté (voir fig. 11) : à ce stade, le disque a pratiquement consommé tout son potentiel, ce qui autorise à ne prendre en compte que la géométrie du disque.

La configuration initiale de la crique est estimée d'après les observations micrographiques. L'aspect fragile du faciès de rupture dans la zone affectée thermiquement suggère que dans les premiers cycles de mise en charge, la plage de matière détériorée par le point de soudure a donné naissance à une crique semi-circulaire de rayon 0.36 mm.

Deux formulations de KI ont été utilisées dans le calcul :

la formule proposée par POPP et COLES (4) (5) avec des facteurs correctifs qui ne tiennent pas compte de la géométrie du barreau

. la formulation de NEWMAN et RAJU (6) qui n'est valable que dans un domaine limité.

La loi de fissuration du matériau représentatif du disque a été déterminée sur éprouvette (fig. 9). Pour tenir compte des limites inhérentes aux conditions initiales sur la taille du barreau et la formulation de KI, le calcul de la propagation s'est déroulé en 3 étapes :

1. Propagation dans le premier barreau d'une crique semi-circulaire (rayon initial 0.36 mm) sous une contrainte de 550 MPa, avec application des deux formules de KI.

2. A partir d'une profondeur fissurée de 3.4 mm, la contrainte appliquée peut être de 550 MPa (contrainte initiale) ou 650 MPa si l'on considère la redistribution de contrainte évaluée après propagation. La formulation de NEWMAN n'est plus utilisée puisqu'on se situe alors en dehors de son domaine de validité.

3. Au delà d'une longueur de crique de 7 mm, le deuxième barreau est adopté.

Les différentes combinaisons envisagées donnent les résultats présentés dans le tableau II. Ils se situent entre 82 et 103 % de la valeur expérimentale, ce qui est une bonne précision. La valeur la plus proche du nombre de cycles réels est obtenue en utilisant la formulation de NEWMAN-RAJU, avec une contrainte non réactualisée. Les courbes N(a) relatives à chaque stade de la fissuration montrent l'importance des premiers millimètres de la propagation : il apparaît en effet que d'après le calcul, près de 60 % de la durée de vie du disque est consommé dans les deux premiers millimètres (fig. 12).

Cette analyse de la propagation d'une crique dans un disque d'essai montre qu'avec l'utilisation des données matériau adéquates, le nombre de cycles à rupture a été obtenu à moins de 15 % de la valeur expérimentale. La simulation numérique a également donné des résultats satisfaisants, puisqu'ils se situent à moins de 20 % de la réalité.

CONCLUSIONS

1. L'alliage base nickel INCONEL 718 possède des propriété de résistance à la propagation de fissures qui dépendent considérablement de la microstructure du matériau. Ce phénomène, mis en évidence essentiellement à chaud, est lié à un effet d'environnement qui se traduit par une fragilisation des joints de grains lorsque les fissures se propagent à l'air.

2. L'utilisation de données de base associée à un calcul sur un disque d'essai a cependant conduit à une bonne évaluation du nombre de cycles correspondant à la propagation d'une fissure jusqu'à rupture de la pièce. Cette bonne concordance est liée en grande partie au fait que les données réelles correspondant au matériau utilisé dans la fabrication du disque, ont pu être établies.

3. Le contrôle de la structure par figeage des opérations industrielles (élaboration du matériau, forgeage, traitement thermique) est à la base de la garantie qui peut être accordée sur la durée de vie des pièces.

REFERENCES

(1) - A. PINEAU - Intergranular creep fatigue crack growth in Ni base alloys. A.S.M. Seminar "Flow and Fracture at elevated temperatures". 1/2 Octobre 1983 - PHILADELPHIE - U.S.A.

(2) - J.P. PEDRON et A. PINEAU - Influence de l'oxydation sur la propagation des fissures à haute température dans l'alliage INCONEL 718 - Mem. Sci. Rev. Met. Décembre 1983 - p. 665.

(3) - P. FLEURET - Ecole des Mines de PARIS. - Analyse d'une rupture observée sur un disque d'essai. Rapport interne SNECMA - 1982

(4) - A. COLES, R.E. JOHNSON et H.G. POPP - Utility of Surface-flowed tensile bars in cyclic life studies - Journ. Eng. Mat. and Techn. - Octobre 1976 - p. 305

(5) - H.G. POPP et A. COLES -Subcritical crack growth criteria for INCONEL 718 at elevated temperature - Proceeding Airforce Conference on Fatigue and Fracture of Aircraft Structures and Materials - Septembre 1970 - DAYTON - U.S.A.

(6) - J.C. NEWMAN et I.S. RAJU - An empirical stress intensity factor equation for the surface crack - Eng. Frac. Mech. vol 15 - N° 1 - 2 - 1981 - p. 185

TABLEAU I

Structure	Température C°	Limite élas. MPa	Charge à rupture MPa	Allongement à rupture %
Duplex à collier	25	1240	1350	18
	650	1000	1080	17
Gros grain	25	1145	1290	24
	650	885	960	17
Grain fin	25	1245	1415	24
	650	990	1130	19

PROPRIETES EN TRACTION MONOTONE

TABLEAU II

KI (première phase)	POPP et COLES (4) (5)		NEWMAN et RAJU (6)	
Contrainte appliquée (deuxième et troisième phases) MPa	550	650	550	650
Nombre de cycles calculés	14700	13350	16600	15250
N calculés/N effectués	0,90	0,82	1,03	0,95

RESULTATS DE LA SIMULATION NUMERIQUE

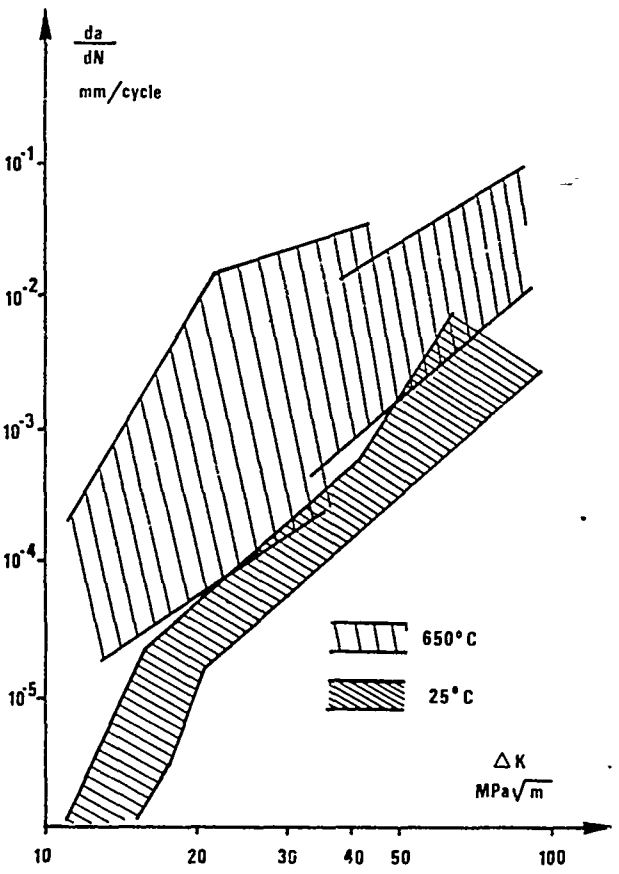

Fig. 1 : Vitesse de fissuration en fatigue continue à 25 et 650° C sur INCONEL 718.

Fig. 2 : Vitesse de fissuration à 650° C pour 3 structures d'INCONEL 718.

a. Fatigue - cycle 20 hz et
cycle 10 s - 300 s - 10 s

b. Fluage

c. Fatigue - cycle 10 s - 300 s - 10 s
Influence de l'environnement

△▲ Gros grain sens long
▽▼ Gros grain sens travers
○● Grain fin
□■ Collier

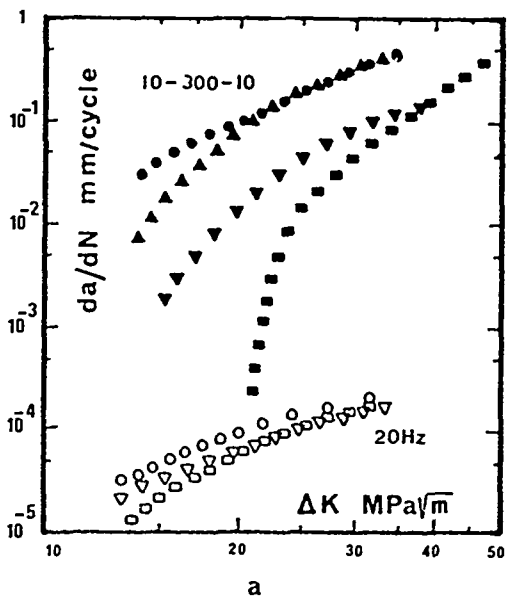

a

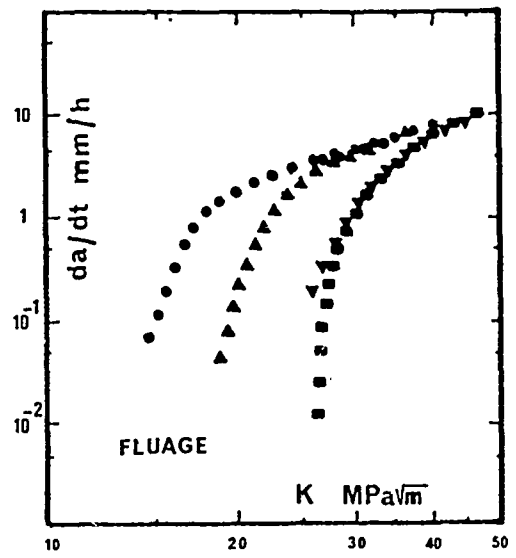

b

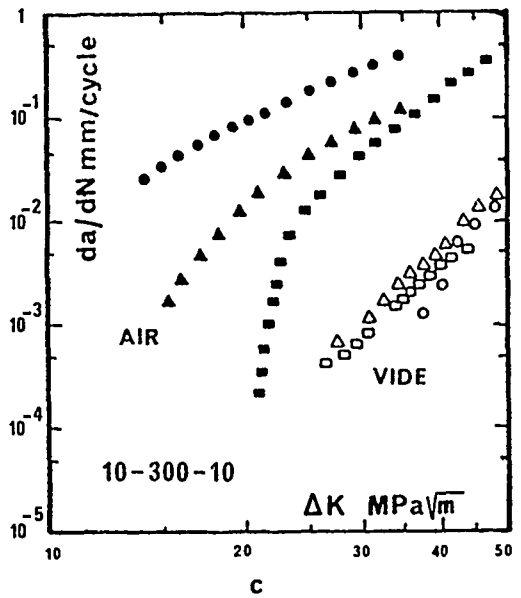

c

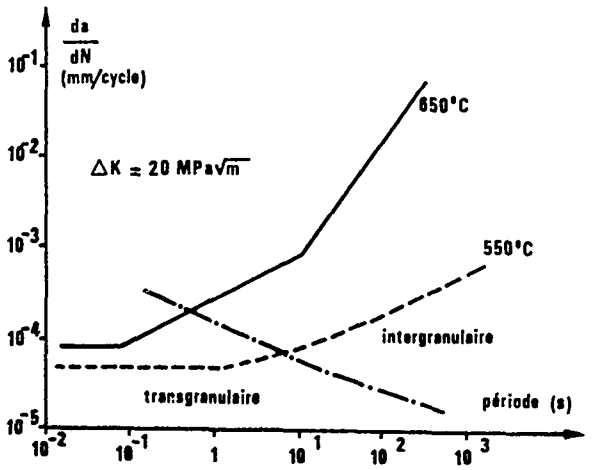

Fig. 3 : Vitesse de fissuration à 550 et 650° C de l'INCONEL 718 en fonction de la période du cycle

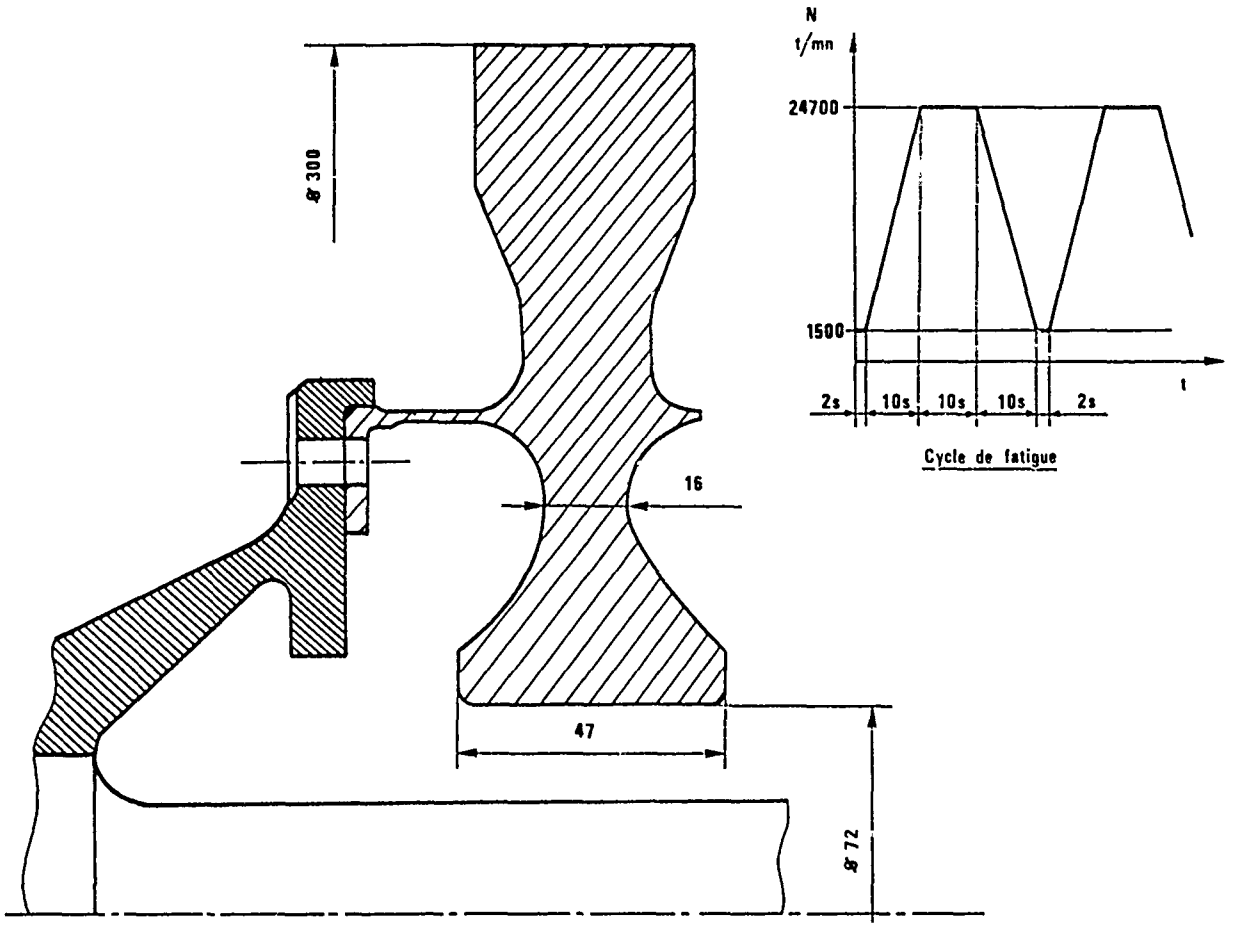

Fig. 4 : Schéma de l'installation

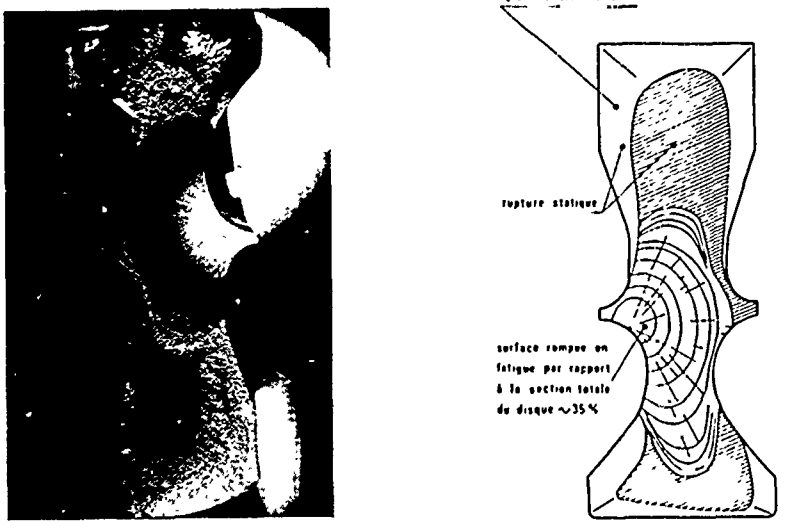

Fig. 5 : Plan de rupture du disque

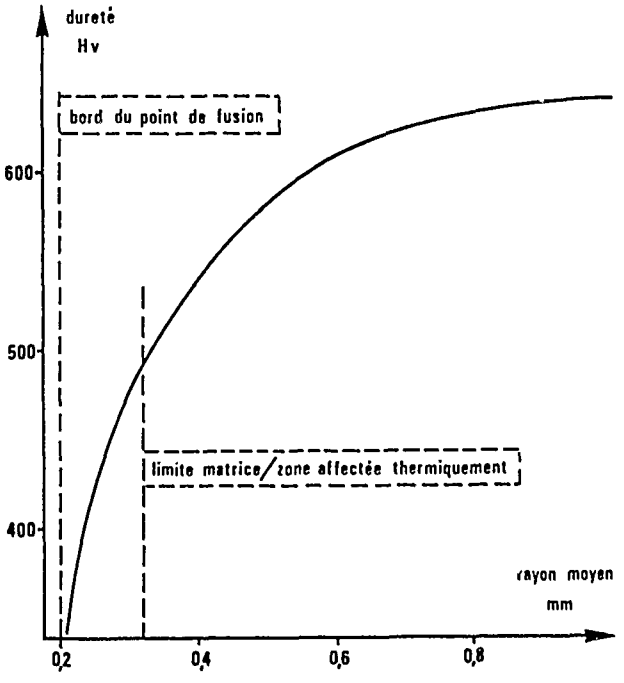

Fig. 6 : Profil de microdureté le long du rayon moyen de la zone affectée.

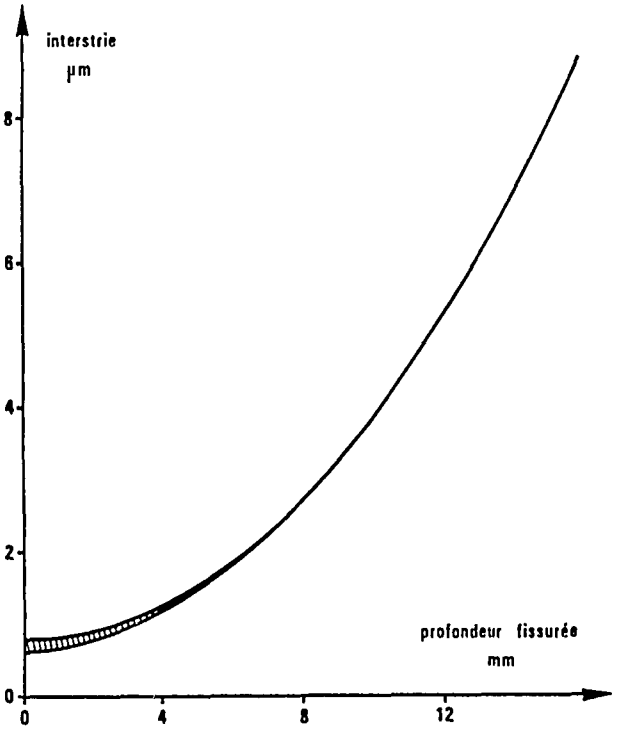

Fig. 7 : Relevé d'interstries sur le disque

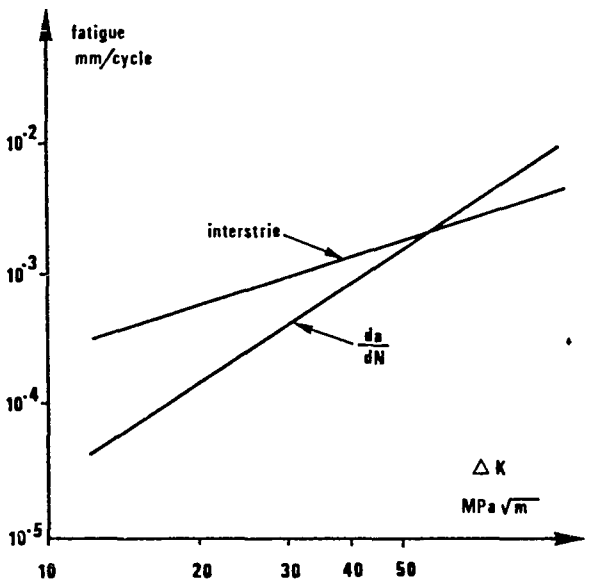

Fig. 8 : Courbes de fissuration et d'interstrie de l'éprouvette CT

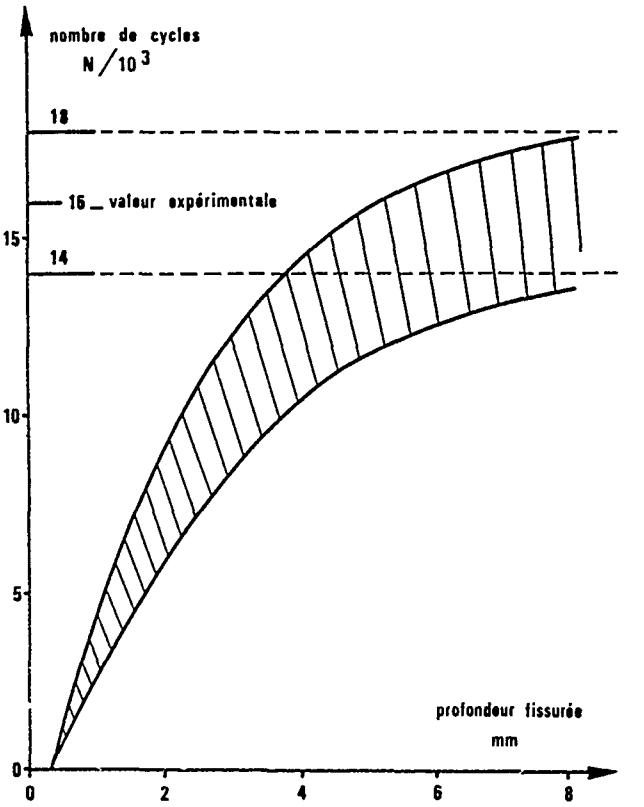

Fig. 9 : Courbe de propagation de la fissure dans le disque

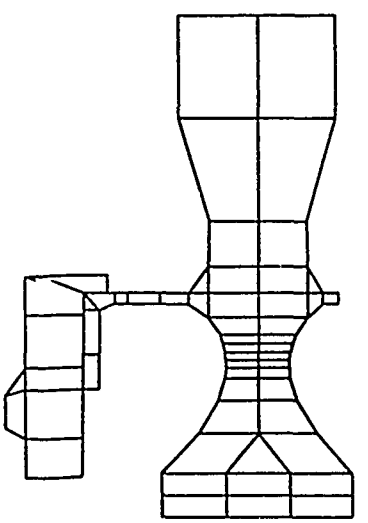

Fig. 10 : Maillage en éléments finis du disque

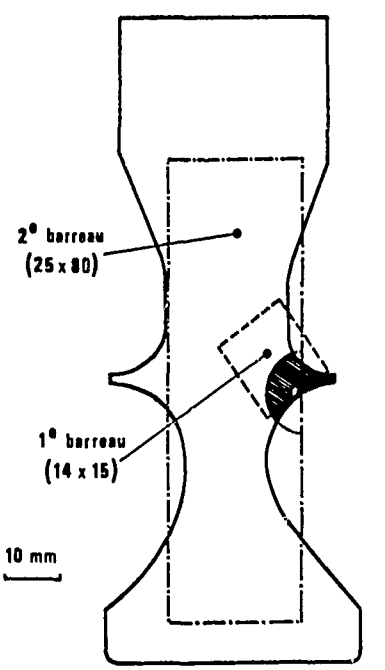

Fig. 11 : Position des barreaux équivalents

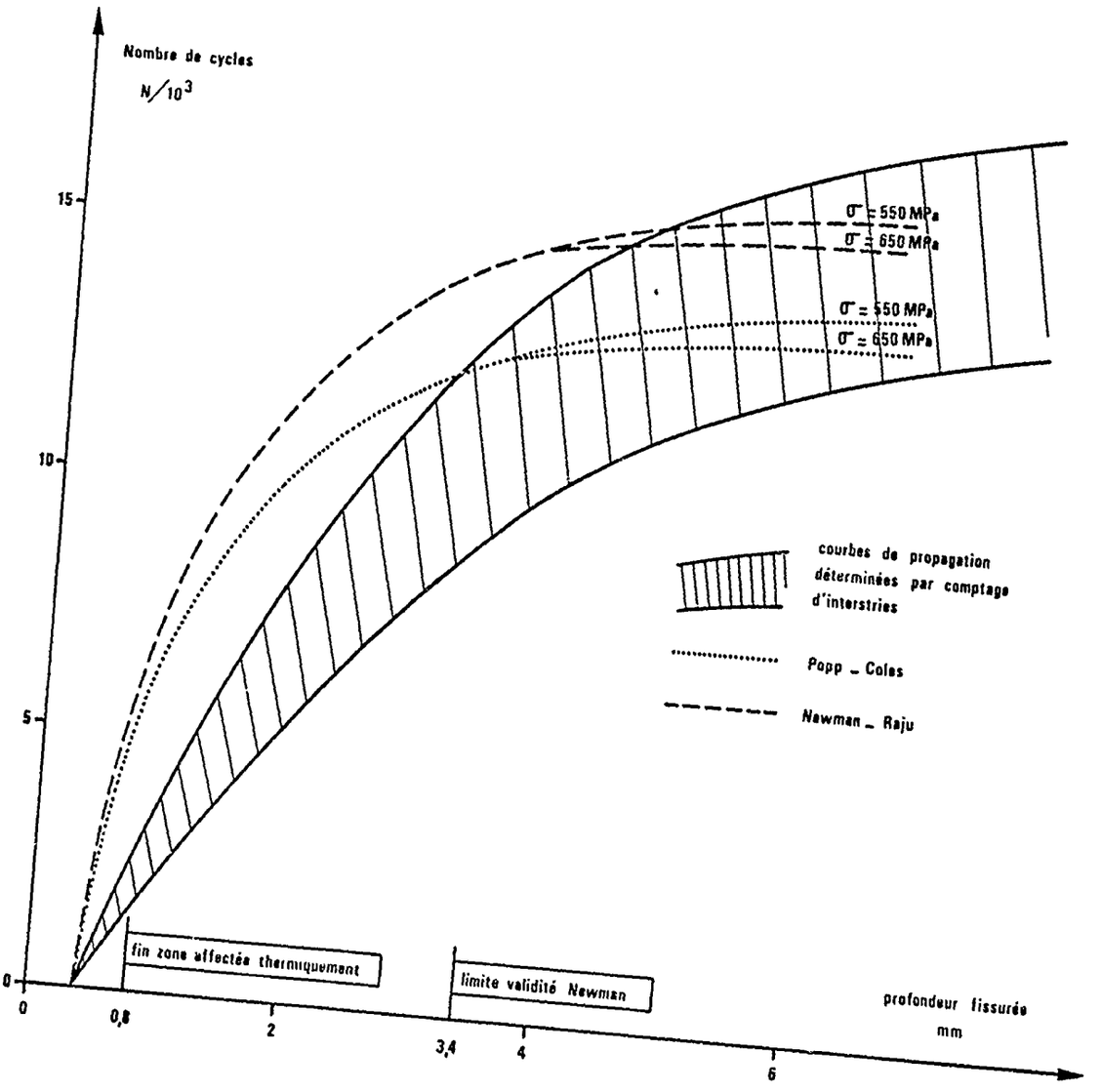

Fig. 12 : Comparaison des courbes de propagation déterminées expérimentalement et par le calcul

DISCUSSION

Dr Bridges, UK

How did you obtain the different grain sizes in your INCO 718?

Author's Reply

Annealing, in the first case. For the ring, it was a mixture of forging and annealing.

A.K.Koul, Ca

How did the speaker draw definite conclusions regarding the environmental effect and microstructure even though he kept his ΔK costant for a given condition? Your K1 and K2 were changing, so how can you differentiate between the effect of K1 and K2 that were changing, even though you kept a constant ΔK? And how could you conclude the effect was environmental not microstructure?

Author's Reply

In the present situation I think that the cracking is ruled by K1 and what we wanted to see was a crack curve for the exact material that was to be used for the disk. You know that there is a certain amount of uncertainty betwen the interspacial spacing measurement and the propagation velocity (this was shown on the Vu-graphs). This test was run at 550°C.

T.M.Edmunds, UK

Your final crack size, taking up 35% of the area, probably implied a K very much larger than the usual K_c we would quote for the alloy which is in line with our experience. Have you got an explanation for that?

Author's Reply

No, I have not.

CUMULATIVE DAMAGE MODELING OF FATIGUE CRACK GROWTH

James M. Larsen and Theodore Nicholas
United States Air Force Wright Aeronautical Laboratories
AFWAL/MLLN, Wright-Patterson Air Force Base, Ohio 45433 USA

SUMMARY

Life predictions of turbine engine structural components utilize fracture mechanics principles to determine fatigue crack growth rates. Fatigue cracks grow under conditions of variable temperature, frequency, hold-time, stress ratio, and stress level. At elevated temperatures, time-dependent material behavior can play a significant role in the material behavior. Cumulative damage models must account for all these variables as well as interaction effects. The earliest modeling involved interaction schemes and, primarily, time-independent material behavior. More recent work has focused on time-dependence and creep fatigue interaction effects. A review of current modeling concepts and problems to be addressed is presented.

INTRODUCTION

During the past two decades drastic changes have occurred in the design criteria and material property requirements for critical structural components in United States Air Force gas turbine engines. In the 1960's, most critical components such as turbine disks and spacers were life limited by the creep and stress rupture properties of their materials. Less than one percent of all rotating components were life limited by Low Cycle Fatigue (LCF). However, demands for improved performance of advanced engines have led to design increases in component operating temperatures and stresses, and the result has been a transition from creep to low cycle fatigue as the dominant life limiting mechanism in the majority of rotating components. In fact, low cycle fatigue has become the life limiting factor for turbine disks in over 75 percent of designs.

Low cycle fatigue, defined by the time required to initiate a crack, is a stochastic process having considerable variability. In order to provide a safe component operating life, the conventional approach has been to use a lower bound on the mean LCF life that is equivalent to a probability of 1/1000 of initiating a detectable crack during the design lifetime of the component. In practice, all components are removed from service after reaching this design lifetime, and this translates into 999 out of 1000 disks being retired from service which are still structurally sound. In an attempt to utilize the remaining life of these 999 disks without sacrificing structural safety, the United States Air Force is implementing a revised life management philosophy termed Retirement-For-Cause (RFC) on some components in advanced engines. Under RFC, components are to undergo periodic inspections and be returned to service if no cracks larger than a specified size are detected. This procedure requires two exacting technologies. The first is the ability to detect cracks larger than a given "detectable size" with a high degree of reliability. The second is the ability to predict crack growth rates accurately and to demonstrate that a crack of the "detectable size" or smaller will not grow to a catastrophic size during one inspection interval.

A capability to accurately predict crack growth in turbine components is also required by the Engine Structural Integrity Program (ENSIP) currently being implemented by the Aeronautical Systems Division of the United States Air Force. Whereas Retirement-For-Cause is being applied to existing engines, ENSIP is a specification for future engines that requires a damage tolerant design approach for all structure critical components. Under this philosophy, flaws or defects must be assumed to exist in the components at the time of production. Design calculations and component testing must demonstrate that such defects will not grow to a catastrophic size within the lifetime of the engine. Finally, the engine design community, in general, has recognized the importance of fatigue in design and is conducting extensive evaluations of fatigue crack propagation rates in materials and components for advanced engines. In this scenario, the ability to analytically predict crack growth under typical engine operating conditions is a key technology. Crack propagation must be predicted under variations of load amplitude, temperature, frequency, load ratio, sustained load hold-time and sequence of loading. This paper attempts to define the key parameters that influence crack growth in turbine components and to present a review of the current capability for crack growth rate prediction for turbine engine materials. In addition, some observations on crack growth behavior in some typical materials will be presented.

FATIGUE SPECTRA

The fatigue spectra imposed on rotating components in an advanced gas turbine engine contain load sequences which differ significantly from the high cycle aerodynamic loading common to airframes. The typical loading spectrum experienced by an engine disk is characterized as low frequency stress cycling resulting primarily from centrifugal forces associated with variations in engine speeds. In the hot section of the engine the stress spectrum is complicated by the superposition of stresses produced by thermal cycling.

The turbine engine fatigue spectra are defined by anticipated and actual aircraft usage field data obtained from pilot interviews and event history recorders which have been installed on selected advanced Air Force fighters to acquire real-time engine operating data. The compilation and characterization of these raw data define representative engine usage for a variety of operational activities including aircraft takeoff, ferry and refueling, bombing runs, maneuvers guided by Terrain Following Radar (TFR), and combat under subsonic and supersonic conditions. Fig. 1 presents a composite plot (Ref. 1) of the full range of operational activities that may occur within a given sortie. Although no single mission would likely contain all of these activities, the plot serves to illustrate the fact that rotating components in advanced engines experience a low frequency loading sequence which includes a mix of fatigue and sustained load segments. A typical stress spectrum is shown in Fig. 2 (Ref. 1). The complete stress spectrum contains both mechanically and thermally induced stresses. In elevated temperature components, the operating temperature also varies as shown in Fig. 2 which represents a specific location on a cooled turbine disk rim.

The problem of predicting fatigue crack growth under combined thermal and mechanical cycling is quite complex. While research is in progress to address this general problem, the present approach most often taken is to model the complete spectrum (combined mechanical and thermal stresses) and reduce the thermal spectrum to a series of isothermal blocks. The typical stress spectrum can be broken down into smaller segments that may be characterized in terms of fundamental parameters such as cyclic frequency (F), stress ratio ($R = \sigma_{min}/\sigma_{max}$; σ is the applied stress), temperature (T), and sustained load hold-time (t_H). In addition to predicting crack growth as a function of these parameters, crack growth modeling must also address synergistic effects such as load sequence and amplitude variations. Creep-fatigue interactions (combinations of fatigue cycles and hold times) and crack growth interactions caused by overloads and underloads must be considered. The general problem of prediction of cumulative damage fatigue crack growth is exceedingly complex, and analytical fatigue models capable of predicting this complex behavior based on fundamental mechanisms are not available. Thus, current cumulative damage predictive capabilities generally rely on the empirical approach discussed in the following section.

ANALYTICAL MODELS

An analytical model of crack growth under gas turbine spectra must have the capability to predict crack growth rate as a function of the primary variables and to interpolate among a finite amount of experimental data. The typical approach involves representing data as da/dN or da/dt (crack growth rate) as a function of ΔK or K (stress intensity) for each combination of variables (T, R, F, t_h). Typical curves exhibit a sigmoidal shape as shown in Fig. 3. A mathematical description of the sigmoidal shape is then introduced. The description can be a hyperbolic sine function, a combination of exponentials, or any other functional form which describes the general shape of Fig. 3 in terms of a number of parameters. These parameters must then be related to the test variables, either directly or indirectly, through additional functional forms. Variations in the test variables result in shifts of the sigmoidal curve. The slope, inflection point, lower and upper asymptotes, and curvature can all change with variations in the test variables while still retaining the general sigmoidal shape. Each parameter in the mathematical model of the curve can be related to one or more or all of the variables. The model should then have the capability for describing data over a wide range of values of the test variables and interpolating between those values. The application of the model requires a systematic procedure to determine the functional relationships through some type of regression analysis of experimental data. Two models which have been developed for this purpose are described below. Both models will be applied to a limited data set to illustrate the predictive capabilities over a range of test variables. Subsequently, a full cumulative damage model that also considers synergistic crack growth variables will be presented.

MSE Model

The Modified Sigmoidal Equation (MSE) was developed by General Electric Co. and was used in an investigation to predict crack growth rates in alloy AF115 (Ref. 2). The basic sigmoidal equation is expressed in the form

$$da/dN = \exp(B)(\Delta K/\Delta K^*)^P (\ln(\Delta K/\Delta K^*))^Q (\ln(\Delta K_c/\Delta K))^D \qquad (1)$$

where da/dN is the crack growth rate per cycle and ΔK the stress intensity range. The equation has the general sigmoidal shape of Fig. 3 with the lower asymptote ΔK^* representing the threshold value of ΔK and the upper asymptote ΔK_c representing the critical or maximum value of ΔK. The equation involves six parameters, ΔK^*, ΔK_c, B, P, Q, and D, each of which, in general, can be related to the 4 test variables T, R, F, and t_H. The parameter B controls the vertical motion of the entire curve. The parameter P provides control of the slope at the inflection point of the sigmoidal curve. The vertical location of the inflection point is controlled by a combination of B, P, and ΔK^*. This three-way interaction makes it extremely difficult to express the parameters of the MSE equation as a function of the test variables. To simplify equation (1) so that the individual parameters can be related to the test variables, alternate parameters are introduced. The purpose of the introduction is to work with

terms which can be easily interpreted physically. These terms are able to describe the vertical and horizontal location of the inflection point of the sigmoidal curve as well as its vertical asymptotes; thus, they can be determined as functions of the test variables. In the application of this model to experimental data, equations were developed relating the six parameters to the four test variables (Ref. 2). Predictions were made of the crack growth rate in alloy AF115, an advanced nickel base superalloy, over a temperature range from 538°C to 760°C, stress ratios from 0.1 to 0.9, frequencies from 0.025 to 2.5 Hz, and hold times up to 5 min. The material behavior ranged from time and frequency independent at 538°C to very time and frequency dependent at 760°C.

Data for alloy AF115 at the intermediate test temperature of 649°C show that over the range of frequencies tested (0.025 to 2.5 Hz) there is apparently no variation in growth rate with frequency for a stress ratio of 0.1. Data at R = 0.9, however, show an increase in growth rate of two orders of magnitude when frequency is decreased from 2.5 to 0.025 Hz. These data are discussed in detail later (See Fig. 18). Data for R = 0.1 and hold-times of 0, 90, and 300 seconds are shown in Fig. 4 at the same temperature. A significant hold-time effect is apparent. From these and other sets of data covering the range mentioned above including 27 test conditions involving 43 tests, the functional relations between the six parameters and the four test variables were established through multiple regression analyses and trial and error. These relationships were limited to linear and power law forms and provide a reasonable representation of the behavior of AF115. These relations and the appropriate constants were incorporated into an interpolative computer code which provides crack growth rate as a function of ΔK and the four test variables. An example of the capability to regression experimental data is shown in Fig. 5 where the MSE equation regression to the data of Fig. 4 is shown along with the original data. In general, the extremely versatile MSE equation was capable of representing the data sets reasonably well.

SINH Model

The hyperbolic sine equation (SINH) was developed by Pratt and Whitney Aircraft (Ref. 1, 3, 4, 5,) to interpolate crack growth rate data over a range of the four test variables T, R, F, and t_H. The equation is expressed in the form

$$\log\ (da/dN) = C_1\ \text{SINH}\ (C_2\ (\log \Delta K + C_3)) + C_4 \qquad (2)$$

which provides the basic sigmoidal shape and constants to vary the shape of the curve and the position of the inflection point. The constant C_1 is a shape factor and is normally set to 0.5 for many materials. C_2 is also a shape factor. The constants C_3 and C_4 control the horizontal and vertical location of the inflection point, respectively. The four constants can be related, in general, to the four test variables. In the development of the model and its subsequent application to several materials, the following functional forms have been established and have been found to be adequate to represent crack growth rate under a wide variety of conditions:

$$\begin{aligned} C_1 &= \text{constant } (= 0.5) \\ C_2 &= a + b_1 \log(1\text{-}R) + b_2 \log (F) + b_3 T + b_4 \log (t_H) \\ C_4 &= c + d_1 \log(1\text{-}R) + d_2 \log (F) + d_3 T + d_4 \log (t_H) \\ C_3 &= e + f C_4 \end{aligned} \qquad (3)$$

The twelve constants (a, b_1, b_2,...) are determined from a least squares minimization technique.

The SINH model was applied to a limited set of data for AF115 (Ref. 6). Data at three frequencies and two hold times at 649°C were used to determine the constants at R = 0.1. The predictions and data for the three hold times are shown in Fig. 6. The dashed curve represents regression results considering all data points. For the lower data set, the right-most data point was found to be in error. Due to its great leverage, this spurious point had an extreme influence on the overall regression analysis. Elimination of the data point from the analysis allowed a much more accurate regression model to be produced as shown by the solid curve. The other curves for t_H = 90 and 300 seconds were essentially unchanged. Comparing the results shown by the solid curves with those of Fig. 5 for the MSE model for the same data sets shows a similar degree of correlation. The regression analysis for the SINH model provided three slightly different curves for three frequencies, although the variations in both the model predictions and the experimental data were extremely small.

COMPARISON OF MODELS

There are numerous similarities as well as many differences between the MSE and SINH models. Both begin with an equation describing a general sigmoidal shape. The MSE model has vertical asymptotes which require special techniques for performing regression analyses on experimental data which may fall outside the asymptotes. The SINH model has four constants (only three are used in most cases) while the MSE model has six. The functional relations between the constants and the four test variables are established for the SINH model and have been used in modeling several materials. The functional relationships for the MSE model are more complex and have been established based on data for one material (AF115). It is not apparent whether these functional forms are valid for other materials. The SINH model has been developed incorporating a sophisticated regression analysis scheme for application to a wide

variety of data sets. No general regression scheme is incorporated into the documented MSE Model. Since very few data on crack growth in the near threshold regime exist for engine materials it is not clear how well either model can predict very low growth rates or how well they can represent the threshold ΔK as a function of the test parameters. The SINH model has, however, been used successfully to represent near threshold crack growth at room temperature in a aluminum alloy (Ref. 7).

Both models, when applied to a limited data set on AF115, were evaluated to determine the variation of crack growth rate with frequency or hold-time while keeping all other test variables constant. Using two fixed values of ΔK and R = 0.1, T = 649°C, plots were made of predicted crack growth rate as a function of cycle time or hold-time for variations in frequency (reciprocal of cycle time) and hold times. The hold times were applied between single cycles at 0.25 Hz. The results are presented in Fig. 7 and show that both models predict similar behavior. It is interesting to note that the MSE model predicts linear relationships in (log) crack growth rate with (log) frequency or (log) hold-time. The SINH model, on the other hand, can predict a non-linear relationship for this behavior.

To our knowledge, the application of the MSE and SINH models to the set of data on AF115 (Ref. 6) is the only direct comparison that has been made of the predictive capabilities of the two models. However, the application of each model to the data was quite different. The constants in the MSE mode had already been established (Ref. 2) for a large data set and the results shown in Fig. 5 simply show the fit to one limited data set illustrating hold-time effects. On the other hand, the SINH model was applied only to the limited data shown in Fig. 4. The data for zero hold-time are for only one frequency although data at other frequencies (which showed no frequency effect) were included in the fit of the MSE model. The inclusion of these additional data would naturally charge the fit in Fig. 6. Another observation in the application of the SINH model is that the fit to a data set is dependent on the users first guess at some of the constants. A non-linear regression analysis will often provide a best fit in the vicinity of the first guess. In the application to data sets, the number of data points of each set, the existence (or elimination) of spurious data points, and the initial guess can all influence the final fit. This requires some degree of experience in the application of the SINH model but also provides a significant amount of flexibility in fitting experimental data. This will be illustrated in the following section which shows the application of the SINH model to complex loading situations.

CRACK GROWTH SYNERGISM

The crack growth models presented above effectively represent crack growth as a function of the primary variables (R, F, T, and t_H) under constant amplitude fatigue. However, it is well known that crack propagation under variable amplitude loading may be retarded, or accelerated due to various load interaction effects (e.g. Ref. 8, 9). For example, if constant load amplitude fatigue is interrupted by a single loading cycle of greater magnitude (i.e. an overload), the rate of subsequent crack propagation will be temporarily reduced under the resumed constant amplitude fatigue. In the extreme, an overload may produce complete crack arrest. Alternately, if a large compressive load (underload) occurs, a period of accelerated crack growth may result under continued fatigue. Load interaction phenomena such as these may significantly affect the life of airframe structures where large overloads may occasionally occur.

By comparison to high cycle airframe spectra, the low cycle fatigue spectra that are imposed on rotating components in turbine engines have little variability. Turbine spectra contain relatively mild overloads (major throttle excursions), and these overloads occur routinely (several times in a given mission). For a rotating component the magnitude of an overload is ultimately limited by the component's burst strength which, in advanced military engines, is only slightly greater than the design stress. As a result, overload stresses are generally much less than one and a half times the normal operating design stress. Thus, the engine spectrum can generally be characterized as rather severe baseline fatigue cycling interrupted by frequently occurring mild overloads.

The magnitude of the load interaction effect produced by such loading has been determined experimentally in elevated temperature testing of the nickel-base superalloy IN100 (Ref. 1, 4). Fig. 8 illustrates test results for crack growth under constant load amplitude fatigue interrupted by a periodic overload occurring every 41 cycles. For the maximum overload ratio (OLR = $\sigma_{overload}/\sigma_{max}$ = 1.5) the result is a factor of 4 reduction in growth rate below that of the constant amplitude cycling. The effect of varying the number of fatigue cycles between the overloads (ΔN_{OL}) is shown in Fig. 9. The crack retardation effect is greatest for case with 40 cycles between overloads and diminishes as ΔN_{OL} is reduced. For testing with ΔN_{OL} = 5, the average crack growth rate is approximately equivalent to that under constant amplitude fatigue alone. For this high frequency of overloading the crack retardation that occurs during the constant amplitude cycling is essentially balanced by the added crack growth due to the overload cycle itself. In the limit as ΔN_{OL} approaches zero, the relative fraction of damage produced by the overload would increase, and the resultant crack growth rate curve would approach the limiting case shown in Fig. 9.

The combined effects on crack growth of overload ratio and the number of cycles between overloads can be described by an interpolative SINH model in a manner similar to that used to represent the effects of the primary variables R, F, T, and t_H. Ultimately, the effects of all the primary and synergistic variables may be incorporated into a single model for predicting cumulative damage crack growth under turbine engine spectra. Such a model was constructed for crack growth in the superal-

loys Waspaloy and IN100, and its predictive capabilities were demonstrated under the mission loading sequences shown in Figs. 10 and 11 (Ref. 1). Under the terms of the demonstration program, the cumulative damage model was used to predict crack growth produced in both compact type and surface flaw specimens under each mission spectrum. Subsequently, crack propagation tests of the two materials were performed under both spectra and using both specimen geometries. Fig. 12 illustrates an example crack growth data set and the corresponding cumulative damage model prediction along with a prediction assuming linear damage summation (i.e. discounting any load interaction effects). The results of all eight demonstration tests may be summarized by calculating the ratio of the predicted to the actual specimen life (N_p/N_A). A ratio of 1.0 indicates perfect correlation, while values less than one indicate conservative predictions. A log-normal probability plot of these life ratios based on the cumulative damage model is presented in Fig. 13. The mean value of these ratios is 1.07 indicating that, on average, the model predicted actual specimen life to within 7 percent. The corresponding mean value for the nonsynergistic life calculation (linear damage summation) is $N_p/N_A = 0.82$.

Among the conclusions that can be drawn from these data is the observation that relatively little crack retardation occurs under the missions tested. On average the synergistic model predicted crack propagation lives only 30% greater than the linear damage summation prediction. This small increase in life may be understood from a consideration of the specific crack retardation process. The maximum degree of crack retardation produced by an overload generally does not occur during the fatigue cycles immediately following the overload. Typically, the process immediately following the overload can be described as delayed retardation and is characterized by a monotonically decreasing growth rate until a minimum is achieved some number of cycles following the overload. Thereafter, crack propagation may be retarded for an extended period. However, under representative turbine engine spectra the overloads occur very frequently, and the retardation process is interrupted and restarted often. It has been shown (Ref. 10) that delayed retardation continues to occur under these circumstances and, in fact, dominates the retardation process. As a result, the full beneficial effect of the overloading is never achieved, and only a modest increase in crack propagation life results.

In addition to limiting crack retardation, the high occurrence frequency for overloads has a second effect. The overloads may occur so often that they, themselves, account for much of the crack propagation produced by a fatigue spectrum. This view is largely accurate when considering the hypothetical missions presented in Figs. 10 and 11 and is often even more appropriate when considering actual engine operating spectra such as that of Fig. 2. Under many actual missions, major throttle excursions (overloads) account for the much of the fatigue damage, and the resulting crack retardation is never fully developed in the few minor fatigue cycles that occur prior to the next major cycle. The general result is a relatively minor load interaction effect for most engine spectra, and although an effective synergistic crack growth model is available, large errors in component life calculations generally do not result if load interaction effects are ignored.

Potentially a greater source of error in calculations of crack growth in elevated temperature components lies with interaction effects produced by a sequence of fatigue cycles and periods of sustained loading. For the type of spectra discussed thus far, the magnitude of most sustained loading is well below the maximum stress level for the fatigue cycles. In this case the relative contribution of the sustained loading to crack growth is very small. However, certain types of aircraft perform activities for which much of the loading spectra is characterized by sustained loading at or near the maximum stress. For these cases "creep-fatigue" interactions can become important at the higher temperatures.

OBSERVATIONS ON TIME-DEPENDENT MATERIAL BEHAVIOR

Modeling of crack growth rate behavior to date has concentrated on alloys in existing engines. Time-dependent crack growth, i.e. effects of hold times, has not been found to be very significant in most cases (Ref. 11). This is because most designs use materials in the elastic region or only slightly into the inelastic strain regime. There are variations in crack growth rate due to frequency, but these variations are not due to purely time-dependent behavior. That is, a decrease in frequency by an order of magnitude does not result in an increase in crack growth rate per cycle by an order of magnitude. As temperatures are increased in new designs, there is a tendency towards more time-dependent material behavior. In particular, the effects of hold times may play a more important role in future modeling exercises. Thus, crack growth under sustained load must be characterized accurately.

Experimental results on a number of materials have shown that at elevated temperatures crack growth can be characterized as purely time-dependent for very low frequencies or under sustained load. Fig. 14 shows results on fatigue crack growth as a function of frequency for Inconel 718 at 649°C for 2 values of maximum K. It can be seen that for frequencies below 0.01 Hz at R = 0.1 the growth rate per cycle is inversely proportional to frequency (-45° slope on log-log plot) or that da/dt, crack growth rate with respect to time, is constant. On this same material, single fatigue cycles with hold times at maximum load between cycles show purely time-dependent behavior for hold times in excess of 10 seconds between 1 Hz fatigue cycles for R = 0.1. For R = 0.5, time-dependent behavior is observed for all hold times. Fig. 15 shows these experimental results for two different values of maximum value of K, the stress intensity factor at R = 0.1, and for one value at R = 0.5. Crack growth rate per cycle is plotted against total cycle time. The total cycle is composed of a 1 Hz

fatigue cycle and a hold-time at maximum load. The data for cycle time equal to one second correspond to the baseline fatigue data at 1 Hz. The solid lines of unity slope represent purely time-dependent behavior. It can be seen that most of the data show time-dependent behavior. In fact, for a very large hold times, the data represent, by definition, the sustained load crack growth behavior since the contribution of the single fatigue cycle can be virtually ignored. Shown also on the plot are dashed lines representing predictions of a linear cumulative damage model to be discussed below.

It is to be noted that K is used as the correlating parameter in both cases (fatigue and creep/fatigue) even when the behavior is purely time-dependent. On the same material, K has been found to provide good correlation with sustained load crack growth rate using three different specimen geometries (Ref. 12). Similar observations have been made on other nickel base superalloys demonstrating that K is an adequate correlating parameter for sustained load crack growth rate. We hesitate to use the terminology "creep crack growth" for sustained load crack growth in these materials because the creep contribution is very small. Instead, crack growth under sustained load, cycles with long hold times, or very low frequencies is an environmentally enhanced process. In the absence of a deleterious environment, in this case air (oxygen), growth rates decrease by over an order of magnitude. Figure 16 shows sustained load crack growth rate in air and vacuum from three separate investigations (Refs. 13 - 15). The data clearly show a significant decrease in growth rate when oxygen is removed from the environment. The time-dependent behavior in the presence of oxygen is thus highly environmentally enhanced which partially explains why K, a linear elastic fracture mechanics parameter, correlates time-dependent crack growth in these materials.

The cyclic crack growth behavior of many alloys at elevated temperatures can generally be categorized as a function of frequency or reciprocal of cycle time over three regions as depicted schematically in Fig. 17. At low frequencies or long cycle times (region 1), behavior is purely time dependent. At high frequencies or short cycle times (region 3) the behavior is purely cycle dependent. At intermediate cycle times (region 2), the behavior is characterized as mixed mode. In Inconel 718 at 649°C, region 2 covers a frequency range from 0.01 to 10 Hz at R = 0.1 as shown in Fig. 14 (Ref. 16). At other values of R, however, the transition frequency changes for the same maximum value of K. Figure 18 shows data for Inconel 718 and AF115 at 649°C for maximum K of MPa-$m^{\frac{1}{2}}$. It can be seen that for AF115 at the same temperature, region 2 does not appear to exist, i.e. the behavior could be characterized as either cycle or time-dependent with no intermediate region. In both of these materials at 649°C, addition of hold times at maximum load increases the crack growth rate. Calculations have shown that the hold-time contribution is readily obtained from sustained load crack growth data. For modeling purposes, sustained load and cyclic growth data can be summed to predict crack growth rates due to cycles with hold times at maximum load (Ref. 16).

Interactions between sustained loads and cyclic loading (creep-fatigue interactions) may be important in typical engine spectra. Linear cumulative damage modeling has been used, rather successfully, to predict growth rates in several cases involving alternate cyclic loading interspersed with hold times at maximum load. In Fig. 15 hold times at maximum load varying between 1 and 500 seconds, interrupted by a single fatigue cycle of R = 0.1, showed time-dependent behavior for hold times greater than ten seconds (Ref. 18). The growth rate can be predicted by summing the contribution of the fatigue cycling and the sustained load portion. The predictions, shown as dashed lines in Fig. 15, correlate extremely well with experimental data for Inconel 718 at 649°C. Similar data, which have been obtained on IN100 at two temperatures, 649°C and 732°C, are presented in Figs. 19 and 20. These figures plot the growth rate per cycle for a single fatigue cycle of 0.167 Hz at R = 0.1 and various hold times as a function of hold-time. Data are presented for 3 values of the maximum stress intensity, 40, 30, and 20 MPa-$m^{\frac{1}{2}}$. The horizontal lines show the crack growth rate prediction due to fatigue only. The lines of unity slope represent predictions due to the sustained load portion only as determined from separate sustained load growth rate tests. The dashed lines are predictions taking into account both contributions and show reasonable correlation with the data. Figure 19 shows that, at 649°C, purely time-dependent behavior does not occur until hold times beyond several hundred seconds are applied. At 732°C, however, time-dependent behavior occurs for hold times of 100 seconds and less. The predictions for very long hold times in both cases are below the experimental data. These differences are attributed mainly to the statistical variability in sustained load crack growth rate data.

Another series of tests which has been conducted to evaluate "creep-fatigue" interactions involves subjecting a specimen to a number of fatigue cycles with a hold-time interspersed between each block of fatigue cycles (Ref. 17). Data for Inconel 718 are presented in Fig. 21 in the form of crack growth rate (da/dt) as a function of the number of fatigue cycles in a block. All fatigue cycles were at 1 Hz with R = 0.1. The data for the number of cycles, N, approaching zero represent sustained loads only. The data for N becoming infinite represent fatigue cycles only. These tests were performed using hold times of 5 and 50 seconds at a maximum value of K of 40 MPa-$m^{\frac{1}{2}}$. A linear cumulative damage prediction obtained by summing the sustained load and fatigue contributions is shown as solid lines in Fig. 20. Predictions considering sustained load only and fatigue only are also shown for comparison. It can be seen that the linear cumulative damage prediction is quite accurate. Note that the growth rate data are plotted on a linear scale. For this material, the contributions due to sustained loading and fatigue are both important for the entire range of N investigated.

Similar data were obtained for IN100 at 649°C and 732°C and are plotted in the same manner in Figs. 22 and 23. The fatigue cycles here are 0.167 Hz at R = 0.1. Fig. 22 shows that the hold times have little influence and that the predictions based on fatigue only are quite good at 649°C. At 732°C, however, both sustained load and fatigue contribute over the range of values for N investigated. The experimental data are somewhat higher than predicted by the linear cumulative damage model, but the trends of both are consistent. A higher sustained load crack growth rate would bring the prediction more in line with the data. This is consistent with the observation of a low prediction in the hold-time data Fig. 19 and, again, is attributed to material scatter in sustained load testing.

In general, our observation has been that sustained loads at maximum load in "creep-fatigue" interactions play an important role in crack growth in engine alloys at high temperatures. It has also been observed that crack growth predictions based on a linear cumulative damage model are quite reasonable. Sustained loads at less than maximum load in "creep-fatigue" interactions have not been investigated to any large extent. If their contribution is numerically small compared to that of the fatigue cycles, they can usually be ignored. If their contribution is not negligible in a linear cumulative model, they cannot be automatically ignored although the magnitude of their contribution may not be determinable from a linear summation basis. In spectrum load experiments on Inconel 718 at 649°C, with sustained loads at 75 percent of maximum fatigue load, linear cumulative damage could not be used. The fatigue overloads had a significant retardation effect on the sustained load behavior. The net crack growth rate was a factor of 40 less than that predicted by sustained load behavior, but over 2½ times that due to fatigue alone (Ref. 17). Similar observations have been made in IN100 at 732°C (Ref. 4). Thus, the effect of fatigue overloads on sustained load behavior appears to be important. This complex problem has received little attention to date.

DISCUSSION AND CONCLUSIONS

Crack growth rate modeling in turbine engine alloys has been concerned primarily with evaluating the effects of stress ratio, temperature, and frequency using stress intensity as a correlating parameter. Hold times at maximum load have also been considered in modeling studies. Both the hyperbolic sine (SINH) and modified sigmoidal equations (MSE) have been used to describe the general shape of crack growth rate curves. Only the SINH equation has been applied extensively to a number of materials over a wide range of conditions. A significant amount of interpolative flexibility is inherent in these models so that, in principle, a wide range of data and combinations of parameters can be represented. These models have been very successful in representing the materials they have been applied to. They have not, however, been applied to any great extent to materials exhibiting significant amounts of time dependent behavior or to very complex mission spectra where hold-time effects are significant.

Certain aspects of material behavior have been ignored or considered unimportant in crack growth modeling. Single overload or underload cycles influencing cyclic crack growth have been found to be relatively unimportant in engine mission spectra. Cyclic overloads influencing sustained load crack growth, however, have been shown to be very important in engine mission spectra, particularly at very high temperatures where time-dependent behavior is apparent. Little work has been done in this area. With the exception of these overload effects, linear cumulative damage modeling has been found to work well under a wide variety of conditions. This concept, combined with interpolative capabilities of a model such as SINH, provides an extremely powerful tool for crack growth modeling under a very wide range of loading conditions. Aspects which have not been addressed in modeling and material behavior studies, which are expected to play important roles in some future applications, include the effects of non-isothermal conditions, the growth of short cracks, closure phenomena, interactions of high and low frequency loading, growth of multiple cracks, crack growth in and near the threshold regime, and crack growth in anisotropic materials such as single crystals.

REFERENCES

1. Larsen, J.M., Schwartz, B.J., and Annis, C.G. Jr., Pratt and Whitney Aircraft, "Cumulative Damage Fracture Mechanics Under Engine Spectra," 1980, Air Force Materials Laboratory Report AFML-TR-79-4159, Accession No. ADA084934.*

2. Utah, D.A., General Electric Co., "Crack Growth Modeling in an Advanced Powder Metallurgy Alloy," 1980, Air Force Wright Aeronautical Laboratories Report AFWAL-TR-80-4098, Accession No. ADA093992*

3. Annis, C.G. Jr., Wallace, R.M., and Sims, D.L., Pratt and Whitney Aircraft, "An Interpolative Model for Elevated Temperature Fatigue Crack Propagation," 1976, Air Force Materials Laboratory Report AFML-TR-76-176, Part I, Accession No. ADA038070.*

4. Wallace, R.M., Annis, C.G. Jr., and Sims, D.L., Pratt and Whitney Aircraft, "Application of Fracture Mechanics at Elevated Temperature," 1976, Air Force Materials Laboratory Report AFML-TR-76-176, Part II, Accession No. ADA044239.*

5. Sims, D.L., Annis, C.G. , and Wallace, R.M., Pratt and Whitney Aircraft, "Cumulative Damage Fracture Mechanics at Elevated Temperature," 1976, Air Force Materials Laboratory Report AFML-TR-76-176, Part III, Accession No. ADA44420.*

6. Christoff, J.R., "Evaluation of Fatigue-Creep Crack Growth in an Engine Alloy," M.S. Thesis, December 1983, Air Force Institute of Technology, Wright-Patterson Air Force Base, Ohio, 45433, USA.

7. Miller, M.S., Gallagher, J.P., "An Analysis of Several Fatigue Crack Growth Rate Descriptions" Fatigue Crack Growth Measurement and Data Analysis, ASTM STP 738, S.J. Hudak, Jr. and R.J. Bucci, Eds., American Society for Testing and Materials 1981, pp 205-251.

8. Broek, D., Elementary Engineering Fracture Mechanics, Third Edition, London, Martinue Nijhoff Publishers, 1982, pp 262-278.

9. Hertzberg, R.W., Deformation and Fracture Mechanics of Engineering Materials, Second Edition, New York, John Wiley and Sons, 1983, pp 562-570.

10. Larsen, J.M., and Annis C.G. Jr., "Observation of Crack Retardation Resulting from Load Sequencing Characteristic of Military Gas Turbine Operation," Effect of Load Spectrum Variable on Fatigue Crack Initiation and Propagation, ASTM STP 714, D.F. Bryan and J.M. Potter, Eds., American Society for Testing and Materials, 1980, pp 91-107.

11. Macha, D.E., Grandt, A.F. Jr., and Wicks, B.J., "Effects of Gas Turbine Engine Load Spectrum Variables on Crack Propagation," Effect of Load Spectrum Variables on Fatigue Crack Initiation and Propagation, ASTM STP 714, D.F. Bryan and J.M. Potter, Eds., American Society for Testing and Materials 1980, pp 108-127.

12. Ashbaugh, N.E., "Creep Crack Growth Behavior in IN718 in Lab Air," to be presented at ASTM 17th National Symposium on Fracture Mechanics, Albany, NY, August 1984.

13. Stucke M., Khobaib M., Majumdar B., and Nicholas T., "Environmental Aspects in Creep Crack Growth in a Nickel Base Superalloy," to be published in the proceedings of the Sixth International Conference on Fracture, December, 1984.

14. Sandananda, K. and Shahinian, P., "The Effect of Environment on the Creep Crack Growth Behavior of Several Structural Alloys," Mat. Sci. and Eng., 43(2), 1980, pp 159-168.

15. Floreen, S. and Kane, R.H., "An Investigation of the Creep-Fatigue-Environment Interactions in a Ni-Base Superalloy," Fatigue of Eng. Mat. and Struct., 2, 1980, pp 401-412.

16. Weerasooriya, T., "Effect of Frequency on Fatigue Crack Growth Rate at High Temperatures," presented at ASTM 16th National Symposium on Fracture Mechanics, Columbus, OH, August 1983; to be published in ASTM STP.

17. Nicholas, T. and Weerasooriya, T., "Hold-time Effects in Elevated Temperature Fatigue Crack Propagation," to be presented at ASTM 17th National Symposium on Fracture Mechanics, Albany, NY, August, 1984.

18. Nicholas, T., Weerasooriya, T. and Ashbaugh, N.E., "A Model for Creep/Fatigue Interactions in Alloy 718," presented at ASTM 16th National Symposium on Fracture Mechanics, Columbus, OH, August 1983; to be published in ASTM STP.

* Technical Report may be obtained from the National Technical Information Service (NTIS), using the Accession No., write to: The United States Department of Commerce, 5285 Port Royal Road, Springfield VA 22161.

ACKNOWLEDGEMENT

The authors wish to acknowledge the support of Project 2307P102, the Materials Laboratory, Air Force Wright Aeronautical Laboratories, Wright-Patterson Air Force Base, Ohio, USA. The technical assistance of Edward R. Cox and Jay R. Jira is also gratefully acknowledged.

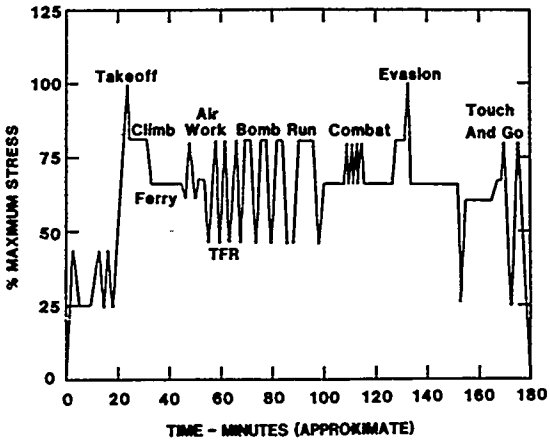

Fig. 1. Composite loading spectrum for an advanced turbine engine (Ref. 1).

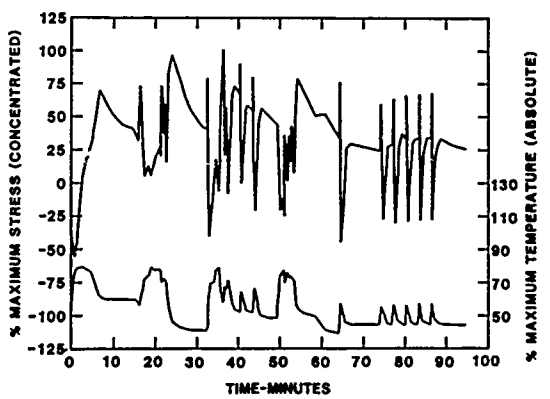

Fig. 2. Typical stress and temperature spectra for a cooled turbine disk rim. (Ref. 1)

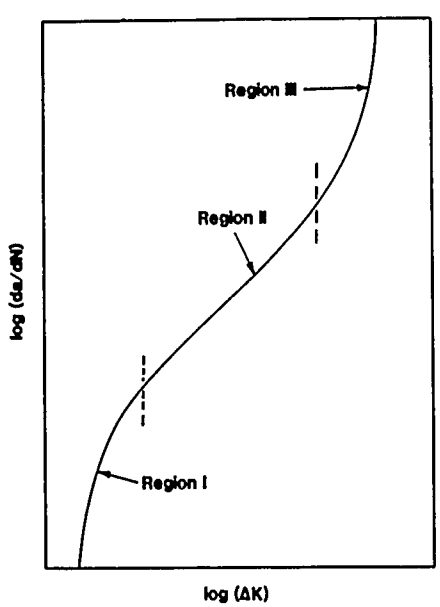

Fig. 3. Schematic of typical sigmoidal shape of crack growth curve.

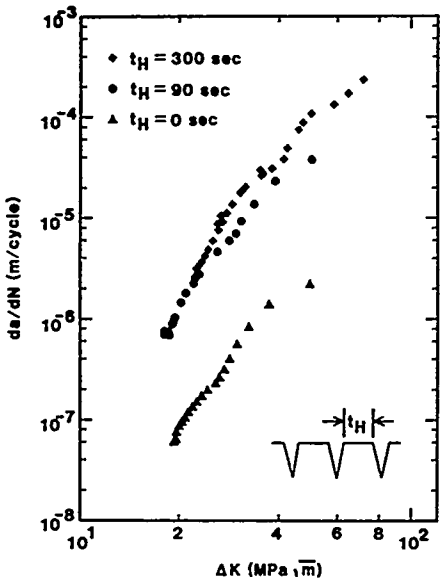

Fig. 4. Experimental data showing effect of hold-time on crack growth in AF115 at 649°C. R = 0.1, f = 0.25 Hz (Ref. 2).

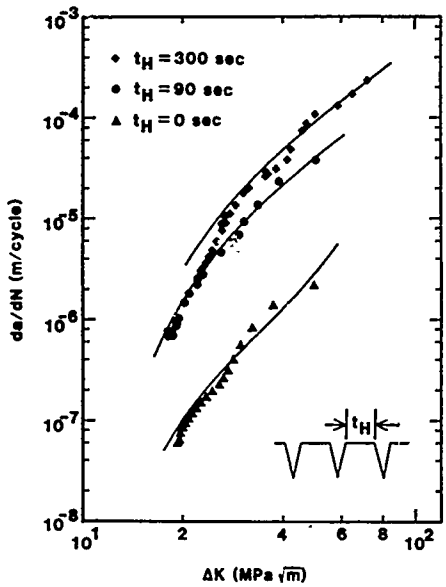

Fig. 5. Analytical predictions of MSE to hold-time data of Fig. 4. (Ref. 6).

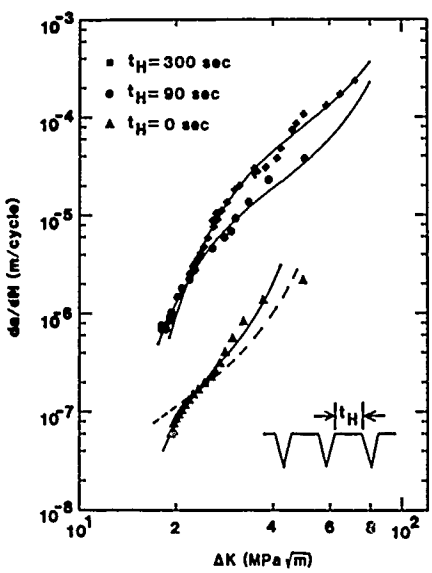

Fig. 6. Analytical predictions of SINH to hold-time data of Fig. 4. (Ref. 6).

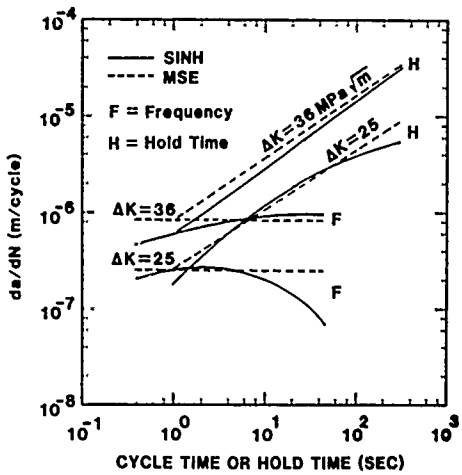

Fig. 7. Predictions of variation with frequency or hold-time for MSE and SINH models. (AF115; 649°C). (Ref. 6).

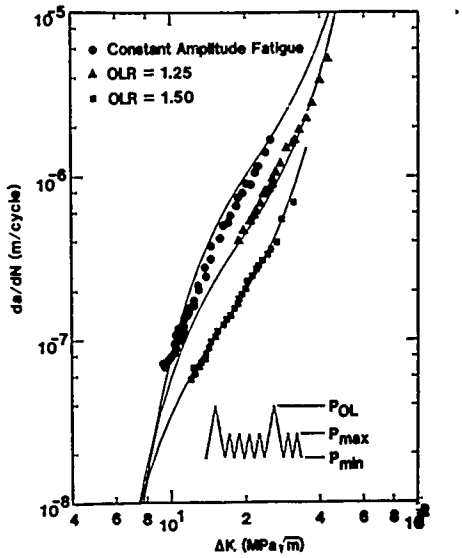

Fig. 8. Effect of overload ratio on fatigue crack propagation in IN100 at 649°C, R = 0.5, ΔN_{OL} = 40 (Ref. 1, 10).

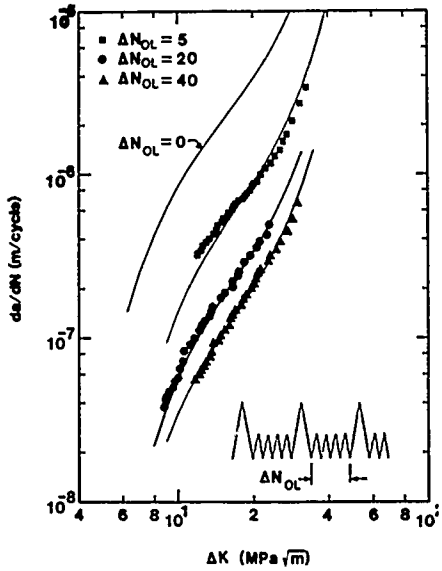

Fig. 9. Effect of number of cycles between overloads on crack propagation in IN100 at 649°C, R = 0.5, OLR = 1.5. (Ref. 1, 10).

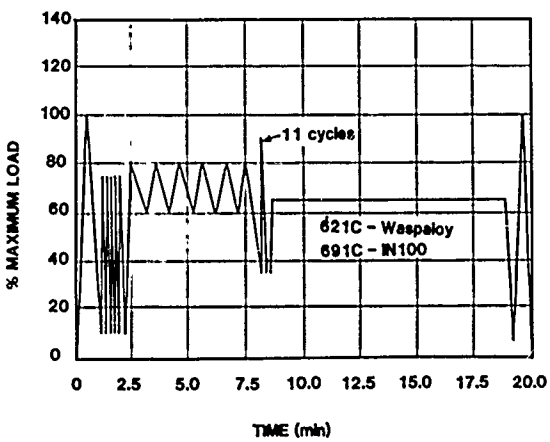

Fig. 10. Crack propagation model demonstration mission No. 1. (Ref. 1).

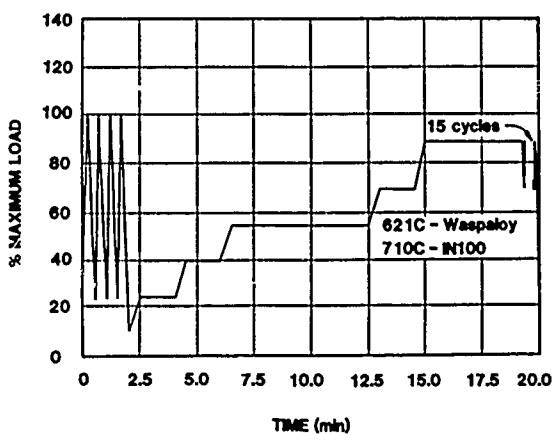

Fig. 11. Crack propagation model demonstration mission No. 2. (Ref. 1).

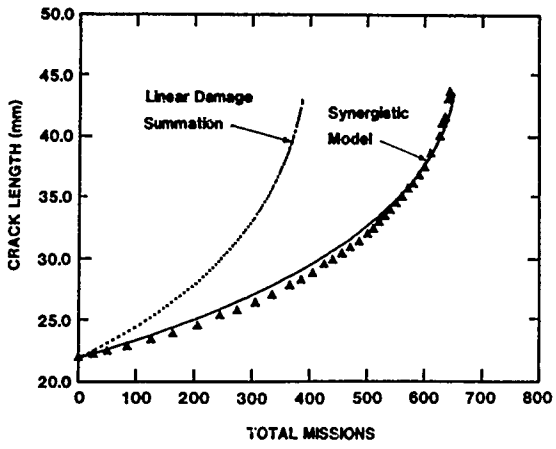

Fig. 12. Example demonstration results for crack propagation model, IN100, 691°C, Mission 1. (Ref. 1).

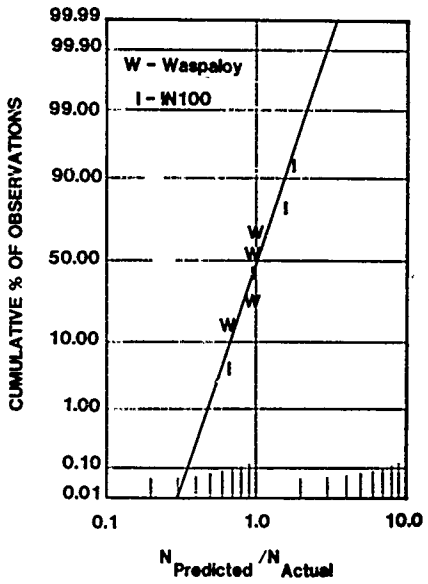

Fig. 13. Demonstration test results for cumulative damage crack propagation model. (Ref. 1).

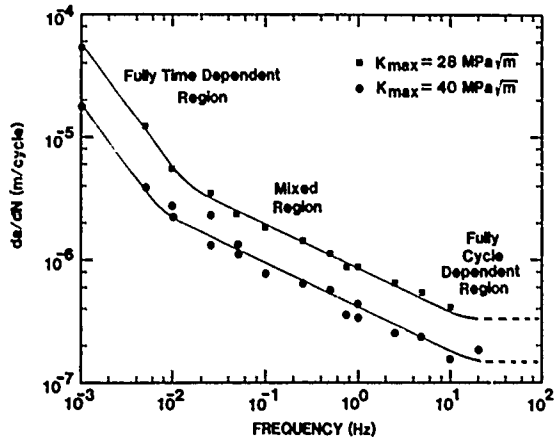

Fig. 14. Effect of frequency on fatigue crack growth rate in Inconel 718, 649°C, R = 0.1. (Ref. 16).

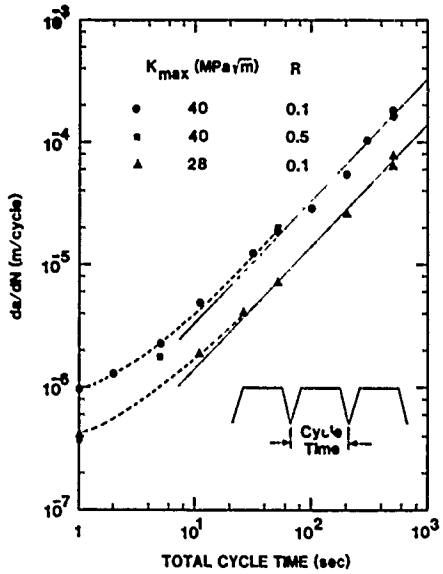

Fig. 15. Crack growth rate for 1.0 Hz fatigue cycle with hold-time at maximum load. Material is Inconel 718, 649°C, R = 0.1. Dashed lines show linear cumulative damage model predictions.

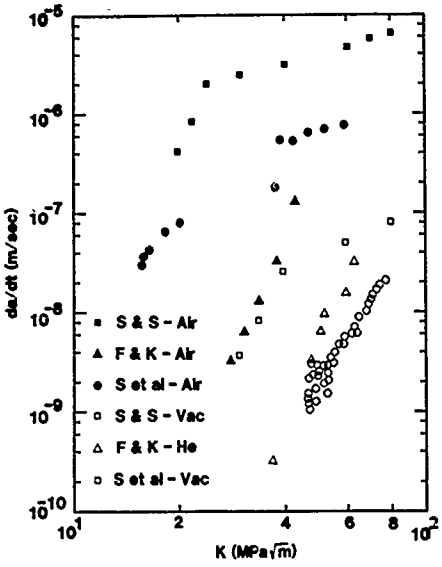

Fig. 16. Sustained load crack growth behavior of Inconel 718 at 649°C obtained in various environments. (S et al, S & S, F & K are Ref. 13, 14 and 15 respectively).

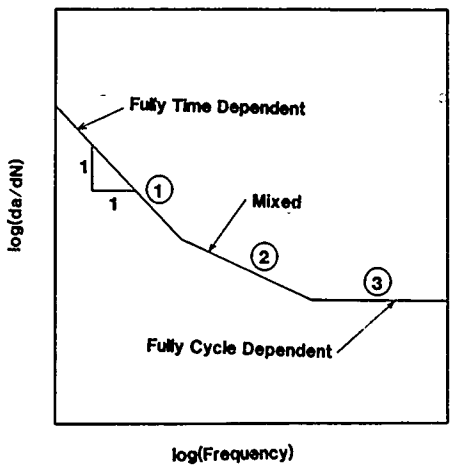

Fig. 17. Schematic of cyclic crack growth rate as function of cycle time (reciprocal of frequency) showing various regions.

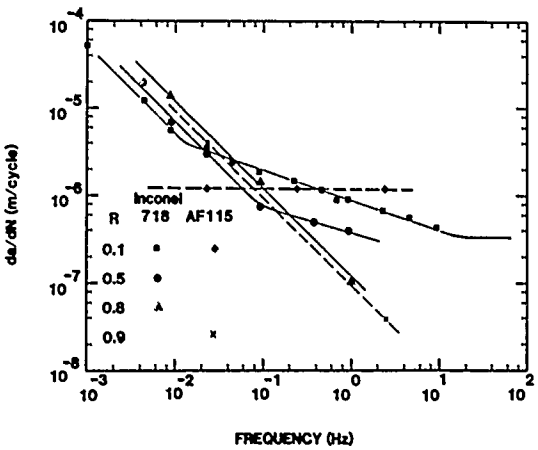

Fig. 18. Effect of frequency and stress ratio on crack growth rate in Inconel 718 and AF115 at 649°C, K_{max} = 40 MPa-m$^{\frac{1}{2}}$. (Refs. 2 and 16).

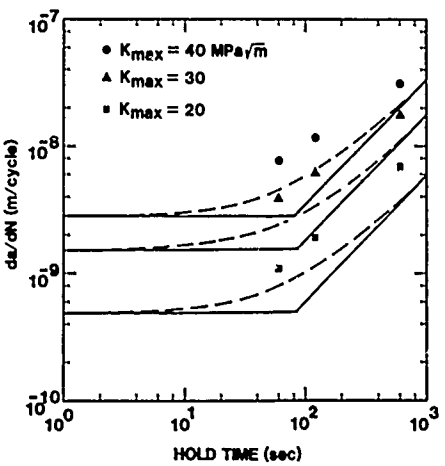

Fig. 19. Crack growth rate for a 0.167 Hz fatigue cycle with hold-time at maximum load. Material is IN100, 649°C, R = 0.1. Dashed lines show linear cumulative damage model predictions. (Data from Ref. 4).

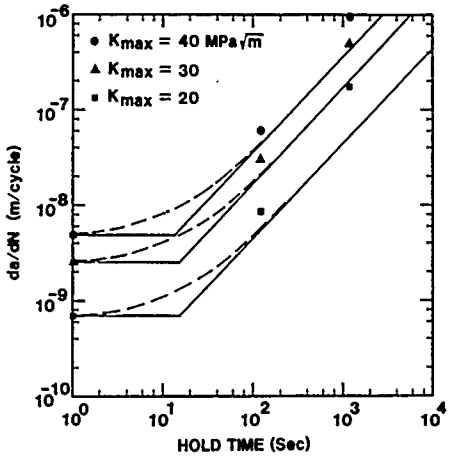

Fig. 20. Crack growth rate for a 0.167 Hz fatigue cycle with hold at maximum load. Material is IN100, 732°C, R = 0.1. Dashed lines shown linear cumulative damage model predictions. (Data from Ref. 4).

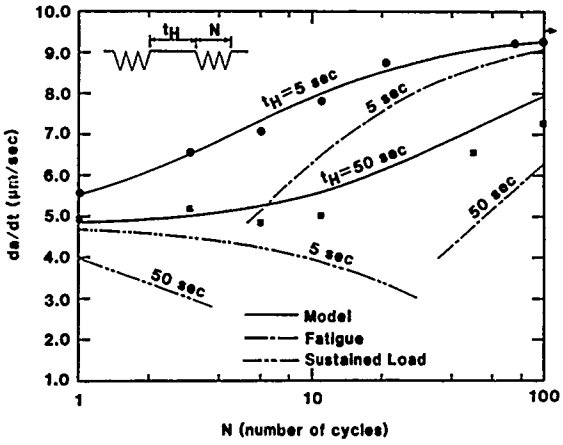

Fig. 21. Crack growth rate for N cycles with hold at maximum load in Inconel 718, 649°C, R = 0.1. Solid lines show linear cumulative damage model predictions. Frequency is 1.0 Hz.

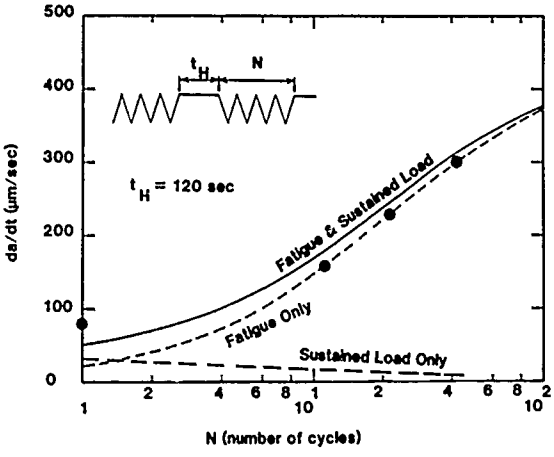

Fig. 22. Crack growth rate for N cycles with hold-time at maximum load in IN100, 649°C, R = 0.1. Solid lines show linear cumulative damage model predictions. Frequency is 0.167 Hz. (Data from Ref. 4).

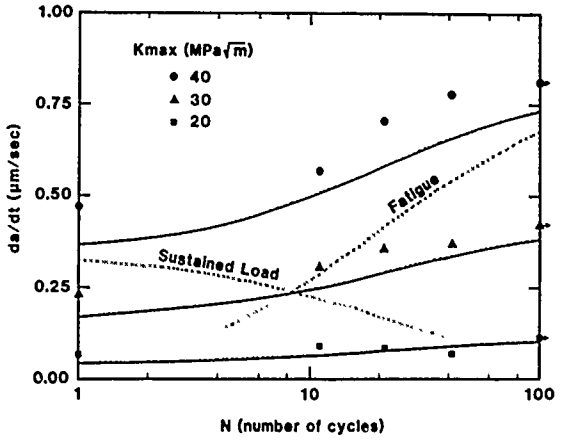

Fig. 23. Crack growth rate for N cycles with hold at maximum load in IN100, 732°C, R = 0.1. Solid lines show linear cumulative damage model predictions. Frequency is 0.167 Hz. (Data from Ref. 4).

DISCUSSION

R.Tadros, Ca

How confident are you when quoting LCF life based on the crack growth data available in the literature at this stage, bearing in mind that other material behaviour studies related to growth of short cracks, closure phenomena, interactions of high and low frequency loading, growth of multiple cracks, crack growth in and near the threshold regime and crack growth in anisotropic materials, have not been fully covered at this stage?

Author's Reply

Confidence in crack growth calculations requires that one does not rely on unknown factors in the areas you mentioned. Confidence in specific calculations is attained by avoiding the unknown range or by developing the appropriate data to adequately answer the specific materials/mechanics questions posed by the given problem. This approach may lead to overly conservative calculations, and not all problems can be solved satisfactorily. The full implementation of a damage-tolerant approach to design of turbine engines requires that additional research be conducted in the variety of areas you mentioned.

D.W.Hoeppner, Ca

In Turbistan activity an attempt is being made to develop a standard load sequence for: (a) evaluation and comparison of materials; (b) evaluation and comparison of manufacturing methods; (c) verification of fatigue life methods; (d) input to fatigue life methods and prediction. This standard load sequence is useful to both the safe life and damage tolerant approaches. In relation to the work you reported, has the US Air Force or your lab or your contractors developed a plan to develop a standard load sequence?

Author's Reply

To my knowledge, neither the US Air Force nor any Air Force contractors currently have plans to develop a standard load sequence for use specifically in evaluations of materials or manufacturing methods. Our approach, as discussed in this paper, has been to attempt to understand the effects of the various components of engine missions and to use this knowledge to guide development of materials and manufacturing methods. Toward this end, the AFWAL Materials Laboratory is conducting various in-house projects to examine interacting effects between cycle-dependent and time-dependent crack growth, and a new contractural programme in the area of cumulative damage modelling will begin in July 1984. In addition to this materials research, the Air Force does have a number of Accelerated Mission Test spectra (as discussed by W.R.Taylor at this meeting) that are used to address various questions of engine durability. These spectra are defined based on specific engine usage, and may be updated as conditions warrant.

D.W.Hoeppner, Ca

In the MSE and SINH models you very nicely described use is made of the threshold parameter. My colleagues and I have used these as well as the four parameter Weibul function, on which since 1974 I have concentrated extensive research. However, in all of these the "goodness of fit" is determined by the threshold as well as other factors. How do the US Air Force or your contractors (GE & PW in this case) obtain the "accurate" threshold inasmuch as we do not have a standard test technique to generate the threshold and the threshold is dependent on microstructure, waveform, etc.?

Author's Reply

To date, the MSE and SINH models have generally not been used to represent crack growth data in the near-threshold regime. Most current damage tolerant life calculations start at values of stress intensity range well above the threshold (K_{th}) due to high stress levels in these components and the starting crack size that is given by inspectability limits. As methods of nondestructive evaluation (NDE) continue to improve, the starting crack size for the damage tolerant calculations will be reduced, and near-threshold crack growth will become more important. However, as you mentioned, there are a number of questions regarding data of ΔK_{th} under realistic engine operating conditions. Research at the Air Force is in progress to address these questions.

D.W.Hoeppner, Ca

Comment — In your oral presentation you mentioned that "small crack" data and "long crack" data often are comparable even below the current "inspection threshold." However, I'm sure you'll agree, when a "large grain" material is involved and we must deal with crystallographic anisotropy (the extreme being a single crystal) the "small crack" data can be significantly different from "long crack" data. In fact, use of K_I as a correlating parameter is not valid in these cases. Dependent on the crystal size, the crack size when this occurs could be much larger than the inspection threshold. This point may have been covered in your last slide under anisotropy effect as well as in your paper under the same topical heading.

Author's Reply

I generally agree with your comment and would like to mention that the Air Force has a number of in-house and contractural research activities in progress in the areas of both the growth of small cracks and crack growth in anisotropic materials such as single crystals.

PROBLEMS AND POSSIBILITIES FOR LIFE EXTENSION IN GAS TURBINE COMPONENTS

A.K. Koul and W. Wallace
Structures and Materials Laboratory
National Aeronautical Establishment
National Research Council
Montreal Road, Ottawa, Ontario K1A 0R6 Canada
and
R. Thamburaj
Department of Mechanical and Aeronautical Engineering
Carleton University, Ottawa, Canada

SUMMARY

The structures and materials community is presently engaged in a number of thrusts aimed to increase reliability, and to extend the lives of engine components both safely and cost effectively. Processes such as hot isostatic processing, crack repair, and new approaches to engine component lifing based on damage tolerance concepts are reviewed.

Data showing the beneficial effects of hot isostatic processing on the stress-rupture properties of new and service exposed Ni-based superalloy turbine blades are presented. Creep design methods that are generally used to highlight the service induced degeneration effects are critically analyzed. A new life prediction method that systematically analyzes the creep degeneration effects with increasing service life is proposed.

Results indicating the successful application of a damage tolerance based maintenance methodology in Canadian Forces J85 engine compressor and turbine discs are discussed. Possibilities of enhancing engine component durability through improved machining techniques and reheat-treatments are also discussed.

1. INTRODUCTION

Over the past twenty-five years considerable work has been performed to investigate the deterioration of turbine engine components in service, and to develop improved designs and degradation resistant materials. The aim has been to improve performance, achieve longer life and to provide trouble free operation.[1-4] Engine components can be separated into two major classes, i.e. those whose deterioration affects only the achievement of maximum thrust and fuel efficiency and those whose deterioration threatens the continued safe operation of the engine. This latter group comprises most of the large rotating components of the compressor and turbine sections such as shafts, discs, wheels and spacers. It is also evident that a malfunction of components such as blades and inlet guide vanes can also seriously disrupt the safe operation of the engine.[5]

Turbine discs and blades of marine, aircraft and land based gas turbine engines are generally made from complex Ni-based superalloys in either wrought or cast form respectively.[1,2] These alloys are strengthened by the precipitation of the intermetallic phase Ni_3 (Al, Ti) i.e. γ' in the grain interiors and by the precipitation of this phase and carbides along grain boundaries. Heat-treatments are therefore carefully designed to achieve a proper balance between intragranular and grain boundary strength. These are controlled by the size, shape and distribution of the γ' and carbide particles.

Improvements in component operational capability have essentially been achieved through proper adjustment of the alloy chemistry to increase the γ' volume fraction and to decrease surface degradation.[6] Progress has also occurred in new processing techniques.[7,8] Perhaps the most remarkable developments in this respect have been the introduction of directionally solidified and single crystal blades[9-11], and the manufacture of powder metallurgy compressor and turbine discs.[3,4,9] Improvements in blade design in the form of internal cooling has allowed the use of increasing gas inlet temperatures, which eventually lead to a reduction in specific fuel consumption and higher thrust to weight ratio in dry engine operations.[12,13]

The stage has been reached where dramatic improvements in engine material performance can no longer be expected in the near future and manufacturers and operators alike are beginning to consider ways of extending the lives of gas turbine components by less traditional methods. These approaches have included hot isostatic processing of turbine blades, weld repair of cracks and the development of design and maintenance methodologies based on damage tolerance concepts.[14-17] One important incentive for such initiatives is reduced cost of ownership over the full life cycle of the engine, but the overriding considerations are reliability in performance and safety.

The lives of various engine components are limited by service induced degeneration effects such as fatigue, creep, erosion and a variety of different environmental reactions. The precise form of deterioration however depends on the part, its design function, operating environment and the materials used in manufacture. The life limiting factors of the major turbine engine sections are summarized in Table 1. This paper will concentrate on the life extension possibilities of the major components, namely, turbine blades, and turbine and compressor discs. The purpose of this paper is to examine these life extension methodologies and to review the associated methods of testing and analysis that are required for component substantiation.

2. PROBLEMS AND POSSIBILITIES OF LIFE EXTENSION

The following subsections will deal with the problems and possibilities of life extension in the above mentioned components.

2.1 Turbine Blades

Creep damage has traditionally been recognized as a major form of airfoil deterioration.[12,18] In cooled blades however, the external airfoil surface is impinged by hot gas while internal cooling passages are chilled and consequently severe thermal gradients exist across airfoil walls and severe thermal transients occur during heat-up or cool-down.[12] Therefore, cumulative damage effects of creep and thermal fatigue are considered for accurate in-service life prediction of cooled blade airfoils.[13] Other forms of damage

caused by events such as foreign object ingestion into the engine can also lead to catastrophic failures. Impact due to ingested small objects may form notches and crack-like discontinuities in airfoils and other components that can result in premature failures. Manufacturers must therefore consider impact damage tolerance of all components, perhaps using fracture mechanics concepts.[19]

To present an overview of all life limiting factors in turbine blades is beyond the scope of this paper, but a critical assessment of the major form of damage, i.e. creep, will be carried out here.

2.1.1 Creep Damage Assessment Using Conventional Data Base

Creep testing and its analysis should be realistic and reliable for establishing design life limits for new blades. A number of parameters, classified under the general category of Minimum Commitment Method (MCM) and the Graphical Optimization Procedure (GOP), are available for accurate extrapolation of the short-term creep test data to design stresses.[20] These parameters include the Larson-Miller parameter, the Manson-Haferd parameter, the Monkman-Grant equation and the Dobes-Milicka equation. A considerable number of arguments have, however, centered around the differences in the predominant mode of deformation during short-term laboratory creep testing and those actually encountered by the components during service. In the current context, however, the ability of a method to consistently highlight the service induced degeneration and rejuvenation effects is of utmost importance.

The Larson-Miller (L-M) parameter is the most widely used method for correlating stress, temperature, and time to rupture or more often, life to a specified value of creep strain of ~0.1%.[21,22] The parameter 'P' is defined as,

$$P = T \times 10^{-3} (C + \log t_R) \tag{1}$$

where T is the temperature in °K, t_R is the life in hours and C is a constant assumed to have a universal value of ~20. The temperature and stress dependent life sensitivity of typical blade materials, such as Udimet 700 and IN 100, is indicated in Table 2. Using nominal stress values of 210 MPa and 345 MPa, it is evident that a change of 40°C in metal temperature changes life by more than an order of magnitude. Similarly, an increase in stress from 210 MPa to 345 MPa decreases life by more than an order of magnitude. Table 2 also indicates that IN 100 can sustain 40°C higher operating temperatures than Udimet 700 for similar service life periods.

Creep life data collected over a range of temperatures and stresses for a given material are also presented in the form of L-M parameter scatterbands such as plotted for Inconel Alloy X-750 and IN 738LC in Figures 1 and 2 respectively.[15,23] Superimposed on the new material scatterbands are the data points from service exposed material. The service induced creep damage effects on rupture life are quite evident in some tests, where the data fall below the lower limit of the scatterband for new material. In contrast, some data for service exposed material fall well within the scatterband of the new material. The ability of the L-M method to detect creep degeneration effects is therefore questionable. The success of the L-M parameter in high temperature creep design can perhaps be attributed to its conservative estimates of long term rupture life.[24,25] It has been suggested that C values other than 20 may lead to better correlation of actual stress-rupture data.[24-26] The constant C is said to vary from one material to another and its value can be determined using the method outlined by Furrillo et al.[24] It has also been shown that in a given material, the C value at lower stresses is very different from that calculated at higher stresses, since creep yield phenomenon predominates below a certain stress level.[25] Whether these modifications can distinguish between the service exposed and the new material has not been ascertained as yet, but minimizing the data scatter problems through these modifications is considered unlikely.[23]

Another creep design relationship, defined by Manson-Haferd (M-H) parameter,[27] postulates that for a given material and stress level there exists a unique value of a parameter 'P'' that is related to temperature and time by the equation

$$P' = \frac{T - C'}{\log t_R - \log t'} \tag{2}$$

where T is the temperature in °F, C' and log t' are material dependent constants having values of approximately 100 and 17 respectively for most γ' strengthened Ni-based superalloys. This relation is considered to be more accurate for service life prediction than the L-M parameter, but it is not as widely used for design purposes. The scatterband obtained using the M-H relationship with data for IN 738LC is shown in Figure 3 together with data for service exposed material. A number of service exposed data points fall well within the new material scatterband, thus indicating the inability of this method to detect service induced creep degeneration.

Many relationships have been proposed between the secondary or minimum creep rate ($\dot{\epsilon}$), time to fracture (t_R) and total creep strain (ϵ_R) and these have been used to analyze data from constant load, accelerated uniaxial creep tests. The correlation between $\dot{\epsilon}$ and t_R is most commonly described in the form of a relationship proposed by Monkman and Grant[23], where

$$t_R \dot{\epsilon}^m = C_1 \tag{3}$$

and m and C_1 are material dependent constants. Dobes and Milicka[29] proposed the inclusion of a normalizing parameter (ϵ_R) to modify Equation (3), where

$$\left(\frac{t_R}{\epsilon_R}\right) \dot{\epsilon}^{m^*} = C^* \tag{4}$$

and m^* and C^* are material constants. Neither Equations (3) or (4) are able to avoid the data scatter, or to differentiate between the new and service exposed IN 738LC creep properties, Figures 4 and 5. These complexities have been discussed at length elsewhere[23], but it will suffice to say here that the erratic nature of the tertiary creep component of the overall creep curve in complex engineering alloys is responsible for such difficulties.

In conclusion, the conventional creep data base is unable to consistently highlight the microstructural degradation effects in service exposed turbine blades.

2.1.2 Influence of Defects on Creep Data Base

As mentioned earlier, the use of precision investment cast alloys has considerably improved the turbine blade operational capability. Notwithstanding the economic merits of investment casting, the process is not without problems. Random casting defects such as shrinkage cavities, hot tears, microporosity and inhomogenity can lead to very high scrap rates. Inhomogenities and hot tears can largely be controlled through heat-treatments and casting parameters respectively, but shrinkage cavities and microporosity can only be eliminated by hot isostatic pressing (HIP), Figure 6.[30,31] This involves simultaneous application of heat and pressure to parts in an autoclave.

Stress-rupture properties of investment cast and HIP processed IN 738LC are compared in terms of the L-M parameter versus stress plots in Figure 7. The reduced scatter and the improved properties at the lower limit are noteworthy. Elimination of shrinkage cavities and microporosity therefore allows the use of higher design stresses in components.

The inherent scatter in the stress-rupture data is nevertheless evident in the L-M scatterband for HIP processed IN 738LC blades, Figure 7. However, the data for service exposed material still falls within this reduced scatterband for new HIP processed material, Figure 2, thus demonstrating the problem of detecting service induced degeneration.

2.1.3 Possible Improvements in Creep Data Base

In view of these scatter problems a new creep design relationship based on the isolation of tertiary creep life and strain from the overall creep curve, was recently proposed.[23] Primary plus secondary creep lives ($t_p + t_s$) normalized by their respective primary plus secondary creep strain values ($\epsilon_p + \epsilon_s$) reveal a straight line relationship as a function of secondary creep rate ($\dot{\epsilon}$) in IN 738LC blades on a logorithmic plot, Figure 8. This relationship indicates minimum scatter over a wide range of stresses (350-700 MPa) and temperatures (760-890°C), with a correlation coefficient of ~1.00. The relationship can be represented by,

$$\left(\frac{t_p + t_s}{\epsilon_p + \epsilon_s}\right) \dot{\epsilon}^M = K_1 \qquad (5)$$

where M and K_1 are constants. An M value of unity and a K_1 value of 0.979 was observed for new IN 738LC.

Equation (5) is capable of detecting the service induced degeneration effects in IN 738LC, Figure 8. This can be attributed to the differences in the primary creep data for new and service exposed material. For service exposed material a continuous decrease in t_p and/or an increase in ϵ_p is observed with increasing service life. Microstructurally, these effects might be related to service induced precipitate coarsening, since recovery mechanisms can be considerably accelerated during further creep testing. The influence of service exposure is primarily to decrease the K value in Equation (5), whereas the slope M is of the order of unity in all cases, Figure 8.

2.1.4 Life Extension Through Rejuvenation and Repair

2.1.4.1 Rejuvenation

The major causes of blade replacement at overhaul include loss of material strength and blade airfoil growth beyond acceptable limits which may be as little as 1-2%. Notwithstanding various forms of surface damage caused by erosion, corrosion and impact etc., the internal damage is the prime factor responsible for blade growth during service.[15] Internal damage in Ni-based superalloy turbine blades is related to microstructural changes which occur slowly during service, depending on alloy composition and service operating conditions. During long time exposure under high stresses at high temperatures, structural changes in the form of γ' particle coarsening, grain boundary carbide morphology changes, creep induced cavitation on grain boundaries aligned normal to the stress axis and brittle intermetallic phase precipitation such as σ phase can occur, Figure 9.[32] These microstructural changes are detrimental to properties such as strength, ductility, and notch sensitivity.

Earlier workers[33,34] had suggested that the majority of microstructural changes could be reversed by applying simple reheat-treatments involving complete solutioning followed by controlled ageing. Elimination of creep cavitation damage is, however, unlikely by a conventional reheat-treatment. Irreversibility of service induced primary MC type carbide degeneration adds to the complexities of the problem even further. Inconel alloy X-750 blade data in Figure 10 clearly indicate that after long service exposures it is not possible to restore properties completely by a reheat-treatment alone. Full restoration of creep properties is however possible through HIP rejuvenation processing as evident in Figure 10.[15,32,35]

HIP processing involves simultaneous application of high temperature and high pressure in an autoclave. The combination of heat and pressure collapses internal creep cavities in blades and diffusion bonds the cavity surfaces together. The selected HIP temperature is usually above or close to the γ' solvus temperature in order to ensure that the material flows readily under the hydrostatic pressure. Other factors to consider in the selection of an appropriate HIP temperature include the extent of primary MC carbide degeneration and time-temperature dependence of abnormal grain growth.[36,37] A post-HIP reheat-treatment is generally required to restore the microstructure of the alloy to its pre-service condition.[15] The selection of an appropriate post-HIP reheat-treatment cycle must consider a number of parameters, namely,

(i) Abnormal grain growth of the service exposed material.[37]

(ii) Formation of serrated grain boundaries where applicable.[38-41]

(iii) Grain boundary carbide precipitate morphology.[36]

(iv) Size and shape of γ' precipitates.[36]

These microstructural features are interrelated, and the optimum results are obtained by proper control of solution temperature, cooling rate, partial solution temperature and aging treatment.

A quantitative analysis of microstructural degradation in service exposed turbine blades has traditionally involved creep cavitation assessment using optical metallographic techniques.[42] It has however been suggested that the possibility of ultra-fine creep cavity formation in service exposed turbine blades should not be overlooked in damage assessment procedures.[43,44] Creep cavities may sometimes be too fine to be resolved either by optical or scanning electron microscopy techniques. The existence of ultra-fine cavities can only be verified by stress-rupture testing of the service exposed specimens. A typical example of this behaviour is shown in Figure 11, where service exposed Nimonic 105 turbine blade (62,000 hours exposure) samples did not reveal any distinct creep cavities in the grain boundary regions. However, the improved rupture life of the HIP plus heat-treated stress-rupture specimens over specimens that were merely heat-treated suggests that the latter contained some ultra-fine cavities, Figure 12.

A major criticism of rejuvenation technology has been the irreversibility of blade growth during hipping. The blade airfoil tips can however be machined to meet the original tip clearance specifications. The use of abradable internal seals in the original engine design improves the chances of applying HIP rejuvenation technology even further. It is envisaged that a typical turbine blade can be HIP rejuvenated more than once before blade growth reaches dangerous levels to cause tip rub during engine operation. In the case of coated turbine blades, the coating can be stripped prior to hipping and reapplied before returning them to service.

The HIP rejuvenated X-750 turbine blades discussed in Figure 10 have now been in service for well over 40,000 hours in an industrial gas turbine engine. The rejuvenated blade performance has been monitored on a continuing basis and there is no evidence of accelerated ageing or blade growth to date.

2.1.4.2 Repair

Unlike turbine vanes, where surface degradation, minor impact damage and cracks are repaired by standardized procedures recommended by turbine engine manufacturers[45-48], turbine blade repair is relatively recent.[49-52] The reluctance in repairing rotating airfoil sections can largely be attributed to the failure of traditional welding techniques in meeting the stricter structure-properties requirements consistently. Turbine vanes in many current and past engines are made from cobalt-base superalloys, which possess relatively good weldability and are amenable to repair through traditional fusion welding techniques. High performance turbine blades on the other hand are made from high strength Ni-base superalloys (γ' volume fractions ~25-55%), which frequently exhibit poor welding response and thus present problems, Figure 13. Two basic problems exist in the welding of precipitation hardened Ni-base superalloys.

(1) Hot cracking — This occurs during the weld solidification and cooling sequence due to thermal contraction strains.

(2) Strain-age or post-weld heat-treatment cracking — This occurs during heat-treatment after welding due to residual welding stresses and strains.

Detailed reviews of the mechanisms of these types of cracking have been given elsewhere.[53,54] In general, to minimize cracking, the parent metal should have as fine a grain size as the application will permit and should be welded with the minimum heat input required. However, grain size can not be decreased in a service exposed part.[37] Overageing the base metal prior to welding (which leads to softening and homogenization) and conducting the post-weld heat-treatment in an inert environment are effective ways of reducing crack sensitivity.[55] But, even careful control of welding parameters and pre-weld/post-weld treatments can not ensure a crack-free weld in several high strength Ni-base superalloys. In view of the difficulties with the traditional fusion welding, other techniques that were originally developed for turbine vane repair have been explored.[49-52] These techniques include,

(a) Brazing

(b) Solid-state diffusion bonding[16], and

(c) Transient liquid phase (TLP) bonding.

Several techniques similar to TLP have been developed and are known by names such as,

(i) Activated diffusion bonding

(ii) Diffusion brazing

(iii) Eutectic bonding.

A detailed account of these bonding techniques can be found elsewhere.[50,55]

Ni-base superalloy brazing involves the use of non-gamma prime filler alloy having a melting point below that of the blade alloy and the repair is carried out in vacuum or in a controlled environment. Use of brazing is however limited to minor blade repairs, such as minor impact and environmental damage, due to limited strength and ductility of the brazed joints. Major repairs in high performance blades that operate at very high service temperatures, can not be carried out because of the tendency of the braze to remelt if overheated.

Major repairs through solid-state diffusion bonding are possible where two clean nominally flat surfaces are to be joined. Hot pressing or HIP are commonly used to create the required pressure, but excessive pressures may lead to cracking. Soft interlayers may be used between the surfaces (e.g. Nickel for Ni-base superalloys) to permit the application of lower pressures to achieve interface conformity. The composition and thickness of the interlayer are important factors which govern the mechanical properties of the joint and a number of solute segregation problems can deleteriously affect the overall blade properties. The process however requires elaborate tooling and equipment, which makes it expensive.

Various forms of liquid phase diffusion bonding techniques are of interest. The processes use a thin interlayer or powder overlays of carefully selected composition, that are either placed in between the old and new blade sections or over the degraded airfoil areas respectively. The assembly is then heated to the bonding temperature in a vacuum or in an argon atmosphere. While the parts are held at the bonding temperature, rapid diffusion of alloying elements occurs between the interlayer/overlayer and the base material. This change of composition at the interface causes the joint to solidify isothermally, thus creating a bond. After isothermal solidification has occurred, the joint microstructure generally resembles that of the base metal except for minor compositional and structural variations. Overlay coating results in at least three distinct zones, the base metal, the diffusion zone and the overlay coating. These processes generally do not require elaborate tooling thus making them economically attractive.

Figure 14 shows an example of the quality of powder overlay repair of a heavily degraded Udimet 500 turbine blade.[52] Typical stress-rupture properties of TLP bonded DS MAR-M-200 + Hf airfoil sections are compared with the parent metal data at 980°C in Figure 15.[47] Similar data is presented for Udimet 700 at 980°C and 870°C creep test temperatures respectively in Figures 16(a) and 16(b).[50] These data clearly indicate that the creep strength of TLP bonded specimens are not inferior to those of the base metal properties. Prior to applying TLP or powder overlay repair processes it is necessary to employ strict cleaning and inspection procedures to obtain base metal properties in the repaired blade areas.[52,55]

Finally, the cost effectiveness of HIP rejuvenation plus repair versus turbine blade replacement must be considered in terms of overall life cycle management. As a guideline, rejuvenation and repair cost should be no greater than 65% of replacement cost to justify costs incurred during installation of a rejuvenation-repair line. Experience with industrial gas turbine engines indicates that HIP rejuvenation costs are less than one third of the replacement blade costs.

2.2 Compressor and Turbine Discs

Until the end of 1950's, the main factors considered for compressor and turbine discs were the creep properties of the rims and tensile properties of bore and rim materials to give a satisfactory overspeed margin without burst. However, low cycle fatigue (LCF) was soon realized to be the principal cause of most of the disc failures, and therefore manufacturers began to base life predictions on the LCF crack initiation behaviour of disc materials.

Modern turbine discs experience operating temperatures of the order of 700-800°C and therefore the combined effects of creep, fatigue and oxidation and their synergistic interactions are of concern.[56] It has also been widely recognized that defects may be present in parts as-manufactured, and therefore an understanding of the growth of small cracks from pre-existing flaws is considered important. Sensitive and reliable NDI procedures to detect these flaws have emerged. The methods of testing and analysis to establish cyclic durability of discs have therefore passed through several phases of development, with methods based on fracture mechanics concepts being the most recent to emerge. These latter methods are beginning to assume particular significance in Canada as a result of a number of disc and other component failures where impact induced damage has led to premature failures.

2.2.1 LCF Life Prediction in Compressor and Turbine Discs

Because of the inherent scatter in LCF crack initiation data component lifetimes were first established from specimens data at the lower end of the statistical life distribution curve, typically -3σ from mean, Figures 17 and 18.[17,57] All parts would be rejected at the life limit irrespective of condition, and in-service NDI would be employed to safeguard against premature fracture. By implication, one part in one thousand would be expected to contain a crack of a size in excess of the detection limit at retirement, while the remainder would either be crack free or contain undetectable flaws. For presently available NDI methods the detection limit is about 0.8 mm, depending on material type, crack location, accessibility and confidence level assumed.

Crack initiation data is generated on smooth, strain-controlled LCF test specimens at approximated service temperatures.[58] It is assumed that the specimen simulates the local behaviour of the material at a geometric discontinuity in a disc. The smooth test specimen generally predicts life under repeated single-cycle load application. The actual mission to be evaluated involves a sequence of cycles differing in strain range and mean stress. To determine life for such a mission certain cycles producing negligible damage may be ignored and a cumulative damage evaluation made for the remaining cycles. The smooth specimen testing data base is used for LCF life prediction during disc design. The final step involves verification through spin-pit testing, where stress-strain distributions more typical of flight conditions can be generated. Accelerated mission tests (AMT) and simulated mission endurance tests (SMET) are also conducted to check engine endurance.[59] However, the high cost of component testing dictates the use of test data from smooth specimens and finite element based component analysis for design.[60]

LCF at room temperature (relevant to some compressor discs) is a time independent plasticity process in which the parameter governing the life of a specimen is the alternating plastic strain amplitude for a completely reversed system. The life of a specimen in LCF at low temperatures is given by the Coffin-Manson equation[61],

$$\frac{\Delta\epsilon_p}{2} = \epsilon_f' (2N_f)^c \tag{6}$$

where $\Delta\epsilon_p/2$ is the plastic strain amplitude, ϵ_f' is the fatigue ductility coefficient proportional to the fracture ductility in monotonic tension, N_f the cycles to failure and c the fatigue ductility exponent. Later work indicated that total strain ($\Delta\epsilon$) amplitude (elastic, $\Delta\epsilon_e$, plus plastic, $\Delta\epsilon_p$) correlated better with life. This modified the equation for strain-life data for LCF smooth specimens:

$$\frac{\Delta\epsilon}{2} = \frac{\Delta\epsilon_e}{2} + \frac{\Delta\epsilon_p}{2}$$

or

$$\frac{\Delta\epsilon}{2} = \frac{\sigma_f'}{E}(2N_f)^b + \epsilon_f' (2N_f)^c \tag{7}$$

where σ_f' is the fatigue strength coefficient related to true fracture stress in monotonic tensile test, E the elastic modulus and b is the fatigue strength exponent. To determine the life of a specimen subjected to a number of different cyclic strain conditions, Miner proposed a cumulative damage rule, where

$$\sum_{i=1}^{N} \frac{N_i}{N_{fi}} \simeq 1 \tag{8}$$

where N_i is the number of cycles at a given strain amplitude, and N_{fi} the corresponding life under the same conditions evaluated by Equations (6) or (7).

At elevated temperature (relevant to turbine discs and some compressor discs) time-dependent deformation in the form of creep can occur during cyclic loading.[58,62,63] Under constant amplitude loading, it is possible to develop a variety of steady state hysteresis loop shapes such as shown in Figure 19. It should be pointed out that at low temperatures, only the loop shown in Figure 19(a) need be considered. The life prediction methods developed to cope with these various loop shapes can be classified as, (i) Damage summation, (ii) Strain-range partitioning, (iii) Frequency modification, (iv) Ostergren's method and (v) Majumdar's method. A detailed account of these methods can be found elsewhere[50,63], and therefore only a brief review will be given here.

In damage summation, it is assumed that damage in creep is effectively the same as damage in fatigue and a linear interaction relationship is established.

$$\sum_{i=1}^{N} \frac{N_i}{N_{fi}} + \sum_{K=1}^{q} \frac{t}{t_f} \leqslant D \tag{9}$$

where t is the time duration of the load condition K and t_f is the allowable creep time at a given stress intensity from load, K. A disadvantage of this approach is its inability to account for compressive creep, since monotonic tensile creep data can not be reconciled with the compressive creep behaviour. In addition, if a material undergoes cyclic hardening or softening, the rupture lives calculated on the basis of monotonic behaviour could be very inaccurate. Finally, the long term rupture lives are usually calculated from time-temperature parameters which are themselves in question when used for extrapolating purposes.

Strain-range partitioning (SRP) was developed by Manson and Co-workers[64,65], and uses four basic types of cycles shown in Figure 19(a) to 19(d). Any general loading cycle is considered to be made up of these four basic types and the four basic material-life time correlations are developed to compute the net damage resulting from the relative contribution of these components. The damage per cycle is represented in terms of total plastic strain that consists of different plastic strain fractions pp, pc, cc and cp, i.e.

$$\frac{1}{N_f} = \frac{f_{pp}}{N_{pp}} + \frac{f_{cc}}{N_{cc}} + \frac{f_{cp}}{N_{cp}} + \frac{f_{pc}}{N_{pc}} \tag{10}$$

where pc denotes plastic tensile strain reversed by creep strain in compression and other three strain fractions can be interpreted from Figure 19. Thus the creep and tensile ductilities for the four fractions are measured for the specific time, temperature and environment anticipated for the structure. The applicability of SRP to turbine disc materials was investigated under an AGARD-SMP cooperative testing programme in 1978.[66] The applicability of SRP varies markedly with the material and test conditions. SRP in its current form is said to be unsuitable to either predict the effect of mean stress on life time or to correlate crack propagation.[58,66] At the strain ranges encountered in turbine discs ($\sim 10^{-4}$), the accurate partitioning of various components was found to be impractical.[66]

Equations (6) and (7) simply relate elastic and plastic strain range to the number of cycles to failure. These simple relationships are unable to describe crack initiation under many different types of cycle frequencies and wave shapes at elevated temperatures.[67,68] The methods devised to include these effects are described as frequency modifications. Room temperature fatigue life relationships are therefore modified through frequency (ν) dependent factors, i.e.

$$\Delta\epsilon_p = C_2 \left(N_f \nu^{K'-1}\right)^{-\beta} \tag{11}$$

and

$$\Delta\epsilon_e = \frac{A'}{E} N_f^{-\beta'} \nu^{K''} \tag{12}$$

where C_2, A', β, β', K' and K'' are material constants to be determined. The quantity $N_f \nu^{K'-1}$ is called the frequency modified life, $\Delta\epsilon_p \nu^{\beta(K'-1)}$ is called the frequency modified plastic strain-range and $\Delta\epsilon_e \nu^{K''}$ is the frequency modified elastic strain-range. The wave shape effects are considered through a frequency factor $\left(\frac{\nu_t}{\nu_c}\right)^{\beta c'}$, where ν_t is the tension-going (t) time frequency and ν_c is the compression-going (c) half cycle frequency. The striking feature of this approach is its ability to separate environmental effects in elevated temperature fatigue.[63,67] The method however requires a large data base for evaluation of the parameters for statistical reliability.[58] Under isothermal, uniaxial, time dependent and time independent cycle boundary conditions, the accuracy of predicted lives lie within a factor of two from the observed lives.[58]

Other LCF life prediction methodologies such as Ostergren's method[69] and Majumdar and Maiya's method[70,71] are relatively recent developments in the field. Much work remains to be done to evaluate these methods and to develop the data bases needed for design.[58]

There are two major concerns with the traditional LCF crack initiation approach. The first is the fact that it does not fully account for the possibility of a flaw existing in the new part as-manufactured. Secondly, most of the discs are discarded in a crack free condition and may have residual safe life remaining. Figure 20 for example, from a USAF analysis of the F100 1st stage turbine disc at retirement, indicates that over 80% of the discs should have at least 10 lifetimes remaining.[57]

2.2.2 The Use of Damage Tolerance Concepts in Durability Analysis

Damage tolerance concepts are being considered for use both at the design stage, for stress analysis and for lifing procedures, and to establish intervals for inspection and repair during service. It is assumed that flaws exist in parts as manufactured, at a size just below the NDI detection limit, and these may be located in the most highly stressed regions or hot-spots of the component. It is further assumed that these flaws will grow in-service, at a rate determined by the local stress (mechanical and thermal) distribution around the flaw, the operating temperature and the environment, Figure 21.[72,73] These parameters will vary with time as a function of engine power setting (demand) and the detailed time histories will therefore be a function of the operational mission profile or use. The general objective of the damage tolerance approach is to establish expected crack growth rates for realistic operating conditions and to implement NDI procedures with an appropriate level of sensitivity, reliability, and frequency to ensure that cracks can be detected and if feasible monitored in service to a point where *risk* of rapid or unstable crack propagation becomes severe, Figure 22.[74-76] Flawed parts are therefore retired on an individual basis when their condition dictates. The "critical" crack length, or length at retirement is therefore a function of many variables including material type, component design, operating environment, engine usage, engine use monitoring system employed and NDI procedures employed.

2.2.2.1 Application of Damage Tolerance Concepts

In order to employ damage tolerance maintenance methodology with actual operating components, considerable information should be available to the engine life cycle manager. This includes at least the following:

(i) The condition of material must be known at all times.

(ii) Crack "initiation" sites must be known and must be inspectable.

(iii) A statistically significant distribution of the number of service hours required to propagate a pre-existing flaw to a detectable size must be available.

(iv) Crack growth rates beyond the detection limit must also be known under realistic mission profiles and operating conditions.

(v) Cracks must be detectable.

(vi) Both the critical crack lengths and the limiting safe crack lengths must be known for the actual operating conditions.

(vii) Inspection intervals must be established from (iii), (iv) and (vi) to ensure that a crack does not propagate to beyond the safe crack length during the period between planned inspection, i.e. a safe crack propagation interval.

The data base for item (iii) above should normally be available from manufacturers, since these data are generated during the early stages of disc design. The statistical significance of these data can be represented in the form of Weibull plots, Figure 23, where service exposure time can be plotted against percentage probability of the presence of a detectable crack. A detailed account of a Weibull analyses of LCF data can be found elsewhere.[77] Information regarding the potential crack initiation locations should also be available from the manufacturers, since their spin-pit testing experience gathered during disc design can be useful in this area. The manufacturer should also be in a position to advise on the likelihood of cracks initiating in the bolt holes, disc hub and rim serrations.

The next logical step is to establish the crack growth rates beyond the detection limit under conditions simulating disc rpm's, i.e. the appropriate centrifugal and aerodynamic forces. These forces or loads create a three dimensional stress state ahead of the crack tip that is responsible for crack advancement. Knowing that crack growth rates depend upon the conditions ahead of the crack tip, intense efforts have been made to determine a parameter that would uniquely describe these conditions. So far, three main parameters have been developed, namely, the stress intensity factor (K), the J-integral and the J*-integral. Basically, the stress intensity factor (K) uniquely describes the stress-state ahead of the crack tip. This parameter is suitable for cases in which plastic deformation is limited to a very small zone ahead of the crack tip and fracture occurs under nominally brittle conditions.[78] In cases where significant deformation is possible, the other two parameters may be more applicable.[79] The J-integral is said to describe the stress-strain field ahead of the crack tip while the recently developed J*-integral is believed to describe the stress-strain rate field.[80] However, the difficulties associated with the experimental evaluation of J and J* have inhibited the widespread application of these parameters to correlate crack growth rates.[81] These limitations therefore force the use of the stress intensity factors corresponding to appropriate centrifugal and aerodynamic forces to calculate crack growth rates at varying crack lengths at operating service temperatures. This type of data can be used to define a critical crack length or a dysfunction limit for a given component. Crack lengths greater than the dysfunction limits result in unstable crack growth, i.e. excessive crack growth rates, under service conditions.

In a given set of discs that are manufactured from the same heat and subjected to nominally similar operating conditions, a considerable variation in crack growth rates is generally observed. These variations arise primarily due to localized differences in the microstructure, fabricating history and time-temperature-stress history of the component. Consequently, the life from crack detection to dysfunction also shows a considerable amount of scatter from one part to another. A statistically significant data base is therefore required to establish the lower limit of the service life causing earliest dysfunction. The life distribution to dysfunction can then be superimposed on the detectable crack distribution, using the same Weibull plot, Figure 23, and a 3σ crack propagation interval in terms of number of missions or service hours can therefore be determined. The problem of crack growth rate variations in turbine discs is further complicated by service induced microstructural degradation effects. The microstructure and mechanical properties of most engine alloys can change significantly at higher service temperatures. It is therefore essential to generate dysfunction limits of the

degraded microstructures for accurate prediction of a crack propagation interval. The fracture mechanics based predictions should generally be verified through spin-pit testing of a few selected service exposed discs.

A crack propagation interval, determined experimentally through fracture mechanics testing and calculated on the basis of the above mentioned procedure, may not necessarily correspond to a safe inspection interval in practice. Appropriate severity factors, corresponding to a change in the aircraft role and service environment, need to be considered to determine a safe inspection interval. The predicted crack propagation interval must therefore be divided by an appropriate severity factor to obtain a safe inspection interval in hours or number of missions. It must be pointed out that it is not unusual for an engine operator to use a specific engine in a variety of roles, e.g. training, combat etc., during its lifetime.

2.2.2.2 Damage Tolerance Concepts Applied to J85-CAN40 Engines (A Case Study)

The Structures and Materials Laboratory of the National Research Council of Canada is currently conducting a post-facto investigation of the life cycle management methodology employed with selected J85-CAN40 engine components. These engines are used in Canadian Forces CF-114 Tutor and an after-burner version in the CF-5 aircraft. The rotating J85-CAN40 components such as compressor discs, turbine discs and spacers were supplied with safe life limits specified by the manufacturer. These safe life limits are believed to have been predetermined by the manufacturer using a -3σ crack initiation criterion. After having used the engine up to the specified safe life limits, the service exposed components were subjected to a fluorescent penetrant inspection (FPI) for crack detection. Almost all components were found to be crack-free within the detection capability of the FPI technique. The manufacturer meanwhile appears to have considered the use of fracture mechanics concepts for component life cycle management, and supplied the information on the fracture critical locations, dysfunction limits and safe inspection intervals of various components. These data are summarized in Tables III, IV and V. *It was suggested that parts which are known to have been crack-free at prior inspection may be operated for a maximum of one propagation interval beyond that inspection with minimum additional risk.* The FPI inspected components were therefore returned to service and reinspected at the end of their respective safe inspection intervals.

The NRC investigation has however highlighted a number of inconsistencies with the overall life cycle management of the retired J85-CAN40 components. For example, a large majority of the fourth stage compressor discs and almost all 1st and 2nd stage turbine discs were retired in a crack-free condition.[82] The reasons for these premature retirements remain uncertain at this stage, but it can be concluded that damage tolerance concepts were not applied in their full extent. It is also possible that components such as turbine discs had marginal damage tolerance capability and hence were only capable of tolerating flaws just over the limit of detectability. These hypothesis are purely conjectural at the present time, since the detailed fracture mechanics data was not made available to the investigators.

Despite these uncertainities with the damage tolerance approach followed in J85-CAN40 components, it is noteworthy that components were used well beyond their original safe life limits, Tables III to V. Service lives greater than twice the original safe life limits were obtained in a number of components with no catastrophic results. Some components were returned to service even after a fourth inspection interval. The case study clearly demonstrates that damage tolerance based maintenance methodology can be successfully applied to rotating turbine engine components and lives well beyond the original safe life limits can be obtained.

2.2.2.3 NRC Approach to Post-Facto Investigation of J85-CAN40 Case Study

The aim of the NRC programme is to investigate engine maintenance and failure problems in some detail, which will lead to more efficient life-cycle management of gas turbine engines in the future. The investigation is primarily a learning exercise from an engine users point of view and the major thrusts of the programme are directed in the following areas.

(1) Visual assessment of the cracked parts:

The aim is to identify fracture critical locations in the turbine engine at large and the individual components in particular. Figure 24 illustrates the crack prone locations (marked X) in the engine. Cracking was severe in 5th and 7th stage compressor discs and in spacers on either side of them in the bolt holes. Cracking was less severe in the initial stages of the compressor train. Likewise, there were no cracks in the 8th stage disc which represents the final stage of the compressor. Cracking was absent in the 1st and 2nd stage turbine discs.

(2) Fractographic analysis of cracked parts:

The aim is to identify the predominant mode of failure, crack initiation locations and their causes, and to attempt to correlate striation spacing data with the mission profiles. LCF has been identified as the primary reason for cracking. Crack initiation sites appear to be associated with the sub-surface cavities around second phase particles near machining marks and typical cases of corner crack initiation have also been identified.

(3) Optical and electron microscopy of the retired discs:

The aim is to locate any service induced microstructural changes from the hub to the bore sections of the discs. No obvious differences in the microstructures of the hub and rim sections of a severely cracked 5th stage discs were observed. This was not unexpected since the temperatures experienced by the component were not severe enough to cause significant microstructural degradation.

(4) Microhardness measurements around the cracks:

The aim is to determine plastic zone sizes ahead of the crack tips and to calculate stress intensity factors. The crack tip areas over which cyclic strain hardening or softening has occurred can be revealed by making a series of microhardness measurements in a grid pattern, Figure 25. If Ry should represent the cyclic plastic zone radius, then a theoretical estimate of ΔK is given by[83,84],

$$Ry = C\left(\frac{\Delta K}{\sigma_{ys}}\right)^2 \qquad (13)$$

where σ_{ys} is the yield strength of the material and C is a constant depending upon the material and type of loading. In AM355 compressor discs investigated, the size of the plastic zone did not vary over a range of crack lengths between 2-6.7 mm, thus indicating a constant stress intensity factor over this range of crack lengths.

(5) Finite Element Analysis:

The aim is to have some knowledge of the stress intensity factors (ΔK) operative at varying crack lengths. These stress intensity factors can be determined through finite element techniques under known operating conditions. The numerical analysis can be extended to determine crack growth rates and life times to failure based on existing da/dN versus ΔK data. A preliminary two-dimensional finite element stress analysis was carried out on the 5th stage compressor disc using the mesh geometry shown in Figure 26, and assuming a rotational speed of 16,500 rpm. The calculated stress intensity factor for various bolt hole crack lengths are plotted in Figure 27. It is of interest to note that the ΔK values tend to remain constant over a significant portion of the crack length. This appears consistent with the conclusions reached through the microhardness measurements of the plastic zone sizes.

(6) Crack propagation simulation on compact tension specimens:

The aim is to determine crack propagation rates experimentally under simulated service conditions. The crack propagation in plane-stress or plane-strain conditions will be simulated, depending upon the component dimensions and service temperatures.

(7) Spin-pit testing:

The aim is to confirm the values of crack propagation intervals and dysfunction limits under realistic service conditions.

(8) Non-destructive evaluation of cracks:

The aim is to evaluate the accuracy of various NDI techniques, e.g. FPI, Ultrasonic techniques and Eddycurrent techniques. To check the accuracy of FPI techniques, the crack length data reported for a 5th stage disc was re-evaluated metallographically. All bolt holes were cut out from the same disc and prepared for metallographic estimation of crack lengths. Out of 40 bolt hole locations examined 35 cracks were found, whereas only 25 cracks were picked up during original FPI evaluation. A plot comparing observed and reported crack lengths is given in Figure 28. It is evident that cracks missed out during FPI were in the 1-2 mm range and hence too small to be detected.

2.2.3 Life Extension Through Rejuvenation

Section 2.1.4.1 discussed HIP rejuvenation of turbine blades. In principle the same techniques may be used with turbine discs. Only one study has been reported on the rejuvenation of Waspaloy turbine discs.[14] However, the study focussed on cracked parts, where surface connected cracks had to be sealed and healed. Figure 29 compares the LCF properties of crack repaired plus Hipped specimens with those of uncracked specimens, where uncracked specimens exhibit less scatter than HIP repaired parts. It was concluded that retired crack-free Waspaloy turbine discs could be successfully HIP rejuvenated to restore their original LCF properties. However, the study did not address the fracture mechanics properties of the components.

2.2.4 Component Durability Through Improved Machining Techniques

Section 2.2.2.3 indicated that fine machining cracks near subsurface second phase particles are potential crack initiation sites. The effect of various machining operations, e.g. grinding, turning, rough electro-discharge machining (EDM), EDM plus glass bead blasting, fine EDM and EDM plus abrasive flow machining (AFB), on the surface quality of Inconel alloy 901 was recently investigated in a separate study.[85] Optical metallography was used to quantify the overall surface cracking upon measuring the number and depth of surface cracks over a representative sample length of 5 mm in all cases. The crack counting was carried out manually at a constant magnification of 1200X and the results are presented in Table VI. The traditional machining operations resulted in the largest number and the deepest cracks, whereas EDM samples contained parallel cracks. EDM plus AFM however produced the best quality surface, where crack lengths were considerably reduced, Table VI. The influence of these machining operations on the LCF properties of Inconel alloy 901 have also been evaluated[86], and the results indicate a 3-5 fold increase in LCF life of EDM + AFM samples when compared with samples machined by conventional methods.

3. CONCLUSIONS

(a) Turbine Blades

(1) When used with existing creep data bases, parameters such as the Larson-Miller parameter, the Manson-Haferd parameter, the Monkman-Grant equation and the Dobes-Milicka equation are unable to detect the microstructural degradation that occurs in service exposed turbine blades.

(2) A new creep design relationship that is capable of detecting service induced degeneration effects has been proposed. The relationship considers primary plus secondary creep lives ($t_p + t_s$) normalized by their respective primary plus secondary creep strain values ($\epsilon_p + \epsilon_s$) as a function of minimum creep rate ($\dot{\epsilon}$), where

$$\left(\frac{t_p + t_s}{\epsilon_p + \epsilon_s}\right) \dot{\epsilon}^M = K_1$$

The relationship indicates minimum scatter over a wide range of stresses and temperatures.

(3) Rejuvenation of service exposed turbine blades by HIP processing followed by post-HIP heat-treatments is a viable process for life extension.

(4) Major turbine blade surface degradation, impact damage and cracks can be reliably repaired through various forms of diffusion bonding techniques such as TLP bonding and powder overlay methods. Various investigators have shown that the creep strength of TLP bonds is comparable with that of the base metal properties.

(5) HIP processing of investment cast turbine blades improves their stress-rupture properties by eliminating shrinkage cavities and microporosity.

(b) Compressor and Turbine Discs

(1) LCF models such as the Coffin-Manson equation, the strain-range partitioning and the frequency modified approach have been briefly described. The accuracy of predicted lives lie at best within a factor of two from the observed lives.

(2) The use of damage tolerance concepts for life cycle management of selected engine components has been discussed. A practical application with the J85-CAN40 engines has been reviewed which indicates that benefits may accrue even with older engines designed to initiation based safe-life concepts.

(3) Rejuvenation of turbine discs appears to be feasible but more work needs to be done before it can be commercially applied.

(4) Enhanced durability of turbine engine components is possible if modern machining techniques such as EDM + AFM are employed during manufacture.

REFERENCES

(1) Wallis, P.B. — The Nimonic Alloys. Eds. W. Betteridge and J. Heslop, Chapter 20, Edward Arnold, London, 2nd Edition, 1974, p. 459.

(2) Fawley, R.W. — The Superalloys. Eds. C.T. Sims and W.C. Hagel, Chapter 1, John Wiley and Sons, New York, 2nd Edition, 1972, p. 3.

(3) Gessinger, G.H. — Recent Developments in Powder Metallurgy of Superalloys. Powder Met. Int., Vol. 13, No. 2, 1981, p. 931.

(4) Immarigeon, J-P.A. — Materials for Gas Turbine Hot Section Components. Can. Aero. and Space Journal, Vol. 27, No. 4, Dec. 1981, p. 336.

(5) Koul, A.K., Dainty, R.V. — Metallurgical Investigation of a Turbine Blade and a Vane Failure from Two Marine Engines. Microstructural Science, Vol. 12, 1983.

(6) Decker, R.F., Sims, C.T. — The Metallurgy of Ni-base Alloys, The Superalloys. Eds. C.T. Sims and W.C. Hagel, Chapter 2, John Wiley and Sons, New York, 2nd Edition, 1973, p. 33.

(7) Freche, J.C., Ault, G.M. — More Heat Resistant Turbine Materials. Product Engineering, July 1979, p. 35.

(8) Kear, B.K., Thompson, E.R. — Aircraft Gas Turbine Materials and Processes. Science, Vol. 208, 1980, p. 847.

(9) Moore, J.B., Athey, R.L. — U.S. Pat. 3,519,504, 1970.

(10) Gell, M., Duhl, D.N., Giamei, A.F. — The Development of Single Crystal Superalloy Turbine Blades. Proc. 4th Int. Conf. on Superalloys, ASM, Metals Park, 1980, p. 205.

(11) Stragman, T.E., Hopkins, G.S., Phipps, C.M., Harris, K., Schwer, R.E. — Development of Exothermally Cast Single Crystal Mar-M247 and Derivative Alloys. ibid, p. 215.

(12) Senechal, P. — Fatigue and Creep Considerations in the Design of Turbine Components. Proc. High Temperature Alloys for Gas Turbines, Eds. R. Brunetand et al, D. Riedel Publishing Company, Boston, U.S.A., Conference held in Liege, Belgium, 4-6th October, 1982, p. 273.

(13) Roberts, M.L. — Engine Life, Usage and Cycle Selection. J. Aircraft, Vol. 15, No. 4, 1978, p. 240.

(14) Sundberg, D.V., Comey, D.H. — Hot Isostatic Pressing Rejuvenation of Disks. AiResearch Manufacturing Company of Arizona Technical Report, AFML-TR-79-4093, July 1979.

(15) Cheung, K., Leach, C.C., Willett, K., Koul, A.K. — Hot Isostatic Processing of Service Exposed Turbine Blades. AGARD-CP-317, 53rd Meeting of the SMP Panel on 'The Maintenance in Service of High Temperature Parts', Noordwijkerhout, The Netherlands, 27th September – 2nd October 1981.

(16) Owczarski, W.A.
Paulonis, D.F.
Application of Diffusion Welding in the U.S.A.
Feb. 1981, p. 22.

(17) Annis, C.G.
Van Wanderham, M.C.
Harris, J.C.
Sims, D.L.
Gas Turbine Engine Disc Retirement for Cause: An Application of Fracture Mechanics and NDE.
ASME 80-GT-127, Gas Turbine Conference and Products Show, New Orleans, 10-13 March 1980.

(18) Loferski, M.T.
Turbine Airfoil Life Prediction by Mission Analysis.
J. Aircraft, Vol. 12, No. 4, 1975, p. 400.

(19) Wallace, W.
Unpublished Work, 1984.

(20)
Development of Standard Methodology for the Correlation and Extrapolation of Elevated Temperature Creep and Rupture Data.
EPRI Report, FP-1062, 1979.

(21) Larson, F.R.
Miller, J.
Trans. ASME, 74, 1952, p. 765.

(22) Collins, J.A.
Failure of Materials in Mechanical Design.
John Wiley's Co., Chapter 13, 1981, p. 435.

(23) Koul, A.K.
Castillo, R.
Willett, K.
Creep Life Predictions in Ni-Based Superalloys.
J. Mat. Sci. and Eng., In press, 1984.

(24) Furrillo, F.T.
Purushotaman, S.
Tien, J.K.
Understanding the Larson-Miller Parameter.
Scripta Met., Vol. 11, p. 493.

(25) Koul, A.K.
Larson-Miller Parameter and Its Modified Version.
Scripta Met., Vol. 16, 1982, p. 947.

(26) Chamblen, C.E.
Redden, T.K.
Creep Resistance and High Temperature Metallurgical Stability of Ti-Alloys.
Met. Trans., Vol. 3A, 1972, p. 1299.

(27) Manson, S.S.
Haferd, A.M.
A Linear Time-Temperature Relationship for Extrapolation of Creep and Stress Rupture Data.
NASA Technical Note 2890, March 1953.

(28) Monkman, M.C.
Grant, N.J.
Proc. ASTM, 56, 1956, p. 593.

(29) Dobes, F.
Milicka, K.
The Relation Between Minimum Creep Rate and Time to Fracture.
Metal Science, Vol. 10, 1976, p. 382.

(30) Bailey, P.G.
Scheikert, W.H.
HIP Densification of Castings, Superalloys: Metallurgy and Manufacture.
Proc. 3rd Int. Symp., eds, B.H. Kear, D.R. Muzyka, J.K. Tien and S.T. Wlodek, Claitors, Baton Rouge, La., 1976, p. 451.

(31) Van Drunen, G.
Liburdi, J.
Wallace, W.
Terada, T.
Hot Isostatic Processing of IN-738 Turbine Blades.
AGARD Conference Proceedings on Advanced Fabrication Processes, CP-256, 13, Florence, Italy, 26-28th September 1978.

(32) Floyd, P.H.
Wallace, W.
Immarigeon, J-P.A.
Rejuvenation of Properties in Turbine Engine Hot Section Components by Hot Isostatic Pressing.
Proc. Heat Treatment 81 Conference, Birmingham, England, 15-16th September 1981, p. 97.

(33) Hart, R.V.
Gayter, H.
Recovery of Mechanical Properties in Nickel Alloys by Reheat-Treatment.
J. Inst. of Metals, Vol. 96, 1968, p. 338.

(34) Davies, P.W.
Dennison, J.P.
Sidey, D.
The Recovery of Mechanical Properties of Nimonic 105 by Heat-Treatment after High-Temperature Creep.
J. Inst. of Metals, Vol. 101, 1973, p. 153.

(35) McCall, W.J.
Turbine Blade Life Can be Extended by Reconditioning.
Combustion, Vol. 42, April 1971, p. 27.

(36) Koul, A.K.
Wallace, W.
Microstructural Dependence of Creep Strength in Inconel 700.
Met. Trans., Vol. 13A, 1982, p. 673.

(37) Koul, A.K.
Morphy, D.
Grain Coarsening Behaviour of Ni-Based Superalloys.
Submitted to Met. Trans. A, 1984.

(38) Beddoes, J.
Wallace, W.
Heat-Treatment of Hot Isostatically Processed IN738 Investment Castings.
Metallography, Vol. 13, 1980, p. 185.

(39) Koul, A.K.
Morphy, D.
Serrated Grain Boundary Formation in Ni-Based Superalloys.
Microstructural Science, Vol. 11, 1982, p. 79.

(40) Koul, A.K.
Gessinger, G.H.
On the Mechanism of Serrated Grain Boundary Formation in Ni-Based Superalloys.
Acta. Metallurgica, Vol. 31, 1983, p. 1061.

(41) Koul, A.K.
Thamburaj, R.
Serrated Grain Boundary Formation Potential of Ni-Based Superalloys and its Implications.
Submitted to Met. Trans., 1984.

(42) Thomas, G.B.
Gibbins, T.B.
Influence of Trace Elements on Creep and Stress-Rupture Properties of Nimonic 105.
Metals Technology, March 1979, p. 95.

(43) Loveday, M.S.
Dyson, B.F.
Prestrain-Induced Particle Microcracking and Creep Cavitation in IN597.
Acta. Met., Vol. 31, No. 3, 1983, p. 397.

(44) Koul, A.K.
Wallace, W.
Rejuvenation of Service Exposed Nimonic 105 Turbine Blades-Microstructural Considerations.
NAE-NRC Report, LTR-ST-1242, March 1981.

(45) King, R.W.
Hatala, R.W.
Hauser, H.A.
Welding of Superalloy Turbine Hardware.
Met. Eng. Quarterly, Vol. 10, No. 4, 1970, p. 55.

(46) Young, W.R.
Turbine Airfoil Repair.
10th National SAMPE Technical Conference on 'Materials Synergisms', New York, Oct. 17th-19th, 1978, Vol. 10, p. 924.

(47) Lee, J.W.
Schaefer, R.P.
Voehringer, C.A.
Repair of Directionally Solidified Airfoil Components.
ibid, p. 733.

(48) Stoll, W.
Thermal Joining of High Temperature Resistant Casting Materials.
Proc. 1st International Conference on Welding in the Aerospace Industry — Design, Materials, Welding Methods and Maintenance, Deutscher Verlag für Schweisstechnik, Gimbh, Dusseldorf, West Germany, 1978, p. 80.

(49) Duvall, D.S.
Doyle, J.R.
Repair of Turbine Blades and Vanes.
ASME Reprint No. 73-GT-44, 1973.

(50) Duvall, D.S.
Owczarski, W.A.
Paulonis, D.F.
TLP Bonding: A New Method of Joining Heat-Resistant Alloys.
Welding Journal, April 1974, p. 203.

(51) Van Schaik, T.
Possibilities of Repair Work on the High Temperature Components of Gas Turbines.
VGB Kraftwerkstechnik, Vol. 58, No. 5, 1978, p. 308.

(52) Haafkens, M.H.
Blade Repair and Recovery.
Proc. Conf. 'High Temperature Alloys for Gas Turbines 1982', Eds. R. Brunetand et al, D. Riedel Publishing Company, Boston, U.S.A., Conference held in Liege, Belgium, 4-6th October 1982, p. 931.

(53) Thamburaj, R.
Wallace, W.
Goldak, J.A.
Electron Beam Welding of Powder Metallurgy Superalloys.
IN 'Powder Metallurgy Superalloys', Vol. 1, Metal Powder Report Publishing Services Ltd., Shrewsburg, England, 1980.

(54) Thamburaj, R.
Wallace, W.
Goldak, J.
Post-Weld Heat-Treatment Cracking in Superalloys.
International Metals Reviews, Vol. 28, No. 1, 1983, p. 1.

(55) Thamburaj, R.
Singer, R.F.
Gessinger, G.H.
Joining Techniques for P/M Superalloys.
IN 'Powder Metallurgy of Superalloys', by G.H. Gessinger, Butterworths Monographs in Materials, 1st Edition, 1984, p. 295.

(56) Coffin, L.F.
Creep-Fatigue-Environment Interactions.
Eds. R.M. Pelloux and N.S. Stoloff, The Metallurgical Society of AIME, 1980, p. 1.

(57) Harris, J.A., Jr.
Annis, C.A., Jr.
Van Wanderham, M.C.
Sims, D.L.
Engine Component Retirement for Cause.
Proc. Conference on 'Maintenance in Service of High Temperature Parts', AGARD CP-317, Noordwijkerhout, The Netherlands, 27th Sept. — 2nd Oct. 1981, 5-1.

(58)
Analysis of Life Prediction Methods for Time-Dependent Fatigue Crack Initiation in Ni-Base Superalloys.
Publication NMAB-347, National Academy of Sciences, Washington, D.C., 1980.

(59) Sammons, J. — Derivation and Correlation of Accelerated Mission Endurance Testing. AGARD-CP-293, 56th Symposium of PEP Panel on 'Turbine Engine Testing', Turin, Italy, 29th Sept. — 3rd Oct. 1980.

(60) Norris, D. — Mechanical Testing of Compressors and Turbines for Aircraft Gas Turbine Engines. ibid.

(61) Fuchs, P.O.; Stephens, R.I. — Metal Fatigue in Engineering. John Wiley & Co., New York, 1980.

(62) Plumtree, A. — Creep/Fatigue Interactions in Type 304 Stainless Steel at Elevated Temperature. Metal Science, August/September 1977, p. 425.

(63) McEvily, A.J.; Crosby, S.R. — Lifetime Prediction Methods for Elevated Temperature Fatigue. Conference Proceedings, 'Low Cycle High Temperature Fatigue', AGARD-CP-155, 38th Meeting of the Structures and Materials Panel, Washington, D.C., 21-26th April 1974.

(64) Manson, S.S.; Halford, G.R. — An Overview of High Temperature Metal Fatigue. ibid.

(65) Manson, S.S. — The Challenge to Unify Treatment of High Temperature Fatigue — A Partisan Proposal Based on Strain Range Partitioning. ASTM-STP-520, 1973, p. 744.

(66) — Characterization of Low Cycle High Temperature Fatigue by Strain Range Partitioning Method. AGARD CP-243, 46th Meeting of SMP Panel, Aalborg, Denmark, 11th-12th April 1978.

(67) Coffin, L.F., Jr. — Fatigue at High Temperature. Fatigue at Elevated Temperatures, ASTM-STP-520, 1973, p. 112.

(68) Carden, A.E.; Coffin, L.F., Jr.; Greenstreet, W.L.; Manson, S.S.; Severud, L.K. — Time Dependent Fatigue of Structural Alloys: A General Assessment (1975). ORNL-5073, Oak Ridge, TN: Oak Ridge National Laboratory, January 1977.

(69) Ostergen, W.J. — A Damage Function and Associated Failure Equation for Predicting Hold Time and Frequency Effects in Elevated Temperature LCF. Journal of Testing and Evaluation, Vol. 4, September 1976, p. 327.

(70) Majumdar, S.; Maiya, P.S. — A Unified and Mechanistic Approach to Creep-Fatigue Damage. Proc. of the 2nd International Conference on Mechanical Behaviour of Materials, ASM, August 1976, p. 924.

(71) Majumdar, S.; Maiya, P.S. — A Damage Equation for Creep-Fatigue Interaction. Proc. of the ASME-Metal Property Council Symposium on Creep-Fatigue Interaction, New York, 1976, MPC-3, p. 323.

(72) Tiffany, C.F.; Cowie, W.D. — Progress on ENSIP Approach to Improved Structural Integrity in Gas Turbine Engines — An Overview. ASME 78-WA/GT-13, Annual Winter Meeting, ASME Gas Turbine Division, San Francisco, Dec. 1978.

(73) Harris, J.A., Jr.; Sims, D.L.; Annis, C.G., Jr. — Concept Definition: Retirement for Cause of F100 Rotor Components. Technical Report AFWAL-TR-80-4118.

(74) Besuner, P.M.; Sorenson, K.G. — Retirement for Cause. A Workable Approach for Structural Life Extension and Response to In-Service Problems. EPRI Technical Report NP-855, August 1978.

(75) Hill, R.J.; Reiman, W.H.; Ogg, J.S. — A Retirement for Cause Study of an Engine Disc. AIAA/SAE/ASME 15th Joint Propulsion Conference, Las Vegas, 18-20 June 1979.

(76) Annis, C.G.; Cargill, J.S.; Harris, J.A., Jr.; Van Wanderham, M.C. — Engine Component Retirement for Cause: A Non-Destructive Evaluation (NDE) and Fracture Mechanics Based Maintenance Concept. Journal of Metals, July 1981, p. 24.

(77) Little, R.E. — Review of Statistical Analyses of Fatigue Life Data Using One-Sided Lower Statistical Tolerance Limits. Statistical Analysis of Fatigue Data, ASTM-STP-744, 1981, p. 3.

(78) Irwin, G.R. — Trans. ASME, 79, 1957, p. 79.

(79) Rice, J.R. — Fracture — An Advanced Treatise. Ed. H. Liebowitz, Chapter 3, Vol. 2, Academic Press, New York, 1968.

(80) El Haddad, M.H.
Topper, T.H.
Mukherjee, B.
J. of Testing and Evaluation, Vol. 9, No. 2, 1981, p. 65.

(81) Sadananda, K.
Shahinian, P.
Fracture Mechanics.
Eds. N. Perrone, H. Liebowitz, D. Mulville and W. Pilkey, University Press, Virginia, Charlottesville, 1978, p. 685.

(82) Thamburaj, R.
Koul, A.K.
Wallace, W.
Unpublished Work, 1984.

(83) Bathias, C.
Pelloux, R.M.
Fatigue Crack Propagation in Martensitic and Austenitic Steels.
Met. Trans., Vol. 4A, No. 5, 1973, p. 1265.

(84) Loye, C.
Bathias, C.
Retail, D.
Devanor, J.C.
The Plastic Zone Ahead of Fatigue Crack in 316 Stainless Steel.
Fatigue Mechanisms: Advances in Quantitative Measurement of Physical Damage, ASTM STP 811, 1983, p. 427.

(85) Koul, A.K.
Gladysz, V.
Unpublished Work, 1983.

(86) Dixon, I.
Gladysz, V.
Unpublished Work, 1983.

Table I — Life Limiting Factors for Gas Turbine Parts

COMPRESSORS (COOL PARTS)	TURBINES (HOT ROTORS)	COMBUSTORS (HOT STATIONARY PARTS)
— Discs, Shafts, Spacers, Blades	— Discs, Blades	—
Fatigue) Cracking, Loss Fretting) of Dimensional Wear) Tolerances	Microstructural Deterioration Creep Damage — Loss of Strength and Ductility, Cavitation Low Cycle, High Temperature Fatigue Oxidation Sulphidation Environmental Embrittlement	Thermal Fatigue and Distortion Erosion Sulphidation Oxidation

Table II — Turbine Blade Creep Life Variations with Temperature and Stress Using Larson-Miller Parameter

T_{METAL} (°C)	UDIMET U700		IN100	
	σ = 210 MPa	σ = 345 MPa	σ = 210 MPa	σ = 315 MPa
650	∞ hrs.	∞ hrs.	∞ hrs.	∞ hrs.
700	∞	100,000	∞	∞
760	100,000	4,570	∞	54,000
815	5,250	280	100,000	2,950
870	370	23	6,170	214
930	34	—	484	20
980	—	—	48	—

Table III — Service Life Data of J85-CAN40 Compressor and Turbine Discs

COMPONENT	SAFE LIFE LIMIT* HOURS	SAFE INSPECTION INTERVAL HRS.	LONGEST LIFE COMPONENT HRS.	MEAN LIFE (HRS.)	AVERAGE LIFE EXTENSION (HRS.)
4th Stage Compressor Disc	2333	555	4428.2	3863	1530
5th Stage Compressor Disc	1777	555	4473	3875	2098
6th Stage Compressor Disc	2222	722	5066.4	3971	1749
7th Stage Compressor Disc	2222	722	5066.4	3812.9	1590.95
8th Stage Compressor Disc	2944	722	5066.4	4080	1136
1st Stage Turbine Disc	1111	555	3737.6	2364	1253
2nd Stage Turbine Disc	1111	555	3791.6	2971	1860

*Based on -3σ from Mean Life to Crack Initiation.

Table IV — Dysfunction Criterion Used in J85-CAN40 Turbine and Compressor Discs

COMPONENT	DYSFUNCTION DEFINITION
4th Stage Compressor Disc 5th Stage Compressor Disc	4.5 mm Bolt Hole Crack Radially Inwards
6th Stage Compressor Disc 7th Stage Compressor Disc 8th Stage Compressor Disc	5.08 mm Bolt Hole Crack Radially Inwards
1st Stage Turbine Disc 2nd Stage Turbine Disc	Flange Bolt Hole Crack Initially Radially Outward Subsequent to Radially Inward Cracking

Table V — Maximum Crack Sizes Observed in Service Exposed J85-CAN40 Compressor and Turbine Discs at Retirement

COMPONENT	MAXIMUM CRACK SIZE IN SERVICE RETIRED COMPONENTS-NDI (mm)
4th Stage Compressor Disc	No Record of Cracking
5th Stage Compressor Disc	19.1
6th Stage Compressor Disc	6.4
7th Stage Compressor Disc	7.9
8th Stage Compressor Disc	4.0
1st Stage Turbine Disc	No Record of Cracking
2nd Stage Turbine Disc	No Record of Cracking

Table VI — Extent of Cracking Observed in Differently Machined Inconel Alloy 901 Samples of 5 mm Length

SAMPLE	NUMBER OF CRACKS OF LENGTH (μm)			
	0 — 5	5 — 10	10 — 15	15 — 20
Ground	—	—	25	23
Machined-Turned	—	—	34	15
Rough EDM	—	—	42 (parallel)	14
EDM + Glass Beading	—	—	46 (parallel)	6
Fine EDM	—	4	18 (parallel)	—
EDM + AFM	38	8	—	—

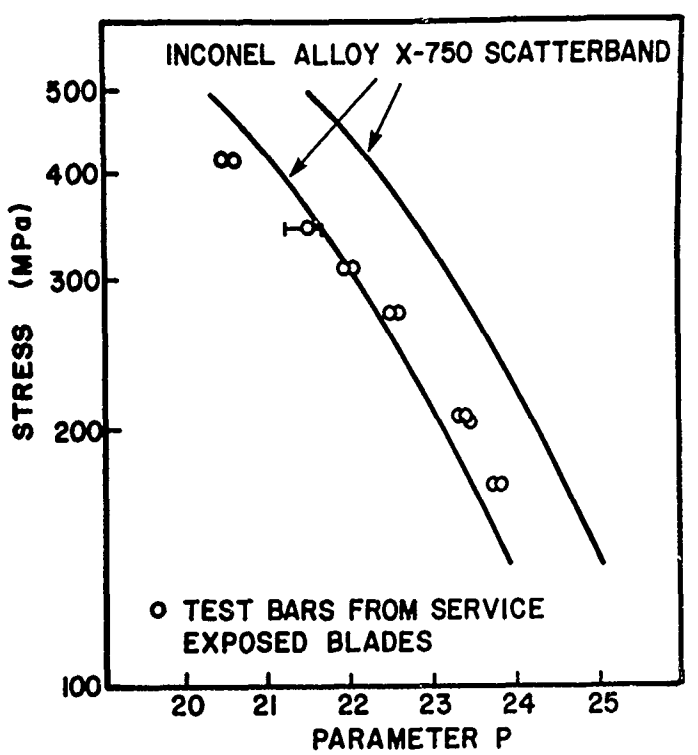

FIG. 1: LARSON-MILLER PLOT [$P = T \times 10^{-3} (20 + \log t_R)$, T IN °K, t_R IN HOURS] OF INCONEL ALLOY X-750 TURBINE BLADES SHOWING NEW AND SERVICE EXPOSED STRESS-RUPTURE PROPERTIES (Ref. 15)

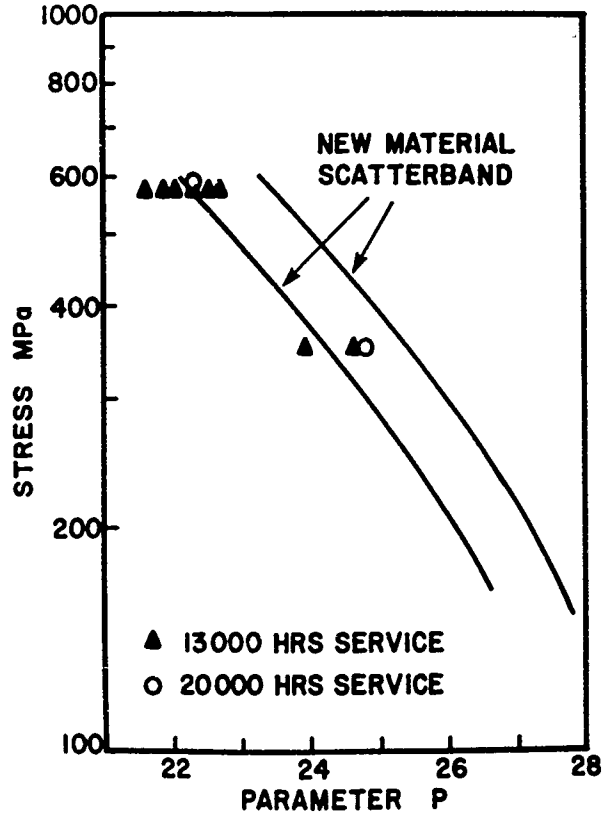

FIG. 2: LARSON-MILLER PLOT [$P = T \times 10^{-3} (20 + \log t_R)$, T IN °K, t_R IN HOURS] OF INVESTMENT CAST AND HIPPED IN 738LC TURBINE BLADES SHOWING NEW AND SERVICE EXPOSED STRESS-RUPTURE PROPERTIES

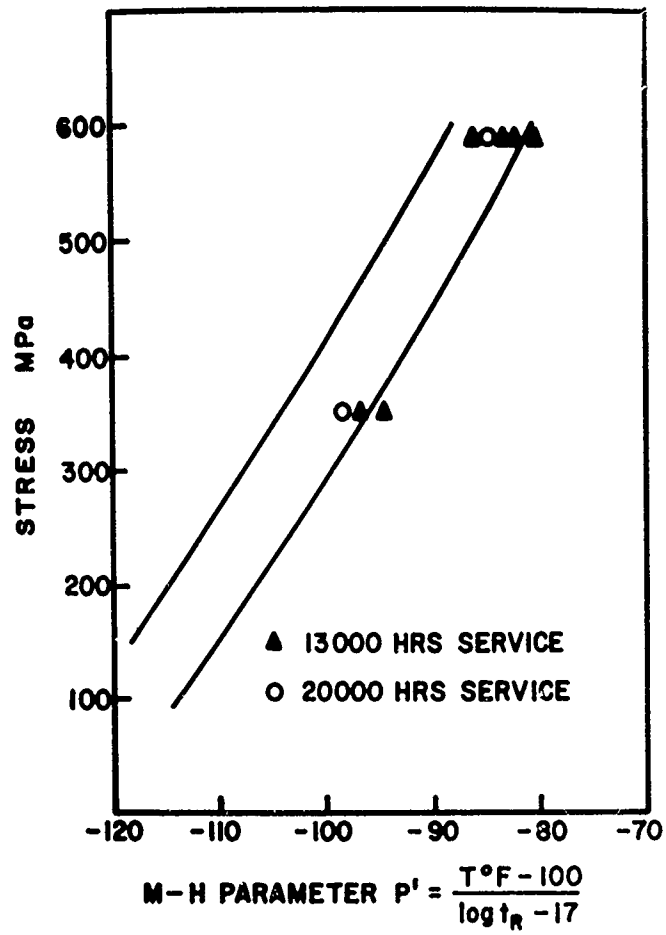

FIG. 3: MANSON-HAFERD PLOT [$P' = (T-100)/(\log t_R - 17)$, T IN °F, t_R IN HOURS] OF INVESTMENT CAST AND HIPPED IN 738LC TURBINE BLADES SHOWING NEW AND SERVICE EXPOSED STRESS-RUPTURE PROPERTIES

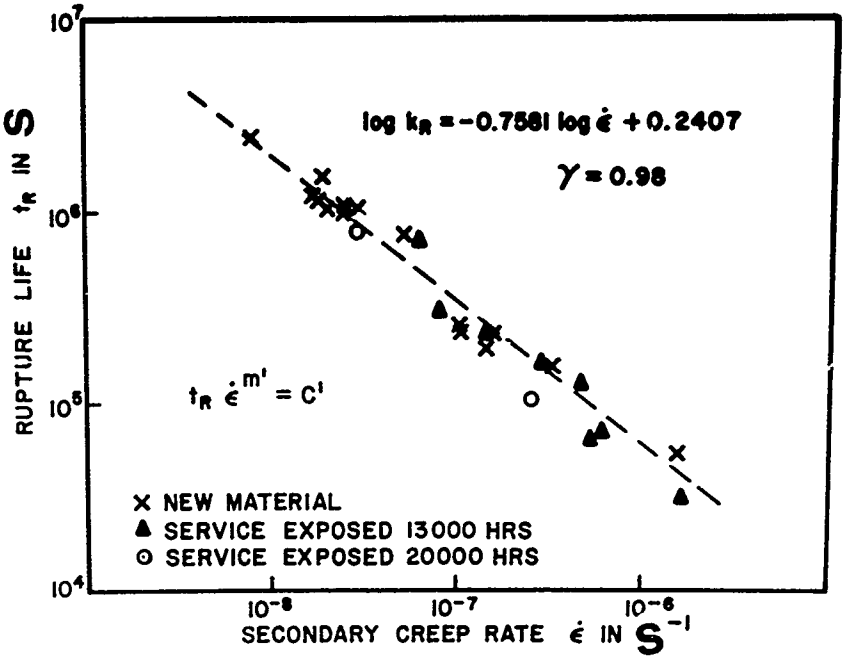

FIG. 4: RUPTURE LIFE VERSUS CREEP RATE PLOT FOR INVESTMENT CAST AND HIPPED IN 738LC TURBINE BLADES IN TERMS OF MONKMAN-GRANT RELATIONSHIP $t_R \dot{\epsilon}^m = C_1$. SUPERIMPOSED IS THE SERVICE EXPOSED IN 738LC CREEP DATA

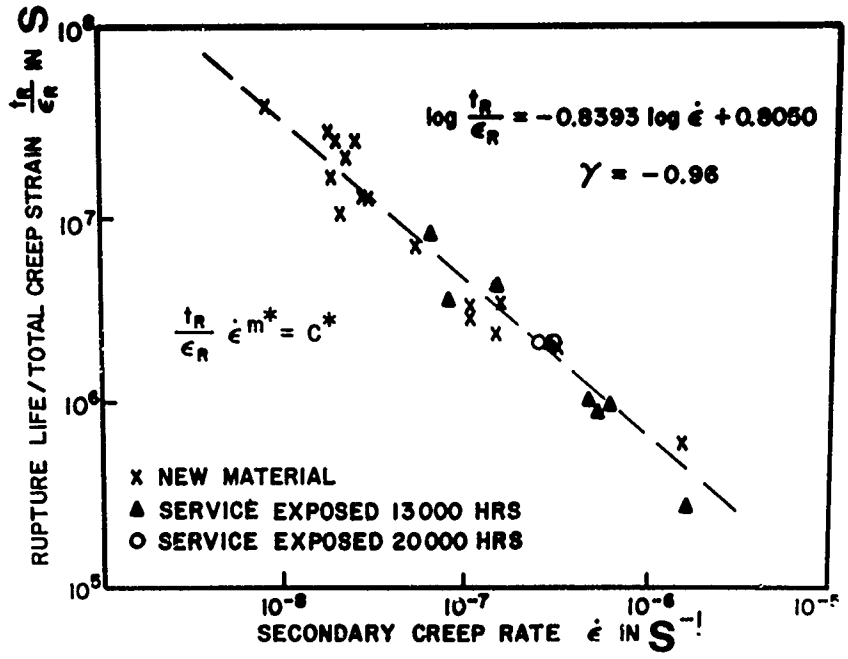

FIG. 5: NORMALIZED RUPTURE LIFE (t_R/ϵ_R) VERSUS CREEP RATE PLOT FOR INVESTMENT CAST AND HIPPED IN 738LC TURBINE BLADES IN TERMS OF DOBES-MILICKA RELATIONSHIP $(t_R/\epsilon_R)\,\dot{\epsilon}^{m*} = C^*$. SUPERIMPOSED IS THE SERVICE EXPOSED IN 738LC CREEP DATA

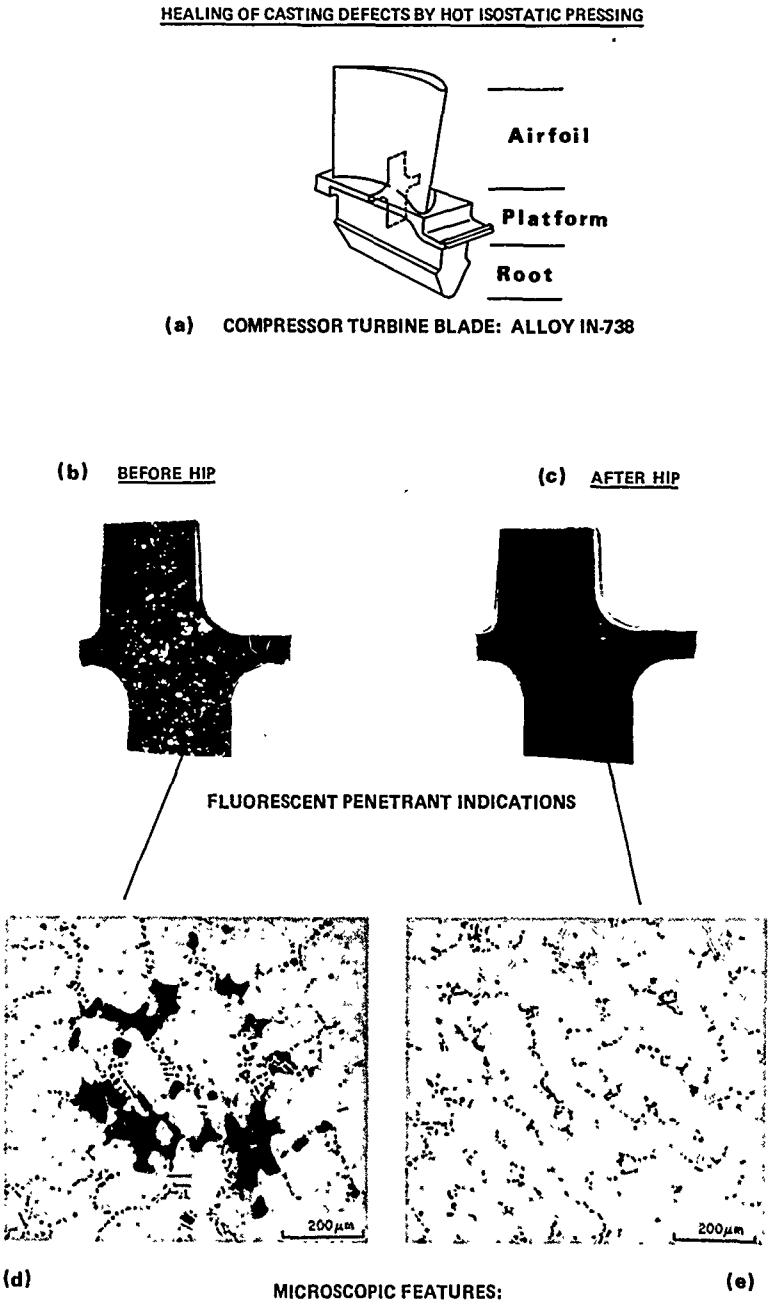

FIG. 6: EFFECT OF HIP PROCESSING ON MICROPOROSITY IN AN INVESTMENT CAST IN 738LC TURBINE BLADE (Ref. 31)

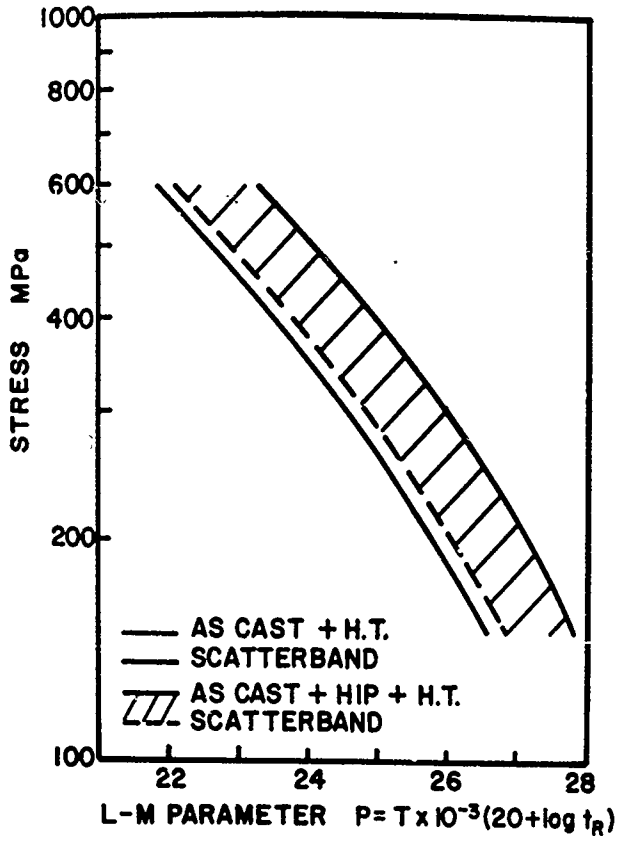

FIG. 7: EFFECT OF HIP PROCESSING ON THE STRESS-RUPTURE PROPERTIES OF INVESTMENT CAST IN 738LC TURBINE BLADES REPRESENTED IN TERMS OF LARSON-MILLER PARAMETER

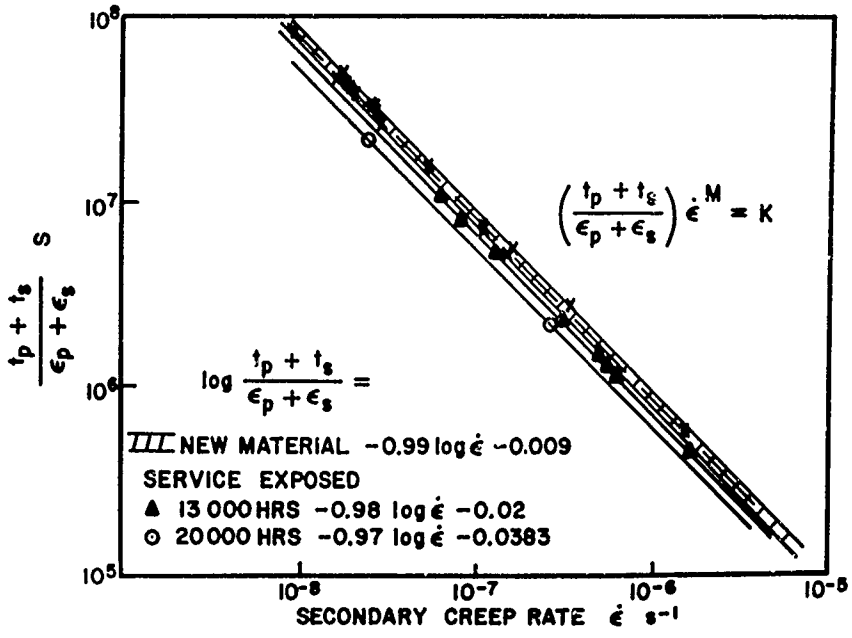

FIG. 8: PRIMARY PLUS SECONDARY CREEP DATA OF INVESTMENT CAST AND HIPPED IN 738LC TURBINE BLADES PLOTTED IN ACCORDANCE WITH $(t_p + t_s/\epsilon_p + \epsilon_s)\,\dot{\epsilon}^M = K_1$, AND SUPERIMPOSED IS THE DATA FROM SERVICE EXPOSED TURBINE BLADES (Ref. 23)

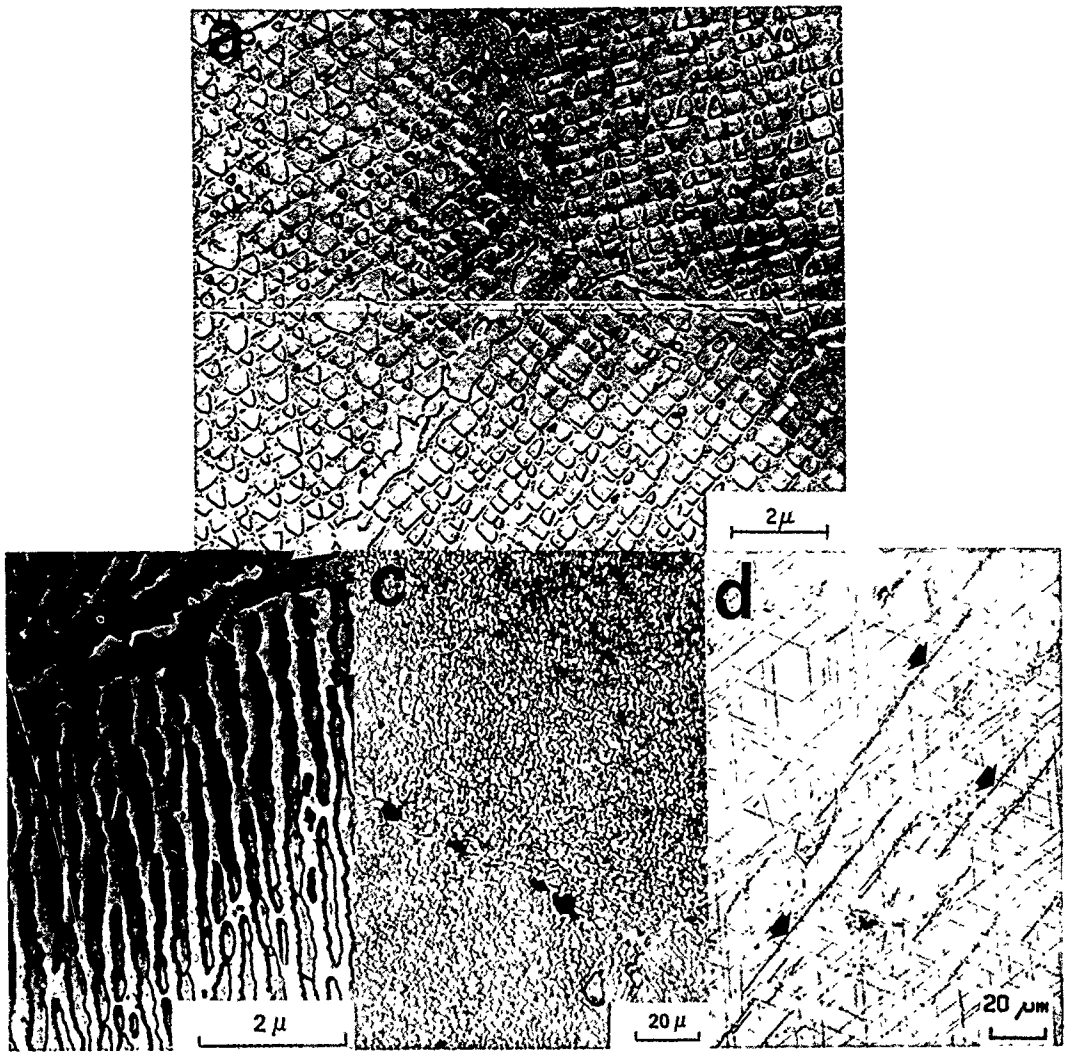

FIG. 9: TYPICAL NICKEL-BASE SUPERALLOY MICROSTRUCTURES: (a) AS HEAT-TREATED; (b), (c), (d) AFTER LONG SERVICE EXPOSURE (Ref. 32)

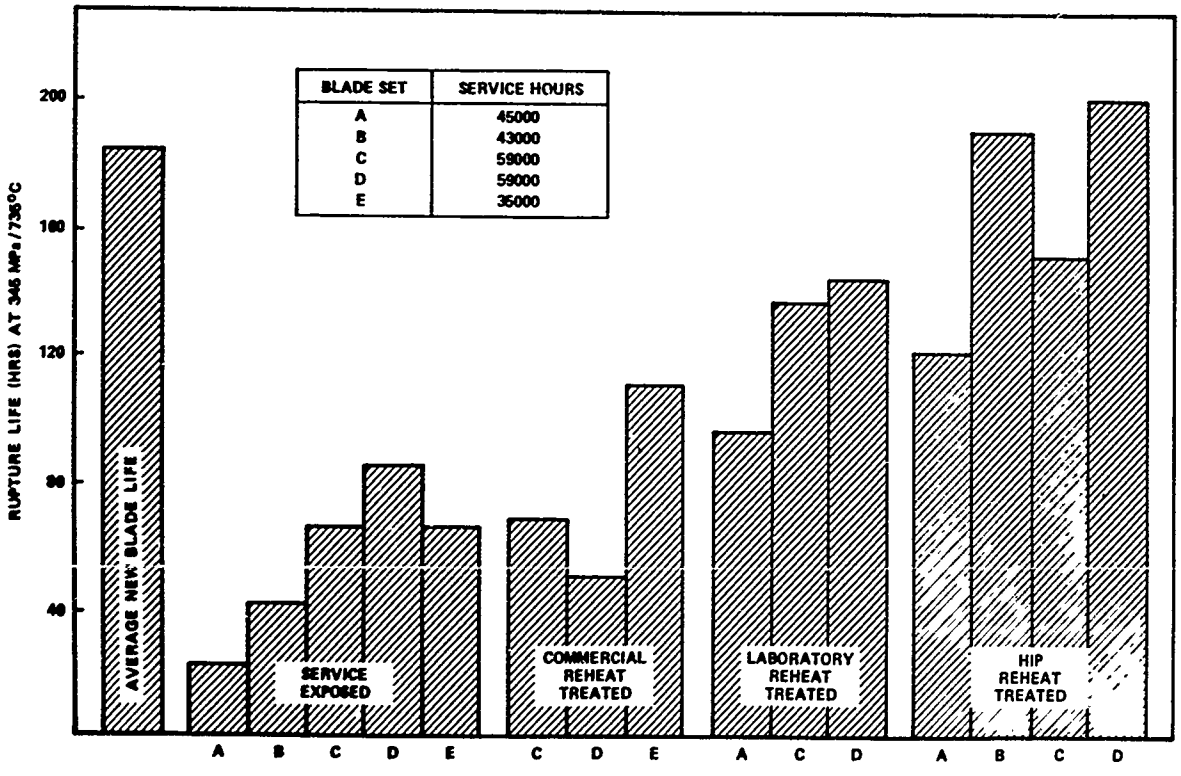

FIG. 10: STRESS-RUPTURE PROPERTIES OF X-750 TURBINE BLADES IN VARIOUS CONDITIONS

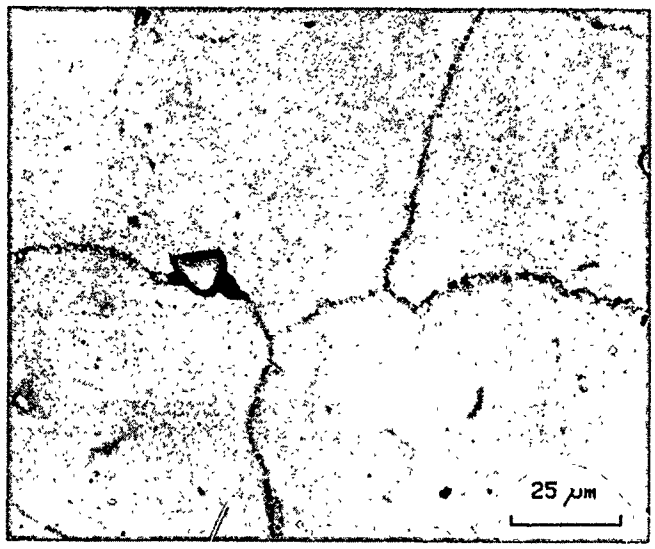

FIG. 11: TYPICAL GRAIN BOUNDARY PREPARATION FOR CREEP CAVITATION STUDIES USING METALLOGRAPHY. THE ABSENCE OF CAVITIES IN SERVICE EXPOSED (62,000 HOURS) NIMONIC 105 TURBINE BLADES IS NOTED (Ref. 44)

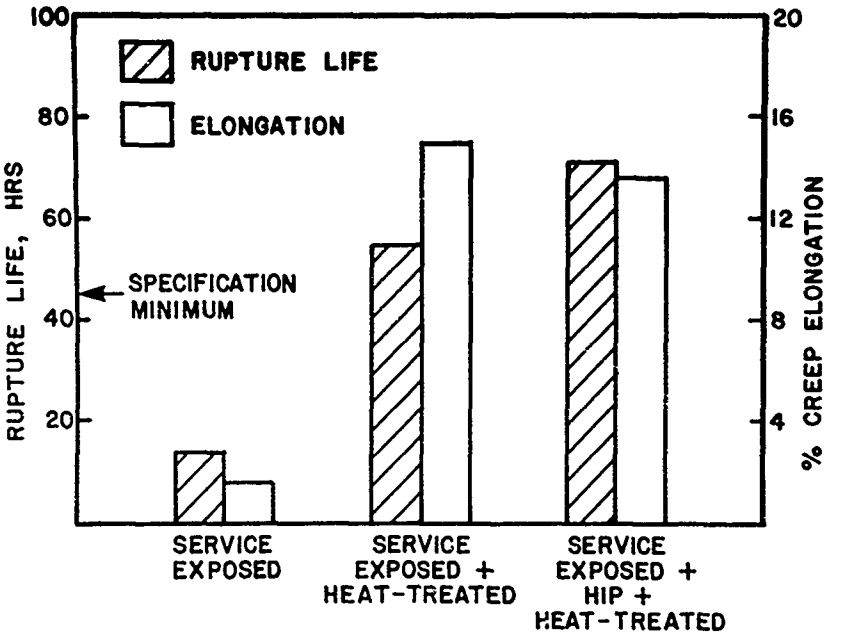

FIG. 12: EFFECT OF HIP PLUS HEAT-TREATMENT ON THE STRESS-RUPTURE PROPERTIES OF SERVICE EXPOSED (62,000 HOURS) NOMONIC 105 TURBINE BLADES

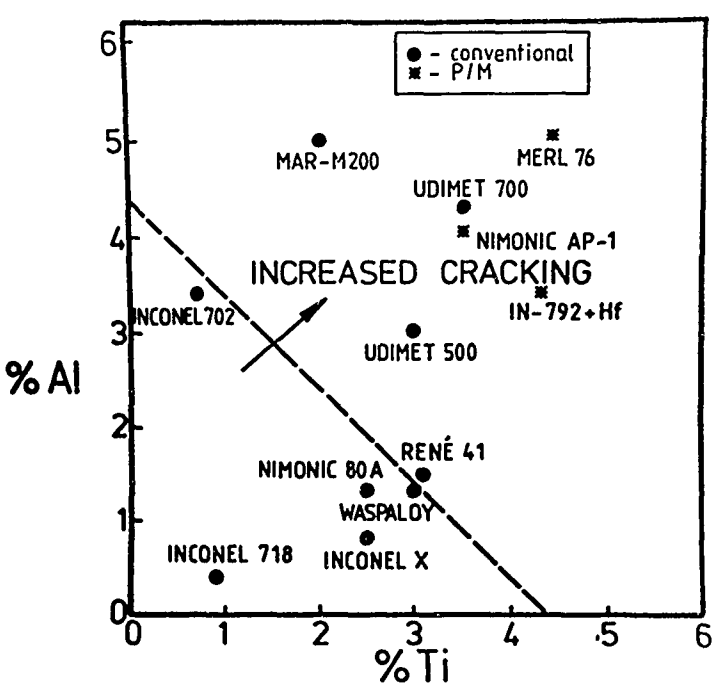

FIG. 13: EFFECT OF Al AND Ti CONTENT ON POST-WELD HEAT TREATMENT CRACKING TENDENCY IN SEVERAL NI-BASE SUPERALLOYS (Ref. 55)

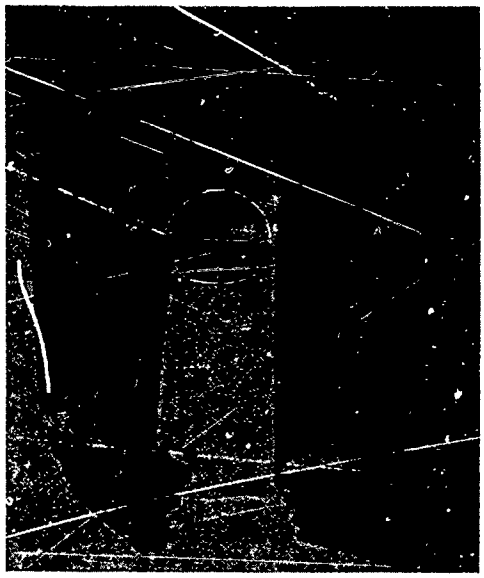

FIG. 14: A HEAVILY DAMAGED UDIMET 520 TURBINE BLADE BEFORE AND AFTER REPAIR WITH A POWDER OVERLAY (Ref. 52)

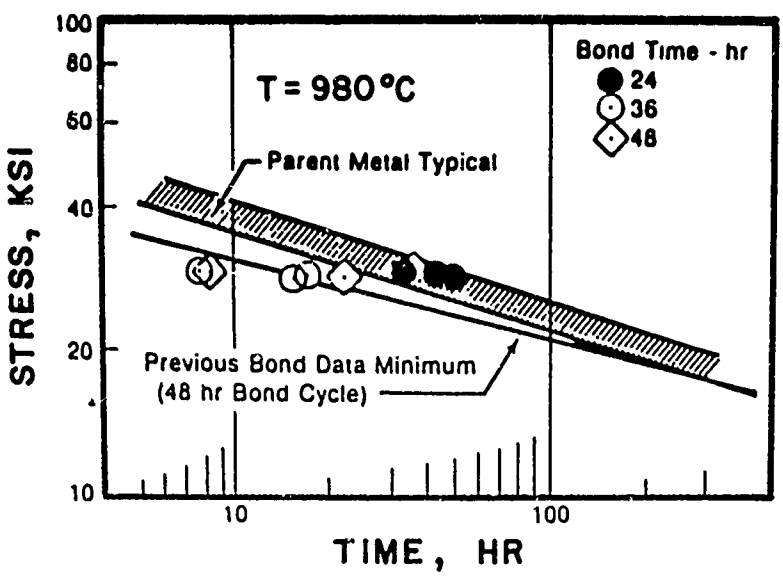

FIG. 15: THE 980°C TLP BOND STRESS-RUPTURE TEST DATA OF DS MAR-M200 COMPARED WITH THE PARENT METAL PROPERTIES DATA (Ref. 47)

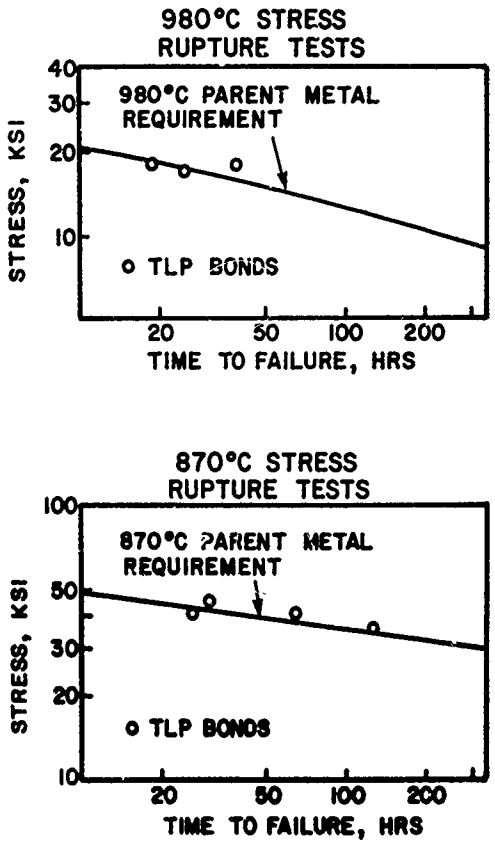

FIG. 16: STRESS-RUPTURE PROPERTIES OF BONDS IN UDIMET 700 MADE AT 1170°C FOR 24 HOURS. (a) 980°C PROPERTIES; (b) 870°C PROPERTIES

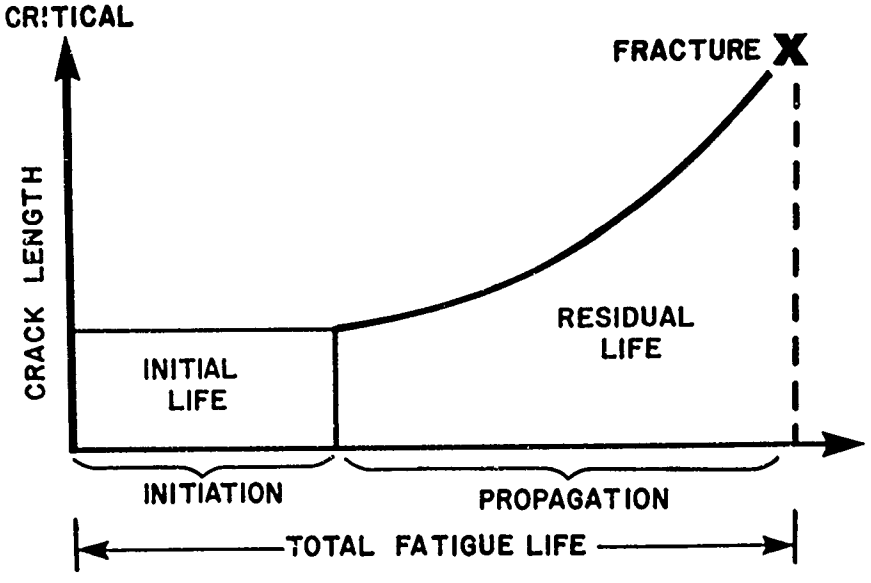

FIG. 17: TOTAL LCF LIFE SEGMENTED INTO STAGES OF CRACK DEVELOPMENT, SUBCRITICAL GROWTH AND FINAL FRACTURE (REF. 17)

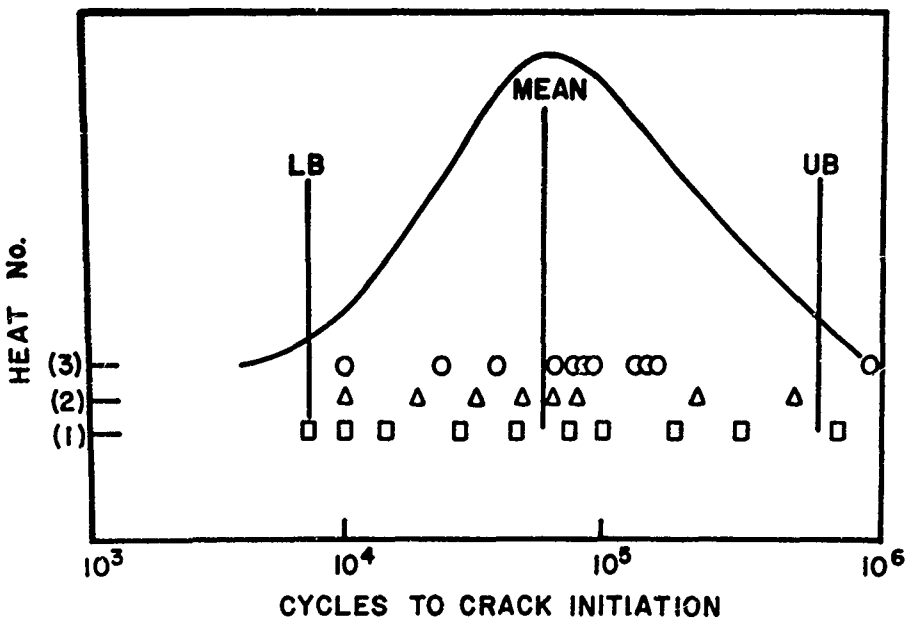

FIG. 18: DISC MATERIAL DATA SCATTER BASED ON LCF CRACK INITIATION APPROACH (Ref. 17)

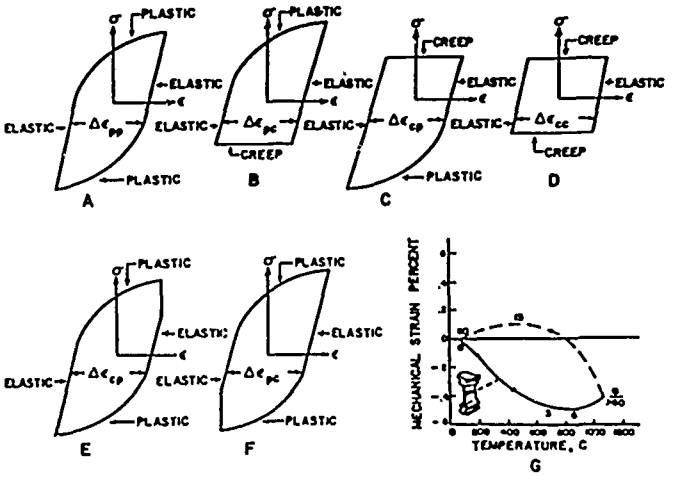

FIG. 19: (a)-(f) DEPICT SIX COMMONLY ENCOUNTERED TYPES OF LCF HYSTERISIS LOOPS, (a)-(d) DEMONSTRATE STRAINS USED IN PARTITIONING APPROACH, (e)-(f) SHOW CONSTANT STRAIN AMPLITUDE STRESS RELAXATION, AND (g) IS A THERMAL FATIGUE CYCLE (Ref. 63)

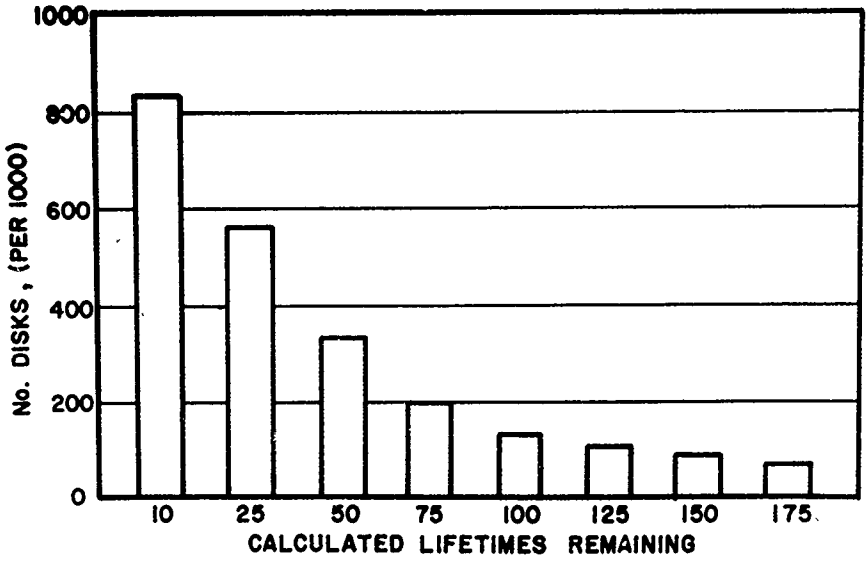

FIG. 20: THE MAJORITY OF DISCS HAVE USEFUL LIFE AFTER RETIREMENT. THE RETIREMENT CRITERION IS BASED ON SAFE LIFE APPROACH (Ref. 57)

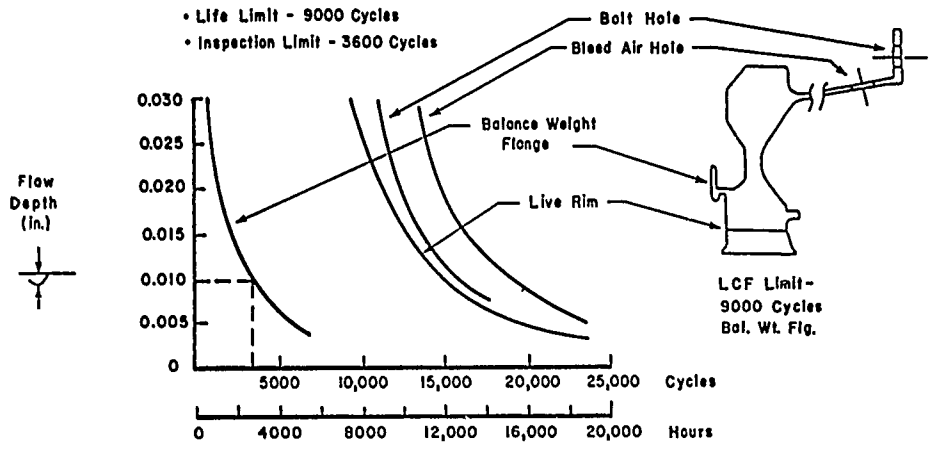

FIG. 21: DETERMINATION OF LCF LIFE LIMITING REGIONS IN A TYPICAL TURBINE DISC (Ref. 73)

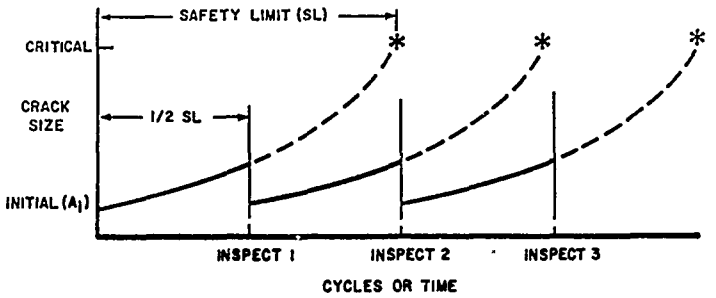

CRITERIA:
- SAFETY LIMIT IS TIME FOR INITIAL FLAW (A_i) TO GROW AND CAUSE PART FAILURE
- INSPECT AT 1/2 SL. INSPECTION INTERVAL 1 LT (DESIGN GOAL) OR 1 DEPOT INTERVAL (MIN DESIGN GOAL)
- APPLIES TO FRACTURE CRITICAL PARTS
- PROD. A_i BASED ON NDE METHOD OR MATERIAL DEFECT DISTRIBUTION
- DEPOT A_i BASED ON NDE METHOD

FIG. 22: USAF DAMAGE TOLERANCE APPROACH TO LIFE MANAGEMENT OF LCF LIMITED ENGINE COMPONENTS

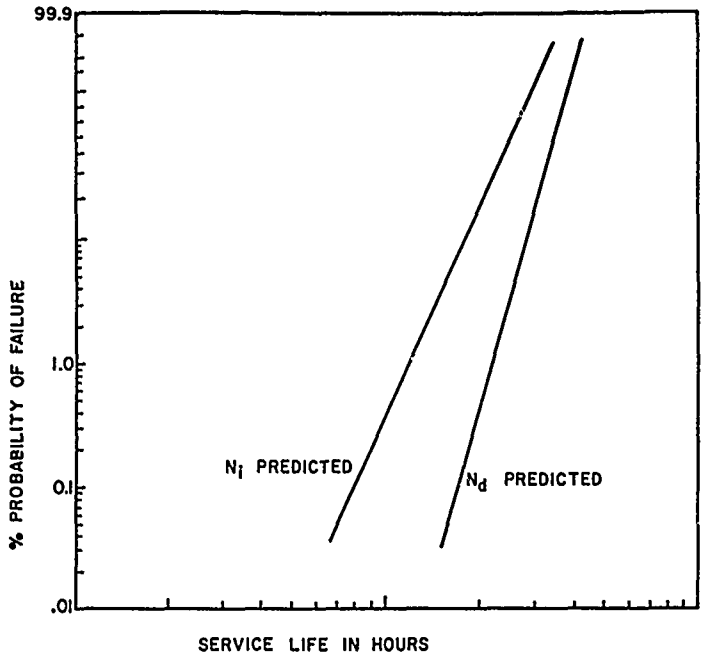

FIG. 23: THE USE OF WEIBULL PROBABILITY PLOTS SHOWING THE NUMBER OF SERVICE HOURS REQUIRED TO PROPAGATE A PRE-EXISTING FLAW TO A DETECTABLE SIZE (N_i) AND TO A DYSFUNCTION LIMIT (N_d) IN ORDER TO DETERMINE A SAFE INSPECTION INTERVAL

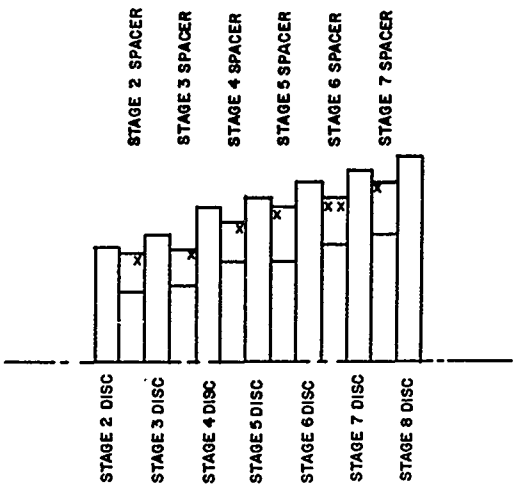

FIG. 24: FRACTURE CRITICAL LOCATIONS (MARKED X) IN VARIOUS COMPRESSOR COMPONENTS OF A J85-CAN40 ENGINE (Ref. 82)

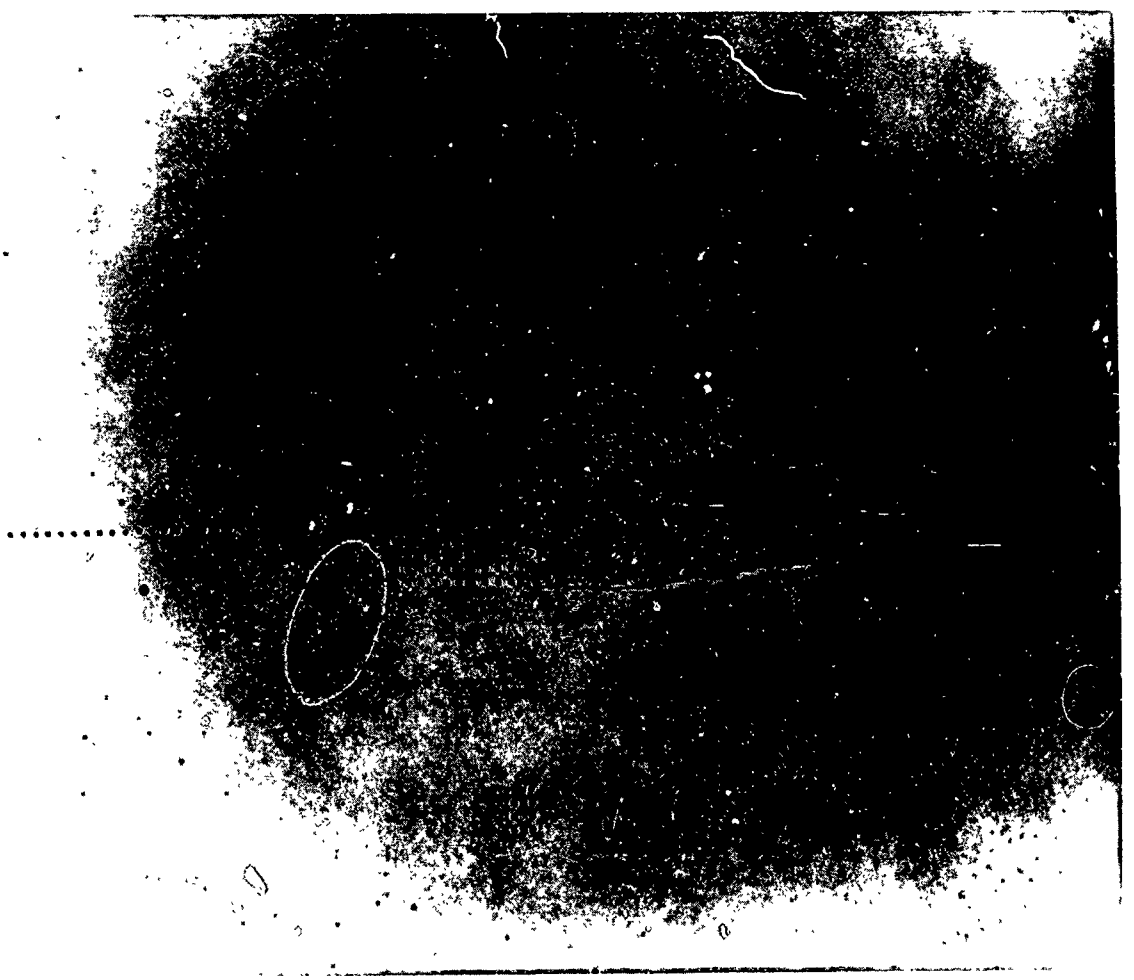

FIG. 25: MICROHARDNESS MEASUREMENTS USED IN A GRID PATTERN TO DETERMINE THE PLASTIC ZONE SIZE IN A 5th STAGE COMPRESSOR DISC IN A J85-CAN40 ENGINE

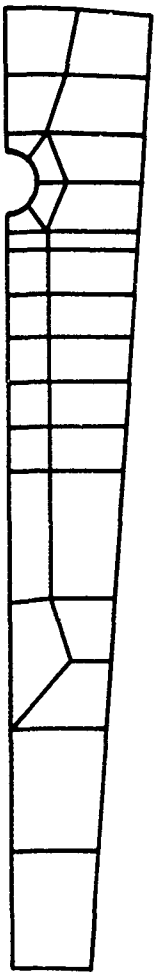

FIG. 26: FINITE ELEMENT MESH
USED TO MODEL A SEGMENT
OF A 5th STAGE J85-CAN40
COMPRESSOR DISC (Ref. 82)

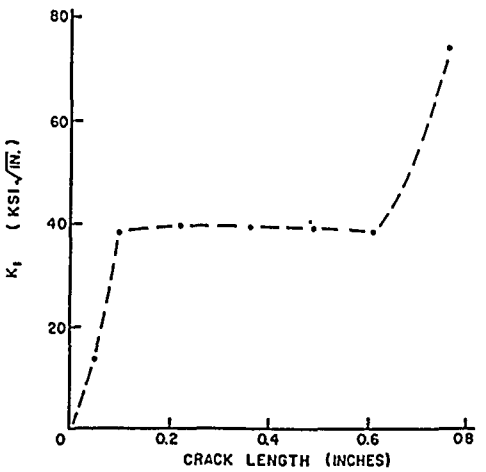

FIG. 27: 5th STAGE COMPRESSOR DISC OF J85-CAN40 ENGINE
ROTATING AT 16,500 RPM SHOWING K_I VERSUS CRACK
LENGTH VARIATION USING FINITE ELEMENT MODELLING

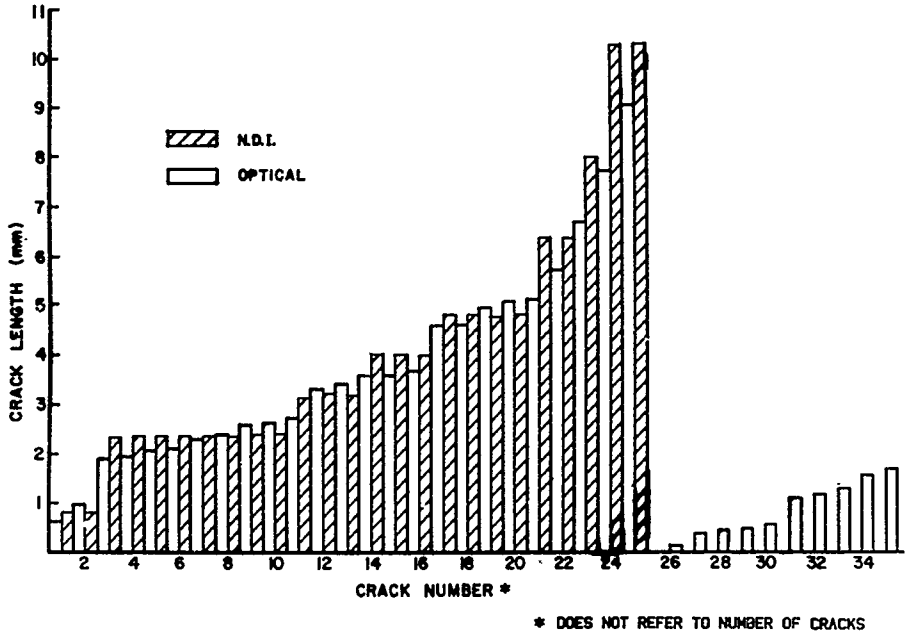

FIG. 28: COMPARISON OF OPTICALLY MEASURED AND NDI (FLUORESCENT PENETRANT INSPECTION) REPORTED CRACK LENGTHS IN A 5th STAGE COMPRESSOR DISC OF A J85-CAN40 GAS TURBINE

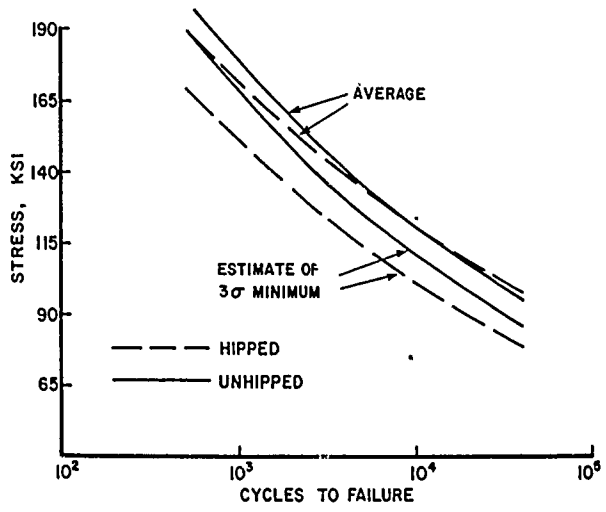

FIG. 29: UNHIPPED VERSUS HIPPED LOAD CONTROLLED LCF PROPERTIES OF WASPALOY TURBINE DISCS AT 540°C

DISCUSSION

M.Y.Nazmy, Switzerland

In one of the creep rupture life parameters that you have used, the secondary creep rate enters. Can you comment on the validity of defining a secondary creep rate of nickel base cast alloys? I believe that one can define a mnimum rather than a secondary or steady creep rate. Can you also comment on the errors that can be expected in using such a parameter which exhibits significant scatter?

Author's Reply

I have discussed the subject of secondary creep rate in IN738LC turbine blades in reference 23 of the paper. I am also aware of the arguments used to define a minimum creep rate as opposed to a secondary creep rate in Ni-base superalloys. If it is assumed that towards the end of the primary creep regime up until an arbitrary point along the creep curve a minimum creep rate did indeed exist in IN738LC material, then t_s and $_s$ terms in equation (5) were given the appropriate values in the data presented in reference 23. It is nevertheless evident that equation (5) indicates minimum scatter over a wide range of stresses and temperatures in IN738LC (contrary to the suggestions made in the question) and the equation is capable of detecting the service-induced degeneration effects systematically (Figure 8).

M.Y.Nazmy, Switzerland

What is the reproducibility of the HIP & H.T. process with respect to the creep life?

Author's Reply

Reproducibility in extending the creep life of service exposed turbine blades through the use of HIP rejuvenation technology can best be judged from the experience gathered on in-service behaviour of the rejuvenated blades. To quote an example, various batches of HIP rejuvenated X-750 turbine blades have now been in-service for well over 40,000 hours without any catastrophic results to date. However, HIP thermal cycles for each batch of turbine blades from the same material should be selected on an individual basis, considering the variations on the operating conditions from one turbine to another. NRC, in cooperation with Westinghouse Canada Inc., has developed a precise microstructural philosophy to combat this reproducibility problem.

A.J.A.Mom, Ne

In your paper you describe that you need, in applying the damage tolerance approach for discs, information on crack growth between a pre-existing flaw up to a detectable size. However, in principle you don't need that information in the damage tolerance approach. In damage tolerance you need only characteristics above the detectable size, that is enough to give you a safe inspection interval. Can you comment on that please?

Author's Reply

Dr Mom's comments regarding the validity of generating a statistically significant data base in terms of the number of service hours required to propagate a pre-existing flaw to a detectable size when considering ENSIP based damage tolerance design approach to lifing are justified in principle. However, the reluctance and scepticism of engine manufacture in applying the damage tolerance based design concepts in their full extent was evident during the course of the meeting. It appears that the manufacturers would like to use shorter inspection intervals in the beginning, until enough confidence in the design procedures is established. The methodology presented in section 2.2.2.1 of the paper appears to satisfy this requirement. In addition, the damage tolerance based maintenance methodology, as applied in J85 CAN40 components, aims to extend the lives of currently operating aircraft turbine engines beyond their original safe life limits as specified by the manufacturer. As pointed out in the text of the paper, N_i curve in Figure 23 for these in-service components should normally be available from the manufacturer, thus requiring little effort on the part of the user in generating these data.

G.A.Webster, UK

I would like to address the problem of measuring the residual life of time exposed material when there is considerable scatter in the original data. It is not sufficient just to quote exposure times, exposure stress and temperature will also determine the amount of damage and deteriorations accumulated in service. Is it possible to say how much life it is expected that your 13,000 hr. and 20,000 hr. exposed material had suffered? It will only be possible to distinguish between the rupture life of original and exposed material if the exposed material has used up a significant proportion of its life.

Author's Reply

It is indeed true that service stress and temperature will largely govern the extent of turbine blade deterioration. The type of equations presented in Figure 8 for different material (IN738LC) conditions can however be used to determine the residual life of a set of service exposed turbine blades. The procedure service imposed blade at near service temperature and stress to determine the secondary or minimum creep rate. Then assuming an allowable creep strain value for use during further service and substituting this and the creep rate value in the appropriate equation in Figure 10 would yield a useful residual creep life value.

DISC FATIGUE LIFE PREDICTIONS FOR GAS TURBINE ENGINES

by
W. J. Evans
M. E. F. Smith
C. H. H. Williams
Materials and Engineering Research Division
Propulsion Department
Royal Aircraft Establishment
Pyestock
Farnborough
Hants GU14 OLS
ENGLAND

SUMMARY

The paper is concerned with the determination of safe cyclic lives for discs in gas turbine engines. It reviews the current procedures which are based on a life to first crack philosophy and, in Britain, require full scale component testing to establish a service safe life. The limitations of this approach are highlighted. It is then suggested that an alternative method based on fatigue crack propagation should overcome some of the limitations. Before this alternative can be adopted, however, it is important to develop quantitative models for the types of crack that occur in engine discs. These cracks tend to be embedded, situated at stress concentration features and subjected to multiaxial stress fields. Some of the published work on such cracks is reviewed and the more relevant models detailed. An experimental programme on the titanium alloy Ti-6-4 is then described in which the behaviour of small cracks is evaluated for stress concentration features in bend specimens and model discs.

1. INTRODUCTION

Disc design in aero gas turbine engines continues to provide a stimulating challenge for the mechanical engineer. The integrity of these components is vital to the safety of the aircraft and yet, of necessity, they are highly stressed to meet the stringent demands of weight and engine efficiency. To maintain standards and ensure that risk levels are acceptably low, engine certification authorities throughout the World have laid down procedures for the design and validation of such components. Initially formulated in terms of tensile strength limits, it was soon realised that factors to cater for the fatigue damage incurred during each flight cycle would also have to be included. Nearly two decades have passed since these more exacting criteria were introduced. This is a sufficient period of time for a reliable assessment to be made of their success. Gunstone (1), for instance, has pointed out that there is only one disc burst per 2×10^6 engine hours in civil operation. Of these failures, only 10% can be attributed to low cycle fatigue (LCF). By this yardstick the lifing rules must be regarded as successful.

However, there are other ways in which success can be measured. For instance, it has been estimated that, because of the safety factors used, about 90% of discs are removed from service having consumed less than 50% of their safe life capability. The criteria, therefore, maybe safe but they are also conservative. On the other hand, a few discs in the remaining 10% may fail prematurely because the lifing criteria are inflexible and unable to cope with conditions that fall outside the strict boundaries within which they have been formulated. It is for these reasons that a number of authors (2,3) have advocated changes in design philosophy and several certification authorities are beginning to develop modified lifing criteria (US Airforce, BRITISH CAA).

The present paper briefly summarises current lifing philosophy particularly in relation to the procedures used in Britain. Limitations are highlighted and areas identified where improvements might be possible. An experimental programme aimed at improving understanding in one of these areas - the growth of small cracks at stress raisers - is then described.

2. DISC LIFING CRITERIA

In Britain, certification requirements for civil engines are controlled by the Civil Aviation Authority through their BCAR (British Civil Airworthiness Requirements) document. Military applications have to conform to the Director General (Engines) specifications RD2100 and RD2300. For disc lifing these requirements are broadly similar. An important common factor is the method by which the engine manufacturer substantiates his declared component design life. Unlike America, the accepted method of establishing the design life is cyclic spin testing of full size components. For large discs, this can be an expensive approach especially when each disc contains several critical design features. Even so, there are instances where full scale testing has unearthed problems that were not revealed during a preliminary laboratory test programme. One such instance has been reported recently (4). Failure in the alloy under evaluation was shown to be controlled by weak microstructural links. The greater the volume of material the better the chance of a weak link being situated in a high stress region. Thus the bigger the volume of critically stressed material the lower the measured fatigue life. In this particular case, a design curve based on limited laboratory data would have given a dangerously optimistic assessment of the service capability of the alloy.

In common with the lifing philosophy adopted in other countries, the British method of determining component safe life is based on a first crack criterion. This is essentially a crack initiation approach in which the component is considered to have become unservicable once a detectable crack -typically 0.75 mm long - is present. In practice, very few components will reach this condition in service. This is because once a life to first crack has been determined from a component test programme it will then be factored to arrive at a safe service life for the part or design feature. The factors are applied to the

mean test life and their magnitude depends on the number of components tested and the degree of scatter in properties shown by the disc material. Typical factors for a well behaved material are shown in Table 1.

Table 1 - Fatigue Scatter Factors

Test Sample Size	1	5	10
Factor	4.00	3.05	2.86

A well behaved material is considered to follow a log normal failure distribution with a ratio for $+3\sigma$ to -3σ fatigue life of 6 (σ is the standard deviation). Some cast materials and powder metallurgy alloys exhibit higher scatter levels and the factors should be adjusted accordingly. For instance if the ratio of $+3\sigma$ to -3σ life is 15 then the factor for a sample size of one becomes 8.13.

Recently, an important alternative method of establishing component safe life has become acceptable. Instead of taking the life to first crack as the design criterion, component tests are run on to burst and the design life is assumed to be 2/3 the number of cycles to failure. The same factors as shown in Table 1 are then applied to the results in order to arrive at the component safe life. This alternative method has been adopted for two related reasons. In the first place, it is recognised that, for many of the modern disc alloys, crack initiation is an ill-defined event that occurs at a comparatively low number of cycles. These alloys spend most of their lives in the crack growth regime. Secondly, most disc components can tolerate cracks that are significantly larger than the 0.75 mm safe life limit. It is argued that the 2/3 burst criterion can benefit from this additional growth without any compromise in safety standards. A comparison of the alternative methods is presented in Table 2 for Ti-6-4 model discs with diaphragm holes (the discs did not fail under test but the cracks were grown to an unstable size as evidenced by the calculated stress intensity factors - K_{IC} values typically are in the range 50 to 95 $MN/m^{3/2}$ (5)).

Table 2 - Comparisons of Lifing Criteria

Maximum speed rev/min	Number of cracks at hole	Life to first crack N_I (cycles)	Life to 'failure' N_f (cycles)	Total length of crack at N_f (mm)	Stress intensity at N_f ($MN/m^{3/2}$)	2/3 burst life (cycles)
43000	2	639	3190	10	89	2130
38700	1	17900	26290	14	82	17530

The higher speed design condition can benefit from the 2/3 burst approach but whether this advantage could be fully exploited would depend on other assessments of the risk involved. Even so, the message in these data is that there could be some advantage in incorporating crack growth criteria into component lifing philosophy. The 2/3 burst approach might not be the ideal way of achieving this but the experience gained in its use should pave the way for more appropriate methods.

3. ASSESSMENT OF THE LIFING METHODS

The important features of current lifing methods can be summarised as:

(a) They are crack initiation based criteria and no allowance is made for the presence of material defects.

(b) The calculation procedure assumes an ideal log normal distribution for component life. Departures from this distribution might increase the risk of inservice failure.

(c) Full size component testing although costly is regarded as an important element in the life calculation procedure because it automatically allows for bulk factors such as microstructural variations, residual stress and biaxiality effects to be modelled.

(d) Except for the pseudo 2/3 burst method, crack growth is not taken into consideration, being regarded as a hidden safety factor.

The apparent success of the method is due in part to the fact that the factors used in the calculation of safe life are large - an additional factor of 2 over those in Table 1 can be invoked to cover 'unquantifiables' such as environment or fretting damage. On the other hand the penalties resulting from the consequent overdesign, together with the possibility that some failure situations are not covered adequately is causing concern in some quarters. It is for these reasons that alternative procedures based on crack growth are being advocated.

4. CRACK GROWTH CRITERIA

The field of fracture mechanics is all encompassing being appropriate for any situation in which crack extension has occured. The significant point for the present paper, however, is the fact that it does provide an effective model for fatigue crack growth. The central parameter in fracture mechanics is the stress intensity factor, K, which describes conditions at the crack tip and has the general form

$$K = G_m \sigma \sqrt{\pi a} \qquad \ldots.(1)$$

G_m is a geometry term which is a function of crack shape and component size, σ is the applied stress and 'a' the crack size. For fatigue situations it has been established that the rate of crack growth, da/dN, can be related directly to ΔK, the range of K per cycle.

$$\frac{da}{dN} = f(\Delta K) \qquad ....(2)$$

A schematic diagram illustrating the form of this relationship is shown in Fig 1. At low ΔK there is a threshold region below which crack growth becomes insignificant (typically with growth rates in the region 10^{-6} - 10^{-7} mm/cycle). As ΔK increases a period of relatively stable growth occurs in which a simple power law can be fitted to the data, $da/dN = c\Delta K^m$. At high ΔK the growth rate accelerates towards component failure.

To estimate the crack propagation life of a component it is necessary to derive the appropriate form of Eq (2) for the material being used, determine K in Eq (1) for the particular geometry and integrate the expression

$$N = \int_{a_0}^{a_1} \frac{da}{f(\Delta K)} \qquad ....(3)$$

between appropriate initial, a_0, and final, a_1, crack sizes. The initial crack size might be a known flaw or microstructural feature. The final size might be that for failure or some lower limit.

Fracture mechanics has been used for some time in airframe design (3) but only sparingly on the engine side. It can, however, in combination with a sophisticated crack detection capability overcome the limitations of the current disc lifing philosophy. Discs need not be removed from service at some predetermined safe life but operated until they are known to contain a crack. Full scale component testing could be reduced to a minimum because it is easier to relate the crack growth behaviour of different geometries through K than it is to equate crack initiation behaviour. A prerequisite to making this change, however, is the successful modelling of the behaviour illustrated in Fig 1 for conditions appropriate to those experienced in engines.

The difficulty as far as engine discs are concerned, and the reason why fracture mechanics has seen limited application in the past, is the fact that stresses in these components can be comparatively high so that critical crack sizes for growth are small. At the sametime, the life limiting areas are usually at stress concentration features and often in thick section material. It is essential, therefore, to quantify the crack propagation behaviour of embedded cracks (corner or thumbnail) situated in stress gradients or regions of plasticity and frequently experiencing multiaxial stress conditions.

5. THE GROWTH OF CRACKS AT NOTCHES

Notch fatigue behaviour has been an area of interest for many years (6). Initially studies were concerned only with life to failure but, as understanding grew, it was realised that a complete treatment of the process would require a division into crack initiation (N_i) and propagation (N_p) regimes:

$$N_f = N_i + N_p \qquad ....(4)$$

The initiation life is usually determined by a local strain approach in which the behaviour of the material at the root of a notch is equated with that of a plain specimen subjected to similar loading constraints (6,7). In addition to stress-strain behaviour, recognition has to be given to the volume of critically stressed material at the notch, mean strain effects and biaxiality (7). Once initiation life has been calculated, total life is determined using equation (3) and growth rate data obtained on large crack laboratory specimens. A difficulty with this approach is the definition of a_0 the crack size on initiation. Various authors have defined this parameter in different ways. Duggan (7), for instance, refers to an engineering crack which is 0.1 mm deep by 0.5 mm long. He then defines N_i as a crack formation life. In practice the size adopted for this initial flaw is determined by the sensitivity of the crack detection equipment. Duggan chose his criterion on the basis of what is possible for component inspection. Laboratory techniques can detect crack growth at sizes well below this level. In fact, as sensitivity is increased N_p is found to make a bigger contribution to the overall life as the crack intiation size approaches alloy microstructural levels (2).

Recognising the importance of the growth regime, a number of authors have begun to address the problem of modelling the behaviour of small cracks (8-9). In particular Haddad et al (8) have introduced ideas that appear to offer significant benefits particularly in relation to the development of embedded cracks at notches. The starting points for their analysis are the threshold stress intensity, ΔK_{th}, in Fig 1 and the smooth bar fatigue endurance limit, $\Delta\sigma_e$, which is the stress range that does not result in failure in, typically, 10^7 to 10^9 cycles. It is important to realise that cracks can form at stresses less than $\Delta\sigma_e$ but do not propagate and that ΔK_{th} is constant only for large cracks. For small cracks ΔK_{th} falls as the crack length is reduced. They then redefine equation (1) for small cracks by adding a constant, l_0, to the crack size:

$$\Delta K = G_m \Delta\sigma \sqrt{\pi(a + l_0)} \qquad ....(5)$$

The geometry factor, G_m, is approximately unity for small through cracks. The constant, l_0, is shown to be related to material structure and is evaluated from the limiting condition when 'a' approaches zero, $\Delta\sigma = \Delta\sigma_e$ and $\Delta K = \Delta K_{th}$:

$$l_0 = \frac{1}{\pi} \left(\frac{\Delta K_{th}}{\Delta\sigma_e}\right)^2 \qquad ....(6)$$

For situations of gross plasticity, the elastic stress intensity is considered to be inappropriate. Hadded at al, therefore, have replaced ΔK in Eq (5) by the Rice 'J Integral'. The J integral is analogous to the strain energy release rate, G, except that it is based on non-linear rather than linear elasticity. For elastic situations J reduces to G so that for plane stress

$$\Delta J_e = G = \frac{\Delta K^2}{E} \quad \ldots.(7)$$

Substituting from equation (5) and taking the elastic strain energy density $W_e = \Delta\sigma^2/2E$

$$\Delta J_e = 2\pi W_e(a + l_0) \quad \ldots.(8)$$

This equation when extended to the plastic case has the form:

$$\Delta J_p = 2\pi f(n) W_p(a + l_0) \quad \ldots.(9)$$

with f(n) a function of the strain hardening exponent, n, and W_p the plastic strain energy density. Following Dowling (10) an approximate analysis for W_p was developed. This analysis was found to rationalise the crack propagation behaviour of short cracks at notches in two steels. Using conventional elastic fracture mechanics analysis, the short cracks were found to grow at a faster rate than large through cracks at the same ΔK. The two sets of data were found to superimpose, however, when the l_0 correction and ΔJ were used.

6. EXPERIMENTAL PROGRAMME ON SMALL CRACK GROWTH

The crack growth models being developed for small cracks at notches have important implications for the development of disc lifing criteria based on fracture mechanics. To be accepted by the industry, however, their validity must be explored for a wider range of conditions than has been attempted so far. As a step in this direction, a research programme was conceived in which the approach of Haddad et al would be evaluated on the widely used compressor disc alloy Ti-6-4. The aim was to improve modelling accuracy through a comprehensive experimental programme and the use of advanced finite element stress analysis.

The research programme was developed to satisfy a number of objectives. In the first place, it was desirable to achieve the highest possible levels of crack monitoring sensitivity. This could only be attained in a carefully controlled laboratory experiment. The edge notch bend specimen shown schematically in Fig 2 was designed to meet this requirement. Most of the data reported here were obtained on a 3.175 mm (1/8 ins) diameter notch with a limited number of tests being carried out on one of 5 mm diameter. Crack growth was monitored by an alternating current (AC) potential drop (PD) method. The system was calibrated by breaking open specimens after a known voltage change and measuring the crack size. A theoretical relationship was developed also (11) which was found to agree with the experimental data. The voltage change was directly related to cracked area as shown in Fig 3. This is a convenient relationship because area is the most appropriate method of describing the size of these small cracks which can vary appreciably in shape, Fig 4. Through attention to detail, such as positioning of current wires, a detection sensitivity was achieved equivalent to a 0.1 mm radius quarter circle corner or semicircular embedded crack.

The second objective was to obtain a meaningful sample of data points at any one stress condition. Material scatter plays an important part in lifing procedures. It is necessary, therefore, to quantify its impact on crack propagation behaviour if reliable minimum life estimates are to be made. A rig was developed to test 5 bend fatigue specimens simultaneously. In all, about 90 specimens were tested over the five loading conditions evaluated.

The final objective was to relate the laboratory bend specimen data to results obtained on the same material in component form. To this end, the model disc shown in Fig 5 was designed and tested on an inhouse cyclic spinning facility. The discs had 6 or 12 diaphragm holes and were tested at speeds in the range 35000 to 42000 rev/min. Tests were stopped periodically and each hole was inspected for cracks by eddy current and optical techniques. Even when a crack was found the test was usually continued so that the rate of growth could be determined. In most tests about 2/3 of the holes developed cracks. This gave a total of 50 failures for the range of discs evaluated. Detection sensitivity though was less than for the bend specimens being about a 0.3 mm radius quarter or semi-circular crack.

The experimental programme encompassed optical and scanning electron microscope observations. These were used to measure striation spacing and to study crack initiation sites. The striation information was used as an additional, albeit approximate, calibration of the crack detection method. Some typical striation measurements and calculated growth rates are given for one test condition in Table 3.

Table 3 - Comparison of Striation Spacing and ACPD Crack Growth Rates

Corner Crack radius (mm)	ACPD rate (mm/c)	Striation Spacing (mm/c)
0.1	0.45×10^{-4}	1.1×10^{-4}
0.3	1.34×10^{-4}	1.6×10^{-4}
0.5	2.23×10^{-4}	2.0×10^{-4}
0.7	3.13×10^{-4}	2.3×10^{-4}

7. MATERIAL AND SPECIMEN PREPARATION

The material used was the titanium alloy Ti-6-4. A chemical analysis gave the composition as 6.36 Al, 4.16 V, 0.15 O_2, 0.12 Fe, 0.02 C, 0.01 N_2, 0.003 H_2. It was obtained as 250 mm diameter pancake forgings which had been given a 3:1 α/β upset. Heat treatment consisted of homogenisation at 1235K followed by an oil quench and anneal at 975K. The microstructure, a mixture of primary α grains and transformed β regions, tended to be coarser towards the centre of the billet. Grain size was in the range 10 to 50 μm. The macrostructure exhibited significant grain flow which can lead to a directional dependence of mechanical properties. This was confirmed by tensile tests on specimens from various positions within the forging. The extremes of behaviour are represented by the curves in Fig 6.

In specimen preparation, care was taken to ensure that the stress concentration features in both bend specimens and discs were machined in the same way. The standard technique was drilling and reaming with the speeds and rates of feed established during a preliminary research exercise. A limited number of 5 mm diameter notch bend specimens were prepared by several alternative methods: grinding, side milling, end milling plus drilling and reaming followed by bead blasting.

8. EXPERIMENTAL RESULTS

8.1 Plain Specimen Fatigue

Strain control tests were carried out in a servohydraulic machine at ambient temperatures and R values (minimum/maximum strain) of -1, 0, 0.5. A Coffin-Manson analysis of the data is given in Fig 7. A cyclic stress strain curve derived from the data coincided with the minimum tensile curve in Fig 6.

8.2 Notch Bar Fatigue

The notch bar specimens were subjected to deflections of zero to 1.5, 1.8, 2.1, 2.5 and 2.8 mm at ambient temperature. In each case, voltage changes, ΔV, were extracted from the ACPD chart traces and plotted on a logarithmic basis against cycles. Two examples of the resultant graphs are shown in Fig 8. These are typical in the sense that centre cracks consistently gave a higher slope than corner cracks. The linear relationship applies to all cracks examined and is representative of growth over crack radii in the range 0.1 to 1.5 mm. From fracture surface studies it was apparent that the cracks were single origin and maintained their quarter or semi-circular shape upto approximately 0.7 mm radius. Beyond that size there was an increasing probability that further cracks would be initiated and that the shape would become more elliptical (Fig 4).

The linear relationship in Fig 8 can be represented by the equation:

$$\log_e \Delta V = \log_e M_0 + \alpha N \qquad \ldots.(10)$$

Since ΔV is proportional to crack area, this equation is strikingly similar to that proposed by Frost and Dugdale (12):

$$\text{Log}_e \text{ (crack length)} = aN + b \qquad \ldots.(11)$$

with a and b constants. Equation (10) implies that crack growth is continuous from the commencement of the test, Fig 9. The parameter, α, is a measure of the rate of crack propagation. Initiation, as detected by the PD measurements, is the point at which the voltage change due to crack growth exceeds the detection threshold for the AC equipment. This is confirmed by Fig 10 which shows that, except for the largest deflection, N_I, the number of cycles to form a 0.1 mm crack, is inversely dependent on α.

Equation (10) also implies that there is a positive voltage change, M_0, at the beginning of the test which is additional to that caused by the growing fatigue crack (Fig 9). The nature of this change is uncertain but it could be due to plastic deformation on loading or to the formation of a flaw. Careful control of the experimental conditions has ruled out any equipment related reasons. Figure 11 illustrates that the value of log M_0 was virtually independent of loading condition for the lower deflections but then increased significantly for the large deflections. An experiment was conducted with 5 mm diameter notches to determine how surface preparation affected the value of M_0. The results are presented in Fig 12. There is an inverse linear relationship between log M_0 and initiation life. It was found that, the shortest lives and the largest M_0 values were obtained with ground surfaces. Examination of the fracture surfaces revealed significant differences between the specimens prepared by grinding and those prepared by drilling and reaming. Cracks in the ground specimens initiated across the width of the notch while the drilled and reamed cracks grew from discrete initiation points as shown in Fig 4. Grinding is known to put the surface layers into tension thereby leading to early crack initiation. Drilling and reaming, on the other hand, causes residual compressive stresses. The M_0 voltage change appears to be a measure of these differences.

Equation 10 can be rewritten in the form:

$$V = M_0 \exp(\alpha N) \qquad \ldots.(12)$$

Assuming the ideal semi- or quarter-circular crack, the calibration curve in Fig 3 can be described by the expression

$$V = cb^2 \qquad \ldots.(13)$$

with c constant and b the crack radius. Differentiating both equations and combining:

$$\frac{db}{dN} = \frac{\alpha b}{2} \qquad \ldots.(14)$$

The Frost and Dugdale analysis results in a similar relationship (12). The growth rates calculated from this equation compared well with striation measurements and optical observations. Some typical values are presented in Table 4.

Table 4 - Crack Growth Rates for Various Bend Deflections

Corner Crack Radii mm	Calculated db/dN mm/cycle for the beam deflections:		
	1.8 mm	2.1 mm	2.8 mm
0.1	4.5×10^{-5}		1.9×10^{-4}
0.3	1.3×10^{-4}	2.3×10^{-4}	5.7×10^{-4}
0.5	2.2×10^{-4}	4.9×10^{-4}	9.5×10^{-4}
0.7	3.1×10^{-4}	7.4×10^{-4}	1.4×10^{-3}
1.0	4.5×10^{-4}	1.0×10^{-3}	1.9×10^{-3}
1.2	5.4×10^{-4}	1.3×10^{-3}	2.3×10^{-3}
1.4	6.3×10^{-4}	1.6×10^{-3}	2.7×10^{-3}

The data in Table 4 are for corner cracks. Similar information was obtained for centre cracks.

8.3 Model Discs

Crack growth measurements for the model discs were not to the same degree of accuracy as for the bend specimens. However, the eddy current measurements were calibrated and appeared to relate well to optical measurements of crack length. Figure 13 is a logarithmic plot of voltage change against cycles. A similar linear relationship to that observed with the PD measurements (Fig 8, Eq 10) was found to apply.

8.4 Stress Analysis

Preliminary stress analysis was carried out using 2D finite elements. It was found, however, that this was inadequate for modelling the behaviour of corner and embedded cracks. A 3D analysis was, therefore, carried out using the GANDALF code. Details on the development of GANDALF have been published by Burton and Ward (13). In essence, the code incorporates a range of non linear solution algorithms to enable problems of differing size and degree of plasticity to be solved efficiently. The code uses a classical time independent plasticity model with a Von Mises yield surface, isotropic hardening and associated flow rule. The plastic analyses of the bend specimen and the disc used the minimum stress strain curve of Fig 6. The beam was modelled at half thickness and typical axial stress contour plots are shown in Fig 14. Through thickness 2D sections for the base of the notch are shown for defelections of 1.8 and 2.8 mm in Fig 15. It was necessary to allow for the observed through thickness and depth variation of stress in the fracture mechanics analysis of the quarter- and semi-circular cracks. A similar set of data was obtained for the disc idealisation in Fig 16.

A 3D finite element analysis of the cracks was not made in the present investigation. Instead, the comprehensive FE analysis of Pickard (14) was adopted. In particular, his stress intensity solutions for corner and centre surface cracks in blocks under uniform stress fields were found to be most appropriate. A number of important assumptions were necessary for this approach to be taken. Firstly, Pickard determined his stress intensity factors with respect to the remote stress field. It was assumed for the small cracks being evaluted (b/H of 0.01 to 0.2), that the 3D plastic stresses adjacent to the crack front could be considered sufficiently remote. This carries the second assumption that the cracks do not significantly change the local stress field. This cannot be correct but the errors will be small for short cracks. The final assumption is that the growth kinetics can be adequately related to ΔK so that a J integral approach is not essential. The justification for this assumption is the observation that a plain specimen, when cyclically tested, deforms plastically initially but after a comparatively few cycles settles down into an essentially elastic deformation mode.

Stress intensity factors determined for corner cracks at a deflection of 2.8 mm are presented in Table 5. The difference between ΔK values for notch root through thickness cracks (Position B) and side face depth cracks (Position A) is apparent.

Table 5 - Stress Intensity Factors for Corner Cracks at 2.8 mm deflection

Units: σ_{xx} = MN/m^2, ΔK = $MN/M^{3/2}$

b mm	db/dN $\times 10^4$ mm/c	Through Thickness		Side face Depth		Average ΔK
		σ_{xx}	ΔK	σ_{xx}	ΔK	
0.1	1.9	960	12	940	12	12
0.3	5.7	975	22	920	21	21.5
0.5	9.5	987	29	900	26	27.5
0.7	13.8	1000	35	700	24	29.5
1.0	19.0	1025	44	500	21	32.5
1.2	22.8	1050	50	380	18	34
1.4	26.7	1075	57	300	15	36

Figure 17 emphasises the difference between through thickness and sideface depth ΔK values when plotted against db/dN for a deflection of 1.8 mm. For comparison the long crack growth rate data of Powell and Henderson for Ti-6-4 (15) have been superimposed on the graph.

The b and db/dN values, however, have been determined on the basis of the increase in cracked area. They represent an average growth condition for which an average ΔK as shown in Table V is more appropriate. The average ΔK values for a deflection of 1.8 mm are plotted in Fig 17. They correlate well with the long crack results. Fig 18 takes this approach further and presents crack growth data in terms of average ΔK for all conditions evaluated. The good correlation with long crack behaviour is maintained irrespective of deflection level and crack geometry. The major discrepancy occurs at low ΔK where the notch bend tests have higher growth rates than would be predicted bt the long crack data.

9. DISCUSSION OF EXPERIMENTAL RESULTS

The deviation at low ΔK shown by the short crack experimental data in figure 18 is similar to that observed by Haddad et al in their work on a steel (8). If their l_0 correction technique is to be used then it is necessary to obtain measurements of ΔK_{th} and σ_e for substitution in Eq (6). Powell et al (15) report a ΔK_{th} of 5 $MN/m^{3/2}$ for long cracks at R = 0 in Ti-6-4. Duggan et al (7) suggest that the endurance limit can be calculated from the elastic component of a fully reversed strain range test through the equation:

$$C_e = \frac{2\sigma_e}{E} N_e^{-\alpha_2} \qquad \ldots.(15)$$

where C_e is the elastic strain range intercept at one cycle, N_e the endurance limit, α_2 the slope of the elastic line and E the modulus. From the R = -1 data used in Fig 7 a value for σ_e of ± 450 MN/m^2 was determined at $N_e = 10^7$ cycles. This value compares favourably with published work which shows that σ_e is orientation dependent in thick section Ti-6-4 but has values in the range ± 427 to ± 565 MN/m^2 (5). Substituting the calculated value of σ_e into Eq (6) gives an l_0 value of 40 μm. Adding this value to the Ti-6-4 crack growth data and replotting according to Eq (5) results in a much improved correlation between short and long crack data as found by Haddad et al, Fig 19.

Hudak (6), whilst supporting the general usefulness of the l_0 concept, expresses concern over the lack of a physical model to account for the observed values. In the present case, this is not a problem because the calculated l_0 is the same order of magnitude as the grain size of the alloy (Section 7). Furthermore the M_0 factor (Eq 12) obtained from the crack growth measurements suggests that some initial crack parameter should exist. It is unlikely that M_0 and l_0 are exactly equivalent. It is more likely that they are the consequence of a common underlying cause. In fact, a careful inspection of Fig 19 reveals that the 40 μm correction is not entirely satisfactory for the 2.8 mm deflection at low ΔK. It requires an l_0 of 80 μm to provide a good correlation with the long crack data. This higher value of course is inappropriate for the lower deflections. It has already been pointed out that M_0 is virtually constant for the 1.8 mm and 2.1 mm deflections - the other deflections used to consruct Fig 19 - but increases significantly for the 2.8 mm deflection. On this basis M_0 and l_0 could be linearly related.

Hoeppner (3) has rewritten Eq (4) in the form

$$N_f = N_n + N_s + N_p \qquad \ldots.(16)$$

where N_n is the number of cycles to nucleate a crack like discontinuity and N_s is the number of cycles to propagate the crack under the influence of local structure and deformation mechanisms. The N_p term is stress dominated and refers to propagation where a continuum approach can be justified. The l_0 term can be identified with the transition between $(N_n + N_s)$ and N_p. The M_0 term arose from an analysis of the continuum crack growth regime. It is a positive voltage offset that is caused by the early plastic deformation and structure sensitive crack growth. In essence M_0 provides a measure of the $(N_p + N_s)$ processes that lead eventually to the development of the l_0 'continuum' crack. A schematic representation of the way in which plastic deformation and crack growth might interact and effect the voltage measurements is shown in Fig 20. Electron microscope observations provide some support for this point of view. Quasi-cleavage facets, Fig 21, were found at most initiation sites. These facets were comparable in size to the alloy grain structure and hence l_0. For crack sizes greater than l_0 striation growth was evident.

A final point on the experimental results concerns the behaviour of the model discs. A similar analysis to the bend specimens was carried out in spite of the less accurate results available. The resultant graph of db/dN against ΔK is given in Fig 22. There is good correlation with the long crack data even though growth was taking placing in a biaxial stress field. This result serves to develop confidence in the ability of fracture mechanics techniques to predict component behaviour.

10. GENERAL SUMMARY

Design criteria for lifing major rotating components in gas turbine engines are based essentially on an understanding of fatigue that was pertinent nearly twenty years ago. The science then was mainly empirical and modelling of the processes responsible for failure was largely qualitative. Over the intervening period there have been significant strides forward in understanding and these have led to the development of meaningful quantitative models. From a technological point of view, conditions are right for a revision of the criteria. At the same time, there is pressure for change as aerodynamicists and thermodynamicists strive to make engines lighter and more efficient.

Quantitatively, the important advance was the application of fracture mechanics ideas to crack propagation. This process began with large cracks - cracks large compared with the alloy structure - for which continuum mechanics theory is appropriate. However, with the realisation that a significant proportion of component life is associated with the development of 'small' cracks, the drive has been to push fracture mechanics concepts towards ever smaller crack sizes and lower growth rates. This trend has

been aided by the improving sensitivity of crack monitoring equipment. The experimental programme presented in the paper, in which embedded crack growth behaviour is related to long crack data, is a further step in this process. It demonstrates that physically small cracks can behave in the same way as long cracks provided the appropriate stress analysis is used. The present results, however, also suggest that a limit for this downward extrapolation approach is being reached. There is a crack size below which continuum ideas cannot be applied. These cracks are now at a size where behaviour is being influenced by local structure. The experimental evidence from large grain materials suggests that once this condition is reached the good correlation between short and long crack behaviour begins to break down (16).

There are, therefore, a number of issues that must be tackled before changes to the lifing criteria can be made with confidence. For instance, is it sufficient to define a lower limit for continuum growth which will then become the initial crack size in a fracture mechanics approach to life? The information presented in the present paper indicates that this route is feasible for fine grain materials. In coarse grained alloys, however, the transition crack size might be so large that the life estimates become unduly pessimistic. If structure sensitive growth must be modelled, then how can this be achieved effectively when most of the important events are below current detection thresholds? The PD measurements reported above would appear to have some potential in this respect. At the sametime, 3D finite element analysis of the region of interest has an important role to play in developing quantitative models. Over the next few years, advances will be made in this area and the effect of factors such as alloy structure (eg defects), environment (vibration, temperature) and surface condition (residual stress) will be quantified. Eventually, this will lead to the development of probabilistic models for this early crack growth.

In conclusion, a change to a fracture mechanics disc lifing criteria has some advantage and is technically feasible. The change must be a step by step process if safety margins are to be maintained and must be mirrored by improvements in other associated fields such as non-destructive testing capability.

11. REFERENCES

1. G. L. Gunstone, "Engine non-containment - the UK CAA view" Assessment of technology for turbojet engine rotor failures, MIT, Cambridge, Massachusetts, NASA CP-2017, 1977, 11-33.

2. R. H. Jeal, "Defects and their effect on the behaviour of Discs", Maintenance in Service of High Temperature Parts, NATO-AGARD-CP317, 1982, 5(1)-5(9).

3. D. W. Hoeppner, "Application of Damage Tolerance Concepts to Short Cracks", Structures of High Fatigue Performance, ICAF, Toulouse, 1983.

4. W. J. Evans, "Low temperature creep and fracture of near α Titanium Alloys", Conference on Creep and Fracture of Engineering Materials and Structures, Swansea, 1984, 395-401.

5. P. J. E. Forsyth and C. A. Stubbington, "Directionality in structure - property relationships", Metals Technology, 1975, 158-177.

6. S. J. Hudak, Jr, "Small crack behaviour and the prediction of fatigue life", J. Enging Matts and Technology, 103, 1981, 26-35.

7. T. V. Duggan, M. T. Lowcock and B. C. Staples, "Predicting crack formation life", Journal of Mechanical Engineering Science, 21, 1979, 263-273.

8. M. H. El Haddad, K. N. Smith and T. H. Topper, "Fatigue crack propagation of short cracks," ASME, 101, 1979, 42-46.

9. M. M. Hammouda and K. J. Miller, "Prediction of Fatigue Lifetime of notched members", Fatigue of Engineering Materials and Structures, 2, 1979, 377-386.

10. N. G. Dowling, "Geometry effects and the J-Integral approach to elastic-plastic fracture crack growth", ASTM STP 601, 1976, 19-32.

11. E. C. Atkinson and M. E. F. Smith, "The detection and measurement of non-through cracks using the AC potential difference method" NGTE Memo 81001, 1982

12. N. E. Frost and D. S. Dugdale, "The propagation of fatigue cracks in sheet specimens" J Mech Phys Solids, 6, 1958, 92-110

13. T. J. W. Ward and C. G. Burton "Design and Implementation of an Efficient 3D Finite Element Code for High Temperature Problems", MAFELAP Conference, Brunel Univ, England, 1984.

14. A. C. Pickard, "Stress Intensity Factors for Cracks with Circular and Elliptic Crack Fronts" "Second Int. Conf. on Numerical Methods in Fracture Mechanics, Swansea, 1980, 599-614

15. B. E. Powell and I. Henderson, "The conjoint action of high and low cycle fatigue", Portsmouth Polytechnic Report, AFSOR-82-0077, 1983

16. C. W. Brown and M. A. Hicks, "A study of short fatigue crack growth behaviour in Titanium alloy IMI685" Fatigue of Engineering Maths and Structures, 6, 1983, 67-76.

12. ACKNOWLEDGEMENT

The authors would like to thank Dr G. F. Harrison, Mr G. W. Timmins, Mr C. Burton, Mr S. Cockrem and Mr P Tranter for their helpful advice and informed technical comment.

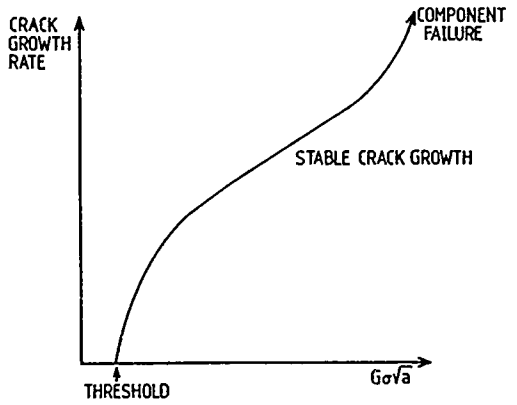

Fig 1. Variation of crack growth rate with stress intensity factor

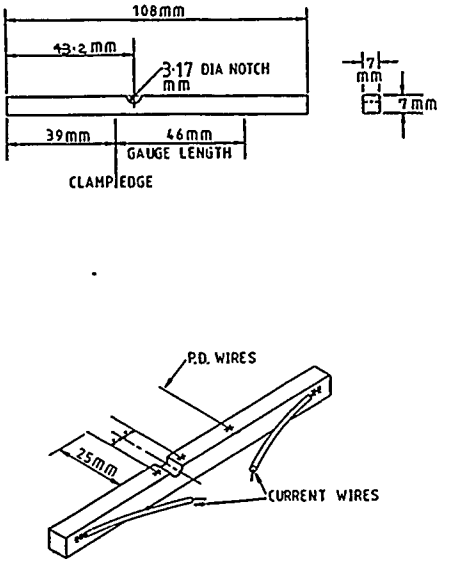

Fig 2. Notch Bend Specimen

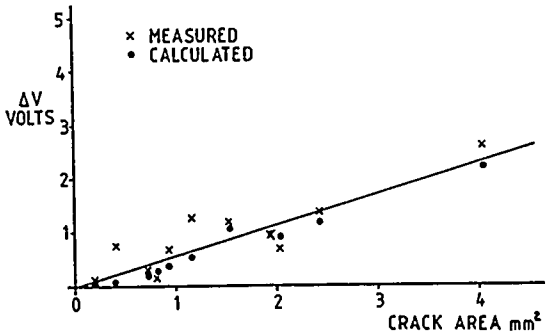

Fig 3. AC(PD) Calibration Curve

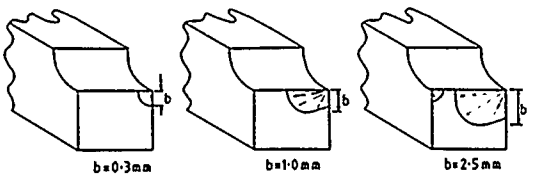

Fig 4. Typical variation of crack shape with depth

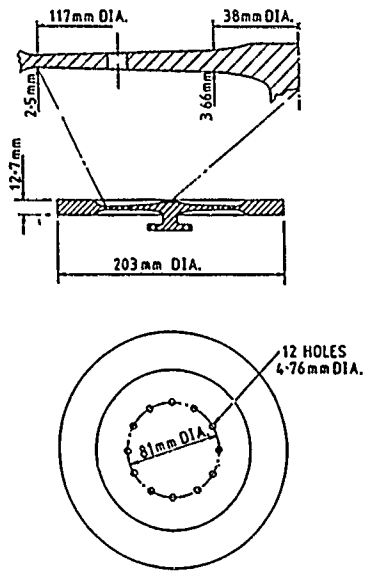

Fig 5. Details of model disc

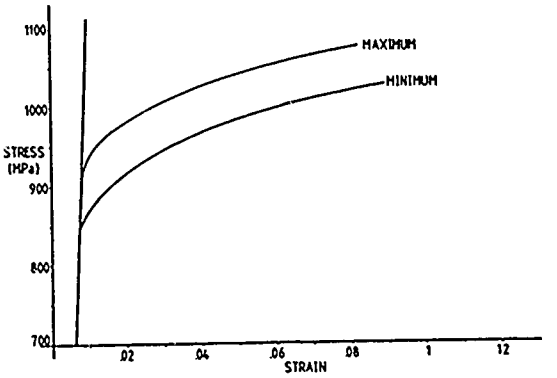

Fig 6. Range of monotonic stress/strain behaviour

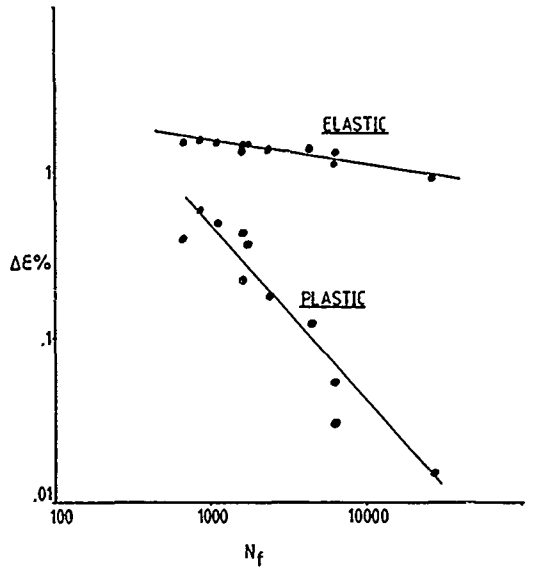

Fig 7. Coffin/Manson analyses of strain control fatigue

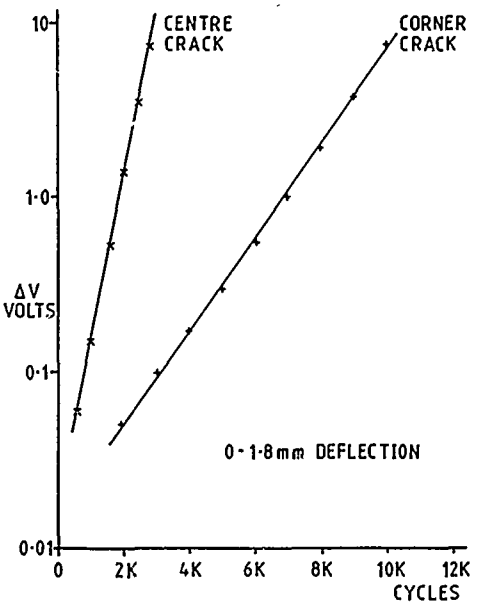

Fig 8. Typical charge of PD with increasing crack size.

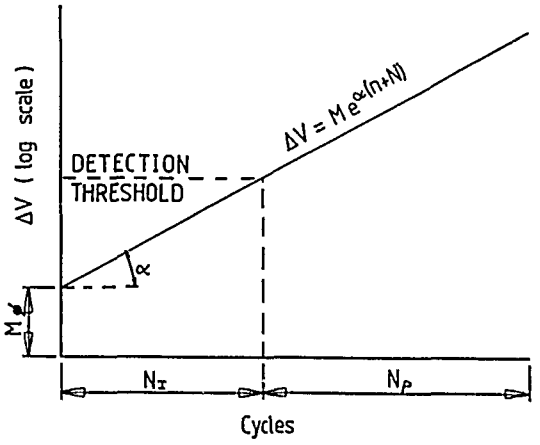

Fig 9. Ideal representation of change of PD with increasing crack size.

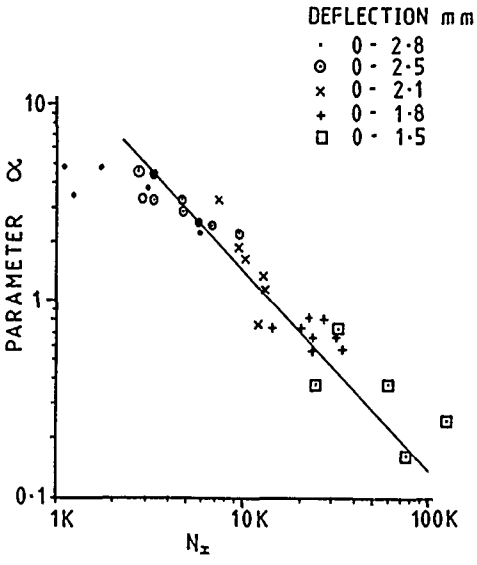

Fig 10. Variation of growth rate parameter α with increasing life to a 0.1 mm crack

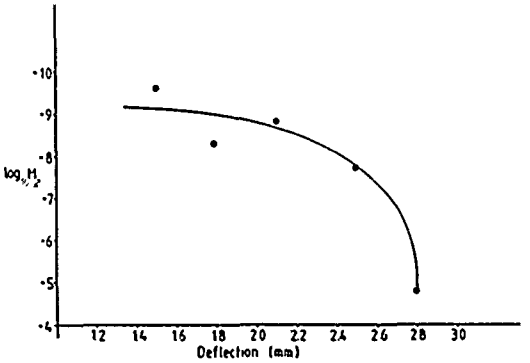

Fig 11. Change of intercept M_0 with loading condition

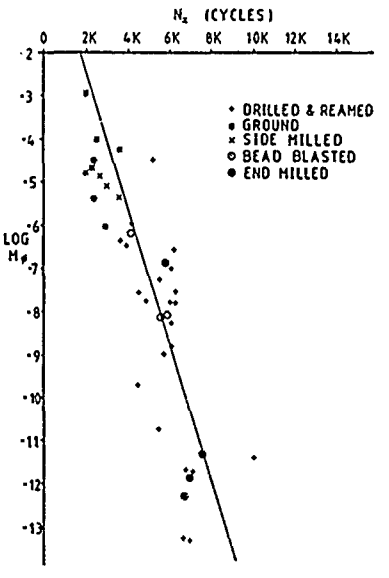

Fig 12. Effect of surface machining methods on M_0 for a deflection of 2.5 mm

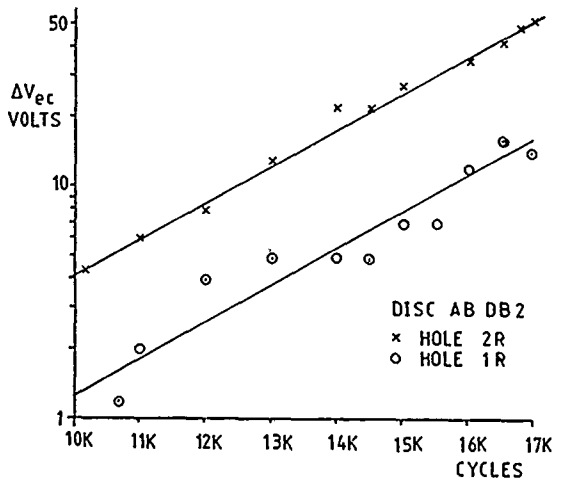

Fig 13. Change of Eddy current reading with crack growth

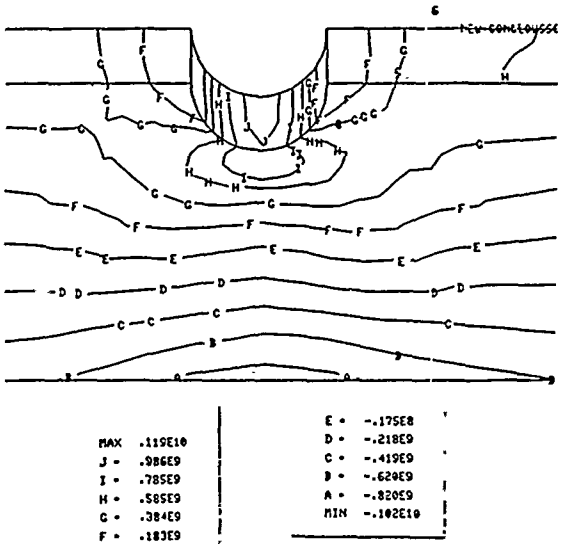

Fig 14. 3D elasto/plastic finite element analysis of notch bend specimen

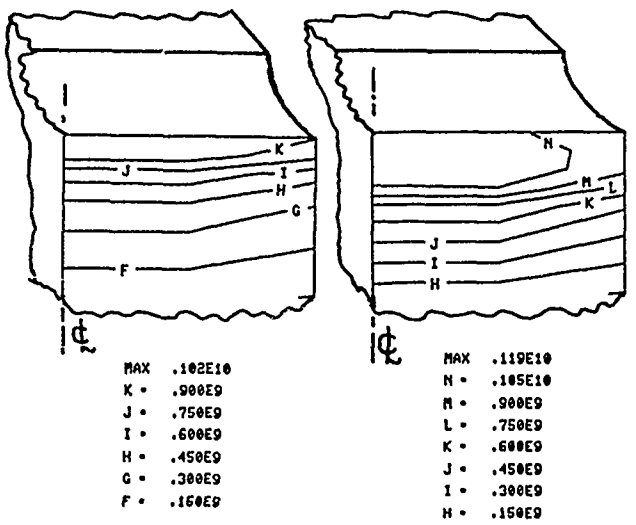

Fig 15A 1.8 mm Deflection 2D cross section of notch root showing axial stresses

Fig 15B 2.8 mm Deflection

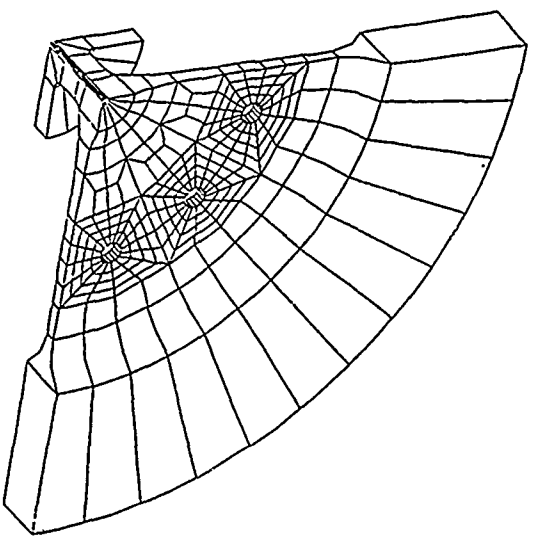

Fig 16. 3D finite element mesh for model disc

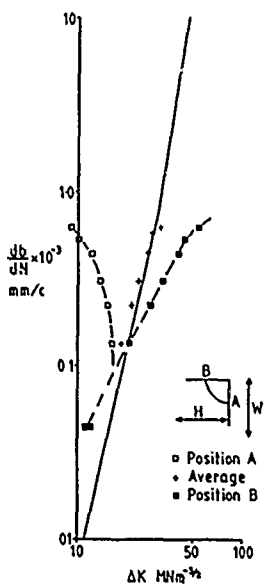

Fig 17. Effect of position on calculated ΔK values

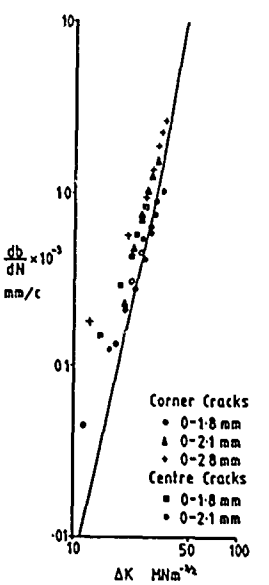

Fig 18. Comparison of short crack growth data with long crack best fit line of Ref 15.

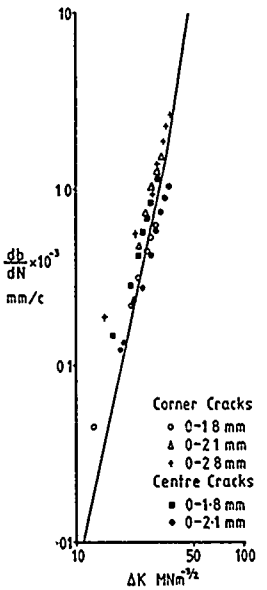

Fig 19. Comparison of short crack growth data with long crack best fit line of Ref 15 + using L_0 = 40 μm

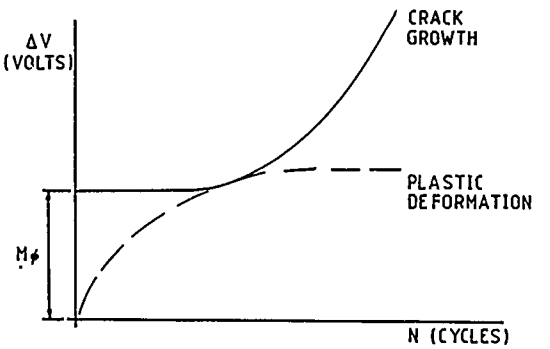

Fig 20. Schematic explanation for M_0 factor.

Fig 21. Facet formation in notch fracture surface

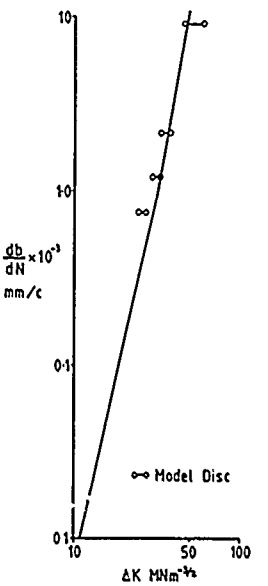

Fig 22. Model disc crack propagation behaviour

DISCUSSION

J.W.Bergmann, Ge

In notched specimens out of structural steels, titanium and aluminium alloys, it was always found that crack initiation took place from several locations in the notch. Some of the small cracks joined and formed the fatigue dominant crack. The same was found in a recent study on small crack propagation in the DFVLR, Cologne. (Small cracks were always greater than grain size.) Was this also true in your investigation? Is it possible to predict this discontinuous forming of large cracks out of small cracks?

Author's Reply

Multiple crack initiation can certainly be a problem. We have experienced it in notch bend tests on powder astroloy and EN 57 steel. Secondary cracking occured also with the Ti-6-4 in the present investigation but not until a significant amount of primary growth (approx. 1.5 mm depth) had been obtained. On the work we have carried out to date, however, it would appear that the calibration of the PD monitoring equipment is unaffected by the presence of these cracks. The voltage change is directly proportional to the increase in total cracked area. In addition, from the limited analysis conducted so far, the linear dependence of voltage change on cycles, as snown in figures 8 and 9 of the paper, still appears to be appropriate. On this basis, we would expect to develop eventually an understanding of multiple crack growth behaviour As for the size of the cracks, for all materials evaluated, at the point of first detection they have been greater than the alloy grain size.

R.Tadros, Ca

You have made a statement saying that the present Safe Life Approach is inadequate. How can you make such conclusion based on the results shown in your paper where fracture crack growth data are used for a known crack location, and using notch bar specimen data which definitely does not cover areas for crack growth in biaxial field, in misotropic materials, close to the threshold limit where specimen data is not representative, in multiple crack growth. You have not studied the effect of frequency loading and thermal fatigue interaction. Can you prove that it is a safer approach at this stage, bearing in mind all the foregoing outstanding questions and what confidence level you will have when using it? Definitely I don't want to sound negative with regard to crack propagation/fracture life estimation. However, I don't think that we can make such a statement unless all the above mentioned points are fully covered and safety is fully demonstrated.

Author's Reply

The question of the adequacy of disc lifing criteria is addressed in the first half of the paper where both strengths and weaknesses of current methods are reviewed. Undoubtedly, a major strength is their safety record, and it is pointed out that any change to the design approach must maintain the standard. The weaknesses relate to the inefficient way in which disc materials are used, the pseudo-scientific basis of the lifing philosophy and the fact that 'non-ideal' material or operating conditions are not adequately catered for. Such inadequacies are untenable as the drive to develop even stronger alloys becomes more difficult. The demands for lighter and more efficient engines will have to be met through the effective use of available materials. Changes in component lifing philosophy would appear to have something to offer in this respect with fracture mechanics based criteria appearing to be particularly advantageous. It is pointed out, however, that before such an approach can be introduced, quantitative models of crack growth behaviour under conditions of relevance to the engine must be developed. The second half of the paper concentrates on one particular aspect of this modelling problem: the growth of non-through cracks at notches. Other aspects are being evaluated, and it is only when the total programme is complete that a full defect tolerant approach can be introduced with confidence.

ENGINE CYCLIC DURABILITY BY ANALYSIS AND MATERIAL TESTING

Albert Kaufman and Gary R. Halford
NASA Lewis Research Center
Cleveland, Ohio 44135

SUMMARY

This paper addresses the problems of calculation of turbine engine component durability. Nonlinear, finite-element structural analyses, cyclic constitutive behavior models, and an advanced creep-fatigue life prediction method, Strainrange Partitioning, have been assessed for their applicability to the solution of durability problems in hot-section components of gas turbine engines. Three different component or subcomponent geometries are examined: a stress concentration in a turbine disk; a louver lip of a half-scale combustor liner; and a squealer tip of a first-stage high-pressure turbine blade. Cyclic structural analyses were performed for all three problems. The computed strain-temperature histories at the critical locations of the combustor liner and turbine blade components were imposed on smooth specimens in uniaxial, strain-controlled, thermomechanical cyclic tests to evaluate the structural and life analysis methods.

INTRODUCTION

Hot-section components of advanced aircraft gas turbine engines are exposed to extreme gas pressure and temperature environments. These operating conditions subject the combustor and high-pressure-stage turbine components to severe thermomechanical cycles that induce repeated inelastic straining and eventual fatigue cracking. Sophisticated analytical methods have been developed to assess the durability of the hot section components.

Nonlinear finite-element computer codes such as ANSYS (Ref. 1) and MARC (Ref. 2) have become available in recent years for calculating inelastic structural response under cyclic loading. The plasticity computations in these codes are based on classical incremental theory using a hardening model to define the yield surface under cycling, a yield criterion, and a flow rule. Generally, the von Mises yield criterion and the normality flow rule are used. Creep computations use a separate creep constitutive model that is not coupled to the plasticity model. Advanced life prediction methods, such as Strainrange Partitioning (Ref. 3), have been proposed for predicting low-cycle fatigue life from the stress-strain history at the critical location.

There is a need to calibrate these analytical methodologies against component experimental data to verify them and to guide their further development. Direct experimental verification from actual engine operation is difficult because the gas conditions are not generally known with sufficient accuracy, because the critical locations of these components are relatively inaccessible, and because the temperatures are beyond the high-temperature capability of state-of-the-art static strain gages. Without confidence in the reliability of the nonlinear structural analysis method or the ability to measure strains, it is seldom possible to verify the life prediction models under actual operating conditions. It is necessary, therefore, to verify these analytical methods with simpler experiments simulating the structural response of the engine component.

This paper addresses the problems of calculating turbine engine component durability. Three different component or subcomponent geometries are considered: a stress concentration in a turbine disk, a half-scale louvered combustor liner, and the squealer tip of a first-stage, high-pressure turbine blade. Nonlinear finite-element analyses, cyclic constitutive material behavior models, and advanced life prediction methods were assessed for their applicability to the solution of durability problems in these components.

Cyclic stress-strain response was obtained both experimentally (Ref. 4) and analytically (Ref. 5) for a two-dimensional representation of the disk notch problem. Three-dimensional nonlinear structural analyses were performed for a half-scale combustor liner (Ref. 6). This liner specimen was constructed in an identical configuration with current-service combustor liners. It was thermally cycled in an induction heated experimental rig. Three-dimensional nonlinear analyses were also performed for the tip region of an air-cooled turbine blade used in the first-stage, high-pressure turbine of a commercial aircraft engine (Ref. 7). This blade had a history of cracking in the squealer tip region. The mission cycle used for the blade analysis was based on full-scale engine factory durability testing.

The computed strain-temperature histories for the critical locations at the louver lip of the combustor liner and the squealer tip of the turbine blade were imposed on smooth specimens in uniaxial strain-controlled laboratory tests. Both structural and life analyses were performed for these thermomechanical test specimens and compared with experimental observations.

The disk notch testing program was a joint effort by the General Electric Co. and Louisiana State University under contract to NASA. Finite-element analyses of the

benchmark notch problems discussed in this paper were conducted at the NASA Lewis Research Center. The combustor liner and blade tip durability studies were performed by Pratt & Whitney Aircraft and the General Electric Co., respectively, under contract to NASA.

DISK STRESS CONCENTRATION

Benchmark notch specimens with discontinuities representative of stress concentrations in turbine disks were cyclically load tested to provide a body of experimental strain measurements taken at the notch root for analytical verification purposes. The specimen design is illustrated in Fig. 1. Specimens were fabricated from a nickel-base turbine disk alloy (Inconel 718). It was not the intent of this program to cycle specimens to failure nor make life prediction calculations.

Benchmark Notch Testing

The test program (Ref. 4) consisted of several axial load patterns, only two of which are of interest herein (Fig. 2). All tests were conducted with a temperature of 650° C maintained in the notch region. Testing was continued until cracks developed or the tensile strain reached 1.6 percent, which was the limit that could be accommodated by the measurement system. The load cycling for pattern I was not fully reversed. However, the notch root strains were great enough that the local stress response would tend toward a fully reversed condition with a mean stress of zero. The frequency was 0.167 Hz. Monotonic step loading was applied for pattern II in five increments, with a dwell time of approximately 1 hr for each increment.

Notch Strain Measurement

Notch root strains were measured with an interferometric strain displacement gage (ISDG) that measures relative displacement between two small indentations at the center of the notch root. These indentations are applied 100 μm apart with a Vickers hardness tester. A schematic of the ISDG system is shown in Fig. 3.

The indentations were illuminated with monochromatic laser light, causing two diffraction patterns to form. These diffraction patterns overlap, creating fringe patterns that can be related to strain, as discussed in Ref. 4. The fringe patterns were tracked by optical scanners. Fringes were recorded by a minicomputer which, in turn, controlled the angular rotation of the scanners. The minicomputer converted the fringe displacements to local notch root strains and stored the data on a diskette.

Finite-Element Analysis

A two-dimensional finite-element model of the specimen test section was constructed as shown in Fig. 4. Because of symmetry, only one-fourth of the test section needed to be modeled. The model used 592 triangular elements, with a total of 335 nodes. Stress and total-plastic-creep strain distributions were obtained at the centroids of the elements using the MARC nonlinear, finite-element computer program.

Cyclic yielding was determined from the stress-strain properties reported in Ref. 4 and the selected hardening model. Two hardening models, combined isotropic-kinematic hardening and kinematic hardening, were selected for evaluation using load pattern I. Monotonic stress-strain properties were used in conjunction with the combined model. A bilinear representation of the saturated cyclic stress-strain curves was used for the kinematic hardening model. The work hardening slope of the kinematic model was determined from energy considerations so that the strain energy would be identical with that of the actual cyclic stress-strain curve. Each load cycle for load pattern I was subdivided into 30 increments. The analyses were terminated at the end of the second load cycle.

Creep analyses were performed with the MARC program for the step loading sequence of load pattern II. The creep properties given in Ref. 4 were correlated by a preprocessor program into a functional relation in exponential form. The creep equations were incorporated into MARC by means of a user subroutine. Creep analyses were performed using both a strain hardening and a time hardening rule.

Comparison of Analyses and Experiments

In Fig. 5 analytical results using both combined and kinematic hardening models are compared with the experimental load-notch strain cycle for load pattern I. Creep was not a significant factor under the continuous cycling, isothermal load conditions of this test. The experimental results demonstrated that a stable load-strain response occurred on the first cycle with only minor strain changes in subsequent cycling. A plasticity analysis using the combined hardening model did not accurately represent the experimental results; it predicted, after initial loading, an elastic response with further cycling (Fig. 5(a)). A second plasticity analysis using the kinematic hardening model exhibited excellent agreement with the experimental results. The kinematic

hardening analysis predicted ratcheting between the first and second cycles and a stable notch strain cyclic response thereafter (Fig. 5(b)). Except for slightly overpredicting the ratcheting, these analytical results are consistent with the experimental cyclic response for load pattern I.

The results of the creep analyses for the step-loading sequence of load pattern II are compared with experimental results in Fig. 6. Agreement was good for initial loading and the first dwell time. However, on subsequent steps the analysis underpredicted the creep strains. The analysis was terminated after the third load step when it became obvious that the discrepancy between analysis and experiment was increasing. Essentially the same analytical results as shown in Fig. 6 were obtained using either strain hardening or time hardening rules.

The reason for the disagreement between experimental and analytical results in Fig. 6 is difficult to determine, as there was some question about the validity of the strain measurement for this test. When the specimen was completely unloaded after the last load step and then reloaded, only 60 percent of the previous total strain was measured. This implies that there was some drift in the displacement measurements during this test as a 40-percent strain recovery would be more than the combined plastic and creep strains before unloading.

HALF-SCALE COMBUSTOR LINER

Liner Durability Testing

An annular combustor liner specimen of the louver type of construction was subjected to thermal cycling in an induction heated experimental rig (Ref. 6). The specimen was half the scale of an actual combustor liner and was fabricated from the same material (Hastelloy X sheet). A conventional combustor liner of the louver type is shown in Fig. 7. The half-scale rig specimen consisted of five complete ring segments. The middle ring was the one studied in the experimental program. Using measured heat flux and cooling airflow rates as input, transient and steady-state, three-dimensional, heat-transfer analyses were conducted. The calculated temperature response (Fig. 8) of the middle louver of the liner specimen closely agreed with measured thermocouple data. The 90-sec test cycle consisted of a 20-sec transient from an isothermal minimum temperature of 504° C to a maximum temperature of 954° C, a 40-sec steady-state portion, and a cooldown back to the original isothermal condition. After the 20-sec heating transient, there was a temperature difference between the knuckle and louver lip of approximately 400° C. A total of 1730 cycles were accumulated on the test specimen. Thermal fatigue cracking was observed at the edge of the louver lip between 1000 and 1250 test cycles.

Finite-Element Analysis

The MARC nonlinear finite-element program, based on conventional tensile and creep properties of Hastelloy X, was used to calculate the structural response of the louver to the thermal cycling. For the analysis, each cycle was subdivided into 78 increments, consisting of 35 thermal load increments during heating, 14 creep increments during the steady-state dwell time, 25 thermal load increments during cooling, and four no-load increments during creep for residual load correction to ensure equilibrium.

A 0.5° segment between adjacent cooling holes was modeled with three-dimensional, 20-node isoparametric elements (Fig. 9). Full 27 Gaussian integration point elements were used around the cooling holes, while reduced integration elements with eight points were used for the remainder of the model to reduce computing time. To minimize round-off error due to the small included angle of the model segment, the program was run in double precision using 640 K words of storage on an IBM 370/3033 computer system. Each analytical cycle required approximately 45 min of execution time.

The effect of the complete shell structure was simulated by applying appropriate boundary conditions. Nodes along radial planes were constrained to move only in those planes. Additional boundary conditions were imposed to simulate the restraint of the fore and aft louvers of the test specimen by relating the nodal displacements of comparable points on the fore and aft louvers to the ratio of the original radii of these louvers.

Figure 10 shows the computed nonlinear stress-strain response at the louver lip critical location for two thermal cycles. Letter designations are given in Fig. 10 so that the response can be followed using the same letter designations given in Fig. 8. Initial yielding occurred on the first cycle after 5 sec heating (B) at a temperature of 732° C. Plastic flow took place between B and C. Creep analyses were conducted between 12.5 sec heating (C) and 60 sec (D) when the heating part of the cycle was completed. Reverse yield was reached 66 sec into the cycle, i.e., after 6 sec of cooling (E). Subsequent loading for the second cycle produced reyielding at a temperature of 893° C (B') as compared with 732° C (B) for the first cycle. The other points indicated for the second cycle (C' to F') occurred at similar times and temperatures as in the first cycle. The predicted stress-strain response had not stabilized after six cycles when the analysis was terminated. Cycles 3 to 6 exhibited similar stress-strain loops, which ratcheted in the negative strain direction. Each succeeding cycle had higher peak tensile stresses but an essentially constant strain range.

Smooth Specimen Simulation

To provide material response data for more direct evaluation of the creep-plasticity models used in the nonlinear analysis of the combustor liner, uniaxial thermomechanical testing was conducted on a smooth, cyclindrical specimen. The experimental system (Ref. 6) is capable of following a prescribed temperature-strain history. The predicted hoop mechanical strain and temperature history for the sixth loading cycle at the louver lip critical location was imposed on the uniaxial specimen. Since the edge of the louver lip experiences an essentially uniaxial stress field, the stress-strain response from the thermomechanical test is considered representative of the actual response producing fatigue failure.

The thermomechanical strain cycling demonstrated that the stress-strain response stabilized rapidly and that there were no significant peak stress changes after the first few cycles. Ratcheting was excluded by the imposed strain controlled test conditions. Reverse plasticity was observed during the cooling portion of the cycles. A MARC analysis was performed for a one-dimensional strain-controlled simulation of the experiment to investigate the ability of the creep-plasticity models to reproduce the experimental results. This analysis used the same material response models as the three-dimensional louver analysis and the same mechanical strain-temperature history as the uniaxial specimen test.

A comparison of the analytical results for the 15th and 30th cycles and the experimental results is shown in Fig. 11. The analytical stress-strain response did not stabilize and showed higher peak stresses than were obtained in the test. These discrepancies were attributed to the uncoupling of the creep and plasticity models. Improving the accuracy of the predicted stress-strain response under cyclic thermomechanical loading may require the use of one of the unified constitutive theories now undergoing development (Ref. 8).

Life Prediction

The cyclic stress-strain and temperature history determined from the structural analysis for the critical location at the louver liner was used directly as input into the life prediction calculations. Similarly, the measured cyclic response of the axially loaded thermomechanical test was used to calculate its probable lifetime and, hence, serve as an independent estimate of the predicted combustor liner life.

Although several advanced life prediction methods have been proposed over the past few years, this discussion is limited to only one, the Strainrange Partitioning (SRP) method of Ref. 3, because of its relative ease of application to the combustor liner durability problem. The life prediction calculations used isothermal SRP data generated at 870° C. This is justified since the SRP properties are not expected to be a significant function of temperature over the range of interest because the ductility of the Hastelloy X alloy is not significantly affected by temperature. Furthermore, only the results for PP (tensile plasticity reversed by compressive plasticity) and PC (tensile plasticity reversed by compressive creep) cycling are required since the hysteresis loop of interest contains only PP and PC components of inelastic strain range.

The inelastic strain range was calculated to be 0.10 percent for the sixth cycle of the finite-element analysis of the half-scale combustor liner. Of this, 0.0706 percent strain range was of the PC type and 0.0294 percent strain range was of the PP type. Hence, the interaction damage rule used in the SRP method for these conditions can be written as

$$1/N_{pred} = 0.706/N_{PC} + 0.294/N_{PP}$$

At an inelastic strain range of 0.10 percent at 870° C, N_{PC} = 7850 cycles to failure and N_{PP} = 10 600 cycles to failure (Ref. 6). The predicted life N_{pred} = 8500 cycles to failure for this case. This life is considerably greater than the 1000 to 1250 cycles to failure life observed for the half-scale combustor liner.

Applying the same calculational procedures to the prediction of the life of the axially loaded thermomechanical test specimen (which sustained a measured inelastic strain range of 0.12 percent), N_{pred} = 6300 cycles to failure. This predicted life is still considerably larger than the observed 1000 to 1250 cycle life of the liner. Although the thermomechanical fatigue specimen noted above was not cycled to failure, independent thermomechanical fatigue tests were conducted on axially loaded specimens of Hastelloy X at the Pratt & Whitney Aircraft Group in support of the combustor liner durability program. As an example, duplicate tests were conducted at 0.0167 Hz over the temperature range 427° to 927° C, out-of-phase (as the case herein), and the resultant inelastic strain ranges were 0.13 and 0.14 percent. Observed thermomechanical fatigue lives were 4944 and 4114 cycles to failure, respectively. Assuming the same fractional partitioning of the inelastic strain ranges of these two tests as for the sixth cycle of the finite-element analysis of the louver lip, the respective predicted lives are 5500 and 4950. Excellent agreement between thermomechanical experiment and prediction, based on isothermal SRP results, is realized in this case. The only discrepancy between predicted and observed lives is encountered for the half-scale component. Hence, some feature as yet to be identified, of the half-scale component, its method of testing, or its analysis must be responsible for the discrepancy. Clearly, the problem is not well

enough understood, and further research is required. Table I summarizes the life prediction results for the Hastelloy X alloy and the half-scale combustor liner.

AIR-COOLED TURBINE BLADE

Engine Durability Testing

The turbine blade under study has been used in the first-stage high-pressure turbine of a commercial aircraft engine. This blade is air-cooled and paired with an adjacent blade on a single three-tang dovetail. The airfoil has a span of 4.47 cm, a chord width of 3.30 cm, and a tip-to-hub radius ratio of 1.13.

A schematic of the blade and the tip region considered in the analysis is shown in Fig. 12. The material is a cast nickel-base superalloy, René 80, with a Codep-B aluminide coating. This blade was selected for study because of its significant creep-fatigue problems which induce cracking in the squealer tip of the blade above the tip cap. As these cracks grow, they cause coolant leakage and consequent overheating and loss of material from the blade tip. Engine efficiency then drops as tip clearances increase. Since centrifugal stresses are negligible near the blade tip, the cracking is primarily a thermal fatigue problem.

Figure 13 shows the mission cycle used for the analysis in terms of turbine inlet and compressor discharge temperatures and engine speed. This cycle is typical of an engine mission except for the condensed cruise time. High transient thermal stresses are induced during the engine takeoff acceleration and during thrust reversal. Creep mainly occurs during cruise between 6.7 sec (the end of acceleration) and 200 sec (the start of thrust reversal).

Metal temperatures were calculated from transient and steady-state, three-dimensional, heat-transfer analyses with known boundary conditions; these were in good agreement with thermocouple measurements from factory engine tests. The calculated metal-temperature, cycle-time profile for the critical tip location is shown in Fig. 14.

Engine durability testing was conducted at the factory to determine component fatigue life. The test cycle departed from a typical flight cycle in including two additional idle-to-takeoff transients per cycle to accelerate the test time. Their influence was accounted for in all life prediction calculations. At the end of 3000 stress-strain cycles (1000 missions) the blades were removed for inspection. All the blades tested were cracked at the blade tip critical location (Fig. 14); the cracks in all but one had progressed below the tip cap, which was 3.8 mm below the squealer tip.

Finite-Element Analysis

The ANSYS nonlinear computer program was used to perform the blade finite-element analysis. Temperature-dependent cyclic stress-strain and creep properties for René 80 alloy reported in Ref. 7 were used for the analysis. A kinematic hardening model was selected for the plasticity calculations, and a power law and a time hardening rule was used for the creep calculations.

Initially, the mission cycle was subdivided into 23 load increments. Inspection of the inelastic results for the first analytical cycle suggested that the number of increments could be reduced to six, provided that a sufficient number of iterations was permitted to ensure convergence of the plasticity solution. Rerunning the initial cycle with the reduced increments gave excellent agreement with the original analytical results. Time steps for the reduced load steps and some of the original load steps are indicated in Fig. 14.

The three-dimensional, finite-element model of the blade tip region above the 75 percent span position is shown in Fig. 15. A total of 580 eight-node isoparametric elements with 1119 nodes was used to model the airfoil shell, squealer tip, tip cap, and ribs. The eight-node element was used because the 16- and 20-node solid elements in ANSYS lacked creep capabilities. Boundary conditions were applied to constrain all nodes at the base of the model to lie on the 75-percent plane of the airfoil. The span length of the model was sufficient to preclude interference of the applied boundary conditions with the stress-strain solution at the squealer tip. Additional boundary conditions were applied to prevent rigid body motion on the 75-percent plane.

Figure 16 shows the stress-strain response at the critical location from the ANSYS nonlinear analysis for the first, second, and seventh mission cycles. Letter designations are given on the hysteresis loops which are consistent with those on the temperature-time response of Fig. 14. Plasticity analyses were performed for the heating portion of the cycle from A to B, and creep analyses during the relatively steady-state portion from B to C. The remainder of the cycle from C to D involved primarily elastic response. As shown in Fig. 16, continued cycling produces ratcheting of the hysteresis loops in the negative strain direction with progressively higher peak tensile stresses during cooling. Although complete stabilization of the hysteresis loops was not achieved when the analysis was terminated after the seventh cycle, the creep strain change per cycle had diminished to less than 35 μin/in for the last

cycle. The computed total strain range per cycle increased from 3082 to 3089 microstrain between the first and seventh cycles, a change of less than 0.3 percent.

Smooth Specimen Simulation

As in the combustor liner study, the validity of the nonlinear analysis was evaluated by means of a uniaxial, thermomechanical test of a smooth, cylindrical specimen. The experimental system which can follow a prescribed strain-temperature history, is described in Ref. 7. The total strain and temperature history at the critical location from the seventh cycle of the ANSYS blade analysis defined the specimen test conditions. An ANSYS analysis was performed for this uniaxial test using the same material properties and creep-plasticity models as the blade analysis.

A comparison of the analytical results for the seventh cycle with the stable test cycle is shown in Fig. 17. The test demonstrated more rapid stabilization of the stress-strain response and a higher tensile peak stress than was predicted by the nonlinear analysis. On the initial cycle, the stress relaxation exhibited in the test was approximately three times greater than that shown by the analysis. These discrepancies between analysis and experiment could also be caused by the uncoupling of the creep and plasticity models. The NASA Lewis Research Center has instituted programs under its turbine engine Hot-Section Technology Project to develop unified constitutive models that will more realistically represent material cyclic behavior by coupling time-dependent and time-independent inelastic strains and avoiding other simplifying assumptions of classical plasticity.

Life Prediction

Similar life prediction procedures as were used for the combustor liner were used to predict the thermal fatigue lifetime of the René 80 turbine blades. The SRP life prediction method was used in conjunction with the ductility normalized (DN) SRP life relations (Ref. 9). Since the ductility of René 80 is a strong function of the temperature, the DN-SRP life relations enable the expected temperature-dependent SRP life relations to be determined from tensile ductility information. Lives were calculated for the blade tip and for the thermomechanically loaded test specimen used in simulating the cyclic stress-inelastic strain response at the critical location. The thermomechanically loaded test specimen was not carried to failure.

Any effects of the aluminide coating on fatigue life were ignored in the calculations presented herein. SRP characterization results and ductility data for René 80 over the temperature regime of interest were obtained from Ref. 7.

Results of the structural analysis and of the measurements made on the axially loaded thermomechanical test specimen revealed that the inelastic strain range was essentially composed of only the PC type strain range. Therefore, the interaction damage rule reduces to the simple statement that the predicted life, N_{pred} is equal to the PC lifetime, N_{PC}. For the temperature conditions existing at the critical crack initiation location on the blade tip, the PC life relation (ascertained from isothermal data at 1000° C plus modification according to the DN-SRP life relations to account for property variations caused by temperature) for René 80 (Ref. 7) is,

$$N_{pred} = N_{PC} = 5.0(\Delta\varepsilon_{PC})^{-1.56}$$

For $\Delta\varepsilon_{PC} = 0.013$ percent as calculated from the ANSYS analysis, $N_{pred} = 4420$ cycles to failure. For the thermomechanically loaded test specimen, $\Delta\varepsilon_{PC} = 0.030$ percent and $N_{pred} = 1200$ cycles to failure. The observed blade tip life was 3000 cycles to failure and is bracketed by the 1200 and 4420 cycle-to-failure predictions of life. Thus, for the blade tip durability problem discussed herein, the hardware lives can be reasonably predicted from the isothermal SRP properties. The reasonably good agreement was obtained, however, only after having modified the 1000° C isothermal SRP life relation for PC straining to account for the substantially lower straining capacity of René 80 at the low temperature end of the thermal cycle. The life prediction results for the René 80 and the turbine blade are shown in Table I.

SUMMARY OF RESULTS

The results of the durability studies of engine hot-section components can be summarized as follows:

1. The nonlinear finite-element structural analyses indicated that the uncoupled creep and plasticity models did not give an accurate representation of the cyclic thermomechanical response of the structures. Tests of uniaxial, strain-controlled specimens with the same strain-temperature histories as computed at the combustor liner and turbine blade failure locations stabilized rapidly. Analytical simulations of these experiments incorrectly exhibited continued cyclic hardening with increasing peak tensile stresses.

2. Analysis of the disk notch problem using kinematic hardening showed excellent agreement with experimental results for continuous load cycling. However, creep analyses of this specimen predicted strains that were low compared with strain measurements under monotonic step loading. It is uncertain whether this disagreement is due to the inadequacy of the creep model or to measurement errors.

3. Life predictions based on isothermal Strainrange Partitioning characteristics and results of the inelastic structural analyses overpredicted the fatigue lives of the half-scale combustor liner and turbine blade tip. The degree of overprediction was not great for the turbine blade tip problem (4420 cycles predicted versus 3000 cycles observed), but substantial error was encountered for the combustor liner problem (8500 cycles predicted versus 1000 to 1250 cycles observed).

4. Life predictions based on isothermal Strainrange Partitioning characteristics were also applied to a few axial strain-controlled, thermomechanical fatigue tests conducted on the combustor liner material. Excellent agreement was obtained between predicted (4950 and 5500 cycles) and observed (4144 and 4944 cycles, respectively) lives for the thermomechanical tests.

5. The significant overprediction of life of the half-scale combustor liner apparently is associated with some feature (as yet unidentified) of the hardware, the method of testing, or the method of analysis.

REFERENCES

1. Kohnke, P. C.: ANSYS Engineering Analysis System Theoretical Manual. Houston, PA, Swanson Analysis Systems, Inc., Nov. 1977.
2. MARC General Purpose Finite Element Analysis Program. User Manual, Vol. A: User Information Manual and Vol. B: Marc Element Library. Palo Alto, CA, MARC Analysis Research Corp., 1981.
3. Characterization of Low Cycle High Temperature Fatigue by the Strainrange Partitioning Method. AGARD-CP-243, London, Technical Editing and Reproduction Ltd., 1978.
4. Domas, P. A., et al.: Benchmark Notch Test for Life Prediction. (R82AEB358, General Electric Co., NASA Contract NAS3-22522.) NASA CR-165571, 1982.
5. Kaufman A.: Evaluation of Inelastic Constitutive Models for Nonlinear Structural Analysis. Nonlinear Constitutive Relations for High Temperature Applications. NASA CP-2271, 1983, pp. 89-105.
6. Moreno, V.: Combustor Liner Durability Analysis. (PWA-5684-19, United Technologies Corp., Pratt & Whitney Group; NASA Contract NAS3-21836.) NASA CR-165250, 1981.
7. McKnight, R. L.; Laflen J. H., Halford, G. R., and Kaufman, A.: Turbine Blade Nonlinear Structural and Life Analysis. J. Aircr., Vol. 20, No. 5, May 1983, pp. 475-480.
8. Walker, K. P.: Research and Development Program for Nonlinear Structural Modeling with Advanced Time-Temperature Dependent Constitutive Relationships. (PWA-5700-50, United Technologies Research Center; NASA Contract NAS3-22055.) NASA CR-165533, 1981.
9. Halford, G. R., Saltsman, J. F., and Hirschberg, M. H.: Ductility-Normalized Strainrange Partitioning Life Relations for Creep-Fatigue Life Predictions. Environmental Degradation of Engineering Materials, Blacksburg, VA, Virginia Tech Printing Department, Virginia Polytechnic Institute and State University, 1977, pp. 599-612.

TABLE 1. - SUMMARY OF LIFE PREDICTION RESULTS

Structure	Material	Temperature range, °C	Frequency, Hz	Inelastic strain range, percent	Observed life, cycles	Predicted SRP life, cycles
Combustor liner[a]	Hastelloy X	504 - 904	0.0111	0.10	1000 - 1250	8500
Axially loaded[b] thermomechanical specimens	Hastelloy X	504 - 904	0.0111	0.12	----	6300
		427 - 927	.0167	.13	4944	5500
		427 - 927	.0167	.14	4114	4950
Turbine blade tip[c]	René 80	344 - 1000	0.0049	0.013	3000	4420
Axially loaded[b] thermomechanical specimen	René 80	344 - 1000	0.0049	0.030	----	1200

[a]Sixth cycle of finite element analysis.
[b]Out-of-phase cycle (maximum temperature at minimum strain).
[c]Seventh cycle of finite element analysis.

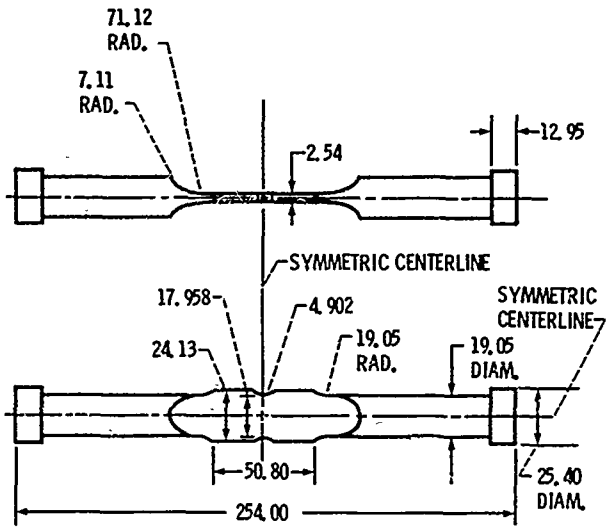

Fig. 1. - Benchmark notch specimen (K_t = 1.9). (Dimensions in mm.)

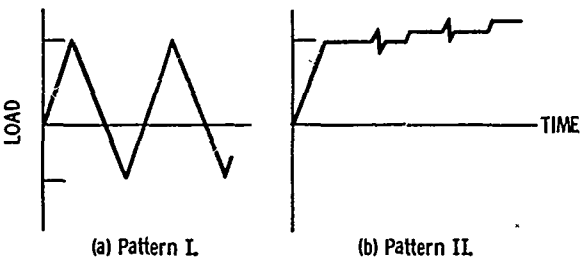

(a) Pattern I. (b) Pattern II.

Fig. 2. - Load spectra for benchmark notch specimen.

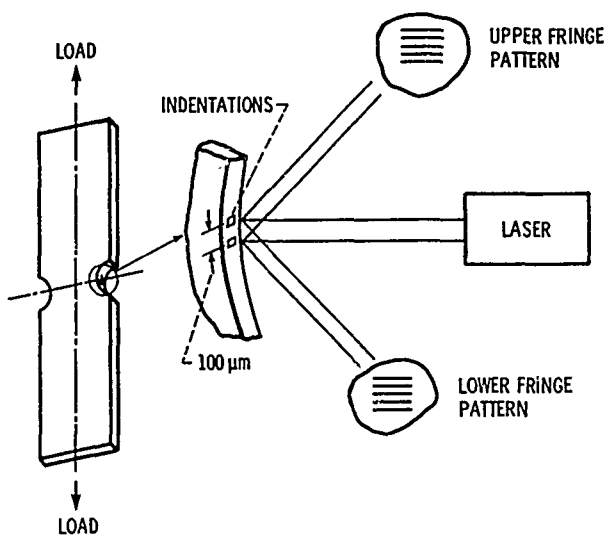

Fig. 3. - Schematic of ISDG.

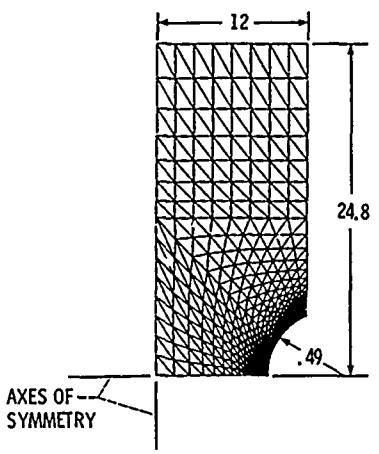

Fig. 4. - Benchmark notch specimen finite-element model. (Dimensions in mm.)

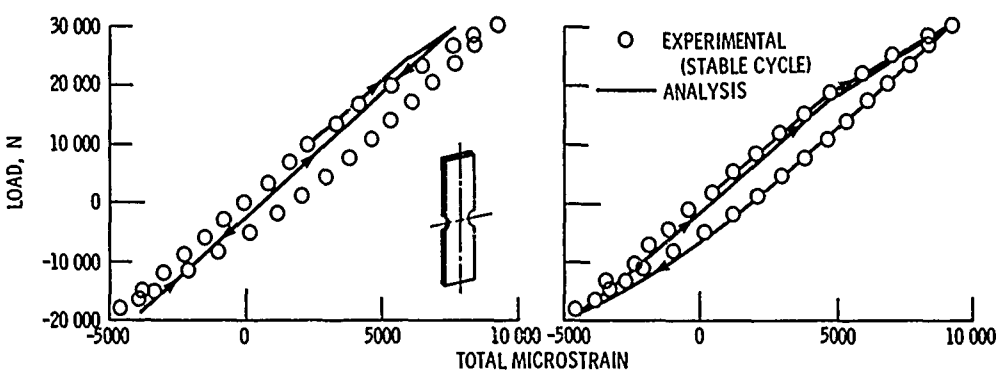

(a) Combined model. (b) Kinematic model.

Fig. 5. - Comparison of benchmark notch specimen experimental and analytical results for load pattern I.

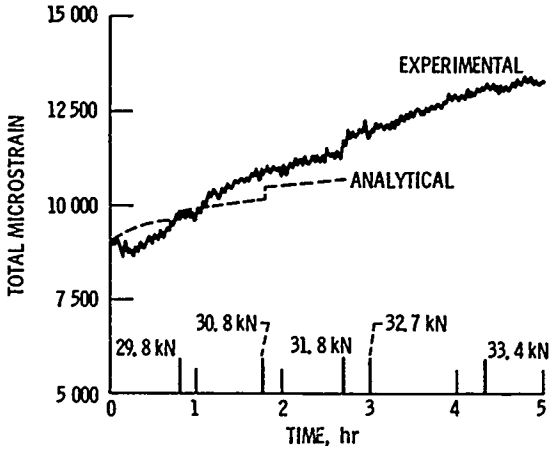

Fig. 6. - Comparison of benchmark notch specimen experimental and analytical results for load pattern II.

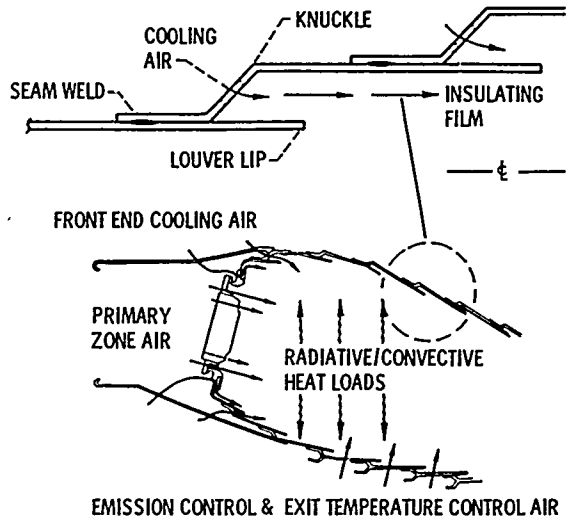

Fig. 7. - Typical louver combustor liner construction and airflow distribution.

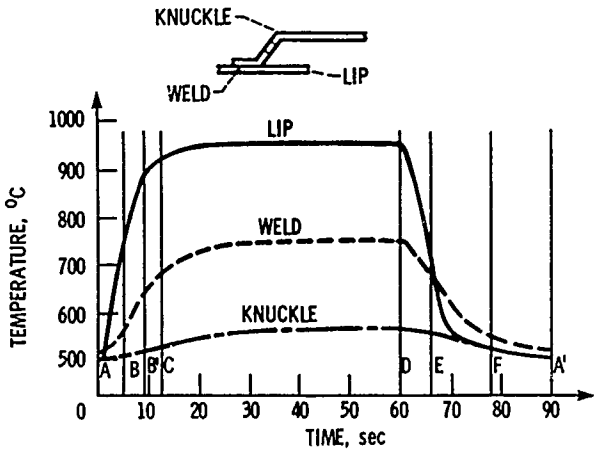

Fig. 8. - Louver temperature response.

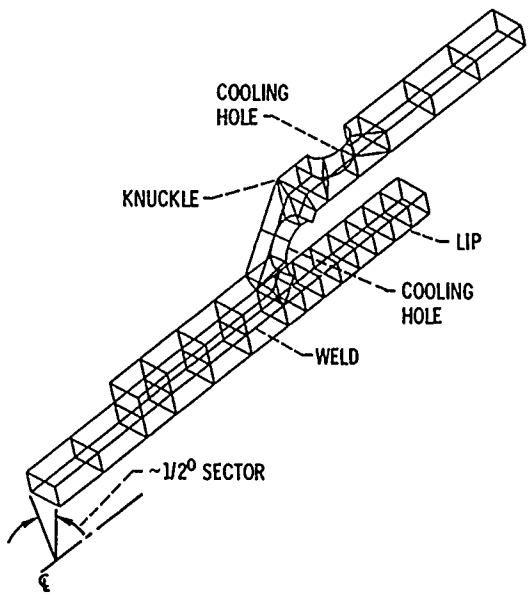

Fig. 9. - Combustor liner finite-element model.

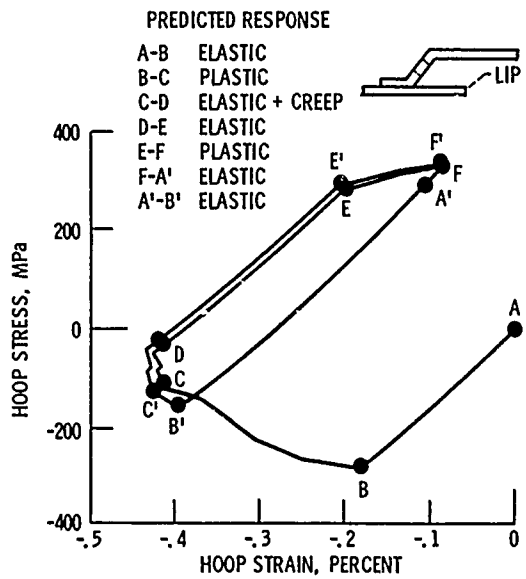

Fig. 10. - Nonlinear analysis stress-strain response at louver lip of combustor liner.

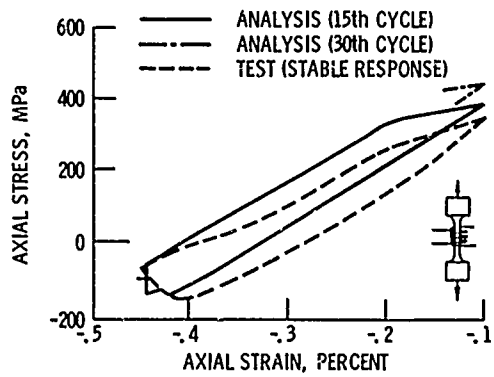

Fig. 11. - Comparison of uniaxial thermomechanical test and analytical results for combustor liner simulation.

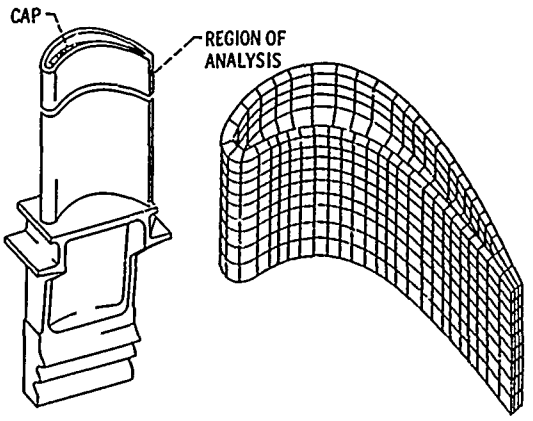

Fig. 12. - First-stage high-pressure turbine blade and finite-element model.

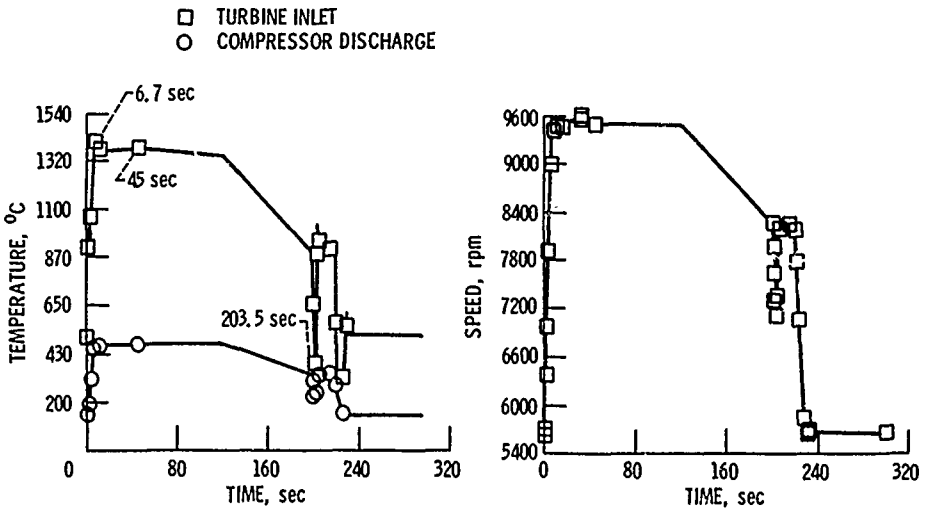

(a) Turbine inlet discharge temperatures.

(b) Core engine speed.

Fig. 13. - Mission cycle used for analysis of turbine blade.

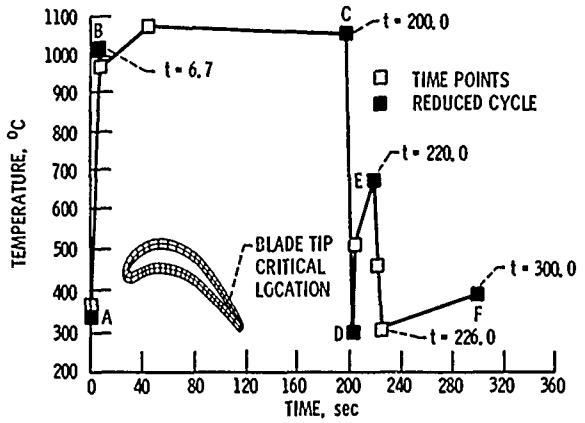

Fig. 14. - Blade metal temperature response at critical location.

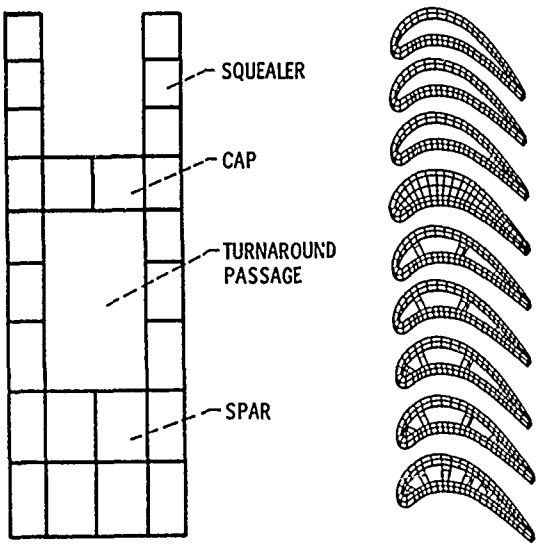

Fig. 15. - Finite-element model of blade tip.

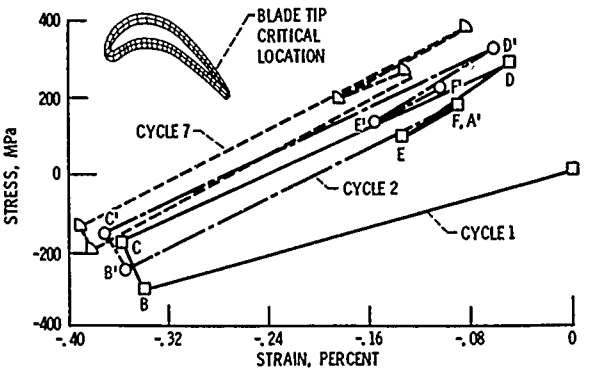

Fig. 16. - Inelastic analysis results: stress-strain response at critical location of turbine blade.

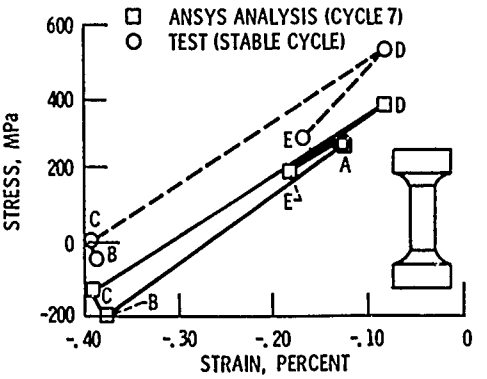

Fig. 17. - Comparison of uniaxial thermomechanical test and inelastic analysis results for turbine blade simulation.

DISCUSSION

M.Y.Nazmy, Switzerland

My question is related to the use of the T.F. in correcting the LCF life for the state of multiaxial stresses. Will this correction take care of the observed overprediction by strain-range partitioning?

Author's Reply

No, the overprediction of life would have nothing to do with any correction for multiaxiality since the stress field at the critical location for all these components is essentially uniaxial.

P.Ramette, Fr

I would like to know if your three-dimensional model of the calculations of stresses for finite elements from the tip of the cooled blade takes into account the geometry of the cooling circuits.

Author's Reply

Internal cooling passages were modelled, as was the tip cap. There were no film cooling holes through the airfoil wall in this configuration.

PREVISION DE DUREE DE VIE A HAUTE TEMPERATURE SOUS CHARGEMENT COMPLEXE

par Georges CAILLETAUD et Jean-Louis CHABOCHE

Office National d'Etudes et de Recherches Aérospatiales (ONERA)
92322 Châtillon Cedex (France)

RESUME

Cet exposé décrit les activités de l'ONERA dans le domaine de la prévision de durée de vie des composants à haute température. Les dernières années ont vu le développement du code d'éléments finis en viscoplasticité cyclique EVPCYCL ; il convient pour les problèmes bidimensionnels (contrainte ou déformation plane, cas axisymétrique), sa particularité essentielle résidant dans les nombreux choix possibles pour les lois de comportement : on peut effectuer des calculs cycliques avec écrouissage cinématique ou isotrope, avec introduction d'un effet de mémoire, de restauration... Les champs de température variables dans le temps sont également acceptés. L'utilisateur dispose de post processeurs graphiques, mais aussi de programme de prévision de durée de vie (faisant intervenir le cumul de dommage en fatigue et fluage).

LIFE PREDICTION AT HIGH TEMPERATURE UNDER MULTIAXIAL LOADING

ABSTRACT

This paper gives an overview of the activities of ONERA concerning the life prediction of high temperature components. In the last few years, the viscoplastic finite element computer code EVPCYCL has been developed ; it is suitable for any two-dimensional problem (plane stress or strain, axisymmetrical case), its main specificity being the choice of various possibilities concerning the constitutive equations : cyclic calculations can be made with kinematic and isotropic hardening, with the introduction of a "memory" effect, of recovery... Variable temperature fields are also accepted. Graphic post-processors are available as well as a life prediction programme (taking into account creep and fatigue damage).

Ce papier donne un aperçu des activités de l'ONERA dans le domaine de la prévision de durée de vie des composants à haute température. Les dernières années ont vu le développement du code d'éléments finis en viscoplasticité cyclique EVPCYCL ; il convient pour les problèmes bidimensionnels (contrainte ou déformation plane , cas axisymétrique), sa particularité essentielle résidant dans les nombreux choix possibles pour les lois de comportement : on peut effectuer des calculs cycliques avec écrouissage cinématique ou isotrope, avec introduction d'un effet de mémoire, de restauration... Les champs de température variables dans le temps sont également acceptés. L'utilisateur dispose de post processeurs graphiques, mais aussi de programme de prévision de durée de vie (faisant intervenir le cumul de dommage en fatigue et fluage).

Après avoir recensé quelques particularités du code de calcul, on analyse les différences de nature entre les diverses lois de comportement possibles. Les différences sont illustrées par des résultats de calcul d'un "disque d'essai de fatigue biaxiale" en Inco 718. La géométrie de cette éprouvette, mise au point et testée à la SNECMA, permet d'obtenir des champs de contraintes equibiaxiales évoluant cycliquement avec la vitesse de rotation et simulant ainsi le type d'efforts que subit un disque de turbine réel. On note finalement que les premiers résultats de prévision de vie semblent très sensibles à la loi de comportement de viscoplasticité cyclique utilisée pour le calcul des contraintes et des déformations.

1 - QUELQUES PARTICULARITES DU CODE EVPCYCL

On ne détaille pas ici le contenu des programmes périphériques au programme d'éléments finis lui-même. Le programme de maillage automatique (BIMAIL) a été fourni par le CETIM*, ainsi d'ailleurs que les moyens de mise en données et de résolution élastique. La partie viscoplasticité et les sorties graphiques ont été réalisées à l'ONERA.

1.1 - La partie "calcul de structure"

La partie "calcul de structure" du programme est très classique : les inconnues sont les déplacements modaux, qui sont reliés aux champs de déplacements et de déformation à l'intérieur de l'élément par les matrices [N] et [B] :

$$(1) \qquad \{u\} = [N]\{q\} \qquad \{\varepsilon\} = [B]\{q\}$$

La déformation totale se partage en une partie élastique, une partie viscoplastique et une partie thermique, si bien que la loi d'élasticité s'écrit :

$$(2) \qquad \{\sigma\} = [D]\{\varepsilon\} - [D]\{\varepsilon_p\} - [D]\{\alpha\vartheta\}$$

La somme des deux derniers termes pouvant être considérée comme une contrainte initiale $\{\sigma_0\}$.

*Centre d'Etudes Techniques des Industries Mécaniques (Senlis).

Le problème se limite donc à la résolution du système linéaire

(3) $$[K]\{q\} = \{F\} + \{F_o\}$$

où la matrice [K] dépend des caractéristiques élastiques du matériau (et pas de la loi de comportement viscoplastique), et du type d'éléments utilisés (on utilise uniquement des triangles isoparamétriques à 6 noeuds), $\{F\}$ et $\{Fo\}$ représente les efforts nodaux équivalents aux efforts extérieurs et aux contraintes initiales. La matrice [K] n'est donc assemblée et triangulée qu'une seule fois pour les calculs isothermes. Dans les problèmes à température variable où les caractéristiques élastiques dépendent de la température, on utilise à l'instant t ($t_i < t < t_{i+1}$) une interpolation linéaire des matrices inverses exactes (il s'agit en fait des matrices après triangulation) définies aux instants t_i et t_{i+1} :

(4) $$K^{-1}(t) = K^{-1}(t_{i+1}) \frac{t - t_i}{t_{i+1} - t_i} + K^{-1}(t_i) \frac{t_{i+1} - t}{t_{i+1} - t_i}$$

On a classiquement besoin d'une soixantaine d'instants t_i pour une bonne description d'un cycle sol-air-sol. Entre ces instants, l'équilibre est toujours respecté, mais la déformation plastique ne sera qu'approchée. On évite ainsi un grand nombre d'assemblage-triangulation (environ 500 à 1000 itérations sont nécessaires par cycle)

1.2 - La partie "algorithme viscoplastique"

Les lois de viscoplasticité sont habituellement écrites sous la forme :

(5a) $$\{\dot{\varepsilon}_p\} = F(\{\sigma\}, \{a_j\}, T)$$

(5b) $$\{\dot{a}_j\} = G(\{\sigma\}, \{a_j\}, T)$$

où les grandeurs $\{a_i\}$ sont des variables scalaires ou tensorielles représentant l'état d'écrouissage du matériau, T est la température.

Une intégration pas à pas en fonction du temps est donc nécessaire : différents algorithmes sont implantés, qui sont soit purement explicites (Euler, "second-ordre"), ou semi-implicite (Euler Cauchy)[1]. Le plus utilisé est l'algorithme du "second-ordre" mis au point et testé à l'ONERA [2] [3] [4]. Dans cette méthode le calcul automatique du pas d'intégration est effectué avant l'incrément de temps en utilisant les dérivées première et seconde de ε_p et a_j, explicites à l'instant t ; si y représente le vecteur des variables d'état ε_p et a_j , on a en effet :

(6a) $$\dot{y}(t) = Y(y(t), t)$$

(6b) $$\ddot{y}(t) = \left(\frac{\partial Y}{\partial y}\right)_t \dot{y}(t) + \frac{\partial Y}{\partial t}$$

Comme l'indique l'organigramme de la figure 1, une particularité de l'algorithme choisi est de ne considérer comme variables à incrémenter que les variables d'états $\{\varepsilon_p\}$ et $\{a_j\}$. On passe de l'instant t à l'instant t + Δt par :

(7a) $$\{\varepsilon_p\}_{t+\Delta t} = \{\varepsilon_p\}_t + \{\dot{\varepsilon}_p\}_t \Delta t + \{\ddot{\varepsilon}_p\}_t \frac{\Delta t^2}{2}$$

(7b) $$\{a_j\}_{t+\Delta t} = \{a_j\}_t + \{\dot{a}_j\}_t \Delta t + \{\ddot{a}_j\}_t \frac{\Delta t^2}{2}$$

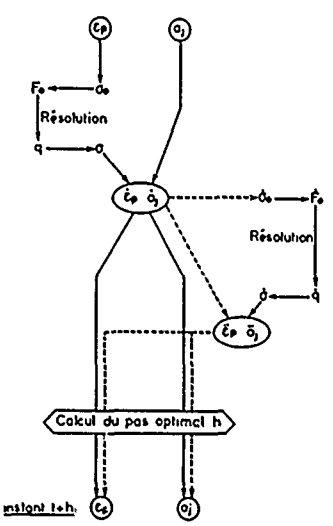

Fig. 1 - Schéma général du calcul de viscoplasticité

Les termes d'ordre 1 sont obtenus après résolution de l'équilibre à l'instant t, connaissant $\{\varepsilon_p\}_t$ par le problème (3), puis par application de la loi de viscoplasticité (5). Les termes d'ordre 2 sont obtenus ensuite par la résolution du problème d'ordre supérieur, connaissant $\{\dot{\varepsilon}_p\}_t$:

(8) $$[K]\{\dot{q}\} = \{\dot{F}\} + \{\dot{F}_o\}$$

où $\{\dot{F}_o\}$ dépend de $\{\dot{\varepsilon}_p\}_t$, $\dot{T}$ et tient compte éventuellement de la variation de [K]. On peut alors évaluer les termes d'ordre 3 de ε_p et a_j, ce qui permet la détermination de la valeur optimale de l'incrément de temps : il est défini en supposant que le terme d'ordre 3 dans le développement de Taylor doit être négligeable devant la somme des termes d'ordre 1 et 2. Le pas Δt est donc obtenu comme solution de l'équation :

$$|\dddot{y}_{(t)}| \frac{\Delta t^2}{6} \leq \eta \left| \dot{y}_{(t)} + \ddot{y}_{(t)} \frac{\Delta t}{2} \right|$$

η étant un facteur de précision dont les valeurs classiques sont de l'ordre de 0,05 [3].

Cette méthode, bien que non mathématiquement fondée, conduit à un algorithme remarquablement sûr. Elle présente d'autre part le gros avantage de ne nécessiter que l'incrémentation approchée de $\{\varepsilon_p\}$ et $\{a_j\}$, l'équilibre et donc les contraintes sont ensuite connus exactement à partir de ces quantités approchées. Cela évite le cumul d'erreurs, assure une certaine stabilité (bien que l'algorithme explicite soit par nature plus instable que l'algorithme implicite) et évite des erreurs non liées à la viscoplasticité, mais à la linéarisation des évolutions thermiques et des évolutions du module d'élasticité.

2 - PREVISION DU COMPORTEMENT CONTRAINTE-DEFORMATION

2.1 - Ecriture des lois utilisées

Il convient maintenant de préciser la forme des lois de comportement accessibles à l'utilisateur. On dispose bien sûr pour les chargements monotones de la loi de Norton et d'une loi de fluage primaire [5]. La loi adaptée aux chargements cycliques introduit une possibilité d'écrouissage isotrope et d'écrouissage cinématique, linéaire ou non [6]. Cette loi peut être étendue pour la représentation d'effets de mémoire complexes : histoire de la température [7], histoire de la déformation maximale [8]. On se borne ici à présenter le modèle "de base", valable pour la plupart des matériaux courants. Il s'écrit :

(9a) $$\dot{\varepsilon}_p = \frac{3}{2} \dot{p} \frac{\sigma' - X'}{J(\sigma - X)}$$

(9b) $$\dot{p} = \sqrt{\frac{2}{3} \dot{\varepsilon}_p \cdot \dot{\varepsilon}_p} = \left\langle \frac{J(\sigma - X) - R - k}{K} \right\rangle^n$$

σ' et X' désignent les déviateurs de σ et de X, $J(\sigma - X)$ le second invariant de $\sigma - X$. Le tenseur X, qui caractérise la position du centre du domaine élastique dans l'espace des contraintes est la somme de X_1 et X_2 avec :

(9c) $$\dot{X}_1 = \frac{2}{3} c_1 \dot{\varepsilon}_p \qquad X_1(0) = 0$$

(9d) $$\dot{X}_2 = c_2 \left(\frac{2}{3} a_2 \dot{\varepsilon}_p - X_2 \dot{p} \right) \qquad X_2(0) = 0$$

On introduit ainsi un écrouissage cinématique linéaire du type Prager (X_1) et un écrouissage cinématique non linéaire (X_2). On peut être amené également dans certains cas à utiliser deux variables cinématiques non linéaires avec des constantes a_1, a_2, c_1 et c_2 différentes.

Le rayon du domaine élastique est initialement égal à k (on choisit R(0) = 0) ; il est susceptible d'évoluer entre le premier cycle et le cycle stabilisé en fonction de la déformation plastique cumulée p :

(9e) $$\dot{R} = b \left(R_s - R \right) \dot{p}$$

On obtient de l'adoucissement cyclique si R_s est négatif, du durcissement cyclique dans le cas contraire.

En conditions cycliques stabilisées, le modèle indiqué ici possède 6 coefficients n, $R_s + k$, K, c_1, c_2 et a_2. Il décrit correctement la courbe d'écrouissage cyclique, chacune des boucles contrainte-déformation et les effets de viscosité (relaxation, influence de la vitesse). Le modèle de base complet permet de décrire en plus l'écrouissage monotone et les effets transitoires jusqu'au cycle stabilité, avec deux coefficients supplémentaires, b et k : la limite élastique passe de la valeur initiale k à $R_s + k$, la vitesse d'évolution étant caractérisée par b.

2.2 - Les différents types de "stabilisation" mécanique

Le but des calculs de contrainte-déformation est d'atteindre les conditions de fonctionnement stabilisées de la structure : le cycle local est alors périodique, avec une superposition éventuelle d'un terme séculaire. C'est sur ces conditions stabilisées que sont basés les modèles qui permettent de prévoir l'amorçage d'une fissure. L'une des grosses difficultés de ces calculs provient de la simultanéité de trois types de "stabilisation".

(i) Le premier est purement lié au matériau, il s'agit de l'adoucissement ou du durcissement cyclique. On conçoit facilement que, sur un élément de volume isolé, la description du comportement par un modèle "complet" conduit à une convergence vers un état cyclique stabilisé lorsque le rayon du domaine élastique est constant (si les sollicitations sont en dehors du domaine élastique). Sur l'élément de volume, le même état peut être atteint directement en utilisant le modèle du cycle stabilisé. La rapidité de la convergence obtenue avec le modèle "complet" est liée à la valeur numérique du coefficient b.

(ii) Il faut retenir ensuite l'effet de relaxation de contrainte moyenne : lié à la fois au modèle et au chargement utilisé, cet effet peut être illustré par le cas d'une sollicitation en déformation imposée avec une valeur moyenne élevée. Il est bien connu que dans de telles conditions un modèle d'écrouissage cinématique linéaire conduit à une adaptation (ou une accommodation) en un cycle avec une contrainte moyenne non nulle, (fig. 2a), alors que la présence du terme de rappel en $\dot{p}$ dans (9d) pour l'écrouissage cinématique non linéaire entraîne une stabilisation progressive autour d'une contrainte moyenne nulle si l'on sort du domaine élastique : il ne subsiste une contrainte moyenne que si l'on reste dans le domaine élastique (fig. 2 b). La rapidité de la chute de contrainte moyenne dans le cas de l'adaptation est liée à la valeur du coefficient C_2 . Il faut remarquer enfin qu'une contrainte moyenne subsiste si l'on superpose une contrainte interne χ_1 linéaire et une autre χ_2 non linéaire.

(iii) La stabilisation "structurale", quant à elle, est liée à la géométrie et au chargement appliqué. Elle est la conséquence des redistributions de contraintes dues à l'écoulement plastique. Elle est seule en cause lorsqu'on utilise la loi de comportement du cycle stabilisé (la stabilisation de type 1 est donc immédiate) et que le chargement est approximativement alterné (pas de problèmes de contrainte moyenne). Dans la plupart des cas, cet effet de structure retarde l'obtention de conditions mécaniques périodiques, l'apparition de la déformation plastique en certains points n'étant que la conséquence du chargement progressif des endroits où s'effectue l'écoulement.

2.3 - Application au disque de fatigue biaxiale

La figure 3 montre la schématisation qui a été choisie pour le disque, ainsi que le maillage en éléments finis (triangles à 6 noeuds). La température est supposée uniforme et constante, les sollicitations mécaniques provenant uniquement de la rotation du disque ; deux chargements ont été étudiés, comportant tous les deux un palier bas à 1500 t/mn :

- à 550°C, avec un palier haut à 27700 t/mn pendant 10 s,

- à 650°C, avec un palier haut à 24000 t/mn pendant 90 s.

A la première température, le matériau est peu visqueux, les redistributions de contraintes seront essentiellement plastiques. A 650°C au contraire la viscosité commence à devenir sensible si bien qu'on observe des déformations pendant la période de maintien. On conçoit donc que les réponses obtenues seront qualitativement différentes à chaque température.

A 550°C, le calcul élastique conduit à des niveaux de contrainte très importants, particulièrement à l'alésage (plus de 900 MPa pour la contrainte équivalente de Mises). On a effectué pour ce chargement deux calculs viscoplastiques, le premier avec la loi du cycle stabilisé (eq. 9a à 9d), le second avec la loi complète (en incluant 9e) : dans ce cas, la valeur de la limite élastique initiale k est plus grande que celle du cycle stabilisé (adoucissement cyclique, R_S =-200 MPa dans 9e). La figure 4 résume l'importante

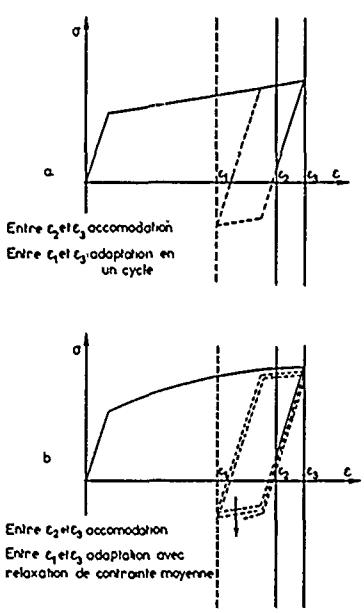

Fig. 2 - Illustration de l'accomodation (——) ou de l'adaptation (----) en déformation imposée
a) avec un écrouissage cinématique linéaire
b) avec un écrouissage cinématique non linéaire (pour simplifier la figure, seul le "squelette" plastique X + R est représenté).

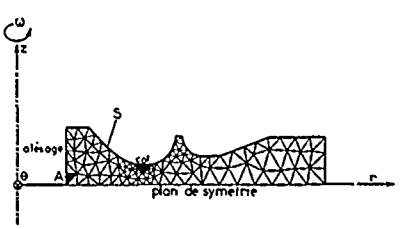

Fig. 3 - Schématisation du disque et maillage utilisé

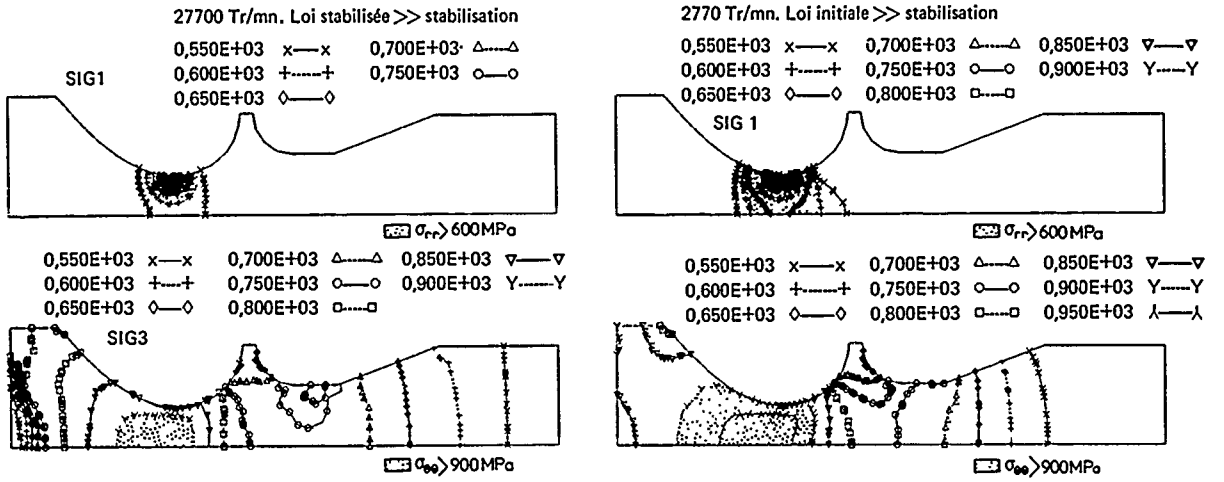

Fig. 4 - Cartes des contraintes radiales et circonférentielles pour la loi du cycle stabilisé (a) et la loi complète (b) à 550°C.

différence qui en résulte, après avoir effectué dans chaque cas 20 cycles de calcul. Un important écoulement s'est produit avec la loi du cycle stabilisé, ce qui diminue nettement les niveaux de contrainte, en particulier à l'alésage (fig. 4a). La loi "complète" contenant l'adoucissement cyclique conduit quant à elle à des cartes de contrainte proche des cartes élastiques (fig. 4b). Cela s'explique (fig. 5) par le fait que, si la première montée fait bien sortir localement du domaine élastique dans les deux cas, il y a moins d'écoulement avec la loi complète ; le matériau ne s'adoucit pas, et l'on est pratiquement accommodé dès le deuxième cycle : les stabilisations du type 1 et 2 (loi de comportement et contraintes moyennes) ne s'effectuent donc pas, la stabilisation structurale étant terminée dès le deuxième cycle. Avec la loi de comportement du cycle stabilisé, l'écoulement cyclique est possible, on assiste donc à une diminution des contraintes moyennes, qui va de pair avec la stabilisation structurale (types 2 et 3).

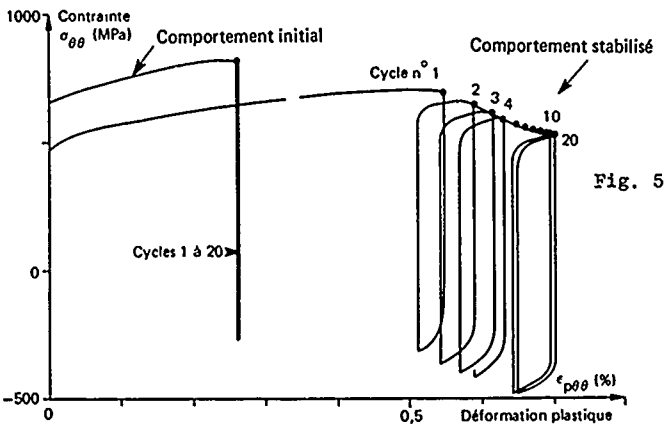

Fig. 5 - Evolution des contraintes et des déformations plastiques circonférentielles en fond d'alésage (triangle A de la Fig.3) avec la loi du cycle stabilisé ; avec la loi complète (loi du cycle initial + adoucissement cyclique) à 550°C.

L'augmentation de diamètre intérieur relevée dans les calculs en ramenant la vitesse à 0 est respectivement de 0,19 mm sur la surface extérieure et de 0,26 mm dans le plan de symétrie pour le premier calcul, et de 0,04 mm et 0,07 mm pour le second. Si l'on compare ces valeurs avec les 0,04 mm relevés après essai à la SNECMA, il semble bien que la loi "complète" soit la plus satisfaisante dans ce cas. Cela signifie, de façon assez paradoxale, qu'un simple calcul monotone suivi d'une décharge permettrait d'obtenir une bonne représentation du cycle stabilisé (tout au moins dans ce cas).

Le second type de chargement, à 650°C, va prouver qu'il n'en est pas toujours ainsi. En effet, même si la figure 6 montre que les cartes de contraintes radiales et tangentielles obtenues à 650°C avec la loi complète sont du même type que celles de la figure 4a (loi complète à 550°C), on constate néanmoins que le "blocage" du cycle contrainte-déformation à l'alésage n'est pas obtenu au premier cycle : une légère redistribution reste présente dans les 30 premiers cycles calculés avec la loi complète (fig. 7a). Il est peu probable cependant que l'on atteigne ainsi l'état d'équilibre de la loi stabilisée (fig. 7c) ; néanmoins il faut noter qu'avec une loi intermédiaire (dans laquelle on a supposé que la courbe monotone était plus basse que dans la loi complète), la redistribution s'amorce et l'état de contrainte tend vers celui qui résulte du calcul avec la loi stabilisée.

La différence de nature entre les deux chargements est résumé sur la figure 8, où l'on a reporté le profil des déformations plastiques sur la surface extérieure du disque : la figure 8b montre qu'un anneau élastique subsiste entre l'alésage et le col dans le calcul à 550°C avec la loi complète, ce qui différencie nettement ce profil de celui de la figure 8a (en particulier pour la déformation circonférentielle). L'écart est moins sensible pour les calculs à 650°C, et dans ce cas la plastification est complète jusqu'au delà du col quelle que soit la loi utilisée.

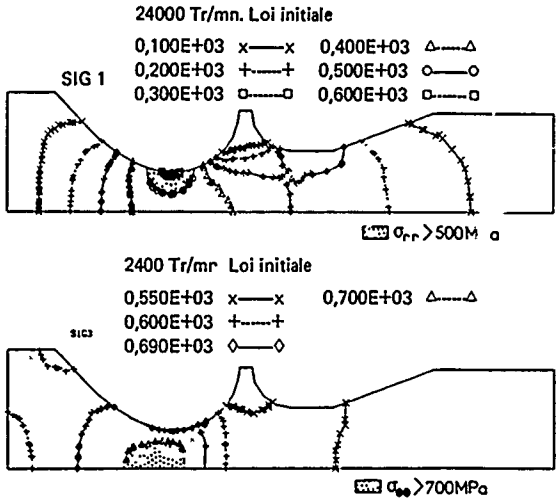

Fig. 6 - Cartes des contraintes radiales et circonférentielles pour la loi complète à 650°C.

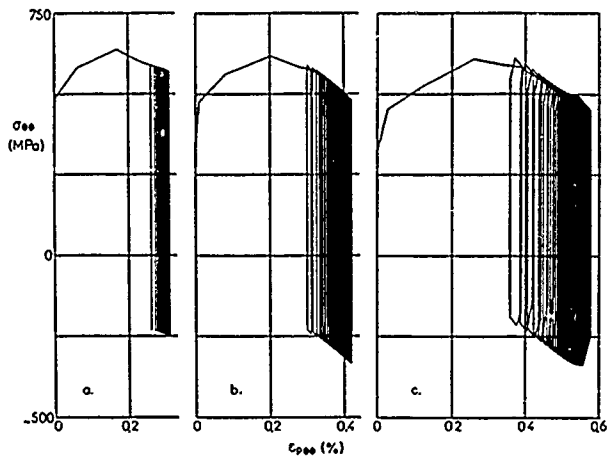

Fig. 7 - Evolution des contraintes et des déformations plastiques circonférentielles en fond d'alésage (triangle A de la Fig. 3).
a) avec la loi du cycle initial.
b) avec une loi intermédiaire.
c) avec la loi du cycle stabilisé.

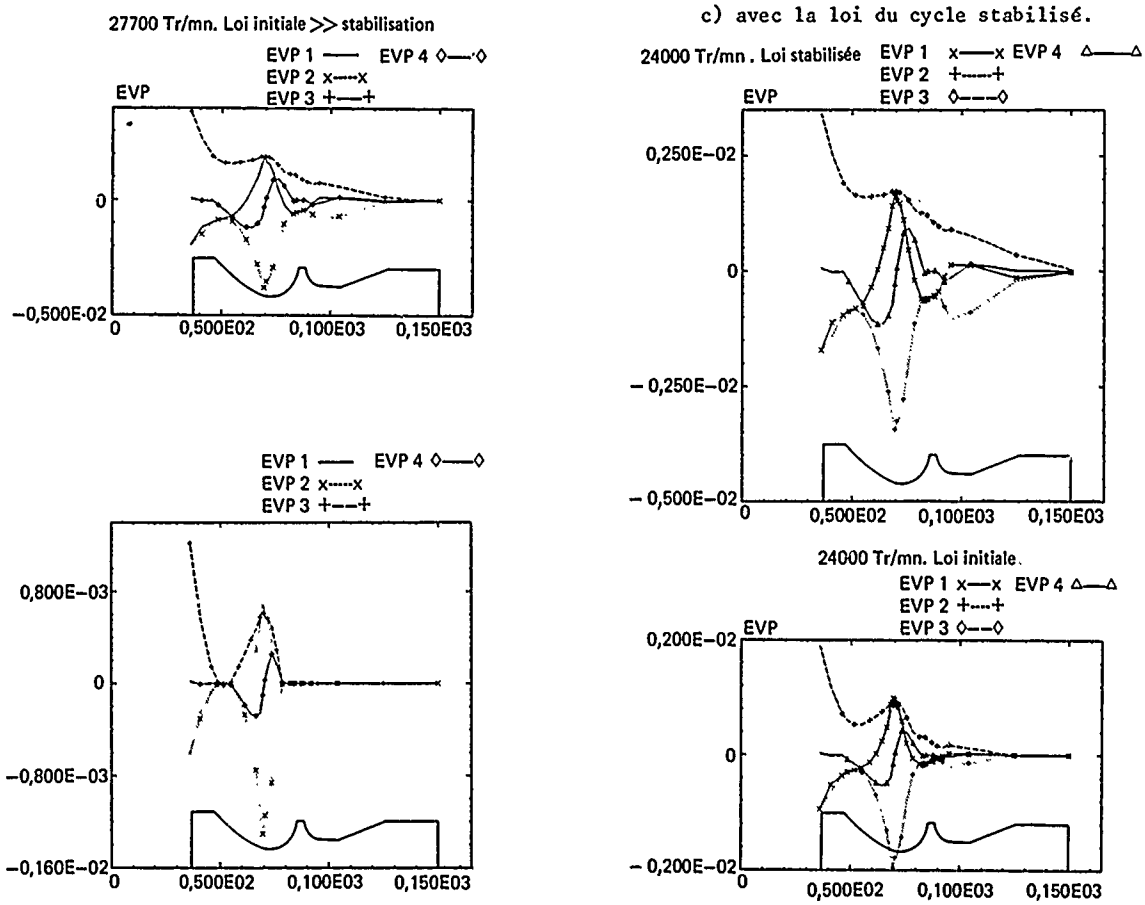

Fig. 8 - Profil des déformations plastiques sur la surface extérieure du disque (surface S de la Fig.3)
a) 550°C, loi stabilisée
b) 550°C, loi complète
c) 650°C, loi stabilisée
d) 650°C, loi complète

3 - PREVISION DE LA DUREE DE VIE

En fatigue-fluage, la prévision de durée de vie s'effectue en utilisant une variable endommagement isotrope [1] dont l'évolution est gouvernée par les invariants de contrainte. Au cours d'un cycle, on cumule ainsi des incréments de fatigue

(10a) $$dD_F = \left[1-(1-D)^{\beta+1}\right]^{\alpha(A_{II},\bar{J}_1,J_{2M})}\left[\frac{A_{II}}{M(1-b\bar{J}_1)(1-D)}\right]^{\beta} dN$$

avec $$1-\alpha = \frac{A_{II} - \sigma_\ell(1-b\bar{J}_1)}{\sigma_u - J_{2M}}$$

et de fluage

$$dD_c = \left\langle \frac{\chi(\sigma)}{A} \right\rangle^r (1-D)^{-k}\, dt \qquad (10b)$$

L'accroissement de dommage de fatigue est donc lié au nombre de cycles, et dépend de J_{2M}, valeur maximale du second invariant du déviateur des contraintes, où $\overline{J_1}$ est la moyenne de la pression hydrostatique sur le cycle $\overline{J_1} = (\sigma_{ii\,max} + \sigma_{ii\,min})/6$ et où A_{II} désigne l'amplitude de la contrainte octahédrale, calculée par :

$$A_{II} = \frac{1}{2} \underset{t_1}{Max}\ \underset{t_2}{Max}\ J(\sigma(t_1) - \sigma(t_2)) \qquad (11)$$

Le dommage de fluage, quant à lui, est lié au temps et dépend de la contrainte équivalente instantanée, celle-ci étant évaluée par une combinaison des premier et deuxième invariants de contraintes [9] : il faut dont intégrer sur un cycle pour obtenir l'accroissement à introduire.

Un tel type d'approche, qui a été mis à l'épreuve en unidimensionnel sur un grand nombre de matériaux [10] [11], prévoit un cumul non linéaire entre fatigue et fluage. Néanmoins, lorsque les temps de fluage calculés par la formule (10b) sont très élevés, comme c'est le cas pour l'INCO 718 à 550°C, on peut calculer la rupture en fatigue pure ; l'intégration de (10a) donne alors :

$$N_F = \frac{\sigma_u - J_{2M}}{A_{II} - \sigma_\ell (1 - b\overline{J_1})} \left(\frac{A_{II}}{M(1 - b\overline{J_1})} \right)^{-\beta} \qquad (12)$$

Cette expression se simplifie bien sûr dans le cas unidimensionnel, où on peut l'écrire en fonction des contraintes maximale et moyenne du cycle σ_M et $\overline{\sigma}$:

$$N_F = \frac{\sigma_u - \sigma_M}{\sigma_M - \overline{\sigma} - \sigma_\ell (1 - b\overline{\sigma})} \left(\frac{\sigma_M - \overline{\sigma}}{M(1 - b\overline{\sigma})} \right)^{-\beta} \qquad (13)$$

ce qui permet de déterminer les coefficients.

Le tableau I résume les valeurs des variables utilisées pour le calcul de N_F dans le cas du calcul à 550°C. On constate que le col présente une amplitude de cisaillement octahédral importante et une faible contrainte moyenne, la première étant plus faible et la seconde nettement plus forte dans l'alésage. Il faut encore retenir que les différences observées entre les deux calculs au niveau des contraintes vont conduire à des estimations bien plus courtes avec la loi complète ; le fait d'utiliser directement la loi du cycle stabilisé conduit donc à un résultat non conservatif.

TABLEAU I -

Comparaison des contraintes (en MPa) au col et à l'alésage pour les deux calculs effectués à 550° C

	Loi stabilisée		Loi complète	
	Col	Alésage	Col	Alésage
A_{II}	595	502	635	504
J_{2M}	788	801	974	889
$\overline{J_1}$	25	207	57	266

Notons enfin que les modèles utilisant une amplitude de déformation plastique sont en échec dans les deux cas : celle-ci est négligeable en tout point pour le calcul avec la loi complète, et elle est non nulle uniquement à l'alésage pour la loi stabilisée, alors qu'expérimentalement la rupture se situe plutôt au col...

4 - CONCLUSION

Le développement de la fiabilité des prévisions de durée de vie de pièces industrielles comporte donc deux points sensibles :

- l'amélioration de la représentation du comportement contrainte-déformation, ce qui passe par une reconnaissance du rôle fondamental de la loi de comportement dans un calcul de structure ; il faut disposer d'équations capables de représenter le comportement monotone, cyclique stabilisé, transitoire (durcissement ou adoucissement), et éventuellement la viscosité du matériau,

- la prise en compte de la multiaxialité du chargement, en incluant des chargements non proportionnels et des chargements comportant une contrainte moyenne.

Il faut également être capable de repérer les phases d'amorçage et de propagation des criques : la durée de vie apparente des disques (jusqu'à éclatement) est le résultat d'un amorçage (parfois sur un défaut) et d'une progression finalement instable d'une petite fissure. Une interprétation correcte des résultats de calcul ne sera donc obtenue que grâce à des examens après rupture [12] ou (et) l'utilisation de méthodes non destructives pour évaluer l'endommagement.

REFERENCES

[1] - J.L. Chaboche - Description thermodynamique et phénoménologique de la viscoplasticité cyclique avec endommagement. Thèse, Publication ONERA 1978-3

[2] - J.L. Chaboche - Prévision de l'amorçage en fatigue à chaud, in "La Fatigue des Matériaux et des Structures" - Editions Maloine, Bathias-Bailon Ed. (1980)

[3] - M. Chaudonneret - Calcul des concentrations de contrainte en élastoviscoplasticité - Thèse et Publication ONERA n° 1978-3

[4] - S. Savalle, J.P. Culié - Méthodes de calcul associées aux lois de comportement et d'endommagement. La Recherche Aérospatiale n° 1978-5, pp. 263-278.

[5] - J. Lemaître - Sur la détermination des lois de comportement des matériaux élasto-viscoplastiques - Thèse, Publication ONERA n° 135 (1971)

[6] - J.L. Chaboche - Viscoplastic constitutive equations for the description of cyclic and anisotropic behaviour of metals. Bull. de l'Acad. Polonaise des Sciences, série Sc. et Techn. Vol. 25 n° 1, pp. 33-42 (1977).

[7] - G. Cailletaud, J.P. Culié, H. Kaczmarek - Mechanical description of viscoplastic and damage behaviour in presence of microstructural instabilities induced by variable temperature. 3rd Symp. on Creep ans Structures, IUTAM (Leicester) 8-12 sept. 1980.

[8] - J.L. Chaboche, K. Dang Van, G. Cordier - Modelization of the strain Memory Effect on the Cyclic Hardening of 316 Stainless Steel - SMIRT5 Berlin (1979)

[9] - Hayhurst D.R. - Creep Rupture under multiaxial state of stress - J. Mech. Phy. Solids - Vol. 20 n° 6 (1972) pp. 381-390.

[10] - J.L. Chaboche, H. Policella, H. Kaczmarek - Applicability of the SRP method and creep-fatigue approach to LCHTF life prediction of IN 100 alloy - in Characterization of low cycle High Temperature Fatigue by Strain Range Partitioning - AGARD Conf. Proc. Aalborg (1978), TP ONERA 1978-13.

[11] - G. Cailletaud, J.L. Chaboche - Life Prediction in 304SS by Damage Approach Conf. ASME-PVP - Paper n° 82-PVP-72, Orlando (1982) - T.P. ONERA 1982-42.

[12] - J.Y. Guedou, A. Pineau, L. Poret - Résistance à la propagation de fissures de l'alliage INCONEL 718 in "Engine Cyclic Durability by Analysis and Testing" AGARD conf. 30 may-1 june 84 (Lisse) - paper 63 B-7

DISCUSSION

R.Tadros, Ca

Have you thought of incorporating time in your analysis in the case of thermal stress problems, not just radial or hoop stress?

Author's Reply

Yes, in the models I presented here there is a time influence because the strain is not entirely plastic but, depending on the stress, is also strain-time dependent. If you have "time" in your analysis then it is not stabilized – you are talking about aging. Well, in the programme there are more complicated versions of the model which are not presented here, and in these models aging has been included.

EXPERIENCES WITH THE MATERIAL BEHAVIOUR AND HIGH TEMPERATURE LOW CYCLE FATIGUE LIFE PREDICTION OF THE IN 738 BLADING ALLOY

M.Y. Nazmy,* H. Wettstein,** and A. Wicki**
* Brown Boveri Research Center
CH-5405 Baden-Dättwil, Switzerland
** Brown, Boveri & Co., Ltd., Gas Turbine Division
CH-5400 Baden, Switzerland

SUMMARY

The (HTLCF) behaviour of the blading alloy IN 738 was studied in air at 850°C. This enabled us to have a basic understanding of the behaviour of this alloy as well as to test the different methodologies used in life time prediction. Another part of the investigation was focused on the influence of different environmental effects on the (HTLCF) behaviour. These environmental conditions were chosen to simulate as much as possible the actual conditions imposed on the gas turbine blades. Mainly sulfur containing environments were utilized for this purpose.

1. INTRODUCTION

A major thrust in the development and use of gas turbines is efficiency through better life-cycle management. Turbine blades, and rotors represent expensive and critical engine components. A reliable and accurate lifetime prediction of these components is essential for optimal use of gas turbines. A major difficulty in predicting the crack initiation life is accounting for the high temperature effects of creep-fatigue interaction and environmental attack. Different methods for high temperature low cycle fatigue (HTLCF) lifetime prediction have been proposed [1 - 4]. The interesting observation that various approaches seem to work well for some alloy systems but not for others can be attributed mainly to the difference in materials response or capacity to absorb the different types of damage. For example, grain boundary sliding and cavitation might occur relatively easily in those systems where there is no pinning of the boundaries by precipitates or carbide particles. In contrast, some systems may be very prone to environmental attack. In many instances in the literature the experimental data were generated to examine the predictive capability of one of the lifetime prediction methods, but in few cases the same core of results from one heat of material is used to evaluate the predictive capabilities of several models [5, 6].

Most of the work done on the effect of environment on the (HTLCF) of nickel-base superalloys involves mainly the difference in behaviour in vacuum vs. air [7, 8]. The effect of air thermal exposure on the (HTLCF) behaviour of the IN 738 superalloy has been reported [9]. Recently, the preliminary results on the influence of exposure in a sulfur containing environment on the (HTLCF) of IN 738 have been supported by the findings on the influence of burner rig prior exposure on the (HTLCF) behaviour of the same alloy [10, 11].

The aim of this investigation is to gain insight into the predictive capabilities of different (HTLCF) lifetime prediction methods as well as into the influence of sulfur containing environment on the (HTLCF) behaviour of the alloy IN 738.

2. EXPERIMENTAL PROCEDURE

HTLCF round specimens with 8 mm in diameter were machined from fully heat treated IN 738 casting. The composition of the alloy (wt. pct.) was 0.09 C, 8.25 Co, 15.95 Cr, 0.011 B, 1.6 Ta, 3.5 Al, 3.45 Ti, 0.7 Nb, 2.48 W, 0.5 Zr, 1.62 Mo, Ni bal. The grain size of this material was found to be ∿ 2 mm. The microstructure of this alloy in the fully heat treated condition consisted of γ' with bimodal distribution in γ matrix, carbide particles of $M_{23}C_6$ type at the grain boundaries, and blocky carbide of MC type distributed at grain boundaries as well as throughout the grains.

The (HTLCF) behaviour was investigated under fully reversed longitudinal strain control conditions using a servo-hydraulic testing machine. Testing was done in air at 700°C, 750°C, and 850°C. Seven types of strain wave shape were used to examin the effect of strain wave shape on the fatigue life at 850°C. These different types of wave shape included fast-fast and slow-slow triangular wave shapes that were done at a strain rate of 10^{-2}, and 10^{-5} s^{-1}, respectively. Tests with slow-fast and fast-slow sawtooth waves were done at a tensile strain rate of 10^{-5} s^{-1} and a compressive strain rate of 10^{-2} s^{-1}, and vice versa. Tests with truncated waves, in which the hold times were varied from 400 to 700 seconds and with a ramp rate of 10^{-2} s^{-1}, were also used. The number of cycles to crack initiation was defined using a failure criterion based on the observed asymmetry in the displacement signals of the LVDT's used to control the longitudinal displacement [12, 13].

In order to investigate the effect of environment on the (HTLCF) of IN 738, prior exposure of specimens was carried out at different temperatures. A number of specimens were placed in a tubular furnace at 850°C embeded in a synthetic ash with the following composition (wt. pct.) 4.3 Na_2SO_4, 22.7 $CaSO_4.2H_2O$, 22.3 Fe_2O_3, 20.6 $ZnSO_4H_2O$, 10.4

K_2SO_4, 2.8 MgO, 6.5 Al_2O_3, 10.4 SiO_2. Air containing 0.015 (vol. pct) of SO_2 and 0.015 (vol. pct.) of So_3 was let to flow through the furnace at a rate of 1 litre/min. The exposure time at 850°C was 1000 hr. The composition of this ash was chosen to simulate the service environment seen by the gas turbine blading material [14]. A number of other specimens were exposed at 700°C, and 750°C for 600 hr under the same environmental conditions mentioned above. In another batch of specimens, the surface of each specimen was coated with a layer of NaCl of ~ 1 mg/mm^2 in thickness prior to their 700°C, and 750°C exposure treatment in the synthetic ash environments.

3. RESULTS AND DISCUSSION

3.1 Lifetime Prediction

The first part of this investigation is concerned with the predictive capability of three different lifetime prediction methods. For this purpose the (HTLCF) data at 850°C is used. A quantitative comparison of the predictive capability of the various methods was established by using the standard deviation defined as follows

$$S = \left[\frac{\sum_{i=1}^{n} [\ln N^i_{calc} - \ln N^i_{obs}]^2}{n - 1}\right]^{1/2} \quad (1)$$

was used. N^i_{calc}, N^i_{obs} are the calculated and the observed numbers of cycles to crack initiation, respectively, and n is the number of data points.

3.1.1 Strain Range Partitioning Method

The concept of strain range partitioning method is discussed in details elsewhere [11]. Using the data on (HTLCF) at 850°C, the known interaction damage rule, and a least square fit program, the constants in the following equation were determined:

$$\Delta\varepsilon_{kj} = A_{kj} N_{kj}^{-\alpha_{kj}} \quad (2)$$

where A_{kj} and α_{kj} are constants depending on the type of strain range component, $\Delta\varepsilon_{kj}$ and N_{kj} are the inelastic strain range and the number of cycles to crack initiation for a specific type of strain range component, respectively. The least square lines for the four types of strain vs life relationships are shown in Figure 1. The observed differences between the different strain range vs life relationships, i.e. the effect of strain wave shape on the (HTLCF) of IN 738, have been attributed to differences in the modes of crack initiation and propagation [12]. The (HTLCF) data correlation of IN 738 at 850°C is shown in Figure 2 with S = 0.38.

3.1.2 Frequency-Separation Methods

The frequency-separation model postulates that the basic parameters necessary to predict the creep-fatigue life are the inelastic strain range, the tension-going frequency, and the hysteresis loop-time unbalance [2]. The basic equation of this model is as follows:

$$N_i = C\, \Delta\varepsilon_{in}^{\beta}\, \nu_t^m \left(\frac{\nu_c}{\nu_t}\right)^K \quad (3)$$

where N_i is the number of cycles to crack initiation, $\Delta\varepsilon_{in}$ is the inelastic strain range, ν_t, is the tension-going frequencyc, ν_c is the compression-going frequency, C, β, m, and K are material constants that depend on temperature. The same set of (HTLCF) data on IN 738 was also used in this method to calculate the constants in Equation (3). The values of C, β, m, and K, as calculated by least square fit computer program, were 21.6, -1.5, 0.0655, and 0.0236, respectively. Figure 3 shows the data correlation using the frequency-separation method with S = 0.41.

3.1.3 Ostergren Method

The measure of deformation used by this model is the tensile hysteretic energy absorbed by the specimen [4]. The observation that the wave shape effect on life was very sensitive when examined from the elastic strain range viewpoint, suggested that a life prediction method that involves stresses, e.g. Ostergren method, may be worthy of consideration [12]. The proposed equation in this method is as follows:

$$N_i = C\, (\Delta\varepsilon_{in} \cdot \sigma_T)^{\beta}\, \nu^m \quad (4)$$

where C, β, and m are material constants, σ_T is the tensile stress in the cylce, v is the frequency, and $\Delta\varepsilon_{in}$ and N_i have the usual meanings. As mentioned earlier, the same set of (HTLCF) data was used to calculate the constants in Equation (4). The least square fit values of these constants were $6.4 \cdot 10^4$, - 1.097, and 0.147 for C, β, and m, respectively. Figure 4 shows the (HTLCF) data correlation using this method with a calculated standard deviation S = 0.39.

From the (HTLCF) lifetime prediction point of view, the strain range partitioning method showed better predictability than that for frequency-separation method. It is noteworthy to point out that the predictability of Ostergren method is comparable to that of the strain range partitioning method.

3.2 Effect of Environments on (HTLCF)

In this part of investigation, precorroded specimens at 850°C, 750°C, and 700°C in sulfur containing environment were tested under (HTLCF) conditions, using a triangular wave shape with a strain rate of 10^{-2} s^{-1}, in air at the same exposure temperatures.

3.2.1 Effect of Prior Exposure at 850°C on (HTLCF)

Figure 5 shows the (HTLCF) results of IN 738 specimens in the unexposed and exposed conditions, in the form of Manson-Coffin plot. It can be seen that thermal exposure for 1000 hr in synthetic ash and air containing (SO_2 + SO_3) lowers the (HTLCF) life compared to that of the unexposed standard condition. This behaviour is in agreement with early reported (HTLCF) preliminary results on IN 738 as well as with the findings of Grünling et al. on the effect of sulfidation on (HCF) of the same alloy [10, 14]. The results on the exposed specimens exhibited a sizable scatter more than that normally exhibited by the results on the unexposed specimens. Similar effect has been reported on the effect of burner rig prior exposure on the (HTLCF) of the same alloy [11].

It has been reported that sulfur containing environment can have different types of corrosion effect on nickel-base alloys depending on the alloy composition, time of exposure, and temperature [15 - 17]. The type of attack that have been observed in this study at 850°C consisted mainly of surface pitting, brittle precipitates formation like chromium sulfide preferably at grain boundaries, and the formation of chromium depleted zones. From metallographic observation of the failed specimens of the exposed type, it was found that crack initiation sites coincided with sulfur affected areas, for example grain boundaries with sulfid particles. A similar mechanism of intergranular crack initiation has been reported on the (HTLCF) behaviour at 900°C of IN 738 specimens coated with (Na_2SO_4 + NaCl) layer [18]. Recently, Woodford and Bricknell have reported that intergranular sulfur penetration in IN 738 causes a reduction in creep life as well as tensile ductility [19]. They attributed this effect to deep intergranular sulfur penetration and embrittlement can occur to depths far in advance of visible corrosion products.

Another effect that results from prior exposure under this sulfidation environment is the change in the constitutive behaviour of the alloy. Figure 6 shows a plot of the cyclic stress range vs the total strain range for the unexposed and exposed types of specimens. From Fig. 6 it can be noted that the cyclic stress range is lower in the exposed tests as compared to the unexpected ones. It can be seen in Fig. 7 that the plastic strain range is higher in the exposed tests as compared to the unexposed ones. Hence, some of the life changes can be attributed to the changes in constitutive behaviour of the exposed specimens. One has to expect that the change in the constitue behaviour of the exposed specimens is time, temperature, and specimen dimensions dependent.

3.2.2 Effect of 750°C Prior Exposure on (HTLCF)

Figure 8 shows the (HTLCF) results of IN 738 specimens in the exposed and the unexposed conditions, in the form of Manson-Coffin plot. Thermal exposure for 600 hr in synthetic ash and air containing (SO_2 + SO_3) lowers the (HTLCF) life compared to that of the unexposed standard condition. However, this effect is not so pronounced as that observed at 850°C. A number of specimens were coated with NaCl layer of ~ 1 mg/mm^2 prior to their exposure. The (HTLCF) results of these specimens are also shown in Figure 8. In spite of the observed scatter exhibited by these results, one can assume that the presence of NaCl may have a synergistic damaging effect. In fact the role of NaCl in the hot corrosion process is not well understood [20 - 22]. In a review by Erdös et al. on mechanisms of hot corrosion, it was suggested that the presence of chlorides may have a disruptive effect on the protective scales by producing cracking and spalling [22]. The extent of this chloride effect on the protective scales depends on different factors like chloride level, temperature, and alloy composition [22]. Figure 9 is a photomicrograph which shows intergranular crack initiation in (HTLCF) of an exposed specimen of the type that was coated with NaCl. Figures 10 a, b, and c are SEM photomicrographs of an area along the crack shown in Figure 9, as well as the chromium and sulfur distributions of the same area. The formation of brittle chromium sulfide particles is evident in this case, and as mentioned earlier the crack initiation exhibited an intergranular mode in the exposed specimens in contrast to the transgranular mode which is usually observed in the unexposed tested specimens.

3.3.3 Effect of 700°C Prior Exposure on (HTLCF)

Figure 11 shows the results on (HTLCF) of the unexposed and the exposed specimens

in the form of Manson-Coffin plot. A number of specimens were also coated with NaCl layer prior to their thermal exposure. At this temperature and for 600 hr exposure time, no clear effect of prior exposure with and without NaCl coating, on (HTLCF) life of IN 738 could be detected. One can explain these results in the light of what has been reported about the existence of an induction period for the hot corrosion process [22]. This induction period could extend to relatively long times depending on the alloy composition as well as on the exposure temperature [22]. Hence, no significant effect of prior exposure, at 700°C and 600 hr, on the (HTLCF) behaviour should be expected if the induction period for IN 738 at these conditions is longer than the exposure time.

The relevance of investigating the environmental effects on the (HTLCF) behaviour of blading alloys to service conditions can be realized in the light of the reported results on fractured gas turbine blades due to high temperature corrosion [23].

4. CONCLUSIONS

1. Using one set of (HTLCF) data three different lifetime prediction methods were evaluated. The strain range partitioning and Ostergren methods both showed comparable predictive capabilities that were better as compared to the frequency-separation method.

2. HTLCF life is affected in a pronounced manner by prior exposure at 850°C in the hot corroding environments studied here. Prior exposure at 750°C in the studied hot corroding environments caused some reduction in the (HTLCF) life of IN 738 specimens. The prior exposure at 700°C for 600 hr in the studied hot corroding conditions did not affect the (HTLCF) life of IN 738 specimens.

3. Initiation mode of cracking was observed to change from transgranular to intergranular when prior exposure was performed in the hot corrosion environment. This was mainly attributed to grain boundary embrittlement by sulfide formation and sulfur diffusion.

REFERENCES

1. MANSON, S.S., The Challenge to Unify Treatment of High Temperature Fatigue - A Partisan Proposal Based on Strain Range Partitioning, Fatigue at Elevated Temperatures, STP 520, Philadelphia, Pa., ASTM, 1973, 744-782.

2. COFFIN, L.F., The Concept of Frequency Separation in Life Prediction for Time-Dependent Fatigue, ASME-MPC Symposium on Creep-Fatigue Interaction, MPC-3, N.Y., ASME, 1976, 349-363.

3. MAJUMDAR, S. and MAIYA, P.S., A Damage Equation for Creep-Fatigue Interaction, ibid, 323-335.

4. OSTERGREN, W., Correlation of Hold Time Effects in Elevated Temperature Low Cycle Fatigue Using a Frequency Modified Damage Function, ibid, 179-202.

5. CHABOCHE, J.L., POLICELLA, H., and KACZMAREK, H., Applicability of the SRP Method and Creep-Fatigue Damage Approach to the LCHTF Life Prediction of IN-100 Alloy, Conf. Proc. on the Characterization of Low Cycle High Temperature Fatigue by the Strain Range Partitioning Method, AGARD-CP-243, 1978, p. 4.

6. NAZMY, M.Y., and WÜTHRICH, C., The Predictive Capability of Three High Temperature Low Cycle Fatigue Models in the Alloy IN-738, Conf. Proc. ICM 4 Mechanical Behavior of Materials, Vol. 1, Pergamon Press, 1983, 183-189.

7. KORTOVICH, C.S. and SHEINKER, A.A., A Strain Range Partitioning Analysis of Low Cycle Fatigue of Coated and Uncoated Rene 80, Conf. Proc. on the Characterization of Low Cycle High Temperature Fatigue by the Strain Range Partitioning Method, AGARD-CP-243, 1978, p. 1.

8. DUQUETTE, D.J., and GELL, M., The Effects of Environment on the Elevated Temperature Fatigue Behaviour of Nickel-Base Superalloy Single Crystal, Metall. Trans., Vol. 3, 1972, 1899-1905.

9. NAZMY, M.Y., The Effect of Environment on the High Temperature Low Cycle Fatigue Behaviour of Cast Nickel-Base IN-738 Alloy, Mat. Sci. and Eng. 55, 1982, 231-237.

10. NAZMY, M.Y., The Effect of Sulfur Containing Environment on the High Temperature Low Cycle Fatigue of a Cast Ni-Base Alloy, Scripta Met., Vol. 16, 1982, 1329-1332.

11. FARRELL, T.R., The Effect of Prior Exposures on IN 738 Low Cycle Fatigue, TMS paper selection, the Metallurgical Soc. of AIME, paper No. A 83-37, 1983.

12. NAZMY, M.Y., High Temperature Low Cycle Fatigue of IN 738 and Application of Strain Range Partitioning, Metall. Trans., Vol. 14 A, 1983, 449-461.

13. NAZMY, M.Y., and MEIXNER, W., Crack Initiation as a Failure Criterion in Low Cycle Fatigue, Material und Technik, Vol. 1, 1983, 33-36.

14. GRÜNLING, H.W., KEINBURG, K.H., and SCHWEITZER, K.K., The Interaction of High Temperature Corrosion and Mechanical Properties of Alloys, Conf. Proc. High Temperature Alloys for Gas Turbines, D. Reidel Publishing Co., Dordrecht, Holland, 1982, 507-543.

15. GOEBEL, J.A., PETTIT, F.S., and GOWARD, G.W., Mechanisms for the Hot Corrosion of Nickel-Base Alloys, Metall. Trans., Vol. 4, 1973, 261-278.

16. HARTNAGEL, W., BAUER, R., and GRÜNLING, H.W., Constant Strain Rate Creep Tests with Gas Turbine Blade Materials under Hot Corrosion Environmental Conditions, Conf. Proc. Corrosion and Mechanical Stress at High Temperatures, London, Applied Science Publishers, 1981, 257-273.

17. ERDÖS, E., and DENZLER, E., On the Oxidation and Hot Corrosion of IN 713 LC, IN 738 LC, and IN 939, Conf. Proc. Behaviour of High Temperature Alloys in Aggressive Environments, London, Metals Society, 1980, 455-463.

18. JIANTING, G., RANUCCI, D., and PICCO, E., Low Cycle Fatigue Behaviour of Cast Nickel-Base Superalloy IN-738 LC in Air and in Hot Corrosive Environments, Materials Science and Eng, 58, 1983, 127-133.

19. WOODFORD, D., and BRICKNELL, R.H., Penetration and Embrittlement of Grain Boundaries by Sulfur and Chlorine - Preliminary Observations in Nickel and a Nickel-Base Superalloy, Scripta Met., Vol. 17, 1983, 1341-1344.

20. HOSSAIN, M.K., and SAUNDERS, S.R.J., A Microstructral Study of the Influence of NaCl Vapor on the Oxidation of a Ni-Cr-Al Alloy at 850°C, Oxidation of Metals, Vol. 12, No. 1, 1978, 1-22.

21. WHITLOW, G.A., BECK, C.G., VISWANATHAN, R., and CROMBIE, E.A., The Effects of a Liquid Sulfate/Chloride Environment on Superalloy Stress Rupture Properties at 704°C, Metall. Trans., Vol. 15 A, 1984, 23-28.

22. CONDÉ, J.F.G., ERDÖS, E., and RAHMEL, A., Mechanisms of Hot Corrosion, Conf. Proc. High Temperature Alloys for Gas Turbines, D. Reidel Publishing Co., Dordrecht, Holland, 1982, 99-148.

23. NAUMANN, F.K., and SPIES, F., Fractured Gas Turbine Blades due to High Temperature Corrosion, Practical Metallography, 18, 1981, 556-559.

ACKNOWLEDGEMENT

The helpful discussions and comments of Dr. C. Wüthrich are greatly appreciated.

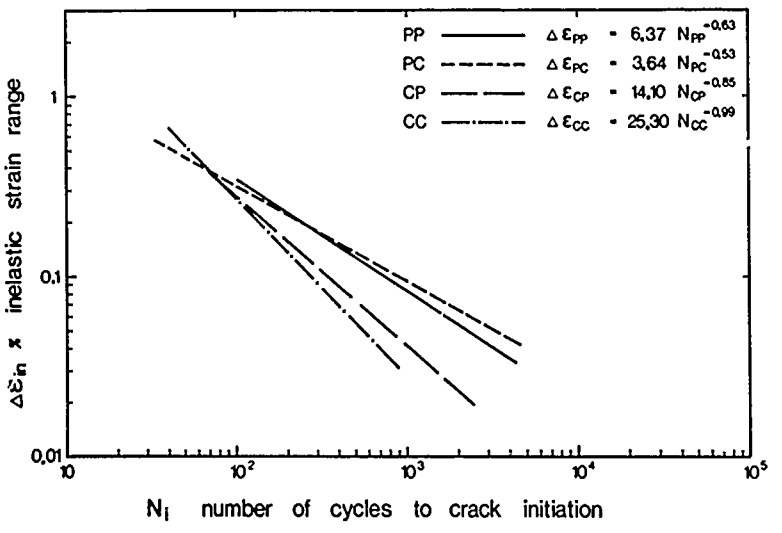

Figure 1: Component strain range vs life relationships.

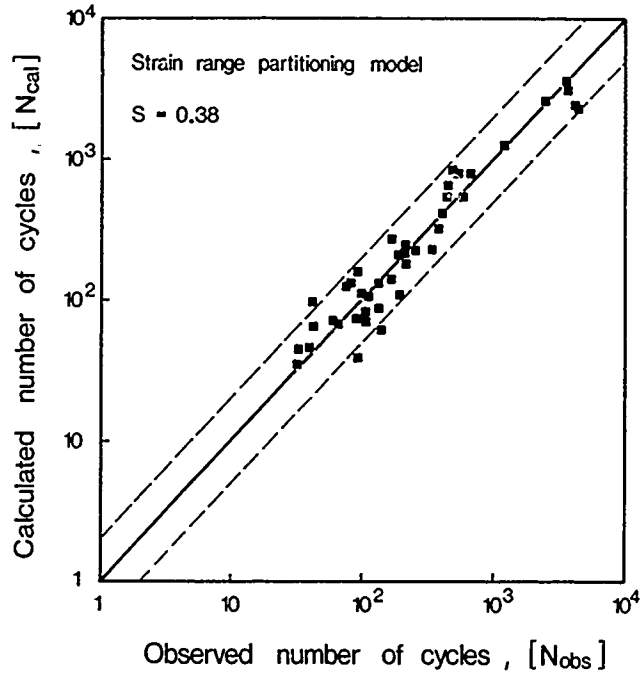

Figure 2: High temperature low cycle fatigue data correlation.

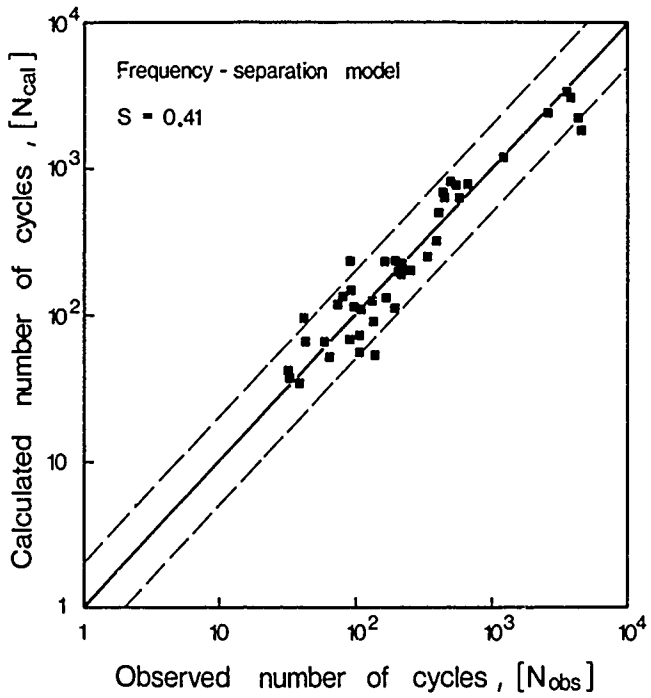

Figure 3: High temperature low cycle fatigue data correlation.

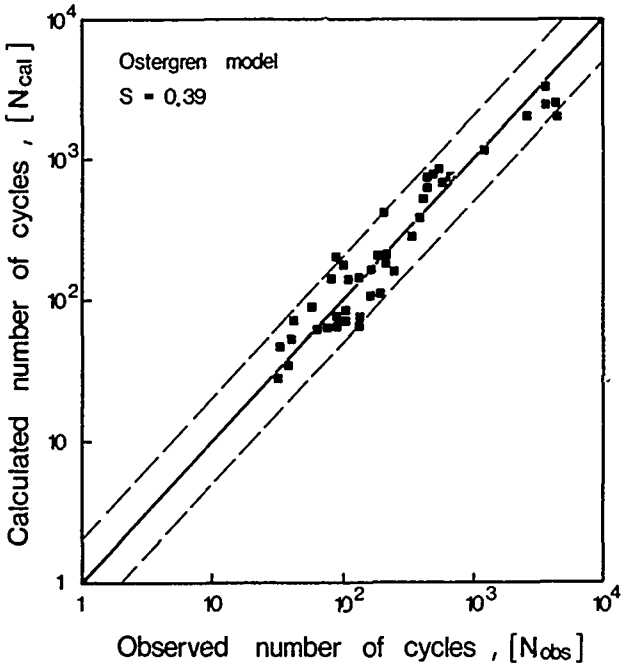

Figure 4: High temperature low cycle fatigue data correlation.

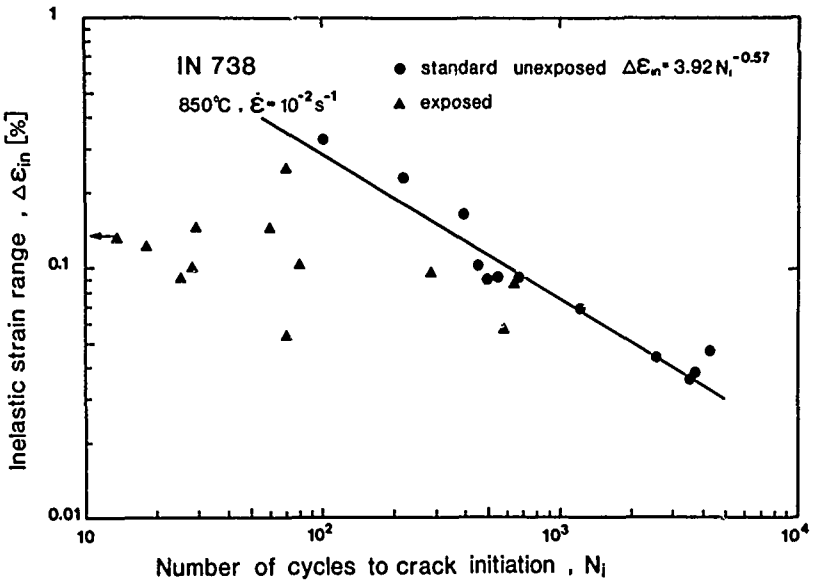

Figure 5: High temperature low cycle fatigue of IN 738 in the standard unexposed and the exposed conditions.

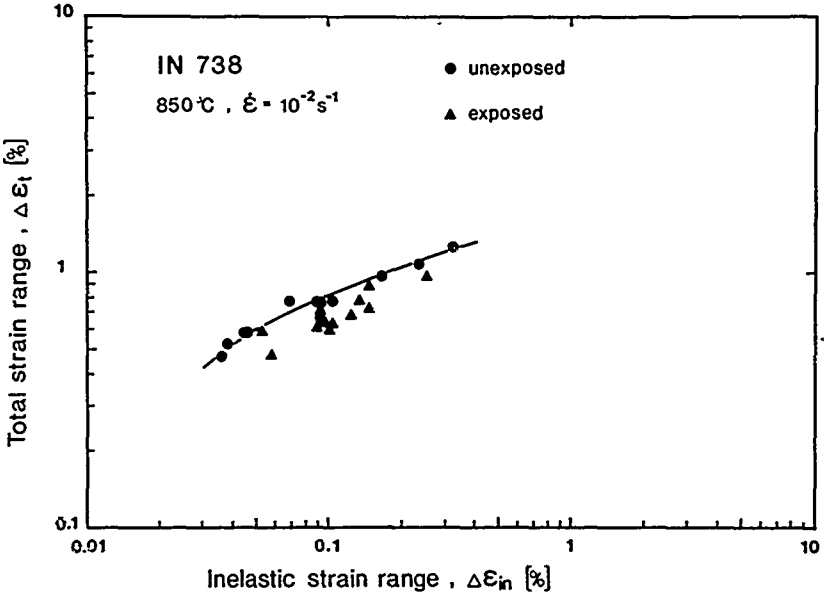

Figure 6: Cyclic stress-strain diagram of IN 738 in the unexposed and the exposed conditions.

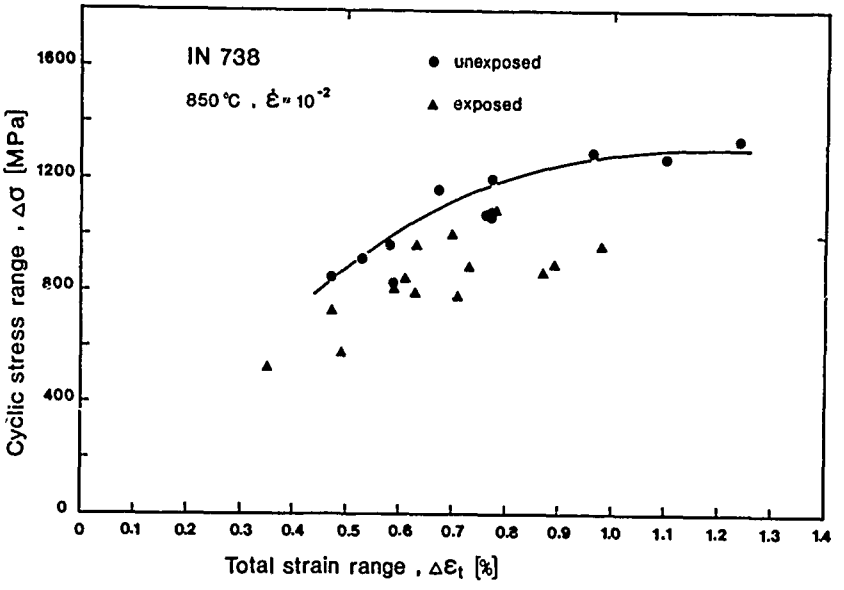

Figure 7: Total strain range vs inelastic strain range diagram of IN 738 in the unexposed and the exposed conditions.

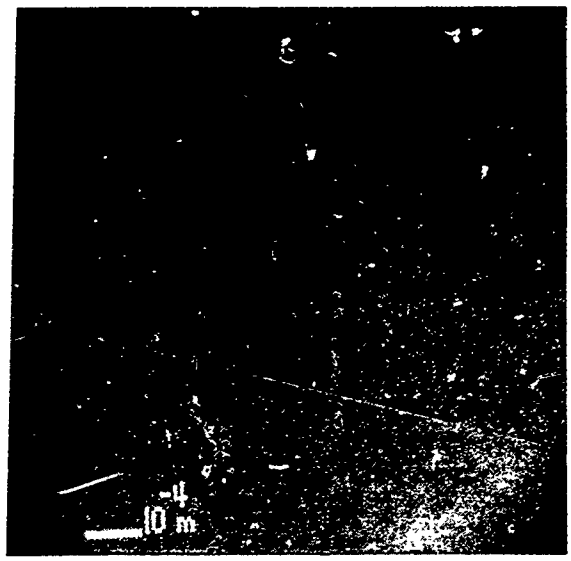

Figure 8: Intergranular crack initiation in high temperature low cycle fatigue in IN 738 precoated with NaCl and exposed in the sulfidation environment at 750°C for 600 hr.

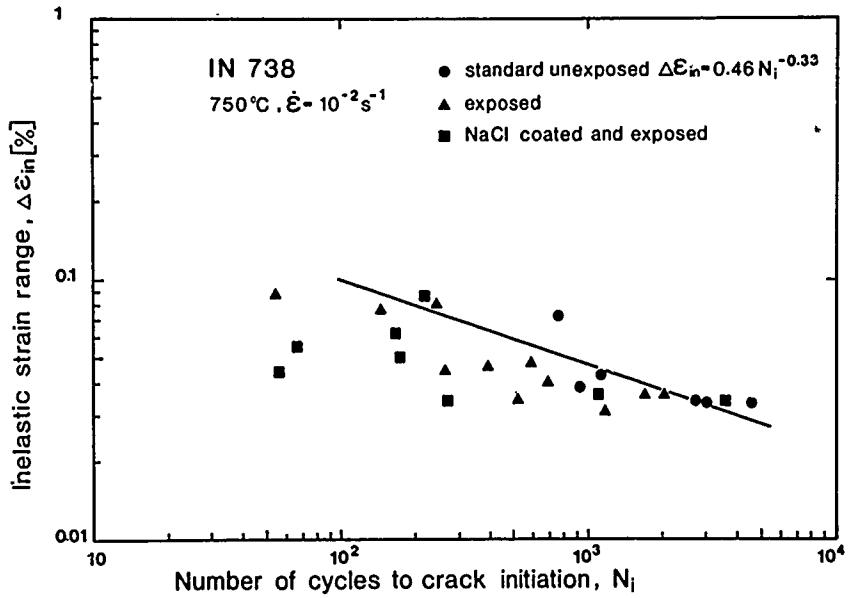

Figur 9: High temperature low cycle fatigue of IN 738 in the standard unexposed and the exposed conditions.

(a)

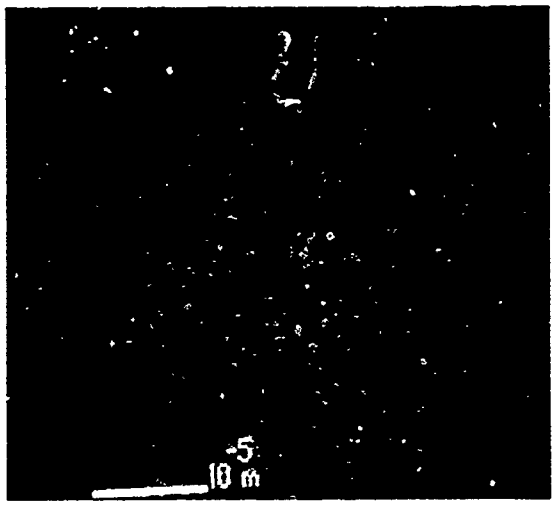

(b)

(c)

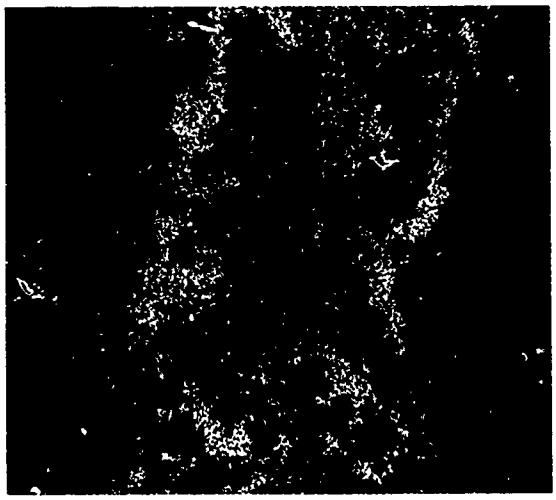

Figure 10: (a) Corrosive intergranular attack in IN 738 precoated with NaCl and exposed to sulfidation environment at 750°C for 600 hr, showing intergranular crack initiation and the formation of brittle sulfide particles mainly chromium sulfide, (b) chromium distribution, and (c) sulfur distribution.

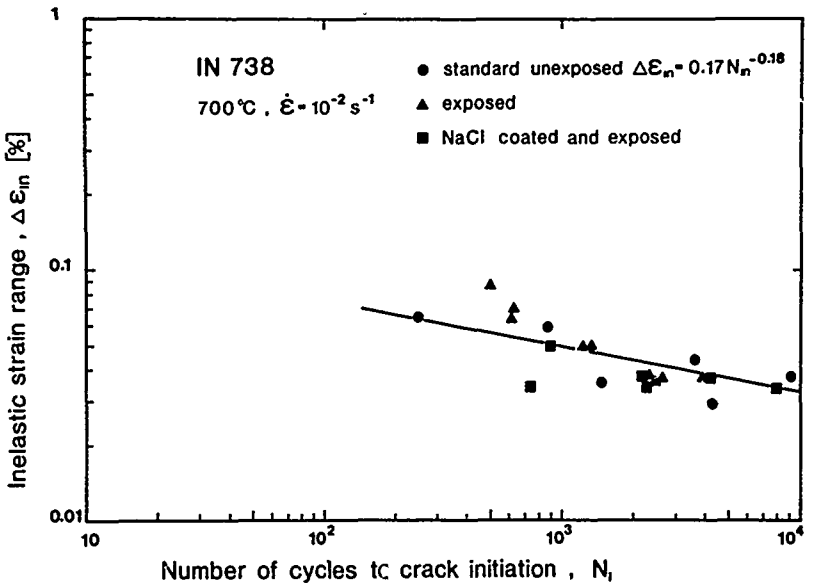

Figure 11: High temperature low cycle fatigue of IN 738 in the standard unexposed and the exposed conditions.

DISCUSSION

D.W.Hoeppner, Ca

How did you decide on your "crack initiation size" of 0.5 mm? Why didn't you select a crack initiation size of 0.1 or 0.3 or 1.0 mm? Isn't your number of cycles to "initiation" really the number of cycles to propagate a crack to a length of 0.5 mm at which point you detect it? How does your experimental detection criterion relate to crack detection on a real blade?

Author's Reply

The definition of the number of cycles to crack initiation is based on a reproducible experimental observation, which is 5% asymmetry in the signal of the used LVDT's. Since the definition of crack initiation is arbitrary to start with, then one can also use another definition for V_i as the number of cycles to initiate and propagate a crack to a 0.5 mm size. Further details on this point can be found in references 12 and 13 in my paper.

D.W.Hoeppner, Ca

Inasmuch as the SRP, frequency modified, and ostergren methods all relate to ideal materials (no discontinuities and/or heterogeneities) and the idealized continuum stress-strain behaviour, as well as empirical end of life criteria, how do you justify using these techniques on a material such as IN738 which is a casting that has pores, carbides, etc. that truly are discontinuities? As well, the material is a polyphase material and I was not aware that these methods were within the physical boundary conditions of these methods. Also, would your correlations of predicted to actual life change with a_i?

Author's Reply

In IN738 alloy as well as in other cast nickel base alloys, crack initiation starts from the surface under LCF condition, i.e. these structural inhomogeneities mentioned do not change the surface crack initiation mechanism. As I have shown in my paper as well as in references 12 and 6, SRP was successfully applied to predict the LCF life of IN738 specimens.

D.W.Hoeppner, Ca

Your specimens were machined from cast blades. How did you establish the specimen machining technique in relation to the cast (and presumably machined) surface of the blades? In relation to this later point, is the "defect" level the same in your specimens as in actual blade surfaces or near surfaces?

Author's Reply

The specimens were machined from cast blocks and their surface finish was done by low stress grinding to avoid introducing any surface machining defects.

A.K.Koul, Ca

In line with Dr Hoeppner's remark about the validity of the term "LCF Crack Initiation" in IN738 blading alloy, I would invite the authors' comments regarding the validity of describing a LCF crack initiation life in aggressive environments containing S_{02}, S_{03} or NaCl, where fracture is invariably intergranular in nature and crack-like discontinuities in the form of $M_{23}C_6$ carbides are already present within the virgin microstructure.

Author's Reply

The definition of crack initiation that I introduced in my investigation was based on the development of approximately 0.5 mm size surface crack regardless of whether the crack initiation made transgranular as in pp type of tests of unexposed material, or intergranular as in the case of exposed specimens.

G.Cailletaud, Fr

You show (figures 5 and 9) that the life of the exposed specimens is lower than the life of the unexposed, nevertheless, the behaviour is different (figures 6 and 7). (1) What would be for the exposed tests the misfit between the experiment and the prediction by the models you have presented? (2) Would it not be possible to use a model with a "micro-initiation" and a micropropagation phase for this type of problem?. We could assume that the micro-initiation phase is shortened due to the exposure period (that corresponds to an early intergranular initiation, see figure 8). So we could represent with only one set of coefficients exposed and unexposed tests. Such an approach has been successfully applied to predict the failure of an austenitic stainless steel in air and vacuum.

Author's Reply

(1) The change in the cyclic stress-strain behaviour of the exposed specimens is not the only reason for the observed difference in life, nevertheless it is an important factor in this respect.

(2) In principle one can apply several other models of life prediction to a certain specific set of data. However, one may find differences between the predictive capabilities of these models, since each model accounts for the damage differently.

CYCLIC ENDURANCE TESTING OF THE RB211-22B CAST HP TURBINE BLADE

by

J S PONSFORD & G K WADDINGTON

ROLLS-ROYCE LIMITED
PO BOX 31
DERBY

SUMMARY

During the design and development of a cast directionally solidified high pressure turbine blade for the Rolls-Royce RB211-22B engine it was recognised that a method of proving the design beyond the normal endurance testing was required in order to simulate the total service life of the turbine blade. This led to the creation of the intensive cyclic endurance programme. The aim of the programme was to prove that the new HP turbine blade was capable of achieving the design objective of a 10,000 hour service life. This paper covers the objectives of the programme, the definition of the endurance cycles and the automation used in running the cyclic tests. The discussion includes comments on the modifications incorporated to ensure that testing was kept representative of the service environment. Also presented are the results of the programme which demonstrated that the design objective would be achieved in airline service.

1.0 INTRODUCTION

The RB211-22B engine entered service in 1972 in the Lockheed TriStar aircraft. The 42,000 lbs of thrust that the RB211 provided was approximately twice the thrust of any engine produced before the arrival of the big fan engines. This jump in thrust had arisen because of the emergence of the wide bodied aircraft. New engine designs were required to meet this challenge.

The RB211, Fig:1, is different from its competitors in that it uses three as opposed to two shafts within the engine. In the LP (low pressure) system the fan is driven by three stages of turbine. The gas generator uses two further shafts, the IP (intermediate pressure) system comprising seven stages of compressor driven by a single stage turbine and the HP (high pressure) system comprising six stages of compressor driven by another single stage turbine. It is the testing of a new design of blade for the single stage HP turbine that is the subject of this paper.

The single stage HP turbine was originally designed as a forged air cooled shrouded blade, but from entry into service reliability was a problem. The combination of high gas temperatures coupled with high rotational speed produced either excessive thermal fatigue or excessive creep in the blade leading to premature failure. It was clear that modifications would be necessary to improve the blade life and reliability in service.

Between 1972 and 1975 two developments of the original forged blade were introduced. On each occasion these redesigns were assessed by a 150 hour certification test (the standard demonstration prior to airline service) and each redesign appeared to be an improvement over the blade in service. Although these changes did improve the reliability and increased the average blade life, the service life was at best 5000 hours. The situation was exacerbated because imminent failure of a blade could not necessarily be detected by regular boroscope inspection of the turbine as the time from first crack to failure was so short. The situation left the airlines with a reliability problem as failures were not predictable and consequently led to unscheduled engine removals.

By 1976 it had become apparent that a reliable blade could not be produced by further development of the existing forged blade. A completely new design was therefore conceived in order to achieve the desired service reliability. In addition to the normal certification testing, intensive cyclic endurance tests were introduced to demonstrate that the new blade design would be successful and reliable in service. These additional trials are discussed in detail in the remainder of this paper.

2.0 DESIGN OF THE CAST BLADE

The new HP turbine blade design was a cast directionally solidified (DS) blade, Fig:2. It featured more surface films, a higher cooling air flow and a superior material with only a few discrete grain boundaries. The design permitted much lower internal temperature gradients and operated at a significantly lower mean temperature. All of these features led to an improved blade life. The objective for the blade was that it should be capable of completing 10,000 hours in service without repair.

The blade is cooled by air tapped from compressor delivery and passed through the blade from two entry passages. High pressure air enters the blade root and passes to both the leading edge passage and the trailing edge triple pass passage. Lower

pressure cooling air enters the shank of the blade and supplies a large radial passage in the centre of the blade. The blade is retained in the disc by a five tooth firtree. Axial retention is provided by a lockplate between the blade and the disc. The inner platform is an integral part of the cast blade and is sealed under centrifugal force by a wire that bridges the gap between adjacent blades. The blade has a tip shroud on which interlocking faces provide twist to hold the blade rigid. Fins on the top of the shroud provide sealing against an abradable static lining.

3.0 THE OBJECT OF THE TESTING

With the background of numerous in-service extruded blade failures and a service life of at best 5000 hours and usually much less, it was necessary to demonstrate to engine operators, the ability of the new cast DS blade to achieve the design claim of 10,000 hours life in service. To this end it was necessary to derive a pre-service test programme of greater severity than normal certification testing.

The object of the test programme was to expose a set of HP turbine blades to sufficient thermal fatigue and creep damage to demonstrate that the blade would survive 10,000 hours in service.

The first task was to examine the operating conditions and environments of the various RB211-22B operators to see how much thermal damage each operator suffered during 10,000 hours of his particular operation. This examination showed that the creep and thermal fatigue damage experienced by virtually all the operators would be surpassed by using a medium length flight plan (Fig:3.1) which was typical of one particular operator. This flight plan (of 108 minutes which implies 5555 flight cycles during 10,000 hours of service life) was then used as the standard by which test bed operations would be assessed.

The engine operating conditions for the cyclic testing were deliberately chosen to represent the most pessimistic conditions in service. In airline operation, maximum power is used only when conditions demand. On approximately 80% of occasions, 90% of maximum power is sufficient and operating in this manner has a powerful conserving effect on component life. For the test bed demonstration no such service derate was assumed for take-off conditions. Also, relative to the steady state conditions of a statistically average new engine, the turbine entry temperature at take-off was increased by 60°C. This represented the cumulative effects of a worst engine, two thirds of total deterioration in service, take-off transient overshoot and other allowances. Similar pessimism of the appropriate allowances was adopted at climb and cruise conditions.

4.0 TEST BED CYCLES

Within certain limits, for a given thrust requirement, as the ambient temperature increases, so the temperatures and shaft speeds within the engine increase. Thus the high pressure turbine blade operating temperatures increase, which coupled with increased centrifugal stress, results in a significant reduction in thermal life, for example a 10°C increase in ambient temperature above ISA increases metal temperature by approximately 35°C which reduces creep and thermal fatigue lives to approximately ¼ and ½ respectively. This sensitivity to ambient temperature means that the test programme had to take account of the variation in day temperatures encountered during airline operation. The table below shows the assumed distribution which is typical of the flight profile chosen:

Occasions	25%	50%	25%	
Take-off	-10	+ 5	+15	
Climb	+ 5	+10	+15	Temperature (°C) relative to ISA
Cruise	0	+ 5	+10	

In terms of thermal damage, the 25% of 'hot' days cause the bulk of the damage with virtually all of the balance being consumed on the 50% of 'normal' days. Thus by specifying two different test bed cycles, one representing 'hot' days and the second representing 'normal' days, it was possible to simulate the thermal damage expected during airline operation. Using the traditional Rolls-Royce method of blade life assessment which is based on mean and peak metal temperatures, it was predicted that 4800 test bed cycles in the mix of 1 'hot' : 2 'normal' cycles would use virtually the same proportions of creep life and thermal fatigue life as used during 10,000 hours (5555 cycles) of worst engine service operation. Furthermore, by adjusting the nominal 1 : 2 mix of cycles, it is possible to compensate for variations of blade metal temperature caused by varying day temperatures on the test bed and maintain the target exposure time of the blade at given metal temperatures.

The test bed cycles are shown in Fig:3.2 and were the best compromise arising from a number of conflicting requirements. One test bed cycle is not equivalent to one flight cycle but it is so designed that the ratio of creep to fatigue life used is the same as during a flight cycle. These life estimates for the flight and test cycles are based on theoretically predicted metal temperatures. With fuel cost and timescale considerations paramount, the duration of each test bed cycle was reduced

to a minimum whilst remaining representative. To this end it was possible to collapse the flight creep damage during climb and cruise into a much shorter duration at a higher temperature. However, care must be taken because unrealistically high operating temperatures can lead to unrepresentative thermal damage which would not be encountered during service operation. The test bed cycles also include a minor excursion after 3½ minutes of take-off running. In theory this feature was not thought to affect either creep or fatigue damage significantly but it was included in order to represent the minor excursions observed on some flights.

In addition to the traditional method of blade life prediction, a second more detailed assessment was made by considering cumulative strain damage. This method was able to predict the locations of maximum creep and fatigue damage within the blade. It also predicted that the blade thermal damage would be greater during 4800 test bed cycles than during 10,000 hours of worst engine operation in service. Therefore by retaining the target of 4800 cycles the pessimistic option was once again taken. Indeed, relative to the typical service operation, the arduous nature of the chosen test programme can be seen on Fig:4 which shows that the test target is between two and three times the life usage after 10,000 hours of typical service life. However, this ratio is necessary as only one blade set was to be tested rather than a larger sample.

5.0 PROGRAMME SCHEDULE & ENGINE CONTROL

The test objective of 4,800 cycles on one set of turbine blades, represented between 700 and 800 hours of engine test running. From previous development experience it was doubtful that one engine would achieve this very arduous objective (equivalent to 10,000 hours in service) without attention to or replacement of some of the engine components. It was therefore decided to provision for three engine builds of 1600 cycles each. Furthermore two engines should be used in order to occupy the test bed fully. It was also clear that even at 1600 cycles unscheduled rejections of engines were likely. To minimise this problem a maximum life between module rework was defined and strip inspection requirements for all engine components established. The testing was also seen as a good opportunity to gain rapid endurance and cyclic experience on newly cleared modifications in other areas of the engine apart from the HP turbine.

It was apparent that if the testing was to provide rapid and consistent cyclic running then an automated system of engine control was required i.e., a system that would run the engine with minimum manpower involvement, and eliminate possible human inconsistency. The electronics necessary to perform this task are relatively simple but the computerised control was a vital ingredient in providing consistent continuous cyclic testing.

The control system was designed to start and stop the engine, operate the throttle and take the engine through the test bed cycle. The system also monitored engine parameters with two control levels on each parameter to guard against unusual engine conditions. The first level, if exceeded, pulled the engine to idle for three minutes then shut the engine down. The second control level was set above the first level with the intention of acting as a reserve if the first level failed or if the engine passed through the first control level too rapidly. If this second level was reached then the fuel to the engine was immediately cut off and the engine turned over on the starter motor to prevent rotor seizure. The computerised system also gave a hard copy readout of specified parameters at defined intervals.

By the end of the cyclic test programme which eventually involved three sets of blades, a total of 7,288 cycles had been achieved over 14 builds. This average of 520 cycles/build was well short of the target of 1600 cycles but still represented a satisfactory programme for three major reasons.

1. All except two builds were terminated with the engine in good running order.

2. The computerised system of engine running worked successfully allowing consistent cycles to be accumulated at a high rate.

3. The experience gained in cyclic endurance running has proved invaluable as this programme pioneered what has become a normal mode of testing for Rolls-Royce.

6.0 TEST EXPERIENCE & RESULTS

The automated test bed control system worked well throughout the testing. The only problem was due to transient overshoot of the IP rotor speed. This overshoot was caused by hysteresis in the variable inlet guide vane control system and resulted in the first control level on IP rotor speed being reached on some cycles and the engine power being reduced to idle. This was overcome by immobilising the first control level on the one parameter during the accelerations and reactivating the system when stable conditions were reached. No other significant problems were encountered with the test bed systems during the total test period.

6.1 Testing Of The First Set Of Blades

The first set of HP turbine blades to be subjected to intensive cyclic endurance testing accumulated a total of 1444 cycles (644 'hot' cycles and 800 'normal' cycles) during two tests. At this point routine boroscope inspection revealed a crack in one HP turbine blade and so the engine was stripped for inspection. The pressure surface of the blades were heavily coated and laboratory inspection revealed that the coating was iron oxide on a base of calcium sulphate. This coating had led to significant blockage of the air cooling holes, overheating and a much more rapid use of blade life, hence the premature crack. A review of high life blades in service showed that this level of material build up had never been experienced on service blades which in most operations accumulated little or no surface deposits. After further investigation, it became clear that the material build up was associated with conditions peculiar to the local atmospheric environment at the time. These conditions were totally unrepresentative of service conditions and in fact severely overtested the blade.

6.2 Testing Of The Second Set Of Blades

It was therefore decided that another set of blades should be tested and that in order to keep the test representative of service experience the blades should be kept clean. The problems caused by excessive dirt were not confined to the HP turbine as there was evidence of dirt accumulation throughout the engine. The best method of tackling the problem lay in filtering the air before it entered the engine; however, whilst this was possible the cost and timescales involved proved unacceptable. It was therefore decided that the HP turbine should be removed from the engine at intervals to allow the turbine blades to be chemically cleaned and inspected. When the second set of blades commenced intensive cyclic endurance testing, they completed 767 cycles before the test was halted due to advancing blockage of the film cooling holes. Boroscope inspections of film hole blockage resulted in this set of blades being cleaned a further six times prior to the end of their testing at 4244 cycles.

The relationship between service and development test cycles and hours was clearly crucial to the success of this programme and a constant monitoring of the engine test conditions was necessary to ensure an accurate simulation of service conditions. During testing of the second set of blades, it became apparent that the average HP compressor delivery temperatures were lower than expected (due to the low day temperatures at the time) and that this in turn was leading to lower than anticipated thermal damage. The mix of 'hot' day cycles to 'normal' day cycles was therefore modified from 1:2 to 1:1 to correct this situation.

At 4244 cycles, routine boroscope inspection discovered one blade with a significant crack. The blades were removed and inspected. Detailed metallurgical examination of the severely cracked blade revealed that the crack originated from an inclusion defect on the suction surface wall 0.25 inches from the trailing edge and just above the root platform. The inclusion material was identified and the point of introduction determined. This resulted in a manufacturing process change to eliminate the problem for service blades.

The remaining blades, which all exhibited minor cracking of various forms, were declared fit to resume testing, although in the event, the test programme on this set of blades was terminated. Metallurgical examination of a number of sectioned blades had revealed higher than expected surface temperatures and when the situation was evaluated it was evident that by 4244 cycles, the blades had already suffered as much creep and more fatigue damage than the 10,000 hours worst engine target, Fig:4. The original predictions of surface temperature had been based on measurements obtained from blades operating in a normal environment. The temperature increase suffered by the test blades was not unexpected and was due to the partial film hole blockage caused by the build up of surface material every 700-800 cycles. Since it was confidently believed that this film hole blockage would not occur in service, there was no reason to continue testing to the original target of 4800 cycles as sufficient thermal damage had already been accumulated.

The removal and cleaning of the blades every 700-800 cycles had facilitated frequent and detailed examination of the blades. It had therefore been possible to find and observe the behaviour of any cracks or other damage at an early stage and monitor propagation throughout the test. There were six areas on the blade which exhibited cracks during testing. Fig:5 shows the crack positions.

Position 1

These cracks originated at the edge of the interlock hardfacing and appeared relatively early in the test programme. After the initial phase, propagation of the crack reduced to an insignificant rate.

Position 2

Radial cracks from the bottom holes of the 2nd pressure surface film row are relatively benign and propagate only slowly. Their appearance was anticipated as the strain analysis had predicted precisely this region as suffering the peak creep strain damage.

Position 3

Cracks near the bottom of the second pass of the triple pass system were first seen on the encrusted first set of blades. Their appearance had been a surprise and only after considerable analysis was it established beyond doubt that these cracks were caused by local overheating associated with surface deposits. The cracks were not expected to appear in a service environment.

Position 4

The fillet radius suffered two forms of related damage. For reasons that only subsequently became apparent, the region was much hotter than expected. This caused both local oxidation and compressive creep. The locally high thermal gradients led to axial cracking. Crack propagation was again slow.

Position 5

The strain analysis had identified the pressure surface aerofoil wall adjacent to the trailing edge passage as the principal region of fatigue damage due to its relatively thin wall section. These axial cracks were therefore not unexpected but once again they propagated only slowly. Laboratory investigation confirmed that the cracking was a function of wall thickness.

Position 6

The appearance of cracks linking leading edge film holes near the aerofoil root was potentially more serious. However, they did not appear until near the end of testing, which was equivalent to a very high service life. The cracks occurred on the external surface and did not penetrate to any significant depth. They were not expected to lead to any imminent blade failure.

The history of the blade cracks is tabled in Fig:6.

It must be emphasised that even after 4244 cycles, the majority of the cracks were very small, typically between .001 and .050 inches in length. Furthermore the rate of crack propagation was very slow. These characteristics are a function of the relatively high ductility and the low number of grain boundaries associated with the material used for the cast DS blade.

6.3 Testing Of The Third Set Of Blades

A third set of blades was also tested but for a limited period only. Initial manufacturing problems had led to a high rate of blade rejection during final inspection due to thin walls between the internal passages and the outer aerofoil. Whilst it was believed that these blades would be satisfactory in service, they were nevertheless outside the tolerances of wall thickness tested on the endurance programme. It was therefore decided that these blades should not be released without a specific evaluation of the thin walls. This third set of blades which included some blade features being tested for the first time, was subjected to 1600 cycles (800 'hot' day and 800 'normal' day cycles).

No significant problems were encountered although cracking in some regions occurred at a lower number of cycles than with the standard wall blades of the previous test. By correlating crack propagation with wall thickness on these two tests, it was possible to establish that a certain amount of wall thinning was acceptable in some regions and that these blades could be released into service.

7.0 THE SUBSEQUENT SERVICE SITUATION

Since entering service in late 1979 the record of reliability of the directionally solidified cast HP turbine blade has been excellent. Over 460 sets have been delivered to the airlines and to date over 1.7m hours of service experience have been accumulated. The longest life set has achieved more than 10,000 hours and cyclic experience on one set has now passed 4850 cycles.

There have been opportunities during this four year period to assess the condition of blade sets after service experience. The report on one set of blades at 5204 hours/1432 cycles is typical. There was very little evidence of foreign matter on the aerofoil surfaces and no blockage of the film cooling holes had occurred. This confirmed that in attempting to simulate service conditions as accurately as possible the decision to clean the second and third sets of intensive cyclic endurance blades was correct.

Three distinct types of crack were evident on the blades. Twenty five blades (out of a set of 102) had pressure surface interlock cracks in the shroud. Twenty nine blades had radial cracking from the bottom holes of the second pressure surface film row. Two blades had trailing edge film row cracks. Cracking at these three sites (Crack types 1, 2 and 5) was identical to that observed during the intensive cyclic endurance testing which had demonstrated that the cracks propagated slowly and without hazard.

There was also evidence of leading edge erosion on all the blades. This erosion is caused by deposits of carbon building up on the fuel burners and then impacting the blade leading edges when shed. The erosion is common on early marks of RB211 and is not peculiar to the cast DS turbine blade. Whilst leading edge erosion may ultimately limit the life of the cast blade in service, the problem itself could not be addressed by the blade design. The solution lies in eliminating the carbon build-up on the burners and this has been achieved on the later marks of RB211.

Only two other types of cracking have been observed in service blades. One type concerns the cooling air tube which is brazed into the blade shank. A very small number of early blades have exhibited hairline cracks in the tube. The possibility of cracked tubes was discovered during other development testing and although the crack risk was very small, a material change was made in 1980 to eliminate the problem. No cracks have been observed with the modified material. The only other type of cracking seen during inspections of service blades has been a very few instances of trailing edge fillet radius cracking associated with compressive creep. The cracking coincides with the tail off of a partial directionally solidified grain. Blades with a partial grain of this type are acceptable within the quality acceptance standard and so cracks of this type are possible. Experience indicates that cracks of this nature do not propagate at a significant rate and do not present a hazard.

Since entering airline service there have been only four engine removals as a result of the cast HP turbine blade. In none of the four cases has the basic design of the blade been the source of the problem. Three of the four removals were caused by manufacturing defects. Three blades with quality problems out of a total of nearly 47,000 blades delivered to the airlines represents only 0.006%. Whilst this is an excellent record, quality control procedures have been introduced to improve the situation still further by ensuring that blades with similar defects are discovered during manufacture. The fourth removal was caused by a small piece of metal, probably swarf, entering the blade through the air cooling hole in the base of the blade and blocking off the air supply. Subsequent investigation led to modification of the assembly quality control procedure.

The general service situation is excellent. Since service introduction in 1979 the blade has proved that the design and reliability have achieved the criteria originally specified. Indeed it is clear that on typical service operation the cast HP turbine blade will last considerably longer than the 10,000 hours originally specified. However even before this situation had been demonstrated in service, there was considerable confidence that no major problems would occur. This confidence was based on the development programme and intensive cyclic endurance testing carried out prior to service introduction. The use of this type of testing to represent service performance convinced Rolls-Royce that the cast directionally solidified turbine blades would finally fix the persistant reliability problem of the RB211-22B HP turbine.

8.0 CONCLUDING REMARKS

Following the successful demonstration of the cast directionally solidified HP turbine blade in the intensive cyclic endurance programme, cyclic testing is now used to test all major developments of the RB211. Component life and reliability lessons learnt during the intensive cyclic endurance programme were used in the design phase of the later RB211-535C and -E4. This allowed production of components that would survive an arduous development cyclic programme and this in turn led to a better product when introduced into passenger carrying service. A comparison between the service introduction of the -535C and the earlier service introduction of the -22B, Fig:7, shows the level of improvement attained. A significant proportion of this increased reliability has come about because cyclic endurance testing, which has its origins in the successful intensive cyclic endurance programme on the DS HP turbine blade, is now a normal part of engine development.

9.0 ACKNOWLEDGEMENTS

We wish to thank the Directors of Rolls-Royce for allowing us to present this paper and also to thank those of our colleagues who helped in its preparation.

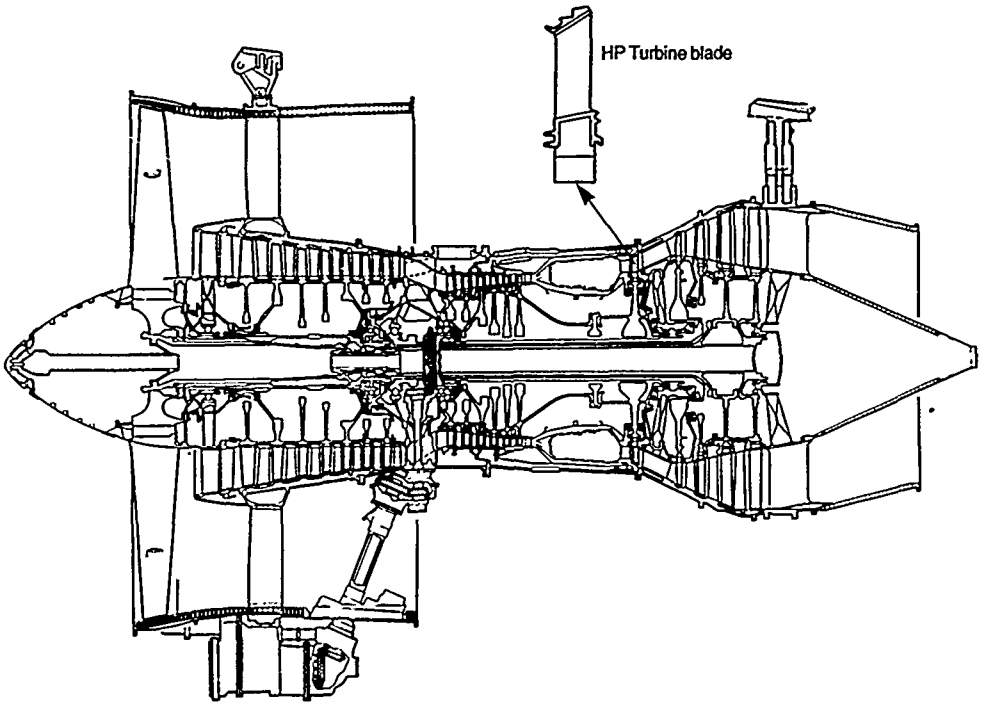

FIG.1 RB211-22B GENERAL ARRANGEMENT

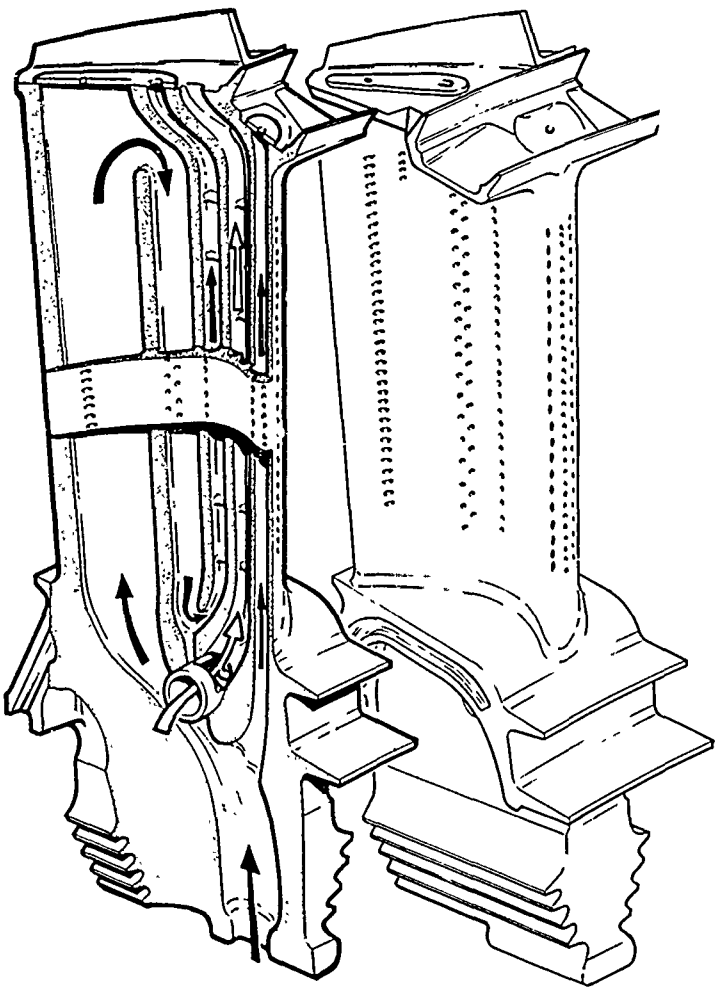

FIG.2 RB211–22B CAST HP TURBINE BLADE

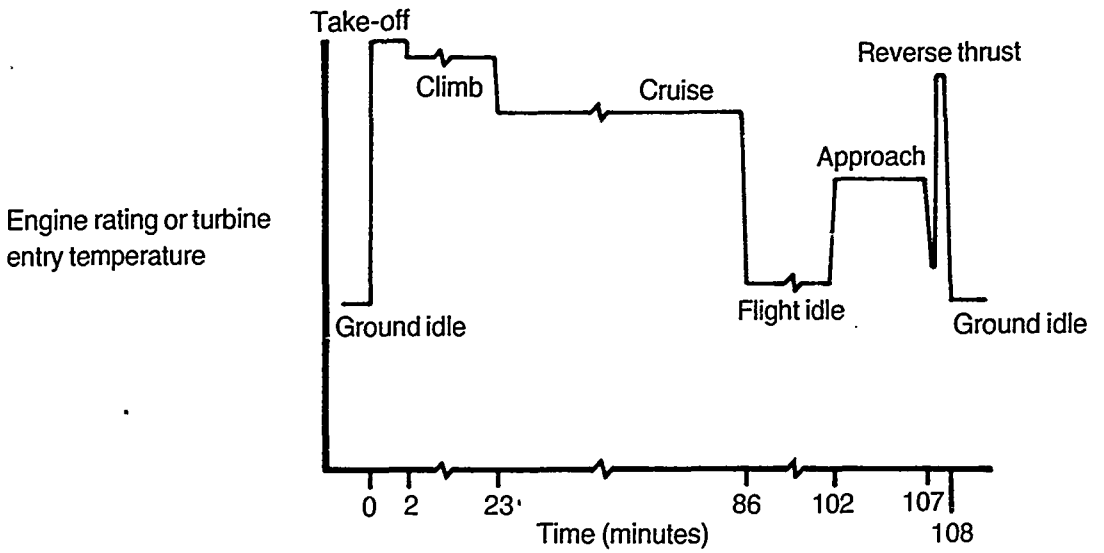

FIG. 3.1 SCHEMATIC REPRESENTATION OF TYPICAL FLIGHT OF RB211–22B

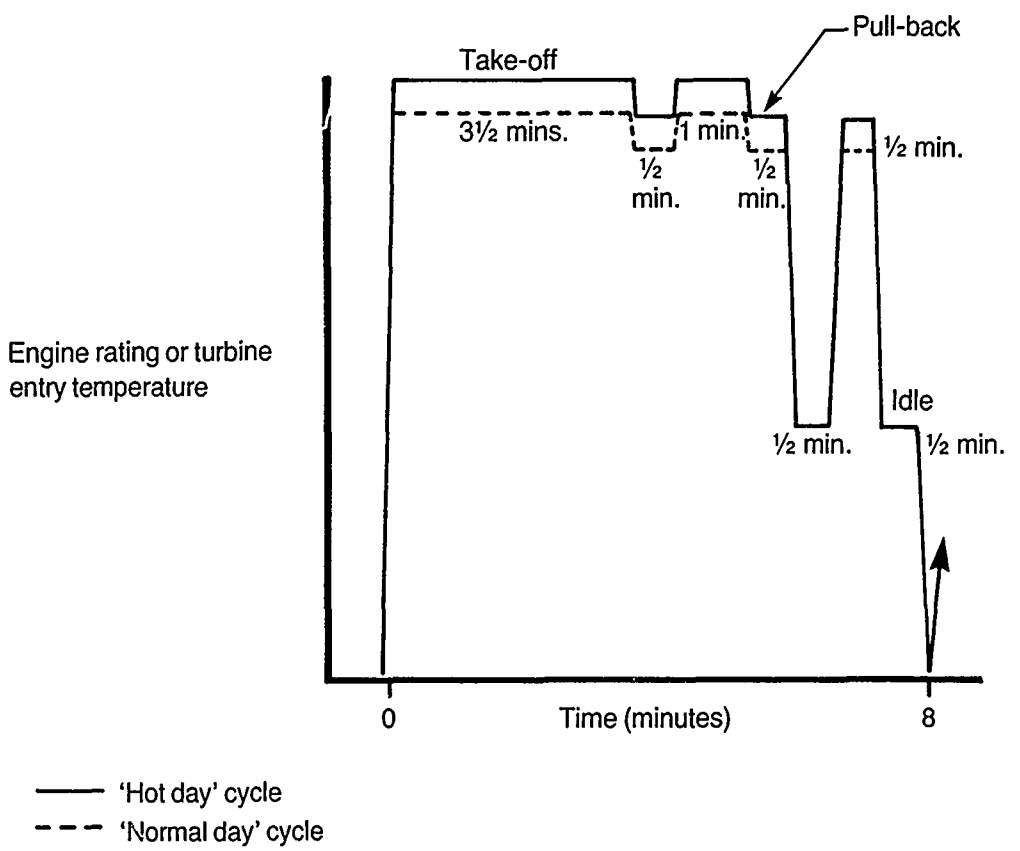

——— 'Hot day' cycle
– – – 'Normal day' cycle

FIG. 3. 2 SCHEMATIC REPRESENTATION OF TEST BED CYCLES

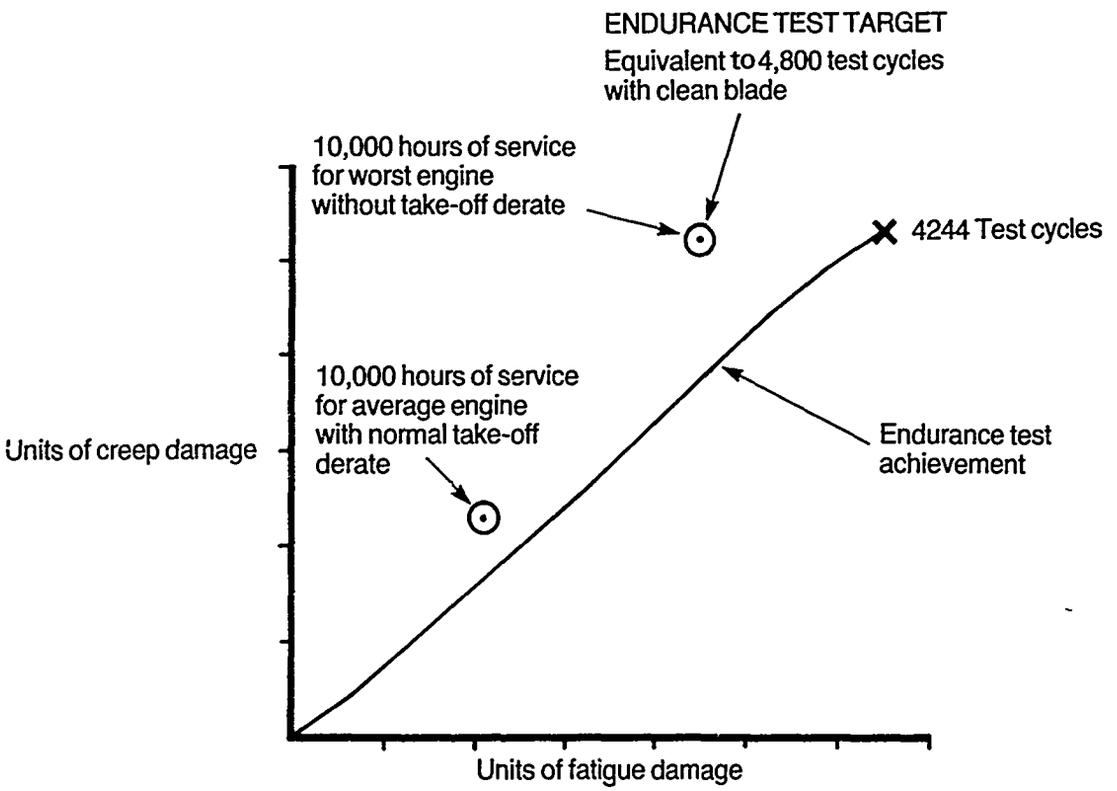

FIG.4 COMPARISON OF THERMAL DAMAGE IN SERVICE AND ON TEST

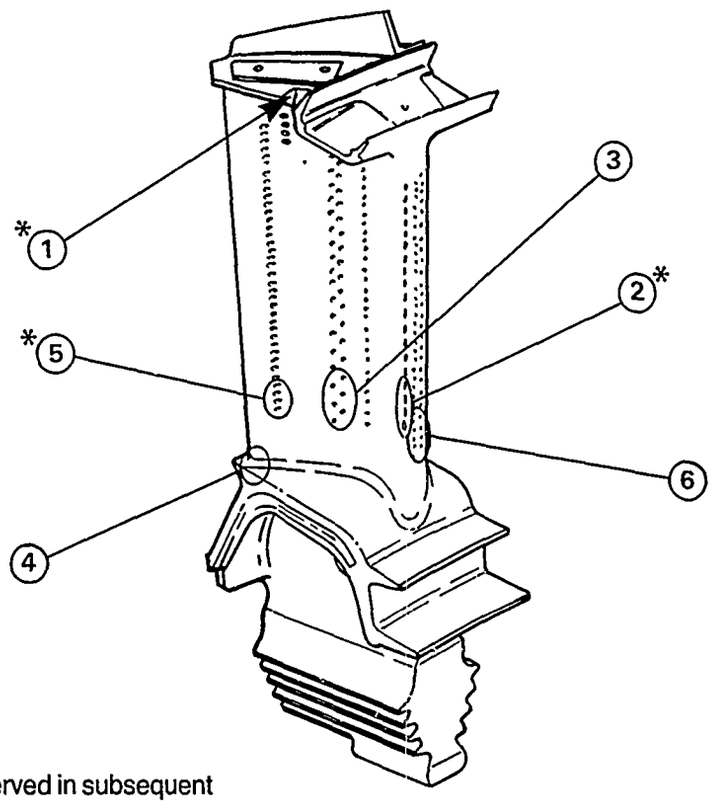

* Cracks observed in subsequent airline service – see section 7.0

FIG.5 RB211–22B DS BLADE CRACK LOCATIONS AFTER 4244 TESTBED CYCLES

HISTORY OF CRACKING ON SECOND SET OF BLADES Fig:6

Number Of Cycles	767	1460	2077	3001	3444	3844	4244	Comments On Cracks At 4244 Cycles
	percentage of blades with particular crack type							
Crack Site								
1. Edge of shroud interlock hardfacing	85%	100%	100%	100%	100%	100%	100%	After initial phase, very slow growth
2. Radial cracks from bottom holes of 2nd pressure surface film row	50%	85%	100%	100%	100%	100%	100%	Affecting holes up to mid height - cracks up to halfway through section
3. Radial cracks near foot of 2nd pass of triple pass cooling system		40%	82%	91%	95%	95%	95%	Up to 0.25 inch in length
4. Trailing edge) oxidation, root fillet) cracking radius)			(5% (' 1%	46% 10%	72% 11%	78% 11%	88% 14%	Up to 0.05 inch in length
5. Axial cracks towards trailing edge from bottom holes of last film row			2%	51%	59%	60%	80%	Maximum length 0.024 inch - typical length 0.001 to 0.010 inch
6. Axial cracking between two leading edge film rows					5%	85%	90%	Extend over lower ¼ of blade - cracks have little depth
Other sites				isolated blades with root platform cracks			one blade with severe crack caused by an inclusion	

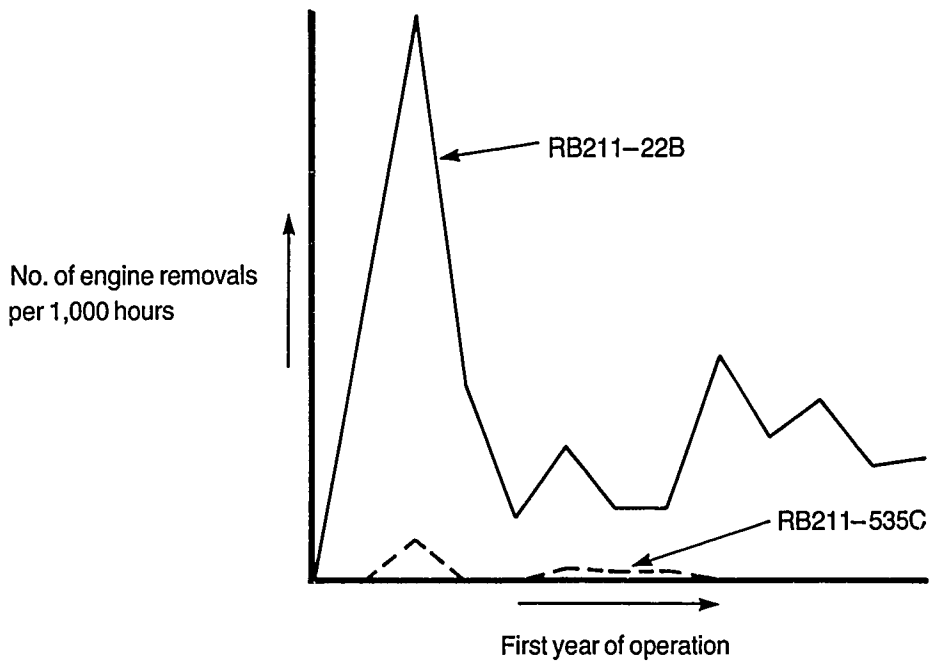

FIG.7 COMPARISON OF FIRST YEAR OF OPERATION RB211-22B Vs RB211-535C

DISCUSSION

D.K.Hennecke, Ge

You said that you want to expand your representative cycle to include the other engine components besides the HP turbine blades. Do you suggest that you can find one cycle that will be representative for all components?

Author's Reply

No, clearly a cycle designed specifically to test one component will not accurately represent the service environment on other components. We do, however, believe it is possible to design a cycle that is reasonably representative of the service environment experienced by the hottest components in the engine. The use of spin pit tests for the cooler components is still the main method of testing those parts to representative service lives.

D.K.Hennecke, Ge

When you ran the tests with the cycle shown in Figure 3.2, i.e., a cycle devised for the HP turbine blades, how did the other components react, especially the combustor, the NGV's, the IP turbine, the turbine discs, and the turbine casing?

Author's Reply

In general, satisfactorily, though as this test was designed specifically to test the H.P. turbine blade, other components were, if necessary, replaced part way through the test rather than allowing them to reach their full lives and stopping the test prematurely as a result of their failure.

P.Ramette, Fr

For an endurance test of HP turbine blades, the dusting of the blades due to combustion products has to be taken into account. Don't you think that the 4200 cycles test that you presented for which the blades have been cleaned six times, every 700 cycles, is not very representative of real test conditions in service?

Author's Reply

The products of combustion that are most harmful to H.P. turbine blades are hard particles of carbon. The testing done did not represent the effect of carbon. However, it was felt at the time that this problem should be addressed by modification to the combustor rather than development of the turbine blade and hence this limitation to the testing was accepted. This approach has subsequently proved correct as carbon erosion has been eliminated by combustion and burner modification.

A.A.Martino, US

Is Rolls Royce developing an AMT for military engines? (The paper showed a civil application).

Author's Reply

The need for Accelerated Mission Testing on military engines is recognized by Rolls Royce. The introduction of cyclic testing for component evaluation is steadily increasing in both civil and military applications. Clearly, the cycle shown in this paper is not intended to be representative of a typical military engine flight.

J.R.Nelson, US

You noted an 8-minute cycle, shutdown, picked up by starter just before complete spooldown, then restart of cycle. We, in USAF, have found cooldown between cycles is important and use motoring of the engine between cycles to gain cooldown Would you please comment.

NOTE. I understand your concern was with the blades which cool down quickly, but you were also looking at the other components, as you stated, and if you are concerned with turbine discs, cooldown is very important.

Author's Reply

The effect of the additional cooling introduced between cycles by stopping the engine would only have a minor effect on the turbine blade which cools relatively quickly. The spooldown that was done as part of the cycle reduced the H.P. rotor to 10% of its maximum speed, compared to an idle speed of 60%. The total time that the shutoff valve is closed is between ½ and 1 minute. This is believed to be sufficient for evaluation of the turbine blade. If cyclic evaluation of the discs is also required then clearly your experience indicates that a longer shutdown time is required.

VERIFICATION OF LIFE PREDICTION THROUGH COMPONENT TESTING

by

Richard J. Hill
Turbine Engine Division
Aero Propulsion Laboratory
Air Force Wright Aeronautical Laboratories
Wright-Patterson AFB OH 45433
United States of America

SUMMARY

This paper gives a status report on the results of current rig and component testing being conducted under the Life Assessment Testing (LAT) approach to turbine engine durability validation. The focus of the paper is the combination of using material of reduced life capability and creating conditions of higher stress to produce short-time failure for cost effective validation of the tools and rules of life prediction. The three components discussed are combustors, compressor disks and turbine blades.

I. BACKGROUND

During the past two decades since the coming of age of Low Cycle Fatigue (LCF) as a dominant gas turbine engine failure mode, the gas turbine engine industry has been struggling with the problem of defining a system of units for component life measurement and a method for component life assessment. Prior to this point in time, the only necessary unit to measure life was hours, and the assessment method was the testing set forth in standards such as MIL-E-5007, and 5009. LCF, however, is a failure mode that results from the repetition of time independent load intensity (stress) events. As such, a new additional unit needed to be established such that all who became involved with defining the life of engine components could communicate on a common basis. Many variations of the term "cycle" have been proposed and used for this additional purpose. However, each "cycle" has only true meaning for a specific engine, manufacturer, organization or design group. Many of these "cycles" appear in Figure 1.

The type of cycles in Figure 1 grew spontaneously and was basically a result of a need to describe the physical limitations of an engine or component, beyond hours, in terms that were understandable to a customer with specific applications. In addition, since most customers demanded a proof test of the engine's cyclic life prior to acceptance of life values, a test had to be devised and conducted which in a very short time (to reduce test costs) would validate a large life value. Thus, adjectives like "advanced," "accelerated," "severe," etc., were combined with the cycles to produce a description of a new test that could be run and be capable of "demonstrating" the inherent long life. These type tests are successful and beneficial when the engine's usage and failure modes are well known and such tests are typically classified as "Accelerated Mission Testing"--AMT. However, during early engine development when an engine is comprised of components of advanced design or material and the intended usage is unclear, AMT results are difficult to quantify and any needed life development effort becomes hard to define and focus. As a result of this difficulty, a new testing philosophy was developed for use in the assessment of advanced development component "design ability." This new approach is based upon the use of failure mode testing by controlling component stress levels during the test as opposed to mission related AMT testing. This testing philosophy is termed Life Assessment Testing (LAT) and it is currently being evaluated as a means of supplying data on the life development of new component configurations by assessing the "tools and rules" used in design.

II. LIFE DEVELOPMENT

Unfortunately, we are unable to design and build engines where each component has an identical life. Therefore, we must try to accurately predict, verify and develop the life of each component in a cost effective, but standard way, so no confusion exists on an engine's structural integrity as a unit.

In the area of component life development, there are major problems such as:

a. Definition of how much life is satisfactory.
b. Establishment of failure criteria.
c. Configuration control during development.
d. Definition of usages.
e. Quantifying boundary conditions on components for each usage.
f. Establishment of durability baselines of components.

Of these problems, the establishment of each component's durability baseline is the most important and currently, most difficult to solve. In addition, it must be solved prior to any use of the component in a production program--it must be characterized during development.

III. DURABILITY BASELINE TEST APPROACHES

As shown in Figure 2, there are basically three approaches to testing components for durability--"whole" life, "potential" life and "reduced" life. In "whole" life, one would test the

actual component under actual, real spectrum loads until failure occurs. This type of testing produces a one-to-one mapping of the test data on actual life expectancy. The "whole" life approach is the best data, but it is also the most expensive and may take a long time to acquire.

The "potential" life approach involves testing the actual component to actual real-time spectrum loads but for only a set percentage of life--not failure. With this method, it is very hard to determine what percentage of life should be exhausted and it is very difficult to quantify the amount of life demonstrated without a calibrated residual life test.

The "reduced" life test approach involves either manipulating the component geometry to produce a "short life" specimen or creating an overstress on the component by changing the environment or both. This method gives a cost effective assessment of the tools and rules of design by allowing the test article to be tested to a failed state in a short test time. The only difficulty in this method is the assurance of maintaining the proper failure mode in the manipulation of the component or the boundary conditions. Methods of higher stress inducement may be faster load rates, use of artificial stress risers, more severe thermal gradients, higher temperatures, use of lower strength (characterized) materials and coatings, high mechanical loading, or combinations of any of these methods.

IV. LIFE ASSESSMENT TESTING (LAT)

The LAT philosophy uses both the "potential" life and the "reduced" life approach to supply a baseline durability characterization of a component's design by validating the "tools and rules" of the design process. These tools and rules are the aero-thermal models, heat transfer models, secondary flow models, stress models, life models and material characterization. The actual testing under LAT can be the testing of a component on either a bench, rig, core or full engine or a combination of these methods. The key to LAT testing is the creation and control of the test by using loads and temperature (stress/strain) rather than mission usage (throttle motion). This requires the LAT tests to be fully instrumented to quantify the component's boundary conditions such that "valid" data is obtained for use in correlation of the tools of design. The instrumentation may be applied for a short duration (first build) and removed for the rest of the test (second build). In addition, other builds may be used to creat a more cost effective program. Most importantly however, the test series must end in "failure" of the component. Failure may be defined as visual distress, crack initiation, fracture to a predetermined crack length or depth, non-recoverable deformation or warpage. The uniqueness of design, material or structural function plus the consequence of "failure" determines which definition is applied to which component. The achievement of failure is the only way of fully quantifying the accuracy of the life prediction. If failure cannot (should not) be achieved in the engine, then a "residual" life test must be run in a subsequent rig or bench test. A durability baseline can only be established on a component through the use of validated tools and rules of design. Without this being done, the testing accomplished on the component is only qualitative in nature and difficult to correlate to past experience.

The LAT approach is currently being applied to combustor liners, turbine nozzles, turbine blades, disks and spacers with success. The remainder of this paper will discuss the application and results of the LAT approach as it is being applied to a cooled turbine blade, a compressor disk and a segmented combustor.

V. LAT APPLIED TO A TURBINE BLADE

A film-cooled turbine blade is a very difficult component to test to validate a life prediction. An attempt at using a "core" engine (compressor, burner, turbine) as a slave test bed to evaluate a turbine blade has been conducted with reasonable success. The LAT turbine blade test involved the two classical failure modes of turbine blades--stress rupture and low cycle fatigue.

1. Blade Rupture Test

The turbine blade was first evaluated in terms of stress rupture design ability by using the "reduced" life test approach. In order to have a higher stress on the airfoil than what normally would be found in the engine environment, ten leading edge suction side cooling holes were omitted from the castings of 43 blades of a blade set. The remaining blades in the blade set were not changed to provide a direct correlation between the modified and unmodified blades. This is shown in Figure 3. In addition, each blade was flow checked to determine the percent of cooling flow consumed by each blade. Complete heat transfer, stress and life analyses were then accomplished in order to predict the actual test time required to form a rupture crack at the "critical" blade location during the core engine test. Both the heat transfer and stress models had prior validation. The goal of this test was to make each airfoil a separate specimen for life prediction validation only. The ordering of life by blade serial number is shown in Figure 4. As shown in Figure 4, the first blade failure was predicted to occur at 48 hours into the core test with subsequent failures predicted up to 200 hours. The test was run with inspections at 50, 90 and 120 hours accumulation with the end result of no measurable distress on any of the airfoils. At the 120 hour timepoint, it was decided to stop the stress rupture test and reinstall instrumentation to precisely determine the temperature of the airfoils without the cooling holes to revalidate the heat transfer predictions.

The results of this heat transfer test showed that the original heat transfer model was in error in that no effect of the loss of cooling flow could be detected. The temperature in the "stress rupture zone" with and without cooling holes was essentially identical. Using this data and re-exercising the blade rupture life prediction model showed that no failure should have occurred within the 120 hour test time. Based upon this data, a switch from "reduced" life to "potential" life testing was made and the rupture blades were removed from the core engine for a residual life test to confirm the stress rupture life calculation. This is discussed below.

2. Blade Low Cycle Fatigue Test

The core engine test bed was refurbished and a mixed turbine blade set was built up. The turbine wheel contained standard airfoils with zero hours of rupture time, 50 hours of rupture time and 90 hours of rupture time prior to this build's testing. In addition, two "rupture" blades from build one were drilled to standard configuration and added to the wheel. Since a synergistic life model was not available, only the non-rupture damaged blades had an LCF life prediction made. The cycle created for damage inducement was thermally severe to the extent that the LCF failure was predicted to occur in 400 thermal cycles. The test was run to 1800 cycles total and the results were that each type of airfoil on the wheel had initiated LCF cracks in the predicted location starting at near the 500 cycle point with one of the first "failures" being the high time rupture airfoil. This data is shown in Figure 5. It should be noted that all cracks could be seen with borescope inspections. Figure 6 shows a typical crack after the completion of the total test duration of 1800 cycles. In comparing the LCF prediction to the first crack formation on the virgin blades (Figure 5), the results were that the prediction was conservative by a factor of two. Considering the material scatter and other variables the LCF life prediction capability was determined to be satisfactory.

3. Residual Life Tests

In order to establish the validity of the rupture predictions and further quantify the LCF predictions, several blades were cut up into small specimens as shown in Figure 7. These specimens were tested by a standard material test method to final failure. Virgin blade, rupture exposure only, LCF exposure only and combined exposure specimens were all tested and compared. The results of this testing were inconclusive due to "size" effects of the specimens and the difficulty in "gripping" them during the test. However, the data did indicate that no life degradation occurred with combined exposure. This residual life test method is currently being refined and tried again on a new set of damaged airfoils. When this data is in hand, a good baseline durability will have been established for this turbine blade.

VI. LAT APPLIED TO A COMPRESSOR DISK

The application of LAT to a compressor disk centered upon validating both stress analyses and life prediction models to create a baseline durability understanding of a titanium compressor disk of advanced design. In order to validate the techniques, the subject disk was analyzed in detail to a composite mission profile. Based on this analysis, an over-stressed, compressed time, spin pit cycle was created to damage the disk in the same failure mode and locations as the real time composite cycle. The spin pit tests conducted correlated very well to the pretest predictions and thus validated the stress and life prediction techniques and thereby established a good baseline durability understanding.

1. Disk Structural Analysis

The purpose of the structural analysis was to identify the critical locations in the compressor disk by defining the stress/strain levels at the critical locations due to the composite mission profile. These analyses provided the basis for establishing a cyclic spin test and life prediction. The mission points were based upon the composite duty cycle shown in Figure 8.

The structural analysis of the compressor wheel involved both two- and three-dimensional (2D and 3D) finite element techniques. The finite element analyses were performed with a contractor propriatary computer program which offered a wide variety of user options and analysis capabilities. The 2D axisymmetric analyses performed during the structural life prediction effort used 12-node axisymmetric isoparametric elements. The 3D stress analyses used 20-node solid isoparametric elements. Because the 2D axisymmetric analysis does not recognize stress concentrations at bolt holes and dovetail slots, it is used to determine "nominal" stresses and to obtain boundary conditions for the more detailed 3D analysis. The implied assumption is that the boundary conditions do not significantly affect the accuracy of results evaluated at points remote from the boundary.

Boundary condition loads, representing the effects of the bolted flange connection and radial pilot fit, were obtained from the 2D axisymmetric analysis. In addition to centrifugal forces, the loads applied to the 3D model included airfoil gas loads, internal cavity pressures, and a temperature gradient.

Results of the first analysis, Run 1, indicated that the 3D model was not sufficiently detailed for accurate stress results. This was evidenced by the existence of large stresses normal to free surfaces, particularly in regions of high stress gradients. Consequently, the 3D model was refined by subdividing the elements along the bottom surface of the dovetail slot and by making the axial spacing of the elements more uniform. Figure 9 shows the progressive refinement of the stress model and Figure 10 shows the reduction of free-surface stress indicating increased accuracy of the 3D model. The final stress "model" consisted of a 2D boundary condition generator and the 3D wheel lug submodel (Run 4) being evaluated at required conditions.

2. Disk Life Model

During the program, several damage accumulation models were compared using standard material life curves and various specimen tests. The specimen tests examined the loading order and magnitude as variables and were representative of engine induced cycle loading. The most accurate model was a nonlinear model of the form shown in Equation 1.

$$D = (n_i/N_i)^{\alpha_i} \qquad \text{Eq. 1}$$

[α_i is a function of the fatigue life (N_i)]

Figure 11 shows the nonlinear damage curve. For mission type loading conditions, the nonlinear rule cumulates damage in the manner illustrated in Figure 12. The illustrated mission consists of n_1 of the N_1 type cycle and n_2 of the N_2 cycle. By adjusting the relative value of alpha for each type of cycle, the longer life cycles can be made more damaging. A functional relationship between alpha and fatigue life (N) is therefore necessary to apply this nonlinear rule.

A second order polynominal in log-log space was judged to provide a good fit for the derived data and is shown in Equation 2.

$$\log \alpha_1 = b_0 + b_1 \log N_1 + b_2 (\log N_1) \qquad \text{Eq. 2}$$

3. Disk Life Prediction

The cycle shown in Figure 13 shows the spin-pit cycle derived to exhaust the life of the disk in the same failure mode (LCF) and location (dovetail slots) as the composite cycle. The test used higher stress and higher temperature (500°F) to accelerate the damage. Using this cycle and exercising the stress and life models gave a mean life prediction of 3981 "mission" cycles. As a further assessment of the life prediction accuracy, a Monte Carlo simulation of the principal variables involved in the test was conducted to determine sensitivity effects. They are as shown in Figure 14.

In addition, one final evaluation of life sensitivity, that concerning the ability to calculate the correct stress level was made. The intent was not to do a Monte Carlo simulation but merely to make a cursory analysis. The analysis was made to determine how the life prediction would differ if the calculated stesses had been 10% lower than the actual stresses. If this occurred, the life prediction would have resulted in a 60% higher life value. However, the correlation between predicted and measured strains for the disk in the spin-pit was excellent at the location of eventual failure (the dovetail slot).

4. Assessment of Disk Life Prediction

The predicted "mean" wheel life of 3981 missions was based on the initiation of LCF cracks in the aft end of the dovetail slots. Furthermore, the analysis predicted that the life scatter band represented by plus and minus two standard deviations was 7726 to 2050 missions respectively.

Two wheels were subjected to cyclic spin tests. In the first wheel, LCF cracks were discovered in 36 dovetail slots after 3000 missions. In the second wheel, cracks were discovered in three dovetail slots after 3110 missions.

Based on the excellent correlation between failure location as well as predicted life, it has been concluded that the analytical life prediction techniques for compressor wheels do a very good job of assessing life. Although the two test wheels initiated cracks slightly earlier than the mean prediction, it is readily recognized that two tests give only limited statistical inference of the true mean wheel life. The true significance of the correlation between the predicted and test results is that the life of a component having a complex geometry and being subjected to variable amplitude loading was predicted analytically with a degree of accuracy commensurate with current needs. In addition, as a result of these techniques being applied to the subject wheel of advanced design, a good durability baseline has resulted. The program also showed the LAT approach of creating an artificial early failure to validate the predictive technique is a valid approach.

VII. LAT APPLIED TO A COMBUSTOR

One of the new design options for combustors is to thermally "release" the hot inner liner from the cool outer shell by flotation and segmentation of the inner liner. This type of design uses small inner wall segments in a "shingle" style of structure to allow for differential thermal expansion to occur. Such a combustor is shown in Figure 15. This type of design effectively eliminates the classical failure mode of Low Cycle Fatigue in combustors. With the elimination of the LCF failure mode, the oxidation/erosion (O/E) failure mode becomes the largest life concern.

Currently, a series of tests are being conducted in a LAT program on 30 segments of a segmented combustor to validate that LCF is indeed no longer a failure mode of concern and to create an adequate prediction capability for an oxidation/erosion failure mode. The testing uses both pre-damaging and reduced strength material as a means of accelerating the rate of damage accumulation in keeping with the LAT philosophy. The testing scenario is shown in Figure 16.

1. Combustor LCF Test

For the LCF portion of the test, 16 segments are being tested as shown in Figure 16, of which, nine segments were pre-damaged in a bench rig for 1100 mechanical and thermal cycles of an engine equivalent strain range. The bench rig was a "4-point bend" rig heated by quartz lamps. Of the nine specimens, four were taken to failure after the engine 1, build 1 test in order to establish a baseline of this test and the remaining five are/will be built up in subsequent core and full-engine tests to accumulate damage at "normal" engine AHT rates. Thus far, a significant number of LCF cycles (2471) have been accumulated with no visable damage. Upon completion of an additional 1350 Type I* cycles 9000 Type III* cycles, all five segments will be taken to the laboratory for final failure in the bench rig for a final residual life determination. As part of the same series of tests, seven segments were tested in a non-predamaged state. Of the seven, four were taken to failure after the engine 1, build 1 test in the same bench rig as the predamaged specimens but at an accelerated rate, and three are used in each build of the core and full engine for a back-to-back comparison to the predamaged segments.

Except for the pre-damaging, all the bench rig testing to failure is being done at strain ranges nearly 10 times greater than the engine produced strain range in order to have cost effective test times. Thus, the results expected from this LCF test are as follows:

a. Correlation of "accelerated" bench testing to "engine condition" bench testing of segments.
b. Correlation of "pre-damaging" to "non-predamaging" of segments.
c. Correlation of "engine" damage to "rig" damage for pre-damaged and non-predamaged segments
d. Assessment of the LCF life models for bench and engine tests.

2. Combustor Oxidation/Erosion Test

The second part of the combustor LAT program was to create an oxidation/erosion model. Since the total test duration available is short (254 hours maximum), a lower strength, characterized material is being used as a means of creating the empirical model in addition to the standard segment material. Both materials are used in the uncoated condition to further accelerate the rate of O/E during the test. Five segments of uncoated standard material A are used as a baseline for the nine uncoated lower strength material B. This test series is also shown in Figure 16. After the first 29 hours of test, four of the lower strength segments were removed due to a "hot streak" induced local burn-through probably caused by a local cooling flow problem. These four segments were replaced with standard segments and together with the remaining five segments will complete the test. The five remaining "controlled" segments are expected to "fail" before the next teardown. Failure of the segments is when the thickness is reduced by.003 inches. Thus, the results expected from this O/E test at the second teardown are as follows:

a. Correlation of "standard" material to "reduced life" material in an uncoated condition.
b. Correlation of "coated" segments to "uncoated" segments of standard material.
c. Creation of an empirical O/E life model via failure of the reduced strength material.

The model under creation will consider the variables of flow angle , temperature, "scrubbing" velocity and pressure. With this new O/E empirical model in place, further LAT testing of this design concept will supply an acceptable durability baseline for the standard material of the design by the time the 254 hours of total test time is accumulated.

VIII. CONCLUSION

Through the component testing described in this paper and other test efforts, it has been determined that the Life Assessment Testing (LAT) philosophy offers a significant cost effective means of using component testing to validate or create life prediction models and methods. Because of the use and control of stress and strain levels during the test, and by executing the test to failure, the engineer gets a controlled assessment of either analytical or empirically-generated life predictions. Component tests can be combined in series or in "piggy-back" fashion in order to utilize the rig, core or full engine test vehicles to maximum potential. As a direct consequence of LAT testing, a quantitative durability baseline for components can be created. Further life development efforts can then be cost effectively focused to expand from this baseline, in any magnitude deemed necessary, to meet future system needs from a life and durability point of view.

* Type I cycle = zero-intermediate-zero throttle excursion

Type III cycle= idle-intermediate-idle throttle excursion

Figure 1. - Test Cycle Terms

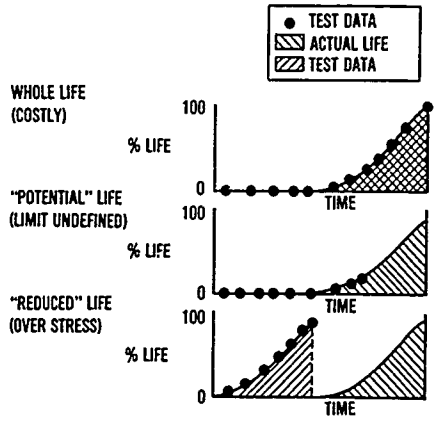

Figure 2. - Durability Test Approaches

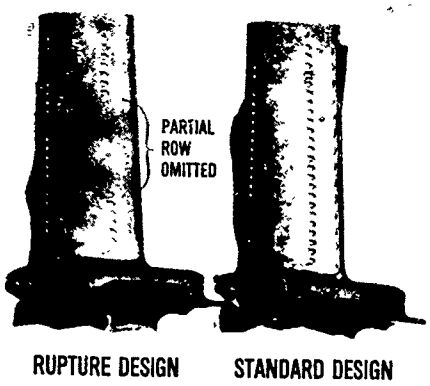

Figure 3. - Test Blade Configuration

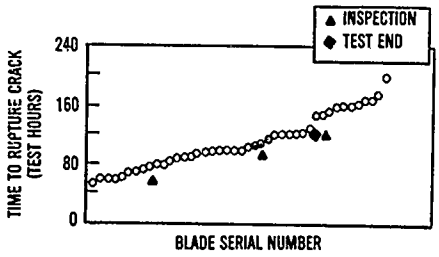

Figure 4. - Rupture Life Prediction Ordering

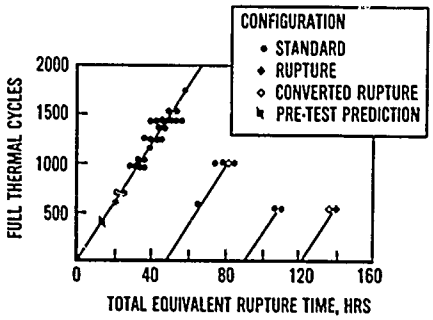

Figure 5. - LCF Test Results

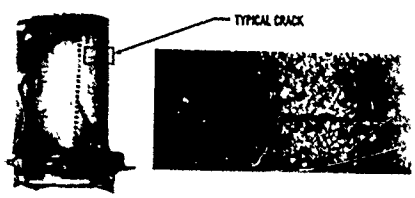

Figure 6. - Cracked Blade

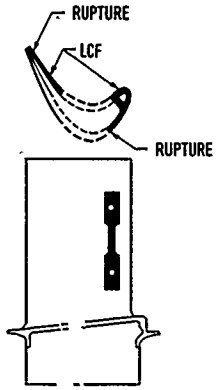

Figure 7. - Residual Life Test

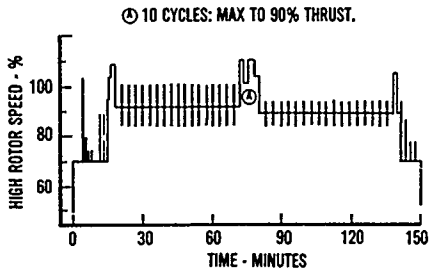

Figure 8. - Composite Duty Cycle

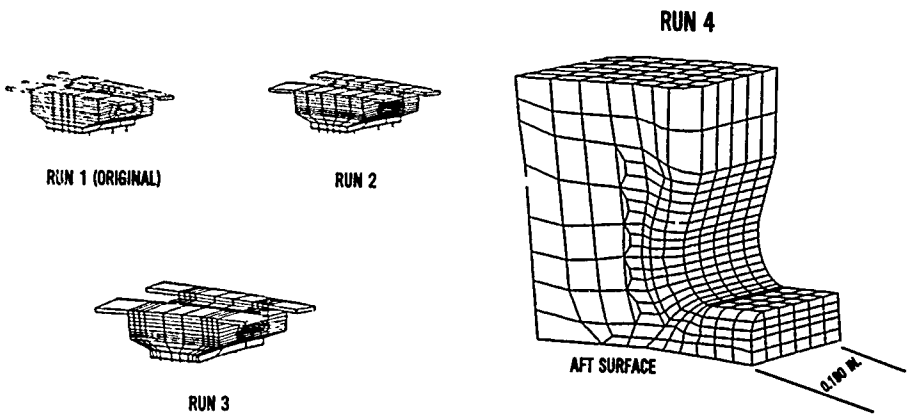

Figure 9. - Wheel Stress Model

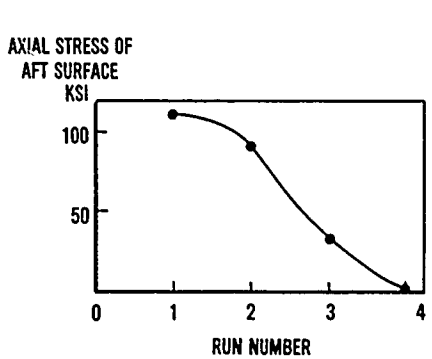

Figure 10. - Stress Model Improvement

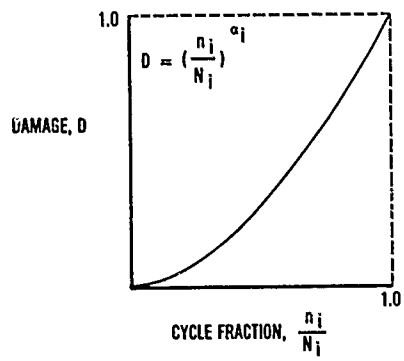

Figure 11. - LCF Damage Model

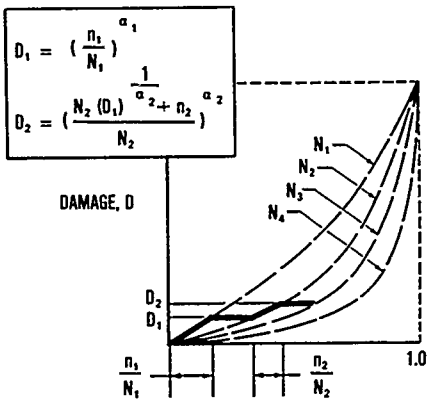

Figure 12. - Mission LCF Damage Model

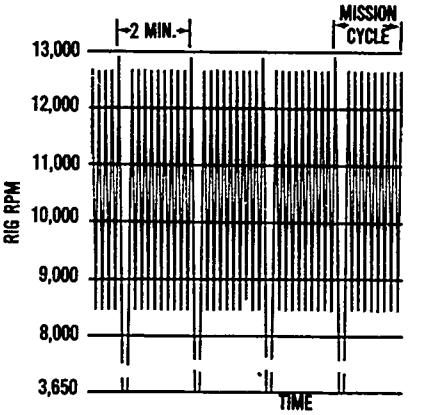

Figure 13. - Spin-Pit Test Cycle

VARIABLE	ERROR	LIFE DEVIATION
DOVETAIL GEOMETRY	MANUFACTURING TOLERANCE	111 MISSIONS
TEST CYCLE	50 RPM	39 MISSIONS
MATERIAL SCATTER	1 STANDARD DEVIATION	1123 MISSIONS
STRESS	10% LOWER	60% HIGHER

Figure 14. - LCF Life Sensitivity Effects

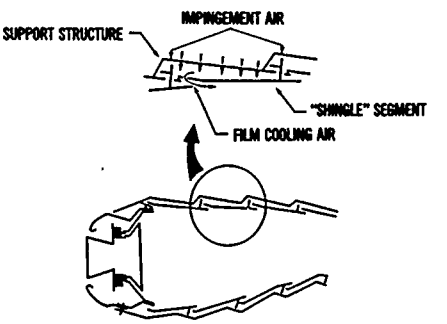

Figure 15.- Segmented Combustor Design

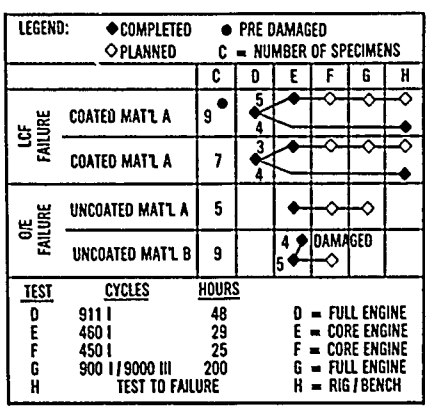

Figure 16. - Combustor Test Plan

DISCUSSION

R.Tadros, Ca,

You have compared LCF test results obtained from different crack locations and different sizes of crack, e.g., in one case three cracks were found and life is quoted, and in another case 36 cracks were found. Don't you think that you have to bring back the life to the same datum, e.g., by doing striation counting, and then you have the relevant lifing numbers to compare with your prediction?

Author's Reply

The programme I described is not yet complete. A striation count will be made and the data will be adjusted in a manner similar to the way you have suggested.

R.Tadros, Ca

In the case of tests in overstress conditions for the purpose of accelerating the tests, have you looked at the situation where plastic deformation can be produced in highly localized stress locations due to the overstress and therefore the LCF test results can be misleading.

Author's Reply

Great care was taken in the creation of the test to insure that local plastic deformation did not alter the prediction beyond what was expected.

D.W.Hoeppner, Ca

The damage parameter used was determined from an LCF data base. How many specimens were used? What test procedure did you use? How did you assure the specimen surface was the same as the disc dovetail slot, particularly the surface quality (finish) and residual stress? Why did you decide on a crack initiation size of 0.030 in.? Why do you call this "initiation" when in fact it is cycles to propagate a crack from some unknown length to the defined detection size? In this sense isn't it cycles to detection?

Author's Reply

(1) There were 100 specimens used in the data base. (2) The test procedure was to ASTM standards using the strain range and mean stress values that were calculated for the critical area of the component. (3) The specimens were generated in such a fashion that the same metallurgical condition was achieved in the test section as that which the dovetail surface would entail — or as near to this as possible. In addition, the specimens were of the same heat of material and produced out of identical forgings. (4) The figure of 0.030 in. for a value of "initiation" was chosen based solely on tradition of an industry practice. (5) The value for "initiation" is indeed a value of number of cycles to propagate the crack from some unknown length to a predetermined size.

D.K.Hennecke, Ge

What cycles did you use for the combustor tests — power settings, number/minute, hold-times?

Author's Reply

The number and type of power settings used in the combustor test are as shown in figure 6 of the paper. A type I cycle is a zero-intermediate-zero throttle excursion and a type III cycle is an idle-intermediate-idle throttle excursion. The intermediate power setting is the maximum thrust of the engine in a non-augmentation condition. The type I cycle gives the maximum thermal strain on the combustor during any flight condition.

MECHANICAL ASPECTS OF HIGH TEMPERATURE COATINGS

Dr. K. Schneider and Dr. H.W. Grünling
Brown Boveri & Cie AG
Dept. ZWT
P.O. Box 351
6800 Mannheim, Germany

High temperature coatings are used for two main functions, either to protect a base metal against corrosion or erosion or to minimize wear. A third function is to reduce the base metal temperature in the case of thermal barrier coatings; however, resistance to hot corrosion and oxidation is again mandatory.

The main functions of such a coating can be fulfilled when the coatings has sufficient resistance to thermal strains and protects the base metal without deterioration. In this paper we describe the strains that arise during the application of a coating - mainly due to thermal expansion mismatch - and during service - due to diffusion, aging and chemical reactions with atmospheres, e.g. the formation of oxides. These strains cause cracks within a coating which reduce its ability to protect the base metal against a corrosion attack.

In the second part of this paper the influence of the coating on the mechanical properties of the coated component is described. In general, a high temperature component is subjected to static loadings - the material undergoes creep - and to cyclic loadings - the component undergoes fatigue. In both cases a coating has some influence either through changes in the material properties due to a different heat treatment or through changes in the surface of a component due to the presence of the coating; hence a coating alters the conditions for crack initiation. From laboratory experience of high temperature coatings applied to gas turbine blades it can be shown that, depending on the type of coating and the method of application, the changes in materials might be positive, negative or negligible.

For all applications it seems to be possible to select coatings without marked effects on the mechanical properties of the base metal. However, it is not always possible to choose the coatings best able to protect the base metal against corrosion or wear, because to achieve mechanical compatibility it is sometimes necessary to use coatings which are not stable for the required lifetimes. In-service examples from gas turbine experience are presented.

1. Introduction

Coatings are used for many engineering applications in order to improve the surface properties of components or structures or to protect them against environmental degradation. Typical examples in high temperature technologies are coatings against (1) high temperature corrosion, (2) erosion and wear, and (3) thermal degradation (overheating)/1/.

Because of its specific task the coating differs from the substrate material in chemical composition, structure and physical as well as mechanical properties. Thus for high temperature applications good chemical and mechanical compatibility between the coating and the substrate material is a main design objective in order to maintain relevant component properties during the designed component life. However, it has to be taken into account that at high temperatures and after sufficient long service times changes occur because of aging, interdiffusion or even environmental effects which additionally may modify specific properties.

In this paper we describe the strains that arise during the application of a coating - mainly due to thermal expansion mismatch - and during service - due to diffusion, aging and chemical reactions with various atmospheres. These strains can cause spallation of coatings or the development of cracks within a coating which reduce its ability to protect the base metal against a corrosion attack. Furthermore, examples of the influence of the coating on the mechanical properties of the coated component are given. In general a high temperature component is subjected to static loadings - the materials undergoes creep - and to cyclic loadings - the component undergoes fatigue. In both cases a coating has some influence either through changes in the material properties due a different heat treatment or through changes in the surface of the component due to the presence of the coating; hence a coating alters the conditions for crack initiation.

Nearly all the examples and test results come from gas turbine materials or from gas turbine field experience but they stand for other high temperature applications as well.

Part of the information presented here is published in /50/. New published data are included to give an up to date version of the subject.

2. Properties of coatings

2.1 Processing

The coating and the substrate are subject to residual stesses during the application process. Stresses can be avoided only when the coating, the interface and the substrate do not undergo phase changes, changes in composition due to diffusion or temperature changes during the production process. It is well known for galvanic chromium coatings that, depending on the deposition conditions, residual stresses develop in the coating which can cause cracking. However, these stresses can be controlled by varying the deposition conditions in such a manner, e.g. by pulse plating /2/, that less harmful compressive stresses are achieved.

For all coatings with a thermal expansion coefficient less than that of substrate (e.g. wear resistant coatings on steel /51/) tensile stresses will develop in the coating at service temperatures above the deposition temperature. To minimize the effect of thermal expansion mismatch coating should be carried out at the highest temperature possible.

That rule might have drawbacks when such a high temperature would cause unwanted changes in properties of the substrate or dimensional instabilities of the part to be coated. So for applications on steel tools a low temperature process like PVD might be prefere in spite of the fact that a high temperature CVD process might reduce stresses at operating temperature /52/.

During thermal spraying of coatings residual stresses develop because the molten droplet hits the substrate, welds to the substrate and is hindered from contracting during the cooling process /3/. These stresses can be so high that cracks appear locally within the sprayed particles, as has been shown for the plasma-sprayed Co-Cr-Al-Y alloy GT 29 on top of Nimonic 75 /4/. The explanation for these cracks is found not only in the cooling process but also in the phase transformation α-Co$\longrightarrow\varepsilon$-Co which leads to a volume contraction of about 1 %. The cooling parameters can be adjusted by preheating the substrate, a procedure which influences the phase transformation and thus the hardness of the coating as well (Fig. 1).

The stresses caused during the application of a coating are dependent on the coating thickness /5/. Even when stress relaxation is possible as a result of high processing temperatures (e.g. with pack cementation or chemical vapour deposition processes) further strains and therefore stresses will be introduced due to the mismatch in thermal expansion coefficients of the coating and the substrate. As a guide-line it is quoted /6/ that the thermal expansion mismatch between the coating and the substrate should be less than $2 \times 10^{-6} {}^{\circ}C^{-1}$ to prevent intolerable strains. This might be valid especially for brittle coatings under tension. However, this mismatch gives a total strain range of 1 %-2 % for a temperature cycle between 500 and 1000°C and so determines the cyclic life of a coating.

Oxides have lower thermal expansion coefficients than metals or intermetallic phases /50/, so that compressive strains always occur in an oxide layer after cooling from the temperature of formation or processing. The greatest strains in this case develop when the interface between the oxide and the substrate remains flat. However, in many cases where oxide scales are formed on metallic surfaces, lateral growth leads to a wavy morphology which may have a much higher strain tolerance /16/. High thermal strains also occur in coatings which consist mainly of intermetallic phases or of chromium- or nickel-based materials.

In the case of oxidation additional strains are introduced into the coating-oxide scale interface by the difference in volume of the coating material and the oxidized coating material /17/, a phenomenon which could even prevent the formation of a dense scale.

Whereas too high strains due to thermal expansion mismatch are to be avoided in metallic coatings, there are applications in the field of thermal barrier coatings where the mismatch results from the need to apply ZrO_2 on top of a metallic bond layer. Here the mismatch in thermal expansion can be used to improve the thermal shock resistance of the coating by producing segmented coatings through plasma spraying of the ceramic layer at low temperature /18/. With this definite cracked structure it is possible to minimize residual stresses in the coating plane and to reduce the tendency towards spalling.

However when using thermal expansion data for coatings one has to keep in mind that this property could be non-uniform and might be influenced by residual stresses, crack networks and phase distributions /55/. There can be found differences by a factor of two in Y_2O_3 stabilized Zirconia coatings depending of pretreatment (Fig. 2). The combined effect of tensile stresses in coatings due to phase changes and of thermal expansion mismatch is made clear in Fig. 3. In a self-fluxing Ni-Cr-Si coating /1/ shrinkage occurs as a result of liquid phase sintering. The time of separation of the coating from the substrate, deduced from the existence of a diffusion zone, may be at the beginning of the sintering process.

2.2 Short-term properties

When external loads are applied to a coated material properties of the coating such as the elastic modulus and the yield stress are important because they determine the strain at which yielding in the coating appears. Figure 4 /7/ shows a plot against temperature of the elasticity modulus as well as other mechanical properties for physically vapour-deposited Ni-Co-Cr-Al-Y coatings 1 mm thick. Apparently the trend is similar to that for a nickel-base alloy. No additional strains should appear when a coated nickel-based alloy is deformed.

The high temperature coatings are not always isotropic which causes the effect that the "socalled" Young's modulus could be load and direction sensitive (Fig. 5). In /53/ it is reported that the modulus of elasticity of plasma sprayed coatings is one order of magnitude below that of a sintered material. Another situation which occurs before yielding of a coating has to be considered: Benson /17/ has estimated that in the fatigue mode the surface becomes more resistant to fatigue crack initiation if the elastic modulus of the coating is greater than that of the substrate.

The next most important properties are the thoughness and the ductility of the coating. High temperature coatings very often consist of or contain phases normally considered as brittle: NiAl, chromium oxides etc. The volume fraction of such phases when embedded in a ductile matrix has to be considerable to be useful in increasing the strength and the creep resistance of a material but it should not lead to a deterioration in the ductility. Therefore the ductility is an important coating property that is measured, for example, in a bending test, where the ducitility is defined as the strain at which the first crack appears /19/. Figure 6 /20/ shows that a temperature exists above which the coating shows improved ductility. This cricital temperature is explained as for bulk materials as the temperature at which dislocations within the coating are able to overcome obstacles /21/. For gas turbine applications it is important that below the transition temperature the strains to cracking are quite low and that above the critical temperature, i.e. during operation of a component, the coating materials become ductile and, if their strength is taken into account (Fig. 4), very tough. When cracks are considered, the constraint of the material is an important factor. Therefore the thinner the coating the higher is the ductility at a given temperature /20/.

The coating does not always have the lowest ductility. With at tough coating (Fig. 7 /22/) the coating-substrate interface can be more brittle than the coating itself because of the better hardening characteristic of the coating (here a plasma-sprayed Ni-Cr-Si coating) by good particle dispersion.

The coating procedure has an influence on the mechanical and physical properties of a coating. In the case of low-pressure plasma-spraying it is reported /54/ that the angle of powder feed into the plasma changes tensile properties singificantly, whereas deposition time has no influence.

In addition, the toughness of a coating will determine the toughness of a coated component, a factor important in cutting steels (Fig. 8/52/).

A similar fact is true for tensile properties in general when there is a significant difference between coating and substrate (Fig. 9 and 10 /56/).

2.3 Effects of annealing, aging and service on short-term porperties of coatings

Every thermal treatment changes the composition of a coating by either transforming the coating from a metastable to a stable state or by interdiffusion of coating elements with the substrate. As shown in Fig. 1 /4/ an annealing treatment can be beneficial for the coating because it can minimize the effects of coating process parameters by producing a microstructure typical of the annealing temperature and thus leading to a certain hardness and toughness. In addition, every heat treatment cycle at high temperature induces a diffusion process at the coating-substrate interface and increases the bonding strength as long as the formation of brittle phases and the development of transformation strains or separations (pore formation) can be avoided.

The thermal treatment can already occur during coating, chemical vapour deposition as shown in Fig. 11 /57/ for TiC deposits. The increase in hardness is due to here change in microstructure. At low temperatures the deposit is very fine grained with a network of cavities whereas at higher temperatures the grain size is larger und the fine cavity network has disappeared.

Long-term annealing produces similar effects due to phases changes or interdiffusion. Hence an Ni-Cr-Al coating on an Ni-Cr-alloy, for instance, might lose aluminium by diffusion into the base metal and so the thermal expansion coefficient of the coating would increase (ref. 24, Fig. 5). The formation of brittle phases, probably by interdiffusion in most cases, has the most important effect on the mechanical properties. However, high temperature coatings loose aluminium or chromium to due the production of oxide scales as shown in ref. 1, Fig. 11, where in a Co-Cr-Al-Y coating the dissolution of CoAl particles by hot corrosion attack is evident. This conversion of the coating into a cobalt solid solution increases the thermal expansion coefficient, reduces the strength of the coating and probably increases the coating ductility. Altogether in this example the mechanical properties of the coating should be improved by the long-term attack. However, it is not optimal for the coating's corrosion resistance because of the lower aluminium content.

Another example has been described in refs. 1 and 25 where a coating with a randomly distributed brittle phase (α Cr) in the outer zone was transformed into a coating with a continuous brittle σ phase layer at the coating-substrate interface. Even with this σ phase layer which is brittle at room temperature no toughness problem arose during service for up to 30 000h.

3. Influences of coatings on mechanical properties

3.1 High cycle fatigue

The high cycle fatigue behaviour of materials is very strongly influenced by the crack initiation conditions. Surface imperfections play an important role. In cast nickel-based alloys and in all castings crack initiation is additionally determined by internal pores. In wrought nickel-based alloys the internal particle size is believed to have an influence. In all cases which components or specimens are subject to alternating bending loads the surface is the most prominent crack initiation site.

Under such conditions coatings can determine the high cycle fatigue properties. The main factors to be taken into account are as follows: (1) the high cycle fatigue endurance limit of the coating; (2) the particle size within the coating; (3) the residual stresses in the coating; (4) the surface roughness; (5) the difference in the elastic moduli /17/. At the high frequencies generally used in high cycle fatigue testing, relaxation effects are not believed to play an important role, even at high temperatures.

Probably all the factors mentioned above determine the results obtained with wrought Udimet 520 tested by rotating bending at room temperature (Fig. 12 /26/). It can be seen that none of the coatings reduces the fatigue limit considerably. The increase in fatigue strength can be temperature dependent (Fig. 13 /27/) so that at medium temperatures a reduction in the fatigue strength is found which probably reverses again at higher temperatures because of the better oxidation and hot corrosion resistance of the coating /28/ /29/.

Especially in castings the fatigue strength shows a wide scatter /29/ /30/ so that only trends can be described. It seems that some coatings (e.g. Pt-Al coatings) reduce the fatigue limit but a more pronounced effect is found with long-term annealing. The explanation is that crack initiation switches from internal pores towards the coating or the coating-substrate interface. Here particle sizes and inclusions play an important role in so far as a surface layer or coating can only determine the crack initiation in fatigue if it is much thicker than the inclusion /17/.

The effect of crack initiation site is pronounced when the internal defects are reduced in number and size. So, a unidirectional solidified material has much higher endurance limit than a coated material because of the shift in crack initiation (Fig. 14) especially at higher strain cycles.

A reduction in the endurance limit is always found when the coating is much more brittle than the substrate, as reported in ref. 31 for a plasma-sprayed Al_2O_3 coating on stainless steel where a reduction of about 30 % in the endurance limit of 10^8 cycles is found at 20 kHz.

The fatigue crack initiation can be described as it was found during the interpretation of coated blade failures (Fig. 15). The coating develops cracks by mechanical bending or thermal shock. The coating thickness is sufficiently large that these cracks together with the loading give rise to a greater stress intensity range than the threshold value ΔK_o for the base metal and fatigue crack propagation is possible. In such a situation a reduction in the coating thickness improves the endurance limit considerably, not only by improving the ductility and toughness of the coating but also by reducing the stress intensity range in limiting the possible crack depth.

3.2 Creep and stress rupture

Creep of a material is mainly a bulk process. The application of a coating can influence creep by the following means: (1) heat treatment due to the coating process; (2) long range residual stresses in the substrate; (3) crack initiation due to the coating, starting from either the surface or the coating-substrate interface; (4) diffusion of coating elements into the base metal (especially along grain boundaries); (5) diffusion of base metal elements into the coating (e.g. oxide-dispersion-strengthened alloys); (6) different creep behaviour of coating and substrate. The last fact (6) is felt especially at low strains/56/ (Fig. 16).

With the exception of the first factor all the other coating effects are more pronounced the higher the coating thickness and the smaller the base metal dimensions. This means that an effect which is not felt within a creep rupture specimen 8 mm in diameter might well be pronounced in a thin-walled cooled turbine aerofoil.

As a further long-term effect it should be mentioned that a coating can positively influence the stress rupture behaviour by reducing the corrosion or oxidation attack from the environment. In some cases, an improvement under hot corrosion conditions is not found owing to early degradation of the coating. This has been observed for aluminide and chromium aluminide coatings on top of IN-100/32/. The action of a thermal barrier coating which reduces the substrate temperature and increases the stress rupture properties will no be mentioned here.

A summary of data of superalloys is reported in ref. 28 where it is concluded that, provided that a suitable heat treatment is carried out after coating, no losses in the creep rupture properties should be seen.

However there seems to be a trend that at high stresses and low temperatures diffusion coatings tend to deteriorate the stress rupture properties probably due to an altered starting γ'-distribution and size.

In some cases, e.g. Pt-Al coatings on IN-738 LC, a deterioration in the stress rupture properties is due to the formation of brittle phases in the coating-substrate interface/37/. This behaviour is more pronounced the thinner the substrate.

3.3 Low cycle fatigue and thermal fatigue

A typical load situation for high temperature materials is thermal fatigue, in general a simultaneous change in temperature and stresses, which leads to local deformation of a component. From the summary of test results reported in ref. 28 it is concluded that no negative effect due to a coating on the low cycle fatigue properties of nickel- and cobalt-based superalloys can be found in cases where the coating can be deform easily, i.e. above the ductile-brittle transition temperature and below a maximum coating thickness. Examples of such test results are shown in Fig. 17/38/. To perform tests more related to operational conditions so-called thermal-mechanical fatigue tests have been used/7//39/ in which the temperature and strain range are cycled. As in all loading conditions where temperature changes occur the thermal expansion mismatch $\Delta E\alpha$ becomes important (Fig. 18 /39/). A common scatter band of different base metals can only be achieved when the mismatch $\Delta E\alpha$ between the coating and the substrate is added to the thermal-mechanical strain range ΔE_{TM}.

In the most common tests for thermal fatigue, however, an attempt is made to simulate the real operation either by using component-simulating sepcimens ("Glenny discs") or by performing cyclic oxidation or hot corrosion tests to investigate the behaviour of the proctecting oxide scale. The experimental parameter is the first crack, a crack size or the weight change of specimen. Typical results for a coated specimen

are shown in Fig. 19 /40/ where the thermal fatigue resistance reflects the brittleness of the coatings tested, as given, for example, by the ductile-brittle transition temperature.

In addition of the effects in metallic coatings the complex structure of thermal barrier coatings gives rise to more thermal fatigue problems. In these coatings defined cracks can improve the thermal shock resistance/43/ as shown in cyclic tests between 75 and 2100°F with ZrO_2-6,6 %Y_2O_3 and (MgO-ZrO_2)/(Co-Ni-Cr-Al-Y) duplex coatings. Microcracks in high density material increase the thermal shock resistance of the ZrO_2-Y_2O_3 coating but not of the MgO-ZrO_2 coating. The very good resistance against thermal cycling can be interpreted /18/ as due to control of residual stresses resulting from a controlled segmentation. Another important parameter in thermal barrier coatings is the bonding between the ceramic and the bond layer and between the bond layer and the substrate, which has to be optimized by an optimized roughness /44/. The microstructure of the oxide is important as well: lamellar structures are to be avoided. Of the physical-mechanical properties the elastic modulus should be kept low to avoid high thermal mismatch. As to the metallic M-Cr-Al-Y layer it is important that it softens at temperatures near 1500°F and can therefore relieve mismatch strains.

The effects of insufficient thermal shock resistance of a coating are shown in Fig. 20 where the chemical resistance of the coating is very good but because of a layer structure, low toughness and insufficient bonding of the layers, spalling did occur in the coating plane. In some cases this caused a deep attack within the base metal.

Another service examples of PtAl-coatings on top in IN 738 LC shows that thermal fatigue cracks in a brittle coating might stop at the base metal at lower temperatures or might cause severe oxidation or hot corrosion at the crack tip (Fig. 21 and 22).

4. Wear-resistant coatings

All descriptions of the mechanical behaviour of coatings given above apply for coatings against wear as well. In addition, the coating is consumed as a result of the wear process during operation of the component.

A low temperatures the very important fretting wear is mainly a mechanical effect in which the mating surfaces weld together and the connections are broken again by the relative movement of the components in contact/17/. When the temperature is increased oxidation or hot corrosion of the surface occurs and the peeled-off particles become very important thus introducing the effect of abrasive wear. Hence for high temperature wear-resistant coatings the oxidation behaviour determines the wear characteristics/45//46/. In Fig. 23 /46/ it is shown that, for a cobalt-based coating matrix, Al_2O_3 inclusions and Al_2O_3-forming coatings behave best at high temperatures whereas Cr_2O_3 and Cr_2C_3-containing coatings should be chosen at low temperatures. Therefore certain temperature ranges are recommended for wear-resistant coatings.

When coatings are applied by plasma spraying or with a detonation gun the bonding is sufficient good for their application on Hastelloy X/47/and cannot be improved by a heat treatment.

Especially for high temperature application the long-term behaviour of the coating is important. In certain environments the hard phase might not show sufficient stability and might transform to other phases. For examples in high temperature gas-cooled reactor helium Cr_3C_2 particles in Cr_3C_2-(Ni-Cr) coatings on Hastelloy X transform into Cr_7C_3 and later into $Cr_{23}C_6$. This transformation is accompanied by a volume contraction which causes spallation of the coating.

As another example, long-term oxidation could lead to the formation of internal oxides, a fact which limits the application of Tribaloy-type coatings at very high temperatures/48/. Oxidation has a direct effect on the wear performance of coatings which is proved by the fact that under non-oxidizing conditions/49/ carbide-carbide couples of mating surfaces are undesirable, whereas in air or under gas turbine conditions chromium carbide behave very well/44/.

5. Discussion and conclusions

All the examples shown before omitted the fact that a coating can work only when the adhesion to the substrate is sufficient. This factor is important not only for high temperature coatings. However because high temperature materials must be oxidation resistant and will develop oxide scales very rapidly a good surface preparation is necessary before the coating process, if possible connected with a diffusion treatment/58/.

In a discussion of the mechanical properties of high temperature coatings and coated components two areas are of main interest: (1) susceptibility of a coating to cracking and spalling; (2) coating-base metal interaction which leads to deterioration of important mechanical properties of the components.

Cracking and spalling may be due to (1) high residual tensile stresses from processing, (2) a marked thermal expansion mismatch, (3) poor ductility or toughness and (4) poor adherence to the substrate material. The base component properties are not directly affected. Coating protection is limited because of premature mechanical coating failures.

Coating-base metal interaction can influence mechanical properties as a result of (1) mismatch of processing parameters (temperature, time, heating and/or cooling rates), (2) interdiffusion and structural changes because of insufficient chemical compatiblity, (3) susceptiblity to crack formation as given above which causes stable crack growth by creep or fatigue in the structural base metal.

In order to prevent deterioration of properties-both after processing and during service-some measures may help to tailor relevant coating properties more appropriately. These are as follows.

(1) Strains and strain ranges can be minimized by adjusting the thermal expansion coefficient and the elastic modulus.

(2) The ductility and toughness can be adjusted with a controlled microstructure which means (a) dispersed brittle phases which are important for protection in a ductile matrix, (b) controlled grain size and phase distribution to avoid stress concentrations during plastic deformation and (c) phase stability at service temperatures.

(3) Good adhesion can be achieved by producing chemical bonding through controlled difffusion.

However, all these measures have to be considered together with the specific loading characteristic that a coated component will be subjected to. A brittle corrosion-resistant coating may work excellently in a small blast furnace gas turbine up to about 720°C but may fail if the temperature and therefore the strain range increase drastically, as found with a galvanic chromium coating/1/.

The potential of mechanical interation between a coating and a component should also be discussed with respect to the coating processing. There are processes in which a special treatment and chemical interaction with the base metal are required (e.g. pack cementation). Such a heat treatment does not necessarily match that required for the best mechanical properties of the component material.

Influences on creep properties at lower temperatures could be attributed to this special "processing mismatch". Coating properties are normally strongly dependent on the base metal composition and cannot be optimized independently. The deep diffusion zone that is always present also influences the mechanical properties of the composite. Hence the range of application of such coatings might be limited especially for thin sections. In contrast, overlay coatings which do not require special heat treatments and do allow a free choice of composition have superior potential. Their composition and structure can more readily optimized in order to meet mechanical requirements as well as to attain phase stability and interdiffusion control.

References

1 H.W. Grünling and K. Schneier, Thin Solid Films, 84 (1981) 1-15.
2 G. Nover, Ch.J. Raub and H. Speckhardt, Metalloberfläche, 34 (1980) 169-173.
3 P. Szelagowski, Ph.D. Thesis, Technische Universität Braunschweig, 1976
4 P. Huber, R. Dekumbis and M. Villat, Plasma Spraying Conf. Essen, 1983.
5 G. Wahl, Z. Werkstofftechn., 7 (1976) 311-315.
6 J. Schlichting, Z. Werkstofftechnik., 7 (1976) 338-340.
7 T.E. Strangman, Thin Solid Films, 45 (1977) 499-506.
16 M. Schütze and A. Rahmel, Proc. DGM "Aufbau von Oxidschichten auf Hochtemperaturwerkstoffen und ihre technische Bedeutung", Augsburg, 1982.
17 D.K. Benson, ASTM Spec. Tech. Publ., 467, 1970, pp. 188-208.
18 D.L. Ruckle, Thin Solid Films, 73 (1980) 455-461.
19 D.H. Boone, AIRCO Temescal, 1976.
20 W. Betz, H. Huff and W. Track, Z. Werkstofftechn., 7 (1976) 161-166.
21 A.R. Nicoll, G. Wahl and U.W. Hildebrandt, in D.A. Holms and A. Rahmel (eds.), Materials and Coatings to Resist High Temperature Corrosion, Applied Science, London, 1978, pp. 233-251.
22 K. Schneider, R. Bauer and H.W. Grünling, Thin Solid Films, 54 (1978) 359-367.
23 R.W. Smith, Thin Solid Films, 84 (1981) 59
24 T.E. Strangmann, E.J. Felten and N.E. Ulion, Am. Ceram. Bull., 56 (1977) 700-705.
25 R. Bauer, H.W. Grünling and K. Schneider, in D.A. Holms and A. Rahmel (eds.), Materials and Coatings to Resist High Temperature Corrosion, Applied Science, London 1978, pp. 233-251.
26 K.H. Keienburg, unpublished results, KWU, Mülheim, F.R.G.

27 G.F. Paskeit, D.H. Boone and C.P. Sullivan, J. Inst. Met., 100 (1972) 58-62.
28 A. Strang and E. Lang, in R. Brunetaud et al. (eds.), High Temperature Alloys for Gas Turbines 1982, Reidel, Dordrecht, 1982, pp. 469-506.
29 K. Schneider, H.G. v. Arnim and H.W. Grünling, Thin Solid Films, 84 (1981) 29-36.
30 K. Schneider, G. Gnirß, B. Trück and H.G. v. Arnim, in R. Brunetaud et al. (eds.), High Temperature Alloys for Gas Turbines 1982, Reidel, Dordrecht, 1982, pp. 685-701.
31 E.S. Umanski, N.I. Afonin, Yu.S. Barisov and A.M. Vyal'tser, Probl. Prochn.., 10 (1977) 112-113 (Engl. trans., (1978) 1267-1269).
32 K.H. Schmitt-Thomas, G. Johner and H. Meisel, Werkst. Korros., 32 (1981) 255-264.
37 A. Strang, CIMAC Congr., Vienna, 1979.
38 A. Strang, in I. Kirman et al. (eds.), Behaviour of High Temperature Alloys in Aggressive Environments, Metals Society, London, 1980, pp. 595-611.
39 G.R. Leverant, T.E. Strangmann and B.S. Langer, in B.H. Kear et al. (eds.), Superalloys, Metallurgy and Manufacture, Claitor's Publishing Division, Baton Rouge, LA, 1976, pp. 285-195.
40 G.W. Goward, Proc. Symp. on Properties of High Temperature Alloys, Las Vegas, NV, 1976, pp. 805-823.
43 B. Gill, J.M. Quets, T.A. Taylor and R.C. Tucker, Jr., ASME Paper 82-GT-266.
44 T.A. Taylor, M.O. Price and R.C. Tucker, Jr., 84th Annu. Meet of the American Ceramic Society, Cinicinnati, OH, 1982.
45 R.C. Tucker, Jr., T.A. Wolfla, J.M. Quets and E.B. Cook, Fall Meet. of the Metallurgical Society of the AIMME, Milwaukee, WI, 1979.
46 J.M. Quets and R.C. Tucker, Jr., Thin Solid Films, 84 (1981) 107-118.
47 T.A. Wolfla and R.C. Tucker, Jr. Thin Solid Films, 53 (1978) 353-364.
48 C.C. Li, Thin Solid Films, 73 (1980) 59-77.
49 D.P. Ferris and C.B. Cameron, J. Vac., Sci. Technol., 12 (1975), 795-799.
50 K. Schneider, H.W. Grünling, Thin Solid Films, 107 (1983), 395-416
51 B.M. Kramer, Thin Solid Films, 108 (1983) 117-125.
52 W. Schintlmeister, W. Wallgram, J. Kanz, Thin Solid Films, 107 (1983) 117-127.
53 H. Grützner, DVS-Berichte 80, 1983, p. 215-218.
54 J.R. Rairden, M.R. Jackson, M.F. Henry, DVS 80,1983, pp. 205-207.
55 C.C. Bendt, H. Herman, DVS 80, 1983, 175-178
56 J.H. Wood, T.R. Farrell, A.N. Beltran, W.F. Schilling, W.J. Ostergreen, Proceeding of the Second, Conference on Advanced Materials for Alternative Fuel-Capable Heat Engines, Monterey 1981, p. 7-45/7-68
57 R.F. Bunshah, Thin Solid Films, 107 (1983) 21-38
58 H.D. Steffens, J. Beczkowiak, DVS 80, 1983, 218-221

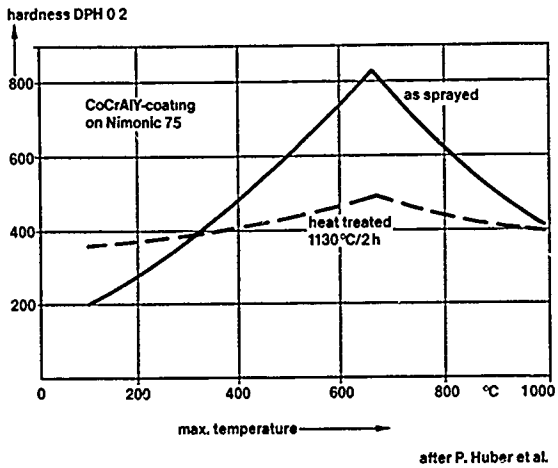

Fig. 1: Correlation between the maximum substrate temperature during spraying and the hardness for a Co-Cr-Al-Y coating on Nimonic 75: ———, as sprayed; ------, heat treated at 1130°C for 2 h.

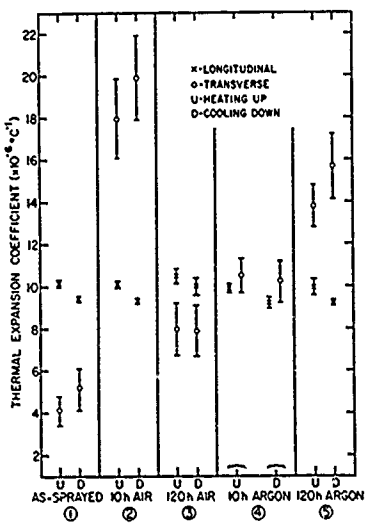

Fig. 2: Summary of thermal expansion coefficients derived from expansion data. The error bars are one standard deviation about the mean value.

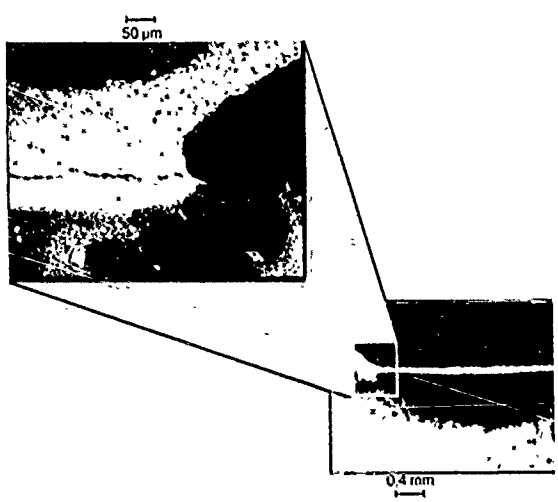

Fig. 3: Shrinkage of a self-fluxing plasma-sprayed coating during application.

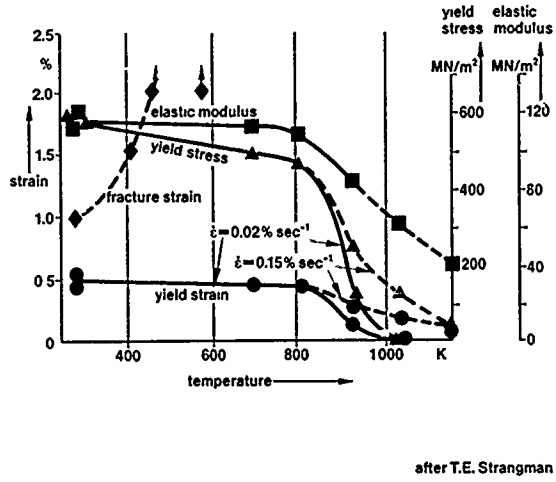

Fig. 4: The mechanical properties of a physically vapour-deposited Ni-Co-Cr-Al-Y coating 1 mm thick.

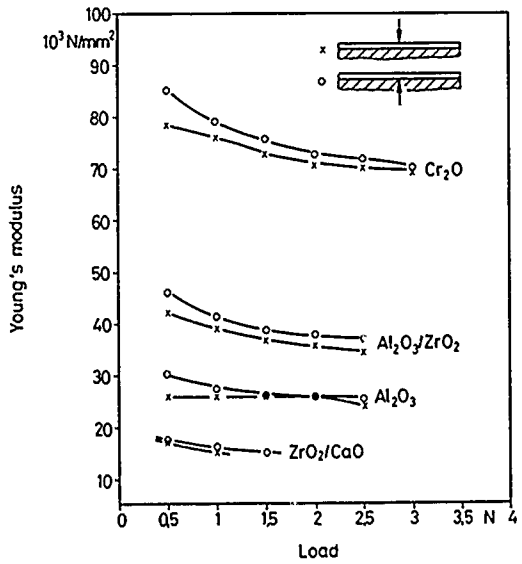

Fig. 5: Young's modulus of stripped off ceramic plasma sprayed coatings as a function of load and direction.

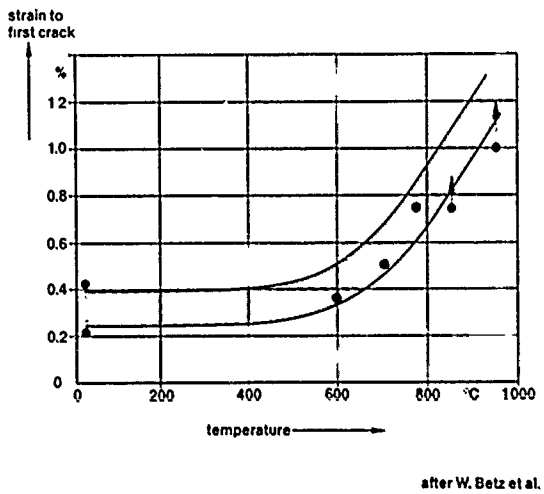

Fig. 6: Ductility of aluminide coatings vs. temperature[20].

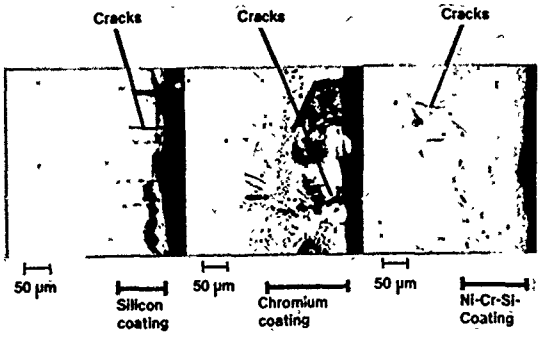

Fig. 7: The cracking behaviour of coated IN-738 LC in bending (18% strain) at room temperature[22].

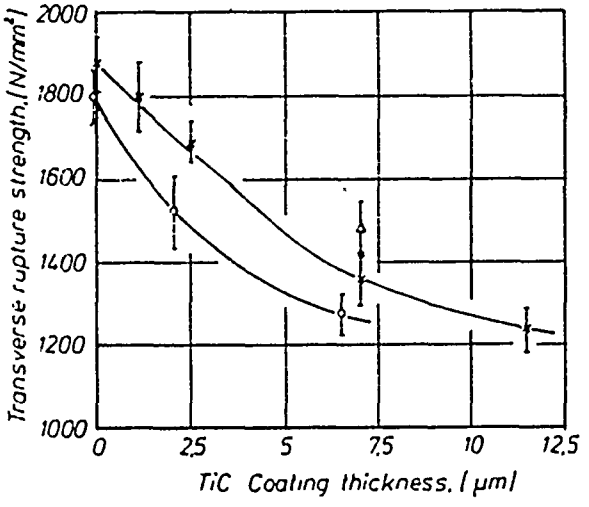

Fig. 8: Dependence of the transverse rupture strength on the thickness of the TIC coating: O, with η layer; Δ, grainy (equiaxed) structure.

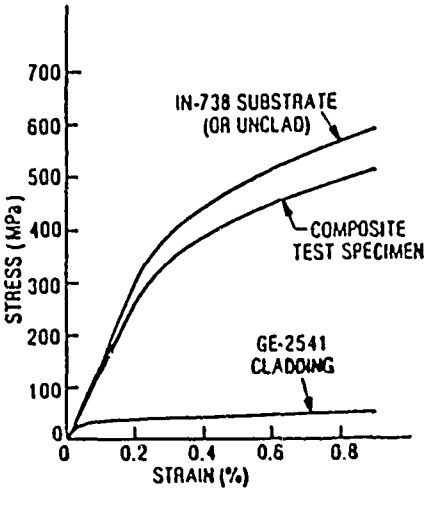

Fig. 9: Calculated 871°C tensile behaviour of GE-2541 CLAD IN 738 tensile bar.

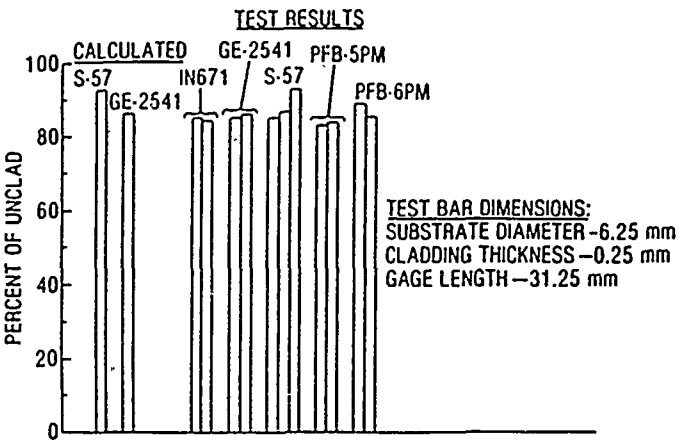

Fig. 10: 0.2% yield strength of CLAD IN 738 tensile bars at 871°C.

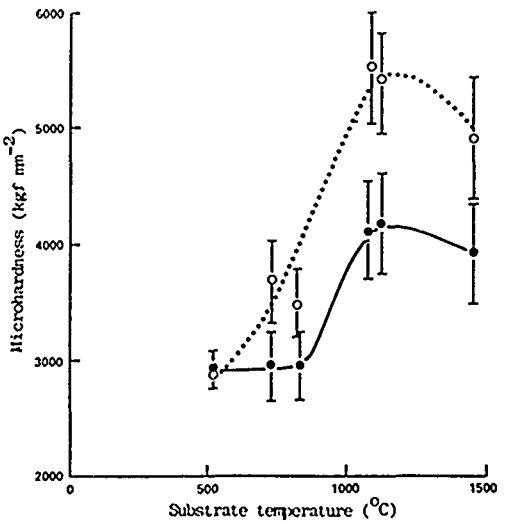

Fig. 11: Variation in microhardness with deposition temperature for TiC[29]: ● diamond pyramid hardness at a load of 50 gf; O , Knoop hardness at a load of 50 gf.

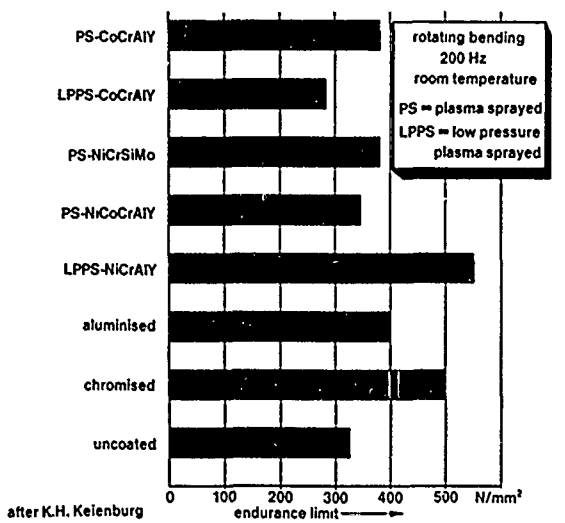

Fig. 12: Fatigue strength of coated and uncoated U 520 tested at room temperature by rotating bending at 200 Hz (PS, plasma sprayed; LPPS, low pressure plasma sprayed)[26].

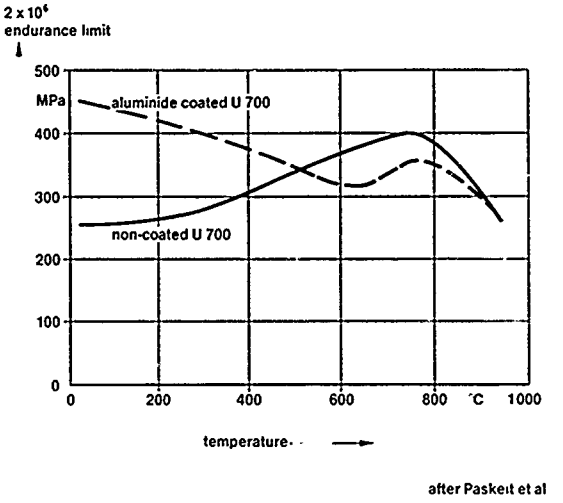

Fig. 13: High cycle fatigue properties of aluminide-coated U 700 (---) and uncoated U 700 (——)[27].

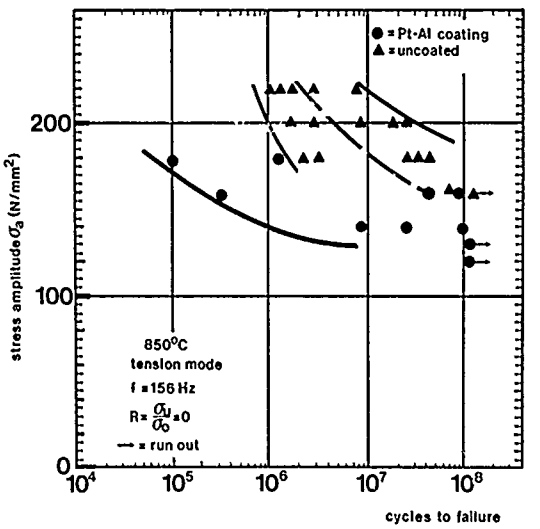

Fig. 14: HCF-properties of unidirectionally solidified IN 738 LC with and without a Pt-Al-coating.

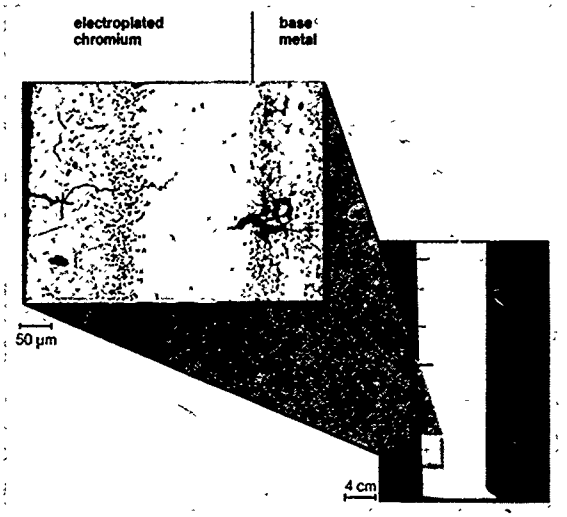

Fig. 15: Blade failure due to fatigue cracks originating from a cracked coating.

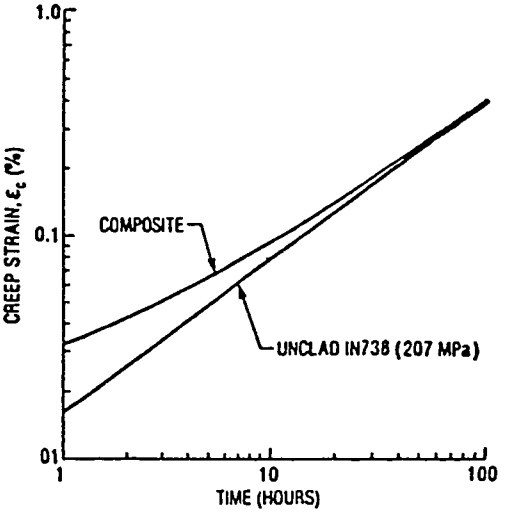

Fig. 16: Calculated constant load creep behaviour of S-57 CLAD IN 738 creep bars at 871°C.

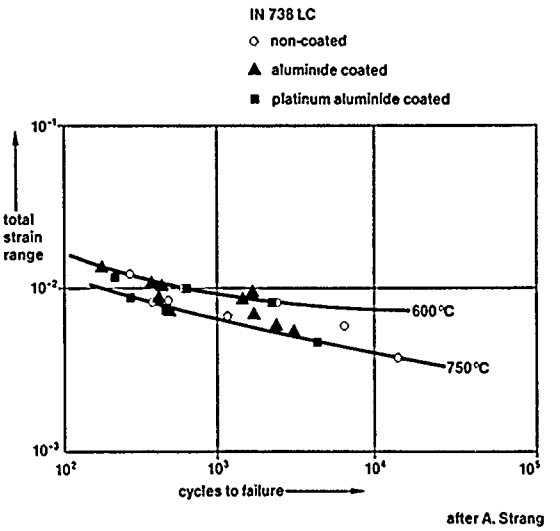

Fig. 17: Low cycle fatigue properties of uncoated (○) aluminide-coated (▲) and platinum-aluminide-coated (■) IN-738 LC [38].

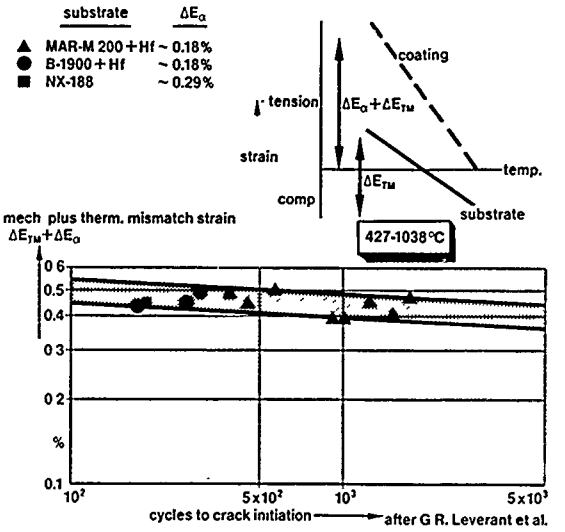

Fig. 18: Crack initiation data for Ni-Co-Cr-Al-Y-coated superalloys: ▲, MAR-M 200 plus hafnium ($\Delta E_\alpha \approx 0.18\%$); ●, B-1900 plus hafnium ($\Delta E_\alpha \approx 0.18\%$); ■, NX-188 ($\Delta E_\alpha \approx 0.29\%$).

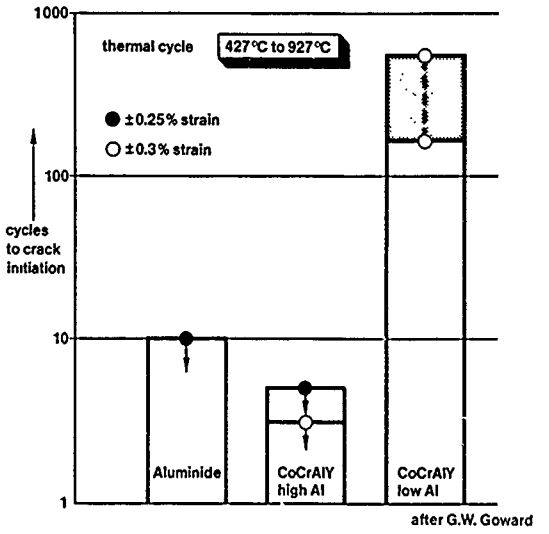

Fig. 19: Thermomechanical fatigue properties of aluminide and Co-Cr-Al-Y coatings (thermal cycle, 427-927°C): ●, ± 0.25% strain; ○, ± 0.3% strain.

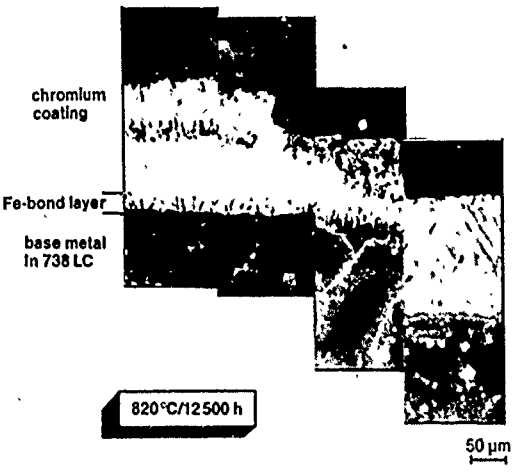

Fig. 20: Spallation of a galvanic coating on a turbine vane (tested at 820°C for 12.500 h).

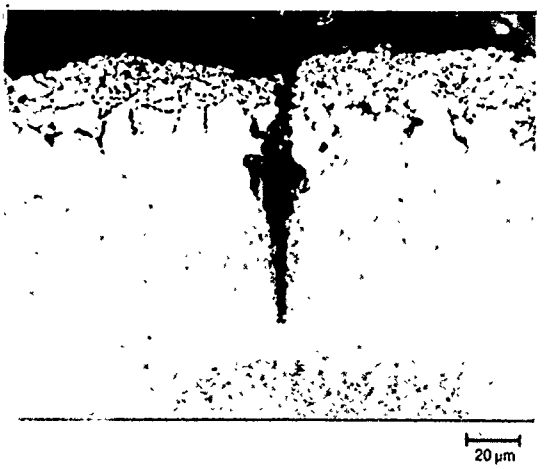

Fig. 21: Crack formation in LDC 2 coating near to the leading edge root area after 6.700 h engine service

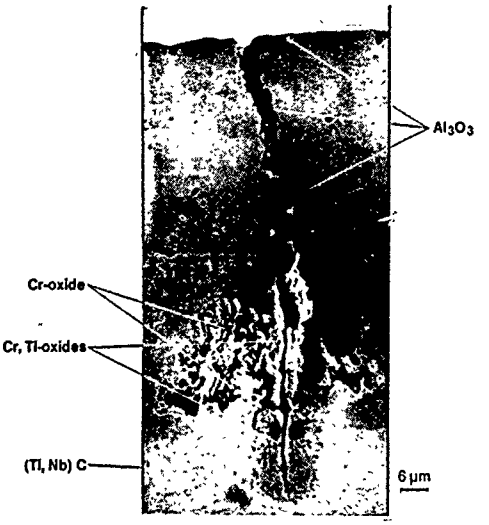

Fig. 22: Oxidized crack in RT 22 coating after 5.000 h engine service

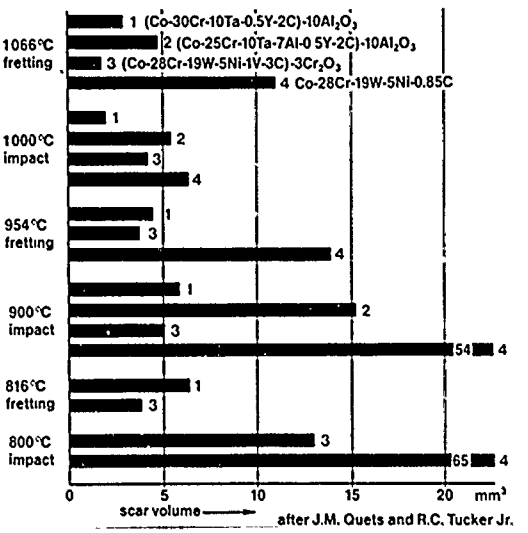

Fig. 23: Impact-sliding and fretting wear test at 200 thermal cycles bars 1, (Co-30%Cr-10%Ta-0.5%Y-2%C)-10%Al_2O_3 ; bars 2, (Co-25%Cr-10%ta-7%Al-0.5%Y-2%C)-10%Al_2O_3 ; bars 3 (Co-28%Cr-19%W-5%Ni-1%V-3%C)-3%Cr_2O_3 ; bars 4 Co-28%Cr-19%W-5%Ni-0.85%C): (a) fretting at 1066°C; (b) impact-sliding at 1000°C; (c) fretting at 954°C; (d) impact-sliding at 900°C; (e) fretting at 816°C; (f) impact-sliding at 800°C.

DISCUSSION

P.Ramette, Fr

Are you considering some coating with porous materials which allow transpiration cooling and do you think that this type of coating could be of some interest?

Author's Reply

Porous coatings which allow transpiration cooling don't seem to be reasonable. Porous structures which allow a homogenous transpiration cooling could have drawbacks when the hot gas is able to close the pores due to deposits.

CFM56-2 - FATIGUE OLIGOCYCLIQUE DU DISQUE DE SOUFFLANTE : DIMENSIONNEMENT ET ESSAIS POUR LA VERIFICATION ET LES AMELIORATIONS

par
A. GUIBERT et G. HERMAN
SNECMA, Centre de VILLAROCHE
77550 MOISSY CRAMAYEL
FRANCE

RESUME

Dans le cadre du programme CFM56-2, la SNECMA a développé (entre autres composants), le disque de soufflante.

L'analyse des contraintes et les vérifications associées ont été incluses dès le début du programme en utilisant aussi bien des techniques fines d'analyses (éléments finis) que des essais sophistiqués de vérification (photoélasticité).

Une partie importante de l'analyse de durée de vie a consisté aussi à comprendre le comportement du matériau (essais sur éprouvettes) et à préparer les essais d'endurance oligocyclique en vraie grandeur.

Les résultats acquis en essais d'endurance en vraie grandeur ont permis les ultimes vérifications et améliorations avant la certification du moteur.

L'ensemble des résultats ainsi acquis a permis la démonstration cohérente de la durée de vie du disque de soufflante.

1 - INTRODUCTION

Dans les turboréacteurs modernes, les objectifs de masse et d'encombrement imposent au constructeur, l'emploi de matériaux performants, et leur utilisation à un niveau de sollicitation très élevé. Cela est particulièrement vrai pour la soufflante du CFM56-2, qui fournit l'essentiel de la poussée du moteur.

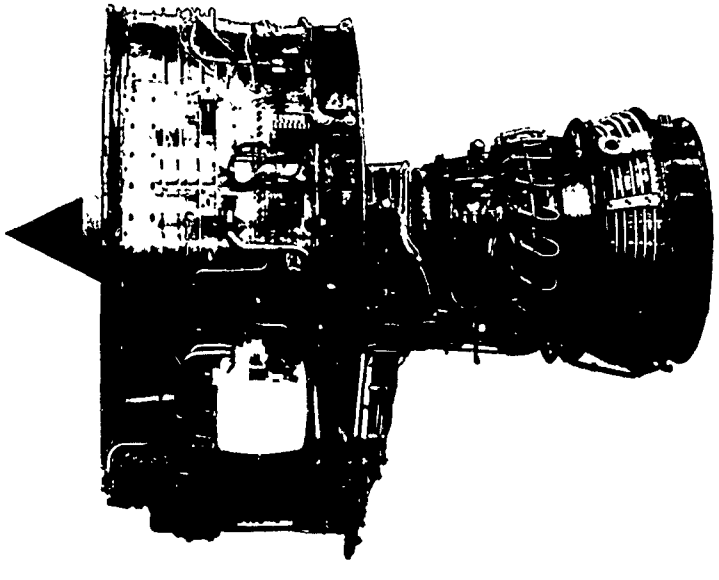

Fig. 1 : CFM56-2

La soufflante du CFM56-2 a un diamètre de 1,7 m et comporte 44 aubes tournant à une vitesse périphérique élevée de 460 m/s et supportées par un disque en alliage de titane TA 6 V, sur lequel elles exercent une traction centrifuge totale de 18 M Newton.

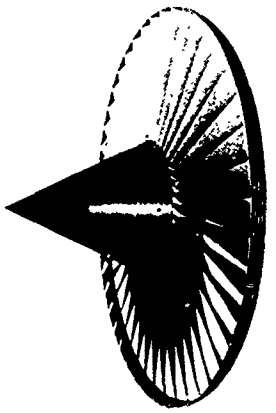

Fig. 2 : Rotor de soufflante

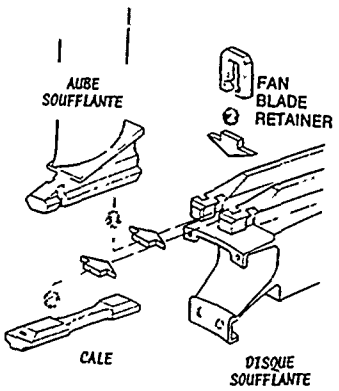

Fig. 3 : Rétention des aubes de soufflante

Il est donc nécessaire de prévoir la durée de vie avec précision, en s'appuyant sur une analyse approfondie des contraintes locales et une bonne connaissance du comportement du matériau.

Pour une pièce fonctionnant à basse température, comme le disque de soufflante, les modes de rupture susceptibles d'intervenir sont :

- la fatigue oligocyclique,
- l'atteinte de la limite de résistance en traction du matériau.

Compte tenu des formes complexes de la liaison disque-aubes, c'est la fatigue oligocyclique qui limite la durée de vie de la pièce.

C'est de la prévision de cette durée de vie cyclique que traitera l'exposé.

Les facteurs influant le plus sur la fatigue oligocyclique du disque sont les suivants :

- variation brusque de section causant une concentration de contrainte,
- fort gradient de contrainte,
- charge élevée en rotation, flexion, forces de liaison avec d'autres composants,
- fonctionnement cyclique sévère : mise des gaz au décollage,
  inversion de poussée,
  arrêt et rédémarrage, etc...

Les définitions retenues pour l'établissement de la durée de vie en fatigue oligocyclique sont les suivantes :

- on définira la durée de vie comme le nombre de cycles de vol, jusqu'à l'amorçage d'une crique,
- l'amorçage d'une crique sera défini comme le développement d'une crique observable, dont les dimensions seront par convention 0,25 mm x 0,75 mm,
- la durée de vie prédite sera définie comme le nombre de cycles de vol que supportera un disque en matériau de caractéristiques minimales, à l'amorçage de crique,
- les caractéristiques minimales de fatigue oligocyclique du matériau, seront celles d'un matériau inférieur de 3 écarts-types à la moyenne.

C'est dans ces conditions que va être présentée la prévision de durée de vie du disque de soufflante CFM56-2.

2 - METHODOLOGIE

La prévision de la durée de vie en fatigue oligocyclique du disque de soufflante du CFM56-2, comme d'ailleurs de celles des autres pièces de ce moteur, est le fruit d'une procédure évolutive.

La méthodologie mise en oeuvre pour assurer, au fur et à mesure de l'avancement du projet, une mise à jour continue de l'analyse des durées de vie, passe par plusieurs étapes (fig. 4) :

- Pré-dimensionnement,
- Dimensionnement avec améliorations,
- Certification,
- Post-certific· ion.

AVANCEMENT DU PROJET	ANALYSE DES CONTRAINTES	ANALYSE DES TEMPERATURES	DEFINITION DU CYCLE DE VOL	DONNEES MATERIAUX	EXPERIENCE ACCUMULEE
Pré-dimensionnement	Modèlisation simple par coques axi-symétriques. Facteurs de concentration de contrainte standard	Calculs thermiques théoriques	Estimation de l'environnement de sévérité maximum	Estimations à partir des charges de rupture;	-
Dimensionnement avec améliorations	Eléments finis et modèles photo-élastiques	Mesure des températures statiques	Mesure des paramètes du cycle de vol élémentaire	Essais de fatigue sur éprouvettes de laboratoire	Performances et températures
Certification	Mesures par jauges de contrainte	Mesure des températures en rotation	Définition de la mission mixée	Essais sur éprouvettes technologiques	Essais cycliques en fosse Cycle C sur moteur
Post-Certificatcn	Mise à jour des modèles et essais	Calculs thermiques complets	- " -	Obtention des courbes matériaux de catégorie supérieure	- " -

Fig. 4 : Etapes de l'analyse

Au cours du franchissement successif de ces étapes, les connaissances que possède le Bureau d'Etudes des divers éléments intervenant dans la prévision des durées de vie, progressent simultanément, de façon à préciser de plus en plus la durée de vie pour les pièces jugées critiques et éventuellement améliorer leur définition (fig. 4).

Dans le cadre de cet exposé, nous aborderons les points suivants, que nous jugeons les plus typiques, pour comprendre l'analyse des durées de vie faite sur le disque de soufflante CFM56-2, jusqu'à la période actuelle, c'est-à-dire, la post-certification :

- Définition du cycle de vol et de la mission mixée,
- Analyse des contraintes,
- Données matériaux,
- Analyse des durées de vie,
- Essais sur pièces réelles et expérience acquise.

3 - DEFINITION DU CYCLE DE VOL ET DE LA MISSION MIXEE

Le paramètre moteur qui influence principalement la durée de vie cyclique du disque de soufflante, est la vitesse de rotation N_{BP}. Elle varie avec :

- le fonctionnement du moteur sur la durée d'un vol,
- la température ambiante.

Les variations de fonctionnement pendant le vol sont définies par un profil typique de cycle de vol (fig. 5).

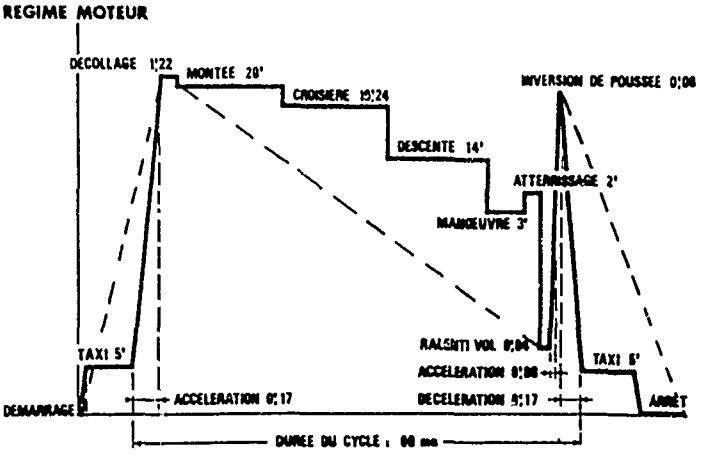

Fig. 5 : Vol commercial type

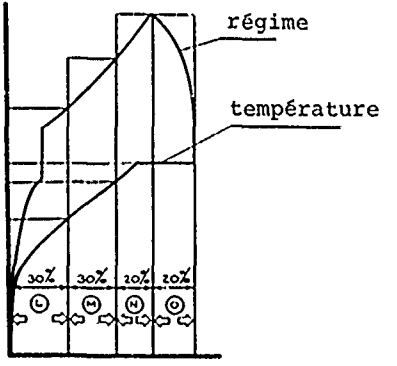

Fig. 6 : Distribution annuelle des régimes

Aux fins de détermination de la durée de vie cyclique, le régime est déterminé pour chaque portion du cycle de vol, ralenti, décollage, croisière, inversion de poussée, etc...

La seconde variable influençant le régime est la température ambiante, qui varie avec la période de l'année et le lieu géographique. La distribution annuelle de température est divisée en 4 valeurs discrètes, désignées par les lettres L, M, N, O, et atteintes respectivement pendant 30 %, 30 %, 20 %, 20 %, des vols (fig. 6).

Ayant établi la gamme de base des régimes utilisés, on fait 2 ajustements pour tenir compte :

- des variations opérationnelles d'utilisation,
- de la détérioration maximale du moteur entre révisions.

Les valeurs du régime BP retenues pour la prévision de durée de vie cyclique, sont représentées fig. 7.

Une durée de vie est calculée pour chaque condition L, M, N, O et la durée de vie totale résulte d'un cumul linéaire :

$$\frac{1}{N} = \frac{0,3}{N_L} + \frac{0,3}{N_M} + \frac{0,2}{N_N} + \frac{0,2}{N_O}$$

PARAMETRES MOTEUR : N_{BP}

REGIME MOTEUR	CONDITION L	CONDITION M	CONDITION N	CONDITION O
Ralenti	1297	1317	1337	1377
Décollage	4689	4865	4932	4927
Montée	4870	4907	4912	4912
Croisière	4772	4813	4818	4818
Descente	2723	2739	2749	2790
Manoeuvre	2978	2998	3008	3050
Ralenti vol	1883	1933	1963	2063
Inversion	4461	4560	4627	4622

Fig. 7 : Paramètres moteurs utilisés pour l'analyse de la durée de vie

4 - ANALYSE DES CONTRAINTES

4.1. Prédimensionnement du disque

Dans la phase dite de prédimensionnement, une première estimation des niveaux de contrainte dans la pièce, est déterminée à partir de calculs théoriques généraux.

Une forme de cycle de vol simplifié est définie où le régime de rotation varie de O à N_{max} et de N_{max} à O, et où les conditions thermiques les plus sévères sont réunies.

Les contraintes sont calculées à partir de modèlisations de la structure sous forme de coques axisymétriques. Les résultats obtenus ainsi sont des valeurs nominales des contraintes radiales, axiales, tangentielles et de flexion dans les sections considérées.

Les valeurs maximum des contraintes de surface sont estimées à partir d'estimations théoriques basées sur des facteurs de concentration de contrainte standard.

4.2. Dimensionnement détaillé

Dans l'étape suivante, une analyse plus détaillée des contraintes est réalisée en vue de la certification, en utilisant des méthodes plus sophistiquées, telles que des calculs éléments finis plus fins, et la photo-élasticité. Les contraintes ainsi calculées sont vérifiées à l'aide de mesures par jauges.

Les zones jugées critiques (fig. 8), ainsi que leurs modes de sollicitation et de rupture (fig. 9) sont étudiées en détail.

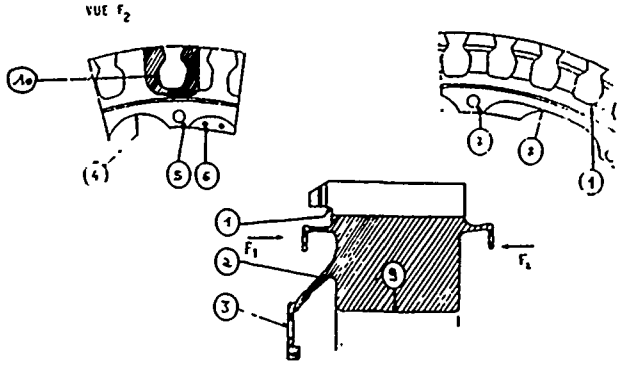

Fig. 8 : Zones critiques analysées

Zone N°	Description de la zone	Mode de sollicitation	Mode de rupture
1	Rayon de raccordement Alvéole/becquet de rétention	Effort radial Kt important	Fatigue oligocyclique
2	Raccordement bride avant	Flexion - Tangentiel	"
3	Trou bride avant	Torsion-flexion-tangentiel	"
4	Feston bride tambour	Tangentiel Kt	"
5	Trou bride tambour	Tangentiel Kt	"
6	Trou équilibrage - Bride tambour	Tangentiel Kt	"
7	Trou bride virole Support de capot	Tangentiel Kt	"
8	Feston bride virole Support de capot	Tangentiel Kt	"
9	Alésage	Tangentiel-axial	"
10	Alvéole	Tangentiel-radial	"

Fig. 9 : Modes de sollicitations et de rupture

4.3. Analyse des contraintes par éléments finis

Dans la vie du projet relatif au disque de soufflante CFM56-2, différentes améliorations ont été apportées et le dessin du disque a évolué de façon à soulager les zones critiques. Nous présentons dans ce paragraphe l'analyse des contraintes effectuée sur la version de production du disque.

Les maillages du rotor compresseur BP complet (fig. 10) et du disque (fig. 11) sont réalisés de façon à déterminer les niveaux de contrainte $\Delta\sigma_1$ et $\Delta\sigma_2$ correspondant à la décomposition du cycle type suivant la méthode du rainflow.

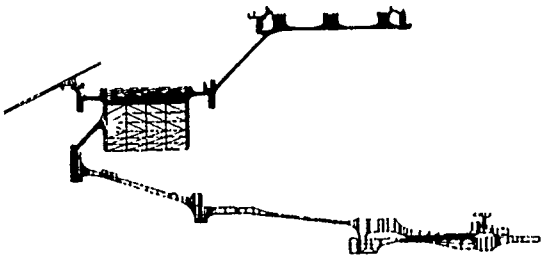

Fig. 10 : Maillage rotor compresseur BP complet

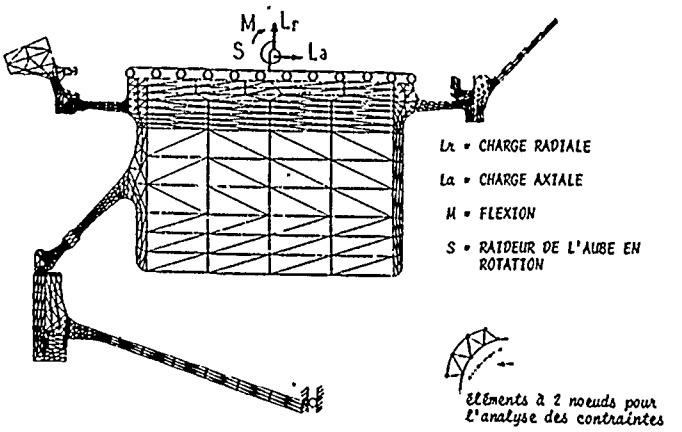

Fig. 11 : Analyse éléments finis du disque

Les calculs sont effectués en considérant les températures les plus sévères rencontrées en fonctionnement au cours d'une année, les propriétés du matériau utilisées étant celles du TA 6 V à 20° C avec une correction minime de température.

Les conditions aux limites du calcul tiennent compte des charges centrifuges dues aux aubes, boulons, entretoises et masses mortes. Les charges axiales induites par les efforts aérodynamiques et les pressions différentielles, sont prises en compte, ainsi que les contraintes d'origine thermique, qui représentent moins de 6 % de la contrainte totale dans tous les cas.

La zone critique du disque située au raccordement alvéole/becquet de rétention, a été analysée en détail pour la certification, et a nécessité l'étude complète du problème de la combinaison de deux facteurs de concentration de contrainte due à la conjonction de deux rayons de raccordement situés dans des plans différents. Une formule empirique conservative a été utilisée pour calculer la contrainte dans cet accident de forme. Elle a été vérifiée par un calcul aux éléments finis 3 D.

Lors de la période suivant la certification, de nouvelles modèlisations par éléments finis 3 D des zones critiques, ont été réalisées (fig. 12) afin d'améliorer la précision sur le calcul des contraintes dans ces zones.

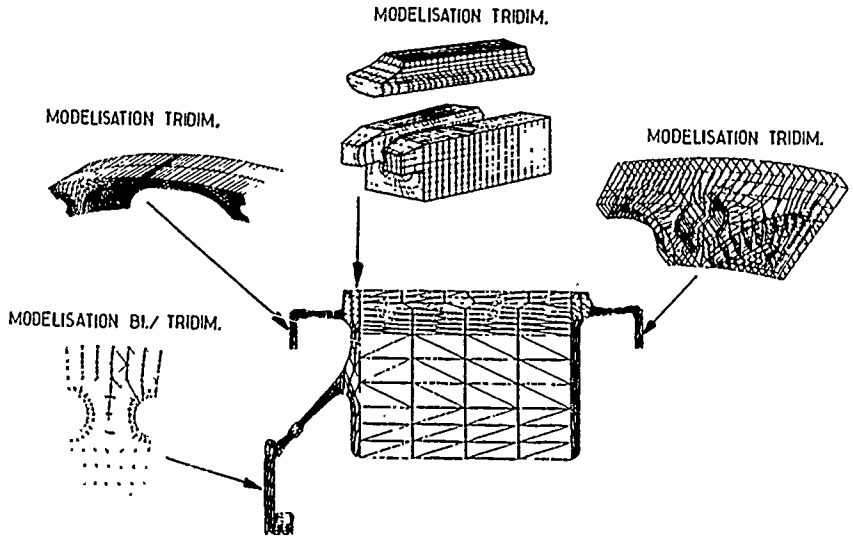

Fig. 12 : Modèles éléments finis

Les valeurs actualisées des contraintes aux points analysés sont représentés fig. 13.

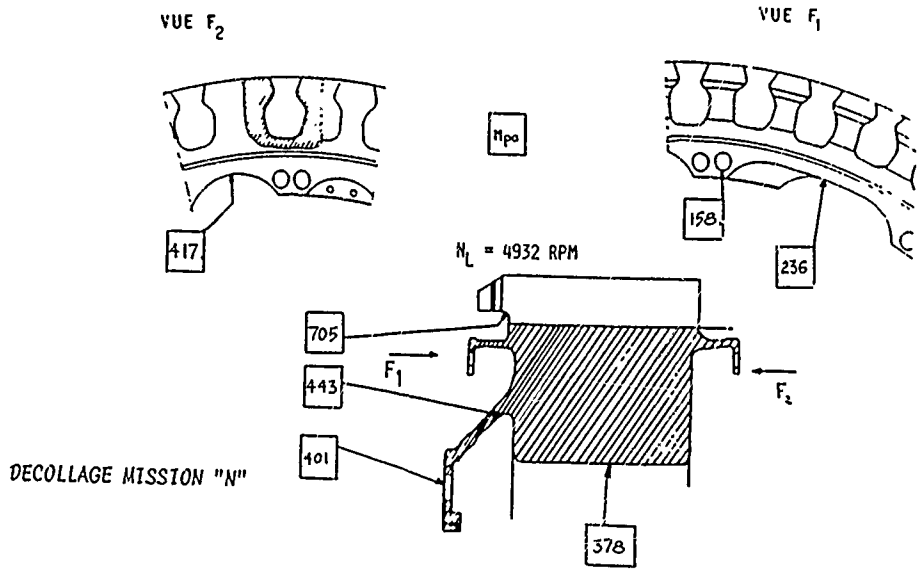

Fig. 13 : Contraintes pour la sollicitation maxi.

Les valeurs de contraintes étant calculées à l'aide de la théorie de l'élasticité, les éventuelles plastifications locales sont prises en compte suivant la méthode exposée au § 6.

4.4. Analyse des contraintes par photoélasticité

Le but de la méthode tridimensionnelle d'analyse des contraintes par photoélasticité est de mesurer des contraintes dans des configurations géométriques complexes présentant des concentrations de contraintes.

Cette méthode est utilisée en complément aux méthodes mathématiques, lorsque l'obtention de la contrainte maximale est incertaine.

Des maquettes en araldite représentatives des pièces sont réalisées, soit par usinage, soit en coulant l'araldite dans un moule de la forme désirée.

La maquette utilisée pour le disque de soufflante est présentée à la figure 14 et un exemple de visualisation de franges isochromatiques au niveau des alvéoles, est montré à la figure 15.

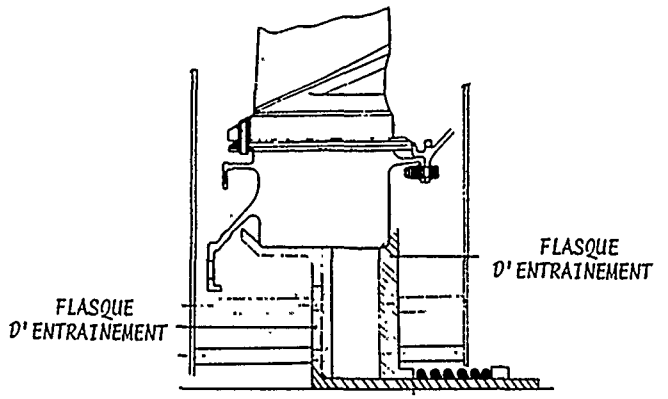

Fig. 14 : Montage d'essai photo-élastique

Fig. 15 : Essai photo-élastique de l'attache d'aube

4.5. Mesures de contraintes par jauges

Les contraintes calculées ont été vérifiées par des mesures par jauges de contraintes sur le disque complet en rotation. Le fonctionnement à basse température du disque, et sa dimension, le rendent particulièrement apte à ces mesures qui ont été effectuées sur le banc de fatigue oligocyclique (fig. 16).

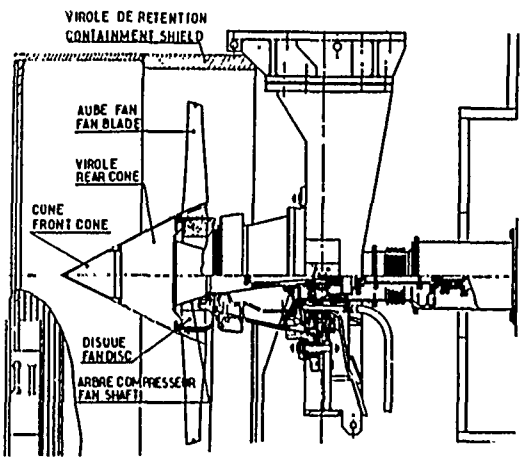

Fig. 16 : Banc d'essais cycliques

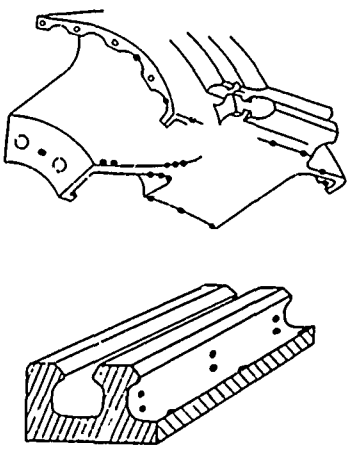

Fig. 17 : Position des jauges

Les jauges ont été placées aux différents points sensibles sélectionnés (fig. 17).

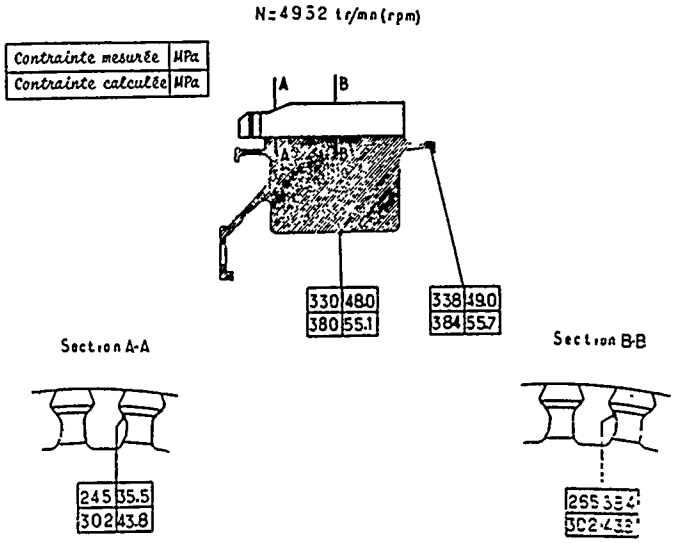

Fig. 18 : *Comparaison calcul-mesure par jauges*

La comparaison entre les valeurs de contraintes calculées et celles mesurées, indique que l'analyse est conservative (fig. 18), du fait de la prise en compte de données pessimistes sur la géométrie et les charges, et de conditions aux limites sévères (problème de la souplesse des liaisons).

5 - DONNEES MATERIAUX

Le matériau du disque, le TA 6 V, doit être caractérisé en fatigue oligocyclique par des essais sur éprouvettes, dont le but est d'établir les relations entre l'état de sollicitation de la matière et le nombre de cycles à l'amorçage de crique. Dans le cas de cette pièce froide, ces relations sont établies à température ambiante.

5.1. Choix de l'éprouvette et du mode de sollicitation

Les points les plus critiques du disque étant soumis à de fortes concentrations de contraintes, il semblerait logique de caractériser le matériau avec une éprouvette entaillée. Mais sur cette éprouvette, de taille réduite puisqu'elle doit être prélevée dans le brut du disque, on ne reproduit ni le gradient de contrainte, ni la taille de la zone plastique de la pièce réelle. De plus, l'usinage de l'entaille peut laisser subsister un écrouissage qui favoriserait la tenue en fatigue.

On a donc développé des essais sur éprouvette lisse qui présente une zone utile de taille réaliste, et dont le mode d'usinage est facile à maîtriser.

Pour les zones de la pièce où le gradient de contrainte est élevé, l'éprouvette simule le comportement de l'élément de matière le plus sollicité. L'ensemble de la pièce travaille dans le domaine élastique et impose son déplacement à cette zone la plus sollicitée. L'éprouvette sera donc essayée à déformation imposée.

La transposition à la pièce réelle des résultats obtenus sur éprouvette en tenant compte de la plastification, sera décrite au paragraphe suivant.

5.2. Fiabilité des résultats

La confiance qu'on peut accorder aux résultats des essais sur éprouvette, valeurs moyennes et écart-type, s'améliore au cours des étapes du projet.

Au stade de la certification, on dispose d'éprouvettes:

- prélevées dans un disque prototype (forgé main)
  un tambour de compresseur BP laminé
- provenant de 2 fournisseurs de matière et de 2 coulées.

Le nombre d'éprouvettes testées permet d'assurer la mise en service.

Après certification, on dispose de nombreuses éprouvettes supplémentaires prélevées dans des disques de série, matricés. 3 fournisseurs et 4 coulées différentes sont pris en compte, ce qui couvre l'ensemble des sources d'approvisionnement.

La confiance dans les caractéristiques moyennes et à -3 écart-type, utilisées pour la prévision de durée de vie cyclique, devient donc très élevée.

Les caractéristiques déterminées à ces 2 étapes du projet sont représentées figure 1 , sur un diagramme :

$$\frac{\Delta\varepsilon}{2} \times E,\ N_R$$

(sur éprouvette lisse, la rupture suit de près l'amorçage de crique)

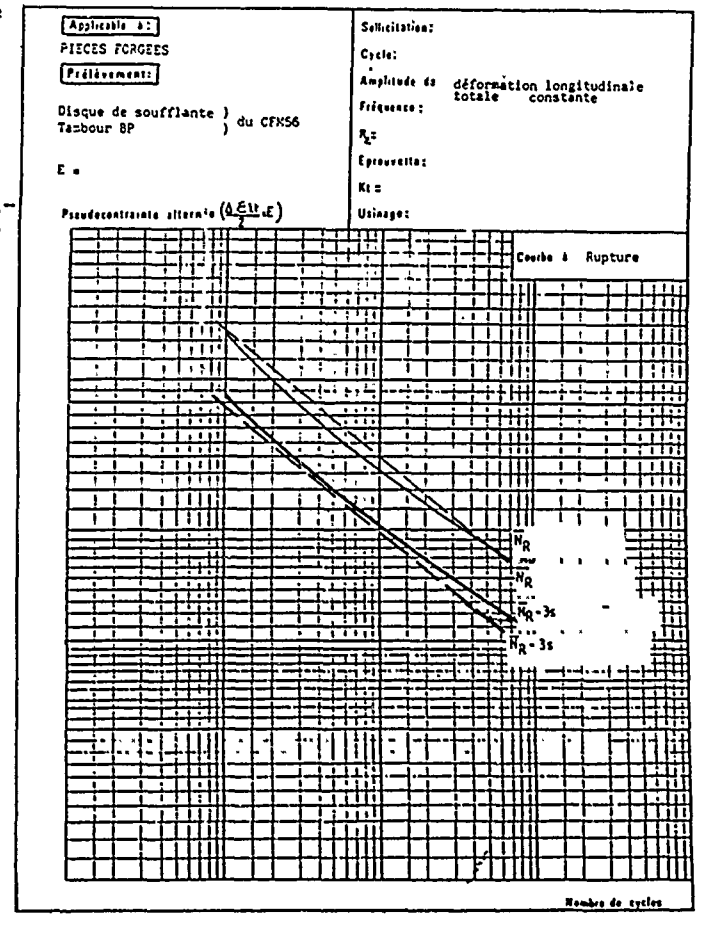

Fig. 19 : Comparaison des données certification et production

6 - CALCUL DE LA DUREE DE VIE

Le profil de la mission-type utilisé pour le calcul de la durée de vie du disque est décomposé en cycles. Les extrêmums de vitesse pendant le vol, sont associés selon la méthode du "rainflow" afin de déceler les alternances de chargements subis par le matériau (fig.20) Le spectre assez complexe de la mission est ainsi ramené à deux cycles.

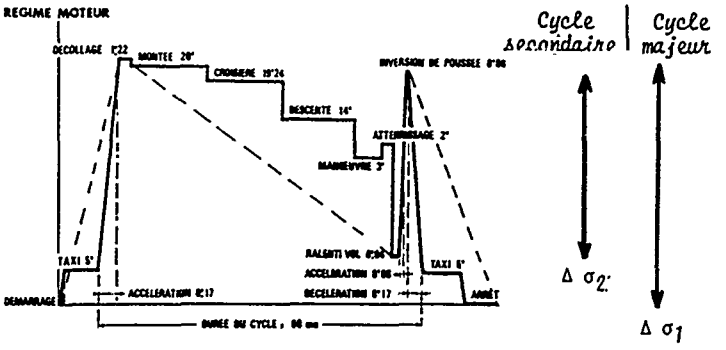

Fig. 20 : VOL COMMERCIAL TYPE - Décomposition en cycles élémentaires

Les calculs d'élasticité ainsi que les mesures par photo-élasticimétrie exposés ci-dessus, sont prolongés afin de déduire de la décomposition en cycles, les allongements Plastiques réels du matériau.

- la zone plastifiée étant de faible volume, l'hypothèse de Neuber :

  σ élast.max. x ε élast.= σ x ε total

  est appliquée sur la courbe de traction cyclique stabilisée obtenue en laboratoire (fig. 21).

- l'endommagement de chaque cycle élémentaire est donné par les caractéristiques en fatigue établies sous la forme de diagramme de HAIG (fig. 22).

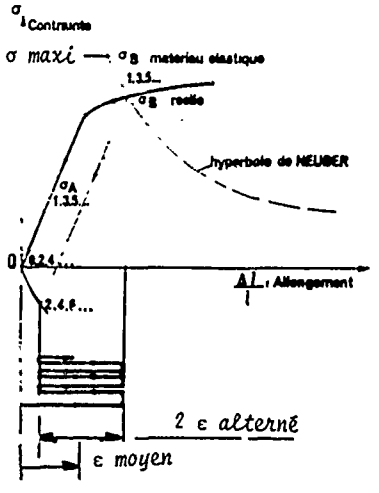

Fig. 21 : Cycle allongement contrainte

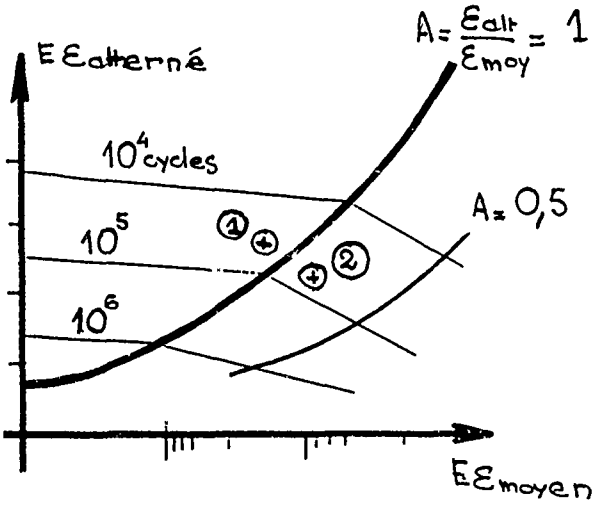

Fig. 22 : Diagramme de HAIG

L'endommagement $\frac{1}{N}$ total de la mission, est selon la loi de MINER, la somme des endommagements des cycles élémentaires :

$$\frac{1}{N} = \frac{1}{N_1} + \frac{1}{N_2}$$

Les résultats pour le point le plus chargé, et pour l'ensemble des points étudiés, au dernier stade de la définition et de l'analyse du disque, sont représentés fig. 23 et 24.

CFM 56 . DISQUE DE SOUFFLANTE . ANALYSE MISSIONS MIXEES

ANALYSE DETAILLEE DE LA DUREE DE VIE EN FATIGUE LENTE DE LA ZONE N°1 *Rayon de raccordement becquet/alvéole*

ETAPES DE L'ANALYSE			L		M		N		O		
			1	2	1	2	1	2	1	2	
(A) Cycles de contraintes locales. σ alt	MPa		344	237	349	247	353	255	351	248	1 cycle première
	KSI	"	49.9	34.4	50.6	35.8	51.2	37.0	50.9	36.0	2 cycle secondaire
	A		1	0.69	1	0.69	1	0.69	1	0.69	
(B) Calcul des durées de vie minimales Courbe post-certification			$N_1 = 6.10^4$	$N_2 = 37\,10^5$	$N_1 = 5.5\,10^4$	$N_2 = 3.\ 10^5$	$N_1 = 5.5\,10^4$	$N_2 = 2.7\cdot10^5$	$N_1 = 5.5\,10^4$	$N_2 = 3.\ 10^5$	
(C) Cumul linéaire d'endommagement			$N_L = 51630$		$N_M = 46480$		$N_N = 45690$		$N_O = 46480$		
(D) Résultats en vols-type mixés $\frac{1}{N} = \frac{0,3}{N_L} + \frac{0,3}{N_M} + \frac{0,2}{N_N} + \frac{0,2}{N_O}$			47700								

Fig. 23 : Calcul de la durée de vie du point le plus chargé

ZONE n°	DESCRIPTION DE LA ZONE	RESULTATS VOLS TYPE MIXES			
		L	M	N	O
1	RAYON DE RACCORDEMENT BECQUET DE RETENTION / ALVEOLE	51630	46480	45690	46480
		47700			
2	RACCORDEMENT BRIDE AMONT	$> 10^5$	$> 10^5$	$> 10^5$	$> 10^5$
		$> 10^5$			
3	TROU BRIDE AMONT	$> 10^5$	$> 10^5$	$> 10^5$	$> 10^5$
		$> 10^5$			
4	FESTON BRIDE TAMBOUR	$> 10^5$	$> 10^5$	$> 10^5$	$> 10^5$
		$> 10^5$			
5	TROU BRIDE TAMBOUR	$> 10^5$	$> 10^5$	$> 10^5$	$> 10^5$
		$> 10^5$			
6	TROU EQUILIBRAGE BRIDE TAMBOUR	$> 10^5$	$> 10^5$	$> 10^5$	$> 10^5$
		$> 10^5$			
7	TROU BRIDE VIROLE ARRIERE DE CAPOT	$> 10^5$	$> 10^5$	$> 10^5$	$> 10^5$
		$> 10^5$			
8	FESTON BRIDE VIROLE ARRIERE DE CAPOT	$> 10^5$	$> 10^5$	$> 10^5$	$> 10^5$
		$> 10^5$			
9	ALESAGE	$> 10^5$	$> 10^5$	$> 10^5$	$> 10^5$
		$> 10^5$			
10	ALVEOLE	$> 10^5$	$> 10^5$	$> 10^5$	$> 10^5$
		$> 10^5$			

Fig. 24 : Durée de vie pour l'ensemble des points

Cependant, ces études de dimensionnement sont sanctionnées par des essais en fosse de survitesse. Ces essais ont pour but de conforter la prévision de durée de vie. Il convient alors de limiter la durée des essais en majorant le régime maximum. Dans le cas du disque fan, le régime maximum sur moteur est 4900 tr/mn, mais la vitesse en fosse varie de 0 à 5400 tr/mn. La démarche ci-dessus est donc reprise pour prévoir l'endommagement du cycle d'essais et son équivalence en "mission-type".

7 - ESSAIS CYCLIQUES EN FOSSE DE SURVITESSE

L'essai est fait sous vide dans une fosse de survitesse. Le disque est monté avec un jeu complet d'aubes ainsi que les pièces voisines (fig. 25).

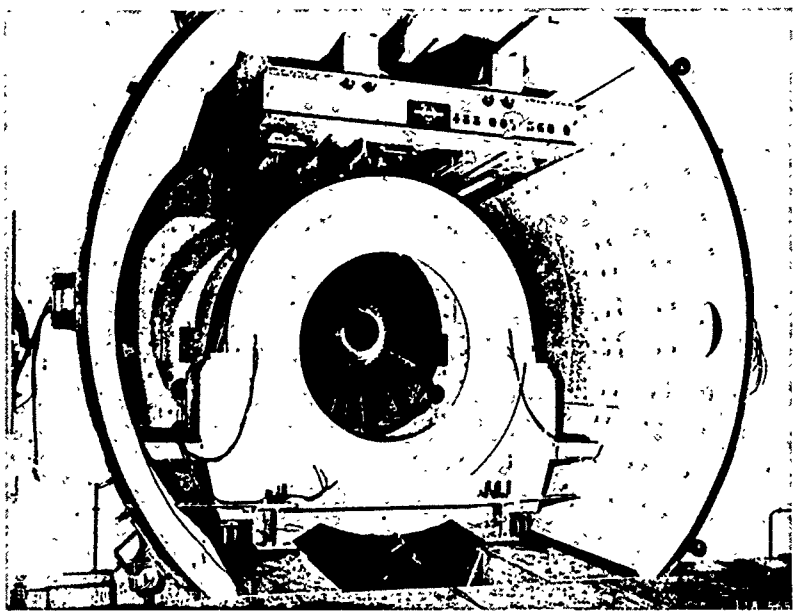

Fig. 25 : Banc d'essais de fatigue oligo-cyclique

La nature du titane et les dimensions de la pièce (présence de pré-contraintes résiduelles) rendent délicate la détection des défauts : c'est pourquoi des contrôles par ressuage sous tension, sont effectués tous les 5000 cycles. Actuellement, les résultats d'essais sont les suivants :

- aucun défaut constaté après 45000 cycles,
- un raccordement criqué à 50000 cycles.

La vitesse de rotation utilisée est de 5400 tr/mn et la caractérisation du disque d'essai, grâce aux anneaux attenants, situe ses performances en fatigue à - 0,9 écart-type. Chaque cycle d'essai est donc équivalent à 1,16 mission-type. L'essai complet est équivalent à 52000 missions-types, ce qui conforte la durée de vie prédite.

Autres essais en cours :

En plus d'une caractérisation métallurgique du titane de plus en plus approfondie, un moteur "fleet-leader" accumule des cycles d'endommagement, très en avance sur la flotte, soit environ 9000 cycles aujourd'hui.

8 - CONCLUSION

Les méthodes de plus en plus précises décrites ci-dessus ont permis d'aboutir à une prévision tout à fait satisfaisante de la durée de vie. Les paramètres métallurgiques influençant le potentiel du TA 6 V, sont aujourd'hui bien connus et les méthodes de calculs fortement automatisées.

Le disque de soufflante est localement plastique au point critique. Les résultats obtenus au terme du dimensionnement montrent que l'hypothèse simplificatrice de NEUBER est justifiée dans ce cas particulier. Cependant, le calcul des zones de formes complexes et fortement plastifiées serait maintenant réalisé par la méthode des éléments finis. La prise en compte des gradients thermiques sera donc aussi possible dans le cas de disques de turbine.

Dans un avenir proche, l'effort de recherche portera sur la connaissance des lois de comportement des matériaux dans le domaine plastique et sous un état de sollicitations complexe . En particulier, les critères d'endommagement devront être précisés et validés ainsi que l'évolution du comportement cyclique du matériau (σ , ε) durant la vie de la pièce : travaux LEMAITRE - CHABOCHE à l'ONERA...)

DISCUSSION

P.P.Meegdes, Ne

Did you, in your test cycle, account for windmilling effects, both on the ground and in the air?

Author's Reply

During windmilling phases of operations, wear is prevented by using coatings. Windmilling is at 2500 rpm.

P.P.Meegdes, Ne

Did you in the calculations account for continued operations with high vibration levels, and/or a fan blade out during take-off?

Author's Reply

We have never experienced a fan blade loss. We have studied this problem and conducted intentional blade loss testing in a spin pit.

VIEW OF FUTURE REQUIREMENTS FOR ENGINE CYCLIC DURABILITY BY ANALYSIS AND TESTING

by
T. E. Farmer
Structures Technology
Group Leader
Pratt & Whitney Aircraft Group
Engineering Division
United Technologies Corporation
P. O. Box 2691, M/S 713-39
West Palm Beach, Florida 33402
United States

SUMMARY

Engine cyclic durability testing today is an integral part of the development program. Cyclic durability testing is employed to substantiate achievement of component life goals. Completion of a comprehensive cyclic life demonstration program establishes component capability, quantifies effects (and amount) of deterioration and prevents costly field retro-fit requirements of sub-standard components. To be comprehensive, a cyclic durability test must employ the latest advances in test procedure, instrumentation and analytical tools for evaluation. While each of these critical disciplines has been advanced in the recent past, a more compatible relation is required between the three to achieve durability demonstration goals of the future.

ABSTRACT

Future requirements of engine cyclic durability analysis and testing must satisfy advancements in technology and configuration in a cost-effective manner. The emphasis on demonstrating engine durability will continue. It is essential that an integrated approach to durability verification be developed and involve component durability analysis, engine measured parameters, laboratory test and engine demonstrated capabilities. Automated analysis techniques must confidently relate test conditions to field operation; non-interference sensors and enhanced data acquisition systems are required for extended test periods; and, engine testing must efficiently address sensitivities, operating limits and cyclic capabilities. Verified component durability prediction systems that are developed will reduce the number of required engine endurance tests. Through coordination of durability analysis, data acquisition and component demonstration testing, more complete knowledge of engine durability will be achieved in a cost-effective manner.

PROBLEM

Future requirements of cyclic durability testing will increase the complexity of the problem. While mission and life goals are extended, competition in the gas turbine engine market increases for the available contracts. Thus, we develop a potentially contradictory requirement for our cyclic durability testing: the best proof of our engine's capability to satisfy a difficult mission goal at the lowest cost!

As shown in Figure 1, cyclic life goals of tactical fighter engines in the U.S. inventory have increased from 2000 cycles in 1970 to six times that goal today. Additionally, the missions have expanded in complexity due to broadened applications for today's tactical fighter.

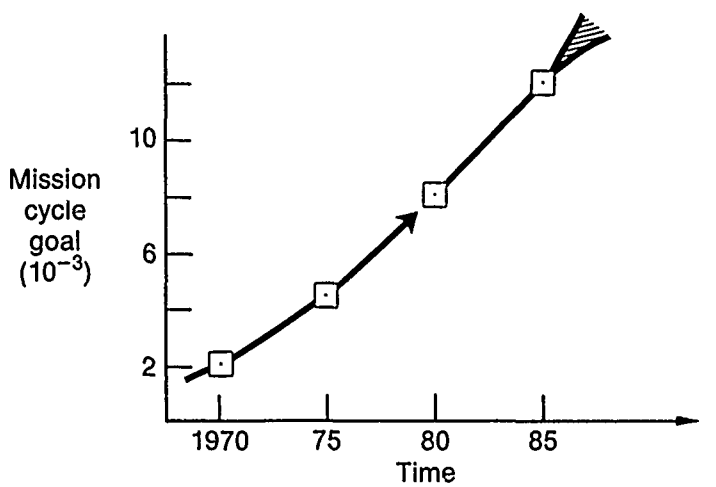

Figure 1. Cyclic Requirements Have Increased

Gas turbine engines in the U.S. inventory must now satisfy damage tolerance requirements which require demonstration of the crack propagation life of critical components and confirmation of inspection capability for detection of component distress. It is no longer sufficient to complete the mission test goal without cracking, the contractor must demonstrate the gas turbine engine's capability with cracks! Not suprisingly, the disciplines of thermodynamics and materials technology have advanced in concert with the cyclic life goals generating an engine configuration considered optimum for the intended usage. Thus, we must confirm ever increasing mission capabilities in a more efficient manner to keep development costs competitive. Incorporation of improved testing techniques, advanced

instrumentation and sophisticated analytical capabilities will offset the complexity of the cyclic durability test problem and allow efficient engine development and demonstration.

DISCUSSION

Advancements in testing procedures and facilities must be pursued to satisfy the cyclic durability test requirements of the future. Improved instrumentation will be used as the link between engine test demonstration results and the advanced analytical techniques. While predictions and early rig data are used to establish the engine operating environment and limits prior to test, the effects of engine operation as established (measured) by reliable instrumentation must be accessed and evaluated by sophisticated, interactive analytical procedures which establish durability limits on a component basis for quick reponse to potential problems.

TEST PROCEDURES

During the last ten years, endurance or Accelerated Mission Testing (AMT) procedures and techniques have improved significantly. Testing efficiencies and mission simulation accuracy have been improved through diligent interface between test, mission analysis and durability groups. For the future, mission simulation accuracy must be maintained, but efficiency will be advanced and an improved assessment of sensitivities will be sought. A key to improved testing efficiency, is the early characterization of the operating environment.

A thorough set of Environmental Characterization Tests will save test time later by enhancing the focus on criticality of components and allowing test cycles, time and operating procedures to most accurately address those prime components of interest in the most efficient manner. Therefore, instrumented testing payoffs increase greatly by measuring the component environmental effects of the widest possible range of mission related procedures and conditions. By confirming the influences of rapid throttle movements, idle/intermediate dwells, surges and other conditions on component temperature, pressure and deflection, the life prediction and demonstration efficiency is improved remarkably.

Understanding of the combined (or sequenced) throttle motion influences on component clearances, loadings and temperatures is critical in establishing mission points for analysis and test; in verifying deterioration due to rubs or distress; and in culling the insignificant mission points from the endurance test plan. A cyclic endurance test cannot accelerate all damage. Wear and other cruise point related distress modes are better evaluated by laboratory bearing, bushing or other dwell test rigs. Figure 2 gives an example of AMT test cycle reduction.

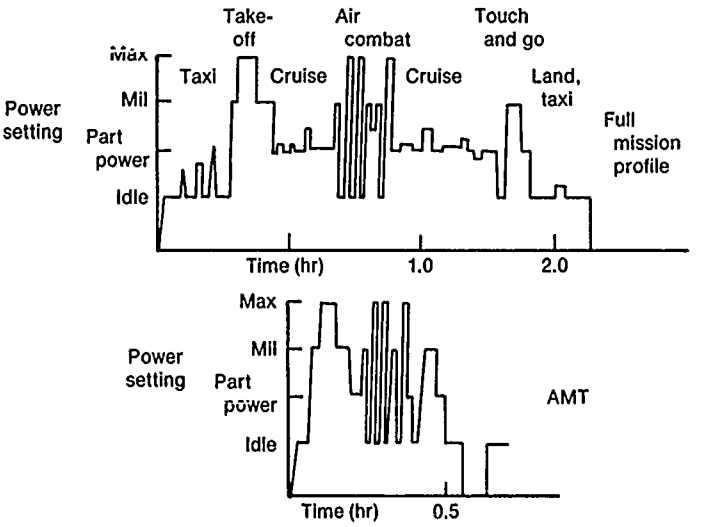

Figure 2. AMT Cycle Compression

The cyclic endurance test must be operated to simulate the primary mission points limiting crack initiation/propagation, creep/stress rupture and overstress/deflection of the engine. Turbine blade life is driven by dwell time at military power and throttle transients from idle to military or maximum power. However, the larger mass of the turbine rotor is very sensitive to the time history at temperature and the related engine speeds. A fully heated high turbine rotor can double its rim stress by a 90 second dwell at idle with an immediate snap acceleration to military power by thus generating a hot bore, cool rim thermal condition with stresses equivalent to those of the centrifugal loading at engine military power. This type operation is critical in establishing the turbine rim cyclic life as shown in Figure 3.

Engine stalls should be induced to evaluate/simulate clearance effects of such mission occurrences. Additionally, rotor unbalance limits must be run to verify additional clearance effects which result in engine deterioration and higher operating temperatures to retain thrust. The interactive test, measurement and analysis of the effects enhances the endurance test cycle by quickly establishing the critical test conditions. (Rate of occurrence of critical mission conditions is based on field interviews and instrumentation and will not be discussed here).

Testing efficiency can be improved with the facilities used. A unique core engine test facility has been in use at Pratt & Whitney Aircraft for two years. This facility allows efficient simulation of full engine operation for the core of multi-spool configurations. Hot section environmental

characterization and durability demonstration can be easily accomplished in the facility shown in Figure 4. This test system can simulate the full range of temperature, pressure and airflow requirements of a core and at the desired rate for rapid throttle transients. Core engine testing of this nature affords excellent opportunity for measurement of critical environmental parameters.

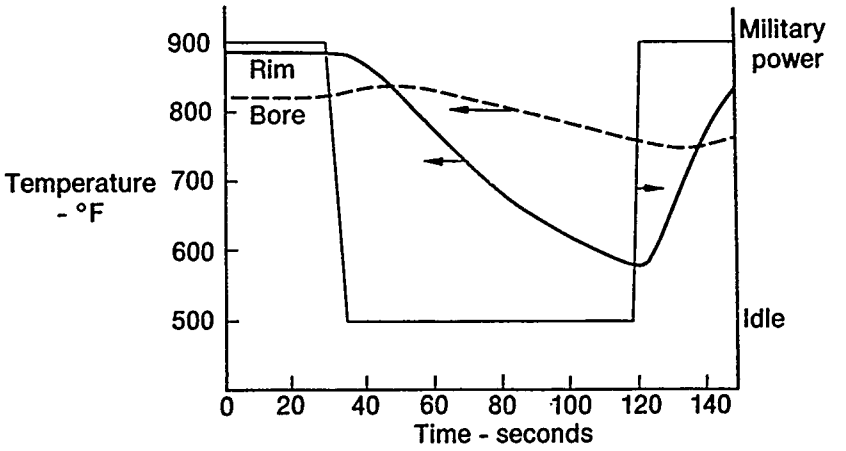

Figure 3. Idle Dwell Effects on Turbine Rotor

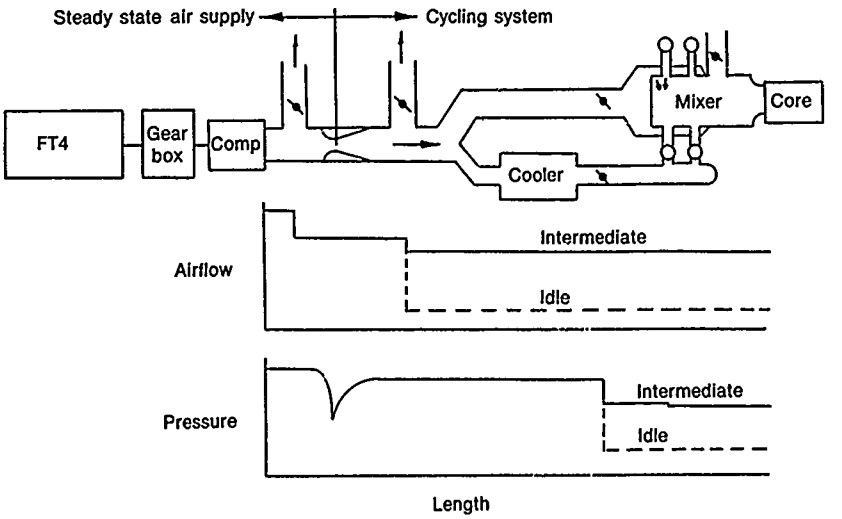

Figure 4. Core Test Facility

INSTRUMENTATION

Advanced instrumentation will be employed in engine durability testing to gain accurate data with minimal effect on the engine performance and durability by sensor configuration and application. While standard slip-ring technology has advanced and will continue to be used as an instrumentation read-out system, as will improved telemetry systems, non-contacting (remote) instrumentation will be a key for successful advanced engine durability testing.

Slip-rings have become smaller and can accommodate 100 channels of data. This trend will continue. Telemetry systems also have advanced in compactness, number of channels and reliability. These are important tools in initial single and multi-spool testing to evaluate component environments and response. However, application of these sensors and the associated leadwork reduce the engine performance, cause configuration revisions and usually diminish component durability through routing and attachment requirements for sensor durability.

These shortcomings will not be experienced with the use of non-contacting deflection and temperature measurement devices. The only detriment to the engine in accommodating this type of sensor is provision for access ports in the static structure. Currently, deflection measurement devices can give rotor/stator clearance read-outs macroscopically. High response units employ laser sensing systems.

Photoelectric Scanning (PES) can currently be employed as a flutter monitor. This optical system can be adapted as shown in Figure 5 to supply real time monitoring of each blade in a stage. By sensing the change in time between subsequent passings of each blade tip, the PES system can establish the presence of non-integral response (flutter). Constant passings are indicative of no resonance or integral (with engine once-per-revolution frequency) order response. Efforts are underway to provide resonance monitoring capability for the PES system. With this system, airfoil response versus engine time and related deterioration will be quantified without affecting engine component durability or performance.

Optical pyrometers offer individual blade metal temperature sensing. This capability, when focused on the life limiting location, can increase endurance test safety and efficiency by allowing real time assessment of airfoil distress. Shutdowns, inspections and teardowns are accomplished as required. This instrumentation has been incorporated into the engine control systems of today.

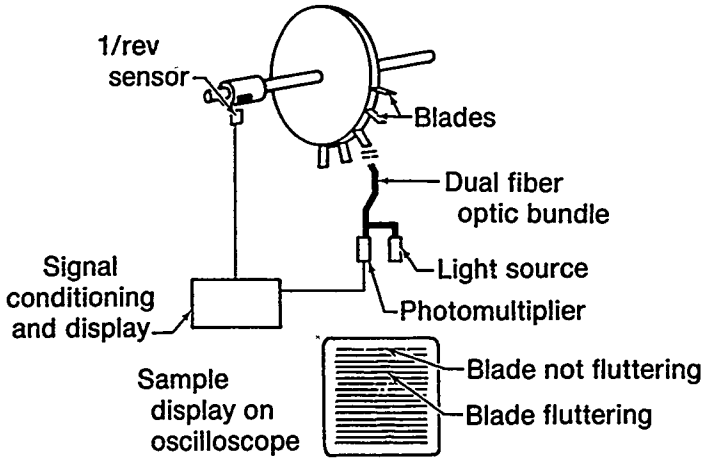

Figure 5. Photoelectric Scanning System Elements

ANALYSIS

Durability prediction has advanced from Manson's equation to non-linear finite element analyses in the last twenty years. Component life prediction has gained from the correlations with engine experience. Today, creep/ fatigue interaction is predicted for the hot section components (Figure 6); crack propagation analysis is a regular requirement in the U.S. engine application. Component modal analysis has been employed to link hardware test and analysis for complex structures. The analytical capabilities will continue to require hardware test correlations. As prediction capability improves the configuration and/or materials are changed to gain further advantage requiring additional correlation.

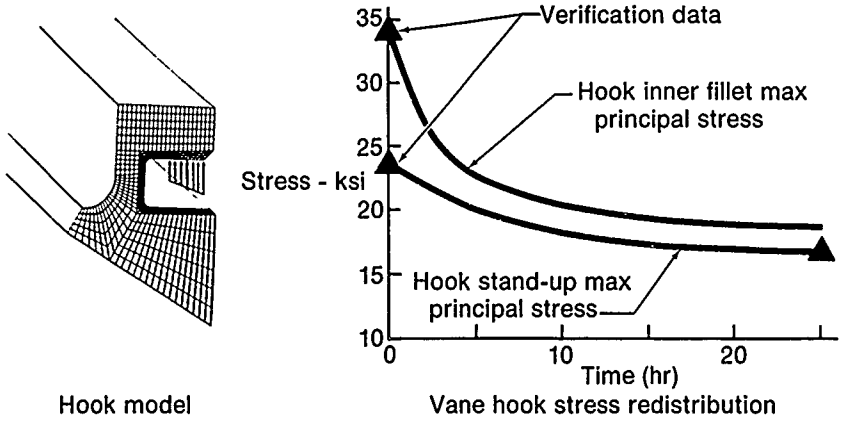

Figure 6. Hot Section Stress Redistribution

CONCLUSION

To achieve the greatest benefit from the advancements, their capabilities must be coordinated. After the environmental characterization engine test, a Life Assessment Test Engine can be dedicated to durability assessment. The endurance cycle engine test accelerates damage by eliminating the less severe mission points, e.g. cruise, idle and slow transients. This test "leads the fleet" by accumulating primary damage cycles and hot time at a much faster rate than the field on the baseline configuration.

Additional acceleration can be achieved for particular engine components by modification of environment and/or material while retaining the same predicted failure mode as the baseline component. For example:

- Reduction of cooling air to a hot section component verifies a life prediction for oxidation or LCF in less time than the baseline.
- Alloys of lesser capability are used to demonstrate design system capabilities quickly to corroborate baseline predictions.

By monitoring the reduced life configurations with non-contacting stress and temperature sensors, safety is maintained during life verification. The entire stage or assembly often would not be of reduced capability. This allows baseline comparison of distress rate. Interactive performance, rotor dynamic and life prediction systems will access the engine data to identify critical shifts in data and highlight near term life limits.

Operation of engine rotors with active cracks has been demonstrated on several occasions. Crack propagation tracking tests are far more efficient single component tests than crack initiation testing, due to reduced material scatter for crack propagation, sensitivity to local stress gradients and improved inspection procedures for tracking propagation rate (Figure 7).

Life Assessment Test (LAT) techniques have been used for years for component durability verification. However, by coordinating the testing activity to maximize the knowledge gained from all available facilities, as shown in Figure 8, a more efficient program is established. Endurance test acceleration knows no limit. The means will be available for rapid, low risk verification of component life limits. Early, thorough characterization, reduced component capability cyclic testing and efficient endurance testing will improve the competitive edge of the out year engine manufacturer.

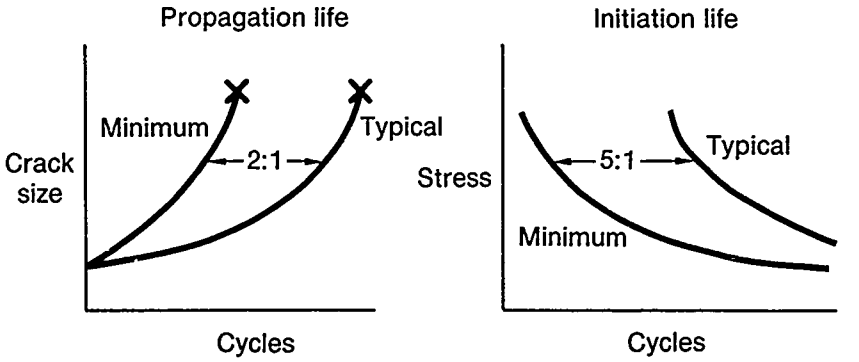

Figure 7. Reduced Scatter of Fracture Mechanics

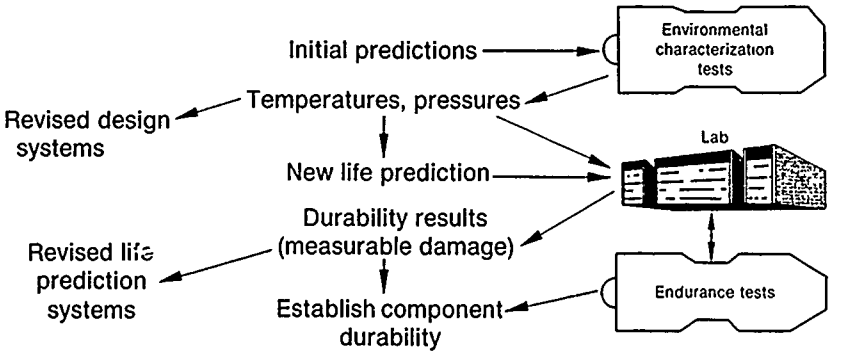

Figure 8. Life Assessment Test Engine

REFERENCES

1. McDonnell, Bernard J., "Accelerated Mission Test - A Vital Reliability Tool." AGARD Propulsion and Energetics Panel, The Hague, Netherlands, March, 1977.

2. Sammons, Jack ,"Using Accelerated Mission Testing as a Tool Within the F100 Engine Component." AIAA/SAE 14th Propulsion Conference, July, 1978.

3. Brown, B. T., "Low Cycle Fatigue Testing Facility." AIAA, June, 1982.

4. Nieberding, W. C. and Pollack, W. C., "Optical Detection of Blade Flutter." NASA, March, 1977.

5. Buchele, Donald R., "Surface Pyrometry in Presence of Radiation From Other Sources With Application to Turbine Blade Temperature Measurement." NASA, December, 1980.

6. Hill, R. J., "Engine Durability Assessment Through the Use of Life Assessment Testing (LAT)." AIAA, May, 1980.

DISCUSSION

G.K.Waddington, UK

What techniques would you suggest for the evaluation of integral flutter in turbine rotors?

Author's Reply

Currently, integral response can only be monitored by strain-gauges applied to the component and, for rotors, read-out through a slip-ring or telemetry system. Studies are under way to employ optical sensing of resonant response.

A.J.A.Mom, Ne

Can you comment on the point that for a damage tolerance approach for disc lifing one needs NDI techniques which should also be able to detect internal defects/cracks; or are internally developing cracks in practice less important?

Author's Reply

While internal defects are currently analysed as 'in service non-inspectable', there is interest in developing improved finished part inspection capability to allow improved safety and perhaps extended usage for components limited by internal defect rupture life.

D.W.Hoeppner, Ca

In your presentation you mentioned the desirability to develop standard test procedures and specimens related to improved design and AMT testing. Would you please comment on this further?

Author's Reply

Universal agreement on material characterization procedures and specimen types can reduce cost of testing of non-proprietary materials by publication and resultant sharing of test results.

REPORT DOCUMENTATION PAGE

1. Recipient's Reference	2. Originator's Reference	3. Further Reference	4. Security Classification of Document
	AGARD-CP-368	ISBN 92-835-0362-7	UNCLASSIFIED

5. Originator: Advisory Group for Aerospace Research and Development
North Atlantic Treaty Organization
7 rue Ancelle, 92200 Neuilly sur Seine, France

6. Title

ENGINE CYCLIC DURABILITY BY ANALYSIS AND TESTING

7. Presented at: the Propulsion and Energetics Panel 63rd (B) Specialists' Meeting, in Lisse, Netherlands, 30 May — 1 June 1984.

8. Author(s)/Editor(s)	9. Date
	September 1984
10. Author's/Editor's Address	**11. Pages**
	206

13. Keywords/Descriptors

Accelerated mission testing
Crack growing
Cyclic testing
Durability of engines
Failure mechanisms
Life assessment of components
Low cycle fatigue
Material characteristics

14. Abstract

The Conference Proceedings contains 19 papers presented at the Propulsion and Energetics 63rd (B) Specialists' Meeting on Engine Cyclic Durability by Analysis and Testing, which was held in Lisse, Netherlands, on 30 May — 1 June 1984.

The Technical Evaluation Report is included at the beginning of the Proceedings. Questions and answers of the discussions follow each paper. The Specialists' Meeting was arranged in four sessions: Engine Utilization and Accelerated Mission Testing Development (3); Critical Material Characterization (4); Life Assessment Methodologies (4); and Component and Engine Cyclic Testing (8).

The Specialists' Meeting surveyed the current state-of-the-art in technological areas related to improving engine life. It considered the technical and economical problems of advanced cyclic testing in the development of engines. Discussed were. relationships between engine utilization and failure modes, accelerated mission testing development, critical material characteristics, component life assessment methods, recent results of component and engine cyclic testing, and future requirements.

AGARD Conference Proceedings No.368
Advisory Group for Aerospace Research and Development, NATO
ENGINE CYCLIC DURABILITY BY ANALYSIS AND TESTING
Published September 1984
206 pages

The Conference Proceedings contains 19 papers presented at the Propulsion and Energetics 63rd (B) Specialists' Meeting on Engine Cyclic Durability by Analysis and Testing, which was held in Lisse, Netherlands, on 30 May — 1 June 1984.

The Technical Evaluation Report is included at the beginning of the Proceedings. Questions and answers of

P.T.O.

AGARD-CP-368

Accelerated mission testing
Crack growing
Cyclic testing
Durability of engines
Failure mechanisms
Life assessment of components
Low cycle fatigue
Material characteristics

AGARD Conference Proceedings No.368
Advisory Group for Aerospace Research and Development, NATO
ENGINE CYCLIC DURABILITY BY ANALYSIS AND TESTING
Published September 1984
206 pages

The Conference Proceedings contains 19 papers presented at the Propulsion and Energetics 63rd (B) Specialists' Meeting on Engine Cyclic Durability by Analysis and Testing, which was held in Lisse, Netherlands, on 30 May — 1 June 1984.

The Technical Evaluation Report is included at the beginning of the Proceedings. Questions and answers of

P.T.O.

AGARD-CP-368

Accelerated mission testing
Crack growing
Cyclic testing
Durability of engines
Failure mechanisms
Life assessment of components
Low cycle fatigue
Material characteristics

AGARD Conference Proceedings No.368
Advisory Group for Aerospace Research and Development, NATO
ENGINE CYCLIC DURABILITY BY ANALYSIS AND TESTING
Published September 1984
206 pages

The Conference Proceedings contains 19 papers presented at the Propulsion and Energetics 63rd (B) Specialists' Meeting on Engine Cyclic Durability by Analysis and Testing, which was held in Lisse, Netherlands, on 30 May — 1 June 1984.

The Technical Evaluation Report is included at the beginning of the Proceedings. Questions and answers of

P.T.O.

AGARD-CP-368

Accelerated mission testing
Crack growing
Cyclic testing
Durability of engines
Failure mechanisms
Life assessment of components
Low cycle fatigue
Material characteristics

AGARD Conference Proceedings No.368
Advisory Group for Aerospace Research and Development, NATO
ENGINE CYCLIC DURABILITY BY ANALYSIS AND TESTING
Published September 1984
206 pages

The Conference Proceedings contains 19 papers presented at the Propulsion and Energetics 63rd (B) Specialists' Meeting on Engine Cyclic Durability by Analysis and Testing, which was held in Lisse, Netherlands, on 30 May — 1 June 1984.

The Technical Evaluation Report is included at the beginning of the Proceedings. Questions and answers of

P.T.O.

AGARD-CP-368

Accelerated mission testing
Crack growing
Cyclic testing
Durability of engines
Failure mechanisms
Life assessment of components
Low cycle fatigue
Material characteristics

the discussions follow each paper. The Specialists' Meeting was arranged in four sessions: Engine Utilization and Accelerated Mission Testing Development (3); Critical Material Characterization (4); Life Assessment Methodologies (4); and Component and Engine Cyclic Testing (8).

The Specialists' Meeting surveyed the current state-of-the-art in technological areas related to improving engine life. It considered the technical and economical problems of advanced cyclic testing in the development of engines. Discussed were: relationships between engine utilization and failure modes, accelerated mission testing development, critical material charateristics, component life assessment methods, recent results of component and engine cyclic testing, and future requirements.

ISBN 92-835-0362-7

the discussions follow each paper. The Specialists' Meeting was arranged in four sessions: Engine Utilization and Accelerated Mission Testing Development (3); Critical Material Characterization (4); Life Assessment Methodologies (4); and Component and Engine Cyclic Testing (8).

The Specialists' Meeting surveyed the current state-of-the-art in technological areas related to improving engine life. It considered the technical and economical problems of advanced cyclic testing in the development of engines. Discussed were: relationships between engine utilization and failure modes, accelerated mission testing development, critical material charateristics, component life assessment methods, recent results of component and engine cyclic testing, and future requirements.

ISBN 92-835-0362-7

the discussions follow each paper. The Specialists' Meeting was arranged in four sessions: Engine Utilization and Accelerated Mission Testing Development (3); Critical Material Characterization (4); Life Assessment Methodologies (4); and Component and Engine Cyclic Testing (8).

The Specialists' Meeting surveyed the current state-of-the-art in technological areas related to improving engine life. It considered the technical and economical problems of advanced cyclic testing in the development of engines. Discussed were: relationships between engine utilization and failure modes, accelerated mission testing development, critical material charateristics, component life assessment methods, recent results of component and engine cyclic testing, and future requirements.

ISBN 92-835-0362-7

the discussions follow each paper. The Specialists' Meeting was arranged in four sessions: Engine Utilization and Accelerated Mission Testing Development (3); Critical Material Characterization (4); Life Assessment Methodologies (4); and Component and Engine Cyclic Testing (8).

The Specialists' Meeting surveyed the current state-of-the-art in technological areas related to improving engine life. It considered the technical and economical problems of advanced cyclic testing in the development of engines. Discussed were: relationships between engine utilization and failure modes, accelerated mission testing development, critical material charateristics, component life assessment methods, recent results of component and engine cyclic testing, and future requirements.

ISBN 92-835-0362-7